

## N O T I C E

THIS DOCUMENT HAS BEEN REPRODUCED FROM  
MICROFICHE. ALTHOUGH IT IS RECOGNIZED THAT  
CERTAIN PORTIONS ARE ILLEGIBLE, IT IS BEING RELEASED  
IN THE INTEREST OF MAKING AVAILABLE AS MUCH  
INFORMATION AS POSSIBLE

REPORT NO. GDC-GPP-79-006 (II)  
CONTRACT NAS8-33527  
JUNE 1980

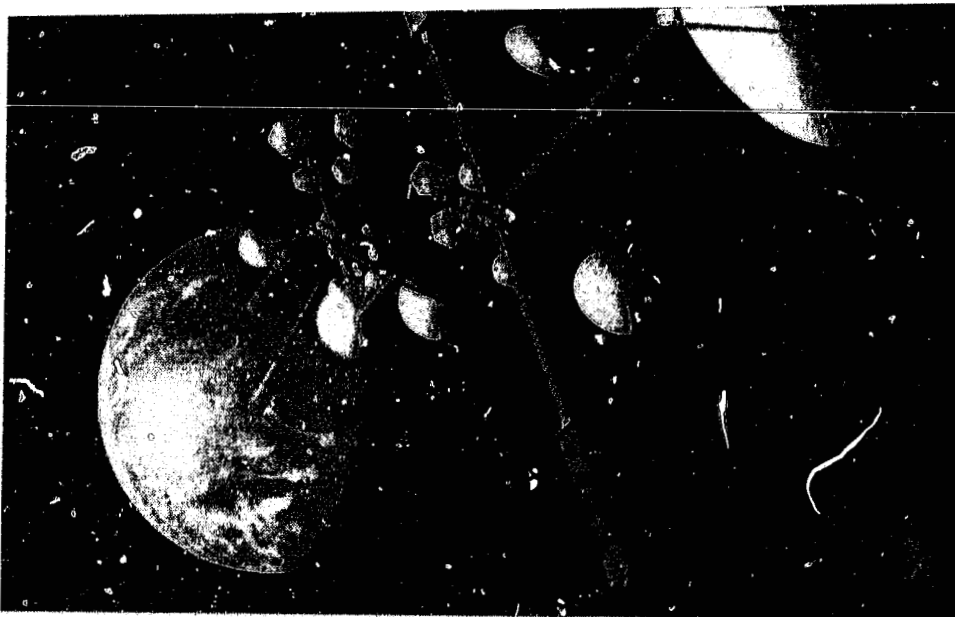
# GEOSTATIONARY PLATFORM SYSTEMS CONCEPTS DEFINITION STUDY

## FINAL REPORT VOLUME II TECHNICAL BOOK 2 OF 3

(NASA-CR-161649) GEOSTATIONARY PLATFORM  
SYSTEMS CONCEPTS DEFINITION STUDY. VOLUME  
2: TECHNICAL, BOOK 2 Final Report (General  
Dynamics/Convair) 413 p HC A18/MI A01

W81-18074

Unclassified  
CSCL 22B G3/15 16497

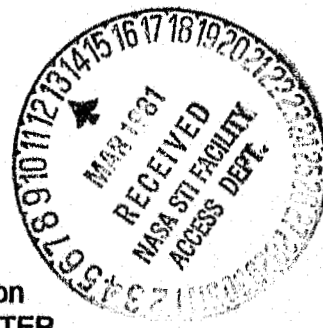


Prepared by

**GENERAL DYNAMICS**  
*Convair Division*  
&  
**COMSAT**

for the

National Aeronautics and Space Administration  
GEORGE C. MARSHALL SPACE FLIGHT CENTER  
Huntsville, Alabama



REPORT NO. GDC-GPP-79-006 (II)  
CONTRACT NAS8-33527

## FINAL REPORT

# GEOSTATIONARY PLATFORM SYSTEMS CONCEPTS DEFINITION STUDY

## VOLUME II TECHNICAL BOOK 2 OF 3

JUNE 1980

Submitted to  
GEORGE C. MARSHALL SPACE FLIGHT CENTER  
National Aeronautics and Space Administration  
Marshall Space Flight Center, Alabama 35812

Prepared by  
GENERAL DYNAMICS CONVAIR DIVISION  
P.O. Box 80847  
San Diego, California 92138

and

COMMUNICATIONS SATELLITE CORPORATION  
COMSAT Laboratories  
Clarksburg, Maryland 20734

GEOSTATIONARY PLATFORM SYSTEMS  
CONCEPTS DEFINITION STUDY  
FINAL REPORT

VOLUME I	EXECUTIVE SUMMARY
VOLUME II	TECHNICAL ANALYSIS, TASKS 1 – 5, 3A
BOOK 1 OF 3	TASKS 1 AND 2
►BOOK 2 OF 3	TASK 3
BOOK 3 OF 3	TASKS 4, 5, AND 3A
VOLUME II(A)	TECHNICAL APPENDIXES
BOOK 1 OF 2	APPENDIX A – G
BOOK 2 OF 2	APPENDIX H – L
VOLUME III	COSTS AND SCHEDULES, TASK 6

This report is submitted in fulfillment of NASA/MSFC Contract NAS8-33527.  
Publication of this report does not constitute approval by the National Aero-  
nautics and Space Administration of the report's findings or conclusions.

1 July 1980

*William T. Carey*  
\_\_\_\_\_  
William T. Carey, Chief  
Applications Group, PS06  
George C. Marshall Space Flight Center  
Huntsville, Alabama

## ACKNOWLEDGEMENT

This study was performed under the guidance and direction of Mr. William T. Carey, Chief of the George C. Marshall Space Flight Center's Space Applications Group. His capable technical direction, liaison activities, and coordination of the many participants and organizations who contributed to this study are gratefully acknowledged. We are particularly indebted to the following for their generous assistance, suggestions, opinions, and contributions in the areas of technical expertise and program planning:

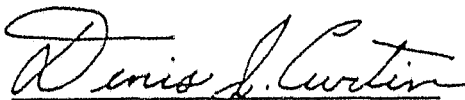
Mr. Ivan Bekey	NASA Headquarters
Mr. Samuel W. Fordyce	NASA Headquarters
Mr. Mark Nolan	NASA Headquarters
Mr. George Knouse	NASA Headquarters
Mr. Clay Hamilton	NASA/MSFC
Mr. Joseph N. Sivo	NASA LeRC
Dr. Burton I. Edelson	COMSAT Corporation
Dr. Robert T. Filep	Communications 21 Corp.
Dr. Fred Bond	Aerospace Corp.
Dr. Reinhard Stammerger	Future Systems Inc.
Dr. Delbert D. Smith	Satellite Communications Magazine

Above all, we wish to thank the study team members at General Dynamics Convair and COMSAT Corporation whose dedication, long hours, and technical competence developed the analyses, data, and recommendations in this study.

While all assistance is acknowledged and appreciated, General Dynamics Convair and COMSAT Corporation accept full responsibility for the opinions, recommendations, and data presented in this report.



Dr. Robert M. Bowman  
Study Manager  
General Dynamics Convair



Dr. Denis J. Curtin  
Subcontract Manager  
COMSAT Corporation

## PREFACE

In today's world of expanding communication, military, and science satellite services, the geostationary orbit is rapidly becoming an extremely valuable and limited earth resource. Nations demand specific positions or "slots" in the orbit corresponding to their geographic longitude, seeking to maximize their territorial coverage and satellite performance. Sovereignty becomes an issue, with several nations at different latitudes and one longitude competing for the common longitudinal slot in the orbital arc. Common carriers within a developed nation demand equal rights for the best slots. Competition has been strong in the developed nations, and the developing nations are now voicing their concern.

At geosynchronous altitude, independent satellites operating at the same frequency must be separated by about 4 degrees of longitude to prevent RF interference (30 dB separation), dictated by the large beam widths of the small affordable ground antennas now in use. About 90 "slots" therefore exist around the world, with about 12 over the U. S. and our northern and southern neighbors.

The frequency spectrum is also a valuable and limited resource that is rapidly approaching saturation, particularly in those regions of low noise and freedom from atmospheric attenuation.

Both resources are now allocated worldwide by the International Telecommunications Union operating through subservient multinational and national agencies. Reallocation cannot solve our basic orbital arc and frequency saturation problems. Recent studies have shown projected traffic demands which will saturate both the geostationary orbital arc and the optimal frequency spectra in the near future. In the U. S. alone, current domestic satellite capacity is about 100 transponders. Projections indicate a five-fold increase in traffic demand for voice, data, and TV distribution in the next 10 years (by 1990); ten-fold by the year 2000. If video and audio conferencing expand as projected, the jump may be to 20 to 50 times the present traffic by 1990 and the year 2000, respectively.

Motivation for the rapid adoption of satellite communications services is primarily economic. Satellite communications provide lower service cost for certain fixed applications, economy of flexibility, and appreciable cost savings over terrestrial operation for mobile services direct to the users. Savings can be increased still further if the cost, complexity, and size of ground stations can be reduced by application of advanced communications and support technologies to a few satellites with expanded capabilities.

What is the solution to our orbital arc and frequency spectrum saturation problems, a solution that also lends itself to reduction of user costs?

One viable solution is the aggregation of many transponders, large antennas, and connectivity switches on board a small number of large orbital facilities. Such facilities, or platforms, can provide common power and housekeeping services to a number of coexistent communications systems, making maximum use of a single orbital slot. Large antennas with multiple spot beams and good isolation, bandwidth reduction, polarization diversity, and system interconnectivity can provide an equivalent transponder capacity over the U. S. at least an order of magnitude greater than the projected traffic demand for the year 2000.

In the public interest, NASA has initiated a program to encourage development of such geostationary platforms, anticipating the need for increased communications and other services in the near decades, at lower costs. In the past two years, initial NASA studies<sup>1</sup> have established the need and requirements for, and the feasibility of these platforms. NASA's George C. Marshall Space Flight Center has been authorized to carry out in-depth studies of geostationary platforms.

This report documents the results of the Geostationary Platform Initial Phase A Study, performed by General Dynamics Convair Division of San Diego with COMSAT Corporation of Clarksburg, Maryland, as subcontractor, under direction of the Marshall Space Flight Center. The performance period was from 1 June 1979 to 30 June 1980.

---

<sup>1</sup> "Large Communications Platforms Versus Smaller Satellites," Future Systems, Inc., Report No. 221 February 1979, prepared for NASA HQ.

"Geostationary Platform Feasibility Study," Aerospace Corp., Report No. ATR-79(7749)-1, 28 September 1979, prepared for NASA/MSFC.

"Geostationary Platforms Mission and Payload Requirements Study," 30 October 1979, prepared for NASA/MSFC.

"18/30 GHz Communication System Service Demand Assessment," 30 June 1979, parallel studies by Western Union and ITT for NASA/LeRC.

"18/30 GHz Communications Service System Study," June 1979, parallel studies by Ford Aerospace & Communications Corp., and by Hughes Aircraft Co. for NASA/LeRC.

## TABLE OF CONTENTS

<u>Section</u>		<u>Page</u>
<b>PART I - OPERATIONAL GEOSTATIONARY PLATFORMS</b>		
<b>BOOK 1</b>		
<b>1</b>	<b>TASK 1: MISSIONS AND PAYLOADS DEFINITION</b>	<b>1-1</b>
1.1	OBJECTIVES	1-3
1.2	INPUT DATA	1-3
1.3	MISSION AND PAYLOAD IDENTIFICATION	1-5
1.4	REQUIREMENTS DEFINITION	1-5
1.4.1	Mission/Payload Groupings	1-9
1.4.2	Traffic Model Development	1-14
1.4.3	Platform Locations	1-16
1.4.4	Payload Architecture	1-19
1.4.5	Payload Requirements	1-39
1.4.6	Mission/Payload Allocation	1-41
1.4.7	Platform Support Requirements	1-54
1.5	REQUIREMENTS DOCUMENTATION	1-57
1.6	RESULTS AND CONCLUSIONS	1-62
<b>2</b>	<b>TASK 2: CONCEPT SELECTION</b>	<b>2-1</b>
2.1	TASK OBJECTIVES	2-1
2.2	INPUT DATA	2-1
2.3	METHODOLOGY	2-2
2.4	ANALYSIS AND RESULTS	2-17
2.4.1	Platform Design Philosophy	2-17
2.4.2	Basic System Trade Studies	2-22
2.4.3	Individual Satellites	2-70
2.4.4	Transfer Vehicle Comparison	2-74
2.4.5	Evolutionary Buildup Options	2-74
2.4.6	Comparison of Best Options	2-87
2.5	SELECTED CONCEPTS	2-87
2.5.1	Mission Set P	2-90
2.5.2	Operational Platform Alternatives	2-90
2.6	CONCLUSIONS	2-90
2.7	REFERENCES	2-105
<b>BOOK 2</b>		
<b>3</b>	<b>TASK 3: CONCEPTS DEFINITION</b>	<b>3-1</b>
3.1	PLATFORMS DEFINITION	3-1
3.1.1	Scope	3-1
3.1.2	Requirements and Constraints	3-3
3.1.3	Conceptual Designs	3-8
3.1.4	Antenna and Feed Designs	3-28
3.1.5	Electrical Power System (EPS)	3-43

**TABLE OF CONTENTS, Contd**

<u>Section</u>		<u>Page</u>
3.1.6	Control of Attitude and Position	3-109
3.1.7	Thermal Control	3-111
3.1.8	Mass Properties	3-119
3.1.9	Stress Analysis	3-123
3.1.10	Structural Dynamics	3-129
3.1.11	Reliability	3-129
3.1.12	Radiation Environment	3-140
3.2	TRANSPORTATION SYSTEMS	3-142
3.2.1	Transportation Requirements	3-142
3.2.2	Module Delivery Transportation Analysis	3-145
3.2.3	Logistics Missions Transportation Analysis	3-156
3.2.4	Debris Disposal Options	3-162
3.2.5	Space Based TMS Options	3-164
3.2.6	Conclusions and Recommendations	3-166
3.3	LOGISTICS PLAN AND MISSION MODEL	3-167
3.3.1	Mission Model	3-169
3.3.2	Logistics Plan	3-170
3.3.3	Flight Operations	3-181
3.4	SPECIALIZED COMMUNICATIONS/ INTEGRATION EQUIPMENT	3-185
3.4.1	Antennas and Feeds	3-185
3.4.2	High Accuracy Pointing Equipment	3-199
3.4.3	Switch Matrices	3-202
3.4.4	On-Board Regeneration	3-210
3.4.5	Interplatform Links	3-212
3.4.6	High Power Amplifiers	3-235
3.4.7	Electromagnetic Compatibility (EMC)	3-240
3.5	REFERENCES	3-247

**BOOK 3**

4	TASK 4: SUPPORTING RESEARCH AND TECHNOLOGY AND SPACE DEMONSTRATIONS	4-1
4.1	OBJECTIVE	4-1
4.2	SCOPE	4-1
4.3	METHODOLOGY	4-2
4.4	ANALYSIS AND RESULTS	4-4
4.4.1	Platform Subsystems	4-4
4.4.2	Communications	4-4
4.5	CONCLUSIONS AND RECOMMENDATIONS	4-73

## TABLE OF CONTENTS, Contd

<u>Section</u>	<u>Page</u>
5      TASK 5: STS INTERFACE REQUIREMENTS	5-1
5.1    ORBITER	5-1
5.1.1 Performance	5-2
5.1.2 Stowage and Deployment	5-2
5.1.3 Operations	5-10
5.1.4 Support Subsystem	5-11
5.1.5 Crew	5-16
5.2    ORBITAL TRANSFER VEHICLE (OTV)	5-17
5.2.1 OTV Performance	5-17
5.2.2 OTV Stowage and Deployment	5-18
5.2.3 Operations	5-19
5.2.4 Support Subsystems	5-22
5.3    SERVICING SYSTEM (TELEOPERATOR)	5-31
5.3.1 Servicing System Performance	5-31
5.3.2 Servicing System Envelope and Mass	5-31
5.3.3 Servicing System Operations	5-32
5.3.4 Support Subsystems	5-32
5.4    CONCLUSIONS AND RECOMMENDATIONS	5-39
 PART II - EXPERIMENTAL GEOSTATIONARY PLATFORMS	
6      TASK 3A: EXPERIMENTAL GEOSTATIONARY PLATFORMS	6-1
6.1    MISSION OBJECTIVE	6-1
6.2    SCOPE OF TASK	6-2
6.3    GROUND RULES AND GUIDELINES	6-2
6.4    INPUT DATA	6-3
6.5    STUDY PLAN	6-4
6.6    ANALYSIS AND RESULTS	6-4
6.6.1 Candidate Technologies	6-4
6.6.2 Candidate Payloads	6-7
6.6.3 Mission Options	6-15
6.6.4 Structural Concepts	6-20
6.6.5 Subsystem Requirements	6-31
6.7    EXPERIMENTAL PLATFORM CONCEPTS	6-39
6.7.1 Candidate Antenna Configurations	6-42
6.7.2 Candidate Platform Configurations	6-44
6.8    TRANSFER VEHICLE OPTIONS	6-83
6.9    EVALUATION	6-84
7      FUTURE WORK	7-1

## LIST OF FIGURES

<u>Figure</u>		<u>Page</u>
1-1	Task Objectives	1-2
1-2	Western Hemisphere Coverage from 110°W, 5° Elevation Angle	1-18
1-3	Atlantic Region Coverage from 15°W, 5° Elevation Angle	1-19
1-4	DTU Coverage, Western Hemisphere	1-23
1-5	0.35° Beam Footprint and Frequency Band Distribution	1-24
1-6	Percent Population Distribution	1-24
1-7	High Volume Trunking Payload Frequency Band and Capacity Distribution	1-26
1-8	HVT Coverage, Western Hemisphere	1-27
1-9	Meeting HVT Demands of the Northeast Corridor	1-30
1-10	Baseline Concept for HVT Multiple Beam Circuit Switched TDMA Communication System	1-34
1-11	Baseline Concept for DTU, FDMA/TDMA Satellite Switched Multibeam Digital Processing Communications System	1-35
1-12	Platform Communications Payload Configuration	1-36
1-13	Matrix Switch Configurations	1-37
1-14	Baseband Processing Systems	1-38
1-15	Mission/Payload Allocation Ground Rules	1-48
1-16	Payload Allocation Summary	1-52
1-17	Platform Support Requirements, Western Hemisphere Location, Communications Payloads Only	1-55
1-18	Platform Support Requirement, Atlantic Location, Communications Payloads Only	1-55
1-19	Platform Support Requirements, Western Hemisphere Location, Communications and Secondary Payloads	1-56

## LIST OF FIGURES, Contd

<u>Figure</u>	<u>Page</u>
1-20 Platform Support Requirements, Atlantic Location, Communications and Secondary Payloads	1-56
1-21 Typical Payload Data Requirements Documenta- tion	1-59
2-1 Basic System Trades Methodology	2-4
2-2 Launch Mode Options	2-10
2-3 Operational Modes for System Trade Studies	2-12
2-4 Evolutionary Buildup Options	2-14
2-5 Increase in Mass Versus Redundancy	2-21
2-6 Mass and Power Estimating Data Sheet	2-35
2-7 Sample Cost Model Output	2-65
2-8 Program Cost Elements - Mission Set N	2-68
2-9 Program Cost Elements - Mission Set V	2-69
2-10 Total Program Costs - Mission Set N	2-70
2-11 Total Program Costs - Mission Set V	2-71
2-12 Mode K Cost Summary - Mission Set N	2-76
2-13 Mode K Cost Summary - Mission Set V	2-77
2-14 OTV Characteristics and Effects - Mission Set N	2-78
2-15 OTV Characteristics and Effects - Mission Set V	2-79
2-16 Transfer Vehicle Comparison	2-80
2-17 Launch Mode Comparison	2-81
2-18 Operational Platform Concept Definition - Alternative #1	2-94
2-19 Operational Platform Concept Definition - Alternative #2	2-95
2-20 Operational Platform Concept Definition - Alternative #3	2-96
2-21 Operational Platform Concept Definition - Alternative #4	2-97
2-22 Cost Comparison - Mission Set P	2-98

LIST OF FIGURES, Contd

<u>Figure</u>		<u>Page</u>
2-23	Cost Comparison - Mission Set V	2-99
2-24	Platform (Bus Plus Payload) Cost Uniformity	2-103
2-25	Mode II Versus Mode III'	2-104
3-1	Concept for Alternative #1	3-2
3-2	Cross Section of the Single Reflector Configuration	3-12
3-3	Packaged View of IPL Antenna and Installation View of IPL Mounted on a Platform	3-13
3-4	TT&C, Typical for Platforms 1 - 6 (Alternative #1)	3-16
3-5	Central Communications Control, Platform 1 (Alternative #1)	3-17
3-6	Central Communications Control, Typical for Platforms 2 - 6 (Alternative #1)	3-18
3-7	GDC Deployable Space Truss Beam	3-22
3-8	Docking System Configuration	3-25
3-9	Soft Docking Concept	3-26
3-10	TT&C (Alternative #4)	3-28
3-11	Central Communications Control (Alternative #4)	3-29
3-12	Pictorial of Six Offset Reflector Antennas	3-31
3-13	Antenna Reflector Deployment Concepts	3-34
3-14	Packaged Height and Diameter Versus Deployed Diameter of Wrap-Rib Antenna (6/4 GHz)	3-36
3-15	Antenna Coverage Example for the Western Hemisphere (CPS)	3-38
3-16	Dual Feed Antenna System	3-40
3-17	The Feed Dimensions of Offset Parabola Are Influenced by the Beam Deviation Factor	3-41
3-18	C-Band HVT Antenna Feed Assembly Showing the Hinge and Pivot Used to Deploy (View of Feed From Back)	3-42

LIST OF FIGURES, Contd

<u>Figure</u>		<u>Page</u>
3-19	Layout of Proposed Transmit Feed Element Assembly for C-Band HVT	3-43
3-20	Power System Weight as Percent of Spacecraft Weight Versus Spacecraft Weight	3-46
3-21	SEPS Solar Panel Configuration	3-50
3-22	SEPS Blanket in Stowed Condition	3-51
3-23	SEPS Solar Array Deployment	3-51
3-24	Power Versus Power Density (W/kg) for SEPS Array at Beginning-of-Life (BOL)	3-53
3-25	Power Versus Power Density (W/kg) for SEPS Array After 16 Years at Geostationary Orbit	3-54
3-26	Solar Array Temperature Profiles (Longest Eclipse) at Geostationary Orbit	3-56
3-27	Effect of Advanced Technology on the Power Density of the SEPS Array at GEO Assuming a 1045 kW EOL Requirement	3-59
3-28	Flat Plate Trough Concentrator (FPT) in SEPS Configuration	3-61
3-29	Two-Dimensional Multiple Flat Plate Concentrator Solar Array (2D-MFFC)	3-62
3-30	Ni-Cd Cells, Ampere-Hour Capacity Versus Weight	3-65
3-31	Energy Density of Ni-Cd Batteries Packaged for Synchronous Orbit Applications	3-67
3-32	Battery Energy Density for Synchronous Spacecraft (Based on Total Spacecraft Power Delivered at Battery Terminals During 1.2-Hour Eclipse)	3-69
3-33	Typical Ni-Cd Battery Life in Synchronous Orbit Based on Computer Analysis	3-70
3-34	Typical Physical Arrangement of a Nickel-Hydrogen Cell [From Esch, Billerbeck and Curtin (4)]	3-72
3-35	Ni-H <sub>2</sub> Cells, Ampere-Hour Capacity Versus Weight	3-74

LIST OF FIGURES, Contd

<u>Figure</u>	<u>Page</u>
3-36 Ni-H <sub>2</sub> Battery Energy Density for Synchronous Spacecraft (Estimated at 60% Depth of Discharge Except Where Noted)	3-76
3-37 Estimated Energy Density for a 1980 to 1985 Design Ni-H <sub>2</sub> Secondary Battery	3-77
3-38 Nickel-Hydrogen Battery Cell Life (Fall, 1975)	3-78
3-39 Eclipse Durations on Different Days - Geosynchronous Orbit	3-79
3-40 Graph for Estimation of Ni-H <sub>2</sub> Battery Mass (kg) With Load Reduction During Eclipse	3-79
3-41 Primary Power Distribution in a Typical Communications Spacecraft	3-82
3-42 Nominal Bus Voltage Trends for Intelsat Spacecraft	3-82
3-43 Typical Solar Array Post-Eclipse Transient	3-83
3-44 Intelsat IV Electrical Power System Diagram	3-85
3-45 Simplified Power System Diagram - Intelsat V	3-86
3-46 Essential Bus Supply for Command and Telemetry Systems	3-88
3-47 EPS DC Section GP Alternative #4 AC/DC Hybrid	3-103
3-48 EPS AC Section GP Alternative #4 AC/DC Hybrid	3-104
3-49 EPS Distribution GP Alternative #4 DC System	3-107
3-50 EPS Control System - GP Alternative #4	3-108
3-51 Three-Channel SADA Fiber Optics Interface	3-109
3-52 North and South Facing Radiators on a Typical Rectangular Payload Package	3-112
3-53 The Convair Thermal Disconnect Allows Replacement of Packages On-Orbit	3-114
3-54 GP Radiator Heat Rejection Performance Varies Strongly with Temperature	3-115
3-55 Subsystem Packages Can Be Located in Replaceable Pie-Shaped Compartments in the Module	3-116

LIST OF FIGURES, Contd

<u>Figure</u>		<u>Page</u>
3-56	Radiator Performance at Winter Solstice	3-119
3-57	Cargo Center of Gravity Limits (Along X-Axis)	3-126
3-58	Alternative #4 Representative Structural Sections	3-130
3-59	Isometric View of the Alternative #4 Platform Finite Element Model	3-131
3-60	Top View of the Alternative #4 Platform Finite Element Model	3-131
3-61	Typical Mode Shape of the Alternative #4 Platform	3-133
3-62	Program Schedule	3-143
3-63	Alternative #1, Platform 2, Launch Configuration	3-146
3-64	Launch Configuration, Alternative #1, Platform 6	3-147
3-65	Allowable Platform Mass Versus ASE Mass For Delivery Mission	3-155
3-66	Alternative #1, Platform Mass Versus ASE Mass Characteristics	3-156
3-67	OTV Delivery/Return Mass Capabilities for GEO Logistics Flights	3-157
3-68	Dedicated TMS Servicer Configuration	3-158
3-69	OTV Delivery/Return Capabilities Without Synchronous Debris Disposal	3-163
3-70	Logistics Mission Model	3-169
3-71	OTV Configuration	3-171
3-72	OTV Low Thrust Performance (Expendable OTV)	3-173
3-73	Teleoperator Maneuver System (Platform Resupply Configuration)	3-174
3-74	Logistics Plan (Three N <sub>2</sub> H <sub>4</sub> Bottles/Platform)	3-183
3-75	Logistics Flight Sequence of Events (Atlantic Constellation)	3-184
3-76	Platform Placement Flight Sequence of Events (Platform 2)	3-189

LIST OF FIGURES, Contd

<u>Figure</u>		<u>Page</u>
3-77	Single Offset Reflector Configuration	3-192
3-78	Dual Offset Reflector Configuration	3-193
3-79	Reflector Gain Loss Versus Surface Tolerances	3-194
3-80	Sidelobe Degradation Due to Surface Tolerances	3-195
3-81	Corrugated Horn With Hybrid Modes	3-196
3-82	Dual Mode Potter Horn	3-196
3-83	Measured Pattern of Broadband Horn, H and 45° Plane, 6.0 GHz	3-197
3-84	Secondary Pattern of a Single Horn with Low Amplitude Peripherals Excited (Additional Beams Shown Separated by One and Two Beamwidths)	3-198
3-85	Main Polarized Gain Contour Plot for the Geometry Shown on Figure 3-84 Using 7 Com- ponent Beams (Center Horn Is At 0 dB Level, Outside Horns Are At -4.77 dB Level with TE <sub>11</sub> Mode Excitation)	3-200
3-86	Cross Polarized Gain Contour Plot For the Geometry Shown on Figure 3-84 Using 7 Com- ponent Beams (Center Horn Is At 0 dB Level, Outside Horns Are At -4.77 dB Level with TE <sub>11</sub> Mode Excitation)	3-201
3-87	BFN Layout For the Experimental Broadband Feed	3-202
3-88	Patterns of Scanned Beams Versus θ <sub>M</sub>	3-203
3-89	Monopulse Tracking Network	3-204
3-90	SS-TDMA System Concept	3-206
3-91	Single-Frequency, Multiple-Beam SS-TDMA Transponder	3-207
3-92	Schematic Diagram of the Simplified MSM	3-207
3-93	Simplified Block Diagram of the DCU	3-208
3-94	ASU Block Diagram	3-208
3-95	Representative Worst Case, Four Consecutive Failures of a Redundant 8 by 8 Switch Matrix Using Only T-Switches	3-209

LIST OF FIGURES, Contd

<u>Figure</u>	<u>Page</u>
3-96 PIN Diode Switch	3-211
3-97 Computed Probability of Survival 8 by 8 Cross-bar Switch	3-212
3-98 MOSFET Switch Implementation	3-213
3-99 Optical Switching Implementation	3-214
3-100 On-Board Regenerative Transponder	3-215
3-101 DQPSK-CQPSK Block Diagram	3-216
3-102 Block Diagram of a Temperature Compensated DQPSK Demodulator	3-217
3-103 CQPSK OBR Block Diagram	3-217
3-104 Equi-symbol Error Rate Curve for Regenerative Repeaters and a Conventional Transponder	3-218
3-105 SS-TDMA Slaved Subnet Work For an Inter-platform Link	3-219
3-106 General and Overall Link - Ground to IPL to Ground	3-221
3-107 Typical Platform - IPL Communications Function	3-222
3-108 Typical Platform Communications Schematic	3-223
3-109 IPL Circuit Using FM Remodulation	3-224
3-110 IPL Circuit Using Heterodyne Repeater	3-224
3-111 Power Versus Bandwidth for FM and Heterodyne Repeaters	3-225
3-112 TDMA Terminal IF Subsystem	3-228
3-113 IPL Transponder Using Baseband Filters	3-229
3-114 IPL Transponder Using Microwave Filters	3-230
3-115 Typical Transponder Layout	3-231
3-116 Block Diagram of Optical IPL System	3-233
3-117 Optical Receiver Block Diagram	3-233
3-118 Optical Receiver Demultiplex Scheme	3-234
3-119 Comparison of Conventional Tube Characteristics With a Corrected Network Characteristic	3-237

LIST OF FIGURES, Contd

<u>Figure</u>		<u>Page</u>
3-120	12 GHz Double Tape Helix Tube Characteristics	3-238
3-121	14 GHz Coupled Cavity Tube Characteristics	3-239
3-122	14 GHz Helix Tube C/I Versus Output Power	3-240
3-123	Various TWTÄ Linearizer Approaches	3-241
3-124	Linearized TWT Performance	3-242
3-125	Schematic of 12 GHz IMPATT Amplifiers	3-243
3-126	Frequency Response of a Double Tuned IMPATT Amplifier	3-244
3-127	High-Power C-Band Amplifier (6 GHz)	3-246
4-1	Platform Subsystems	4-5
4-2	Experimental Geostationary Platform Program Schedule	4-73
5-1	Typical Platform/OTV Payload Package in Orbiter Cargo Bay	5-3
5-2	OTV Airborne Support Equipment	5-4
5-3	Starboard (T-4) Payloads/OMS Delta-V Umbilical Panels and Dump Provisions (Routing Concepts)	5-5
5-4	Port (T-4) Payload/OMS Delta-V Umbilical Panels and Dump Provisions	5-6
5-5	Shuttle Orbiter Payload Interface Locations - Xo 1307 Bulkhead	5-7
5-6	Shuttle Orbiter Payload Physical Interface Locations - Aft Flight Deck General Arrangement	5-8
5-7	Platform Deployment and Checkout, Attached to Orbiter	5-9
5-8	STS Flight Operations - Ascent Phase	5-10
5-9	Cargo Bay Light and TV Camera Locations	5-15
5-10	CCTV Camera Mounting Options	5-16
5-11	OTV Airborne Support Equipment	5-20
5-12	Platform Deployment and Checkout, Attached to Orbiter	5-21
5-13	Platform Delivery Mission, Major Phases, and OTV Requirements	5-22

LIST OF FIGURES, Contd

<u>Figure</u>		<u>Page</u>
5-14	Service System Delivery Mission, Major Phases, and OTV Requirements	5-23
5-15	Platform Support Concept	5-24
5-16	OTV Configuration	5-36
5-17	TMS/Payload Docking Approach	5-37
5-18	Manipulator Arm Concept	5-38
6-1	C-Band Communications System	6-9
6-2	Ku-Band Communications System	6-10
6-3	L-Band Sea Mobile Coverage - Examples of Shaped Beams Frequency Reuse	6-12
6-4	Sea Mobile Payload Concept	6-13
6-5	Interplatform Link Communications System	6-14
6-6	Experimental Platform at 110°W Longitude, 5° Elevation Angle	6-20
6-7	Experimental Platform at 5°W Longitude, 5° Elevation Angle	6-21
6-8	Walking Orbit Propellant Requirement for 95° Geosynchronous Orbit Shift	6-22
6-9	Experimental Platform Deployable Structural Support Concept	6-23
6-10	Semideployable Arm Concept	6-25
6-11	Semideployable Arm Concept - Two Bay, 1/3 Scale Model, Folded	6-26
6-12	Semideployable Arm Concept - Two Bay, 1/3 Scale Model, Deployed	6-27
6-13	Fully Deployable Arm Concept	6-29
6-14	Growth Potential - Full Cargo Bay, Packaged	6-30
6-15	Operational Geostationary Platform Growth - Linear Expansion	6-32
6-16	Operational Geostationary Platform Growth - Lateral Expansion	6-33
6-17	Operational Geostationary Platform Soft Docking Concept	6-34

LIST OF FIGURES, Contd

<u>Figure</u>		<u>Page</u>
6-18	Soft-Docking System Hardware	6-35
6-19	Experimental Platform Attitude Control System	6-36
6-20	Active Stabilization System (Modern Control Theory)	6-37
6-21	Experimental Platform Avionics Subsystem	6-38
6-22	Experimental Platform Communications Subsystem	6-39
6-23	Candidate Antenna Concepts	6-43
6-24	Experimental Platform Concept 1, Deployed - Plan View	6-47
6-25	Experimental Platform Concept 1, Deployed - Side View	6-48
6-26	Experimental Platform Concept 1, Packaged	6-49
6-27	Experimental Platform Concept 2, Deployed - Plan View	6-53
6-28	Experimental Platform Concept 2, Deployed - Side View	6-54
6-29	Experimental Concept 2, Packaged	6-55
6-30	Experimental Platform Concept 3, Deployed - Plan View	6-59
6-31	Experimental Platform Concept 3, Deployed - Side View	6-60
6-32	Experimental Platform Concept 3, Packaged	6-61
6-33	Experimental Platform Concept 4, Deployed - Plan View	6-65
6-34	Experimental Platform Concept 4, Deployed - Side View	6-66
6-35	Experimental Platform Concept 4, Packaged	6-67
6-36	Experimental Platform Concept 5, Deployed - Plan View	6-71
6-37	Experimental Platform Concept 5, Packaged - North-to-South Side View	6-71
6-38	Experimental Platform Concept 5, Packaged - East-to-West Side View	6-72

LIST OF FIGURES, Contd

<u>Figure</u>		<u>Page</u>
6-39	Experimental Platform Concept 5, Packaged - Cross Sections	6-72
6-40	Experimental Platform Concept 6, Deployed - Plan View	6-76
6-41	Experimental Platform Concept 6, Deployed - Side View	6-76
6-42	Experimental Platform Concept 6, Packaged	6-77
6-43	Experimental Platform Concept 6, Packaged - Cross Sections	6-77
6-44	Experimental Platform Concept 6, Packaged - Cross Sections	6-78
6-45	Transfer Vehicle Options	6-83

Foldout

FO-1	Alternative #1, Western Hemisphere, Platform No. 1
FO-2	Alternative #1, Western Hemisphere, Platform No. 2
FO-3	Alternative #1, Western Hemisphere, Platform No. 6
FO-4	Alternative #4, Western Hemisphere, High Traffic Model
FO-5	Alternative #1, Western Hemisphere, Module 1
FO-6	Alternative #4, Western Hemisphere, Module 2

## LIST OF TABLES

<u>Table</u>		<u>Page</u>
1-1	Input Data	1-4
1-2	Candidate Missions	1-6
1-3	Deleted Missions	1-8
1-4	Platform Participant Concerns	1-10
1-5	Mission Functional Classification with Payloads	1-11
1-6	Mission Orientation	1-13
1-7	Mission Pointing Accuracy Requirements	1-13
1-8	Projected Voice, Data and Video Traffic in Equivalent 40 MHz Transponders, Nominal Traffic Model	1-15
1-9	Projected Video Conferencing Traffic in Equivalent 40 MHz Transponders	1-16
1-10	Projected Voice, Video, Data and Video Conferencing Traffic in Equivalent 40 MHz Transponders, High Traffic Model	1-17
1-11	Multiregional Traffic in Equivalent 40 MHz Transponders for the Year 2000	1-18
1-12	High Capacity Direct to User Payload Para- meters to Meet Year 2000 Nominal Traffic Model	1-21
1-13	High Volume Trunking Payload Parameters To Meet Year 2000 Nominal Traffic Model	1-25
1-14	High Volume Trunking Traffic Distribution Over CONUS	1-28
1-15	HVT Payload Capacity Distribution	1-29
1-16	High Capacity Direct-to-User Payload Para- meters To Meet Year 2000 High Traffic Model	1-32
1-17	High Volume Trunking Payload Parameters To Meet Year 2000 High Traffic Model	1-33
1-18	Operational Communications Payload Data I	1-40
1-19	Operational Communications Payload Data II (Western Hemisphere Location)	1-42
1-20	Operational Communications Payload Data III (Atlantic Location)	1-43

LIST OF TABLES, Contd

<u>Table</u>		<u>Page</u>
1-21	Environmental Observations and Position Location Payload Data	1-44
1-22	Candidate DoD Communications Payload Data I	1-45
1-23	Candidate DoD Communications Payload Data II	1-46
1-24	Candidate NASA Science Payload	1-47
1-25	Communications Payload Allocation, Western Hemisphere, 110°W	1-49
1-26	Communications Payload Allocation, Atlantic, 15°W	1-49
1-27	Communications and Secondary Payload Alloca- tions, Western Hemisphere, 110°W	1-50
1-28	Communications and Secondary Payload Alloca- tions, Atlantic, 15°W	1-51
1-29	Time Phasing of Payloads in Weight Increments	1-53
1-30	Platform Support Requirements, Communications Payloads, Nominal Traffic Model, Western Hemisphere Location	1-58
1-31	DoD Candidate Payloads for the Geostationary Platform, Payload 31	1-62
2-1	Mission Sets	2-2
2-2	Payloads	2-3
2-3	Task 2 Trades Methodology	2-5
2-4	Ground Rules	2-5
2-5	Scope and Interrelationship of System Trade Studies	2-6
2-6	Transfer Vehicle Options	2-8
2-7	Launch Mode Cases	2-9
2-8	Operational Mode Options	2-11
2-9	Evolutionary Buildup Options	2-13
2-10	Summary of System Design Options	2-15
2-11	Summary of System Concepts Developed in Trade Studies	2-16

LIST OF TABLES, Contd

<u>Table</u>		<u>Page</u>
2-12	Platform System Design Philosophy	2-18
2-13	Reliability and Servicing Design Impact (Payload and Subsystems)	2-20
2-14	Weight Penalty Assessments	2-21
2-15	STS Upper Stage Options (Cost in Millions of 1980 Dollars)	2-23
2-16	Payload Mass and Power Limits	2-25
2-17	Number of Platforms Required Versus OTV and Mode (Mission Set N)	2-29
2-18	Number of Platforms Required Versus OTV and Mode (Mission Set V)	2-32
2-19	Platform Packaging - Mission Set N	2-38
2-20	Platform Packaging - Mission Set V	2-41
2-21	Servicing Requirements for 16 Year Mission - Mission Set N	2-46
2-22	Servicing Requirements for 16 Year Mission - Mission Set V	2-47
2-23	Baseline TMS Description	2-48
2-24	Servicing Options Capabilities and Costs	2-49
2-25	Servicing Transportation Costs Summary - Mission Set N	2-50
2-26	Servicing Transportation Costs Summary - Mission Set V	2-51
2-27	Transportation Cost Summary - Mission Set N	2-52
2-28	Transportation Cost Summary - Mission Set V	2-55
2-29	Program Cost Summary, Nominal Traffic Model - Western Hemisphere, Mission Set N	2-59
2-30	Program Cost Summary, High Traffic Model - Western Hemisphere, Mission Set V	2-62
2-31	Launch Case I Cost Elements	2-72
2-32	Case I' Individual Satellite Description	2-73
2-33	Individual Satellite Mode Program Cost Summary	2-75

LIST OF TABLES, Contd

<u>Table</u>		<u>Page</u>
2-34	Evolutionary Buildup Options - Mode H Versus Mode K	2-83
2-35	Buildup Mode J Comparisons	2-85
2-36	Best Overall Options - Mission Set V	2-88
2-37	Key to Coding of Options	2-89
2-38	Funding Spread Analysis Results	2-89
2-39	Program Cost Summary - Mission Set P	2-91
2-40	Preliminary Program Costs, Alternatives #1 through #4	2-100
2-41	Trade Study Results Summary	2-101
3-1	Payloads and Platform Assignments - Western Hemisphere Alternative #1	3-4
3-2	Payloads and Platform Assignments - Atlantic Alternative #1	3-5
3-3	Communication Payload Definitions, Western Hemisphere, Nominal Traffic Model, Alternative #1	3-6
3-4	Requirements for Stationkeeping and Attitude Control	3-7
3-5	Link Calculation of a 32/25 GHz IPL	3-14
3-6	Estimate of the Number of 40 MHz and 1 GHz Bandwidth Channels Required for Each Communications Payload Alternative #1	3-19
3-7	Data Bus Requirements for the Constellation Members Alternative #1	3-19
3-8	Alternative #4 (Western Hemisphere) Payload Assignments	3-20
3-9	Alternative #4, Communications Payloads Definitions (Western Hemisphere, High Traffic Model)	3-21
3-10	Estimate of the Number of 40 MHz and 1 GHz Bandwidth Channels Required For Each Communications Payload, Alternative #4	3-30

LIST OF TABLES, Contd

<u>Table</u>	<u>Page</u>
3-11 Communication Payload Definitions, Western Hemisphere, Nominal Traffic Model, Alternative #1	3-32
3-12 Alternative #4, Communications Payloads Definitions (Western Hemisphere, High Traffic Model)	3-33
3-13 Packaged Antenna Reflector Dimensions	3-35
3-14 Antenna Type Trade Study Parameters	3-37
3-15 Summary of Intelsat Spacecraft Characteristics	3-45
3-16 Recent Design Prismatic Nickel-Cadmium Cells	3-64
3-17 Synchronous Spacecraft Battery Weight Analysis	3-67
3-18 Ni-Cd Spacecraft Battery Energy Density Calculations	3-68
3-19 Comparison of Cell Operating Features	3-73
3-20 Ni-H <sub>2</sub> Battery Weight Analysis	3-75
3-21 Growth of Intelsat Spacecraft	3-81
3-22 Geostationary Platform Alternative #1 Power Requirements	3-94
3-23 Solar Array Sizing Using Advanced SEPS and Concentrator Technology GP Alternative #1	3-96
3-24 Battery Storage Sizing with Ni-H <sub>2</sub> Cells GP Alternative #1	3-97
3-25 Equipment List GP Alternative #1	3-98
3-26 Geostationary Platform Alternative #4 Power Requirements	3-100
3-27 Alternative #4 EPS AC/DC Hybrid	3-101
3-28 Alternative #4 EPS DC System	3-105
3-29 Radiation Exchange Factors and Properties for Thermal Analysis	3-116
3-30 Thermal Analysis Results for Simple Heat Pipe Concept	3-118
3-31 Thermal Analysis Results for Variable Conductance Heat Pipe Concept	3-120

LIST OF TABLES, Contd

<u>Table</u>		<u>Page</u>
3-32	Operational Platform No. 1 Weight Summary	3-121
3-33	Operational Platform No. 2 Weight Summary	3-122
3-34	Operational Platform No. 6 Weight Summary	3-123
3-35	Operational Platform Alternative #4 Weight Summary	3-124
3-36	Operational Platform Alternative No. 4 Payload Weight	3-125
3-37	Alternative #1 Minimum Structural Sections	3-127
3-38	Alternative #4 Minimum Structural Sections	3-128
3-39	Modal Frequencies of the Alternative #4 Platform	3-132
3-40	Description of the First Eleven Mode Shapes	3-132
3-41	Solar Cell Configurations	3-141
3-42	Solar Cell Configuration Totals	3-141
3-43	OTV/Platform Launch Mass (For 6,895 kg Reference Payloads)	3-148
3-44	Delivery Mission OTV Characteristics	3-149
3-45	Delivery Vehicle Flight Performance Analysis (for 6,895 kg Reference Payload)	3-150
3-46	Platform No. 1 Delivery Performance Analysis	3-152
3-47	Platform No. 2 Delivery Performance Analysis	3-153
3-48	Platform No. 6 Delivery Performance Analysis	3-154
3-49	Logistics Mission Launch Mass	3-159
3-50	Logistics Mission OTV Characteristics	3-160
3-51	Logistics Vehicle Flight Performance Analysis	3-161
3-52	TMS Debris Disposal Mission - Flight Performance Analysis	3-165
3-53	Summary of Logistics Flight Options	3-168
3-54	OTV Performance Characteristics	3-172
3-55	Teleoperator Maneuvering System Characteristics	3-175
3-56	Resupply Logistic Weights	3-176
3-57	Alternative Logistics Considerations	3-177

LIST OF TABLES, Contd

<u>Table</u>		<u>Page</u>
3-58	Trade Study of TMS Basing Mode	3-180
3-59	Trade Study of Debris Disposal Mode	3-182
3-60	Flight Operations - Logistics Flight (Atlantic Constellation)	3-186
3-61	Flight Operations - Placement Flight (Platform 2)	3-190
3-62	Typical MSM Specifications	3-210
3-63	FM Crosslink	3-226
3-64	Heterodyne Crosslink	3-227
3-65	Weight/Power Summary	3-232
3-66	IPL Tracking Windows	3-234
3-67	Satellite TWTA Status	3-235
3-68	Solid-State Amplifier	3-236
3-69	Amplifier Performance	3-245
4-1	Space Construction	4-6
4-2	Active Control of Large Space Structure	4-9
4-3	Solar Array	4-12
4-4	Power Management System	4-15
4-5	Power Management System Control	4-18
4-6	Power Management Component Technologies	4-21
4-7	Secondary Power Source	4-24
4-8	Increased Performance RCS/Propulsion Subsystem	4-27
4-9	Thermal Management	4-30
4-10	Automated Remote Docking and Servicing	4-33
4-11	High Speed, High Capacity, Satellite Switch Matrix	4-37
4-12	Improvement of Deployable Antenna Reflector Surfaces	4-40
4-13	Phased Array Antennas	4-44
4-14	Lens Antennas	4-47
4-15	MBFRA Feed Assemblies	4-50

LIST OF TABLES, Contd

<u>Table</u>		<u>Page</u>
4-16	Interplatform Links (IPLs)	4-54
4-17	Intraconstellation Links (ICLs)	4-59
4-18	Electromagnetic Compatibility/Interference	4-63
4-19	Fiber Optics Data Transmission	4-67
4-20	30/20 GHz High Power Amplifiers	4-70
4-21	Recommendations for Technology Advancement	4-74
5-1	Orbiter Cargo Bay Lighting and Illumination	5-14
5-2	Total ACS Impulse for Low-Thrust OTV Mission, Platform Delivery	5-28
5-3	Total ACS Impulse for Round Trip OTV Platform Servicing Mission (No Disposal of Expended Components in Debris Orbit)	5-29
5-4	Servicing Flight Operations, Atlantic Constellation	5-33
6-1	Platform Technologies to be Demonstrated for Future Operational Platform Use	6-5
6-2	Advanced Communications Technology Candidates, Platform Related	6-6
6-3	Advanced Communications Technology Candidates, Nonplatform Related	6-6
6-4	Candidate Communications Payloads	6-8
6-5	Candidate C-Band and Ku-Band Payloads	6-11
6-6	Candidate Communications Payload Characteristics - Experimental Geostationary Platform	6-16
6-7	Secondary (DoD and Science) Payload Candidates in Tentative Order of Priority	6-17
6-8	Experimental Platform Mission Options	6-18
6-9	Power Requirements, Experimental Platform Concept 2	6-40
6-10	Power Subsystem Weight Estimate, Experimental Platform Concept 2	6-41
6-11	Existing, Deployable Antenna Concepts for the Experimental Geostationary Platform	6-44

LIST OF TABLES, Contd

<u>Table</u>		<u>Page</u>
6-12	Experimental Platform Concepts - Payload Allocation and Platform Weight Summary	6-45
6-13	Experimental Platform Concept 1, Payloads and Technologies	6-50
6-14	Experimental Platform Concept 1, Antenna Characteristics	6-51
6-15	Experimental Platform Concept 1, Weight Estimate	6-52
6-16	Experimental Platform Concept 2, Payloads and Technologies	6-56
6-17	Experimental Platform Concept 2, Antenna Characteristics	6-57
6-18	Experimental Platform Concept 2, Weight Estimate	6-58
6-19	Experimental Platform Concept 3, Payloads and Technologies	6-62
6-20	Experimental Platform Concept 3, Antenna Characteristics	6-63
6-21	Experimental Platform Concept 3, Weight Estimate	6-64
6-22	Experimental Platform Concept 4, Payload and Technologies	6-68
6-23	Experimental Platform Concept 4, Antenna Characteristics	6-69
6-24	Experimental Platform Concept 4, Weight Estimate	6-70
6-25	Experimental Platform Concept 5, Payloads and Technologies	6-73
6-26	Experimental Platform Concept 5, Antenna Characteristics	6-74
6-27	Experimental Platform Concept 5, Weight Estimate	6-75
6-28	Experimental Platform Concept 6, Payloads and Technologies	6-79

LIST OF TABLES, Contd

<u>Table</u>		<u>Page</u>
6-29	Experimental Platform Concept 6, Antenna Characteristics	6-80
6-30	Experimental Platform Concept 6, Alternative #1, Weight Estimate	6-81
6-31	Experimental Platform Concept 6, Alternative #2, Weight Estimate	

## GLOSSARY

ACOSS	Active Control of Space Structures
ACS	attitude control system
AFC	automatic frequency control
AIL	Avionics Integration Laboratory
APS	auxiliary power subsystem
APSK	amplitude and phase shift keying
APU	auxiliary power unit
ASE	airborne support equipment
ASU	acquisition and synchronization unit
BER	bit error rate
BFN	beam forming network
BOL	beginning of life
BOSS	baseline optical surveillance system
BSM	baseband switch matrix
CADSI	communications and data systems integration
C&W	caution and warning
CCC	central communications control
CER	cost estimating relationship
C/I	carrier/interference
CITE	cargo integration test equipment
CMG	control moment gyro
COMSAT	Communications Satellite Corporation
CONUS	Contiguous United States
CPS	customer premise services (same as DTU)
CQPSK	coherent quadriphase shift keying
CRT	cathode-ray tube
CSC	Computer Sciences Corporation
CTE	coefficient of thermal expansion
DARPA	Defense Advanced Research Projects Agency
DCU	distribution control unit
DDT&E	design, development, test and evaluation
DEU	Display Electronics Units
DHS	data handling system
DMS	Data Management System
DMSP	Defense Meteorological Satellite Program
DNSP	Defense Navigation Satellite Program
DoD	Department of Defense
DOD	depth of discharge
DoE	Department of Energy
DORA	double rolled array
DPS	Data Processing system
DQPSK	differential quadriphase shift keying
DSCS	Defense Satellite Communications System
DSN	deep space network

## GLOSSARY, Contd

DTU	direct to user (same as CPS)
EHF	extra high frequency
EIRP	effective isotropic radiated power
EMC	electromagnetic compatibility
EMU	extravehicular mobility unit
EOL	end of life
EPC	electronic power conditioner
EPS	electrical power subsystem
ESA	European Space Agency
EVA	extravehicular activity
FCC	Federal Communications Commission
FDMA	frequency division multiple access
FDM/FM	frequency division multiplex/frequency modulation
FET	field effect transistor
FMECA	Failure Modes and Effects Criticality Analysis
FPR	flight performance reserve
FPT	flat plate trough
FRUSA	flexible rolled up solar array
FSI	Future Systems, Inc.
FSS	frequency selective subreflector
GDC	General Dynamics Convair Division
GDTTSS	General Dynamics Tetrahedral Truss Structure
	Computer Program
GEO	geostationary orbit
GFE	government-furnished equipment
GFP	government-furnished property
GN&C	guidance, navigation and control
GOICM	Ground Operations and Integration Cost Model
GP	Geostationary Platform
GPC	General Purpose Computer
GRARR	Goddard range and range rate
GSE	ground-support equipment
GSFC	Goddard Space Flight Center
G/T	gain-to-noise temperature ratio
HALO	High Altitude Laser Optics
HPA	high power amplifier
HVT	high volume trunking
ICL	intra-constellation link
I/F	interface
IF	intermediate frequency
IFSM	intermediate frequency switch matrix
IM	intermodulation
IMPATT	type of power-transmitting diode
IMU	inertial measurement unit
IOC	Initial Operational Capability
IOTV	Interim OTV

## GLOSSARY, Contd

IPL	inter-platform link
IR	infrared
ISP	specific impulse
ITU	International Telecommunications Union
IUS	inertial upper stage
IVA	intravehicular activity
JPL	Jet Propulsion Laboratory
JSC	Lyndon B. Johnson Space Center
km	kilometer
KSC	John F. Kennedy Space Center
LaRC	Langley Research Center
LASS	Large Advanced Space System
LCC	life cycle cost
LEO	low earth orbit
LeRC	Lewis Research Center
LH <sub>2</sub>	liquid hydrogen
LLLTV	low light level television
LO <sub>2</sub>	liquid oxygen
LSS	large space structures
MBA	multibeam antenna
MBFRA	multiple beam frequency reuse antenna
MCC	Mission Control Center (at JSC)
MCDS	Multifunction Control and Display System
MDM	multiplexer-demultiplexer
MMP	Mission Mass Properties (program)
MMS	Multimission Modular Spacecraft
MMU	manned maneuvering unit
MOSFET	metal oxide silicon field effect transistor
MSFC	Marshall Space Flight Center
MSM	microswitch matrix
MTBF	Mean Time Between Failures
MUX	multiplex
NASA	National Aeronautics and Space Administration
nm	nautical miles
NPV	net present value
OBR	onboard regenerator
OLS	optical line scanner
OMJ	ortho-mode junction
OMS	orbital maneuvering subsystem
OOA	On-Orbit Assembly
OPF	Orbiter Processing Facility
OSR	optical solar reflector
OSS	orbital servicing system
OSS	Office of Space Science (NASA)
OSTA	Office of Space and Terrestrial Applications
OTV	orbital transfer vehicle

## GLOSSARY, Contd

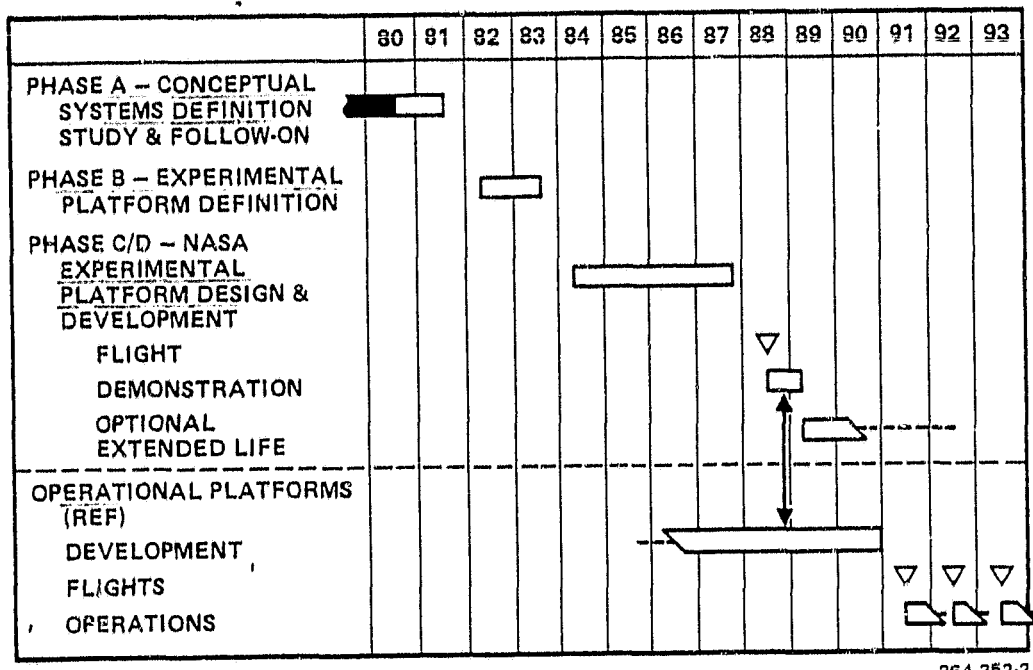
PCM	Pulse Code Modulation
PCR	payload changeout room
PDI	Payload Data Interleaver
PEP	power extension package
PETA	Parabolic Expandable Truss Antenna
P/L	payload
POP	perpendicular to orbit plane
PSP	payload signal processor
Q	quality factor (energy stored/energy lost)
QPSK	quadriphase shift keying
RAU	remote acquisition unit
RCS	reaction control subsystem
RF	radio frequency
RFI	radio frequency interference
RIU	remote interface unit
RMS	remote manipulator system
ROI	return on investment
RTOP	Research and Technology Operating Plan
SADA	solar array drive assembly
S/C	spacecraft
SCF	Satellite Control Facility
SCR	silicon controlled rectifier
SEP	solar electric propulsion
SGLS	space ground link subsystem
SPST	single pole single throw
SRT	supporting research and technology
SS	solid state
SSLCC	Space System Life Cycle Cost
SS-TDMA	satellite-switched time division multiple access
SSUS	spin-stabilized upper stage
STDN	space tracking and data network
STS	Space Transportation System
T&C	telemetry and command
TDMA	time-division multiple access
TDRS	Tracking and Data Relay Satellite
TDRSS	Tracking and Data Relay Satellite System
TMS	Teleoperator Maneuvering System
T/R	transmit/receive
TRIAC	type of regulator tube
TSO	time-sharing option
TT&C	telemetry, tracking and command
T/W	thrust-to-weight ratio
TWT	traveling wave tube
TWTA	traveling wave tube amplifier
ULP	ultra-lightweight panel
USB	unified S-band

## GLOSSARY, Contd

UV	ultraviolet
VCHP	variable conductance heat pipe
VPF	vertical processing facility
WAP	Work Authorization Plan
WBS	Work Breakdown Structure
W <sub>p</sub>	weight of propellant
W <sub>t</sub>	weight
X <sub>o</sub>	X-axis of Orbiter
X <sub>p</sub>	X-axis of payload
Y <sub>o</sub>	Y-axis of Orbiter
Y <sub>p</sub>	Y-axis of payload
Z <sub>o</sub>	Z-axis of Orbiter
Z <sub>p</sub>	Z-axis of payload
ΔV	delta (incremental) velocity

## SUMMARY

The George C. Marshall Space Flight Center (MSFC) has the responsibility within the NASA for the geostationary platform - to initiate conceptual studies, develop feasible concepts, coordinate user needs and technology requirements, and promote activities aimed at system hardware solutions to the projected service demands of the 1990s. The schedule, as shown here, provides for a National Aeronautics and Space Administration (NASA) experimental platform in 1988 to validate required technology, and operational platforms with launch dates in the 1990s.



264.352-2

Projected Development Schedule for Geostationary Platforms

On 31 May 1979, General Dynamics Convair was placed under contract to do the Initial Phase A Concepts Definition Study for the Geostationary Platform. NASA/MSFC's planned approach includes a review of communications, military and science payloads, and mission models, development and analysis of operational and experimental platform

concepts, identification of communications and platform technology requirements, and development of supporting programmatic data. Primary objectives of the study are to select and conceptually define operational geostationary platforms based on time-phased mission and payload requirements, and to develop attendant costs, schedules, and supporting research and technology (SRT) requirements. This data will be used as a basis for definition of the NASA experimental geostationary platform, which will be the subject of follow-on studies, although some preliminary precursor work on the experimental platform was done during this initial phase of the study.

Six tasks were defined in the Statement of Work (SOW) for this study:

Task 1 - Further Define Candidate Missions and Payloads.

Task 2 - Define Candidate Approaches/Concepts and Conduct Analyses and Trades Leading to Selected Concepts.

Task 3 - Define Selected Approaches and Concepts.

Task 4 - Define Supporting Research and Technology and Recommended Space Demonstrations.

Task 5 - Define Requirements On and Interfaces With STS Hardware Elements.

Task 6 - Define and Develop Cost and Schedule Data.

This document, Volume II of the final report, summarizes the technical and programmatic work performed in satisfying Tasks 1 through 5 of the Statement of Work and Study Plan requirements for these tasks. It contains in-depth discussions of the study elements, engineering data, and system and programmatic trades generated during the study. Parts 1 and 2 of this volume address operational and experimental geostationary platforms, respectively. Extensive data tables and drawings are documented in the appendixes (Volume II Supplemental Data), where appropriate.

Task 6, Cost and Schedules Data, is treated separately (Volume III of the Final Report), per data procurement document instructions.

A summary of Task 1 through 5 results follows.

In Task 1, candidate geostationary platform missions and payloads were identified from COMSAT, Aerospace, and NASA studies. These missions and payloads were cataloged; classified with respect to communications, military or scientific uses; screened for application and compatibility with geostationary platforms; and analyzed to identify platform support requirements. Two platform locations were then selected (Western Hemisphere - 110°W, and Atlantic - 15°W), and payloads

allocated based on nominal and high traffic models considering communications payloads only, and considering communications plus secondary [Department of Defense (DoD) and science] payloads. In all cases, candidate payload requirements and characteristics were defined on three-page candidate payload data summary forms (Appendix E).

In Task 2, candidate platform concepts were defined and analyzed, and trade studies performed leading to recommendation of selected concepts. Of 30 Orbit Transfer Vehicle (OTV) configuration and operating mode options identified from data supplied by NASA/MSFC, 18 viable candidates compatible with the operational geostationary platform missions were selected for analysis. Each was considered using four platform operational modes - 8 or 16 year life, and serviced or nonserviced, providing a total of 72 OTV/platform-mode options. Standard platform concepts were defined for each of the 72 options for both the nominal and the high traffic models, and payloads reallocated to these 144 options based on OTV performance capability and payload weight and power. For final trade study concept selection, a cost program was developed considering payload and platform costs and weight; transportation unit and total costs for the Shuttle and OTV; and operational costs such as assembly or construction time, mating time, and loiter time. Servicing costs were added for final analysis and recommended selection.

The 144 candidate concepts were screened and the nine best options for combinations of launch and operating modes, transfer vehicles, and evolutionary buildup modes were analyzed. Four were recommended and selected by NASA for further study. Alternative #1 was designated for definition in Task 3. Alternatives #2, 3, and 4 were deferred to the follow-on study for further definition.

Task 3 defines concept Alternative #1 as a data base for further geoplatform analyses in this study, in sufficient detail to identify requirements for supporting research and technology, space demonstrations, GFE interfaces, costs, and schedules. Alternative #1 consists of six platforms in geostationary orbit (GEO) over the Western Hemisphere and six over the Atlantic, to satisfy the total payload set associated with the nominal traffic model. Each platform is delivered to low earth orbit (LEO) in a single shuttle flight, already mated to its LEO-to-GEO transfer vehicle and ready for deployment and transfer to GEO.

Although Alternative #4 was deferred to the follow-on study for further definition, it was looked at briefly in this initial study for comparison of configuration and technology requirements. Alternative #4 consists of two large platforms, one over the Western Hemisphere consisting of three docked modules, and one over the Atlantic (two docked modules), to satisfy a high traffic model. The modules are full-length orbiter cargo-bay payloads, mated at LEO to OTVs delivered in other shuttle flights, for transfer to GEO, rendezvous, and docking.

Alternatives #2 and 3, deferred to the follow-on study for definition, are respectively single-shuttle flight platforms docked at GEO and multiple-shuttle platforms in constellation at GEO.

Task 3 was expanded somewhat to include a preliminary feasibility study of an experimental platform to demonstrate communications and platform technologies required for the operational platforms of the 1990s. Six configurations were conceptually developed to consider a wide variation in payloads, structure, number of shuttle flights, and compatibility with available OTV performance characteristics. Results of this task (3A) are reported in Part 2 of this volume.

Task 4 identifies the SRT and space demonstrations required to support the 1990s Operational Platforms as typified by Concept Alternatives #1 and #4.

Task 5 identifies the requirements on and interfaces with STS hardware elements supporting the geostationary platform program, including the shuttle, orbital transfer vehicles, teleoperator, etc., to provide integrated support requirements to these programs.

The body of this volume concludes with a short preview of work to be accomplished on the follow-on study, in which operational platforms will be further characterized and concepts for an experimental geostationary platform further developed. Central to the further characterization of operational platforms will be the development of a multislot communications architecture using low-risk communications technology. Work on experimental geostationary platform concepts will concentrate on identifying affordable configurations compatible with potential upper stages.

## SECTION 3

### TASK 3: CONCEPTS DEFINITION

Making use of inputs from Tasks 1 and 2, this section defines concepts for Task 3 - Platforms Definition (3.1), Transportation Systems (3.2), Logistics Plan and Mission Model (3.3), and Specialized Communications/Integration Equipment (3.4).

#### 3.1 PLATFORMS DEFINITION

It is the objective of this task to prepare conceptual designs that will demonstrate feasibility of mission concepts. Such designs have been prepared for the mission configuration chosen, in cooperation with NASA, for preliminary study. This is known as Alternative #1. Alternatives #2, #3, and #4 are to be defined in a follow-on study.

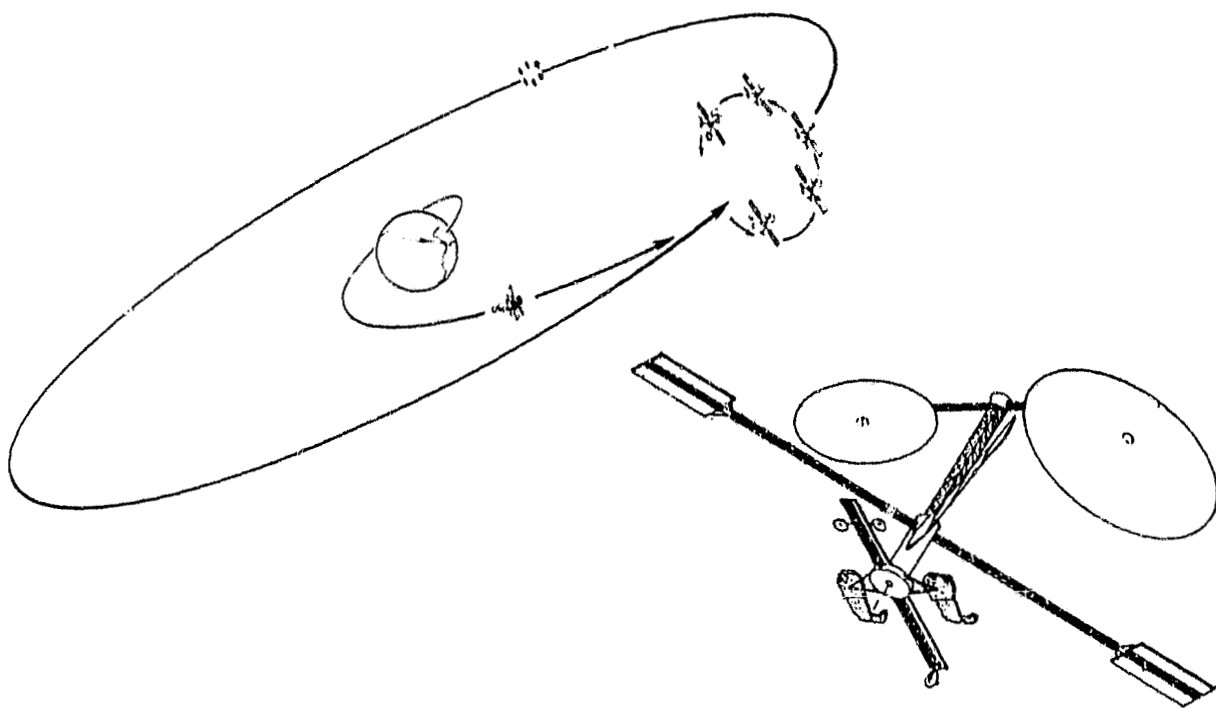
However, efforts have been made under bid and proposal funding, to set forth a preliminary definition of Alternative #4, the results of which are included herewith for the record.

3.1.1 SCOPE. From the mission models established in Tasks 1 and 2, two sets of payloads were defined to handle different predicted levels of traffic; namely, nominal traffic model and high traffic model. The mission concept of Alternative #1 is:

- a. Nominal traffic model.
- b. Two constellations, with six small platforms in each, located in stationary orbit at 15°W and 110°W longitude, respectively.
- c. Each platform is to be launched in a Shuttle Orbiter sharing the cargo bay with an orbital transfer vehicle (OTV).
- d. The OTV is the NASA low thrust expendable design.
- e. After deployment and checkout in low earth orbit (LEO) the OTV transports the platform to geostationary earth orbit (GEO).

Alternative #1 is illustrated diagrammatically in Figure 3-1. OTV performance and the constellation configuration are described in Sections 3.2 and 3.3, respectively.

Packaging of the platforms and payloads into the Shuttle, along with their associated OTVs, proved to be a very challenging task, available space in the Shuttle bay being only 7.925m (26 ft) in length. Initial review showed that foldable design concepts existed for reflector dishes, masts and arms, but nothing was found for feeds. First cut estimates on some feed sizes were many



264.352-136

Figure 3-1. Concept for Alternative #1

meters in maximum dimension with little obvious prospect for folding or assembly in orbit. Much effort was devoted to devising prospective concepts for compacting feed designs and then folding them to meet packaging requirements. To accomplish this, it was necessary to postulate several technological developments in feed design. These are discussed in Section 3.1.4.

As a result of the efforts spent to develop viable packaging concepts, attention paid to operational subsystems was forced into a subordinate role. Solar panels and batteries were sized to meet overall power requirements with allowance made for degradation; central radiators have been provided that can dissipate the total heat load; momentum wheels and hydrazine propellant are included to provide total momentum balance requirements for attitude control and stationkeeping; and a brief stress analysis has been made for the thrust loading condition between LEO and GEO. However, much remains to be done in regard to system design, and we feel that a pulsed plasma reaction control system (RCS) should definitely be considered.

The Western Hemisphere constellation was chosen for study. The payloads to be considered are listed in Section 3.1.2. These were divided into six groups of very roughly equal power and weight and assigned to platforms numbered 1 through 6, also shown in Section 3.1.2.

As mentioned previously, an additional study was made on mission concept Alternative #4. This is defined as follows:

- a. High traffic model.
- b. Two large platforms in geostationary orbit at  $15^{\circ}\text{W}$  and  $110^{\circ}\text{W}$  longitude respectively.
- c. Each platform to consist of three modules to be transported separately and docked at GEO to form a single large platform.
- d. Each module to be launched in a single Shuttle flight occupying the entire cargo bay. Module to be deployed/assembled at LEO.
- e. Each module to be mated at LEO with an OTV launched in a separate Shuttle flight.
- f. The OTV is the NASA low thrust two stage reusable vehicle (also see following paragraph).

It should be noted that Alternative #4 was originally conceived with the high thrust reusable OTV. However, preliminary stress analysis indicated that this would impact the structure and the low thrust OTV was chosen instead. This is discussed in Section 3.1.9. The small configuration of Alternative #1 had no difficulty with  $T/W = 0.05$  as specified. The large configuration of Alternative #4 could not tolerate the loading due to  $T/W = 0.31$  as specified, but could tolerate  $T/W = 0.035$  of the low thrust vehicle.

**3.1.2 REQUIREMENTS AND CONSTRAINTS.** Payloads for the nominal traffic model were obtained from Tasks 1 and 2 along with preliminary weights and power requirements. The payloads were then assigned to six platforms in each constellation in such a way as to roughly distribute both weight and power about equally. These assignments are shown in Tables 3-1 and 3-2.

As the work progressed, particularly in the area of conceptual feed design, more realistic figures were developed. It also became clear that the payloads fell into two distinct classes: 1) communications payloads, which are large and hard to package and require folding and 2) scientific observation payloads, which are generally compact\* and create no great packaging problems. Table 3-3 contains detailed information on communications payloads for the Western Hemisphere (Alternative #1) including updated weights based on the conceptual design studies, and pointing requirements for the individual antennas.

The requirements for system lifetime is 16 years with consumables being replenished at 8 years. Requirements for stationkeeping and attitude control of the platforms are shown in Table 3-4. It will be noted that pointing

---

\*An exception is Payload 27, the RF interferometer, which must be provided with orthogonal baselines each of 100 m.

Table 3-1. Payloads and Platform Assignments - Western Hemisphere Alternative #1

P/L No.	Payload Function	Antennas/Sensors	Platform 1		Platform 2		Platform 3		Platform 4		Platform 5		Platform 6		
			Mass (kg)	Power (W)	Launch Yr:1992	Mass (kg)	Power (W)	Launch Yr:1993	Mass (kg)	Power (W)	Launch Yr:1994	Mass (kg)	Power (W)	Launch Yr:1995	
1.1	CPS, Ku Band	(3) 6 m (3) 4 m	1600	6500	1040	5700	1145	700	700				1040	5700	1040
1.2	CPS, Ka Band	(1) 15 m (1) 6 m			980	3200									5700
2.1	HVT, C-Band														
2.2	HVT, Ka Band														
3	TV Distribution	(2) 1.5 m													
4	Tracking and Data Relay	(2) 5 m, (1) 2 m, (1) Array	425	630											
5	Educational TV	(4) 2.5 m, (4) 1.5 m	620	400											
6	Direct to Home TV	(1) 1.5 m, (1) 10 m	515	2100											
7	Air Mobile	(1) Array, (1) Horn	260	1200											
9	Land Mobile	(1) 20 m (2) 3 m	685	4000	139	300	130	300	300	300	130	300	130	300	130
11	Inter Platform Link	(1) 10 m													
12	Data Collection														
15	Lightning Mapper	(1) 1 m (7) Helices	320	300											
18	Atmospheric Sounder	(1) 0.4 m	185	50											
19	Visual and IR Radiometer	(1) 1 m	500	100											
20	Microwave Radiometer	(1) 4.5 m	136	150											
27	RF Interferometer	(7) Antennas on 100 m x 100 m Baseline	120	220											
31	DMSR Data Relay	TBD	165	100	195	100									
54	DOD EHF Experiment	3 x 3 x 3 ft	230	500											
55	DOD Laser Communication Experiment	TBD	320	550											
32	Advanced OLS Cloud Imager	TBD	150	150											
38	Aerosol and Cloud Height Sensor	Telescope, 0.75 m <sup>3</sup>	50	100											
42	Global UV Radiance	0.43 m <sup>3</sup> UV Imaging Spectrometer	50	20											
52	BOSS Evaluation	0.5 m dia IR Telescope, 1m <sup>3</sup>	150	400											
33	Materials Exposure	TBD	10	25											
43	Magnetic Substorm Monitor	0.1 m <sup>3</sup>	10	5											
56	Fiber Optics Demo	TBD	10	30											
71	Earth Optical Telescope	1.5 x 2 m	1100	2000											
		Total Mass, kg	2550	5100	5100	2110	8220	2645	5980	2660	1971	8400	1940	6600	6600
		BOL Power, W													
		EOL Power, W													

Table 3-2. Payloads and Platform Assignments - Atlantic Alternative #1

P/L No.	Payload Description			Platform 7 Launch Yr:1993		Platform 8 Launch Yr:1994		Platform 9 Launch Yr:1995		Platform 10 Launch Yr:1996		Platform 11 Launch Yr:1998		Platform 12 Launch Yr:1999	
	Payload Function	Antennas/Sensors	Mass Power (kg) (W)	Mass (kg)	Power (W)	Mass (kg)	Power (W)	Mass (kg)	Power (W)	Mass (kg)	Power (W)	Mass (kg)	Power (W)	Mass (kg)	Power (W)
1.1	CPS, Ku Band	(3) 6 m	1600 6500			1600	6500								
1.2	CPS, Ka Band	(3) 4 m	1040 5700									1040	5700	1040	5700
2.1,10.1	HVT, C-Band	(1) 15 m	1145 700	1145	700							980	3200		
2.2,10.2	HVT, Ka Band	(1) 6 m	980 3200												
3	TV Distribution	(2) 1.5 m	515 4000	515	4000							620	400		
4	Tracking and Data Relay	(2) 5 m, (1) 2 m, (1) 1.5 x 1.5 m Array	425 680					425	680						
5	Educational TV	(4) 2.5 m, (4) 1.5 m	620 400					620	400						
6	Direct to Home TV	(1) 1.5 m, (1) 10 m	515 2100									515	2100		
7	Air Mobile	(1) 1 x 1 Array, (1) 1.2 x 2 m Horn	260 800			260	900								
8	Sea Mobile	(1) 1 x 1 m Array, (1) 14 M, 2 x 0.2 m Horn	515 600							515	600				
9	Land Mobile	(1) 20 m	685 4000					685	4000						
11	Inter-Platform Link	(2) 3 m	130 300	130	300	130	300	130	300	130	300	130	300	130	300
12	Data Collection	(1) 10 m	130 100							130	100				
17	Lightning Mapper	(1) 1 m (7) TBD Helices	320 300					320	300						
18	Atmospheric Sounder	(1) 0.4 m	185 50							185	50				
27	RF Interferometer	(1) TBD Helices, 120 x 120 m Baseline	120 220									120	220		
31	DMSP Data Relay	TBD	195 100	195	100										
39	Solar Flare Monitor	TBD	100 100	100	100										
40	Solar Flare Isotope Monitor	TBD	13 6	13	6										
41	Ion and Proton Sensor	TBD	3 6	3	6										
44	Charged Particle Monitor	TBD	5 10	5	10										
73	Chemical Release Module Observation	0.5 x 1.5 m + mount	200 250							200	250				
75	Imaging Spectrometer	0.5 x 7.5 x 2.0 m	350 150	350	150										
76	Fabry-Perot Interfero- meter/Photometer	0.5 m dia x 2.5 m long	150 200										150	200	
77	FR Occultation Instrument	0.5 m x 1.0 x 2.5 m	200 800					200	400						
79	Low Light Level TV	1.0 m dia x 2.5 m long	300 1000							300	1000				
81	Microwave Sounder	10 m Antenna with Steer- able Feed	50 200							50	200				
84	Bistatic Forward Incoher- ent Scatter Radar	2.3 m Antenna with Steerable Feed	700 100									700	100		
Total Mass, kg BOL Power, W BOL Power, W				2461		1990		2380		2490		1805		2020	
					5372		7700		6080		5700		8320		
					5100		5100		5380		4100		8100		
														6300	
														6000	

Table 3-3. Communication Payload Definitions, Western Hemisphere, Nominal Traffic Model, Alternative #1

P/L No.	Payload Description	Band	Frequency (GHz)		Beams			Antennas			Power (watts)			Mass (kg)			Geographic Coverage*	
			Up	Down	No.	Beam-width (deg)	Pointing Accuracy (deg)	Aperature Size (m)	Focal Length (m)	Dish Size (m)	No. of Transponders	Total RF	Total Input	Dish	Feeds	Other Avionics	P/L Total	
1.1 Customer Premises Service	Ku	14	11	170	0.35	0.035	6 <sup>1</sup>	10.8	6/5.1	400	890	6,500	43	654	472	1,600	NA	
		14	11	30	0.35	0.035	6 <sup>1</sup>	10.8	6/5.1	400	800	6,500	43	115	472	1,600	CA	
		14	11	60	0.35	0.035	6 <sup>1</sup>	10.8	6/5.1	400	800	6,500	43	230	472	1,600	SA	
1.2 Customer Premises Service	Ka	30	20	170	0.35	0.035	4 <sup>1</sup>	7.2	4/2.7	400	2,500	11,500	16	38/104	566	1,040	NA	
		30	20	30	0.35	0.035	4 <sup>1</sup>	7.2	4/2.7	400	2,500	11,500	16	38/104	566	1,040	CA	
		30	20	60	0.35	0.035	4 <sup>1</sup>	7.2	4/2.7	400	2,500	11,500	16	38/104	566	1,040	SA	
2.1 High Volume Trunking	C	6		65	0.35	0.035	6/0.35	16.8x10	20.0	17	125	125	700	104	257	204	1,145	NA, SA, CA
2.2 High Volume Trunking	Ka	30	20	21	0.20	0.020	6 <sup>2</sup>	7.2	6	100	1,000	3,200	40	400	460	980	NA	
		30	20	9	0.20	0.020	6 <sup>2</sup>	7.2	6	100	1,000	3,200	40	400	460	980	CA, SA	
		30	20	6	0.20	0.020	6 <sup>2</sup>	7.2	6	100	1,000	3,200	40	400	460	980	SA	
3	TV Distribution	Ku	17	12	61	1.00	0.100	1.5	3.0	1.5	75	750	4,000	13	489	515	NA	
			17	12	61	1.00	0.100	1.5	3.0	1.5	75	750	4,000	13	489	515	SA, CA	
4 Tracking and Data Relay	S/Ku	2.2/15	2.1/14	1	2.0/0.3	0.040	5	1.5	5	1	26/1.5	680	24	309	425	Hemispheric		
		2.2/15	2.1/14	1	2.0/0.3	0.040	5	1.5	5	1	26/1.5	680	24	309	425	Hemispheric		
		15	13	1	0.7/0.8	0.100	2	1.0	2	1	30	680	TBD	309	425	Ground Station		
		2.2	2.1	20	8.00	0.100	(30x30 Array)	2.5x2.5	1	TBD	680	TBD	309	425	Hemispheric			
5 Educational TV (Used CPS Channel for Uplink)	S	2.5	1	3.50	0.300	2.5	1.5	2.5	16	96	400	71	549	620	CONUS - Pacific Time Zone			
		2.5	1	3.50	0.300	2.5	1.5	2.5	16	96	400	71	549	620	CONUS - Mountain Time Zone			
		2.5	1	3.50	0.300	2.5	1.5	2.5	16	96	400	71	549	620	CONUS - Central Time Zone			
		2.5	1	3.50	0.300	2.5	1.5	2.5	16	96	400	71	549	620	CONUS - Eastern Time Zone			
		2.5	1	5.50	0.500	1.5	0.9	1.5	16	96	400	71	549	620	Mexico, CA			
		2.5	1	5.50	0.500	1.5	0.9	1.5	16	96	400	71	549	620	SA - North			
		2.5	1	5.50	0.500	1.5	0.9	1.5	16	96	400	71	549	620	SA - Central			
6	Direct-to-Home TV	Ku	14	0.7	1	1.00	0.100	1.5	0.9	1.5	8	800	2,100	52	463	515 Ground Station		
		UHF	14	0.7	6	3x4	0.300	10	6.0	10	8	800	2,100	52	463	515 Hemispheric		
7 Air Mobile	L	1.6	1.5	1	Shaped	0.500	(12 Helix Array)	1x1	2	200	1,200	65	195	260	Hemispheric			
		C	6	5	1	18.00	(Horn)	1x1	2	20	1,200	65	195	260	Hemispheric			
9	Land Mobile	UHF	0.9	0.8	21	1.5	0.100	20	15.0	20	100	1,000	4,000	340	344	680 CONUS, Alaska, Hawaii, Virgin Islands		
11	Interplatform Link	K/Q	32	25	2	0.3	0.030	2.4	1.0	2.4	2	130	300	67	63	130 To other platforms		
12	Data Collection	UHF	0.4	0.4	4	5.0	0.100	10	5.0	10	4	4	100	35	95	130 Hemispheric		

\*NA = North America; SA = South America; CA = Central America

= Feeds included in antenna mass

<sup>1</sup>Circular/parabolic reflector; FSS subreflector

<sup>2</sup>Offset/Cassegrain

Table 3-4. Requirements for Stationkeeping and Attitude Control

Attitude	
Pitch	$\pm 0.05^\circ$
Roll	$\pm 0.05^\circ$
Yaw	$\pm 0.1^\circ$
Stationkeeping	
Constellation Longitude:	$\pm 0.03^\circ$
Constellation Latitude:	$\pm 0.03^\circ$
Platform to Platform Spacing:	$\pm 1$ km

requirements of several payloads call for higher accuracy than the platform tolerances. This is resolved by providing special high accuracy (or vernier) pointing capability in these antennas themselves. This can be done electronically, by beam steering with monopulse sensing or, special gimbals at the antennas and/or feed mounting points. The former appears to be most desirable. This is discussed further in Sections 3.1.4 and 3.4.3.

Due to the large size of the platforms, it is considered highly desirable - if not a firm requirement - to provide local thermal control at the "black box" level. This would be most important for feeds and matrix switches where large amounts of heat are generated. As stated earlier, the present study has provided central radiators with capacity to handle the total load and development of detailed designs to provide local cooling is an important item for future study. This is discussed in Section 3.1.7.

An effort has been made to locate RCS propellant bottles in positions that would be accessible for servicing or replacement. However, viable design details will be an important subject for future study, and the same is true of attitude control system design particularly with respect to the effects of low frequency structural modes.

The requirements for a system lifetime of 16 years with consumables (batteries and RCS propellant) replenished at 8 years, implies a high level of reliability and is discussed in Section 3.1.11.

Finally, the design of airborne support equipment (ASE) is a major item that must be covered in future work. The current study has provided approximately 0.3m radial clearance within the Shuttle bay for ASE, and an allowance of greater than 10 percent of the combined platform/payload weight has been made for it.

**3.1.3 CONCEPTUAL DESIGNS.** Conceptual designs have been made of Alternative #1, Platforms 1, 2, and 6 for the Western Hemisphere constellation. These were chosen because:

- a. Platform 1 appeared to be most challenging.
- b. Platform 2 carried the large interferometer payload.
- c. Platform 6 carried the high priority CPS Ka-band payload.

Some results are also presented for a preliminary layout of Alternative #4.

#### **3.1.3.1 Alternative #1.**

**Introduction.** This alternative is based on the nominal traffic model, and Platforms 1, 2, and 6 in the Western Hemisphere constellation have been chosen for study. Payload assignments were shown in Table 3-1. At the beginning of work it seemed impossible that the required payloads, along with a viable platform structure could ever be packaged to fit into the available cargo space - i.e., a cylinder 7.925m by 4.572m diameter (26 ft by 15 ft diameter). For this reason, packaging was given a very high priority when making all design decisions. A radial clearance of approximately 0.3m inside the cargo bay was reserved, as a goal, to provide space for installing ASE. This envelope was penetrated at several points but for the most part it has been kept available. The ASE has not been designed, but is counted on to provide support and strength during launch as well as a handling cradle for both ground manipulation and deployment at LEO.

**Packaging Considerations.** The main consideration in packaging the geostationary platform in the Shuttle for Alternative #1 was the choice of a transfer vehicle. Previous studies had implied that the platforms would likely be volume rather than mass constrained. NASA memo PD01-80-16 directed GDC to use a maximum payload length of 26 feet thereby making the allowable payload length for the Centaur, IOTV or OTV the same. For these studies the payload length starts just aft of the forward cabin (station 582).

A design objective that has been met was to design a platform wherein the structure and payloads were deployable as one unit and to have all subsystems preinstalled. This objective allows for precheckout procedures to be run on a complete assembly prior to deployment at LEO. It is not dependent on EVA operations (except for corrective action) thereby minimizing Shuttle stay time in orbit.

Existing concepts of antennas were utilized consistent with antenna requirements. Given a choice, the antenna that exhibited the minimum volume was utilized. The same consideration was applied to the platform structure.

Platform 1. Previous studies segregated the various payloads onto six platforms based on mission priorities and mass distribution. Platform 1 was deemed to be the most difficult from a packaging standpoint. Figure FO-1 shows the view from Earth of the deployed platform. (Foldouts are placed at the back of the book). The biggest driver was the feed array for Payload No. 2.1 (HVT C-band). In order to meet our deployment philosophy, the feed was divided into three segments, which allowed it to be packaged. In addition, it was decided to arrange the feed arrays at the base of the platform, thereby placing the "active" hardware in the vicinity of the central core structure. The "passive" elements or main reflectors are mounted on deployable structures, thereby minimizing electrical line runs.

The platform central core structure houses the avionics, attitude control system, power and switching gear. From this central core a deployable mast (an Astro Research Corp. concept) supports two smaller versions of the "astromast" that in turn become the structural supports for two large main reflectors. To the top of the central mast the interplatform link antenna is mounted to provide a clear line of sight to the other platforms in the constellation (see Figure FO-1, Sheet 2). In order to avoid running communications and power lines up the mast an alternative position is shown for the IPL in Figure FO-1, Sheet 4.

For the solar array, the Lockheed solar electric propulsion system (SEPS) concept was utilized with minor variations. This concept exhibits excellent packaging characteristics and has been developed into a viable concept. In order to prevent shadowing of the solar panels, they are mounted radially from the central hub via an astromast (see Figure FO-1, Sheet 3).

To support the smaller payloads, two semideployable arms are mounted to the central core. The overall length of the arms is fixed allowing the smaller payloads and subsystems to be mounted. During deployment, the arms are rotated to a horizontal position and an open latticework is deployed providing the torsional and bending stiffness for the arms (see Figure FO-1, Sheet 4).

Not shown in the above figure is the design concept for the ASE. In order to provide support for the payload during launch and/or abort loads, an ASE cradle is required that will support all elements of the payload. This is an important subject for further work.

For deployment, the transfer vehicle with the payload attached is rotated to approximately a 75-degree position from the horizontal axis of the Orbiter. In this position, the payload can be deployed without interfering with the Orbiter. The platform is designed for controlled and sequential deployment. Each element of the platform can be deployed and checked out prior to initiating the deployment of another part of the structure.

For servicing at GEO, a docking port is provided on the platform for the Teleoperator to dock while it performs the service operations (remove and/or replace propellant tanks, batteries, etc.).

Platform 2. Platform 2 is similar in concept to Platform 1. The platform consists of a central core structure about which the antennas are cluster-mounted. As with Platform 1, the size of the feed arrays becomes a large driver in the packaging concept. In order to provide a platform where all subsystems and antennas could be prepackaged yet be fully deployable without aid from EVA, the feed arrays and subreflectors are mounted on articulated arms about a centralized telescoping mast that provides a compact volume-efficient package (see Figure FO-2).

In this concept, all subsystems, ACS propellant tanks, batteries, reaction wheels, etc., are mounted within the central core structure. The deployable radiator, for thermal control, is derived from a rigid panel deployable radiator system concepted by the Vought Corporation. The radiator panels fold "accordian" fashion for stowage and the radiator fluid is transferred between adjacent deployed panels across the hinge line using fluid swivels.

The solar array concept is the same as Platform 1, except that it is mounted to the central core through a rigid structure. The only deployment actions required are to rotate the arms to the horizontal position; the "astromast" then deploys the panels.

Due to the large baseline required for the RF interferometer, four astromasts are mounted within the central core and, when deployed, exhibit a slight angle to the horizontal. This places the end mounted helix antennas in the same plane with the three helix antennas on the top of the telescoping mast. The ASE design and deployment operations will follow the same philosophy as for Platform 1.

Platform 6. Platform 6 is almost identical in design to Platform 2, the only difference being in the complexity of the packaging design. Due to the smaller antennas and fewer payloads, greater freedom in design was available. The solar panels, radiator, and packaging of subsystems is almost identical to Platform 2 (see Figure FO-3).

ASE design and deployment would be the same as noted for Platform 1.

Platforms 1, 2, and 6 were chosen for preliminary packaging and deployment layouts, as it was felt that they covered the complete range of difficulty. Based on these layouts, it is assumed that Platforms 2, 4, and 5 would be less of a challenge.

Communication Links Between Payloads. When a ground signal originates in the area covered by the Atlantic constellation and is to be transmitted to a receiving station covered by the Western Hemisphere constellation, it must be relayed by a long range link between the two constellations. We describe this long range link by the term "interplatform link" (IPL). This term was well established before development of the concept of "constellations" and we see no

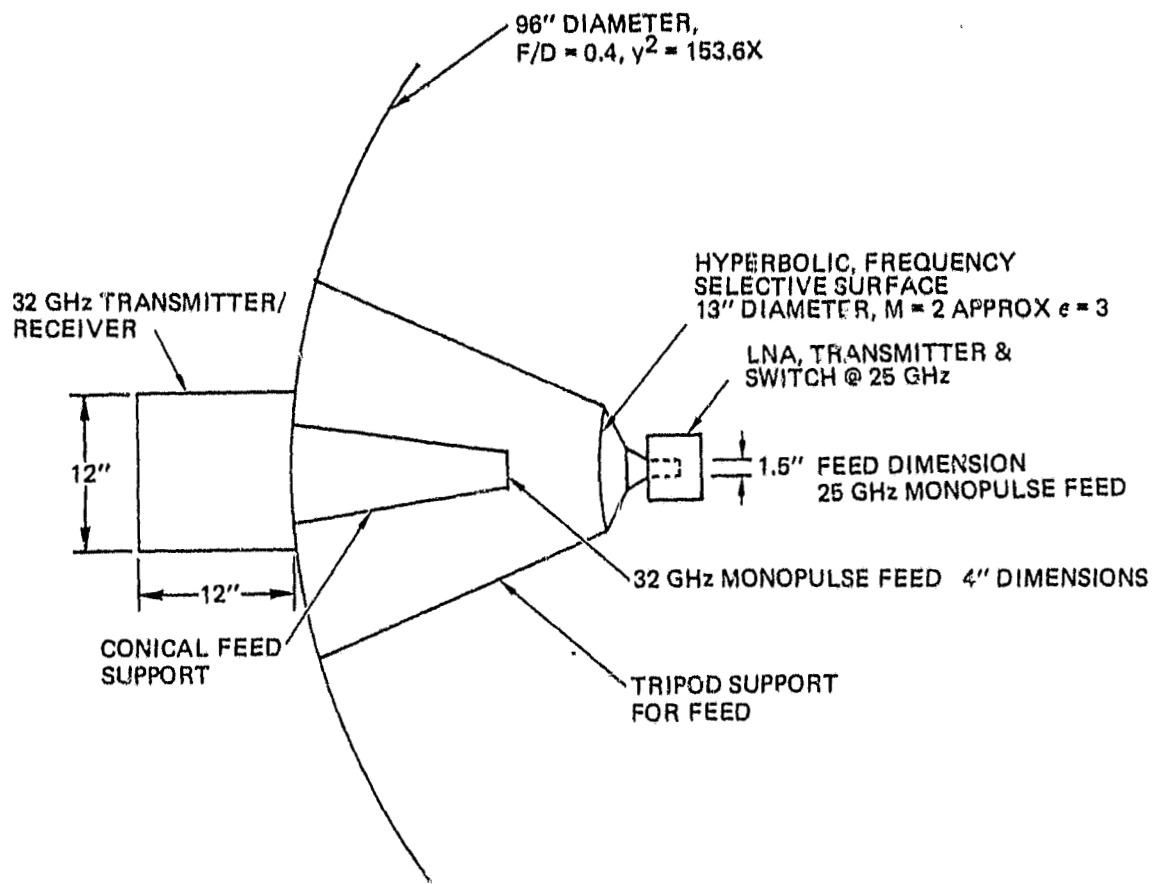
reason to change it. However, the constellation concept introduces, in addition, the need for a short range communications link between platforms within a constellation. Since the requirements for the new short range link will not be the same as for the IPL we have introduced the term "intraconstellation link" (ICL) to describe it.

Estimates of the volume of traffic transmitted on the IPL average near 10 percent of the total data bandwidth of the terminals. Greater percentages of the total platform bandwidth will probably be required in the future to further relieve congestion on the multiple ground station links that are otherwise used. Estimates of the IPL data bandwidth far exceed the capability of the 32/25 Intelsat links. Existing higher frequency communications allocations or optical links will be pressed into service to provide additional bandwidth.

The relationship between the IPL linking the highly separated platforms or constellations and the ICL has not been investigated fully. The data rate requirements for the ICL are very high for the "merry-go-round" type of constellation (see Figure 3-2 and Section 3.3). The ICL terminal is configured the same as the IPL terminals described in the following paragraphs with several exceptions. The tracking rates are higher since terminal separations are smaller. The data rates and information bandwidths of the ICLs are much greater than the IPLs. The pointing accuracy of the ICL is reduced by using larger beamwidth antennas.

Two configurations of the IPL were investigated. Both operate at 32/25 GHz. A single parabolic reflector antenna combines the two frequencies on the reflector with a frequency selective subreflector (FSS). Prime focal point feeding of the reflector is accomplished by low loss transmission through the subreflector at 25 GHz. The Cassegrain antenna is excited at 32 GHz, where the subreflector is highly reflective. Figure 3-2 shows a cross-section of the single reflector configuration. The magnification of the Cassegrain system is limited to approximately 2 by placing the feed near the subreflector. The 2.4m reflector antenna provides gains of 53 dB and 55 dB at 25 and 32 GHz and beamwidths of 0.35 degrees and 0.27 degrees, respectively. The frequency selective subreflector has precise insertion and reflective phase requirements to achieve antenna gain requirements. The feeds at both frequencies serve transmit and receive functions. T/R switches select the operating mode of the antenna assembly to be compatible with the antenna at the other end of the link. Receive monopulse provides antenna steering information after initial computer aided acquisition. Acquisition may also require a faster scan sequence to obtain monopulse tracking lock-on. Transmission occurs on the sum pattern only, while reception is accomplished with both sum and two axis difference patterns. The IPL antenna is gimbal mounted with computer control and servocontrol capability.

Figure 3-3 shows the IPL antenna mounted on a platform mast with broad coverage of the geostationary arc and in a packaged configuration. The solid surface reflector is folded in a TRW "Sunflower" arrangement. The subreflector



264,352-137

Figure 3-2. Cross Section of the Single Reflector Configuration

and both feed assemblies remain in fixed relative positions. The other configuration of IPL antenna uses dual reflectors. Both reflectors of the second configuration are mounted on a common stabilized subplatform and electrically boresighted to a common pointing angle. The advantage of this approach is higher efficiency resulting from the elimination of the frequency selective sub-reflector. This configuration, however, has poor packaging characteristics and is more difficult to position because of larger subplatform dimensions.

Separations between IPL terminals result in large propagation space loss. The separation between Western Hemisphere and Atlantic constellations is nominally 32,000 miles. The space loss at 32 GHz is 217 dB.

Table 3-5 shows a sample link power budget calculation. The required transmitter power is 400 watts in this example. RF power reduction methods include reduction of receiver noise bandwidth and in-receiver noise figure. The antenna gain can also be increased, but acquisition and tracking difficulties increase. Data transmission to satellites within the constellation requires very

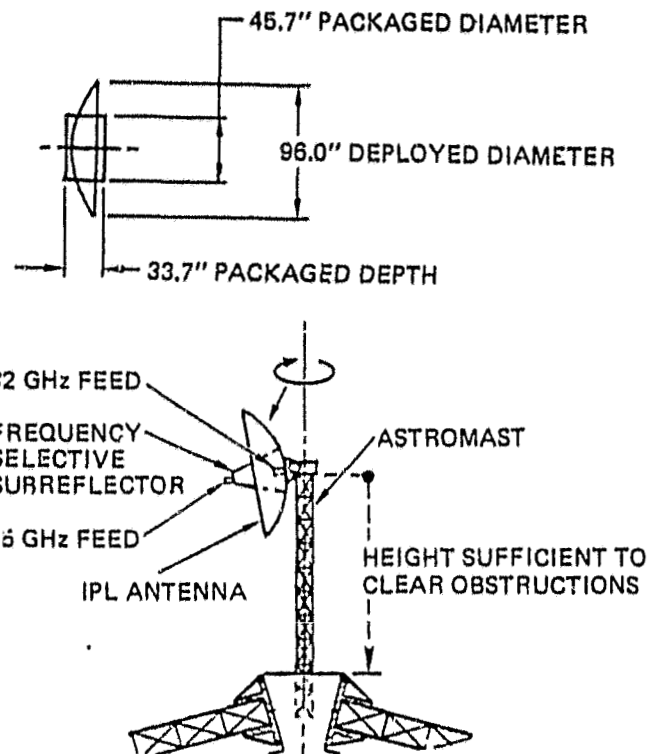


Figure 3-3. Packaged View of IPL Antenna and Installation View of IPL Mounted on a Platform

low power RF amplifiers since the interterminal distances are comparatively short. Tracking gimbal angular rates are higher for the constellation terminals.

Geoplatform Command, Data and Communications Links, Alternative #1. The GP command and data links fall into two categories: those associated with moderate data rate functions such as payload power switching, tracking for stationkeeping, and housekeeping data and those involved in controlling high data rate communications and scientific payload links. These categories are discussed under telemetry, tracking, and command (TT&C) for moderate data rates and central communications control (CCC) for the high data rate functions.

TT&C. The constellation platform proposed for Alternative #1 will have a dedicated ground station for system operation. The individual communication payloads will in some cases have their own separate ground stations. The tracking function for stationkeeping can be provided with provision in the dedicated ground stations link (requires more than one ground station for tracking geometry), by using TDRSS, or possibly with GPS. Selection of one or more of these tracking methods is to be examined further during GP pre-design phase.

Table 3-5. Link Calculation of a 32/25 GHz IPL

Parameter	Value
Terminal Separation (32 GHz)	32,000 miles
Free Space Loss	217 dB
Receiver Input Level	
KT	-204 dBW
Required C/I	20 dB
Noise Figure	10 dB
Noise Bandwidth	90 dB
Total	-84 dBW
Antenna Gain (32 GHz)	
Receive	55 dB
Transmit	55 dB
Pointing Error Loss	
Receive	1 dB
Transmit	1 dB
Losses	1 dB
Required Transmit Power	26 dBW

Previous tracking systems have included Azusa, Globetrack, minitrack, C-band beacon, radar, SGPS, GRARR, and USB. A major deficiency of these systems is the inability to continuously track low earth orbit satellites. Two new systems going into operation, TDRSS and GPS will substantially improve this situation. TDRSS will have two satellites in GEO with 130 degree longitudinal spacing giving near continuous coverage for LEO, and 100 percent coverage with 1200 km altitude decreasing to 38 percent coverage at GEO. GPS initially will have 6 satellites in 12-hour orbits giving near continuous coverage for LEO, followed by an 18-satellite full-up system providing 100 percent coverage for LEO. Studies have shown that GPS should also be suitable for GEO satellite tracking.

Since TDRSS cannot provide 100 percent coverage at GEO, the operating plan is to use STDN ground stations for GEO tracking and to augment the TDRS in LEO coverage. The accuracy of TDRS tracking is less for satellites with the same orbital inclination due to geometry. Less than one-half orbit tracking with TDRS results in reduced accuracy for geometry reasons. Noncontinuous tracking that requires orbit prediction has error sources of drag variation and the gravity harmonics.

At GEO, the accuracy of STDN and GPS is in the order of 100 meters 3 sigma. For low inclination LEO, TDRSS accuracy is in the order of 700 meters 3 sigma, while GPS continuous tracking accuracy in the full-up configuration is in the order of 10 meters 1 sigma.

The TT&C block diagram in Figure 3-4 illustrates the interconnections of the GP control and data processor via a fiber optics bus to the platform subsystems. The tracking function is shown with TDRSS, and GPS as an alternate. With TDRSS the range and range rate information is developed at the White Sands station, whereas with GPS, the information is obtained on the platform. The stationkeeping computation and control is perceived as being done at the GP dedicated ground station. The orbital data from GPS would have to be transmitted from the platform and for TDRSS from White Sands or GSFC.

The GP commands would be transmitted, and the GP housekeeping data would be received, on the link from the GP dedicated ground station to the GP control and data processor. TDRSS also provides telemetry and command links in addition to the tracking function; however, it has to be shared with other users.

CCC. The central communications control is illustrated in Figure 3-5 for Platform 1 with the central communications controller being updated by the GP dedicated ground station to operate the 16 by 16 matrix switch controller, the communications payloads communication functions, and the scientific payload high data rate functions. The mux-demux combines lower bandwidth communications channels into the 1 GHz matrix switch channels. The matrix switch routes the 1 GHz channels to another constellation GP over the IPL, to the other platforms in its own constellation over ICLs to the GP dedicated ground station link, and to other communications 1 GHz channels within Platform 1. The high data rate scientific payload channels are directly muxed on to the downlink and do not go through the communications matrix switch. In case of GP dedicated ground station link failure, a recovery mode is indicated through the STDN ground station.

For some of the platforms (2 through 6)(Figure 3-6), a smaller 8 by 8 matrix switch is utilized since the IPL is not required (only the ICL), and the high data rate link to the GP ground station is provided only on Platforms 1 and 4 (4 for redundancy and added capacity, along with another IPL).

Data routing between payloads in each platform of the constellation is coordinated by the platform switch and the data bus. Data transfer between the platforms and timing synchronization is accomplished by the ICL. Data rates of the data buses, switches, and ICLs are estimated at between 20 and 30 percent of the total data rates of all the payloads of each platform. Table 3-6 shows the number of 40 MHz transponders associated with the communications payloads of Alternative #1. The number of equivalent 40 MHz interconnect transponders is shown as one quarter of the payload transponders. The 40 MHz transducers are multiplexed onto 1 GHz bandwidth data buses. Table 3-7 shows the broadband data bus requirements for the corresponding platforms of the constellation.

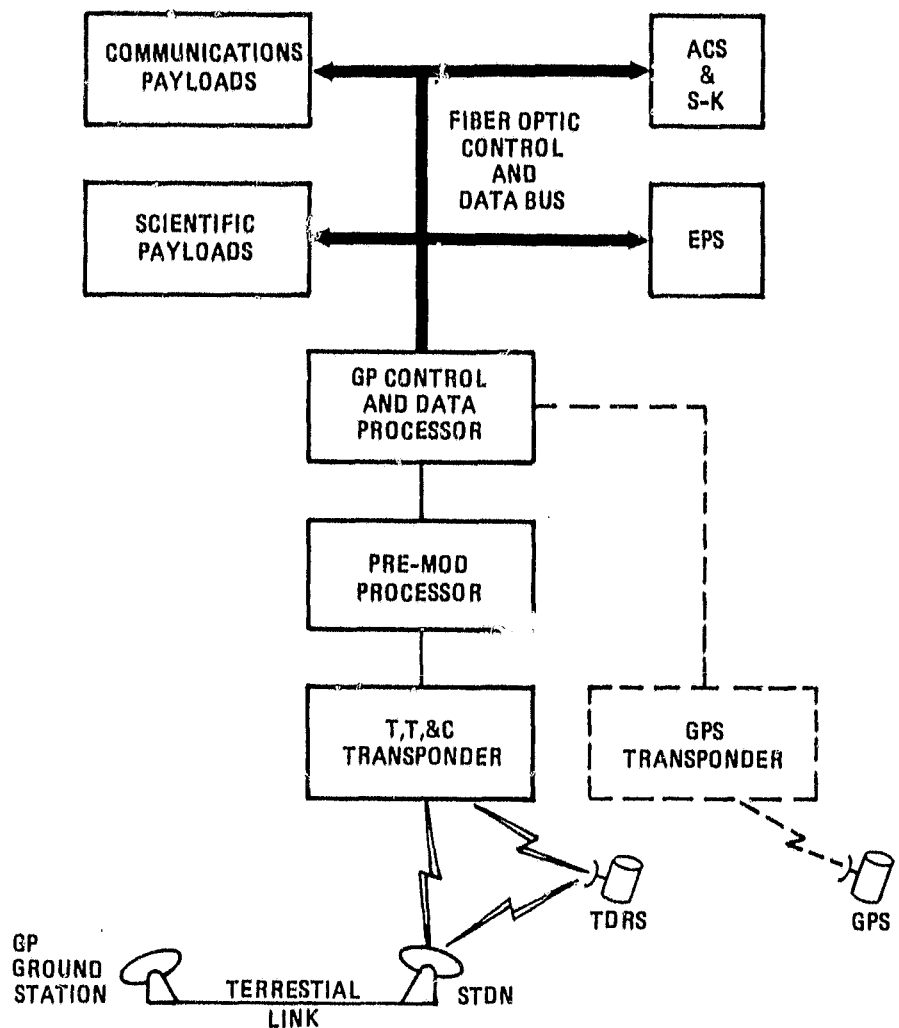


Figure 3-4. TT&C, Typical for Platforms 1 - 6 (Alternative #1)

The IPL and ICL bandwidth requirements are equal to the payload interconnect bandwidths. In the higher bandwidth platforms, the data is split between the IPL and the ICL. For lower bandwidth platforms, we permit full bandwidth capability on both links. Each platform has switching requirements below that provided by a 16 by 16 matrix switch. The bandwidth of the data bus switch is significant and broadband optical data bus and switch design will be required. High quality lasing diode sources and low dispersion fiber optics transmission lines will be necessary.

**3.1.3.2 Alternative #4.** Additional studies were made of Alternative #4 under bid and proposal funding and are presented herewith for information.

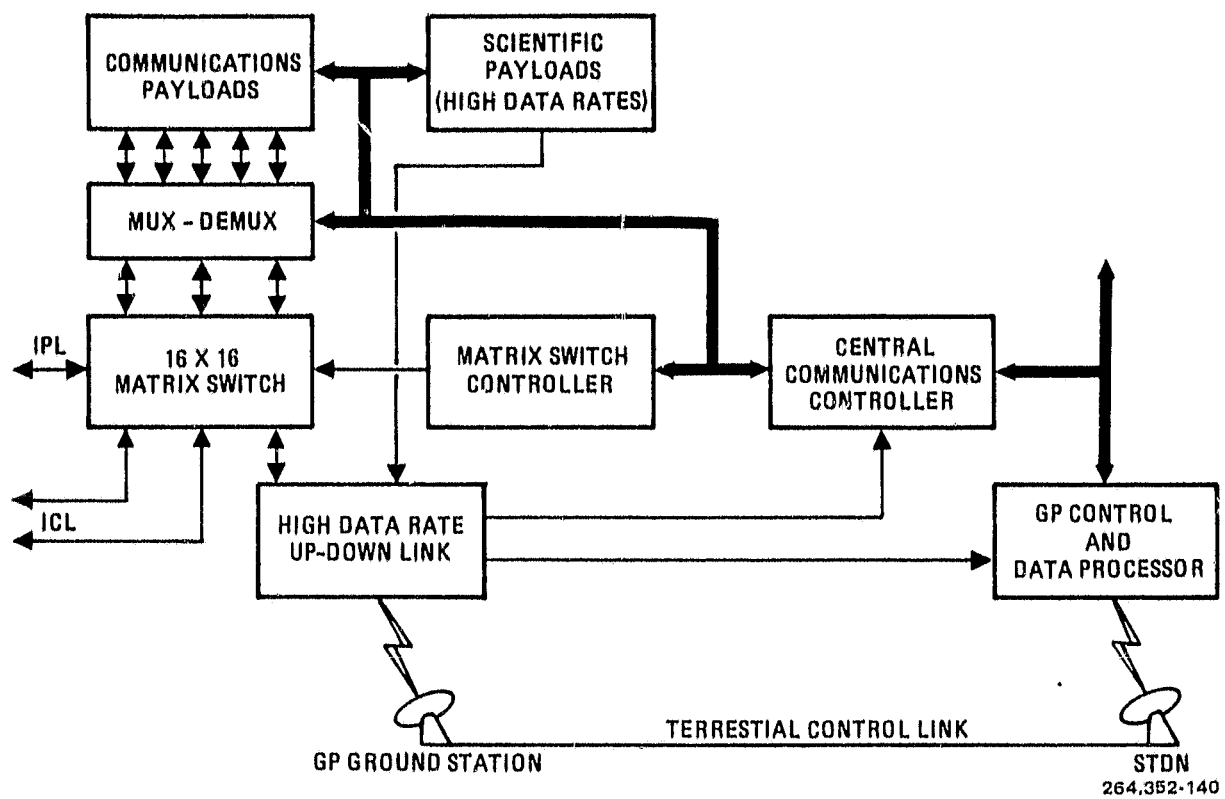


Figure 3-5. Central Communications Control, Platform 1 (Alternative #1)

Introduction. This alternative is based on the high traffic model and the Western Hemisphere platform has been chosen for study. It is a single large platform consisting of Modules 1, 2, and 3. Each module is launched in a separate Shuttle flight and occupies the entire cargo bay. Each module meets, and is mated with, a two stage reusable OTV at LEO. After transfer to GEO the three modules are docked to form the single platform. The payload list and the module assignments are summarized in Table 3-8. Data and requirements for the communications payloads are shown in Table 3-9.

In spite of the fact that each of these modules has an entire Shuttle bay to itself, packaging continues to be a very challenging task since they are so much larger than the corresponding platforms of Alternative #1. In this highly preliminary study, the assembled platform was laid out first and divided into modules. Module 1, incorporating the 60m antenna, was chosen for the first packaging effort. Its various components were then folded by themselves, each as compactly as possible; these were then loaded into the Shuttle bay to fill the volume as efficiently as possible, allowing 0.3m radial clearance for ASE, but without regard for the logistics of unpacking and assembly at LEO. This demonstrated that Module 1 can be fitted into the cargo bay, but it fails to indicate whether or not the packaging scheme is viable for the required mission. The size of the feed for the 60m antenna is 14.2m by 8.0m (46.6 ft by 26.2 ft)

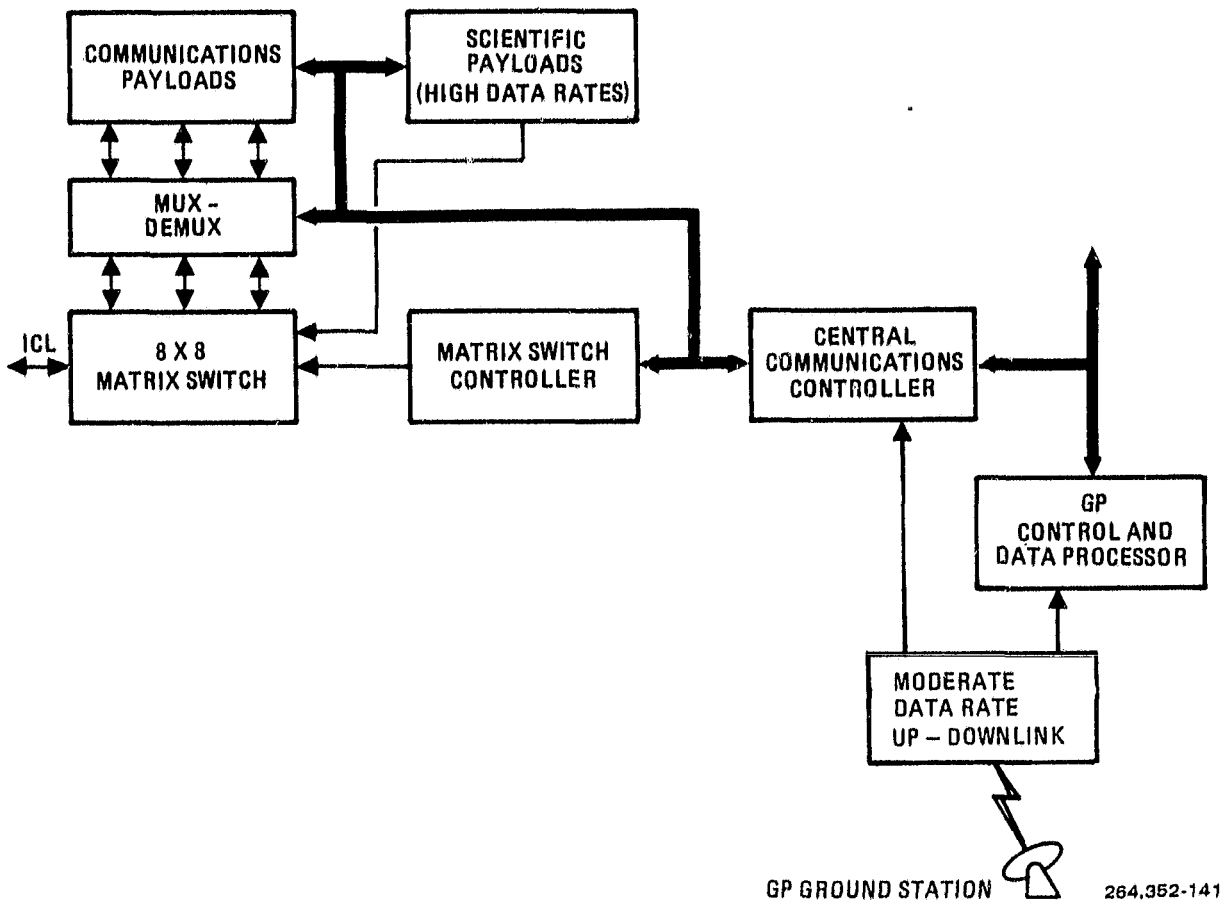


Figure 3-6. Central Communications Control, Typical for Platforms 2 - 6 (Alternative #1)

including all design assumptions and technological improvements invoked for Alternative #1 (see Section 3.1.4). This implies the need for significant folding of the feed.

The experience gained in packaging Module 1 is an important first step in devising a conceptual design to meet mission requirements. This is the stage of the work at the time of writing. The next step is to develop a logical unpacking and assembly sequence that is compatible with the packaging. Much use will be made of EVA and the remote manipulator system (RMS).

Most of the platform structure has been designed around the GDC deployable space truss beam made of low CTE graphite composite material. This is feasible due to the basically larger structure than Alternative #1, as well as the larger available packaging volume in the cargo bay.

The original OTV choice for Alternative #4 was the high thrust two stage reusable version with T/W = 0.31. Preliminary stress analysis indicated that this would impose a severe penalty on the structure if transferred from LEO to

Table 3-6. Estimate of the Number of 40 MHz and 1 GHz Bandwidth Channels Required for Each Communications Payload Alternative #1

Payload	Platform Number	Number of Transponders	Estimated Interpayload Transponders (25%)	Equivalent 1 GHz Channels
1.1	2	400	100	4
1.2	5, 6	400	100	4
2.1	1	125	32	2
2.2	4	100	25	1
3	1	75	16	1
4	3	4	1	1
5	3	16	4	1
6	5	8	2	1
7	2	4	1	1
9	3	30	8	1
11	All	2	0.5	1
12	3	4	1	1

Table 3-7. Data Bus Requirements for the Constellation Members Alternative #1

Platform	No. of Payload Interconnect Buses*	
	Without IPL, ICL	With IPL, ICL
1	3	9
2	5	10
3	4	8
4	1	3
5	5	10
6	4	8

\*Each bus = 1 GHz Capacity.

Table 3-8. Alternative #4 (Western Hemisphere)  
Payload Assignments

Description	Payload No.
Module No. 1	
CPS Ku-Band	1.1
HVT C-Band	2.1
Land Mobile	9
Interplatform Link	11
Module No. 2	
CPS Ka-Band	1.2
HVT Ka-Band	2.2
TV Distribution	3
Tracking and Data Relay	4
Educational TV	5
Direct to Home TV	6
Air Mobile	7
Data Collection	12
Lightning Mapper	17
Atmospheric Sounder	18
RF Interferometer	27
DNSP Data Relay	31
Module No. 3	
Materials Exposure	33
ACOSS/Halo Demonstration	34
Advanced On-Board Signal Processor	36
Solar Flare Monitor	39
Solar Flare Isotope Monitor	40
Energetic Proton Heavy Ion Sensor	41
Magnetic Substorm Monitor	43
Charged Particle Monitor	44
Cryogenic IR Radiator	51
BOSS Evaluation	52
Gemini Evaluation	53
EHF System	54
Aircraft Laser Relay	55
Fiber Optics Demonstration	56
Earth Optical Telescope	71
Chemical Release Module	73
Cryogenically Cooled Limb Scanner	78
Low Light Television	79
Microwave Sounder	81

Table 3-9. Alternative #4, Communications Payloads Definitions (Western Hemisphere, High Traffic Model)

P/L No.	Payload Description	Band	Frequency (GHz)		Beams		Antennas			Power (watts)			Mass (kg)		Geographic Coverage*		
			Up	Down	No.	Beam-width (deg)	Pointing Accuracy (deg.)	Aperature Size (m)	Focal Length (m)	Dish Size (m)	No. of ponders	Total RF	Total Input	Dish Feeds	Other Avionics		
1.1	Customer Premises Service	Ku	14	12	2,270 <sup>1</sup>	0.10	0.01	20/16.7	36.8	20.0	1,000	1,000	13,000	140	1,911	1,064	5,732 Western NA
			14	12	2,270 <sup>1</sup>	0.10	0.01	20/16.7	36.8	20.0	1,000	1,000	13,000	140	1,911	1,064	5,732 Eastern NA
			14	12	430 <sup>1</sup>	0.30	0.03	6/5	10.8	6.0	1,000	1,000	13,000	60	223	1,064	5,732 SA
			14	12	430 <sup>1</sup>	0.30	0.03	6/5	10.3	6.0	1,000	1,000	13,000	60	223	1,064	5,732 CA
1.2	Customer Premises	Ka	30	20	2,000 <sup>1</sup>	0.10	0.01	10/6.7	18.4	10.0	1,000	4,000	28,000	100	690	1,064	2,996 Western NA
			30	20	2,000 <sup>1</sup>	0.10	0.01	10/6.7	18.4	10.0	1,000	4,000	28,000	100	690	1,064	2,996 Eastern NA
			30	20	430 <sup>1</sup>	0.30	0.03	4/2.7	7.0	4.0	1,000	4,000	28,000	70	106	1,064	2,996 SA
			30	20	430 <sup>1</sup>	0.30	0.03	4/2.7	7.0	4.0	1,000	4,000	28,000	70	106	1,064	2,996 CA
2.1	High Volume Trunking	C	6	4	62	0.09	0.02	60/40 (15x25/ 10x17)	90.0	60.0	62	25	1,200	500	1,197	709	2,797 CONUS and S. Canada
			S	4	43	0.35	0.07		20.0	25.0	43	25	1,200	121	270	709	2,797 SA and CA
2.2	High Volume Trunking	Ka	30	20	30	0.10	0.02	10/6.7	18.4	10.0	100	400	3,000	100	223	161	1,205 Western NA
			30	20	60	0.10	0.02	10/6.7	18.4	10.0	100	400	3,000	100	223	161	1,205 Eastern NA
			30	20	5	0.20	0.04	6/4	15.0	6.0	100	400	3,000	75	124	161	1,205 SA
			30	20	5	0.20	0.04	6/4	15.0	6.0	100	400	3,000	75	124	161	1,205 CA
3	TV Distribution		17	12	61	1.00	0.10	1.5	3.0	1.5	75	750	4,000	13	+	489	515 NA
			17	12	61	1.00	0.10	1.5	3.0	1.5	75	750	4,000	13	+	489	515 SA and CA
4	Tracking & Data Relay	S/Ku	2.2/15	2.1/14	1	2.0/0.3	0.04	5	1.5	5.0	1	26/1.5	680	24	+	309	425 Hemispheric
			2.2/15	2.1/14	1	2.0/0.3	0.04	5	1.5	5.0	1	26/1.5	680	24	+	309	425 Hemispheric
			15	13	1	0.7/0.8	0.10	2	1.0	2.0	1	30	680	TBD	+	309	425 Ground Station
			2.2	2.1	20	8	0.10	(30x30 Array)		2.5x	1	TBD	680	TBD	+	309	425 Hemispheric
3-21	Educational TV (Uses CPS Channel for Uplink)	S	2.5		1	3.50	0.30	2.5	1.5	2.5	16	96	400	71	+	549	620 CONUS Pacific Time Zone
			2.5		1	3.50	0.30	2.5	1.5	2.5	16	96	400	71	+	549	620 CONUS Mountain Time Zone
			2.5		1	3.50	0.30	2.5	1.5	2.5	16	96	400	71	+	549	620 CONUS Central Time Zone
			2.5		1	3.50	0.30	2.5	1.5	2.5	16	96	400	71	+	549	620 CONUS Eastern Time Zone
			2.5		1	5.50	0.50	1.5	0.9	1.5	16	96	400	71	+	549	620 Mexico and CA
			2.5		1	5.50	0.50	1.5	0.9	1.5	16	96	400	71	+	549	620 SA - North
			2.5		1	5.50	0.50	1.5	0.9	1.5	16	96	400	71	+	549	620 SA - Central
			2.5		1	5.50	0.50	1.5	0.9	1.5	16	96	400	71	+	549	620 SA - South
6	Direct-to-Home TV	Ku	14	0.7	1	1.00	0.10	1.5	0.9	1.5	12	1,200	2,500	52	+	593	645 Ground Station
		UHF	14	0.7	6	3x4	0.30	10	6.0	10.0	12	1,200	2,500	52	+	593	645 Hemispheric
7	Air Mobile	L	1.6	1.5	1	Shaped	0.50	(12 Helix Array)		1x1	2	200	1,200	65	+	195	260 Hemispheric-Aircraft
		C	6	5	1	18.00	0.50	(Horn)		1x1	2	20	1,200	65	+	195	260 Hemispheric-Control Centers
9	Land Mobile	UHF	0.9	0.8	21	1.50	0.10	20	15.0	20.0	100	1,000	4,000	340	+	344	684 CONUS, Alaska, Hawaii, Virgin Islands
11	Interplatform Link	EHF	32	25	2	0.30	0.03	2.4	1.0	2.4	2	130	300	67	+	63	130 To Other Platforms
12	Data Collection	UHF	0.4	0.4	4	5.00	0.10	10.0	5.0	10.0	4	4	100	35	+	95	130 Hemispheric

\*NA = North America; SA = South America; CA = Central America

+ = Feeds included in antenna mass

<sup>1</sup>Maximum number of beams capability

to GEO in the assembled/deployed configuration. For this reason, the OTV was changed for Alternative #4, to the low thrust two stage reusable version with  $T/W = 0.035$ . For comparison, it should be noted that the low thrust expendable OTV with  $T/W = 0.05$  was specified for the smaller structures of Alternative #1. This created no problem but we had no occasion to analyze this for a higher thrust case. It is probable, however, that the smaller modules of Alternative #1 would be less sensitive to larger values of  $T/W$ .

Alternative #4 - Docked Configuration. The configuration of Alternative #4 (see Figure FO-4) consists of three modules docked together. The three modules were tentatively assigned payload missions considering priorities and weight assignments. An additional requirement was to provide the power supply (100 kW) in the first module.

Each module with its subsystems and payloads packages into a single Orbiter bay. In LEO, the module is assembled and/or deployed. Two OTV stages are brought up in separate Shuttles after the module has completed its operational checkout. The stages are mated together and interfaced to the module for transfer to GEO.

Since the packaging problem of the structure is not quite so severe as it was in Alternative #1, the GDC deployable space truss beam (Figure 3-9), made of low CTE graphite composite material, is used in many places instead of the Astromast, which consists of fiberglass.

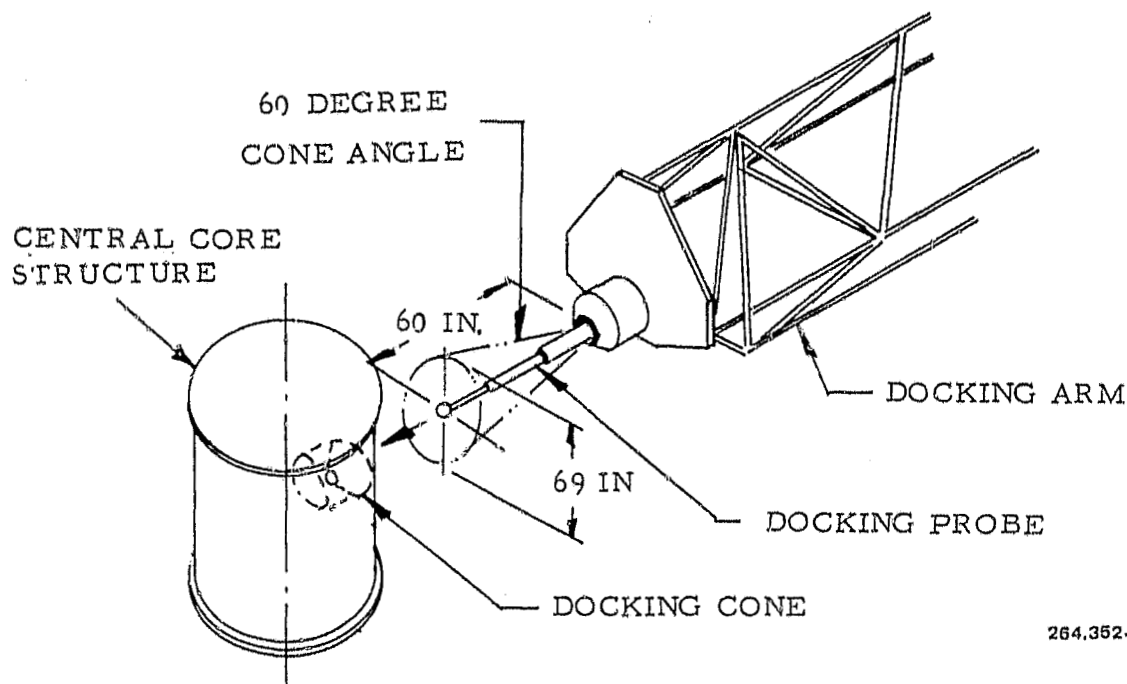


Figure 3-7. GDC Deployable Space Truss Beam

## Module 1

Module 1 is essentially a long beam with a central core structure at its midpoint (see Figure FO-5). The beam is a tetrahedral structure (diamond shape in cross sections) presently under development by General Dynamics Convair. The solar panels are mounted to these beams, which places them in an outboard position, which prevents shadowing from the payloads. A design objective was to mount the feed arrays (active elements) on the platform beams and to mount the main reflectors (inactive elements) on deployable masts.

As with other concepts, feed arrays were a major driver in packaging. For example, Payload No. 2.1 for the 60m antenna requires an array 8 by 14.2m, well beyond the cargo bay limits. Therefore, the array was divided into four elements (see Figure FO-6) in order to fit within the cargo bay diameter. For the most part, the Lockheed "wrapped rib" concept for the main reflectors was chosen for its efficient packaging dimensions. For high frequency antennas (such as Payload No. 11 - interplatform link) the TRW "Sunflower" concept was used because of its higher surface accuracy.

To maintain a high volumetric packaging efficiency, the central core structure (which becomes the interface for the two main beams of the platform) were packaged in a telescoping manner and provided room for other elements of the platform. The mast structure is the same concept as the main platform beams. Astromasts, pantograph beams, and others studied to date do not exhibit the structural stiffness or packaging efficiencies for large structure (90m) required in this concept.

Due to the high density packaging requirements for Alternative #4 (three Shuttle flights for structure and payload), the preliminary concept was aimed at investigating the packaged elements of the platform versus the available cargo bay volume. The concept as delineated for Module 1 (packaged configuration) takes the packaged platform elements and arranges them in a manner to maximize the volumetric efficiency of the cargo bay. This preliminary exercise indicates that all elements of Module 1 can be packaged and transported in one Shuttle flight. This concept differs from Alternative #1 (where the design produces a completely automated deployable platform) in that the build-up of Alternative #4 Module 1 requires RMS and EVA operations. Elements of Module 1 would be removed from the Orbiter bay in a predetermined sequence, deployed, and/or assembled to other elements until the platform is complete.

A design goal in further evaluations would be to take grouping of payloads such as Payload No. 2.2 (see Figure FO-4, Module 2), which consists of 2 ten-meter and 2 six-meter antennas, a central mast, a lateral supporting structure and perhaps the feed arrays and design them into an integral deployable unit. This unit could then be removed from the Orbiter bay in LEO, deployed, and installed on the platform structure. This concept would minimize EVA and RMS operations and be a hybrid of Alternatives #1 and #4, as presently depicted.

### Module 2

Module 2 is similar in design to Module 1, except the structure exhibits a "T" section (see Figure FO-4). A central core structure forms the main interface for three radial arms that form the platform. The large arm contains a docking probe and latches for joining to the central core of Module 1.

Again, the same design philosophy was used for Module 2 as 1 (install the active elements on the structure and the passive elements on masts above the structure).

Figure FO-6 depicts the packaged sizes of the elements that make up Module 2 and how they are packaged in the Orbiter bay.

### Module 3

Module 3 contains those payloads that are not deployable such as the DoD or science payloads with the exception of Payload No. 81 (a 10m antenna).

The platform structure is comprised of three rigid arms arranged about a central core structure (see Figure FO-4). In the packaged configuration, the three radial arms are rotated parallel to the axis of the central core. The arms are sized for length so that they will fit within the cargo bay length. The payloads are installed at various locations of the radial arm with the exception of the 10m antenna, which is mounted on the central core. This concept allows Module 3 to have all payloads and subsystems preinstalled and allows for complete deployment of the platform without EVA or RMS operations. One of the three radial arms will contain a docking probe for attachment to the central core of Platform 2.

### Docking System

Docking of two very large, low density flexible structures is an area of advanced technology requiring thorough analysis and evaluation. Previous studies have been conducted by General Dynamics Convair in which impact (hard) nonimpact (soft), single-point, and multiple-point docking systems were evaluated. It was concluded that a single-point, active/passive soft docking system would be an optimum for this application.

Alternative #4 configuration readily lends itself to this concept.

Primary functions of the docking system and requirements for design of the structure and mechanisms, are:

- a. Initial capture.
- b. Shock attenuation, the energy required to bring the relative velocity between the two impacting bodies to zero without damage.

- c. Mating, after the two bodies have been initially coupled and the relative velocities are zero.
- d. Latching, the structural connection applied by multiple latches that secure the two bodies together.

In addition to the structural mating of two structures, consideration will be given to the mating of a power, communications, and fluid interface between the two structures.

The basic docking concept is shown in Figures 3-8 and 3-9. Assume that Module 1 is already in geosynchronous orbit and that Module 2 has been placed in GEO orbit in preparation for docking to Module 1. Module 2 will be called the "chase" module. The chase module incorporates the active docking mechanism with an extendable probe 5 feet in length that can be steered within a 60 degree cone angle. At a distance of 5 feet or less between the modules, the chase craft probe is extended and steered until contact is made with the passive docking port in Module 1 and locked in. Draw in of the two modules follows, until full contact of the conical surface is made and they are latched together. This contact method minimizes the absorption energy required, resulting in an optimum and simplified damping system.

IPL. The IPL shown in the Alternative #4 platform is similar to the Alternative #1 constellation links, except that data bandwidths are significantly larger to handle the high traffic model data rates. An optical data link is used in addition to the 32/25 GHz data link. The RF link provides coarse pointing information to align the optical system. The optical system utilizes a fine scale auto-track capability to maintain critical alignment. The required stability of the optical platform will be near several arc seconds.

Geoplatform Command, Data, and Communications Links Alternative #4. As with Alternative #1 GP, the command, data, and communications links fall into two categories: the normal satellite control and housekeeping functions; and the high data rate communications and scientific imagery links.

TT&C. The tracking link poses somewhat the same considerations for Alternative #4 as for Alternative #1. The relative accuracy requirements are not as stringent for Alternative #4 as for Alternative #1 since proposed spacing of 9 km (18 km diameter) between constellation platforms does not have to be maintained for docked modules. Figure 3-10 illustrates tracking by either GP ground station, TDRSS, or GPS. The command and data link would be from the GP ground station. The GP control and data processor operates over a fiber optics bus to the GP subsystems and payloads. Optocouplers are utilized at docking interfaces for noncontact data transmission.

CCC. The central communications control of GP Alternative #4 is more complex on the per individual platform basis, needing a 20 by 20 switch and docking

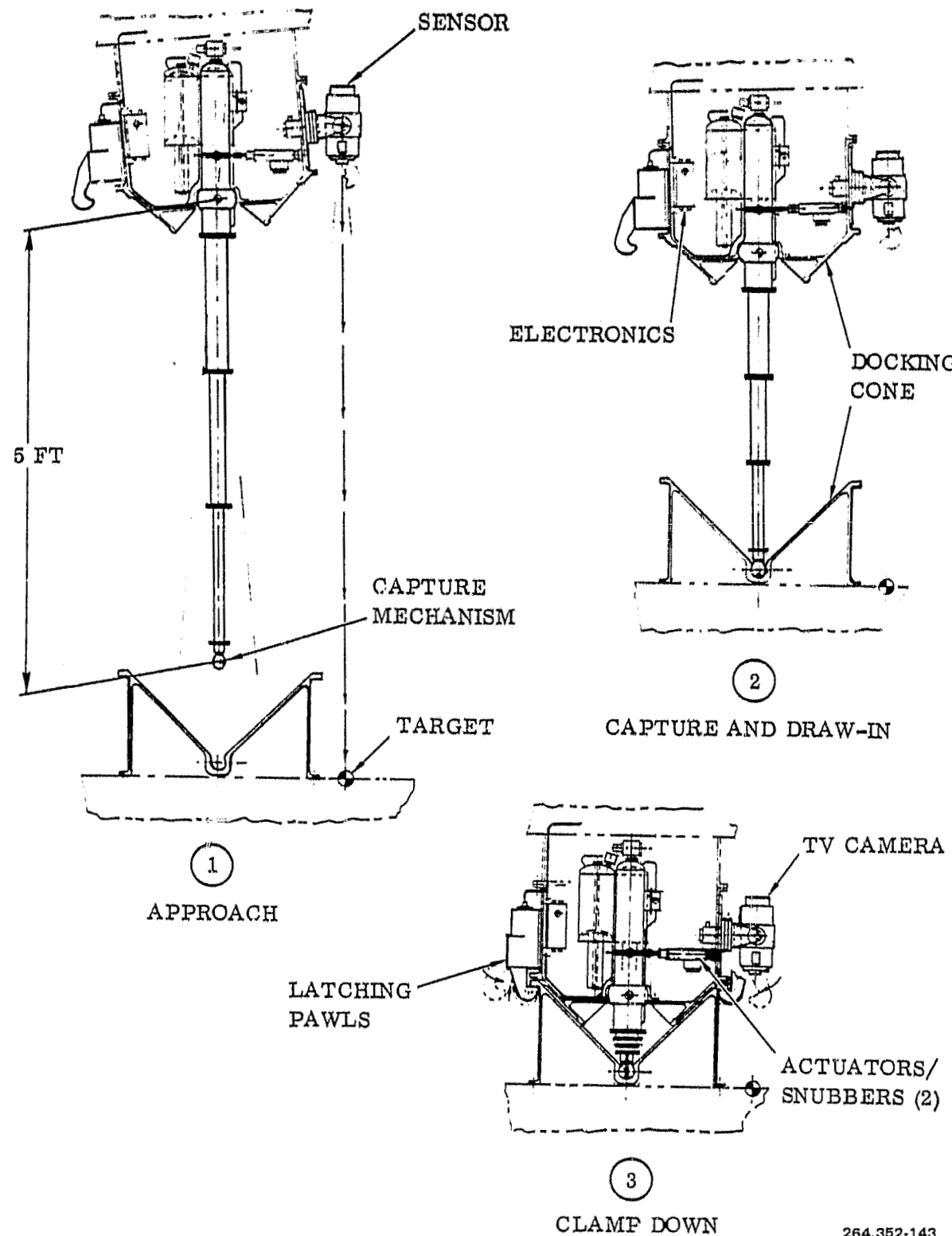
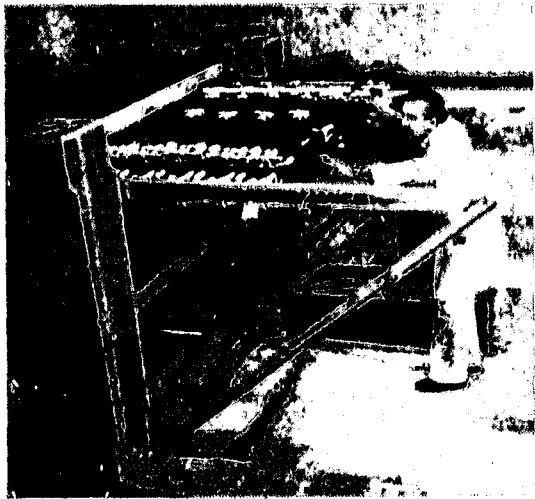
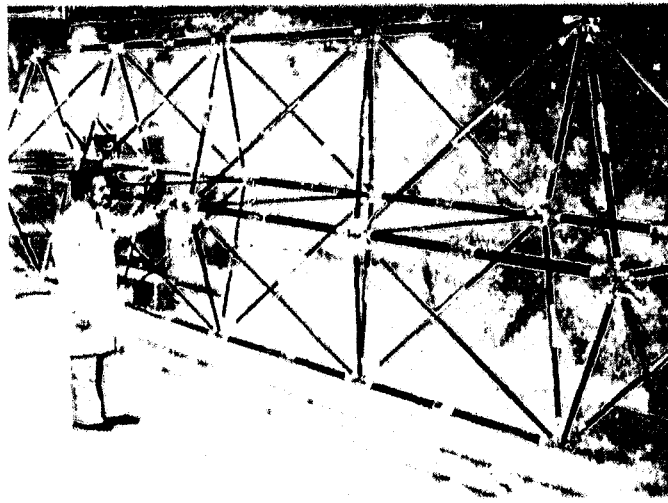


Figure 3-8. Soft Docking Concept



FOLDED

CVC800222



DEPLOYED

CVC800235

264,352-144

Figure 3-9. Docking System Configuration

interface couplers. The total CCC is simpler since ICLs are eliminated, being replaced with optical fiber links, as shown in Figure 3-11.

The platform configuration (Alternative #4) eliminates the need for ICLs and reduces the interpayload bandwidth requirements (see Section 3.1.3.1, — "Communication Links Between Payloads"). Interpayload bandwidths decrease since direct routes are maintained rather than linkage through multiple ICLs as in the constellation configuration of Alternative #1. Table 3-10 shows the number of 40 MHz transponders associated with each communications payload and the number of equivalent 40 MHz interconnect transponders. The platform interpayload transponder requirement is 10 percent of the payload bandwidth. The table shows that 19 channels with 1 GHz data bandwidth are required to interconnect the separate payloads in the platform. A 20 by 20 switch is installed in Module 1 of the platform to perform data bus interconnection. Large bandwidth of the optical switch, data bus, and connection components of the platform is necessary. The data bus lines must interface between the three modules of the platform. The very close tolerance optical connections at both docking ports require fine control of the locally flexible interconnect mechanisms. The high data rate optical transmission and switching is an area requiring research and development activity.

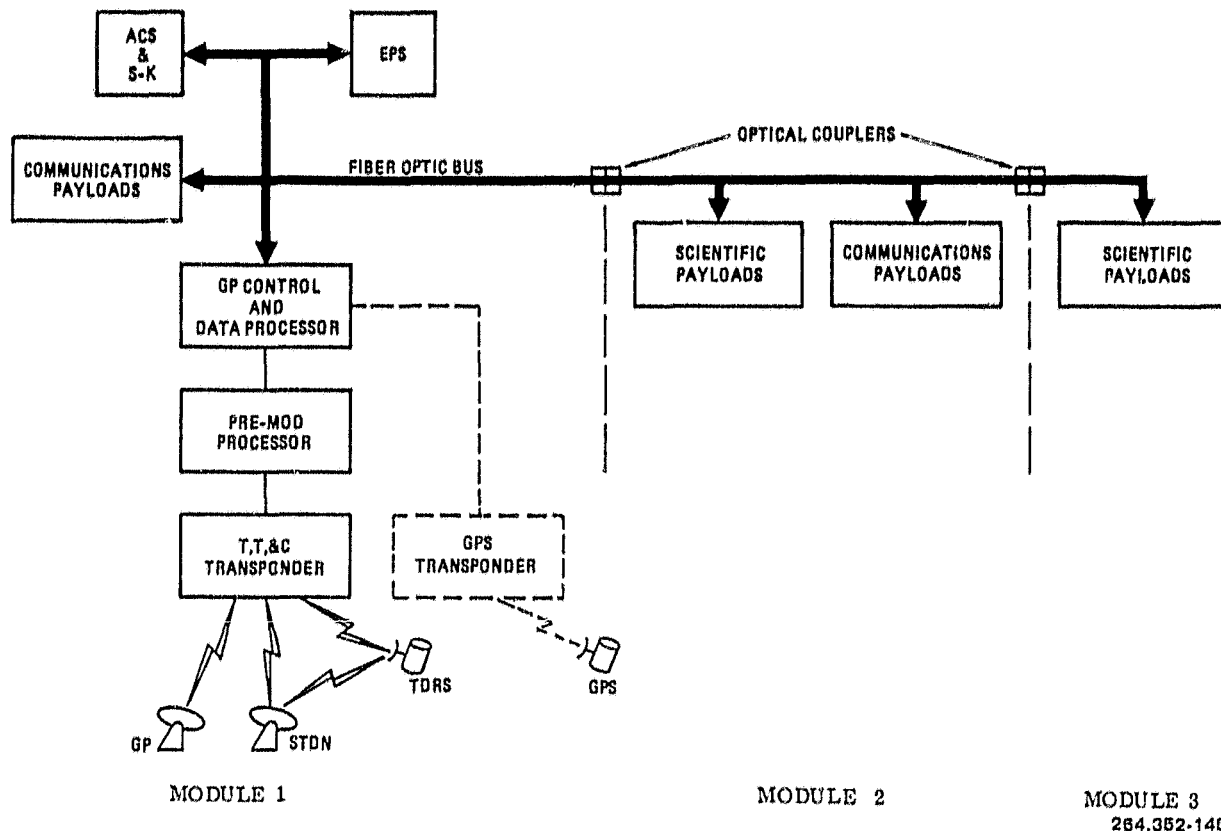


Figure 3-10. TT&C (Alternative #4)

**3.1.4 ANTENNA AND FEED DESIGNS.** Present Intelsat and related communications satellites are saturating both orbital arc and frequency resources. Only greater frequency reuse and the use of higher frequency communications bands will permit extension to future traffic demands. The antennas that we have investigated for the 1990s timeframe are therefore large and have complex feed assemblies. A variation in design has been introduced for a more flexible future concept. The same payload antenna has therefore been configured a number of ways on the several different platforms that support that payload. We have evaluated the following antenna candidates for application to Alternatives #1 and #4.

- Offset paraboloid reflectors.
- Offset Cassegrain reflectors.
- Offset confocal reflectors.
- Phased array antenna.
- Lens antennas.

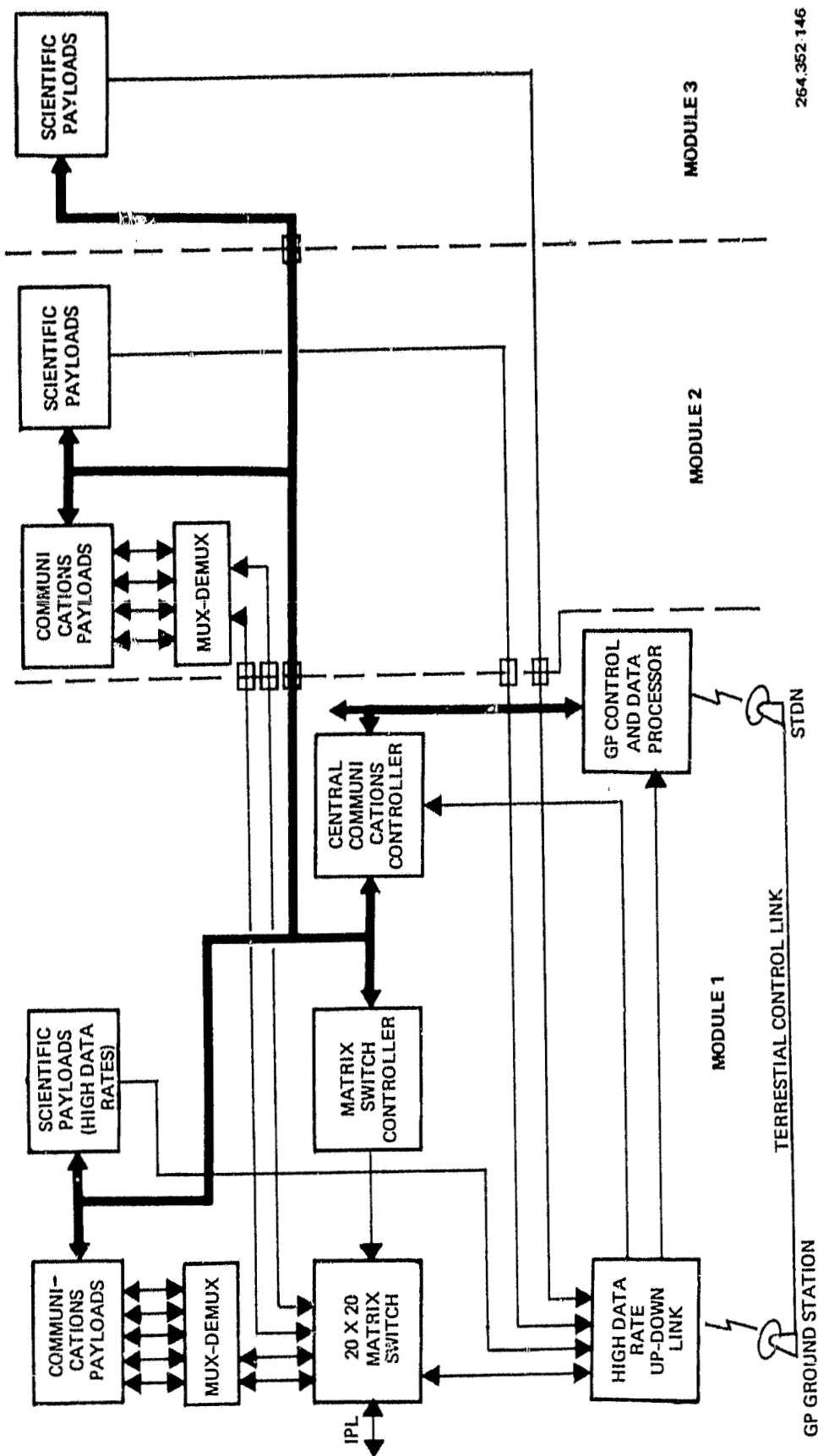


Figure 3-11. Central Communications Control (Alternative #4)

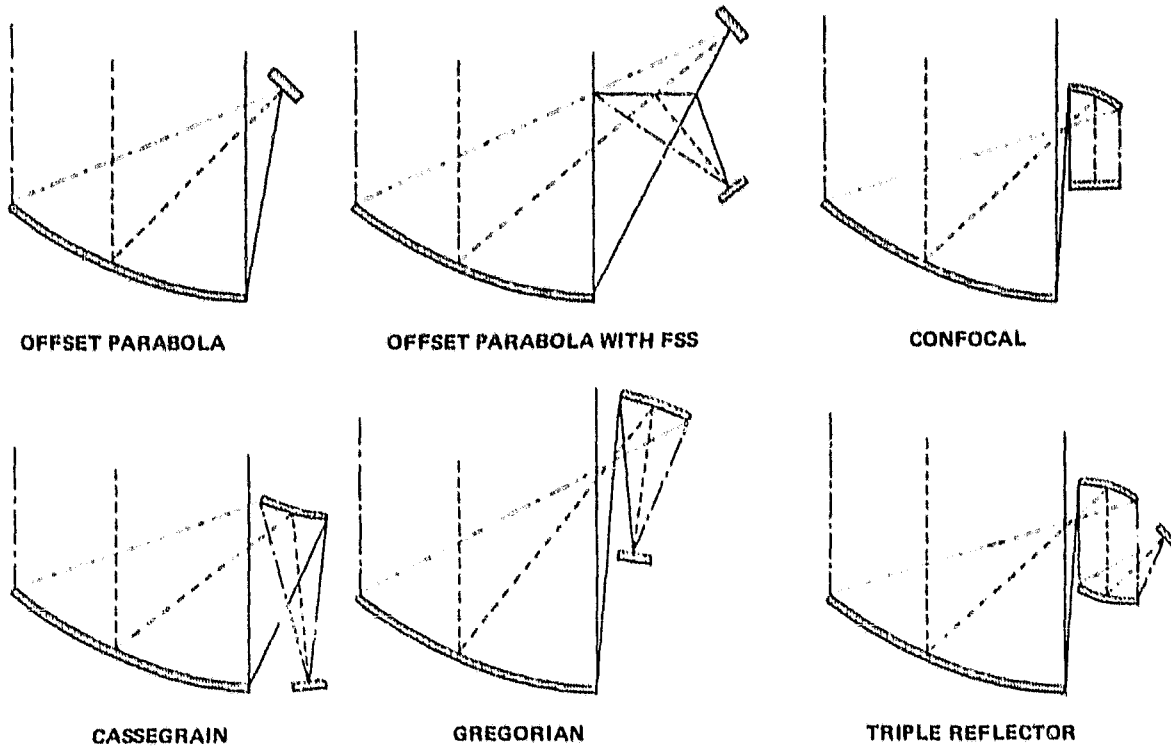
Table 3-10. Estimate of the Number of 40 MHz and 1 GHz Bandwidth Channels Required For Each Communications Payload, Alternative #4

Payload No.	Number of Transponders	Estimated Interpayload Transponders 10%	Equivalent 1 GHz Channels
1.1	1000	100	4
1.2	1000	100	4
2.1	400	40	2
2.2	200	20	1
3	75	7.5	1
4	4	0.4	1
5	16	1.6	1
6	12	1.2	1
7	4	0.4	1
9	100	10	1
11	2	0.2	1
12	4	0.4	1
Total channels required in switch:			19

Figure 3-12 shows six offset reflector antennas. Each antenna has MBFR.

ability by incorporating multiple displaced feed elements near the antenna focal point. The lens antenna and phased array have greater scan angle capability than the reflector antennas.

**3.1.4.1 Antennas Selected.** Tables 3-11 and 3-12 show the communications related payloads for the nominal and high traffic model GEO platforms. These are the same as Tables 3-3 and 3-9 reproduced at this point for convenience. Each entry in the tables represents a single antenna and many of the characteristics of the selected antenna. All of the antennas shown in the tables are offset paraboloids. Some have planar frequency selective surfaces (FSS) to combine transmit and receive functions on a single reflector. The remaining antennas have feed assemblies that combine the solid state amplifiers, receivers, beam forming network (BFN), ortho mode junctions, polarizers if required, and feed horn into a single transmit/receive assembly. The single most difficult problem identified in the antenna design has been the large dimensions of the feed assembly and the packaging of these assemblies for placement at LEO.



264,352-147

Figure 3-12. Pictorial of Six Offset Reflector Antennas

The offset paraboloid has the smallest feed assembly of the reflector antennas that are capable of scanning the required angular distance. Using the offset paraboloid and combined receive-transmit feeds, therefore, results in minimum sized feeds. The feed designs are discussed further in Section 3.1.4.7. The reflectors used in the selections have either parabolic or dual focus contours.

**3.1.4.2 Antenna Reflector Packaging.** Large reflectors and their packaging for transport have been extensively studied. Three types of reflector deployment mechanisms have been used on the geostationary platform: General Dynamics PETA; Lockheed wrap rib; and TRW sunflower.

Figure 3-13 shows these antennas in a deployed and partially deployed state. Both solid and mesh surfaces have been used on the PETA and wrap rib reflectors. Only graphite epoxy surfaces have been used on the sunflower reflector. The sunflower antenna has the best tolerance specifications and therefore it is used at the higher frequency communications bands. Table 3-13 shows the packaged dimensions of the reflectors used on the platforms. The wrap rib antenna shows the highest ratio between deployed and packaged dimensions for the larger antenna sizes. However, the expandable truss PETA antenna has a higher ratio for the smaller antennas. The packaged dimensions of both the wrap rib and, to a lesser extent, the PETA antennas, increase with increasing frequency. This is caused by the requirement to control the reflective surface at more

Table 3-11. Communication Payload Definitions, Western Hemisphere, Nominal Traffic Model, Alternative #1

P/L No.	Payload Description	Band	Frequency (GHz)		Beams		Antennas			Power (watts)			Mass (kg)			Geographic Coverage*		
			Up	Down	No.	Beam- width (deg)	Pointing Accuracy (deg)	Aperature (m)	Focal Length (m)	Dish Size (m)	No. of ponders	Total RF	Total Input	Dish	Feeds	Other		
1.1	Customer Premises Service	Ku	14	11	170	0.35	0.035	6 <sup>1</sup>	10.8	6/5.1	400	800	6,500	43	654	472	1,600 NA	
			14	11	30	0.35	0.035	6 <sup>1</sup>	10.8	6/5.1	400	800	6,500	43	115	472	1,600 CA	
			14	11	60	0.35	0.035	6 <sup>1</sup>	10.8	6/5.1	400	800	6,500	43	230	472	1,600 SA	
1.2	Customer Premises Service	Ka	30	20	170	0.35	0.035	4 <sup>1</sup>	7.2	4/2.7	400	2,500	11,500	16	38/104	566	1,040 NA	
			30	20	30	0.35	0.035	4 <sup>1</sup>	7.2	4/2.7	400	2,500	11,500	16	38/104	566	1,040 CA	
			30	20	60	0.35	0.035	4 <sup>1</sup>	7.2	4/2.7	400	2,500	11,500	16	38/104	566	1,040 SA	
2.1	High Volume Trunking	C	6		65	0.35	0.035	16.9x10	20.0	17	125	125	700	104	257	204	1,145 NA, SA, CA	
					4	65	0.35	0.035	15x25	20.0	25	125	125	700	156	424	204	1,145 NA, SA, CA
2.2	High Volume Trunking	Ka	30	20	21	0.20	0.020	6 <sup>2</sup>	7.2	6	100	1,000	3,200	40	400	460	980 NA	
			30	20	9	0.20	0.020	6 <sup>2</sup>	7.2	6	100	1,000	3,200	40	400	460	980 CA, SA	
			30	20	6	0.20	0.020	6 <sup>2</sup>	7.2	6	100	1,000	3,200	40	400	460	980 SA	
3	TV Distribution	Ku	17	12	61	1.00	0.100	1.5	3.0	1.5	75	750	4,000	13		489	515 NA	
			17	12	61	1.00	0.100	1.5	3.0	1.5	75	750	4,000	13		489	515 SA, CA	
4	Tracking and Data Relay	S/Ku	2.2/15	2.1/14	1	2.0/0.3	0.040	5	1.5	5	1	26/1.5	680	24		309	425 Hemispheric	
			2.2/15	2.1/14	1	2.0/0.3	0.040	5	1.5	5	1	26/1.5	680	24		309	425 Hemispheric	
			15	13	1	0.7/0.8	0.100	2	1.0	2	1	30	680	TBD		309	425 Ground Station	
			2.2	2.1	20	8.00	0.100	(30x30 Array)	2.5x2.5	1	TBD	680	TBD			309	425 Hemispheric	
5	Educational TV (Uses CPS Channel for Uplink)	S	2.5	1	3.50	0.300	2.5	1.5	2.5	16	96	400	71		549	620 CONUS - Pacific Time Zone		
			2.5	1	3.50	0.300	2.5	1.5	2.5	16	96	400	71		549	620 CONUS - Mountain Time Zone		
			2.5	1	3.50	0.300	2.5	1.5	2.5	16	96	400	71		549	620 CONUS - Central Time Zone		
			2.5	1	3.50	0.300	2.5	1.5	2.5	16	96	400	71		549	620 CONUS - Eastern Time Zone		
			2.5	1	5.50	0.500	1.5	0.9	1.5	16	96	400	71		549	620 Mexico, CA		
			2.5	1	5.50	0.500	1.5	0.9	1.5	16	96	400	71		549	620 SA - North		
			2.5	1	5.50	0.500	1.5	0.9	1.5	16	96	400	71		549	620 SA - Central		
			2.5	1	5.50	0.500	1.5	0.9	1.5	16	96	400	71		549	620 SA - South		
6	Direct-to-Home TV	Ku	14	0.7	1	1.00	0.100	1.5	0.9	1.5	8	800	2,100	52	463	515 Ground Station		
		UHF	14	0.7	6	3x4	0.300	10	6.0	10	8	800	2,100	52	463	515 Hemispheric		
7	Air Mobile	L	1.6	1.5	1	Shaped	0.500	(12 Helix Array)	1x1	2	200	1,200	65		195	260 Hemispheric		
		C	6	5	1	18.00	0.500	(Horn)	1x1	2	20	1,200	65		195	260 Hemispheric		
9	Land Mobile	UHF	0.9	0.8	21	1.5	0.100	20	15.0	20	100	1,000	4,000	340	344	680 CONUS, Alaska, Hawaii, Virgin Islands		
11	Interplatform Link	K/Q	32	25	2	0.3	0.030	2.4	1.0	2.4	2	130	303	67	63	130 To other platforms		
12	Data Collection	UHF	0.4	0.4	4	5.0	0.100	10	5.0	10	4	4	100	35	95	130 Hemispheric		

\*NA = North America; SA = South America; CA = Central America

= Feeds included in antenna mass

<sup>1</sup>Circular/parabolic reflector; FSS subreflector

<sup>2</sup>Offset/Cassegrain

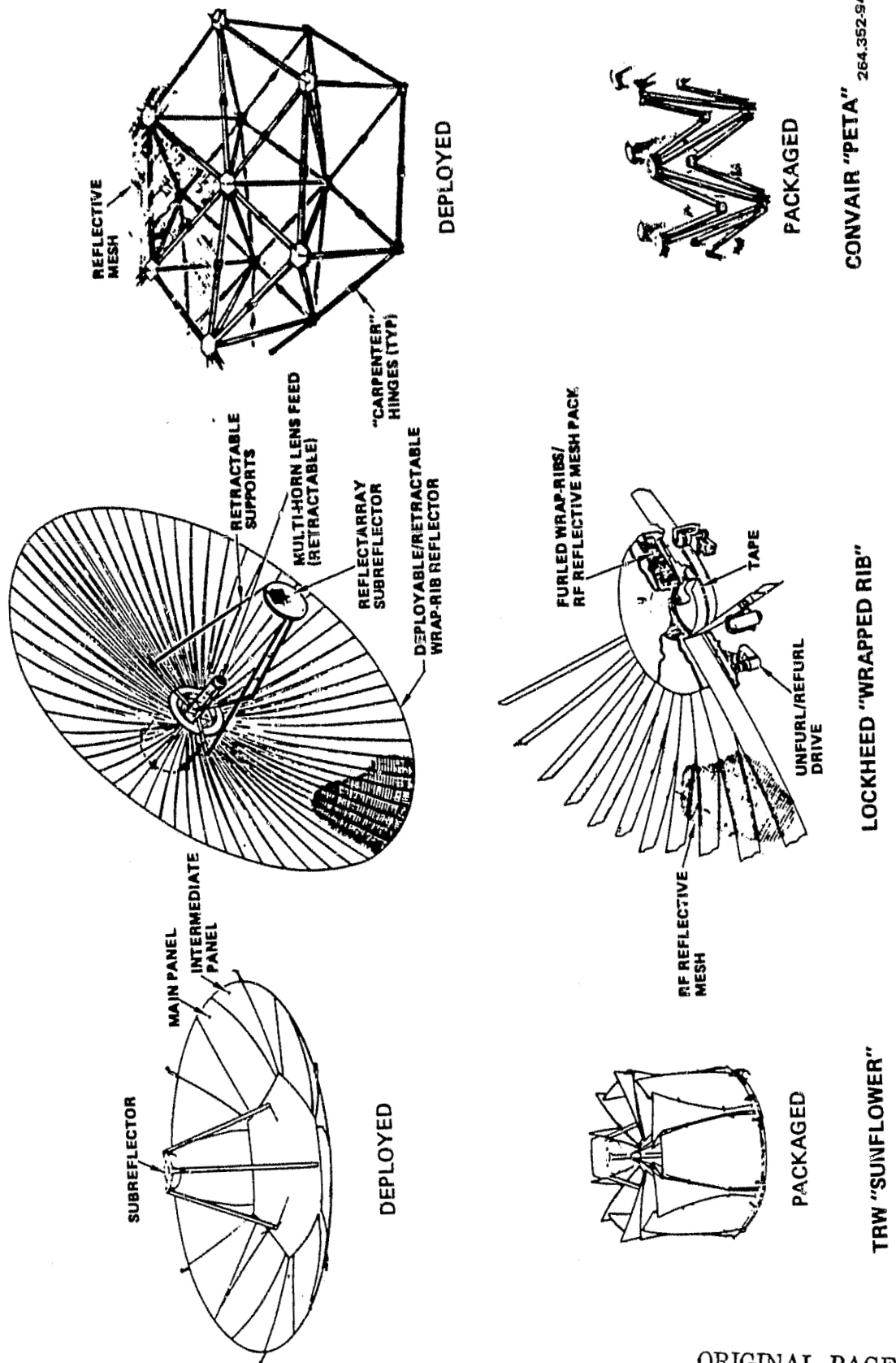
Table 3-12. Alternative #4, Communications Payloads Definitions (Western Hemisphere, High Traffic Model)

P/L No.	Payload Description	Band	Antennas						Power						Mass					
			Frequency (GHz)	Beam- width (deg)	Pointing Accuracy (deg)	Aperature Size (m)	Focal Length (m)	No. of Ponders	Dish Size (m)	No. of Trans- ponders	Total RF	Total Input	Dish	Feeds	Other	P/I	Total	Geographic Coverage*		
1.1	Customer Premises Service	Ku	1.4	12	2.270 <sup>1</sup>	0.10	0.05	20/16.7	36.8	23.0	1,000	1,000	13,000	140	1,311	1,064	5,732	Western NA		
			1.4	12	2.270 <sup>1</sup>	0.10	0.01	20/16.7	36.8	20.0	1,000	1,000	13,000	140	1,911	1,064	5,732	Eastern NA		
			1.4	12	430 <sup>1</sup>	2.30	0.03	6/5	10.3	6.0	1,000	1,000	13,000	60	223	1,064	5,732	SA		
			1.4	12	430 <sup>1</sup>	3.30	0.03	6/5	10.8	6.0	1,000	1,000	13,000	60	223	1,064	5,732	CA		
1.2	Customer Premises	Ka	30	20	2,000 <sup>1</sup>	0.10	0.05 <sup>+</sup>	13/6.7	18.4	10.0	1,000	1,000	23,000	100	650	1,364	2,996	Western NA		
			30	20	2,000 <sup>1</sup>	0.10	0.01	16/6.7	18.4	10.0	1,000	1,000	26,000	100	690	1,684	2,996	Eastern NA		
			30	20	430 <sup>1</sup>	9.39	0.03	4/2.7	7.0	4.0	1,000	1,000	28,000	70	106	1,064	2,996	SA		
			30	20	430 <sup>1</sup>	0.30	0.03	4/2.7	7.0	4.0	1,000	1,000	28,000	70	106	1,064	2,996	CA		
2.1	High Volume Trunking	C	6	4	62	0.09	0.02	60/40	90.0	60.0	62	25	1,200	500	1,197	709	2,797	CONUS and S. Canada		
			6	4	43	0.35	0.07	(15x25) <sup>1</sup>	20.0	25.0	43	25	1,260	121	270	709	2,797	SA and CA		
2.2	High Volume Trunking	Ka	36	20	30	0.10	0.05	10/6.7	18.4	10.0	100	100	400	100	3,000	100	223	161	1,205	Western NA
			30	20	60	0.10	C.02	19/6.7	18.4	10.0	100	100	400	100	3,000	100	223	161	1,205	Eastern NA
			30	20	5	0.20	0.04	6/4	15.0	6.0	100	100	400	100	3,000	75	124	161	1,205	SA
3	TV Distribution		17	12	61	1.00	6.10	1.5	3.0	1.5	75	750	4,000	13	+	489	515	NA and CA		
3-1	Tracking & Data Relay	S/Ku	2.2/15	2.1/14	1	2.0/6.3	0.04	5	1.5	5.0	1	26/1.5	680	24	+	309	425	Hemispheric		
3-2			2.2/15	2.1/14	1	2.5/0.3	0.04	5	1.5	5.0	1	26/1.5	680	24	+	309	425	Hemispheric		
3-3			15	13	1	0.7/0.8	0.10	2	1.0	2.0	1	30	680	TBD	+	309	425	Ground Station		
			2.2	2.1	20	8	0.10	(30x30 Array)	2.5x	2.5	1	TBD	680	TBD	+	309	425	Hemispheric		
5	Educational TV (Uses GPS Channel for Uplink)	S	2.5	1	3.50	0.30	2.5	1.5	2.5	1.5	15	96	400	71	+	549	620	CONUS Pacific Time Zone		
			2.5	1	3.50	0.30	2.5	1.5	2.5	1.5	16	96	400	71	+	549	620	CONUS Mountain Time Zone		
			2.5	1	3.50	0.30	2.5	1.5	2.5	1.5	16	96	400	71	+	549	620	CONUS Central Time Zone		
			2.5	1	5.59	0.50	1.5	0.9	1.5	16	96	400	71	+	549	620	CONUS Eastern Time Zone			
			2.5	1	5.50	0.50	1.5	0.9	1.5	16	96	400	71	+	549	620	Mexico and CA			
			2.5	1	5.50	0.50	1.5	0.9	1.5	16	96	400	71	+	549	620	SA - North			
			2.5	1	5.50	0.50	1.5	0.9	1.5	16	96	400	71	+	549	620	SA - Central			
			2.5	1	5.50	0.50	1.5	0.9	1.5	16	96	400	71	+	549	620	SA - South			
6	Direct-to-Home TV	Ku	14	14	1.60	0.10	1.5	0.9	1.5	12	1,200	2,500	52	+	593	645	Ground Station			
			UHF	14	6	3x4	0.30	10	6.0	10.0	12	1,200	2,500	52	+	593	645	Hemispheric		
7	Air Mobile	L	1.6	1.5	1	Shaped	0.50	(12 Helix Array)	1x1	2	200	1,230	65	+	195	260	Hemispheric-Aircraft Control Centers			
		C	6	5	1	18.60	0.50	(Horn)	1x1	2	20	1,200	65	+	195	260	Hemispheric-Control Centers			
9	Land Mobile	UHF	0.9	0.8	21	1.50	0.10	20	15.0	23.0	100	1,000	4,000	340	+	344	684 CONUS, Alaska, Hawaii, Virgin Islands			
11	Interplatform Link EHF		25	2	0.30	0.03	2.4	1.0	2.4	2	130	300	67	+	63	130 To Other Platforms				
12	Data Collection	UHF	1.4	0.4	4	5.00	0.10	10.0	5.9	10.0	4	4	100	35	+	95	130 Hemispheric			

\*NA = North America, SA = South America; CA = Central America

+ = Feeds included in antenna mass

Max number of beams capability



ORIGINAL PAGE IS  
OF POOR QUALITY

Figure 3-13. Antenna Reflector Deployment Concepts

264.352-94

Table 3-13. Packaged Antenna Reflector Dimensions

Antenna Diameter Deployed (m)	Frequency (GHz)	Lockheed "Wrap Rib"			GD Expandable Truss Thickness (m)	Diameter (m)	Thickness (m)	Diameter (m)
		Thickness (m)	Diameter (m)	Thickness (m)				
60.0	6/4	0.76	4.00	5.88	8.96	—	—	—
25.0	6/4	0.33	1.63	2.45	3.73	—	—	—
20.0	14/11	0.35	2.44	1.96	2.99	—	—	—
16.7	6/4	0.33	1.27	1.64	2.49	—	—	—
10.0	30/20	—	—	0.98	1.49	3.70	3.60	—
3-35	6.0	0.25	0.66	0.59	0.90	2.20	2.10	2.10
6.0	14/11	0.25	1.37	0.59	0.90	2.20	2.10	2.10
6.0	30/20	—	—	0.59	0.90	2.20	2.10	2.10
4.0	14/11	0.20	1.01	0.39	0.58	1.56	1.70	—
4.0	30/20	—	—	0.39	0.58	1.56	1.70	—
2.4	32/25	—	—	—	—	0.86	1.14	—

closely spaced points. The wrap rib requires more ribs to accomplish surface control at higher frequencies. The PETA has an increased number of wire interconnects. The sunflower antenna has a poor packaging ratio and is heavy. The solid surface sunflower antenna is the only type with sufficient surface accuracy to provide necessary antenna gain and sidelobe levels at the higher frequency communications bands. Figure 3-14 shows a graph of packaged dimension versus the deployed diameter of a wrap rib antenna operating at the 6/4 GHz communications band.

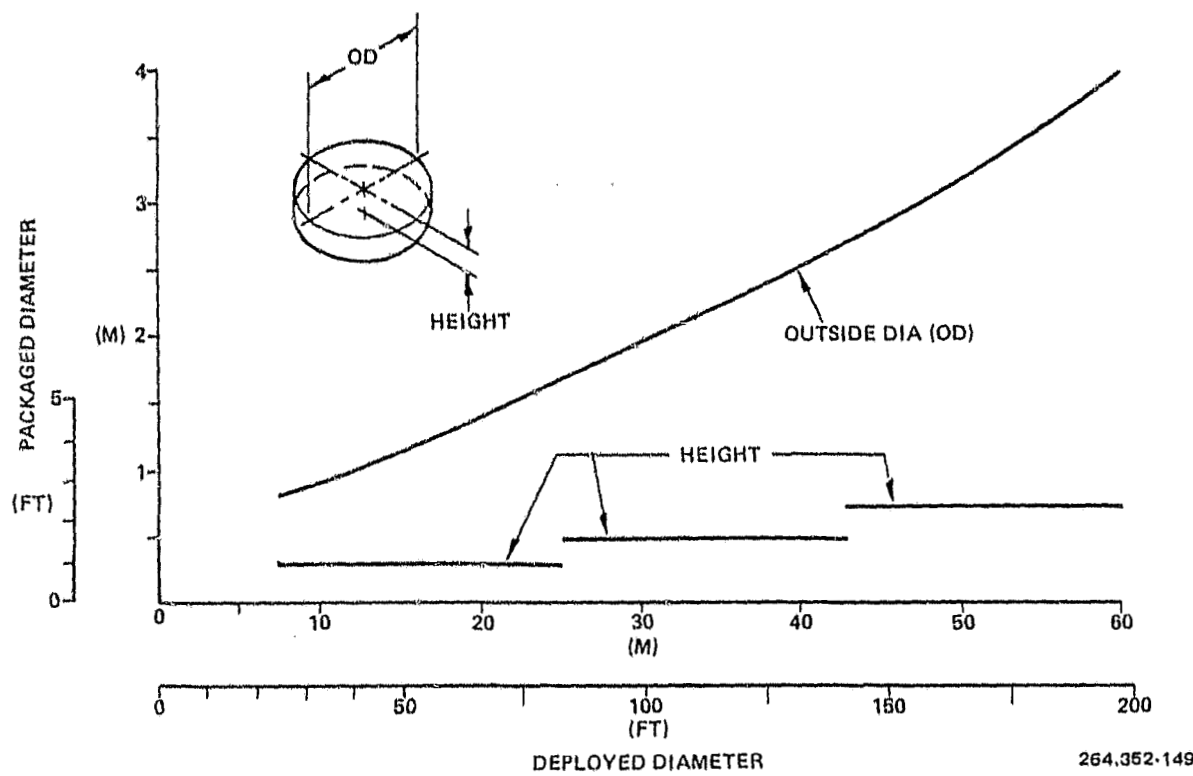


Figure 3-14. Packaged Height and Diameter Versus Deployed Diameter of Wrap-Rib Antenna (6/4 GHz)

**3.1.4.3 Antenna Selection Criteria.** The antenna selection for each payload is determined in a trade study of antenna capability versus system parameters. Approximate performance ratings of the four major antennas types are given in Table 3-14 for six of the antenna requirements that have proved to be selection drivers. The scan angle capability is a critical requirement since frequency reuse of each antenna is determined by the resulting antenna coverage. Phased array antennas have very good scan capability without major impact on the reuse factor since multibeam capability is limited. The lens antenna also has good scan capability and its multibeam capability is determined by a separate feed assembly, as are the reflector antennas. The lens is highly complex with element numbers equal to those of the phased array antenna. The scan capability of the offset parabola and offset Cassegrain are fundamentally different.

Table 3-14. Antenna Type Trade Study Parameters

Antenna Type	Approximate Scan Angle Capability		Approximate Focal Lengths			
	Scan Performance	Antenna Complexity	Feed Complexity	Feed Size		
Offset Parabolas	15 Beamwidths	Poor to Medium	Long	Low	High	Medium
Offset Cassegrain	5 to 6 Degrees	Medium	Medium	Medium	High	Large
Phased Array	80 Degrees	Very Good	Flat Surface	Very High	None Required	None Required
Lens Antenna	>20 Beamwidths	Good	Long	High	Medium	Medium

The maximum scan angle of the offset Cassegrain is approximately six degrees, while the parabola has a limitation based on the antenna beamwidth. For narrow beams, the offset Cassegrain has a clear advantage in terms of scan angle. In most payload antenna systems, the coverage requirements are not met by a single antenna.

Traffic models determine the antenna coverage. Figure 3-15 shows an example of a payload coverage requirement. Approximately 600 beams cover the populated regions of the Western Hemisphere. The total coverage scan angle is approximately 17 degrees. The CPS example has a triangular grid spacing allowing use of the three frequency adjacent beam separation. The frequency reuse of an antenna system providing the above example coverage is about 200.

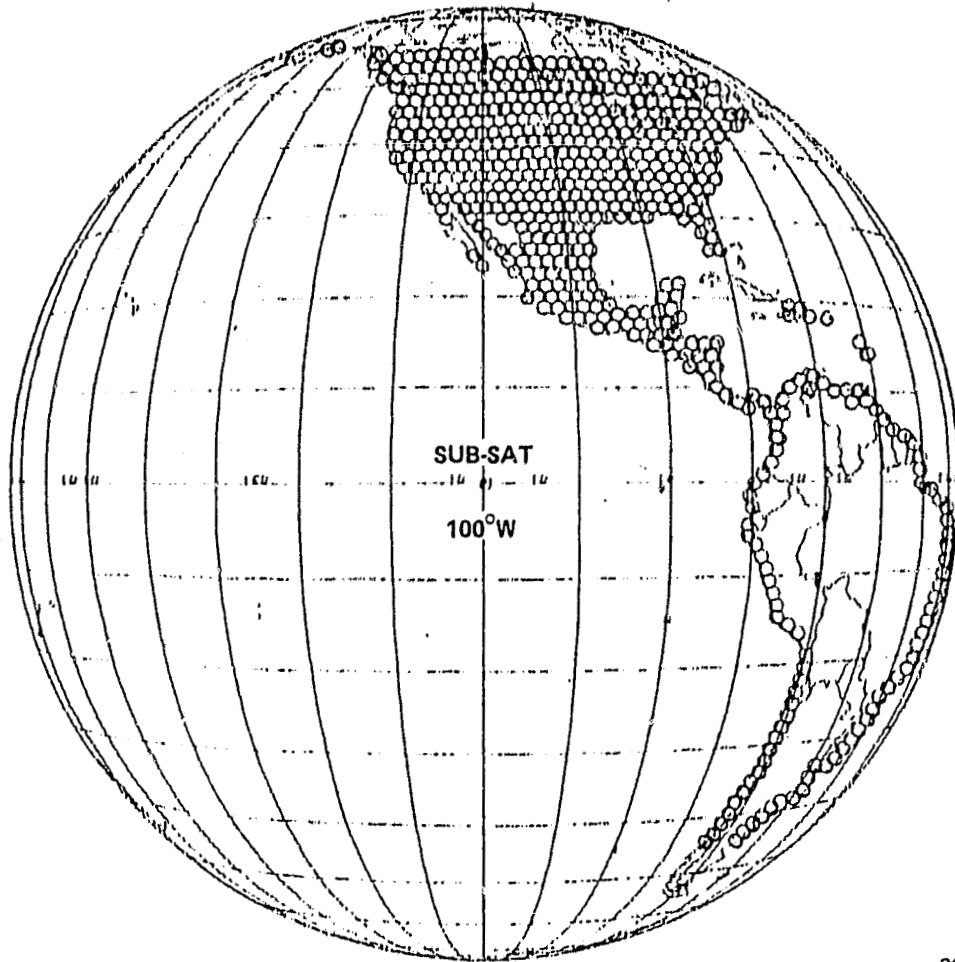


Figure 3-15. Antenna Coverage Example for the Western Hemisphere (CPS)

ORIGINAL PAGE IS  
OF POOR QUALITY

The beamwidth in the example coverage model is 0.25 degrees; therefore, separation between beams operating at the same frequency would be 0.5 degrees. Tailored feed excitation and phasing provide sidelobe levels below about 30 dB at the two beamwidth separation. The C/I for a single interfering beam is 30 dB without cross polarized beams and approximately 28 dB with cross polarized beams excited. Adding the interference contribution of all six close-in beams, the C/I is 20 dB. The C/I value is the incoherent addition of the interfering sidelobes.

3.1.4.4 Selection Process. The number of antennas needed for the coverage is first determined for each payload. The scan characteristics of the candidate antennas provide individual antenna coverages. The number of antennas is minimized for many coverage diagrams when the individual antenna coverages are asymmetrical. Two antenna techniques have been evaluated to provide elliptical shaped coverages. The first is an asymmetrical reflector with parabolic curvature in one direction and spherical in the other direction. The radius of curvature of the spherical surface is nominally twice the focal length of the parabolic surface. With the introduction of added feed complexity to correct sidelobes introduced by the spherical surface, the scan capability can be increased. A second method of providing an asymmetrical scan coverage is provided by dual focus reflectors. The reflector dimensions are increased to offset decreases in reflector efficiency. The resulting antenna has significantly improved scan capability.

The number of reflectors are decreased by using the reflector for both transmission and reception within a common payload. Two ways of doing this have been shown in the platforms: by using frequency selective subreflectors and by combining transmit and receive functions in a common broadband feed assembly. Figure 3-16 shows such an antenna. Some authorities believe that frequency selective subreflectors will not be available in the required time period, and that emphasis should be on broadband feed assemblies. All agree that considerable development is needed.

The 20 GHz feed looks into and reflects from the subreflector to form a Cassegrain antenna. The full main reflector is illuminated by the 20 GHz feed system. The 30 GHz feed looks through the subreflector in a standard offset paraboloid. Only a part of the main reflector is illuminated by the 30 GHz feed. The reflector outside of the 30 GHz region is also dichroic to transmit the 30 GHz spillover and therefore prevent sidelobe level buildup. The combined transmit and receive feed assembly requires a greater amount of additional work than the FSS approach does - e.g., broadbanding of the feed assembly components and introduction of elaborate BFNs and receiver/transmit modules.

The next phase is the determination of the focal length and feed size to obtain the required scan angle from the antenna mechanical boresight. Feed complexity is traded off for reduced focal length. As the focal length is decreased, more elements are required to reduce sidelobe levels in each beam. The feed

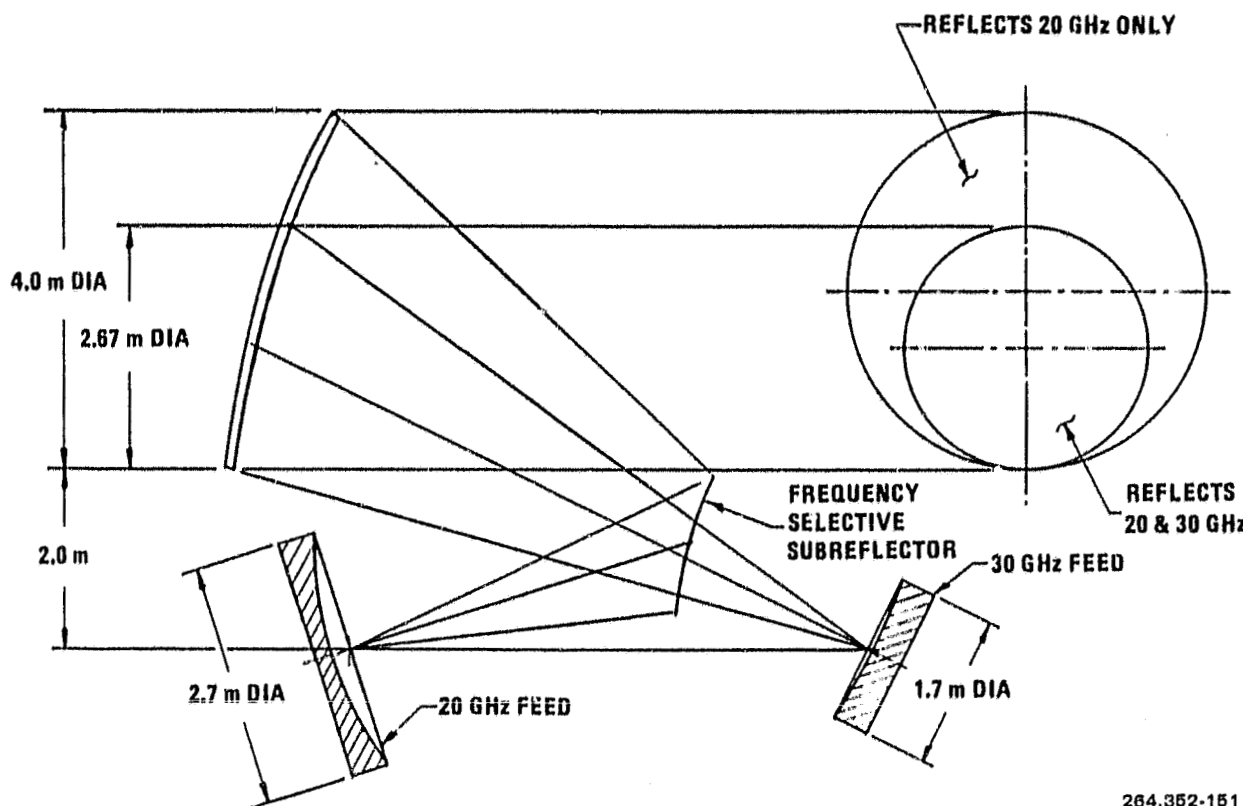


Figure 3-16. Dual Feed Antenna System

dimensions are controlled by the beam deviation factor shown in Figure 3-17. The feed displacement angle is larger than the beam scan angle by the reciprocal of the factor.

**3.1.4.5 MBFRA Feed Assemblies.** The feed assemblies described in the previous sections are large, very complex (particularly for the combined feeds), and heavy. Most of the electronics associated with the payloads have been combined with the feed assemblies to reduce RF transmission lines to tens of centimeters instead of many meters. Methods of deploying the large number of RF transmission lines required for each beam include fiber optics type of data transfer systems which provide the large data rates, deployability, and light weight required for interconnects to the baseband processors and large switches that are located in the central core structures.

The size of the feed assemblies for the GEO platform has been minimized during this study based on Shuttle Orbiter capability. More efficient antenna systems could be made but would have larger feed assemblies. Thus one of the greatest feed problems for the 1990s timeframe will be their dimensions. The actual feed assemblies will require significant deployment or space assembly capability. The present minimized dimension feeds have limited deployment capability. Figure 3-18 is a drawing of the HVT C-band antenna feed for the nominal traffic

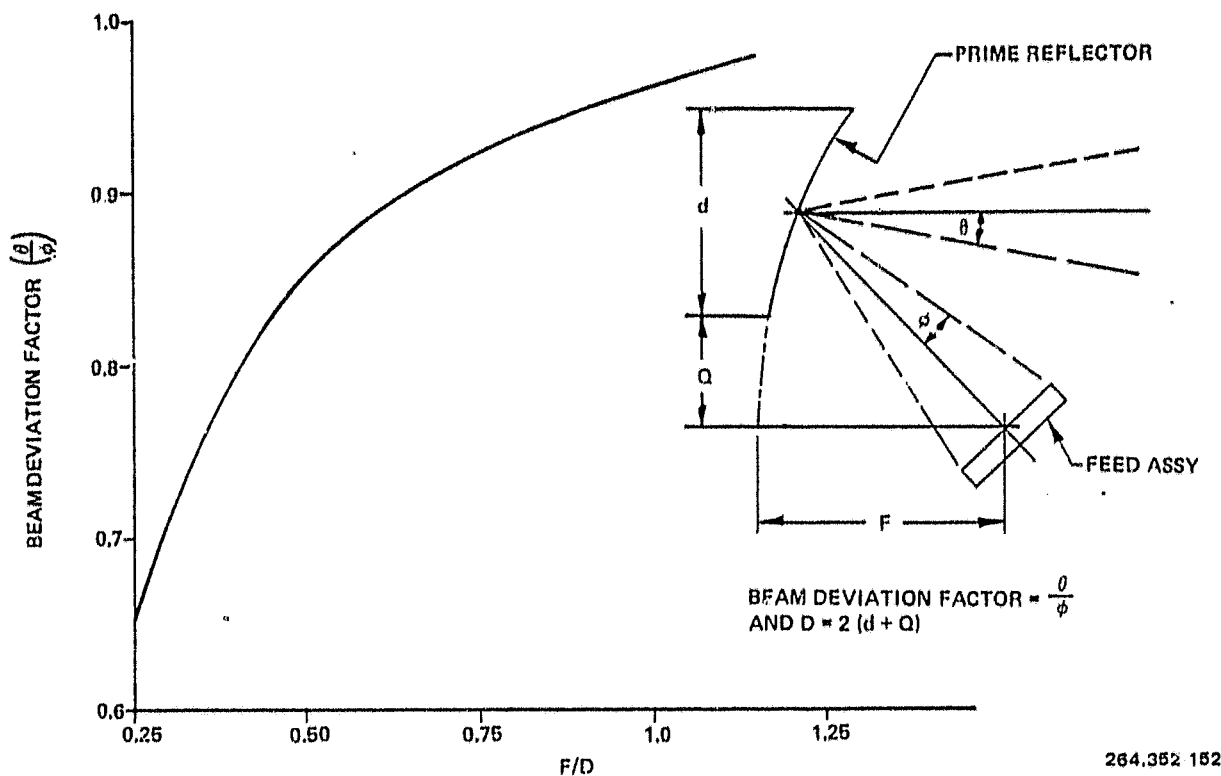


Figure 3-17. The Feed Dimensions of Offset Parabola Are Influenced by the Beam Deviation Factor

model. The circles in the framework represent individual feed elements. For placement within the Shuttle, the assembly is hinged in the center and a small section near the bottom is rotated to lie against the remaining elements (see also Figure FO-1). The HVT feed for the high traffic model is broken into four circular sections, each one filling the available diameter of the Shuttle (see Figure FO-3). Dual shaped reflector antenna systems having very good scan capability have feed sizes several times larger than these. The scan capability of the shaped dual reflector is well known and nearly beamwidth independent. Therefore the antenna is a very likely candidate for the GEO platform for large reflector/high frequency systems.

The feed assemblies will be highly complex structures combining the feed elements and beam forming networks as a minimum, and probably incorporating receiver and power amplifier components to reduce RF transmission line requirements. The transmission lines are very difficult to deploy and are massive when a very large number of beams is anticipated. When transmit/receive components are placed on the assemblies, heat radiators will be required for temperature stabilization. Figure 3-19 shows a drawing of an individual transmit feed element assembly for the HVT C-band application. A receive feed element assembly is similar except that the transmit module is replaced by a receive module behind the BFN. All the components are aligned with the horn except

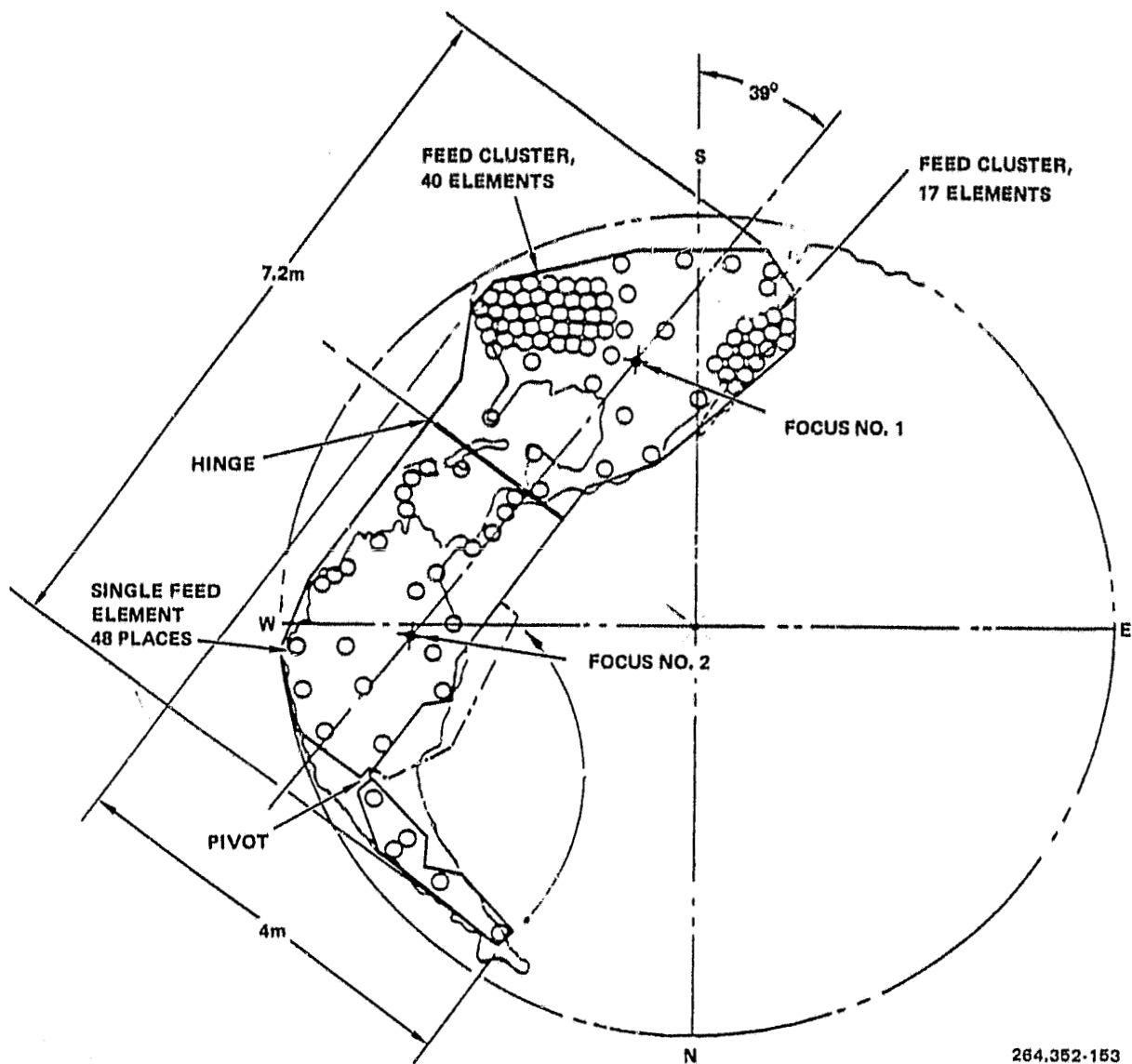
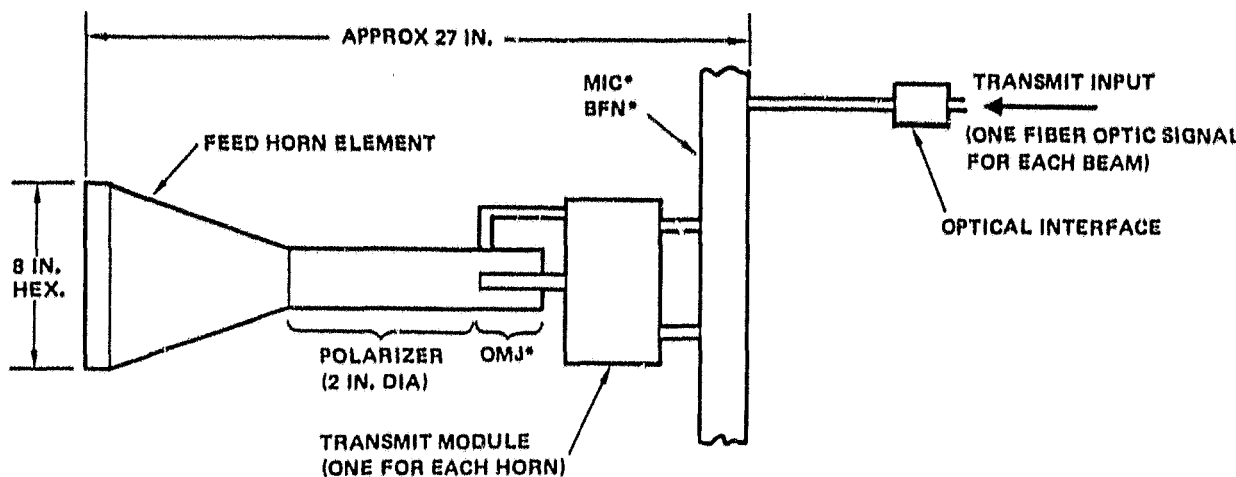


Figure 3-18. C-Band HVT Antenna Feed Assembly Showing the Hinge and Pivot Used to Deploy (View of Feed From Back)

the beam forming network. Each transmit module, including a power amplifier, is connected to a particular feed horn element. The BFN interconnects transmit inputs with those feed horn elements associated with a specific beam.

The BFN also makes interconnection between the receive module and those feed horn elements required for a specific beam. In the general case, the BFN provides reconfigurability by including variable phase shifters and variable power dividers in the corporate feed stripline assembly. Generally, also, the transmit and receive inputs will be connected to a common feed horn, or a common set of seven clustered (triangular lattice) feed horns, through the BFN. Feed assemblies with the complexity described are on the drawing boards or are



\*OMJ = ORTHO-MODE JUNCTION

MIC = MICROWAVE INTEGRATED CIRCUIT

BFN = BEAM FORMING NETWORK

**NOTE:**

"RECEIVE FEED ELEMENT ASSEMBLY" IS SIMILAR EXCEPT "RECEIVE MODULE" IS BEHIND BFN.

264.352-154

Figure 3-19. Layout of Proposed Transmit Feed Element Assembly for C-Band HVT

being prototyped for narrow band feed systems, and very limited reconfigurability for the lower frequency communicated bands. Considerable work remains to be done to achieve wide band operation of each feed component and a high degree of beam reconfigurability. Reconfigurability is highly desirable in the high reuse narrow beam antenna systems to provide an electronic stabilization capability. Otherwise, mechanical antenna reflector stabilization is necessary to locate the beams with much greater accuracy than can be supplied by platform stabilization. Mechanical stabilization has poor reliability. To provide accurate beam pointing, several ground station beacons will be tracked with a separate receiver set and a modification of the BFN. Four feeds or four clusters of feeds that are centered on the beacons are arranged in a monopulse configuration within the BFN and are utilized to determine precision angular departures caused by errors in stabilization. The angular error information is fed to a beam control computer that controls the beam forming network to correct both uplink and downlink beam pointing angles.

**3.1.5 ELECTRICAL POWER SYSTEM (EPS).** The electrical power system can be divided into four functional categories: power generation, energy storage, power distribution, and power management. The discussion of EPS will first cover these four functional areas, and then the EPS discussion will relate to GP Alternative #1 and GP Alternative #4 applications.

The six platforms for Alternative #1 that are planned are projected to be launched over an eight-year period. The docked platform for Alternative #4 was planned for launch over a four-year period. This may well imply that two different designs will be used for Alternative #1; namely, a design for the first three launches that represents the best proven technology in 1989-1990 time-frame and an updated design using the newer technology available in 1993-1995. This is the approach that was taken here. Two separate designs were considered.

Since these platforms are designed for 16-year missions providing commercial communications service, the key design goal must be high reliability. Consequently, to be attractive to typical communications satellite users, proven technology with a demonstrable 16-year lifetime must be used, particularly in those areas where servicing is not planned.

The approach taken will be to first determine the actual end of life (EOL) solar array power requirement for each launch. Following the initial assumption of two different designs, one for the first three launches and the other for the second three launches, the primary and secondary power system technology applicable to both designs will be reviewed. From there, estimates are made of the possible design characteristics.

3.1.5.1 Power Generation. The presently foreseen acceptable power source for the GP is solar arrays. Other sources, such as nuclear and thermoelectric, are not deemed viable at this time.

Solar Array Requirements. Following the initial assumption that there will probably be two designs and that high reliability is most important, the possible types of solar cells and solar arrays that might be used were first studied. An analysis of the previous development of commercial communications satellites indicates that solar cells and solar arrays chosen for these missions had been developed a minimum of 3-4 years before they were considered in the satellite design (and a minimum of 5-6 years before they were flown on the satellites). For the platform array design, this means that the first platform launched in 1992 will probably be using technology developed no later than 1986-1987. The development of the COMSAT violet solar cell was announced in 1972 and flown first in 1978. The development of the nonreflective cell was announced in 1974 and will not be flown commercially until late 1980.

There are two possible conflicting factors that may affect this time factor. A large amount of funding is presently going to develop solar cells for terrestrial purposes. Some breakthrough there or the development of very large production facilities may lead to the shortening of the development-to-commercial flight use cycle. However, the requirement for twice the lifetime of present satellites would counteract this with the tendency to rely on well proven (often meaning long developed) technology. For these tradeoffs, these two factors were considered along with where the present technology trends seem to be leading.

It was mentioned earlier that because the launches were spread out over eight years, two designs were considered. In their 1979 paper, Slifer-Billerbeck (Reference 1) have shown that following the historical trends in the development of the Intelsat series of satellites, the amount of weight available to the power system has been a very slowly decreasing function with time (see Table 3-15) to about 17.6 percent for Intelsat V and 15.9 percent for TDRSS. In Figure 3-20, this trend was continued out to include the OTV projected for use with the operational platforms. This led to the same number as for TDRSS, namely, 15.9 percent or 1,096 kg of the 6,895 kg of the geostationary orbit (GEO) payload would be available to the power system. Furthermore, Slifer-Billerbeck have shown that about 36 percent of the power system is devoted to the solar array on Intelsat V. For the platform design, this first cut means there would be 395 kg available for the solar array.

Table 3-15. Summary of Intelsat Spacecraft Characteristics

Spacecraft	I	II	III	IV	IV-A	V
S/C Power (W)	40	75	120	400*	500	1,000
S/C Mass (kg)	38.6	86.2	151.5	700	790	1,014
Power Subsystem Mass (kg)	>6.22	>24.8	34.9	137	148	178
Power Subsystem Mass Ratio	>0.161	>0.287	0.230	0.194	0.187	0.176

The first three launches have a raw load power requirement at EOL (the critical design point) of 5606, 8506, and 5986W. However, typical designs include addition of 10 percent for battery charge (nominal for GEO missions), 5 percent for load growth, a 10 percent design contingency (these are commercial missions demanding full power at EOL), and 10 percent for the distribution and conditioning losses. This results in final EOL power requirements of about 7,763, 11,772, and 8,283W, respectively. For the second three launches, the EOL power requirements would be about 3,850, 11,825, and 9,764W. Clearly, the design driver for the first three launches is the need to be able to provide 11.77 kW of array power within the 395 kg envelope. The design driver for the second three launches would be 11.82 kW. This presumes a solar array (including the solar array drive assembly) delivering a power density of about 29.8 W/kg after 16 years at GEO at the operating temperature to deliver the 11.77 kW. Our first design effort goal will be to determine what level of technology is needed to deliver this power density after a 16-year mission and our second will be determine if there are designs available that could improve this EOL power density and thereby save weight.

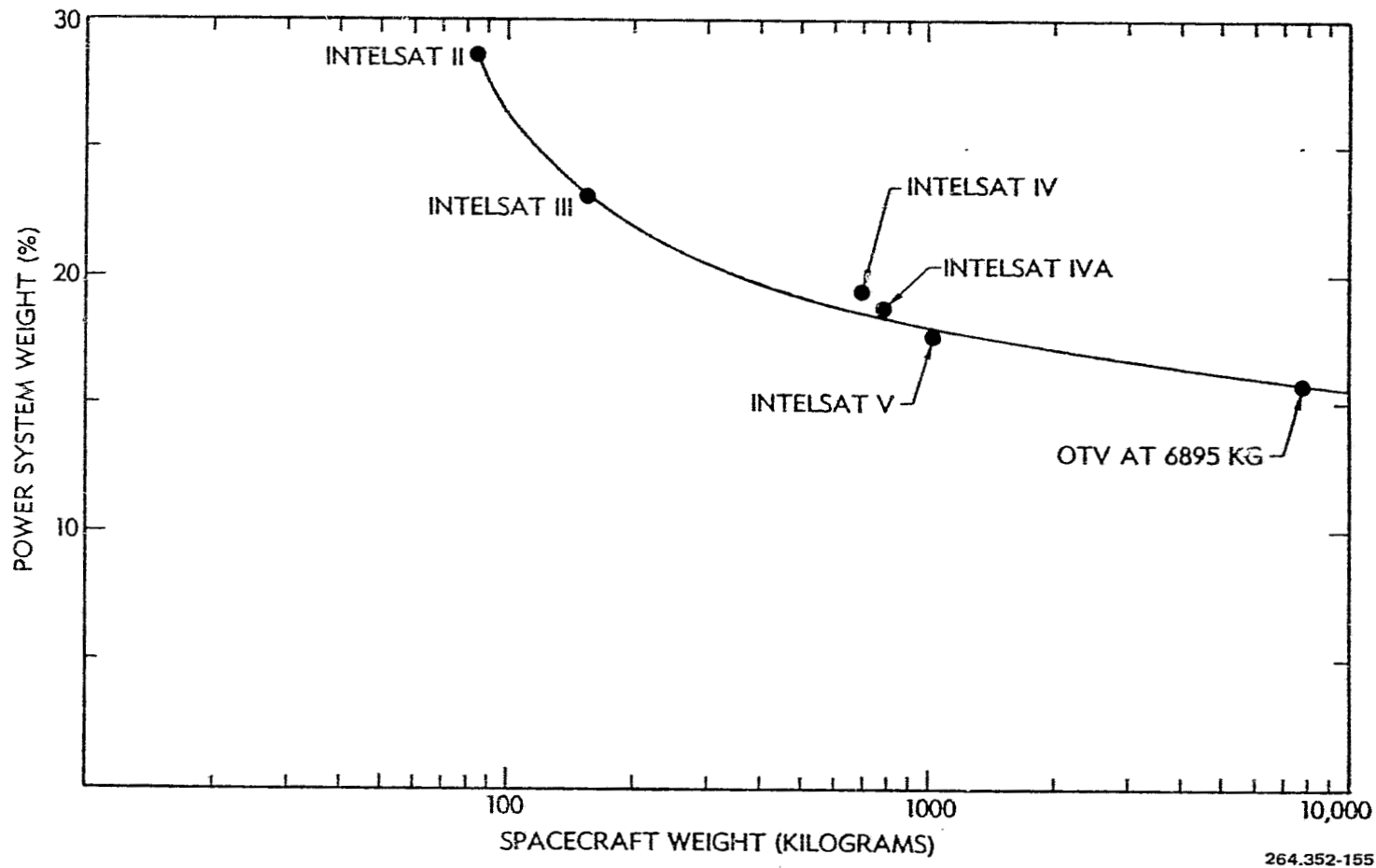


Figure 3-20. Power System Weight as Percent of Spacecraft Weight Versus Spacecraft Weight

Solar Cells. There are only two types of solar cells that can be considered at this time for space use — either silicon solar cells or gallium arsenide solar cells. Silicon solar cells are the only solar cells used at the present time on commercial spacecraft. Gallium aluminum arsenide solar cells have been under development for several years and appear to offer significant future promise.

Silicon Solar Cells. Silicon solar cells are presently available in production with an area of  $1 \text{ cm}^2$  to several  $\text{cm}^2$ , in thicknesses from  $50 \mu\text{m}$  to  $300 \mu\text{m}$  and to efficiencies of over 15 percent. For at least fifteen years, it has been stated that silicon solar cells would soon be superseded by some other type of solar cell or power source. Silicon solar cells are a moving target because they will be the mainstay of the 1980s and perhaps beyond. Recent technology trends have been directed toward decreasing thickness of the devices from the typical  $250\text{-}300 \mu\text{m}$  to  $50\text{-}100 \mu\text{m}$ , while maintaining or improving efficiency and reducing radiation damage. In the short term, the trend will be to develop the capability of handling, welding, and fabricating arrays with the  $50\text{-}100 \mu\text{m}$  2 by 2 cm or larger cells of 12-13 percent efficiency. Implementation of these cells into solar arrays offers 20-30 percent improvements in power density directly. At the same time, work will continue on producing these thin cells at efficiencies up to 15 percent or more so that their power output is comparable with the best of the present day thicker cells.

The very high efficiency silicon solar cells are typically manufactured with etched surfaces on the top of the cell to make the surfaces nonreflective. Unfortunately, this also increases the absorptance (i.e.,  $\alpha > 0.9$ ) of the cells so that they operate at a higher temperature in space. Since silicon solar cells have a negative temperature coefficient for power, this increased temperature can negate some of the efficiency improvement. To counteract that, the rear surface of the cells is treated to make it reflective to the photons not used by the cell so that the unused energy is reflected back out of the cell, thereby reducing the cell temperature. The goal in this effort is to lower the absorptance so that it is comparable to or less than conventional cells (i.e.,  $\alpha > 0.7$ ).

The long-term goal in silicon solar cell research is to produce an 18-percent efficient cell that suffers little radiation degradation. This effort (Reference 2) is underway, but it will be a number of years before it is known whether these devices will be available in time for use on the early platform missions.

Gallium Arsenide Solar Cells. The gallium aluminum arsenide solar cells have been under development for several years. Theoretically, they should offer higher efficiency than silicon cells with less radiation degradation and, in addition, the possibility of radiation annealing. A number of research papers have been published and efficiencies of 16-18 percent have been discussed. To date, however, there are no gallium arsenide solar cells available commercially for use or testing. Small research level quantities are being made and used for laboratory tests. Recent discussions with researchers in this area indicate a goal of 18-percent cells in pilot production in about three years (Reference 3).

Before any credibility can be given to the cells it is essential that at least pilot production quantities at even lower efficiencies be available for testing by the user community.

The whole question of radiation performance and annealing has to be looked at closely. There is hope that the cells will degrade less than silicon cells, however, there are some indications (References 3, 4) that the present cells cross over silicon performance between  $10^{15}$  and  $3 \times 10^{15}$  1 MeV electrons/cm<sup>2</sup>. This corresponds to a typical dose for a 5-10 year mission with 150 micron coverslips. Similarly, the annealing question is still open. It would be a tremendous advantage if the cell damage could be annealed out at 200C or less.

Until these questions and questions of actual cell mass, cost, and availability are resolved, gallium arsenide research should push ahead.

Choice of Solar Cell for the Geostationary Platform. For the first three launches, the focus is on using silicon solar cells. The approach for the second three launches is more speculative, being either a planar or concentrator silicon system or a concentrator gallium arsenide system.

Solar Array Tradeoff. There are three types of lightweight, deployed solar arrays that are potential candidates for these missions, namely, flexible fold-out solar arrays of the solar electric propulsion stage (SEPS) type (Reference 5), the ultra lightweight panel (ULP) (Reference 6), and the rollout solar arrays like the flexible rolled up solar array (FRUSA) (Reference 7), space telescope (Reference 8), and the double rollout array (DORA)(References 9, 10). For the high power required here, rigid honeycomb sandwich panel deployed arrays do not offer the necessary power density and also require too much volume.

SEPS Solar Array. The SEPS solar array (Reference 5) consists of two wings. each approximately 4m wide by 32m long. It is designed to produce 25 kW beginning of life (BOL) using an 8-mil silicon cell, a 6-mil fused silica cover, a 1-mil Kapton substrate, and a 28 gm (1-oz), copper printed circuit interconnect. The array has a BOL specific power of 66 W/kg. This is achieved through the use of graphite-epoxy structures and an aluminum flat conductor cable harness.

The array blanket consists of solar panels connected by piano-hinge joints. During launch, the folded array is compressed between two rigid panels that comprise the array containment box. An even distribution of compression load over the folded blanket is achieved with aluminum honeycomb panels. Each wing is supported by an extendable and retractable lattice structure mast constructed of fiberglass, with an aluminum or graphite-epoxy canister.

The blanket tensioning system consists of negator powered reels from which tensioning cables are unwound. The reels are mounted under the array containment box floor. The negators provide constant tension in the cables

during array deployment. Figures 3-21 through 3-23 show different parts of the SEPS array.

Ultra Lightweight Panel (ULP). The ULP (Reference 6, 10) type solar array was developed by the West German Government for possible use in their direct broadcast satellite program. The final development and qualification of the array was jointly funded by Intelsat and the West German Government. The solar array was designed for use on a three-axis stabilized spacecraft with sun oriented solar arrays in the 1-10 kW power range.

The basic array is semirigid, consisting of a yoke, a blank panel to prevent shadowing by the spacecraft, and the active panels with flexible solar cell blankets. Each of the current 3.8 by 1.15m by 0.0025m-thick panels consists of a rigid carbon fiber boxbeam frame. The solar cell substrate is a flexible Kapton-carbon fiber cross-laminate suspended within the frame. The solar cells are mounted to this blanket.

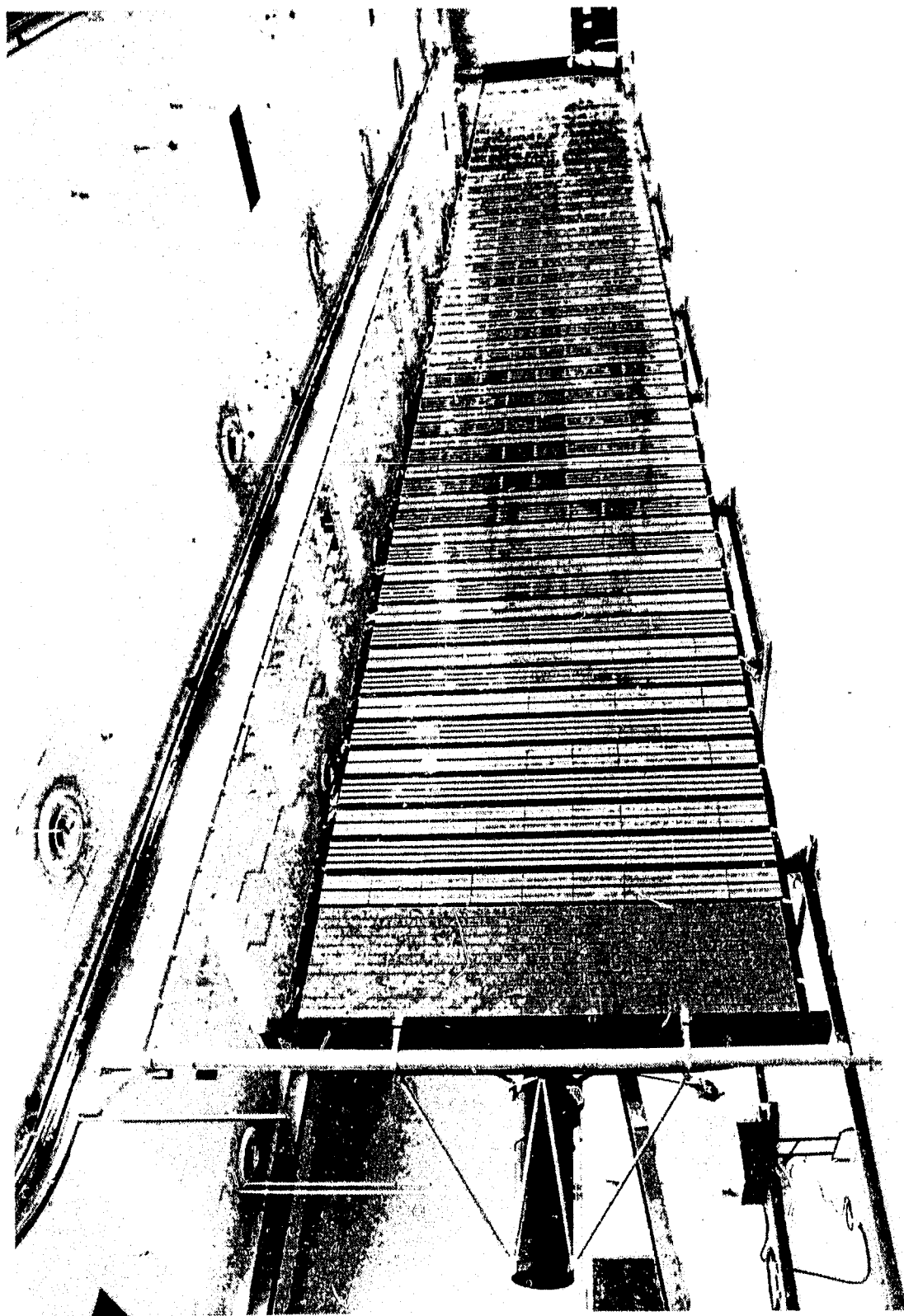
Pretensioned spiral springs at the interconnecting hinges are used for deployment. A closed cable loop controls the panel flatness during deployment. Hinges on each panel are latched to provide rigidity after deployment.

This type of array offers the distinct advantage of providing transfer orbit power directly by having the outboard panel face the sun in the stowed position. It does suffer from some stowage volume problems, particularly at the high power levels.

Rollout Solar Arrays. The flexible rolled-up solar array (FRUSA) (Reference 7) flew successfully in 1971. The flexible rolled-up solar array power system consists of a pair of drum-mounted [5.25m by 1.8m (16 by 5-1/2 ft)] flexible solar cell arrays; an orientation mechanism that maintains the array in a sun-pointing attitude; a power conditioning and storage subsystem that provides regulated AC and DC voltages, controls battery charging, and supplies housekeeping power during eclipse periods; and an instrumentation subsystem to monitor structural, thermal, and electrical performance.

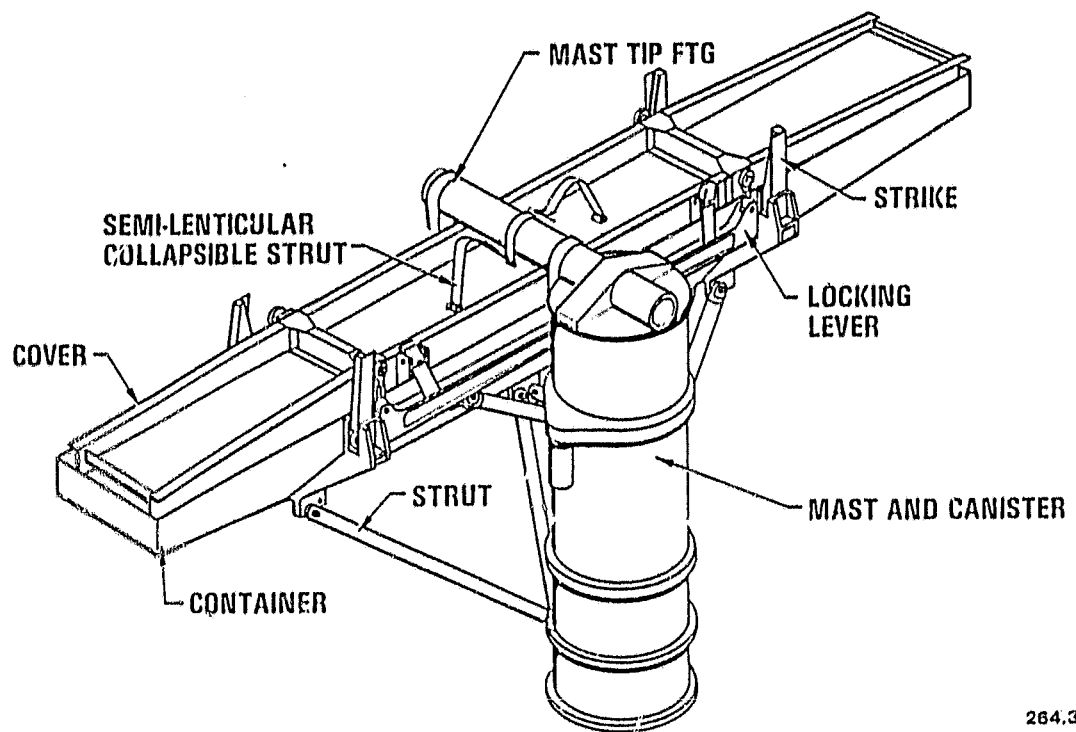
Array power is transferred through flexible flat cables in the drum assembly and through two slip-ring assemblies in the orientation mechanism to the power conditioning unit mounted in the spacecraft. The power conditioning unit provides regulated and unregulated power to the system.

During the last few years, the basic FRUSA array has been used as a base and redesigned to fly as the primary power source for the space telescope (Reference 8), where it will have a BOL capability of 26.9 W/kg. The two-year EOL power density is 20.9 W/kg.



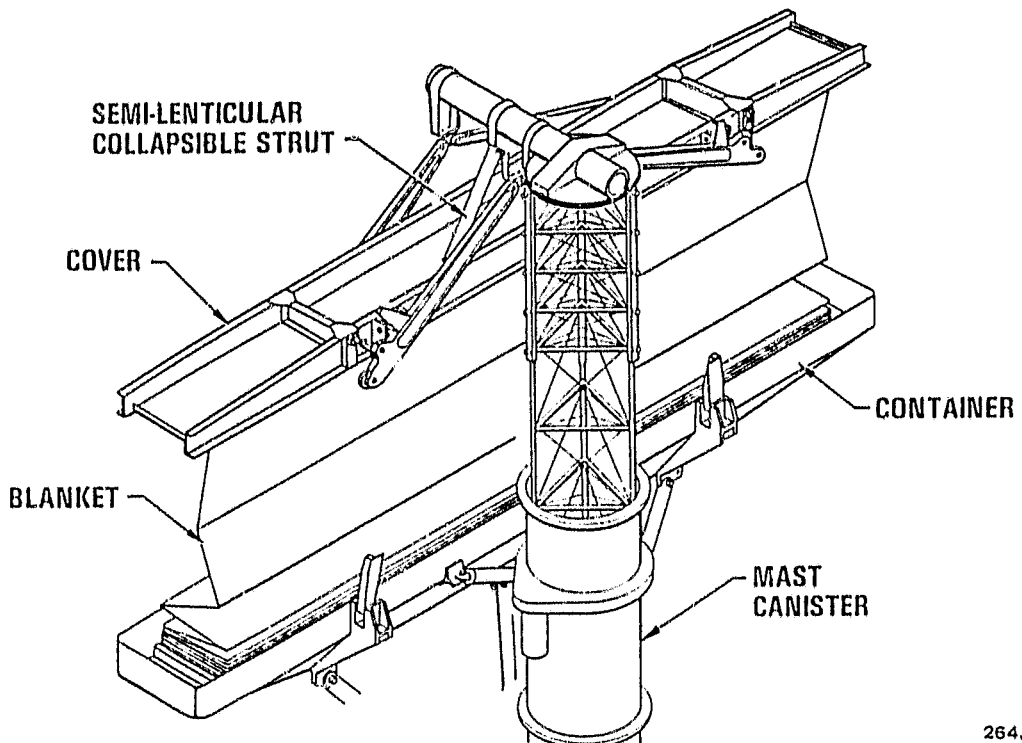
264.352-156

Figure 3-21. SEPS Solar Panel Configuration



264,352-157

Figure 3-22. SEPS Blanket in Stowed Condition



264,352-158

Figure 3-23. SEPS Solar Array Deployment

The double rollout solar array (References 9, 10) (DORA) has been under development for several years. It consists of a flexible blanket coiled up on a stowage drum with cushioning between the blankets to prevent cell breakage. The deployment mechanism is made up of two double spool STEM cassettes at the drum ends for storage of the 4 bi-stems. The tips of the STEM booms are connected by articulated STEM traverses so that the traverse, 2 bi-stems and the storage drum form the support frame for the blanket during and after deployment. The overall system includes a central tube, torque tube, drive motors, multielement tension springs, cushioning stowage drums and wire loops with guides.

Comparison of the Arrays. All three types of arrays can do the job. At the higher levels (Reference 10), the ULP suffers from stowage constraints and less power density than the rollout (and flexible foldout) concepts, but it does provide transfer orbit power. For the higher levels, the choice is between rollout and flexible foldout arrays. There are questions of stowage volume, power density, complexity, and transfer orbit power provision that can be debated for each type of array.

For this study, it was decided to use the flexible, foldout, SEPS-type array as the baseline. Both the space telescope rollout array and DORA array are still under development but the continuing need for more power on the space transportation system (STS) will force the continued development of a SEPS-type array for the power module and the power extension package (PEP). Consequently, there will be a lot of experience with this type of array. The SEPS-type array is then a good candidate, at this time, for the geostationary platform. If the rollout development continues for a GEO application, it should be reexamined at a later date but the rest of the analysis for all six launches is based on using a SEPS array. For the first three, a planar-type array is considered, while for the latter three launches concentrator approaches are examined.

The SEPS Design at GEO - Problems and Potential. The basic SEPS solar array has been designed to provide 25 kW of power at BOL and delivers about 66 W per kg at BOL for the array alone without any yoke, telescoping assembly, or solar array drive assembly (SADA). For the geostationary platform, the interest is in the power and power density at EOL, 16 years.

Since the initial array power required is considerably less than the present SEPS design, estimates were first made for what the array characteristics would be at BOL for lower powers as shown in Figure 3-24 (Reference 11). These were made using the same solar cell, blanket, mast, etc., as used on the original SEPS and assuming a stiffness such that the bending frequency is 0.04 Hz. Furthermore, since the interest is in 16-year life performance, estimates were made of the probable degradation of the solar array characteristics. Figure 3-25 shows a plot of array power at EOL in kilowatts versus power density for a SEPS solar array after 16 years at GEO. The operating temperature of about

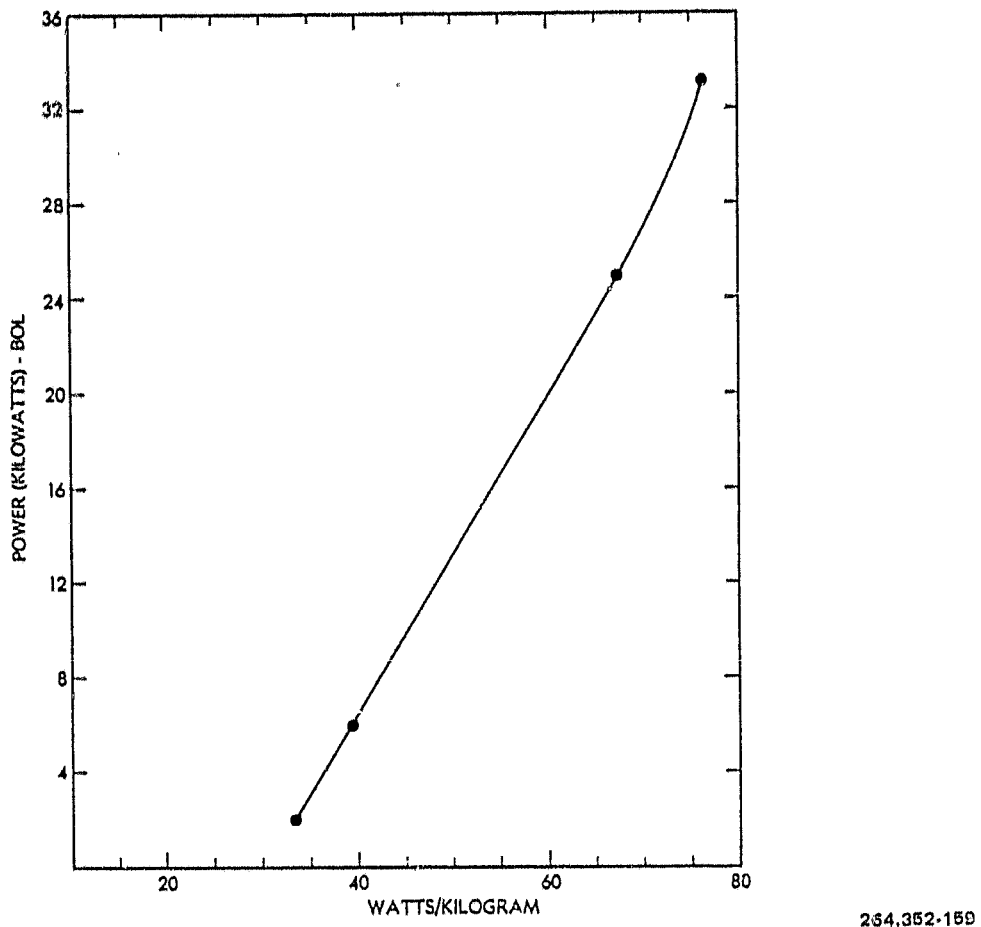


Figure 3-24. Power Versus Power Density (W/kg) for SEPS Array at Beginning-of-Life (BOL)

60C (as in the published SEPS data) was assumed and, as in the basic SEPS design, this power density is optimistic since it does not include the yoke, telescoping mast, and SADA weights. At 10.45 kW this results in a power density of about 34.6 W/kg (EOL), and if estimates of the mass of the yoke and SADA are included, the power density at EOL is about 30 W/kg. These estimates are determined by calculating the effect of 16-year expected particle radiation, ultraviolet, and thermal cycle environment on the solar cells presently used in the SEPS array.

It was mentioned earlier that an initial analysis of the system with the OTV to be used for the platform showed that about 395 kg would be available for the solar array and that this implied a power density requirement of 29.8 W per kg. It appears that a SEPS-type solar array can meet this requirement.

Problems In Using the Current SEPS-Type Array Design at GEO. A major problem in designing solar arrays for spacecraft at GEO is providing transfer orbit power. Typically, the solar arrays are not deployed until GEO is

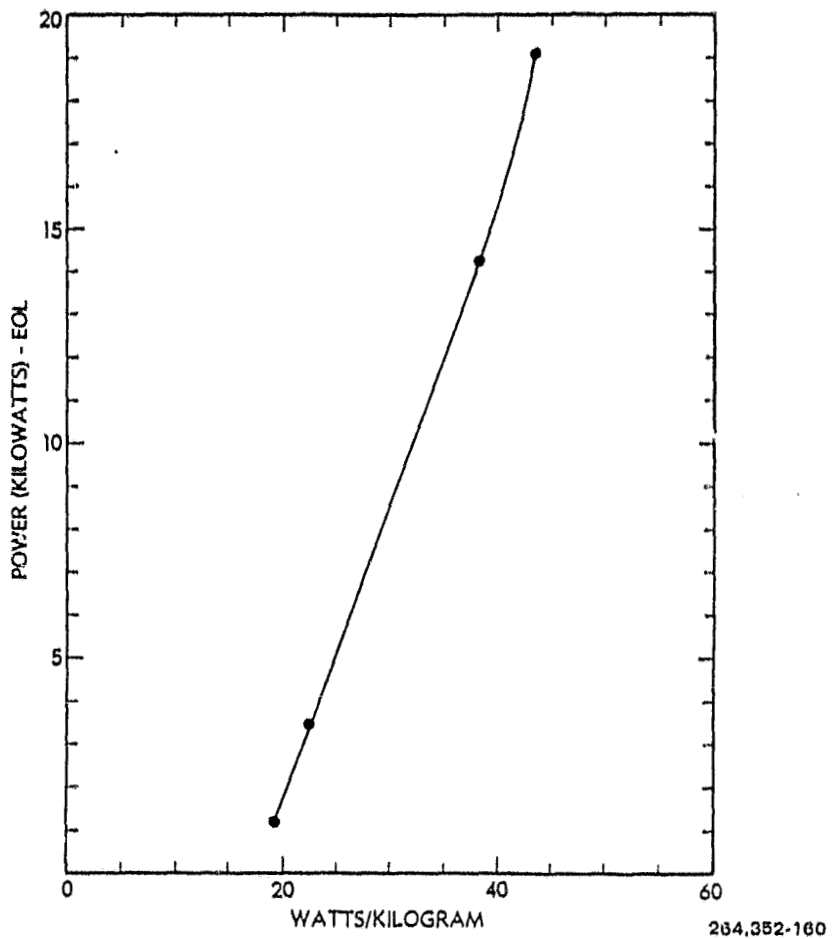


Figure 3-25. Power Versus Power Density (W/kg) for SEPS Array After 16 Years at Geostationary Orbit

achieved and some means for supplying power is required while the spacecraft is being acquired and prepared for apogee motor firing. In rigid, deployed solar arrays, this is accomplished by having the outermost panels of the array face outward in the stowed position.

The typical flexible substrate array is launched with the solar cell blanket completely rolled up or folded up so no power is available during transfer orbit. This is a severe problem for GEO missions. Several solutions are possible. On CTS (Reference 12), two rigid panels were mounted over the stowed flexible array and discarded as the stowed array was deployed. Another solution is to design the system so that the rigid arrays used for the transfer power are attached to the stowed flexible array so that they can be deployed and used as part of the final array - the so-called hybrid array. It has also been suggested that the flexible arrays can be partially deployed during transfer orbit, and then either retracted during transport to GEO or left partially deployed.

The resolution of this problem may not be simple. The cleanest solution is to redesign the SEPS so that in its GEO configuration it is a hybrid array. Whether the array can be deployed and retracted or transferred from low earth orbit (LEO) to GEO in the partially deployed state will involve knowledge of the OTV gravity forces. Furthermore, one may have no certainty that even low gravity forces will not, in some way, affect later complete deployment. It might be simpler to be sure the OTV will impart very low gravity forces and deploy the array completely in transfer orbit. This is a key area needing further study.

The SEPS array was originally designed for the Halley's flyby-type mission but has also been generally considered for the relatively short missions at LEO. In the former case, the array was expected to see a high temperature of 250C and one long thermal cycle to -150C with long durations at each end and perhaps 16-percent degradation (25 kW to 21 kW) over five years. In this orbit and at LEO, the array will experience a considerably different environment than at GEO. The amount of irradiation at GEO will be greater including trapped electrons and protons and solar flare protons.

The thermal environment is also different. At LEO, there is a considerable amount of earth albedo so the array stays warm and even though the array goes into eclipse more often, the thermal cycles are much less severe. At LEO, the array may be thermal cycled numerous times between 70C or 80C and -100C. At GEO, because of the low earth albedo and other factors, the very lightweight array will be thermal cycled between 60C and -185C to -200C. Furthermore, as Figure 3-26 shows, it is not just the temperature extremes that are a potential problem, but the very high rate of temperature change during the exit from eclipse. These rapid changes can cause degradation to interconnects, weld joints, cell structure, etc. At GEO, this is modified somewhat by the fact that there are only about 90 eclipses (and thermal cycles) per year. This tougher thermal environment at GEO has to be carefully accounted for in the blanket design and testing including the cells, adhesives (type, amount, and thickness), coverslides, weld joints, interconnects, wiring, etc.

There is a growing body of knowledge accumulating on how to design lightweight arrays for 3-8 years (References 13, 14) at GEO, but what might be required to achieve a 16-year orbit is not yet known. It may be a straightforward extrapolation to go to 16 years, but it is possible that there may be problems that can only be determined through rigorous testing (e.g., unexpected fatigue failures).

Another major solar array problem at GEO has been the potential effect of solar substorm particles injected into the earth's magnetic field after a geomagnetic substorm. Significant static charge buildup and arc discharges (References 15 through 17) result from environmental charging of the insulator surfaces to the extent that the electrical breakdown value is exceeded and discharges can occur. The worst case of charge buildup on a solar array blanket occurs when

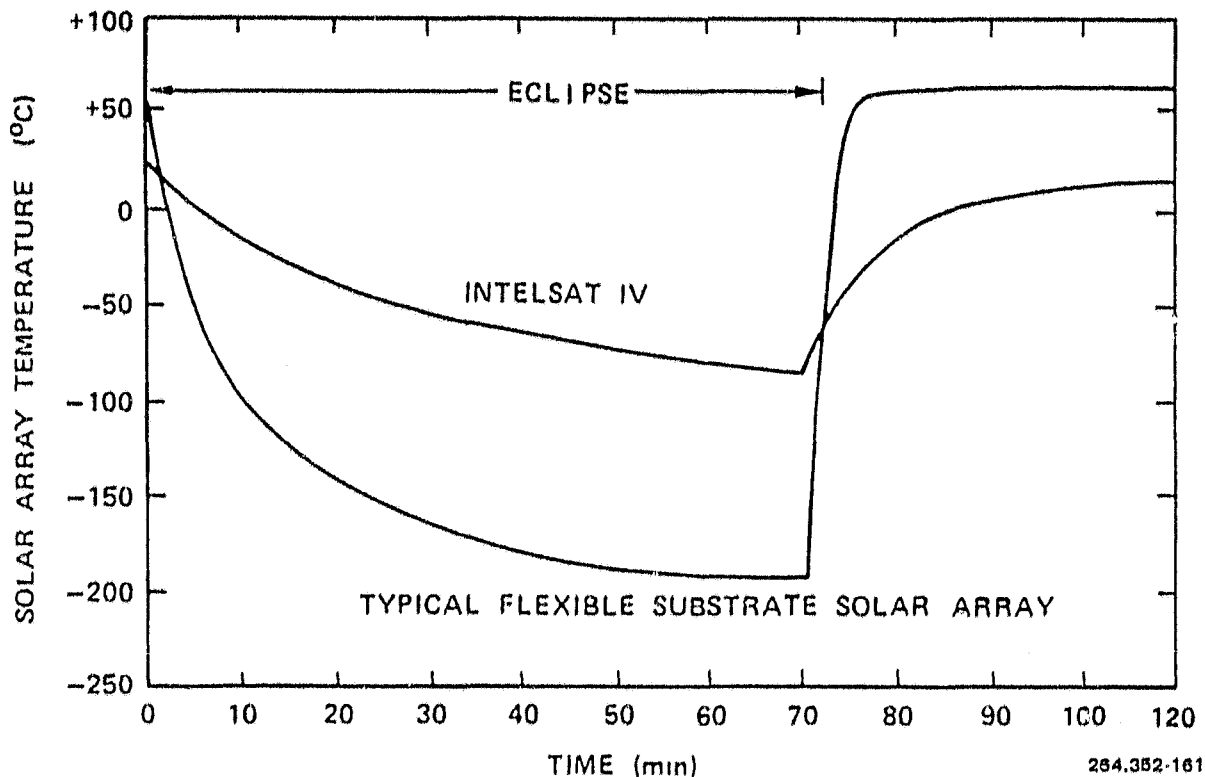


Figure 3-26. Solar Array Temperature Profiles (Longest Eclipse) at Geostationary Orbit

the nonconductive materials on the blanket are not solar illuminated (e.g., the rear surface of the blanket or an inboard area shadowed by the satellite). In such cases, no photoemission of electrons occurs to lower the potential.

The present SEPS solar array design uses a Kapton substrate and, consequently, the rear surface is an insulator. This will have to be modified for use at GEO to provide a low potential rear surface. There are a number of ways to accomplish this. For instance, the rear of the Kapton blanket can be laminated with a carbon fiber weave (References 6, 19) or a high conduction material can be sprayed on the rear surface. In any case, this potential problem must be solved and its solution will increase the array weight.

It is recognized that in terms of power density, the SEPS-type array is a viable candidate for geostationary platforms use, but that it may require redesign to provide transfer orbit power and to be able to perform in the significantly different environment at GEO. Some engineering effort must be undertaken to modify the present design for use at GEO.

Potential for Improving the EOL Power Density on a SEPS-Type Array at GEO. Trying to estimate the 16-year EOL performance of a solar array that will be designed 8-10 years from now and be launched 12-15 years from now and reach

EOL 28-30 years from now is, of course, a speculative exercise. As was mentioned earlier, a blend of past solar array history, present developments and future development projections is used here.

Assuming that the SEPS-type array can be modified for GEO, the next step in the analysis was to determine how far a SEPS-type system might be improved by including higher performance cells and possibly a lighter weight structure. To do this, different types of advanced silicon solar cells were analyzed for their effect on array performance. The approach was first to determine the effect of using solar cells that appear at this time to have a good chance of being developed and qualified for these missions, and second, solar cells that NASA and other researchers in this field are studying as a future development that may be achievable in time for these missions. These analyses are based on providing 11.77 kW at EOL, 16 years at GEO.

Use of Thin High-Efficiency Silicon Solar Cells. In the first case, it was assumed that the current 200 micron solar cells with 150 micron covers and a VOL output of  $17.3 \text{ mW/cm}^2$  (12.8 percent efficient in the SEPS design) are replaced by 50-micron thick cells with 50-micron thick covers and a BOL output of  $20 \text{ mW/cm}^2$  (14.8 percent efficient). With these particular solar cells, two different cases were studied.

- a. Thin, High Efficiency (80 mW) Solar Cell with a High Absorptance and Operating Temperature. Since this device is now being produced only in experimental quantities, there is a limited amount of information available. The first published data on the performance of these cells under irradiation was analyzed to estimate the performance after 16 years at GEO (Reference 18). This data was combined with the predicted degradation for a 50-micron ceria doped coverslip in orbit, predictions of the overall performance degradation due to thermal cycling, micrometeroids, random failures, etc. For an initial estimate, the other array characteristics were frozen and only the blanket was changed. However, even though the SEPS characteristics were frozen, estimates were made of the mass of a yoke, telescoping mast, and SADA for use at GEO. For a longer thermal cycle life, Invar interconnectors were used. An estimate was also made of the effect of laminating carbon fiber to the blanket to reduce magnetic substorm charge buildup (References 6, 19).

It was determined that the power density of the complete array including SADA, yoke, telescoping mast, SEPS structure and blanket, using 50 micron cells and covers at 16 years EOL at GEO, was about 36-38 W/kg. The lower figure includes an estimate of the effect of charge protection on the blanket mass.

No attempt was made to determine the effect of providing transfer orbit power since this appears to be an open question. However, it is likely that if a hybrid array with a rigid panel is used to provide transfer orbit power, it will decrease the power density.

- b. Thin High-Efficiency (80 mW) Solar Cell with a Low Absorptance and Operating Temperature. The gain here is in increased power from the lower operating temperature, which allows for reduction in size and weight of the blanket.

Using the same criteria as in the first case, the power density at EOL would be about 38-40 W/kg.

In a and b above, it was assumed that the structural mass was not affected by the decreased size and mass of the blanket. However, it is likely that the structural mass of the array would also decrease as the blanket does. This may be modified by the need to have the array survive the 16-year environment (e.g., concerning material embrittlement, can a SADA work for 16 years, etc.). For a first estimate, it was assumed the mass of the yoke, telescoping mast, structure, etc., decreased 30 percent. This results in a power density of a) 80 mW, high  $\alpha$  cell of 46-49 W/kg and b) 80 mW, low  $\alpha$  cell of 50-53 W/kg. Consequently, as expected, the reduction in mass of the structural elements will also have a major effect.

#### Conclusion:

- a. 80 mW, 50  $\mu\text{m}$  cell with high  $\alpha$ ; no change in structural mass - 36-38 W/kg EOL.
- b. As in a, but cell has low  $\alpha$  - 38-40 W/kg EOL.
- c. 80 mW, 50  $\mu\text{m}$  cell, but assume 30 percent reduction in structural mass.
  1. High  $\alpha$  cell 46-49 W/kg EOL.
  2. Low  $\alpha$  cell 50-53 W/kg EOL.

Use of advanced cell resulting from NASA Research. The present SEPS solar cell is replaced with a cell resulting from advanced NASA solar cell research. The goal of this research (Reference 2) is an 18 percent silicon solar cell that suffers little degradation due to radiation. For this analysis, it was assumed that by the late 1980s, this cell will have been developed and that 18 percent ( $24.3 \text{ mW/cm}^2$ ) BOL capability cells in 50  $\mu\text{m}$  thicknesses will be available that only degrade 20 percent due to radiation in 16 years. For this analysis, it was also assumed that the array structural weight has been decreased 30 percent.

- a. 18 percent, 50  $\mu\text{m}$  cell with high absorptance. The EOL power density for the complete array including yoke, SADA, etc., is about 53-55 W/kg EOL.
- b. 18 percent, 50  $\mu\text{m}$  cell with low absorptance. The EOL power density is in the range of 56-58 W/kg EOL.

Figure 3-27 summarizes the results of the analysis on advanced solar cell technology. At this time, it appears feasible to expect that a SEPS-type array using thin planar silicon solar cells should be able to achieve 45-50W per kg at

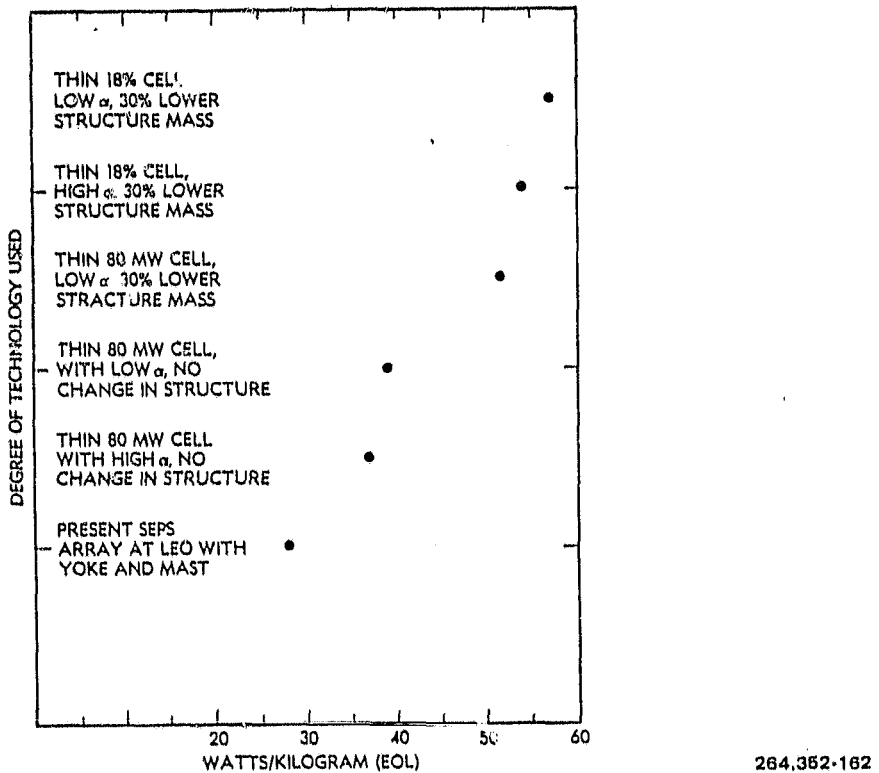


Figure 3-27. Effect of Advanced Technology on the Power Density of the SEPS Array at GEO Assuming a 1045 kW EOL Requirement

EOL 16 years. This assumed the 80 mW, 50  $\mu\text{m}$  cell with an absorptance between  $\alpha > 0.9$  now and the  $\alpha \approx 0.61$  under development and a substantial reduction in array mass. As Figure 3-27 and the previous discussion have indicated, it may be possible to go well beyond that if the higher performance cells can be developed. For example, if a 42V bus is assumed, the 11.77 kW could be provided with approximately 140,000 2 by 4 cm, 50  $\mu\text{m}$  thick solar cells having an initial performance of 80 mW/2 by 2 cm cell and a 45C in-orbit operating temperature.

It has been mentioned earlier that historical precedence indicated that the solar array would utilize about 395 kg or 29.8 W per kg. The previous analysis implies that the array for the 11.77 kW case should be available for about 235-260 kg. It must be strongly emphasized that this analysis presumed that the major research items can be accomplished and that the SEPS-type array will be designed for use at GEO. Furthermore, the analysis made no assumption about man's involvement at LEO or GEO. Comparing the initial 395 kg possibly available with the 260 kg that may be needed leaves considerable margin for contingency mass growth.

Concentrator Solar Arrays. Solar array concentrators offer the potential advantages of a high power-to-mass ratio and a reduction of the number of solar cells required to produce a given power. A number of studies of concentrator concepts are under way. However, they are still in preliminary stages, and any attempt to characterize a concentrator system is of necessity highly speculative. Three concentrator arrays are considered for possible use on the second three launches.

Two concentrator designs were considered for a solar array with an EOL capability of 11.77 kW. Even though this is directed toward the later launches, 11.77 kW was used for comparison with the previous analysis. The first is a silicon flat-plate trough (FPT) concentrator array (Figure 3-28) with a BOL geometric concentration ratio ( $C_g$ ) of 2. The second is a back-lit two-dimensional multiple flat-plate concentrator (2D-MFPC) (Figure 3-29) using gallium arsenide solar cells with a  $C_g$  of 7 (Reference 20). Aluminized Kapton was assumed as the reflecting material for both concepts. The reflectance used was 0.85 at BOL, and 0.74 at EOL (Reference 21). The EOL reflectance is of doubtful accuracy (Reference 22), however, and it does not account for micrometeoroid effects, thermal cycling effects, or UV degradation. Little is known at present concerning the properties of reflecting materials in geosynchronous orbit. This uncertainty must be resolved before concentrator arrays can be accurately evaluated.

FPT Silicon Concentrator Array. The flat-plate trough concept was chosen for the silicon array because of its simplicity and the ease with which it can be incorporated into a SEPS-type configuration (Reference 23). The upper practical limit of  $C_g$  for this configuration is approximately 2 (Reference 24). This is compatible with a silicon array at GEO because for  $C_g \geq 2$ , higher temperatures rapidly reduce the efficiency of the array (Reference 22).

The analysis was done for three cases. The first uses an 80-mW, 50  $\mu\text{m}$  silicon cell with low  $\alpha$  (0.61), the second uses an 18-percent efficient, 50- $\mu\text{m}$  silicon cell with low  $\alpha$  and little radiation degradation, and the third repeats the second with no reflector degradation. For  $C_g = 2$ , and  $\alpha = 0.61$ , the array temperature is on the order of 90C at autumnal equinox and 80C at summer solstice. It has been assumed for these analyses that the blanket and reflector mass constitute 54 percent of the total array mass (excluding yoke and SADA).

- a. 80 mW, 50  $\mu\text{m}$ , 2 by 2 cm silicon solar cell,  $\alpha = 0.61$ . It was determined that the total array power-to-mass ratio including blanket, reflectors, mast, SEPS structure, yoke, and SADA was about 51 W/kg at 16 years. This array has a total mass of 230 kg. It requires approximately 100,000 fewer cells than the planar configuration, but the reflectors have a mass of approximately 30 kg, which offsets much of the reduced blanket mass.
- b. 97.4 mW (18 percent), 50  $\mu\text{m}$  silicon solar cell,  $\alpha = 0.61$ . The above analysis was repeated for an 18-percent efficient, 50- $\mu\text{m}$ , 2 by 2 cm cell with only 10 percent radiation degradation at 16 years. The power density

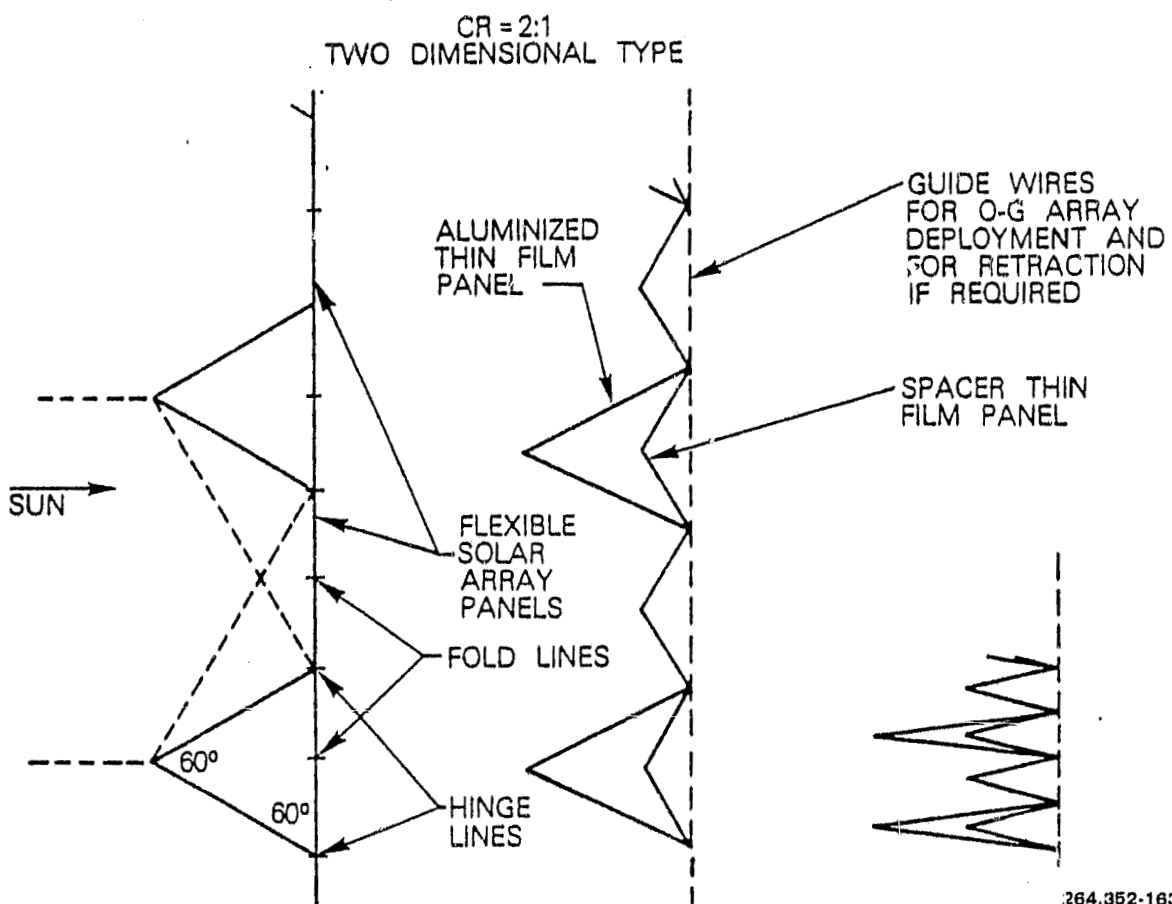


Figure 3-28. Flat Plate Trough Concentrator (FPT) in SEPS Configuration

including the yoke and SADA was determined to be about 60 W/kg EOL. The total mass of this array was about 197 kg. This array requires about 130,000 fewer cells than the planar array.

- c. 18 percent, 50  $\mu\text{m}$  silicon cell,  $\alpha = 0.61$ , zero reflector degradation. This analysis was done in order to get an idea of the sensitivity of the power density to variations in reflector degradation. Assuming that the aluminized Kapton retained the same reflectance (0.85) at 16 years as at BOL, the power density was determined to be about 65 W/kg EOL (95 W/kg BOL), including yoke and SADA. Thus, including yoke and SADA with no reflector degradation, the EOL power density is about 8-percent higher than it is with 13 percent degradation in reflectance. A major limiting factor in increasing the power density appears to be the mass of the yoke and SADA, which remained constant for all the above cases.

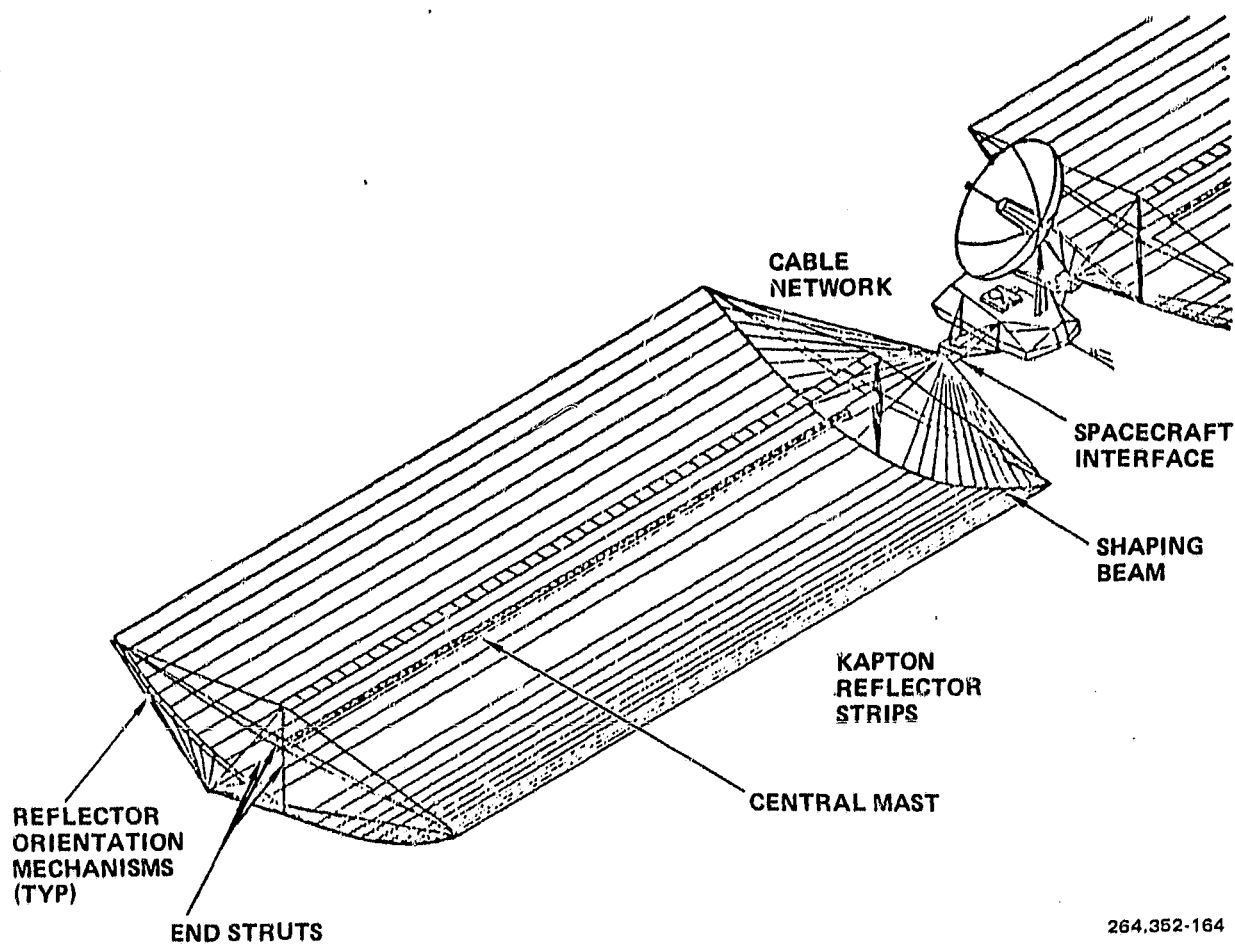


Figure 3-29. Two-Dimensional Multiple Flat Plate Concentrator Solar Array (2D-MFPC)

Conclusion:

- 80 mW, 50  $\mu\text{m}$  cell, low  $\alpha$ ; 51 W/kg EOL.
- 97.4 mW, 50  $\mu\text{m}$  cell, low  $\alpha$ ; 60 W/kg EOL.
- 97.4 mW, 50  $\mu\text{m}$  cell, low  $\alpha$ , no reflector degradation; 65 W/kg EOL.

2D-MFPC Gallium Arsenide Concentrator Array. The two-dimensional multiple flat plate concentrator consists of a series of stretched flat plate mirrors that direct sunlight onto a long narrow FRUSA-type solar array that faces the mirrors with its back to the sun (Figure 3-29). Both the mirrors and the solar array are rolled up during launch and deployed from canisters as the central mast deploys and pushes the end beams apart (Reference 20).

The analysis was done for two cases. The first incorporates an 18 percent efficient, 50  $\mu\text{m}$ , 2 by 2 cm GaAs solar cell (Reference 20) with  $\alpha = 0.751$

(Reference 25). The second repeats the first with no reflector degradation. For  $C_g = 7$  and  $\alpha = 0.751$ , the array temperature is on the order of 250C at autumnal equinox and 240C at summer solstice. The analysis does not consider annealing of radiation damage. The blanket and reflector mass assumedly constitute 50 percent of the total array mass, excluding the yoke and SADA.

- a. 97.4 mW, 50  $\mu\text{m}$  GaAs solar cell,  $\alpha = 0.751$ . The total array power density including the yoke and SADA was found to be about 73 W/kg EOL. The array has a total mass of about 163 kg. It requires only about one fifth as many cells as a silicon planar array, but at  $C_g = 7$  the reflector mass is approximately two times that of the blanket.
- b. 97.4 mW, 50  $\mu\text{m}$  GaAs solar cell,  $\alpha = 0.751$ , no reflector degradation. The power density with no reflector degradation including the yoke and SADA was found to be approximately 78 W/kg EOL. Including the yoke and SADA with zero reflector degradation, the EOL power density is about 4 percent higher than it is with 13 percent degradation in reflectance. This increase is less than that for the silicon concentrator array because, for the GaAs array, the yoke and SADA constitute a larger percentage of the total array mass than for the silicon array. Thus, the yoke and SADA more sharply limit the increase in power density.

#### Conclusion:

- a. 97.4 mW, 50  $\mu\text{m}$  GaAs cell,  $\alpha = 0.751$ , 13 percent reflector degradation; 73 W/kg EOL.
- b. 97.4 mW, 50  $\mu\text{m}$  GaAs cell,  $\alpha = 0.751$ , no reflector degradation; 78 W/kg EOL.

From the above analysis it would appear that, in terms of power density, concentrator arrays offer only marginal improvement over planar arrays at GEO for a 11.77 kW system. However, at this early stage this can be only a highly tentative conclusion. Reductions in mass, more efficient GaAs cells, radiation annealing, or higher concentrations coupled with heat pipes or other active cooling systems (Reference 26) could make concentrator systems more attractive. A firm conclusion concerning the desirability of concentrator solar arrays at GEO cannot be reached until more is known about specific properties of the system components.

**3.1.5.2 Energy Storage.** The present space energy storage method is based on batteries with a few exceptions involving interplanetary spacecraft which use radio isotope power sources. Some development support is underway on flywheel kinetic energy storage with high peak power capability. Batteries are proposed for the GP, at least until development of other methods shows improvement in weight and operating performance.

Nickel-Cadmium Cell. The rechargeable sintered plate nickel-cadmium (Ni-Cd) alkaline cell has been used to supply primary power during eclipse on all geo-synchronous commercial communications spacecraft, and indeed in a high percentage of all spacecraft flown to date. In particular, the backlog of orbital experience, the high-rate deep discharge capability, and long storage life appear to be key qualifications of this cell.

The analysis performed here consists of first establishing the relationship between cell ampere-hour capacity and weight. A large number of cells were surveyed some time ago in Reference 27. This information has been updated to reflect the performance of recent cells that have been used in operational synchronous orbit missions. These data have been analyzed in Table 3-16, plotted, and the resulting curves shown in Figure 3-30. Although some R&D work on lighter Ni-Cd cells is being done, no large-scale changes in this relationship appear likely.

Table 3-16. Recent Design Prismatic Nickel-Cadmium Cells

---

General Electric Category 42B 015 AB 53 Cell Used on Intelsat IV

Typical Weight	655.4 g
Rated Capacity	15.0 A-hr
Actual Capacity	21.5 A-hr to 1.0V
Cell Energy Density at 100% DOD	$\frac{21.5 \text{ A-hr} \times 1.2\text{V}}{655.4 \text{ g}} \times \frac{1000 \text{ g}}{2.2 \text{ lb}}$
	17.9 W-hr/lb (39.4 W-hr/kg)

General Electric Cell Used on Intelsat V

Typical Weight	1050 g
Nominal Capacity	34.0 A-hr
Actual Capacity	38.0 A-hr to 1.0V
Cell Energy Density at 100 Percent DOD	$\frac{38.0 \text{ A-hr} \times 1.2\text{V}}{1050 \text{ g}} \times \frac{1000 \text{ g}}{2.2 \text{ lb}}$
	19.7 W-hr/lb (43.4 W-hr/kg)

---

Several important facts have come to light regarding performance characterization of the Ni-Cd cell and the philosophy of integrating it into a synchronous spacecraft power system. Most of the available experience data indicate no loss and actually a slight increase in total ampere-hour capacity to zero volts, with time and cycling. On the other hand, it is known that cell terminal voltage, either on charge or on discharge, is quite variable and somewhat difficult to predict. It is a function of cell design, current, state of charge, temperature,

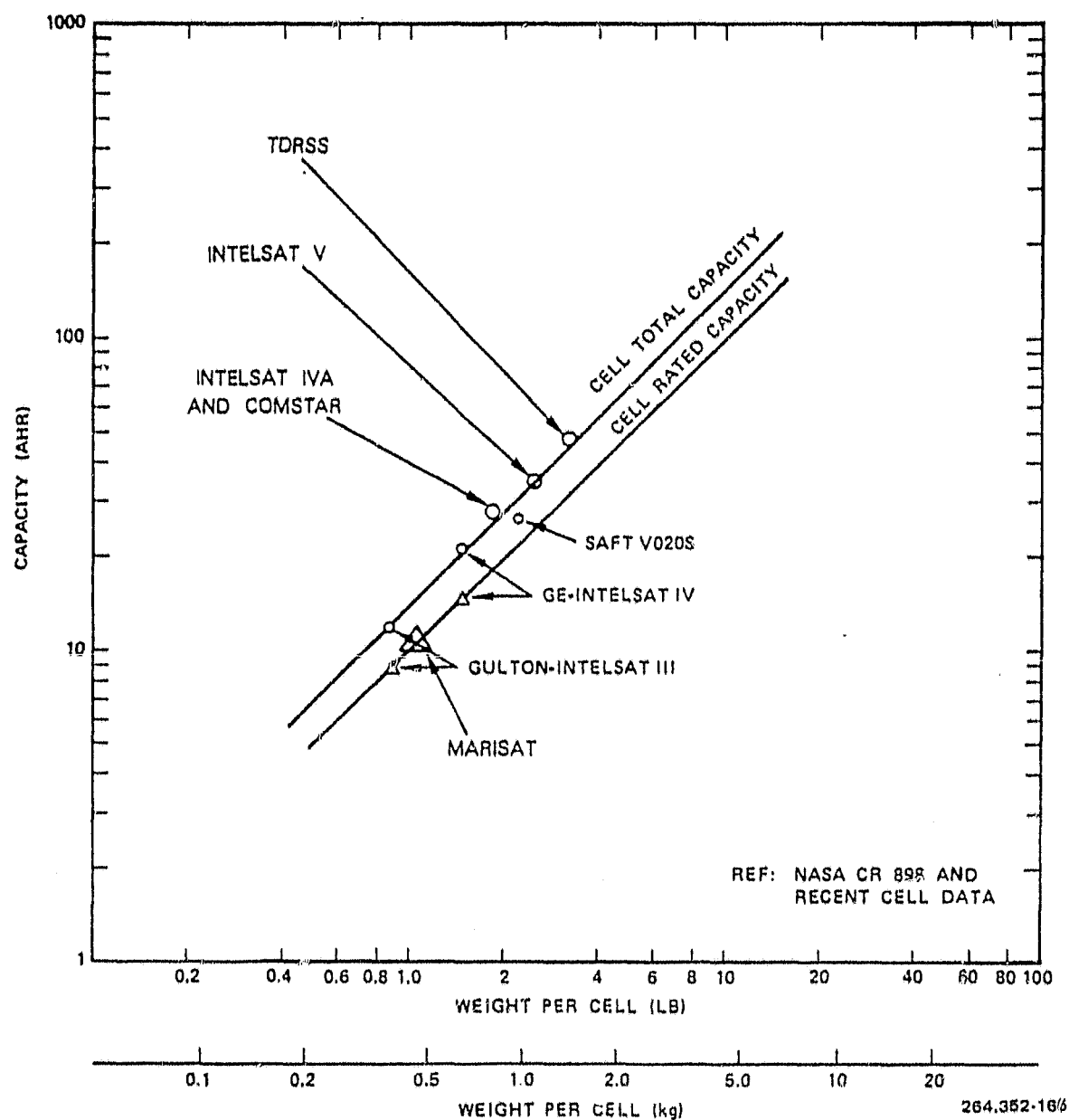


Figure 3-30. Ni-Cd Cells, Ampere-Hour Capacity Versus Weight

contaminant levels, and previous reconditioning history. Therefore, it appears logical to consider the cell as a circuit element that is a source of current or ampere-hours rather than as a constant voltage device.

Second, the importance of cell temperature should be recognized. The Ni-Cd battery is one of the most temperature-sensitive devices in a typical communications spacecraft. In order to operate to the deep depth of discharge that is essential to high energy density, it is necessary to fully charge the cell. Hence, the temperature of all the cells in a stack must be below 75F, since the charge efficiency drops off very rapidly at higher temperatures. Also, the

nylon separator degradation causes profound effects on cell overcharge protection. Its effect on cell life has been shown to be a log function of temperature (Reference 28). Minimum temperatures of 30F to 40F have been experienced with quite satisfactory results, and lower temperatures down to zero Fahrenheit can be used if the charge rates are carefully controlled. In summary, cool temperatures are an essential ingredient to a long-life Ni-Cd battery design.

In order to satisfy the thermal requirements outlined previously, and particularly to minimize cell-to-cell temperature variations, even in much smaller power systems, designers have often found it necessary to disperse the cells in small packages mounted on the structure in a number of locations. Alternatively, heat pipes could be used to provide uniform temperatures throughout the stack as implemented in the two kilowatt long life battery project, in Reference 29.

Long-term laboratory tests, Reference 30, have demonstrated that one or more deep discharges beyond the normal operating depth partially restores cell voltage, thus improving both maximum energy density and battery useful lifetime. This reconditioning process has been used extensively in orbit to improve the end of discharge voltage performance of Ni-Cd batteries in communications spacecraft.

It has become a routine procedure in all the Intelsat IV and IVA satellites, and in the COMSTAR and MARISAT birds to perform two successive discharges down to 1.0 volts/cell prior to each eclipse season. Resistive loads are used, typically discharging the batteries at about a C/30 to C/60 rate. The effects of this procedure are quite regular and can be predicted ahead of time with a computer model (Reference 31). The overall effect of reconditioning can be characterized as a significant reduction in the long term degradation of battery terminal voltage during discharge. This increases the battery energy density available at end of mission and narrows the input voltage range of the using equipment.

Ni-Cd Batteries. Detailed battery component weights have been analyzed for several flight spacecraft, as shown in Table 3-17. The average weight of the cells was about 83 percent of the total battery weight, with about 12 percent devoted to structure and the remaining six percent used for electronics and connectors. This information, together with the cell ampere-hours per pound, and an end of mission voltage estimate can be used to estimate the watt-hours per pound for complete spacecraft batteries.

The reliability requirements for individual cells are quite stringent in order to ensure full operation for five years or more. One approach that has been used to surmount this problem is to add one or two extra cells in series to the stack to accommodate shorted cells, and to use diodes or a transistor switch to bypass open-circuited cells, Reference 32. An alternative approach that has been used is to provide a spare battery stack in parallel; this stack can then be switched in when needed (Reference 33). Both of these designs have been analyzed and the energy density curves versus depth of discharge are shown in Figure 3-31.

Table 3-17. Synchronous Spacecraft Battery Weight Analysis

Battery	Weight (kg)	Percent of Total Weight
<b>Intelsat IV*</b>		
Cells and Insulation (50 cells)	32.7	83.4
Structure and Connectors	4.8	12.3
Electronics (diodes)	1.7	4.3
Total	39.2	100.0
<b>Intelsat V*</b>		
Cells and Insulation (56 cells)	57.4	88.4
Structure	4.0	6.2
Electronics and Connectors	3.5	5.4
Total	64.9	100.0

\*The mass of two complete batteries which comprise the complete spacecraft energy storage system are listed.

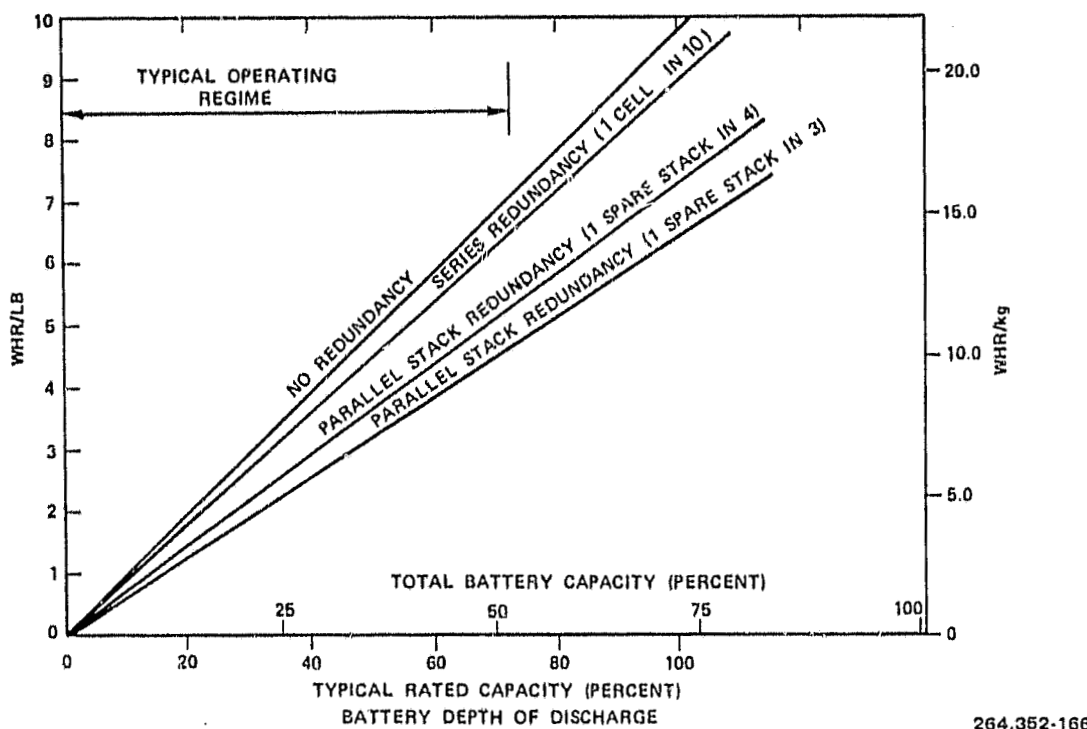


Figure 3-31. Energy Density of Ni-Cd Batteries Packaged for Synchronous Orbit Applications

264.352-166

It is necessary to determine the battery depth of discharge which can be used in a synchronous operational satellite. The Intelsat IV program has provided considerable operational experience on a number of spacecraft at a maximum depth of discharge of about 57 percent of rated capacity (~40 percent of total capacity). Intelsat V is operating at about 52 percent of total capacity. The energy density achieved on these spacecraft has been calculated in Table 3-18 and is plotted in Figure 3-32, along with data obtained from numerous other synchronous communications spacecraft providing full service through eclipse.

Table 3-18. Ni-Cd Spacecraft Battery Energy Density Calculations

---

Intelsat IV Battery

Weight	=	86.4 lb
Battery Stack Energy Density at 100 Percent DOD	=	$\frac{21.5 \text{ A-hr} \times 1.18\text{V} \times 50}{86.4 \text{ lb}}$
	=	14.7 W-hr/lb
Battery Stack Energy Density at 100 Percent Rated Capacity	=	$\frac{15.0 \text{ A-hr} \times 1.22\text{V} \times 50}{86.4 \text{ lb}}$
	=	10.6 W-hr/lb
Maximum Operating Energy Density at Battery Terminals	=	$\frac{7.0\text{A} \times 1.2 \text{ hr} \times 1.22\text{V} \times 50}{86.4 \text{ lb}}$
	=	5.94 W-hr/lb (13.08 W-hr/kg)

Intelsat V Battery

Weight	=	64.96
Battery Stack Energy Density at 100 Percent DOD	=	$\frac{38 \text{ A-hr} \times 1.18\text{V} \times 56}{64.96 \text{ kg}}$
	=	38.7 W-hr/kg
Maximum Operating Energy Density at Battery Terminals	=	$\frac{911\text{A} \times 1.2 \text{ hr}}{64.96}$
	=	16.83 W-hr/kg

---

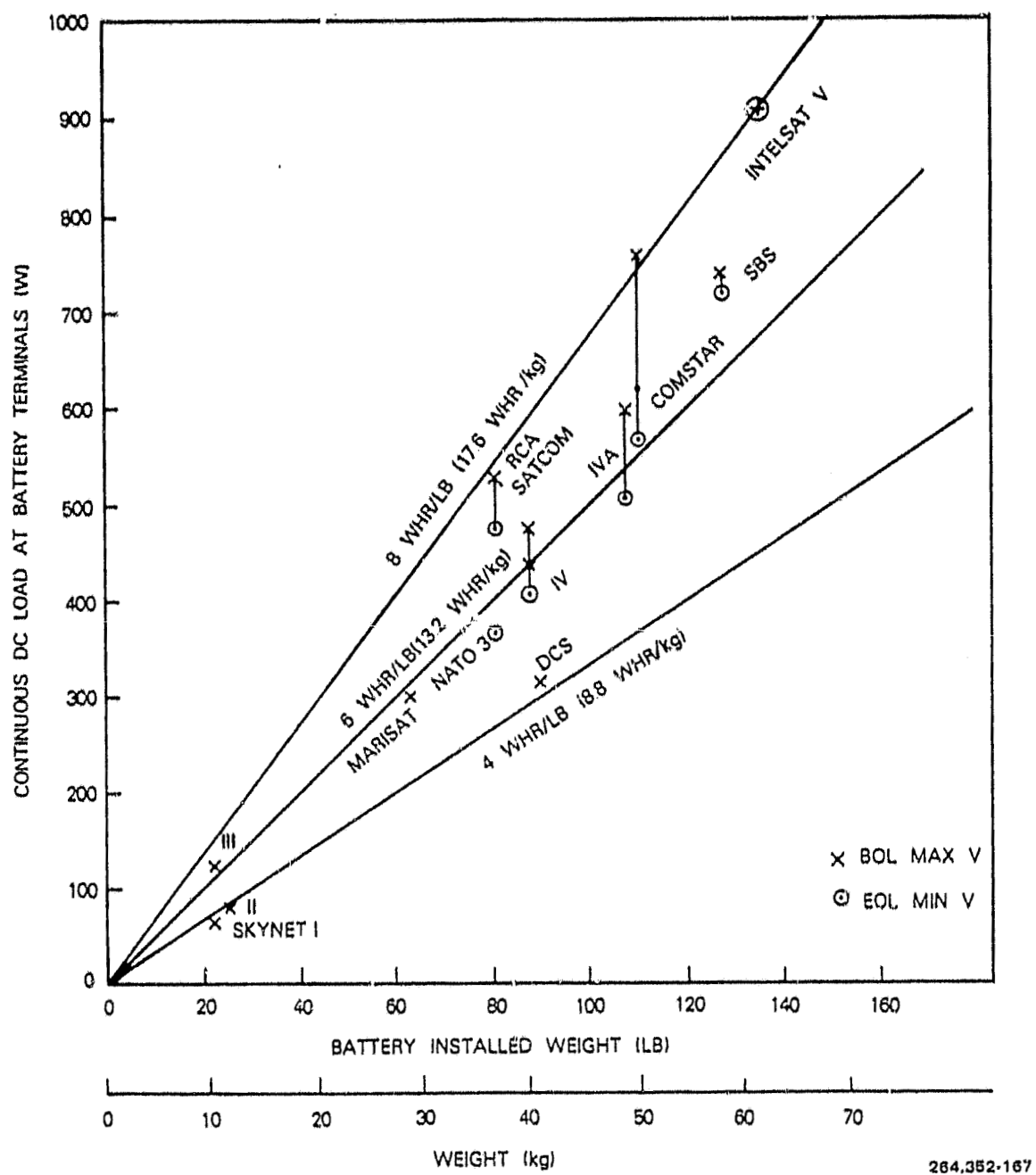


Figure 3-32. Battery Energy Density for Synchronous Spacecraft  
(Based on Total Spacecraft Power Delivered at Battery Terminals During 1.2-Hour Eclipse)

Ni-Cd Battery Life. A large body of data is presently available on the synchronous orbit mission life of present state of the art aerospace Ni-Cd batteries. Most of these are prismatic cells with chemically impregnated plates, undrawn nylon separator material, and about 35 percent KOH aqueous electrolyte, manufactured by General Electric Co.

Computer modeling and statistical analysis of this data indicates that battery mission lifetime is typically controlled by cell degradation in a wearout mode. The discharge voltage at end of longest eclipse decays as a function of the number of discharge cycles to the second power. This can be modeled as an increase in cell internal impedance with time, since a synchronous satellite regularly experiences 90 eclipse cycles per year. Thus, for any selected minimum voltage on discharge, the mission life of a battery is a function of discharge current.

An example taken from computer predictions on an actual flight battery is shown in Figure 3-33. This plots battery life to one volt/cell after 1.2 hour eclipse for a typical 28 ampere-hour Ni-Cd battery. It is assumed that this battery has been seasonally reconditioned to 1.0 volts/cell since launch. To support a given power load with this type of battery, there is a tradeoff between battery initial capacity and load (i.e., battery DOD). Further, this becomes a tradeoff between battery mass and mission life, as shown in Figure 3-31.

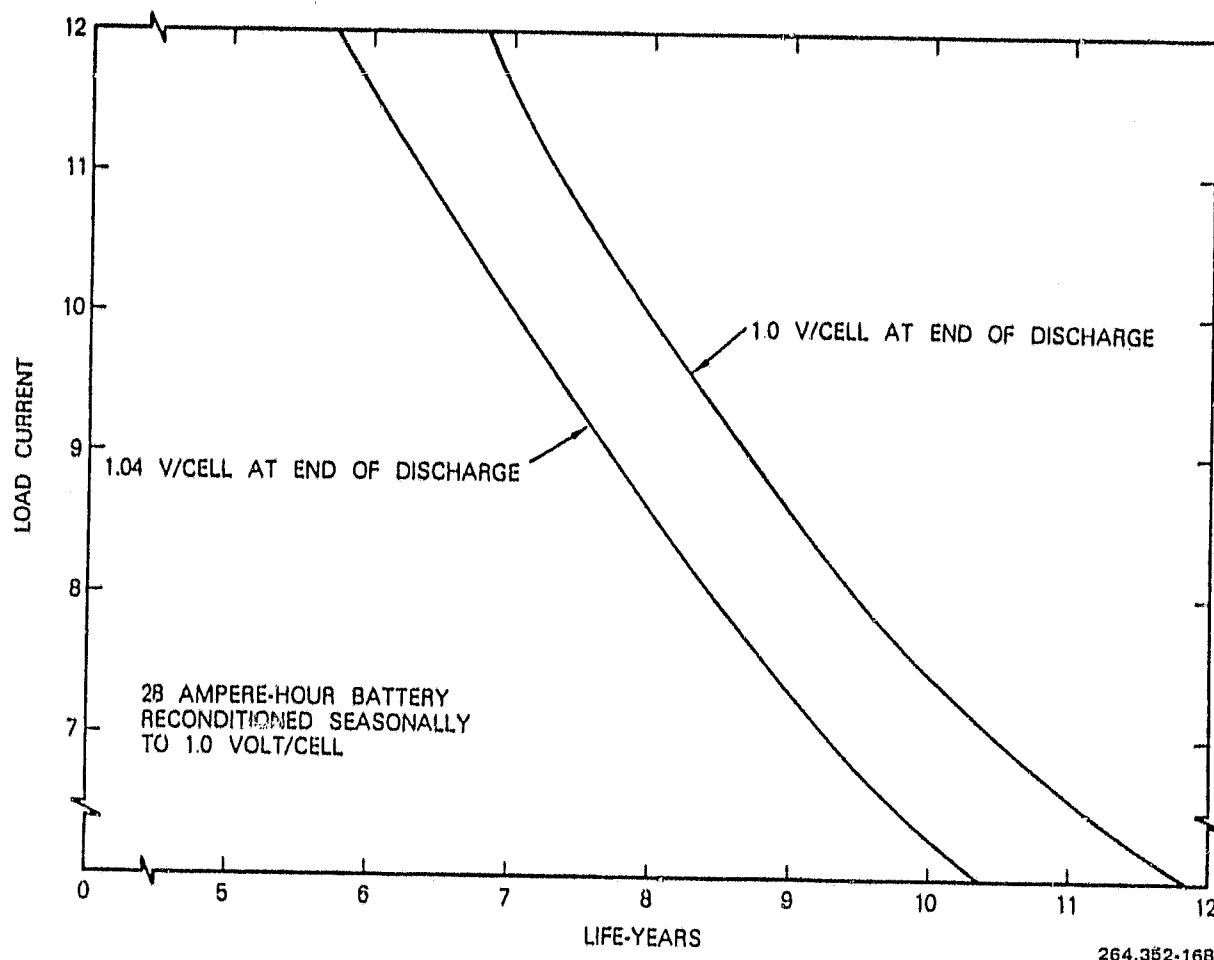


Figure 3-33. Typical Ni-Cd Battery Life in Synchronous Orbit Based on Computer Analysis

Improvements in cell design or in-orbit operating modes could improve this situation. For instance, one important degradation phenomenon in this cell is the swelling and development of microcracks in the positive plate, leading to redistribution of electrolyte into the positive plates and separator dryout. The use of electrochemically deposited positive plates promises to provide a significant life improvement by reducing this impedance buildup with time, Reference 30. Also, improvements in in-orbit storage and reconditioning techniques may further improve performance. However, it is not yet possible to quantify these effects precisely.

The Nickel-Hydrogen Cell. The aerospace nickel hydrogen cell, which was invented in 1972, Reference 35, consists of a sintered nickel positive electrode, a porous separator containing an aqueous potassium hydroxide solution, and a gas electrode negative consisting of a platinum black catalyst teflon bonded to a conductive screen.

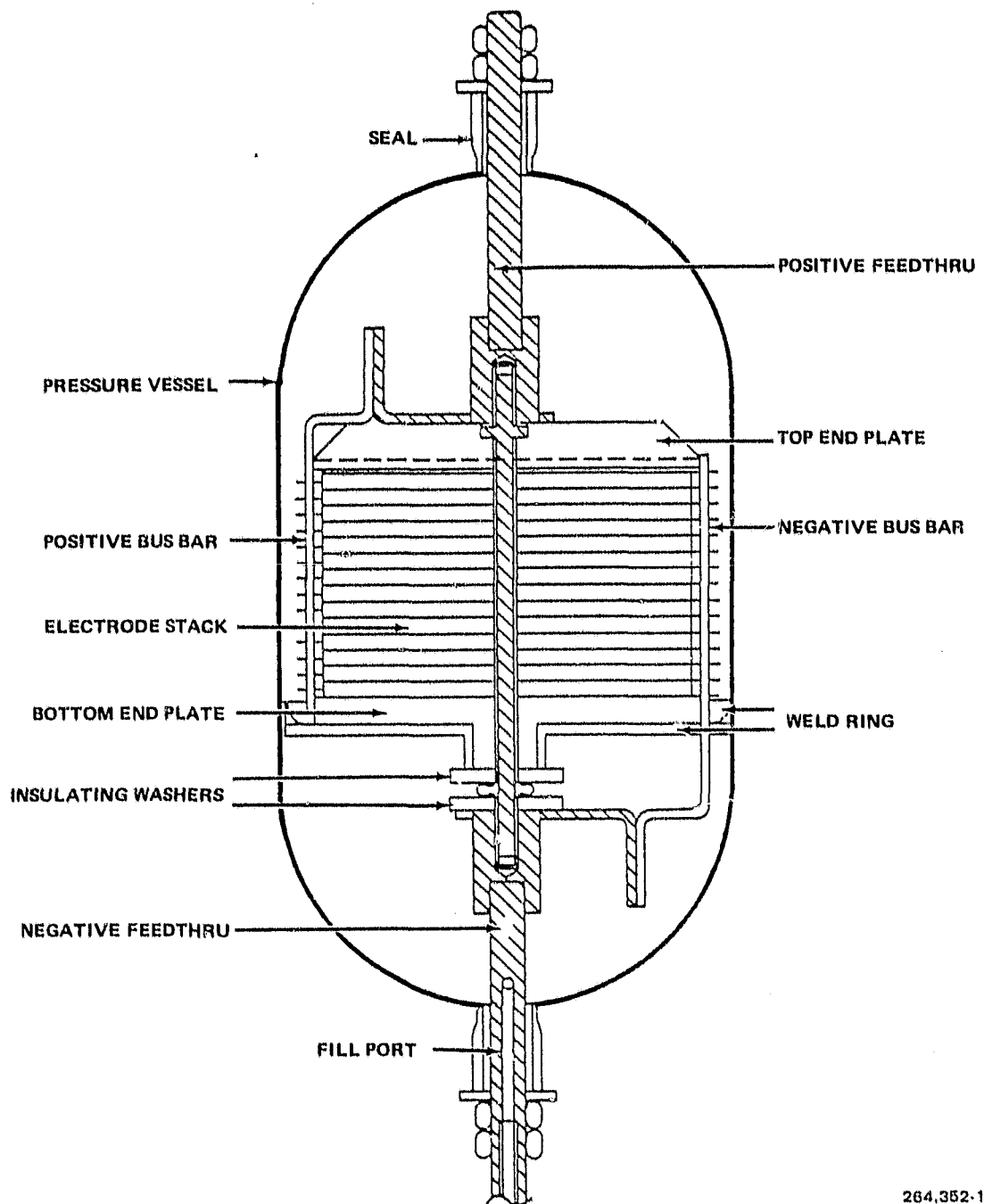
One typical physical arrangement is shown in Figure 3-34. The electrodes, separators, and inert plastic screens that allow gas access to the electrodes are contained in a stack between end plates. The annular space between the electrode stack and the outer pressure vessel is used for hydrogen gas storage. The gas pressure typically ranges from about one to 20 atmospheres. The pressure vessel is made from age-hardened Inconel 718, typically 0.5 mm (0.020 in.) thick. Ziegler type plastic compression seals are used at the electrical feedthroughs.

This cell has a number of desirable attributes. Electrochemically, both the nickel electrode and the gas electrode are quite stable and efficient. The positive electrode used in most designs of these cells consists of a porous plaque impregnated with nickel, using an electrochemical deposition process of the type pioneered by Bell Laboratories. Many tests of both Ni-Cd (Reference 30) and Ni-H<sub>2</sub> cells have demonstrated this plate has even less swelling and micro-cracking under deep discharge conditions than the quite stable chemically impregnated plate flown previously.

The overall energy efficiency of the cell can be inferred to be the same or slightly better than Ni-Cd from the charge and discharge voltages, which are each about 50 millivolts higher than the typical Ni-Cd voltages. (Roughly 1.50V on charge and 1.25V on discharge).

The cell tolerates both overcharge and reversal quite well. At rates of charge appropriate for geosynchronous, like C/10 to C/20, the hydrogen pressure increases linearly with state of charge, and then becomes constant when the cell is fully charged. Some of the key electrochemical features of the cell performance are compared with Ni-Cd in Table 3-19.

To charge or discharge these cells at very high rates could cause large temperature differentials between the electrode stack and the outer case. It can be seen from the vapor pressure curves of Reference 36 that if this differential



264,352-169

Figure 3-34. Typical Physical Arrangement of a Nickel-Hydrogen Cell  
[From Esch, Billerbeck and Curtin (4)]

exceeds about 10C, condensation of water can occur on the inner wall of the case. This makes it unavailable unless a wick system is provided to return it to the reaction. Thus, the design options are to control the temperatures by selection of appropriate charge and discharge rates, which has been done in

Table 3-19. Comparison of Cell Operating Features

Parameters	Type of Alkaline System	
	Ni-Cd	Ni-H <sub>2</sub>
Satisfactory Operating Temperature	5-20C	20C
Inherent Overcharge Protection (C/10 current)	Yes	Yes
Inherent Reversal Protection	No	Yes
Metal Electrode Utilization	Ni: 80%-85%; Cd: Large Excess Required	80%-85%
Metal Electrode Stability	Stable	Stable
Electrode Insolubility in KOH	Ni: Yes; Cd: Slight Solubility	Yes
Separator Uniformity Requirement	Moderate	Moderate
Electrolyte Management	State of the Art	State of the Art
Overall Watt-Hour Efficiency	70 Percent	70 Percent
Approximate Ratio of Thermal to Electrical Output on Discharge	0.1	0.1

most applications so far, or to augment the heat transfer paths out of the stack if extremely high currents are anticipated. Normally, this is not a problem in synchronous orbit applications.

The mass of present state of the art single-cell type Ni-H<sub>2</sub> cells is characterized in Figure 3-35. The mass of each of the cells flown or about to fly is plotted, along with new developmental cells being built in various labs, and the general trends expected from computer parametric analysis of optimum designs. As one can observe from the trend of the computer generated curve, the energy density of the cell increases with cell capacity up to about 50 ampere-hours, and then remains relatively constant at the larger capacities.

The Intelsat V cells, (Reference 40) have an energy density at 100 percent depth of discharge of about 49 watt-hr/kg in a 35 amp-hr size. Early Intelsat V flights use Ni-Cd. Flights F5 and on use Ni-H<sub>2</sub>. Cells in a larger size and with some design refinement in the pressure vessel details can reach higher energy densities. Some cells in a 50 amp-hr size have more recently been built and weigh 750 grams. This means they have achieved an energy density of about 60 watt-hrs/kg at 100 percent DOD. This cell appears to be a reasonable

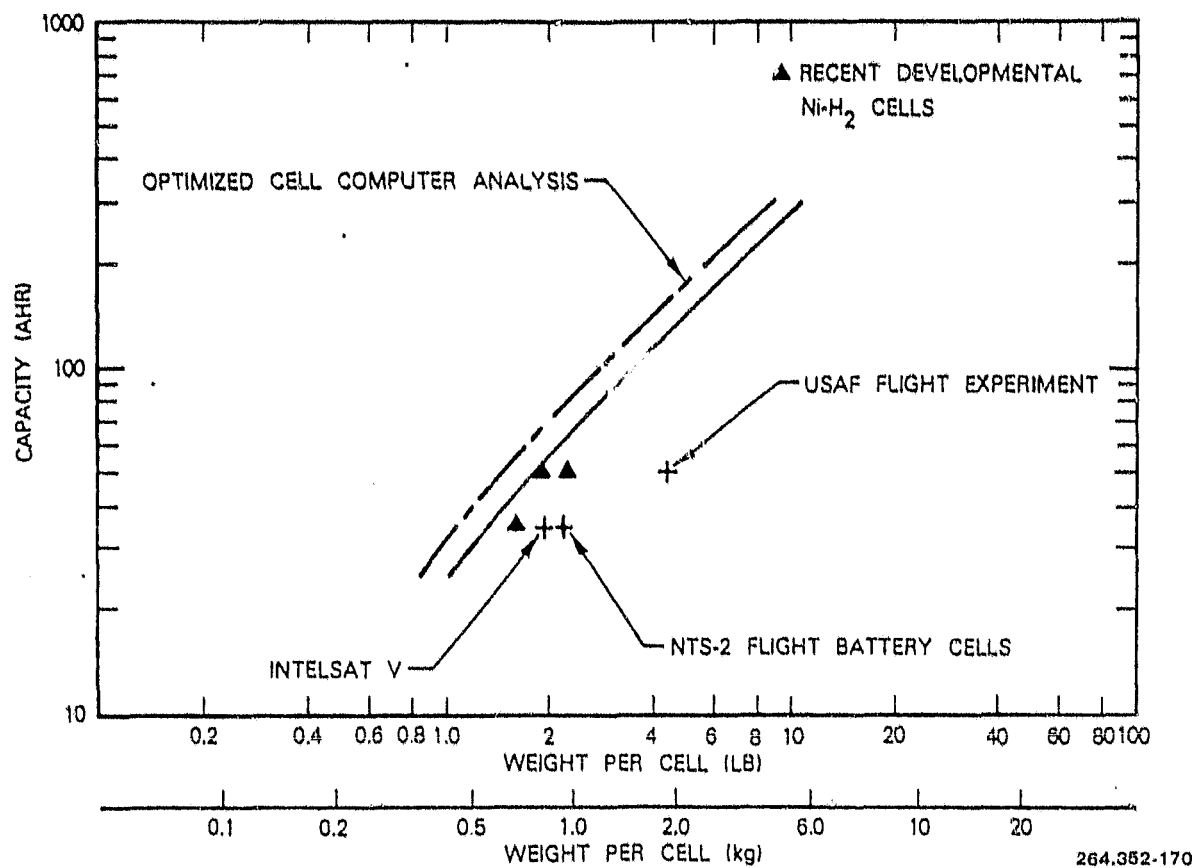


Figure 3-35. Ni-H<sub>2</sub> Cells, Ampere-Hour Capacity Versus Weight

baseline for extrapolation of a cell mass versus capacity curve, following the trends published in Reference 37. This is shown as the solid curve presented in Figure 3-35.

It is interesting to compare these cell weights with Ni-Cd. The early flight experiment cells are observed to be slightly heavier or equivalent to Ni-Cd cells of the same capacity. There is every indication that the Ni-H<sub>2</sub> cells can be safely operated at a deeper DOD and thus produce a higher operating energy density than the nickel-cadmium. The more recently designed Intelsat V cells are above the Ni-Cd curve at 35 ampere-hours, and it is expected that optimized flight cells in the region of 50 A-hr and above should be considerably higher, as shown by curves.

Nickel-Hydrogen Batteries. Several nickel-hydrogen batteries have been designed and built for successful flight experiments, References 39 and 40, and work is presently underway on qualification of a battery designed for operational use in a series of communications satellites, Reference 40. The mass of these batteries has been analyzed in Table 3-20. The actual output power numbers and eclipse times have been adjusted to scale them to synchronous orbit where necessary, and the data are plotted in Figure 3-36.

Table 3-20. Ni-H<sub>2</sub> Battery Weight Analysis

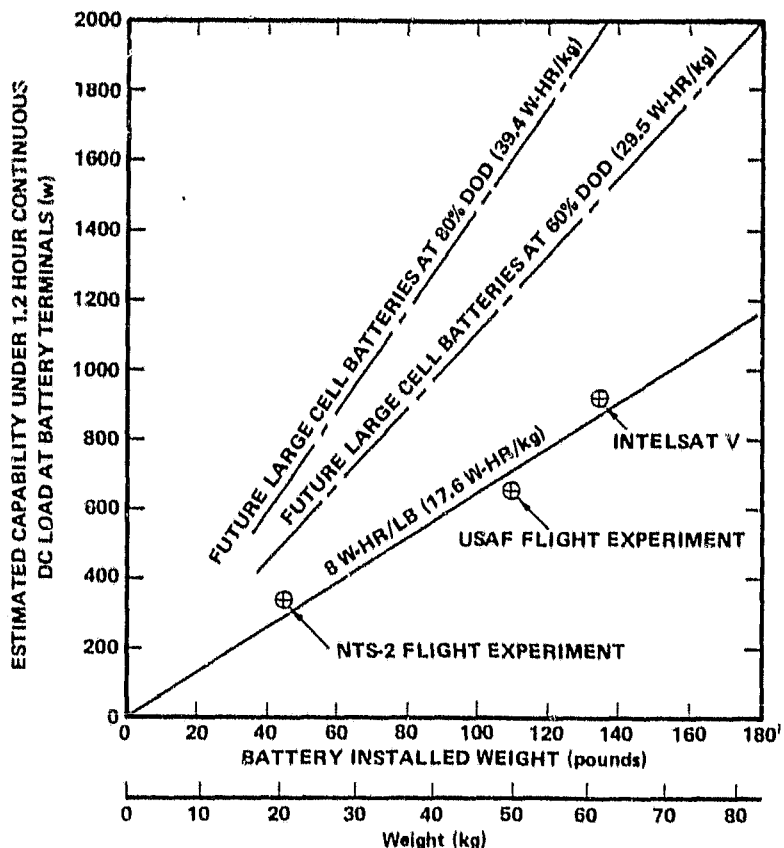
Battery	Mass	Percent of Total Weight
<b>NTS-2 Flight Experiment</b>		
Cells (14)	14.3	70.1
Structural and Thermal	5.1	25.0
Connectors, Wiring, FTC	1.0	4.9
<b>Total Mass</b>	<b>20.4</b>	<b>100.0</b>
<b>USAF Flight Experiment</b>		
RNH-50-9 Cells (21)	39.7	80.7
Electrical Insulation	0.9	1.8
Structure and Thermal	7.3	14.8
Heaters, Wiring, and Connectors	1.3	2.6
<b>Total Mass</b>	<b>49.2</b>	<b>100.0</b>
<b>Intelsat V</b>		
Cells (54)	48.0	79.8
Structure and Thermal	8.3	13.8
Connectors, Heaters, Diodes, and Wiring	3.8	6.3
<b>Total Mass</b>	<b>60.1</b>	<b>100.0</b>

It is clear from the weight analysis that a sizable portion of the battery mass in all of these designs, ranging from 14 to 25 percent, is devoted to the structural/thermal features on the package. Much of this is associated with the thermal aspects of removing heat from the cells during discharge, while maintaining uniform temperatures along the length of the individual plate stacks. It appears reasonable to assume that future refinement of the mechanical and thermal designs will result in some modest reduction of this mass fraction. A study of this is reported in Reference 41.

Looking at battery designs aimed at multikilowatt power levels, where it is appropriate to design the power system to use a cell with a capacity of 50 A-hr or more, and starting from mass/capacity data derived in recent development work (Reference 38), a battery energy density can be calculated as follows:

$$\text{Useful Energy/kg} = \text{Cell ED} \times \text{Mass Fraction} \times \text{DOD}$$

$$\begin{aligned} \text{Useful Energy/kg} &= 60 \text{ W-hr/kg} \times 0.82 \times 0.60 \\ &= 29.5 \text{ W-hr/kg at 60 Percent DOD} \end{aligned}$$



264.352-171

Figure 3-36. Ni-H<sub>2</sub> Battery Energy Density for Synchronous Spacecraft  
(Estimated at 60% Depth of Discharge Except Where Noted)

If deeper depths of discharge prove feasible as expected for nickel-hydrogen batteries, it may be possible to increase the energy density with the existing single cell devices to:

$$\text{Useful Energy/kg} = 60 \times 0.82 \times 0.80 = 39.4 \text{ W-hr/kg at 80 Percent DOD}$$

This relationship together with the slight reduction for redundancy provisions is shown plotted in Figure 3-37.

Life. There are strong indications that the in-orbit operating life of Ni-H<sub>2</sub> batteries will be significantly better than that experienced with nickel-cadmium. Several problems associated with Ni-Cd, such as cadmium dendritic growth, loss of overcharge protection due to nylon degradation, and rapid over-pressure failure when reversed have been eliminated in the new Ni-H<sub>2</sub> cell designs. The electrochemically deposited nickel oxide plates have significantly reduced the degradation due to swelling and microcrack formation during cycling (Reference 38). These batteries seem operable at deeper DOD for many more cycles, substantiated by initial laboratory testing. An early estimate on the cyclic life by TRW is reproduced from Reference 42, as shown in Figure 3-38. Tests are continuing at several laboratories, but since the cells do have a longer life, a number of long duration tests will be needed to quantify it.

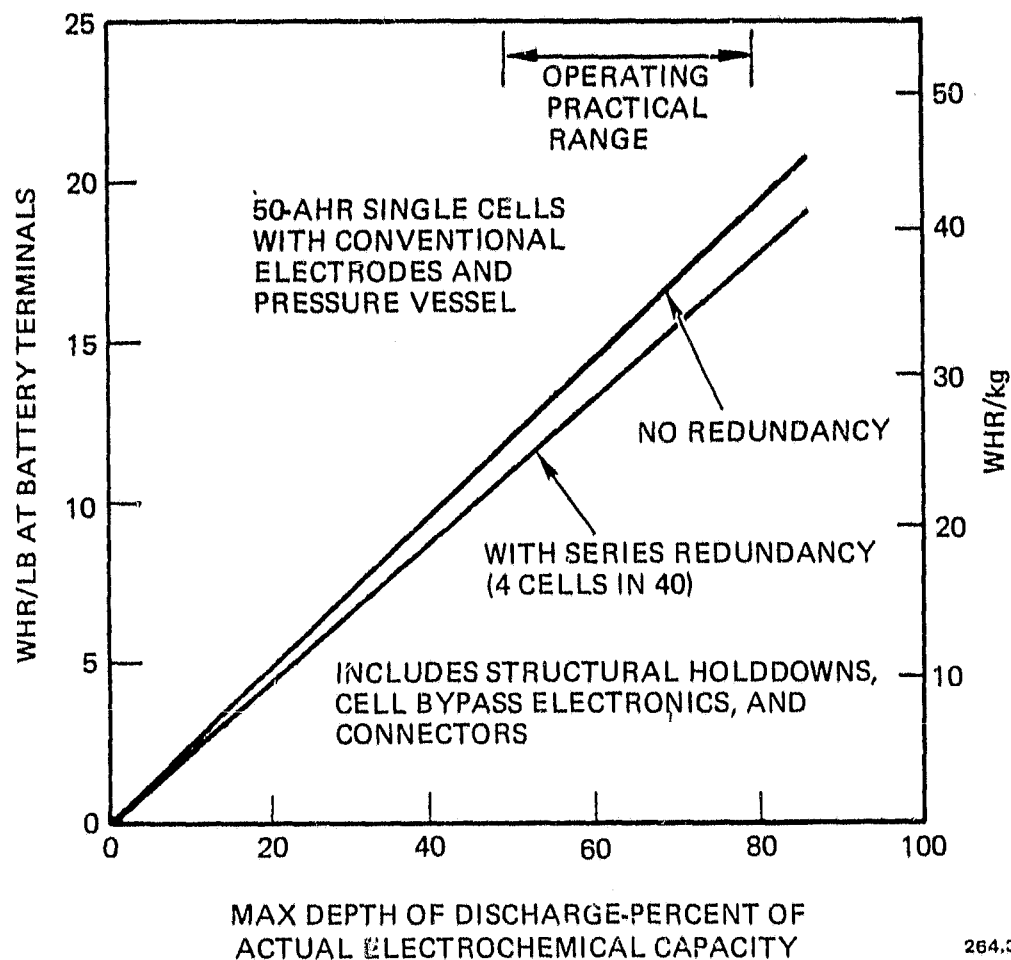


Figure 3-37. Estimated Energy Density for a 1980 to 1985 Design Ni-H<sub>2</sub> Secondary Battery

Effects of Reduced Eclipse Load on Battery Mass. In geosynchronous orbit the spacecraft is continuously sunlit except during two periods lasting approximately 45 days each, centered on the Spring and Fall equinoxes. The duration of the eclipse varies each day as shown in Figure 3-39.

Since the satellite eclipse occurs near local midnight on earth at the subsatellite location, the amount of traffic being handled at that time of day is often quite low. This is particularly true if the satellite is positioned over the more westerly of the earth terminals that are communicating. With some types of communications service it may be possible to plan to reduce the number of high power transmitters used during eclipse, thus making significant savings in battery mass.

There are other implications of this design approach including changes in overall spacecraft thermal balance, and the more detailed considerations of thermal and electrical cycling on TWT life.

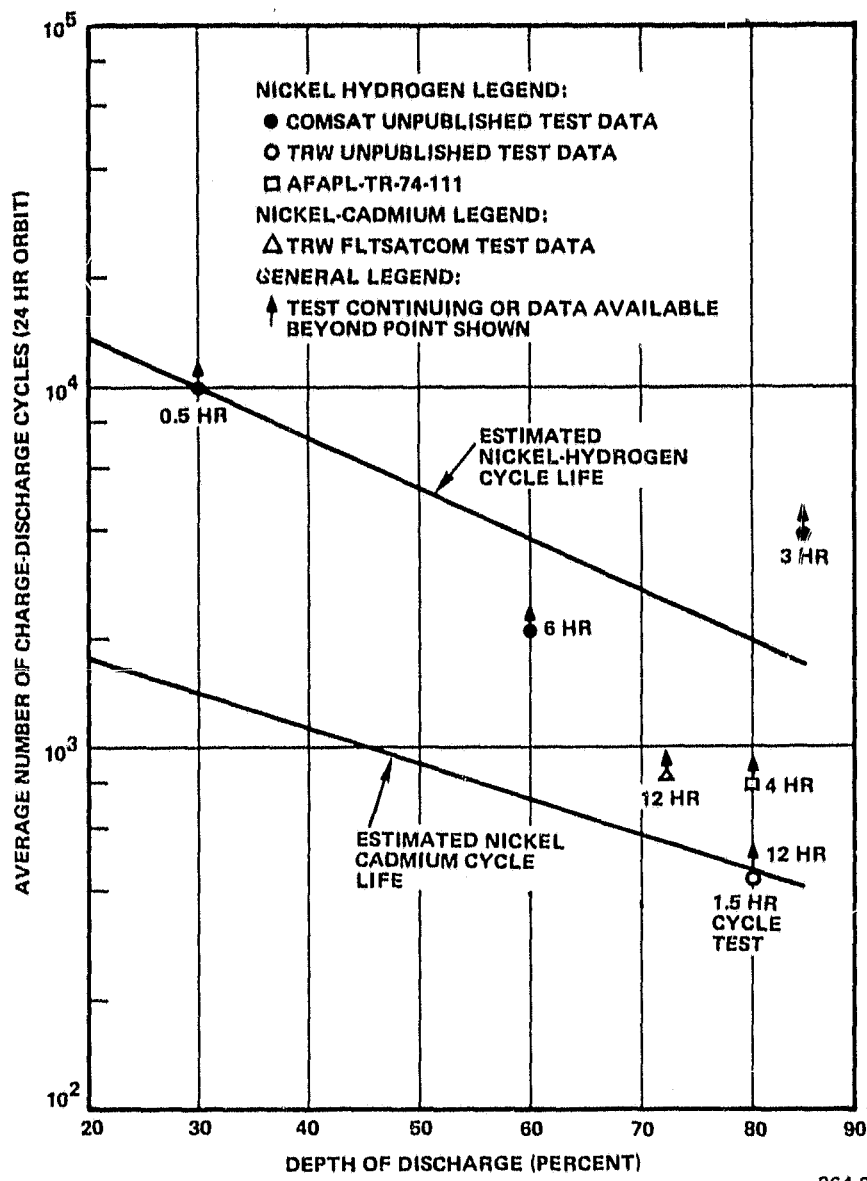


Figure 3-38. Nickel-Hydrogen Battery Cell Life (Fall, 1975)

The mass of a battery using Nickel-Hydrogen cells can be obtained from Figure 3-40. Various cell and battery development timeframes are represented here, ranging from the existing designs typically at about 17.6 W-hr/kg, up to extrapolated future designs yielding 29.5 W-hr/kg at 60 percent DOD and 39.4 W-hr/kg at 80 percent DOD. The latter performance improvements may be expected to be achieved in the next 5 to 10 years.

**3.1.5.3 Power Distribution and Management.** The design of power systems for synchronous communications satellites has passed through several evolutionary

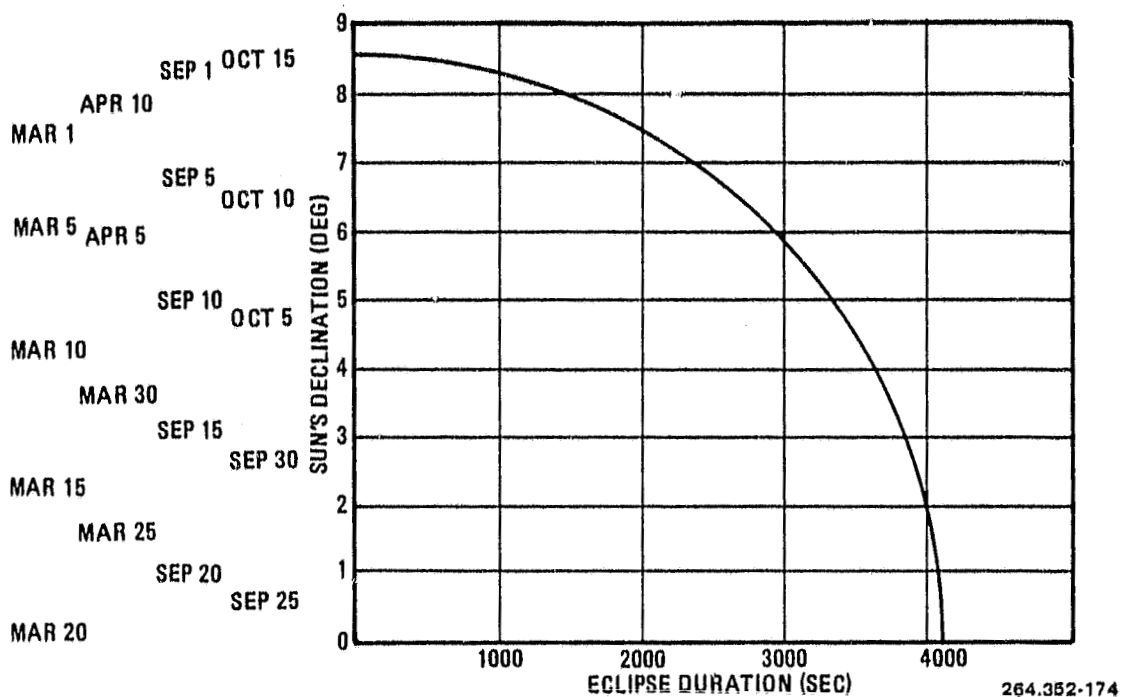


Figure 3-39. Eclipse Durations on Different Days - Geosynchronous Orbit

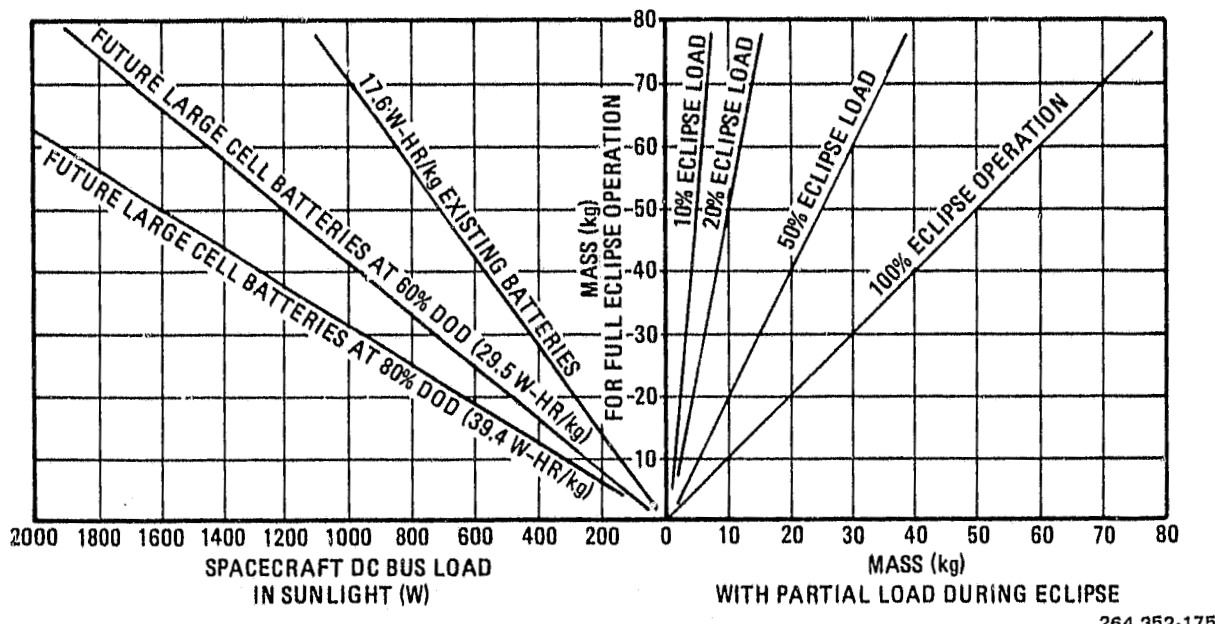


Figure 3-40. Graph for Estimation of Ni-H<sub>2</sub> Battery Mass (kg) With Load Reduction During Eclipse

stages in reaching its present state of development. The characteristics of the power systems of the successive series of Intelsat spacecraft offer an interesting example.

Basic information (Reference 43) on the power level and design lifetime of each series are shown in Table 3-21. A quantity of one to eight flight spacecraft of each type was produced. The DC power requirements have increased in consonance with the number of communications channels required. It is an interesting sidelight that the DC power has approximately doubled each time a basically new design was laid down.

As mentioned earlier, the design of commercial communications spacecraft is beginning to stabilize and become an evolutionary process. A more detailed examination of the power system loads tends to reinforce this view. The ratio of power required by each of the subsystems is quite similar from one spacecraft to the next. Figure 3-41 shows the breakdown of power loads for a typical microwave repeater satellite (Reference 44). These proportions are quite similar for either the drum spinner or the body-stabilized spacecraft, even though the various subsystems are quite different physically and functionally. The "housekeeping" equipment requires only about 13 percent of the total power, while almost 87 percent is allocated to the communications system. Of this, the majority (some 82 percent of the primary power) goes directly to the high-voltage power supplies for the traveling wave tube transmitters in the existing satellite system. Thus, the spacecraft design is quite economical in terms of power required for functions subordinate to its central mission. Also, the dominance of the efficiency and mass of the high voltage supplies becomes evident.

This situation is changing slightly and will continue to change in the future as FETs and other solid-state devices begin to displace traveling wave tubes in the lower end of the frequency spectrum. However, the efficiency, mass, and reliability of the power supplies for these transmitters will obviously continue to be quite significant since they process such a large proportion of the spacecraft power.

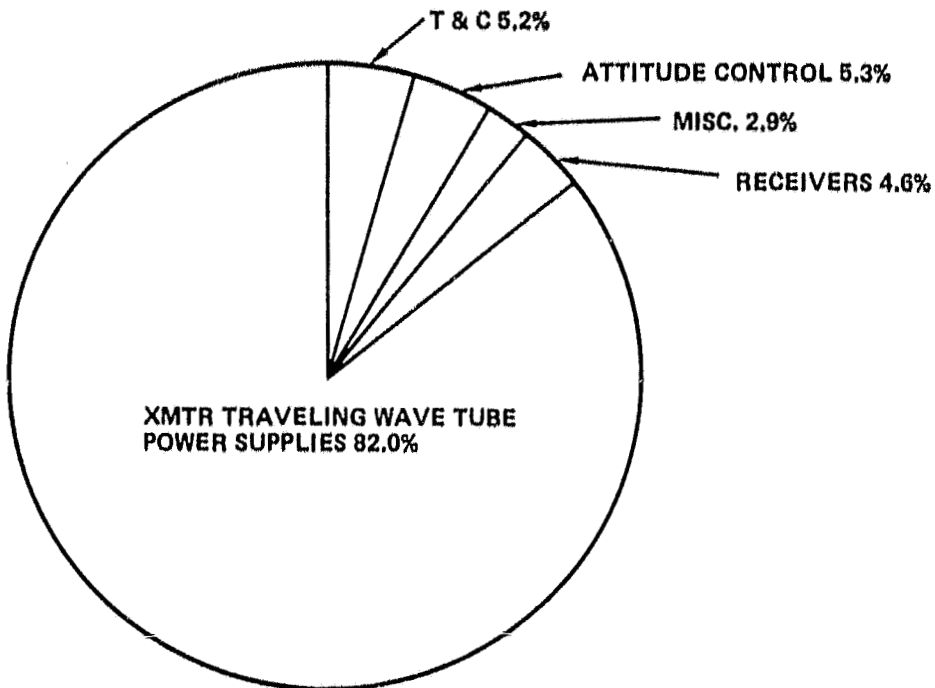
Primary Bus Voltage Selection. As the overall electric power requirements on the spacecraft have increased, the primary bus voltage has gradually been increased, as shown in Figure 3-42. The Intelsat II, IV, and IV-A spacecraft use an unregulated main bus design. The normal voltage in sunlight is relatively constant, as shown here. However, following the eclipse period which occurs about 90 times per year, as the cold array enters sunlight, the solar cell voltages are much higher (their temperature coefficient is roughly 0.5 percent per degree C). With a body-mounted array like Intelsat IV, the peak voltage is about 45 to 50V. Lightweight deployed arrays get much colder, as discussed in the solar array section, resulting in much higher post-eclipse transient voltages. A typical voltage plot is shown in Figure 3-43. Both the Intelsat III and Intelsat V designs use a regulator to control the bus voltage during sunlight operation. Larger spacecraft with deployed arrays will continue to require this feature.

Table 3-21. Growth of Intelsat Spacecraft

		Intelsat Satellite					
		I	II	III	IV	IV-A	V
Year of First Launch		1965	1967	1968	1971	1975	1979 to 1980
Drum Dimensions (cm)	Diameter Height	72.1 59.6	142 67.3	142 104	238 282	238 282	— —
Overall Deployed Height (cm)	—	—	—	528	590	1585	—
Mass (kg)	At Launch In Orbit	68 38	162 86	293 152	1385 700	1469 790	1870 1014
Primary Load Power (W)	40	75	120	400	500	975	—
Active Transponders	2	1	2	12	20	20-30	—
No. of Telepho Circuits	240*	240	1200	4000	6000	12000 + 2 TV	—
Design Lifetime (Yr)	1.5	3	5	7	7	7/10**	—

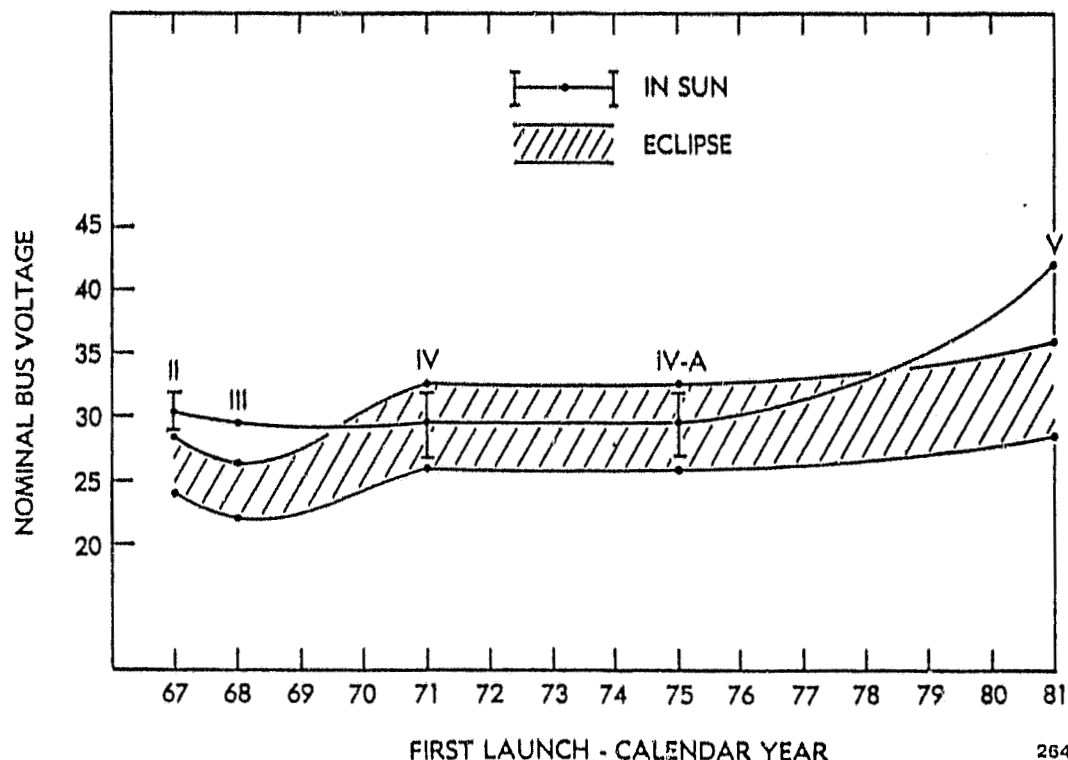
\*No multiple access.

\*\*Incentive 7 years; design 10 years.



264.352-176

Figure 3-41. Primary Power Distribution in a Typical Communications Spacecraft



264.352-177

Figure 3-42. Nominal Bus Voltage Trends for Intelsat Spacecraft

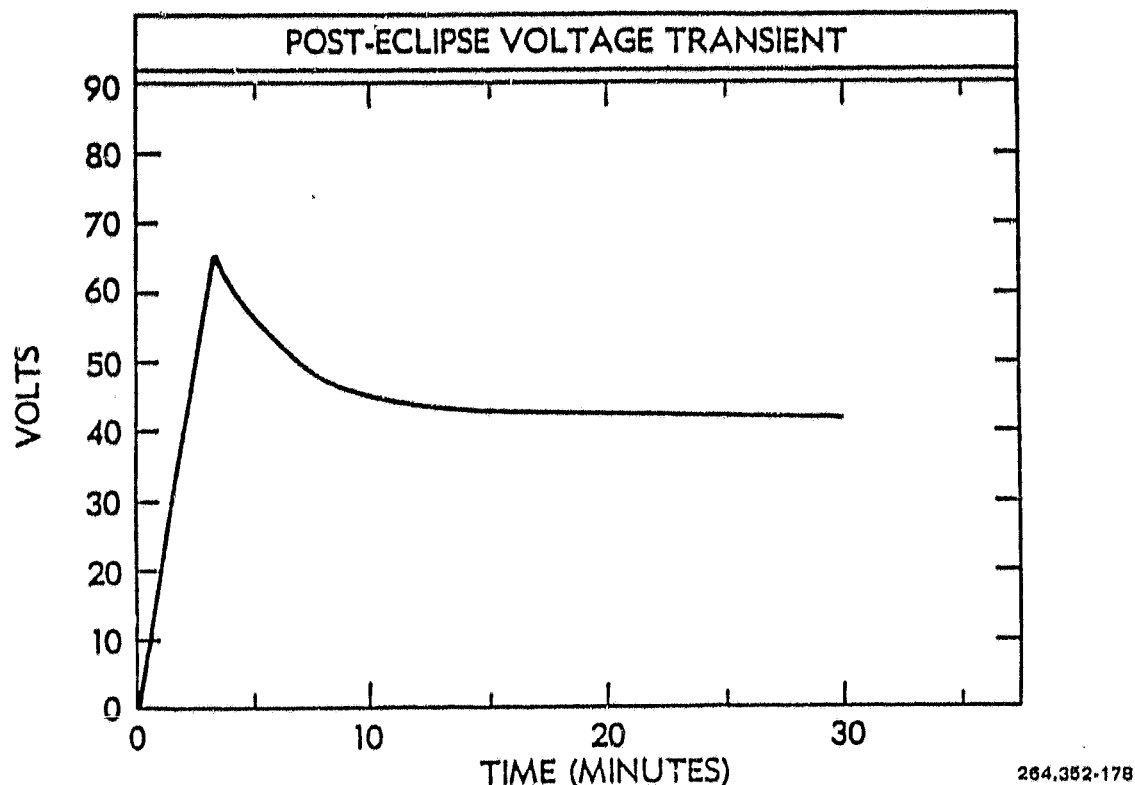


Figure 3-43. Typical Solar Array Post-Eclipse Transient

A secondary factor in the selection of bus voltage levels is the availability of battery cells in a suitable ampere-hour size. Once the eclipse power load on a given bus is determined and a maximum depth of discharge in the longest eclipse (72 minutes) is specified, a selection of the number of cells in series determines the cell ampere-hour capacity. This can be expressed in an energy balance equation as follows:

$$\begin{aligned}
 \text{Eclipse time} \times \text{load watts} &= \text{number of series cells} \\
 &\quad \times \text{cell discharge voltage} \\
 &\quad \times \text{percent DOD} \times \text{cell amp-hrs}
 \end{aligned}$$

$$1.2 P_L = n \times 1.2V \times \text{Percent DOD} \times \text{CAP}$$

Simplifying this expression, it becomes:

$$P_L = n \times \text{Percent DOD} \times \text{CAP}$$

With the eclipse load and maximum depth of discharge as given quantities, a selection of the bus voltage during discharge (approximately  $n \times 1.2V$ ) determines the cell capacity that is required. In the Ni-Cd cells, if this comes out to be a size that has not been previously built and flown, a new cell will

have to be designed and qualified. Since this is expensive, time consuming, and certainly not risk-free, the bus voltage is often changed slightly to move to an available size.

If Ni-H<sub>2</sub> cells are used and the capacity is much below 50 A-hr, the computer studies have shown that the cell energy density begins to decrease rapidly. In this case, it may be desirable to decrease the bus voltage or combine several loads so as to move to a larger cell size.

Multiple Bus Considerations. In a high-capacity communications satellite, the design must be arranged so that failures will cause it to "degrade gracefully" rather than to fail catastrophically. Within the power system, one concept that has been promulgated and implemented successfully in a number of domestic and international communications spacecraft is the multiple primary bus concept.

First of all, a "protected bus concept" is used; no single discrete component failure within the power system can short the bus to ground, and all external loads are isolated with fuses or current limiters. The analogue to the approach taken in the design of large-scale terrestrial power distribution systems is seen in the latter guideline.

The multiple bus concept goes beyond this to provide additional protection in several ways. Firstly, the division of the spacecraft into two or more major sections with independent power supplies and their associated loads protects against the unlikely but possible fault in a main bus connector, standoff, wire insulation or other "passive" component. An example of this type of failure was the loss of Seasat due to a short from the single primary bus to ground in the slip ring assembly after 100 days in orbit. The multiple bus type of power system is designed to survive this type of difficulty, retaining a sizable portion of its communications capability following such an event.

This multiple bus concept can be implemented in a number of ways. In some cases, it is convenient to simply split the primary loads into two equal portions and then build two identical power systems, each supporting half the spacecraft load. This has been done on several designs for operational series of spacecraft, including Intelsat IV and IV-A COMSTAR, and Intelsat V. The Intelsat IV and Intelsat V power system diagrams are shown in Figures 3-44 and 3-45 to demonstrate this type of configuration. In each of these, a key design feature is the employment of separate command and telemetry systems on each bus that can control and monitor all portions of the spacecraft. Thus, if one bus goes down, the full T&C capability is available for failure diagnosis and command into appropriate work-around modes.

Loss of one bus in a two-bus spacecraft early in the mission would not necessarily mean loss of half of its communications capacity. At this early stage, the remaining solar array may have 20 to 30 percent more than its EOL power available, plus whatever power margin was built in to cover uncertainties in design, manufacture, and environmental effects. In some cases, this is 10

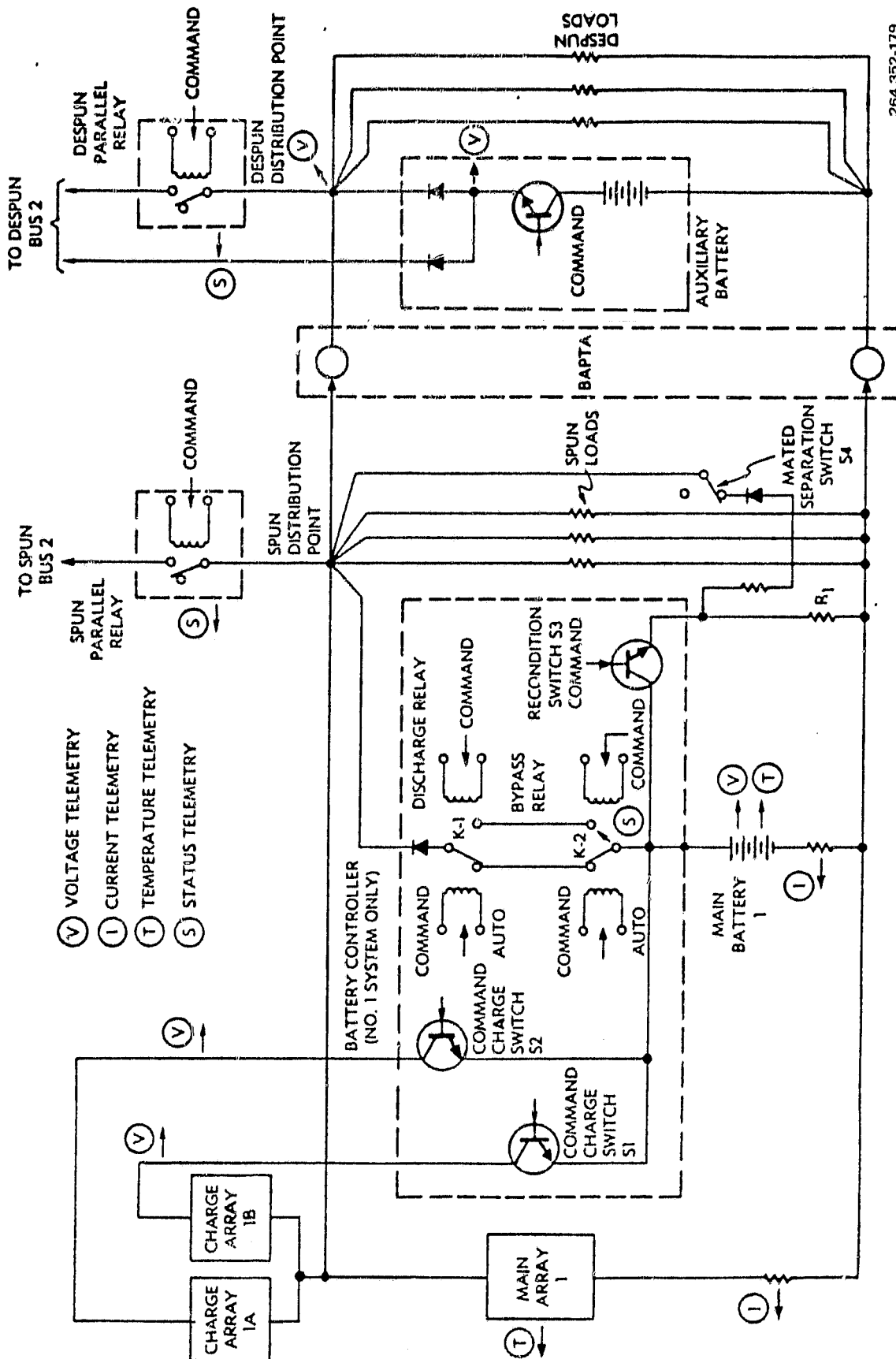


Figure 3-44. Intelsat IV Electrical Power System Diagram

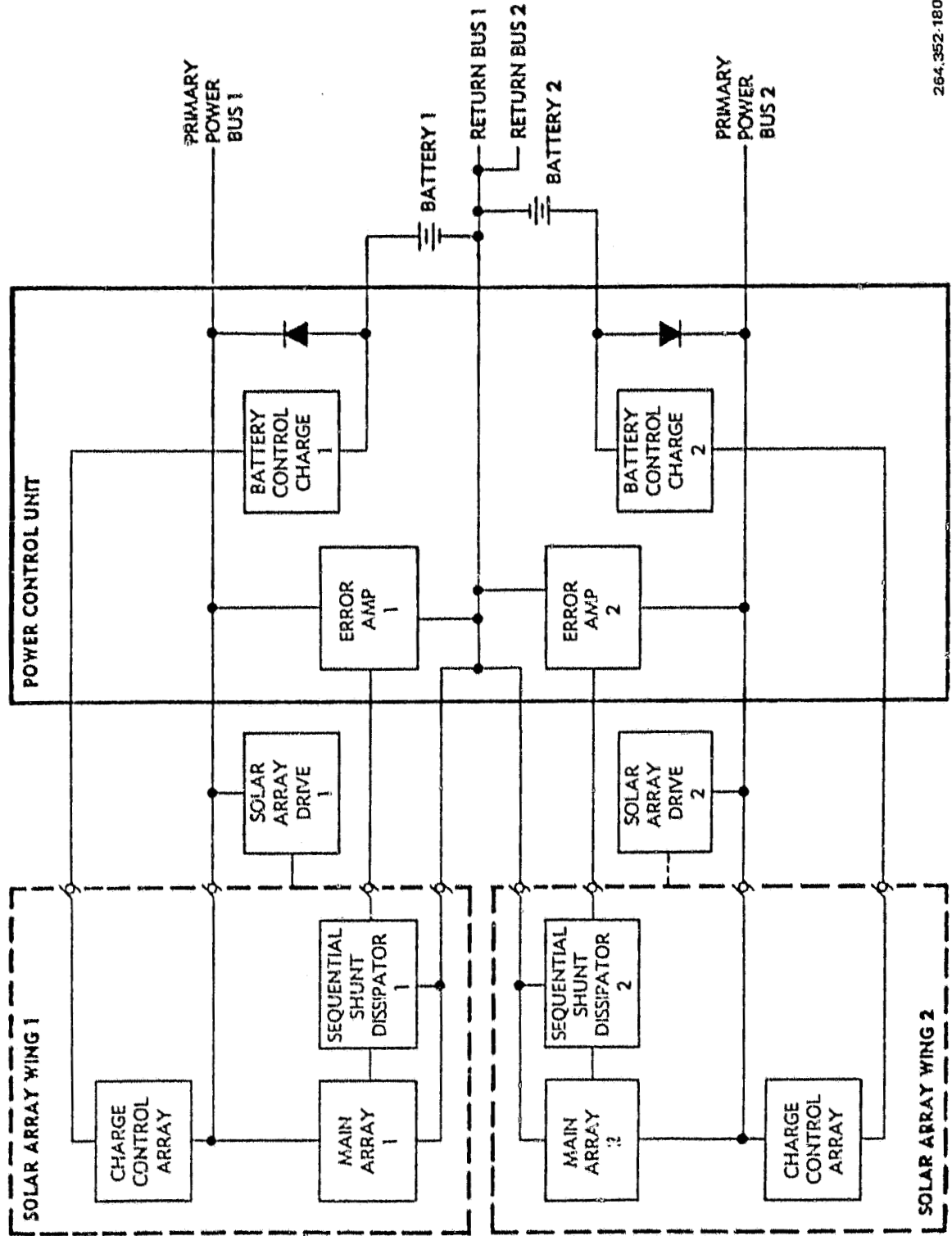


Figure 3-45. Simplified Power System Diagram - Intelsat V

percent of the initial array power leading to a maximum of 30 to 40 percent additional power early in life. Also, the batteries can typically be operated at greater DOD during eclipse at some sacrifice in life.

However, a key question is whether the communications load can be configured to utilize this additional power. This is closely intertwined with the way that the output TWT or solid-state amplifier redundancy is implemented, since in many designs the output amplifiers are set up in narrow bands side by side in the frequency spectrum. Clearly one cannot substitute tube K for tube A simply because it is convenient for the power system engineer.

One frequently considered scheme in a dual bus system is to provide a double-pole switch at each of these amplifiers so that it can be powered from either of the two buses. This appears to be an eminently straightforward design, but in actuality it requires a very detailed investigation of the circuitry and the components to ensure that the bus integrity is not compromised. For instance, a very careful examination of the switching relays is needed to ensure that an insulation fault or some type of armature malfunction cannot result in the two buses being connected together.

Topologies for Larger Systems. Another basic conceptual approach that can be taken in designing the electric power system is to plan to use two or more main buses for the principal communications and housekeeping loads, and provide a separate highly protected essential bus to supply the command, or command and telemetry systems. The power for these can also be or'ed off a main bus to make the T&C power redundant. This type of design has been used on a number of U.S. and European spacecraft, and is analogous to the aircraft system concept of a separate essential bus for primary flight instruments used in almost all commercial airliners today.

One possible implementation is shown in Figure 3-46. Here, the command system and telemetry system are powered by a separate small solar array. The voltage in sun is higher than the main bus, back biasing the or'ing diodes, causing the command and telemetry to draw all of their power from the essential bus solar array. The zener diode is used to limit the maximum voltage when the array reenters sunlight following an eclipse. During the one percent of the mission time that the spacecraft is in eclipse, this scheme would use current provided from the main batteries to power the T&C. Presuming that a duplicate system is connected to main bus 2, these functions would be operational in eclipse even with one battery failed.

In supplying this multibus type of design to larger spacecraft, it is easy to conceive of a power system with three, four, or even more primary power buses. This decision will be based on several practical considerations, including the size of the communications load increments, the capacity of available battery cells, and the amount of compartmentation desired to limit the impact of a bus fault.

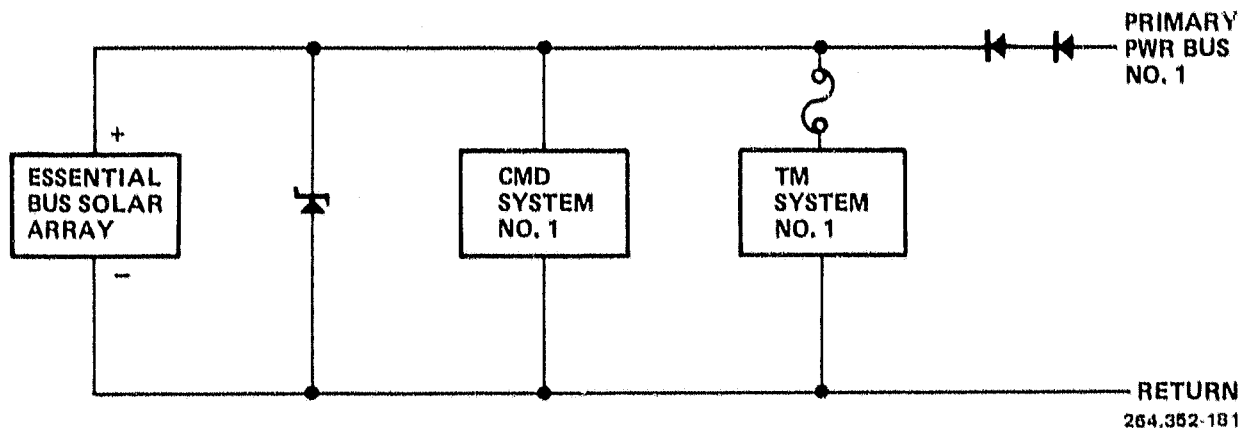


Figure 3-46. Essential Bus Supply for Command and Telemetry Systems

Summary of Power System Design Ground Rules. In the course of developing a number of commercial communications spacecraft, several design concepts or ground rules for power systems have evolved that are now being implemented in ongoing programs. These are primarily aimed at providing a very high probability of uninterrupted service for the full mission lifetime. They have a secondary goal, almost equally important, of ensuring that, when the spacecraft finally loses some of its capability, it degrades "gracefully", shedding channels without interrupting the remaining operational channels, and giving adequate time for replacement by other spacecraft. Some of these concepts are as follows:

- a. Avoidance of catastrophic failure. The design shall be arranged so that no single component failure shall compromise full mission operation. This stems from the standard reliability considerations, but is especially important in any permanently connected portion of the primary power bus.
- b. Protected bus concept. All power system loads must be designed to unload the main bus in case of a fault. This is arranged by means of overcurrent shutdown, fusing, or use of fusible components such as fusible resistors. In the latter two cases, it is essential to provide sufficient source current from the batteries to open the fusible component rapidly.
- c. Multiple main buses. Whenever the design permits, the loads are grouped so that several completely independent primary buses can be used, each with its own separate solar generator and battery. The primary bus circuits must have redundant wiring.
- d. Essential bus for critical functions. The command receiver with associated power switching and sometimes certain essential telemetry and attitude control functions are operated from a low-current bus that can draw power from several sources.
- e. Defined unloading sequence. The undervoltage shutdown levels are selected to shed communications loads in a defined sequence to unload the bus. Essential housekeeping functions are retained at much lower voltages, with the command system still functioning after all other loads are dropped off the bus.

- f. Automation at the earth end of the command and sensing links. When there is an even choice between hardware automation of sensing and power control functions in the spacecraft and software implementation at the earth station, the latter is preferable to gain simplicity and associated reliability in the spacecraft.
- g. Load contingency planning. In the design phase a load growth margin of 5 to 10 percent is carried for new equipment, tapering to 0 as all final flight hardware power requirements become measured values.
- h. Adequate primary power sizing to provide the required end-of-mission power with high confidence. The design includes an allowance to account for component and process variations, measurement errors, and variability in long-term degradation estimates. Statistical probability analysis shows that this is typically 5 to 10 percent above the nominal end-of-mission power for  $3\sigma$  confidence with contemporary solar array designs.
- i. Reliability approach. A combined random failure and wear-out life analysis, tempered by previous experience, is used to evaluate power system designs. As mentioned earlier, the wear-out life aspect is particularly significant in the case of batteries. Of course, the usual flight-approved, high-reliability burned-in components are used, and the equipment is put through a bench burn-in test, coupled with realistic environmental testing.

AC Bus Considerations. There is a possibility of using an AC power distribution rather than the conventional DC power distribution system for these spacecraft. Undoubtedly, when spacecraft power systems become very large, the advantages of low-loss transmission of high power with high voltage AC will assert themselves. In the meantime, one of the key questions is at what power level this change to AC distribution systems will take place.

In the existing microwave relay satellites, almost all of the communications load power is converted to square wave AC. Some 82 percent of the power in a typical spacecraft of this type feeds into the traveling wave tube electronic power conditioners (EPCs), as shown in Figure 3-41. This current flows into the EPC and is chopped to square wave AC with a typical frequency of 10 to 20 kHz. This is fed into the primary of a transformer, which produces the high voltage outputs that are rectified and filtered to end up with the high voltage DC needed at the TWT. The overall efficiency of this DC-DC conversion process is presently very close to 90 percent.

From a simplified theoretical perspective, the major portion of the spacecraft power could be distributed at low voltage DC, low voltage AC, high voltage AC, or high voltage DC, depending on where one elects to fan out from the main power system to the individual load boxes. For the AC distribution systems, the subsets of square wave, sine wave, and multiphase systems are possibilities that could be examined.

All of the existing commercial communications spacecraft perform the power distribution function at low voltage DC. A number of studies have addressed the relative advantages and problems of using low voltage AC distribution. These include work done for Intelsat (Reference 47), the West German GfW (Reference 48), and several European Space Agency (ESA) funded studies (Reference 49 through 51). The latter are continuing, and it is also understood that an ESA study is presently underway at British Aircraft Corporation.

The early work by AEG/Telefunken reported in Reference 48 describes development of a 1.5 kW sine wave inverter. Paralleling of square wave inverters on the main bus has some problems since slight phase differences can cause overloading due to equalizing currents flowing between them, while sine wave inverters are inherently more tolerant of this condition. The Dornier paper, Reference 49, brings out the point that only a very small portion of the load in these spacecraft consists of linear loads and that in cases where the output rectifiers are operating at low duty cycle (i.e., in the peak detection mode), the sine wave will produce more noise than a square wave distribution system.

The AC bus concept was developed further, as reported in Reference 50. The focus of this effort was development of a composite 2-kW square-wave inverter built up from modules to provide one-in-four redundancy. A common oscillator clocks the four modules, and the four outputs are in series so that all the inverters will have identical currents. Each 700W module consists of a biphase input switch feeding a current driven transistor bridge circuit operating at 20 kHz.

Most communications spacecraft power system studies so far highlight several key areas related to the AC bus power distribution concept. These are:

- a. Electromagnetic interference effects (EMI).
- b. Reliability impact.
- c. Mass tradeoffs.
- d. Load switching.

The EMI effects of using square-wave AC bus power is a multifaceted subject of important consideration on communications spacecraft. The conducted interference (EMC) portion is quite straightforward and consists of defining a bus noise spectrum and then designing each black box to operate suitably in the presence of this input.

The radiated and magnetically induced portions of the problem are more difficult to pin down. The radiated noise is generated by peak voltage changes at a source ( $V_{p-p}$ ) and the amount of noise picked up is governed by capacitance effects, or said another way, by radiant transmission theory. Obviously, the amplitude of the driving voltage, and the length, orientation, and characteristic impedance of the receiving element determines the amount of noise received. With a given amplitude of the AC bus voltage, the amount of noise

received. With a given amplitude of the AC bus voltage, the amount of noise coupled to other conductors by this mode is dependent on the impedance of the receiving line, and large noise voltage spikes can be produced in high impedance signal and data lines. One typical approach for controlling the capacitive coupling of AC bus noise is by a coaxial shielding of the control and data lines.

Looking at the other aspect, the magnetically-induced noise is generated by current changes at a source ( $dI/dt$ ) and can be considered a transformer effect. The voltage induced in a secondary conductor depends directly on the rate at which lines of magnetic flux cut it. Since the magnetic lines are further apart at a distance from the primary conductor, the rate at which they cut the secondary will be lower. Thus, the noise voltage induced in the secondary will be a function of the configuration and spacing of the two conductors and the rise time of the bus current waveform. The induced waveform will consist of spikes occurring whenever the polarity of the bus current is reversed. The amount of current magnetically coupled into a secondary conductor increases as the load impedance as its output decreases. Thus, the alternating bus current will tend to induce noise spikes in other low impedance bus lines. One common approach for controlling the magnetic coupling is to minimize the net magnetic field by twisting the AC bus feed and return lines together. Since the currents are flowing in opposite directions, the magnetic fields around the wires tend to cancel each other. This prevents the use of the spacecraft structure as a ground return.

Some tests of AC bus noise control were carried out during the course of the ESA funded investigations. Initial tests with twisted pair AC bus and coaxial signal leads showed negligible noise pickup (Reference 49). Later tests were to be carried out with an AC power harness routed through the Helios spacecraft. More recently, the SBS communications spacecraft is being successfully implemented with a power system design that can continuously draw low frequency repetitive current pulses as large as 3A from its 30 Vdc main buses. Although this is not an AC bus system per se, it does have a sizable AC current component riding on the 12A nominal DC drain.

The spacecraft reliability impact of changing from a number of smaller inverters at each load to one centralized inverter can be largely alleviated by going to some type of modularized inverter with automatic redundancy of the type described in Reference 50.

In regard to the issue of saving mass by changing to an AC bus, most power system studies so far (Reference 47) have found that in the 1- to 10-kW range, no significant mass advantage can be gained in changing to the AC bus. This is largely because the mass of the inverters of conventional design appears to be reasonably linear with power level, and the mass of one large inverter, including redundancy, comes out to be nearly the same as the total mass of a number of smaller inverters placed at each load.

Advanced devices and techniques are becoming available that will reduce inverter mass. For example, the advent of high-power, high-voltage power FET devices suitable for space application will allow inverter frequency to be

significantly increased, resulting in a decrease in the mass of the heavy inductive and capacitive components. This would not seem to change the one versus many inverter trade discussed above.

However, monolithic high voltage solar cells are under development (Reference 51) by NASA, and an on-chip sine wave inverter has been proposed (Reference 52). An unconventional inverter design of this type offers the possibility of source redundancy and mass reductions that could make the spacecraft AC bus more attractive at the 1- to 10-kW level in the future.

The problems of power load switching at high voltage and high current have a bearing on the AC versus DC bus selection. Magnetic latching relays are conventionally used to perform the command switching functions in most of the present spacecraft. Larger, higher current versions can be obtained as the power requirements increase. However, when the voltage gets up to the vicinity of several hundred volts DC or more, it becomes difficult to interrupt the load since circuit inductance results in high voltages, which can cause avalanche breakdown and ionization of molecules in the arc. Both magnetic blowout and gas jet extinguishment are used in high power switchgear, but these techniques have not been generally applied in the devices of interest here. Of course, vacuum relays could be used but they are large, bulky, and not noted for reliability. Transistor switches are limited to similar voltage levels by their collector to emitter breakdown characteristics.

The AC bus switching is considerably easier. Relays are available that are quite capable of handling voltages and currents in the range up to 500V and up to 50A or more at 60 Hz. However, frequency and voltage waveform of the AC source can be important. Immediately after the current through an arc is interrupted in the switching process, the gas is hot and ionized. It takes some time for the gas to cool and regain its dielectric strength. The time to 50 percent dielectric recovery has been measured (Reference 53) as 50 to 60 ms for 50 Hz sine wave, and as small as 3 ms after short duration arcs lasting 20 - 2000 ms. Thus, the rise time of the AC bus square wave might have an effect on relay switching performance.

SCR and TRIAC solid-state switches are well-developed and appear quite attractive for switching AC main power loads. Devices are available with breakdown voltages up to 1200V or so, and currents of hundreds of amperes. The satisfactory operation of this type of switch is frequency-dependent for two reasons. First, rapid changes in applied voltage can cause spurious turn-on of this type of switch (Reference 54). Typical values of the maximum allowable rate of change of bus voltage lie in the range of 10 to 200 V/ $\mu$ s. Using the best value of this parameter and a 1-percent transition time for the square-wave results in a maximum AC frequency of 5 kHz. Lengthening the rise time of the square wave at the expense of some additional losses could extend the frequency capability of the system. The second SCR device limitation is the turnoff time, which must be less than 1/2 cycle. With typical turnoff times ranging from 10 to 60  $\mu$ s, the best devices are limited to about 50 kHz.

### 3.1.5.4 EPS GP Alternative #1.

Power Requirements GP Alternative #1. The power requirements for GP Alternative #1 are tabulated in Table 3-22. It allows for a 5 percent load contingency factor, and a 10 percent solar array design margin, in addition to the estimated array degradation to allow for measurement uncertainties, micrometeorite damage, excessive UV darkening, and greater than anticipated solar flare activity. Platforms 1 through 3 and 5 have the array EOL based on 16 years since the load requirements essentially continue for the full duration. Platforms 4 and 6 use the two year solar array EOL since substantial unloading occurs at that time for the remainder of the mission. The energy storage requirements are based on full load power for the maximum eclipse duration of 1.16 hours.

Solar Arrays GP Alternative #1. The solar array power requirements, array area, reflector area, number of solar cells, and estimated weight are tabulated in Table 3-23. For Platforms 1 through 3, thin silicon solar cells with an efficiency of 13.5 percent and a 16 year degradation of 23 percent are postulated. For Platforms 4 through 6, concentration arrays utilizing Ga-Al-As cells with 13.4 percent efficiency at 125C and only 5 percent degradation in 16 years with self annealing are used. The array construction is SEPS requiring either retraction during thrusting or a low thrust orbital transfer vehicle. Large area solar cells are used since array production cost is a strong function of cell size, and cell cost is not so heavily influenced by cell size. Since it is difficult to predict cell and array characteristics some 12 to 16 years in advance of use, this solar array sizing is given as an indication of actual realization.

Energy Storage GP Alternative #1. The weights of a Ni-H<sub>2</sub> battery system, charge discharge thermal losses, DOD, and reserve capacity are listed in Table 3-24. A 72-cell battery consisting of three 24-cell packs in series for a 80 to 100 Vdc battery voltage is used. The number of batteries is 4 with 35 A-hr cells for Platforms 1 and 4, and 50 A-hr cells for the other platforms. Cell bypass electronics are used so the reserve capacity can be used for bad cell loss without requiring redundant batteries. A higher DOD is used in later platforms as space usage experience and manufacturing experience is accumulated.

Electronics EPS GP Alternative #1. A typical sizing of the power electronics for GP Alternative #1 is presented in Table 3-25. For purposes of sizing, an unregulated DC bus system was assumed with an array voltage of 100-115 Vdc, a battery voltage of 80-100 Vdc, and a distribution bus voltage of 80-115 Vdc. Section 3.1.5.3 discusses AC and DC power distribution. For larger systems, an AC system is preferable. For small platforms as in Alternative #1, a DC system may be preferable because of the experience factor. If the small platform is a precursor of larger follow-on platforms, than an AC system should be used on the small platform in order to gain space operating experience for application to the larger platform. The sizing is based on 4 array buses, 4 battery chargers each with 2 array bus input and redundancy for reliability, a microprocessor implemented battery controller with internal redundancy,

Table 3-22 . Geostationary Platform Alternative #1 Power Requirements

	Platform 1	Platform 2	Platform 3	
Communications and Science Payload				
2.1 HVT C-Band	700W	1.1 DTU Ku-Band	6,500W	4 Tracking and Data Relay
3 TV Distribution	4,000	7 Air Mobile	1,200	5 Educational TV
11 Interplatform Link	300	11 Interplatform Link	300	9 Land Mobile
31 DNSP Data Relay	100	27 RF Interferometer	220	11 Interplatform Link
				300
				12 Data Collection
				18 Atmospheric Sounder
				50
				52 Boss Evaluation
				400
				55 DoD Laser Command
				Experiment
				550
BOL Total	5,100W	8,220W		6,480W
2 Year and 16 Year EOL	5,125W	8,000W		5,480W
Platform Systems				
ACS and S-K	209W	209W		209W
TT&C	297W	297W		297W
Load Contingency	282W	425W		299W
16 Year EOL Total	5,888W	16 Year EOL Total	3,931W	16 Year EOL Total
Power Losses and Storage				
Distribution Loss	87W	134W		94W
Battery Charge	559W	845W		594W
Conditioned/Regulated				
Loss	524W	792W		557W
16 Year EOL Total	7,058W	16 Year EOL Total	10,702W	16 Year EOL Total
Array Design Margin	705W	1,070W		753W
Array EOL Power	7,763W	11,772W		8,283W
Energy Storage	8,210W-Hr	11,748W-Hr		9,401W-Hr

Table 3-22. Geostationary Platform Alternative #1 Power Requirements, Contd

	Platform 4	Platform 5	Platform 6	
<b>Communications and Science Payload</b>				
2.2 HVT Ka-Band	3,200W	1.2 DTU Ka-Band	5,700W	1.2 DTU Ka-Band
11 Interplatform Link	300	6 Direct to Home TV	2,100	11 Interplatform Link
17 Lightning Mapper	300	11 Interplatform Link	300	19 Visual and IR
33 Materials Exposure	25	20 Microwave Radio-		Radiometer
38 Aerosol and Cloud Height Sensor	100	meter	150	54 EHF System
42 Global LIV Radiance	20	32 Advanced OLS Cloud Imager	150	
43 Magnetic Substorm Monitor	5			
56 Fiber Optics Demonstration	30			
71 Earth Optical Tele	<u>2,000</u>			
BOL Total	5,980W		8,400W	6,600W
2 Year and 16 Year EOL	3,500W		8,100W	6,000W
<b>Platform Systems</b>				
ACS and S-K	209W		209W	209W
TT&C	297W		297W	297W
Load Contingency	<u>253W</u>		430W	353W
2 Year Total	6,739W	16 Year EOL Total	9,036W	2 Year Total
				<u>7,461W</u>
<b>Power Losses and Storage</b>				
Distribution Loss	80W		136W	112W
Battery Charge	503W		855W	706W
Conditioned/Regulated Loss	<u>425W</u>		723W	597W
2 Year Power	7,747W	16 Year EOL Power	10,750W	2 Year Power
				<u>8,876W</u>
Array Design Margin	<u>775W</u>		<u>1,075W</u>	<u>888W</u>
Array 2 Year Power	8,522W	Array 16 Year EOL	11,825W	Array 2 Year Power
				<u>9,764W</u>
Energy Storage	8,403W-Hr		11,906W-Hr	9,477W-Hr

Table 3-23. Solar Array Sizing Using Advanced SEPS and Concentrator Technology GP Alternative #1

GP	Required BOL Power		No. 5x5 Solar Cells	Concentration Ratio	Array Area m <sup>2</sup>	Reflector Area m <sup>2</sup>	Arrays and SADA Wt. (without Shadow Clearance Structure)		Solar Cell Type
	BOL Power	Solar Cells					Area m <sup>2</sup>	Wt.	
1	10.48 kW	10.72 kW	22,595	1	61.57	0	105.70	kg	THIN SI
2	15.65 kW	16.07 kW	33,893	1	92.36	0	140.55	kg	THIN SI
3	11.12 kW	11.25 kW	23,724	1	64.65	0	109.59	kg	THIN SI
4	9.12 kW	9.45 kW	11,297	2	30.79	61.58	82.23	kg	GA-AL-AS
5	12.83 kW	13.23 kW	15,816	2	43.10	86.20	94.81	kg	GA-AL-AS
6	10.32 kW	10.39 kW	12,426	2	33.86	67.72	81.93	kg	GA-AL-AS

Table 3-24. Battery Storage Sizing with Ni-H<sub>2</sub> Cells GP Alternative #1

Year	Energy Storage Capacity Required W-hr	Energy Storage Capacity Baseline W-hr	Reserve Capacity* (percent)	DOD (percent)	Weight** (kg)	Thermal Losses W Charge	Thermal Losses W Discharge
1992	8,444	9,828	16.5	75	334	121	1,902
1993	11,999	14,040	17.0	75	455	168	2,643
1994	9,593	14,040	46.4	75	455	132	2,077
1996	7,072	9,828	48.2	80	334	102	1,599
1997	12,241	14,040	22.3	80	455	175	2,755
1998	9,822	14,040	52.5	80	455	142	2,230

\*Determined by the number of batteries.

\*\*Does not include weight of structure for mounting batteries (fixed or replenishable), or weight of thermal control.

Table 3-25. Equipment List GP Alternative #1

	1	2	3	4	5	6		
	Qty	Wt (kg)	Qty	Wt (kg)	Qty	Wt (kg)	Qty	Wt (kg)
Solar Array - ULP (Technology) (SEPS)	2	112.4 (105.7)	2	149.1 (140.6)	2	117.0 (109.6)	2	119.2 ( 82.2)
Battery	4	334.0	4	455.0	4	455.0	4	455.0
Battery Charger, Redundancy	4	36.0	4	36.0	4	36.0	4	36.0
Battery Monitor and Control, Redundancy	1	7.0	1	7.0	1	7.0	1	7.0
Power Switching Redundancy	2	16.2	2	16.2	2	16.2	2	16.2
Drive Electrics Dual	2	10.0	2	10.0	2	10.0	2	10.0
Load Converter/Regulator High Power, Redundancy (to be supplied by payloads)	2	22.0	2	22.0	2	22.0	2	22.0
Load Converter/Regulator Medium Power, Redundancy (to be supplied by payloads)	4	16.0	4	16.0	5	20.0	7	28.0
Power Conductors Dual		26.0		33.0		30.0		35.0
Power Control Unit Redundancy	1	7.0 (579.9)	1	7.0 (742.8)	1	7.0 (712.8)	1	7.0 (671.4)
Total		586.6		751.3		720.2		708.4
								754.6
								697.7

Excludes array shadowing clearance structure, thermal mounting surfaces, and thermal radiators.

dual drive electronics for dual drive motors for each SADA, power switching with backup modes and redundancy, a corresponding microprocessor implemented power controller with internal redundancy and the load converter/regulations with internal redundancy. The load converter/regulators are sized but would be provided by the payload suppliers. A dual bus system is used, with a third bus for critical platform subsystem loads (ACS, etc.). A contingency factor in the order of 5 percent is not included but should be added for miscellaneous connectors, status monitoring wiring, etc. For internal redundancy a weight increment of +29 percent was used above a nonredundant unit.

### 3.1.5.5 EPS GP Alternative #4.

Power Requirements GP Alternative #4. The power requirements for GP Alternative #4 are listed in Table 3-26. The same contingency factors are used as in Alternative #1. A 6 year EOL array is used since the scientific experiment power requirements for Module 3 will gradually diminish from the 6th to the 16th year. Since the modules are docked, TC&C and TCS power are required only on Module 1. The prime energy storage is on Module 1. Modules 2 and 3 require power in the order of 660 watts for 24 hours prior to docking with Module 1. This is shown as being supplied by energy storage. A trade needs to be made of solar array versus short life battery storage for this short term power requirement.

Solar Arrays GP Alternative #4. A SEPS derived array was utilized consisting of two wings mounted on two SADA with three 4 meter by 46 meter arrays per wing. The silicon cell technology of Section 3.1.5.4 was used to arrive at the array configuration in Table 3-27.

Energy Storage GP Alternative #4. A Ni-H<sub>2</sub> battery system with 75 percent DOD and a battery voltage of 264-336 Vdc with ten 24 cell packs in series for each battery and twelve batteries total was sized for Module 1 as tabulated in Table 3-27.

Electronics EPS GP Alternative #4. The electronics are listed in Table 3-27. The system configuration is given in Figure 3-47 and 3-48. Advantages of the AC system are:

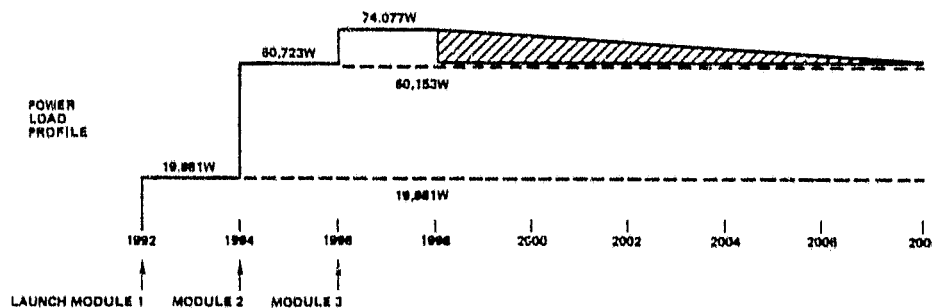
- a. Reduced switching noise.
- b. Simple power system isolation.
- c. High degree of flexibility.
- d. Noncontact power transfer across docking interfaces.
- e. Lower weight payload AC/DC and AC/AC converters as opposed to DC/DC and DC/AC payload converters for a DC system.
- f. Regulated AC provided by the DC/AC converters.

Table 3-26. Geostationary Platform Alternative #4 Power Requirements

Module 1	Module 2	Module 3	
1.1 GPS Ku Band	13,000W	1.2 DTU Ka Band	28,000W
2.1 HVT C Band	1,200	2.2 HVT Ka Band	3,000
9 Land Mobile	4,000	3 TV Distribution	4,000
11 Intersatellite Links	300	4 Tracking and Data Relay	680
BOL Total	18,500W	5 Educational TV	400
		6 Direct to Home TV	2,500
		7 Air Mobile	1,200
		12 Data Collection	100
		17 Lightning Mapper	300
		18 Atmospheric Sounder	50
		27 RF Interferometer	220
		31 DNSP Data Relay	100
		BOL Total	40,550W
		33 Materials Exposure/Unrecovered	25W
		34 ACOSS/HALO Demonstration	500
		36 Advanced Onboard Signal Processor	200
		39 Solar Flare Monitor	100
		40 Solar Flare Isotope Monitor	6
		41 Energetic Proton Heavy Ion Sensor	8
		43 Magnetic Substorm Monitor	5
		44 Charged Particle Monitor	10
		51 Cryogenic IR Radiator	-
		52 BOSS Evaluation	400
		53 GEMINI Evaluation	1,800
		54 EHF System	500
		55 Aircraft Laser Relay	550
		56 Fiber Optics Demonstration	30
		71 Optical Telescope	2,000
		73 Chemical Release Module	250
		78 Cryogenically Cooled Limb Scanner	6,000
		79 Low Light Television	1,000
		81 Microwave Sounder	250
		BOL Total	13,652W

PLATFORM SYSTEMS

ACS and S-K	216W	316W	316W
RCS	76W	76W	76W
TC&C	332W	--	--
TCS	757W	--	--
	19,881W	40,842W	13,924W



Total Load Power	74,077W
Load Contingency	3,704W
6 Year Total	77,781W

Power Losses and Storage

Distribution Loss	1,167W
Battery Charge	6,810W
Conditioner/Regulator Loss	6,222W
6 Year Power	91,980W
Array Design Margin	9,198W
Array 6 Year Power	101,178W
Energy Storage:	
Module 1	98,797 W-hr
Module 2	15,840 W-hr
Module 3	15,840 W-hr

Table 3-27. Alternative #4 EPS AC/DC Hybrid

LAUNCH DATE: 1992

COMPONENT SOA DATE: 1989

Solar Array

SEPS Derivative		
Maximum Power Load	78.52 kW	
Array BOL Power	108.82 kW	
Concentration Ratio	1	
Array Area	625 m <sup>2</sup>	
Number 5 × 5 cm Cells, SI	229,358	
Arrays and SADAs Weight without shadow clearance structure, retracted for transfer to GEO)	854 kg	

Battery

Ni-H <sub>2</sub> 75 percent DOD Technology		
Energy Storage Capacity Required	16 Yr	106.78 kW-hr
	6 Yr	125.09 kW-hr
Energy Storage Capacity		140.40 kW-hr
Reserve Capacity		12.2 percent
Number of Cells per Pack	24	
Number of Packs per Battery	10	
Number of Batteries	12	
Battery System Weight without thermal mounting structure and thermal radiator weights)	4502 kg	
Thermal Loss Discharge	21.56 kW	
Thermal Loss Charge	1.37 kW	

Electronics

Gimbal Drive's Electronics, 2 Redundant Units	15 kg
Battery Chargers 12 Units Redundancy	48 kg
Battery Controller Redundancy	15 kg
Power Switching Redundancy 6 Units (20, 18, 12)	50 kg
Power Controllers Redundancy 3 Units (10, 6, 6)	22 kg
DC/AC Converter/Regulator 10 kW Redundancy 7 Units (including 1 spare)	258 kg
DC/AC Converter/Regulator 5 kW Redundancy 3 Units	61 kg
Coupling Transformer 10 kVA 10 Units (including 2 spares)	77 kg
Power Conductors DC Buses	100 kg
Power Conductors AC Buses (15.6, 95.1, 2.4)	113 kg

Table 3-27. Alternative #4 EPS AC/DC Hybrid, Contd

Power Conductors Load Buses (2.7, 3.6, 4.6)	11 kg
Connectors, Etc.	15 kg
AC/DC Payload Converter/Regulator (payload supplied)	
AC/AC Payload Converter/Regulator (payload supplied)	
Bus/Converter Protection and Monitor Assembly	8 kg
Solar Array Monitor Assembly (2 units)	10 kg
Power Management Controller Redundancy	10 kg
Miscellaneous and Contingency	40 kg
	<hr/>
	853 kg
	<hr/>
EPS Total	6209 kg

- g. Freedom to select AC bus voltage for maximum system efficiency.
- h. Array and battery voltage can be optimized.
- i. High efficiency conversion.

In Table 3-28, a less conservative unregulated DC system is sized for GP Alternative #4. An array and battery voltage with roughly 2 times the AC/DC system corresponding voltages is used (Figure 3-49). This reduces the number of batteries and chargers by one-half. It also increases the array plasma losses and poses operation at a voltage with little experience.

The solar array and battery weights are comparable. The battery charger weights would be comparable for the same array and battery voltages. The unregulated DC system does not have DC/AC converter/regulation, but this is counterbalanced by lighter weight AC/DC - AC/AC payload converters compared to DC/DC - DC/AC payload converters. The payload converters operate from a regulated AC bus for the AC/DC hybrid system, and from an unregulated DC bus for the DC system.

In essence, the AC/DC hybrid system may weigh somewhat more than the unregulated DC system. The advantages of AC power over DC will usually offset the slight DC system weight advantage. Each application has to be examined in detail, with higher power systems definitely using AC transmission.

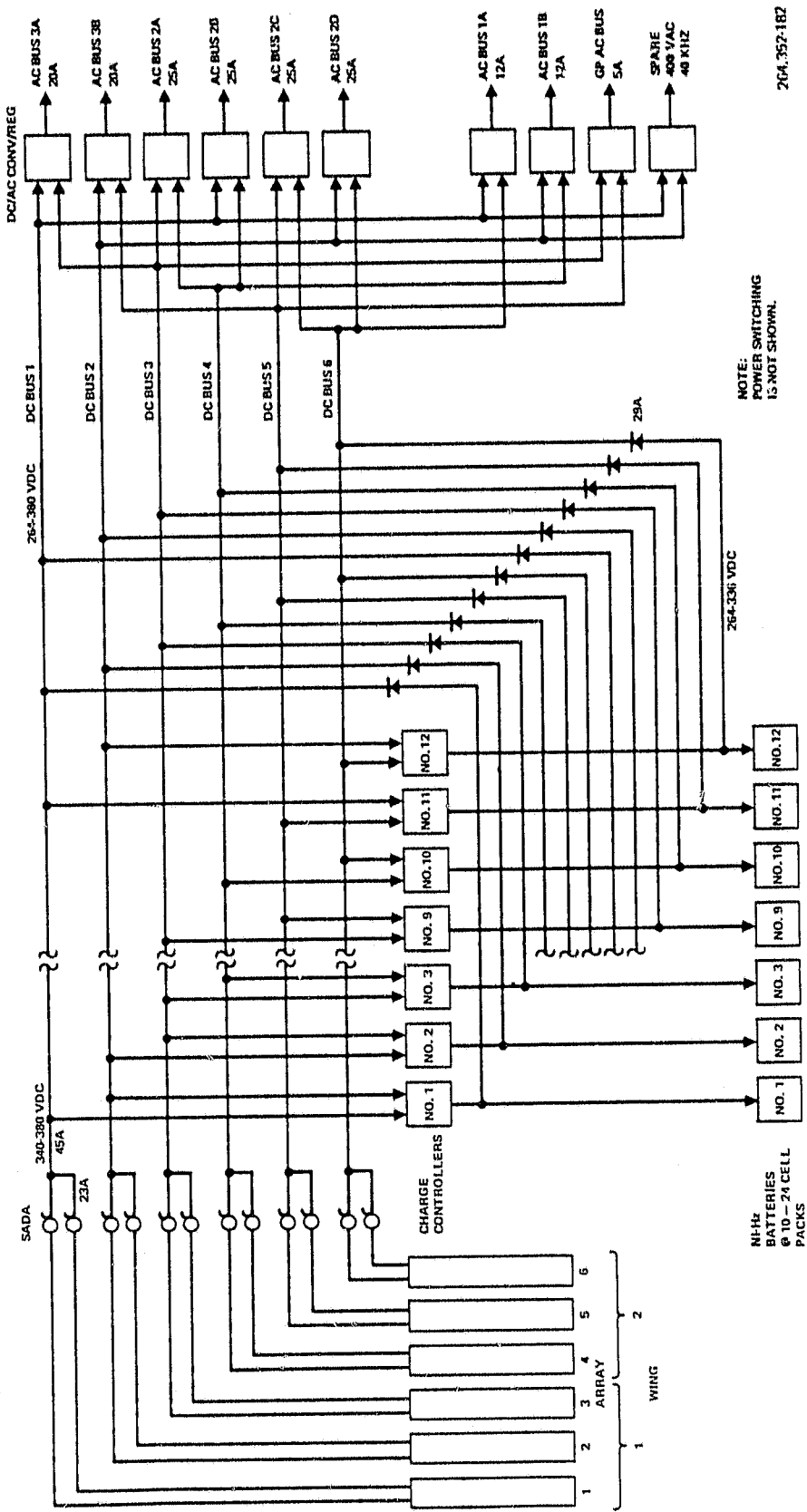


Figure 3-47. EPS DC Section GP Alternative #4 AC/DC Hybrid

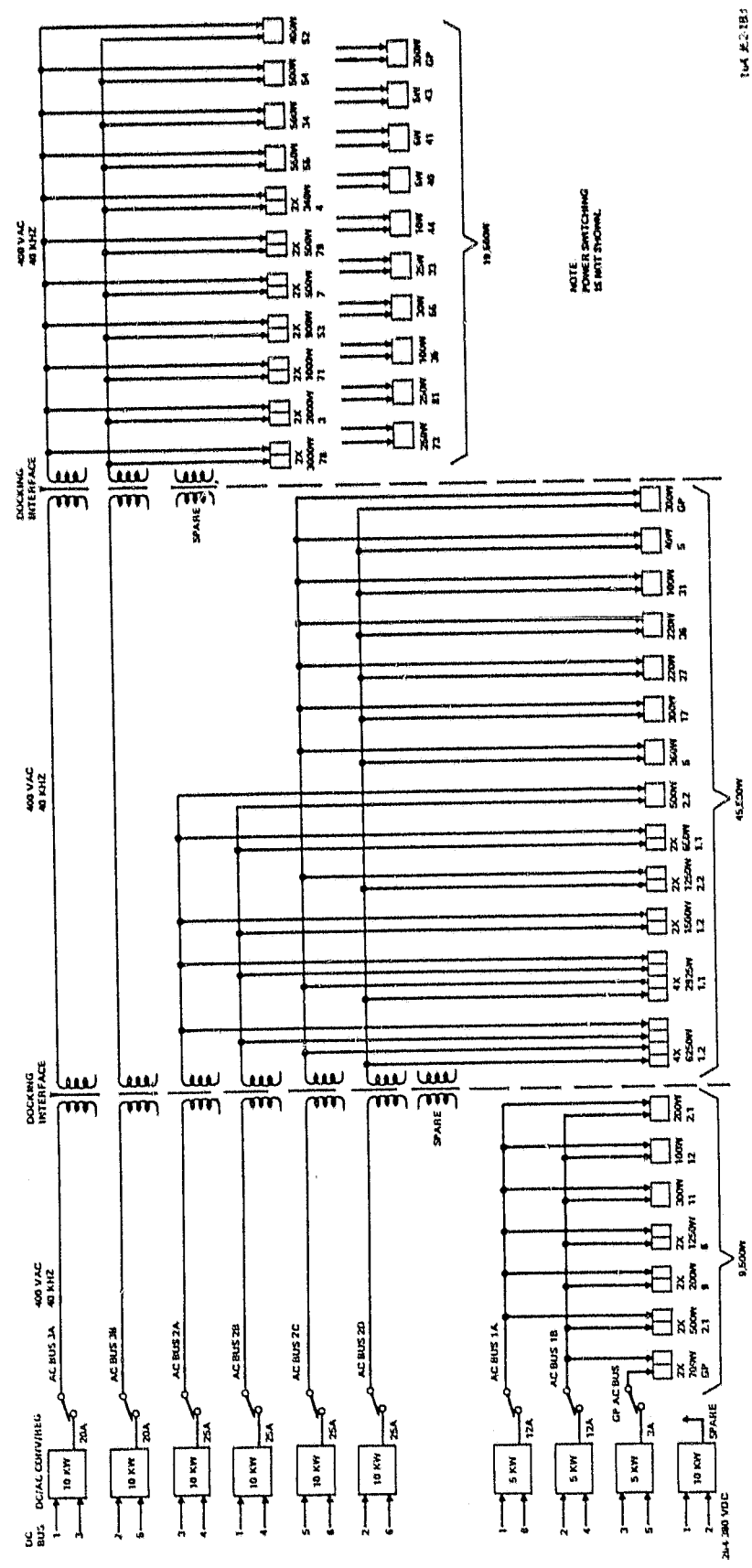


Figure 3-48. EPS AC Section GP Alternative #4 AC/DC Hybrid

Table 3-28. Alternative #4 EPS DC System

---

LAUNCH DATE: 1992  
COMPONENT SOA DATE: 1989

Solar Array

SEPS Derivative		
Maximum Power Load		78.52 kW
Array BOL Power (+0.5 percent LL, -20 percent CL, +0.5 percent LRL, -1.0 percent Net)		107.73 kW
Concentration Ratio	1	
Array Area	619 m <sup>2</sup>	
Number 5 × 5 cm Cells, SI	227,064	
Arrays and SADAs Weight (without shadow clearances structure, retracted for transfer to GEO)	854 kg	

Battery

Ni-H <sub>2</sub> 75 percent DOD Technology		
Energy Storage Capacity Required	16 Yr	105.71 kW-hr
	6 Yr	123.84 kW-hr
Energy Storage Capacity		140.40 kW-hr
Reserve Capacity		13.4 percent
Number of Cells per Pack	24	
Number of Batteries	6	
Battery System Weight without thermal mounting structure and thermal radiator weights)	4502 kg	
Thermal Loss Discharge	21.34 kW	
Thermal Loss Charge	1.36 kW	

Electronics

Gimbal Drive's Electronics, 2 Redundant Units	15 kg
Battery Chargers 6 Units Redundancy	30 kg
Battery Controller Redundancy	15 kg
Power Switching Redundancy 6 Units (20, 18, 12)	50 kg
Power Controllers Redundancy 3 Units (10, 6, 6)	22 kg
Docking Connectors Redundancy 2 Units	20 kg
Power Conductors DC Buses	
Arrays to Batteries	39.5 kg
Batteries to Module 1	4.9 kg
Batteries to Module 2	61.5 kg
Batteries to Module 3	24.2 kg

Table 3-28. Alternative #4 EPS DC System, Contd

Power Conductors Load Buses	11.0 kg
Connectors, Etc.	15.0 kg
DC/DC Payload Converter/Regulator (payload supplied)	
DC/AC Payload Converter/Regulator (payload supplied)	
Bus Protection and Monitor Assembly	80 kg
Solar Array Monitor Assembly (2 units)	10.0 kg
Power Management Controller Redundancy	10.0 kg
Miscellaneous and Contingency	40.0 kg
	<hr/>
	376.1 kg
	<hr/>
EPS Total	5372 kg

Power Management GP Alternative #4. The EPS power management is depicted in Figure 3-50. The EPS operates as a subsystem of the main GP control and data bus. The power management controller is the interface unit and the EPS supervisory controller. A fiber optic bus connects the microprocessor implemented elements of the EPS. Fiber optic couplers at the docking interfaces eliminate electrical contacts for this function. A rotary fiber optic joint is used for solar array monitor data transmission through the SADA. A form of this rotary joint is shown in Figure 3-51.

3.1.5.6 Research and Technology. A number of items need research and technology pursuit to achieve operational application. These include:

- a. Development of advanced, high efficiency silicon and gallium arsenide solar cells with low absorptance and low radiation degradation.
- b. Design of a large SEPS type or other high power density array for use at GEO including provision for transfer orbit power, little or no blanket charge buildup, and survivability for 16 years in the GEO environment.
- c. Development of radiation resistance concentrator surfaces.
- d. Low cost solar array fabrication techniques.
- e. Replenishable Ni-H<sub>2</sub> battery packs with adequate thermal interfaces and maximized operating life.
- f. Fuel cell systems for follow-on platforms.
- g. AC power components and interfaces, and system level development.
- h. Microprocessor implementation of power management, battery controller, power controllers, array drive and monitors, and associated intradata bus.

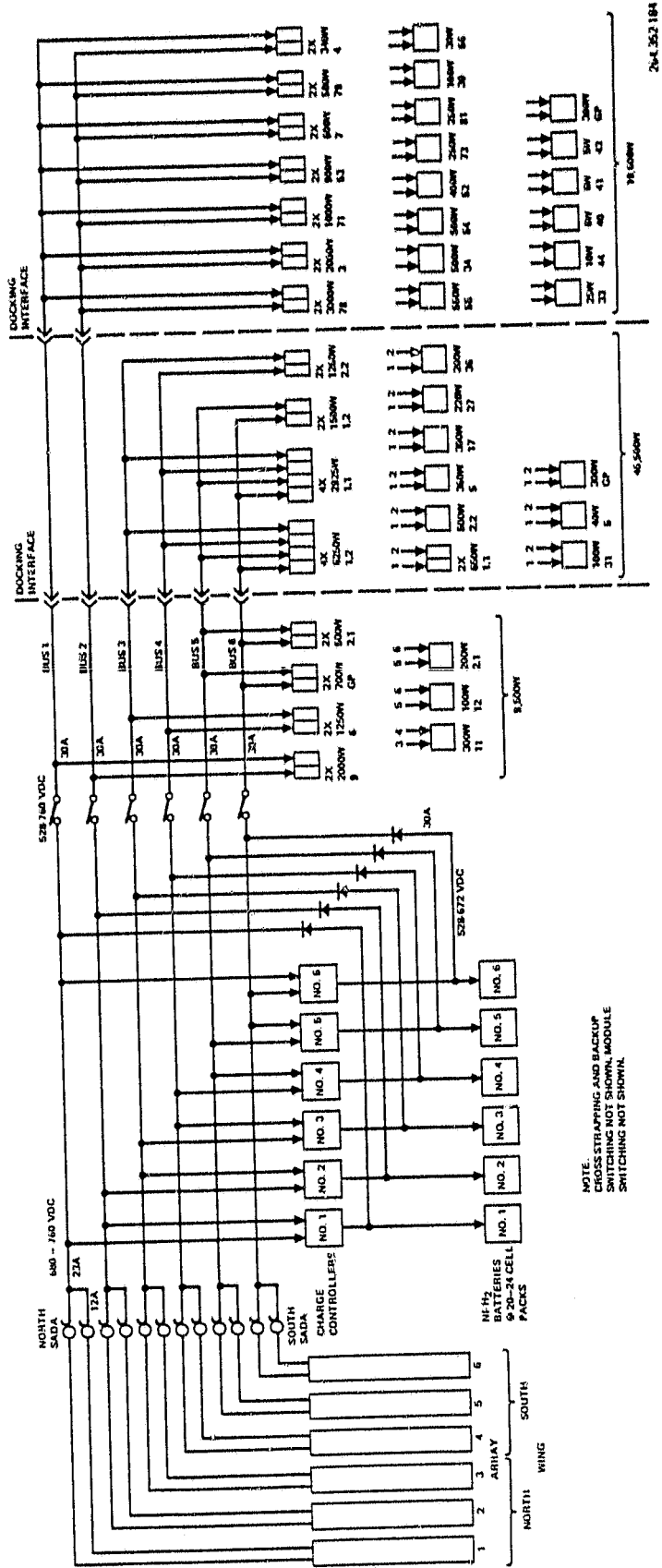
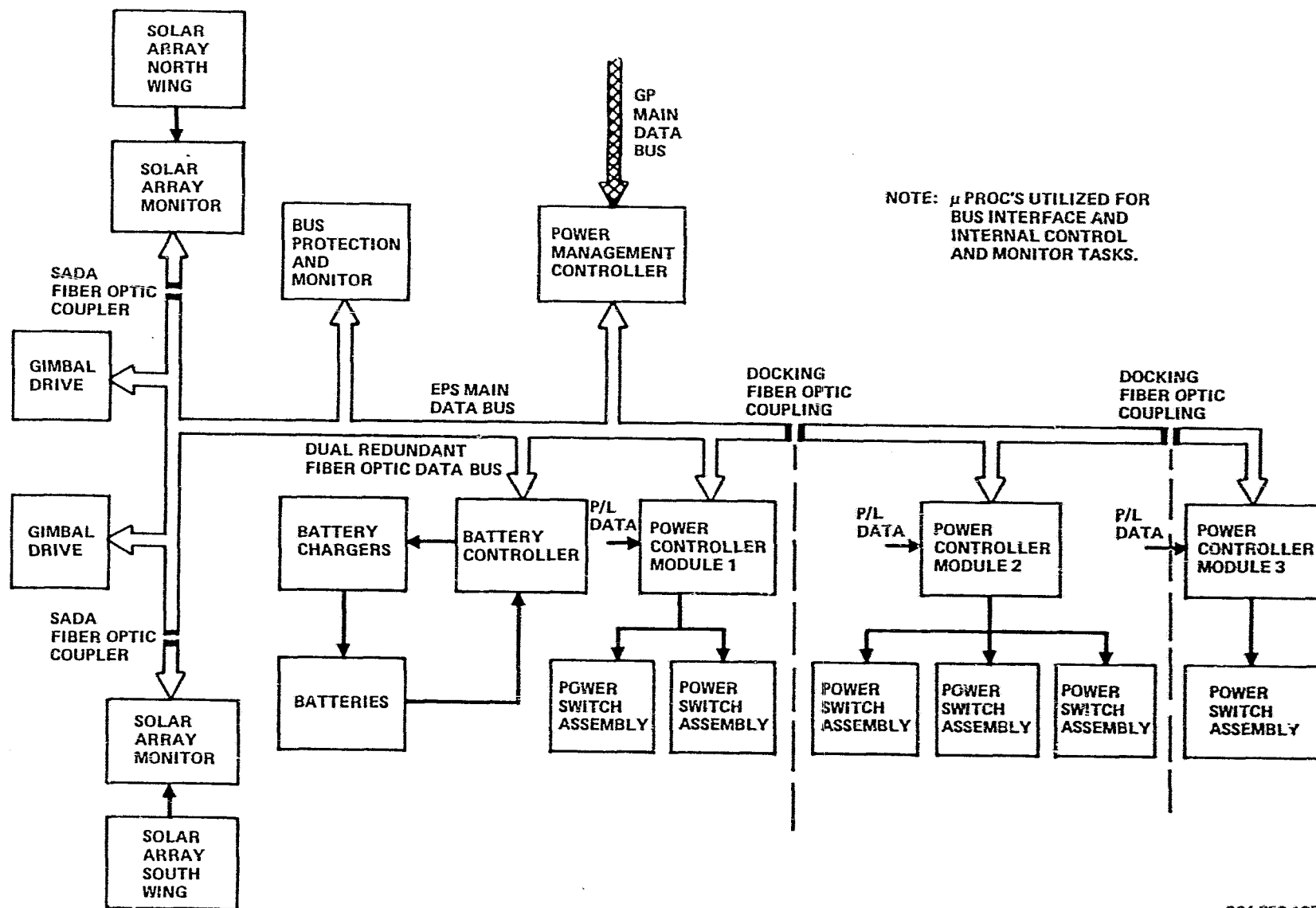


Figure 3-49. EPS Distribution GP Alternative #4 DC System



264.352-185

Figure 3-50. EPS Control System - GP Alternative #4

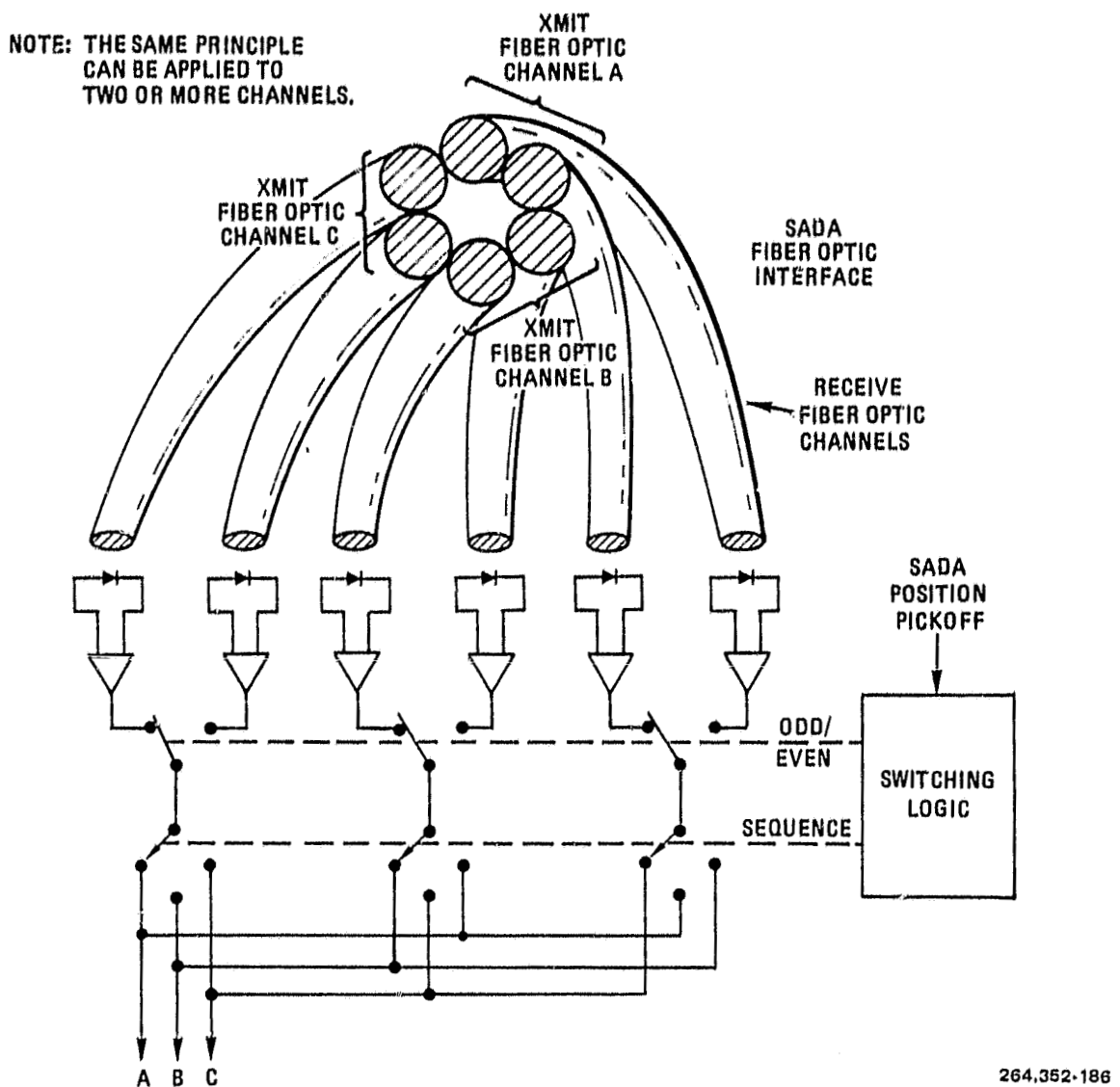


Figure 3-51. Three-Channel SADA Fiber Optics Interface

**3.1.6 CONTROL OF ATTITUDE AND POSITION.** Most of the attitude control and stationkeeping requirements can be met with straightforward control system designs that are well within the state-of-the-art. This includes attitude error sensing, computation and logic, and force and torque generation. The exceptions are transients associated with docking for servicing and the possible need for active structural damping of the very long period modes. In the following paragraphs numbers refer to Platform 1 of Alternative #1. General discussion applies to all cases.

**3.1.6.1 Attitude Sensing.** The basic attitude reference system is maintained in a strapped-down platform using rate integrating gyros and a computer. Update of the attitude is provided by use of horizon sensors and yaw sensors. Although the accuracy usually associated with a geosynchronous horizon sensor (0.05

degrees) is not suitable for use in holding the platform to 0.05 degrees, the major instrument error sources can be calibrated out. These removable error sources include long-term drift in detector responsivity, instrument temperature changes as the platform slowly rotates with respect to the sun, seasonal earth radiance variations, and static alignment.

**3.1.6.2 Stationkeeping Requirements.** The platform will require north-south stationkeeping to prevent a buildup in orbital inclination and east-west corrections to prevent drift toward the stable points. An equivalent velocity of 46 m/s per year is needed for inclination drift and this correction must be applied in the vicinity of the node resulting from the uncorrected drift. The east-west velocity requirement varies with distance from the stable point, but the worst case identified in this study is 5.3 m/s per year at 15°W longitude. The orbital position at which the longitudinal drift correction is applied is not critical.

**3.1.6.3 Torque Generation.** In some of the configurations, the platform mass distribution results in gravity gradient instability. This is actually not as serious as it sounds since the gravity gradient torque is nominally zero at the reference orientation although any deviation from that orientation can result in a torque in a direction to increase the error. In addition, gravity gradient torques can be handled without any increase in propellant requirements above those needed for stationkeeping. Bias torques from gravity gradient in roll and yaw, although fixed in body axes, rotate relative to inertial space and thus can be handled entirely by angular momentum exchange. Any bias torque in the pitch axis will integrate up to a large value if uncorrected, but this integrated torque can be stored in a wheel and dumped by proper application of the east-west stationkeeping thrust. Unbalance to solar pressure in the roll-yaw plane (pitch disturbance) will be oscillatory and also can be handled by angular momentum exchange. Any solar pressure unbalance in the pitch-yaw and pitch-roll planes will result in torques that will integrate to large values over time. Either of these torques can be dumped with controlled unbalance of the east-west stationkeeping impulse. The solar pressure torque that lies in the orbit plane perpendicular to the uncorrected line of nodes can also be dumped with proper application of the north-south stationkeeping impulse.

Thus, the predominant environmental attitude disturbance torques can be handled by a properly sized angular momentum system and controlled unbalances in the stationkeeping impulses. Compared to the stationkeeping requirements, additional propellant requirements for attitude control are "noise level".

**3.1.6.4 Active Structural Control.** The long period structural modes of oscillation computed for Alternative #1 present potential problems in the areas of amplitude buildup and attitude system bandwidth limitations. Amplitude buildup could occur as the result of harmonic excitation from disturbance sources such as thruster firings, thermal shocks from occultation, and movement of antennas with mechanical gimbaling, if any. The usual practice of

limiting the attitude control bandwidth so that the system corners well below any important modes could result in too soft a control system to effectively meet the pointing and stability requirements. Both potential problem areas can be solved by the application of active structural damping techniques. These techniques range from relatively simple systems that behave much like passive dampers to advanced high performance state feedback systems. More work is needed to define an active damping system for this application.

**3.1.6.5 Docking Transients.** The usual docking transient to be considered is that from the momentum transferred by the actual impact. In configurations with most of the mass lumped in a centerbody, a negligible change in moment of inertia will occur when the teleoperator mass is added to the centerbody; if it were to be docked at the end of a relatively long antenna arm however, this would no longer be true. The mass properties change combined with the need for a higher bandwidth attitude system to minimize the pointing error from impact requires further study.

**3.1.7 THERMAL CONTROL.** Passive thermal control of the GP payloads can be achieved, but not without an impact on the platform configuration. Radiator heating by infrared radiation emitting from the platform structure, antennas, solar arrays, and other payloads should be kept to a minimum. This requires that the geometric view factors from the radiators to these external bodies be as small as possible.

To achieve high valued view factors from each radiator to space, several general observations on the platform configuration can be made:

- a. The east-west dimension of the platform should be maximized while the north-south dimension is minimized. Impact of this overall shape on the pointing accuracy needs to be evaluated.
- b. The long dimension of the solar arrays should be in the north-south direction. In this manner the solar arrays are prevented from sweeping over the payload radiators (which would periodically reduce the radiators' view to space and provide an undesirable source of infrared radiation). Locating the solar array rotating axis onto the earth side of the platform truss will further these objectives.
- c. A separate subsystem equipment module should be provided. The module would be the prime source of power for all of the communications payloads. This eliminates the requirement of a battery thermal control system in each payload. The module would have its own radiators, which will maintain batteries and other subsystem packages at a lower temperature than is generally required for communications electronics.
- d. The payloads should be distributed on the platform in a manner providing minimum heat exchange between the payloads.

**3.1.7.1 Thermal Design for Heat Rejection From Distributed Payloads.** The individual payloads are assumed to be widely separated and distributed over the GP. Each payload is assumed to be a rectangular package with north and south-viewing radiators whose size is dependent on the payload internal heat dissipation (see Figure 3-52). Heat pipes in the radiators provide nearly uniform temperatures over the radiator surface. The exposed four sides of the package are insulated as is the inside surface of the radiators. The radiators are connected by a central web (perpendicular to the plane of the platform) on which the dissipating electronics are located. Heat pipes on the web interconnect the north and south radiators to reduce seasonal effects. As the sun incidence angle on the north radiator reaches a peak 23.5 degrees at the summer solstice, some of the absorbed energy is transferred to the south radiator and both radiators reside at essentially equal temperatures. Likewise, the radiators reside at nearly equal temperatures as the sun shines on the south radiator during the winter solstice.

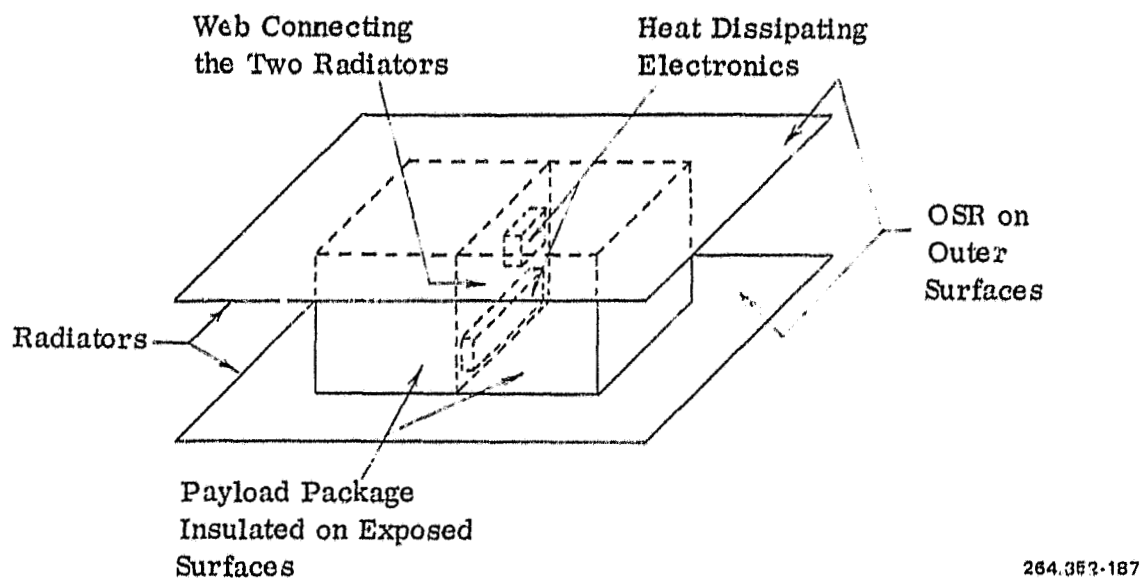


Figure 3-52. North and South Facing Radiators on a Typical Rectangular Payload Package

The radiators are assumed to be covered with quartz optical solar reflectors (OSRs). This material has a sufficiently high emittance and an acceptable rate of solar absorptance degradation. Recent data derived from COMSTAR spacecraft indicate the degradation of solar absorptance proceeds from an initial value of 0.11 at rates between 0.015 and 0.030 per year, with the former value more probable. These data have been taken for only a few years and extrapolation to a 16 year mission is only estimated. Nevertheless, this data has been used in the payload package thermal analysis that follows later. It is very desirable that the degradation rates for OSRs be better defined before the final platform design is begun.

**3.1.7.2 Thermal Design For Module Equipment.** Heat dissipating subsystem equipment on the geostationary platform will be located in a central cylindrical module. Specific mounting arrangements for this equipment have not been identified. To reject heat dissipated in the packages enclosed in the module and prevent excessive temperatures, the heat must be transported to an external radiator system. Adding to the complexity of the heat rejection system is a requirement for servicing and replacement of packages. That is, the package must be in intimate thermal contact with the heat transport medium, and yet be removable and replaceable. Three methods (one active and two passive using heat pipes) of rejecting heat from module packages are discussed below. Active systems are generally unlimited in the total power they can reject because very large radiator sizes can be employed. On the other hand, heat pipe lengths (and thus radiator sizes) are limited by the heat pipe maximum capillary pumping pressure. Further definition of specific subsystem packages, heat dissipation levels, allowable temperatures, and the mounting arrangement are required before a preferred approach can be identified.

**Active Cooling.** Active heat rejection can be accomplished by pumping a fluid through coldplates beneath the packages and out through a deployed radiator. In this case the package replacement requirements can be met using the General Dynamics Convair thermal disconnect (patent pending) shown in Figure 3-53. The coldplate has ribs integrally milled into it on the side opposite the packages. The radiator cooling loop tubing passes back and forth between the ribs. Joining takes place with the tubing depressurized. Normal operating pressure of the cooling system provides the required contact pressure.

The radiator design for an active cooling system could be one employing rigid panels that are deployed with a scissors mechanism (see Figure FO-6). This is a rugged yet deployable radiator concept. Required radiator area per net watt of heat rejection depends on the radiator temperature; the higher the temperature, the greater the heat rejection. However, package cooling capability is reduced with increasing fluid temperature. Maximum fluid temperature is established by the allowable package temperature. Figure 3-54 shows the dependency of heat rejection performance on radiator temperature. Shuttle radiators operate at an outlet temperature of 40F. Some communications electronics can operate with a coolant temperature as high as 100F. Most likely the radiator would operate at a temperature between 40 and 100F, resulting in a heat rejection performance of  $19 \pm 7$  watts/ft<sup>2</sup>.

The most serious problem with the use of active thermal control on the GP is the requirement for long life. Redundant pumps would be required since they are subject to failure and yet must operate continuously for the life of the platform. In addition, meteoroid penetration becomes a serious problem with the few fluid loops of a pumped fluid system.

**Passive Cooling.** Two passive cooling concepts (heat pipes only) that could be used to reject heat from module packages were investigated. In both concepts, the packages are located in pie-shaped compartments in the module (Figure 3-55).

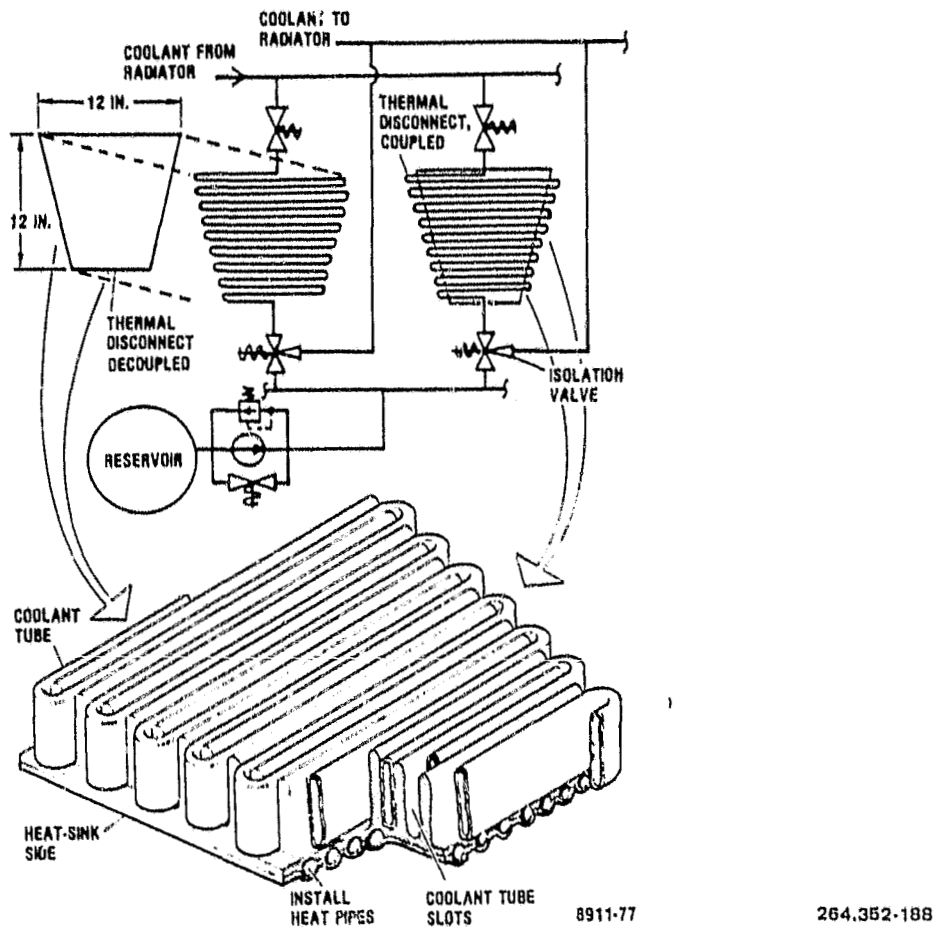


Figure 3-53. The Convair Thermal Disconnect Allows Replacement of Packages On-Orbit

The first passive thermal control concept employs heat pipe radiators projecting out from opposite sides of the cylindrical module. Each radiator has north/south faces, and the long edge is aligned east/west. The radiators are thermally connected to cylindrical heat pipes on the module wall. Packages are mounted on the cylindrical wall of the pie-shaped compartment. Deploying the radiators and getting the dissipated heat from the packages into the cylindrical wall pose difficult problems. Machined sawtooth interfaces between the replaceable unit and the cylinder wall would aid heat transfer by increasing contact area. This concept uses a common radiator to service packages with differing heat rejection and temperature requirements, which can result in system cooling inefficiencies.

The second passive concept employs individual radiators for each pie-shaped compartment. The compartment with its package group and radiator is replaceable as a unit. The radiator is deployed by rotating it from a stowed position where it is tangent to the circumference with its long edge parallel to the module centerline. In the deployed position, the long edge is perpendicular to

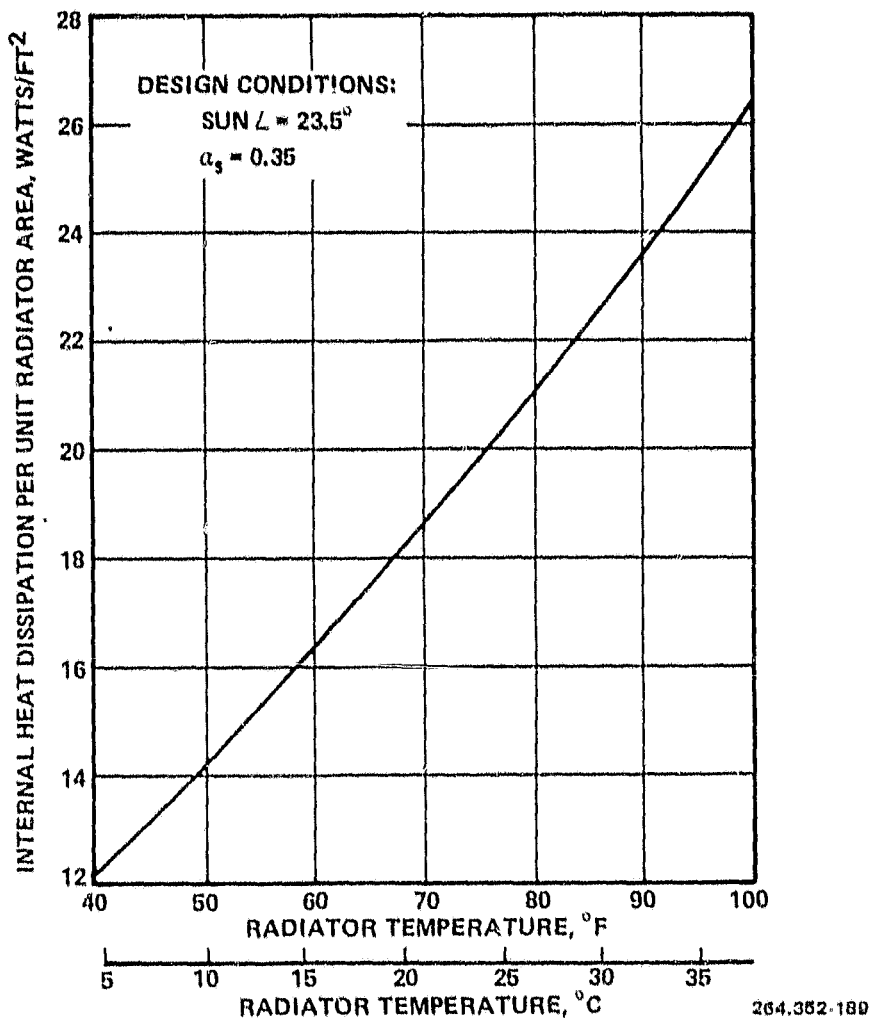


Figure 3-54. GP Radiator Heat Rejection Performance Varies Strongly with Temperature

the centerline. The radiator has north/south faces when deployed. Replacement units are brought up in a module with similar pie-shaped compartments. The operational and service modules berth with centerlines aligned. Empty spaces in the service module can receive the faulty units to be replaced. The service module is then clocked about its centerline to install the new units.

**3.1.7.3 Thermal Analysis of Typical Payload.** Two passive radiator design concepts of the configuration described in Section 3.1.7.1 were analyzed for a 2 kW communications packages. A 20-meter diameter solid antenna (worst case design) was assumed to be located directly in front of the package and 8 meters away. Three structural members (10 cm diameter and 9 meters long) were assumed to partially block the view to space of each radiator. Radiation interchange factors ( $F$ ) were computed for the radiator to space, structure and antenna. A list of the assumed conditions and properties is shown in Table 3-29. The beginning of life (BOL) solar absorptance ( $\alpha_s$ ) for second surface mirrors was assumed to be 0.11. At the present, the predicted degradation of

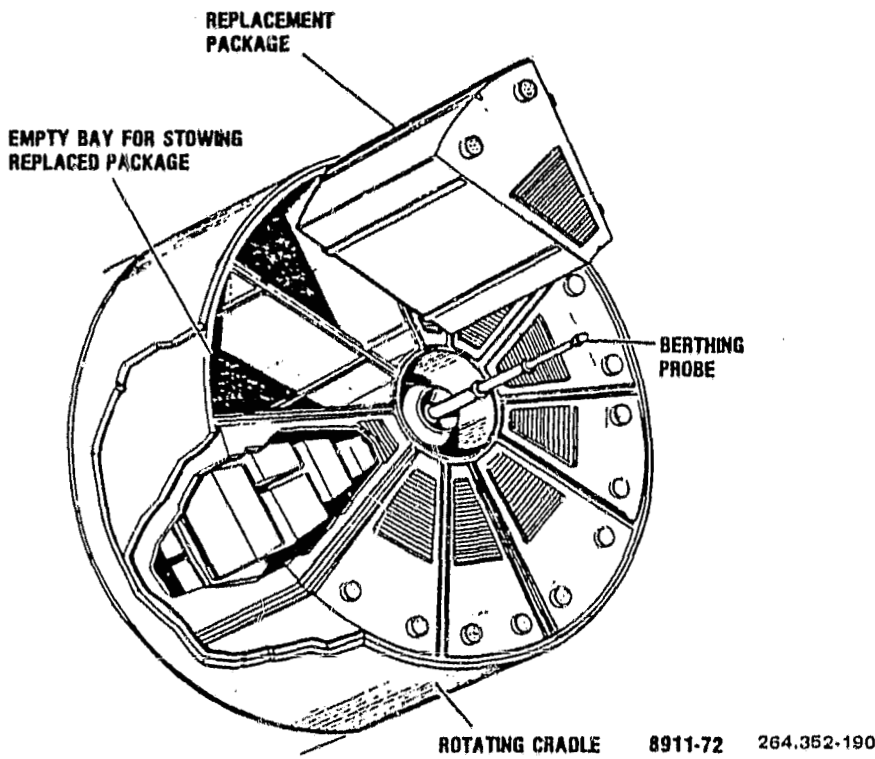


Figure 3-55. Subsystem Packages Can Be Located in Replaceable Pie-Shaped Compartments in the Module

Table 3-29. Radiation Exchange Factors and Properties for Thermal Analysis

$F_{r-st}$	0.03322
$F_{r-ant}$	0.08314
$F_{r-space}$	0.6634
$\epsilon_r$	0.78
$\alpha_T$	0.59, 0.35

$\alpha_s$  is 0.015/year. However, some flight data on existing spacecraft indicate a possible degradation rate of 0.03/year. These two rates projected for a 16 year life result in an end of life (EOL)  $\alpha_s$  of 0.35 and 0.59, respectively.

Single Fluid Heat Pipe Concept. The first design concept incorporates simple heat pipes placed along each radiator to reduce radiator gradients. Simple heat pipes were also used on the interconnecting web. Heat dissipated by the electronics is transported to the radiators by the interconnecting heat pipes. Winter solstice (maximum insolation) with a worst case  $\alpha_s$  of 0.59 at EOL was selected as the hot design condition. A maximum radiator temperature of 40C

(104F) was selected as being acceptable for TWTS and other payload electronics. The structure and dish antenna temperatures were computed to be 50C (122F) and 60C (140F), respectively. This resulted in an internal dissipation per unit radiator area ( $Q_i/A_r$ ) of 17 W/ft<sup>2</sup> and a total radiator area of 118 ft<sup>2</sup> for a 2 kW payload. For this design at autumnal equinox (no solar heating), the radiator temperature was 3C (37F). Finally, a steady state heat balance was made for end-of-eclipse conditions and a radiator temperature of -19C (2F) was computed. This did not take into account the heat capacity of the package and was therefore a very conservative number. In actuality, it should be significantly warmer.

Next, it was decided to repeat the above calculations assuming the more likely  $\alpha_s$  degradation rate of 0.015/year resulting in  $\alpha_{EOL}$  of 0.35. For winter solstice and a radiator temperature of 40C (104F), the  $Q_i/A_r$  was 23.2 W/ft<sup>2</sup>, resulting in a required radiating area of 86 ft<sup>2</sup>. For autumnal equinox, the radiator temperature was 20C (68F) and at end of eclipse (steady state) was 1C (34F). A summary of analysis results for the simple heat pipe concept is presented in Table 3-30.

Variable Conductance Heat Pipe Concept. Because there is some doubt in the high degradation rate 0.03/year for  $\alpha_s$  and the obvious desire to operate the electronics at a cooler temperature, the second design incorporated the use of variable conductance heat pipes (VCHP) between the electronics and the radiators. As before, simple heat pipes were used in the radiators. It was decided to design around winter solstice,  $\alpha_{EOL}$  of 0.35, and a radiator temperature of 20C (68F). This was accomplished for a  $Q_i/A_r$  of 14 W/ft<sup>2</sup> and a radiator area of 142 ft<sup>2</sup>. This was only a 20 percent increase in area for a 20C (36F) decrease in operating temperature. Another advantage of the VCHP operation is that the radiator will operate at 20C (68F) for all seasonal environments including eclipse. This is accomplished because a VCHP will vary the active radiator area to maintain a designed operating temperature. Therefore, at autumnal equinox the active radiator area is reduced to 85 ft<sup>2</sup> while maintaining a 20C (68F) radiator and down to 66 ft<sup>2</sup> at end-of-eclipse (steady state).

The VCHP design has the advantage of being able to function satisfactorily even if the solar absorptance becomes higher than the predicted 0.35 and of achieving this without increasing the radiator space. Should the solar absorptance increase further, the VCHPs will act as the simple heat pipes and continue to reject heat at 14 W/ft<sup>2</sup> while the radiator temperature increases. For the design case of  $\alpha_{EOL} = 0.59$  the radiator temperature is 34C (93F). The performance of this radiator is shown in Figure 3-56. A summary of analysis results for the variable conductance heat pipe concept is presented in Table 3-31.

Table 3-30. Thermal Analysis Results for Simple Heat Pipe Concept

	$\alpha_s = 0.59$	$\alpha_s = 0.35$
<b>Winter Solstice</b>		
$S, \text{ W}/\text{ft}^2$	130	130
Solar angle, $\sigma$ , deg	-23.5	-23.5
$T_{\text{structure}}, ^\circ\text{C} (^{\circ}\text{F})$	50 (122)	50 (122)
$T_{\text{dish}}, ^\circ\text{C} (^{\circ}\text{F})$	60 (140)	60 (140)
$T_{\text{radiator}}, ^\circ\text{C} (^{\circ}\text{F})$	40 (104)	40 (104)
$Q_i/A_{r_2}, \text{ W}/\text{ft}^2$	17	23.2
$A_r, \text{ ft}^2$	118	86
<b>Autumnal Equinox</b>		
$S, \text{ W}/\text{ft}^2$	125	125
$\sigma, \text{ deg}$	0	0
$T_{\text{structure}}, ^\circ\text{C} (^{\circ}\text{F})$	44 (111)	44 (111)
$T_{\text{dish}}, ^\circ\text{C} (^{\circ}\text{F})$	57 (135)	57 (135)
$T_{\text{radiator}}, ^\circ\text{C} (^{\circ}\text{F})$	3 (37)	20 (68)
$Q_i/A_{r_2}, \text{ W}/\text{ft}^2$	17	23.2
$A_r, \text{ ft}^2$	118	86
<b>End of Eclipse</b>		
$S, \text{ W}/\text{ft}^2$	0	0
$\sigma, \text{ deg}$	0	0
$T_{\text{structure}}, ^\circ\text{C} (^{\circ}\text{F})$	-157 (-251)	-157 (-251)
$T_{\text{dish}}, ^\circ\text{C} (^{\circ}\text{F})$	-157 (-251)	-157 (-251)
$T_{\text{radiator}}, ^\circ\text{C} (^{\circ}\text{F})$	-29 (-2)	1 (34)
$Q_i/A_{r_2}, \text{ W}/\text{ft}^2$	17	23.2
$A_r, \text{ ft}^2$	118	86

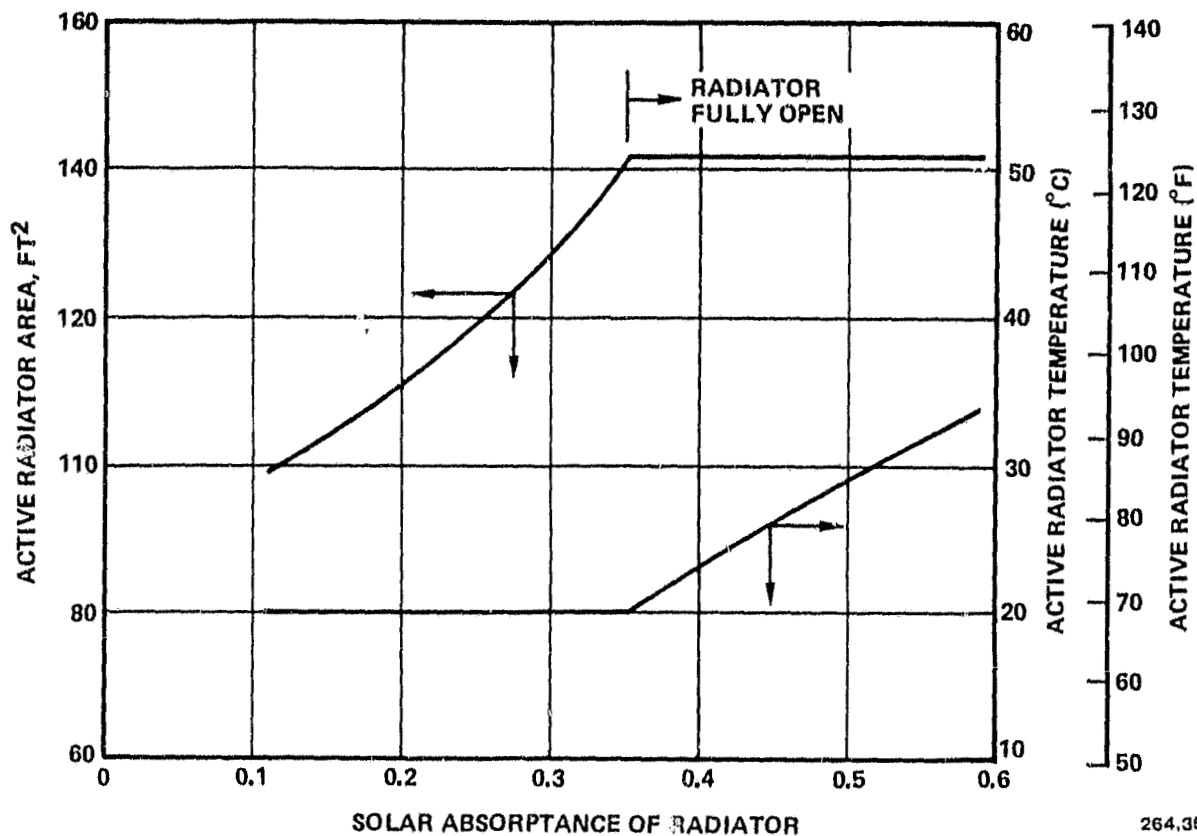


Figure 3-56. Radiator Performance at Winter Solstice

### 3.1.8 MASS PROPERTIES.

**3.1.8.1 Weight.** The weights of Alternative #1, Platforms 1, 2, and 6 are shown on Tables 3-32, 3-33, and 3-34, respectively. The low thrust orbital transfer vehicle (OTV) has been offloaded to meet the mission requirements. The ACS propellant for Platforms 1 and 6 has an 8-year supply of ACS propellant. Platform 2 has been offloaded to a 6-year capability at launch due to the OTV capability of 6895 kg. Operational Platform Alternative #4 consists of three modules, as shown in Table 3-35. The weights shown are preliminary estimates used to allocate payloads to each module in an effort to maintain a module-plus-payload weight less than the 19,505 kg capability of the high thrust reusable OTV.\* Table 3-36 shows the payloads allocated to each module.

\*It was necessary to change to the low thrust reusable OTV due to impact on structure. The capability of this from LEO to GEO is 16,878 kg and the average module weight from Table 3-35 is 16,212 kg; this is a potentially feasible approach, therefore, but considerable rearrangement will be needed in a further study.

Table 3-31. Thermal Analysis Results for Variable Conductance Heat Pipe Concept

Winter Solstice	
S, W/ft <sup>2</sup>	130
Solar Angle; $\sigma$ , deg	-23.5
T <sub>structure</sub> , °C (°F)	50 (122)
T <sub>dish</sub> , °C (°F)	60 (140)
T <sub>radiator</sub> , ( $\sigma_s = 0.35$ ), °C (°F)	20 (68)
T <sub>radiator</sub> , ( $\sigma_s = 0.59$ ), °C (°F)	34 (93)
Q <sub>i</sub> /A <sub>r<sub>2</sub></sub> , W/ft <sup>2</sup>	14
A <sub>r</sub> , ft <sup>2</sup>	142
Autumnal Equinox	
S, W/ft <sup>2</sup>	125
$\sigma$ , deg	0
T <sub>structure</sub> , °C (°F)	44 (111)
T <sub>dish</sub> , °C (°F)	57 (135)
T <sub>radiator</sub> , °C (°F)	20 (68)
Q <sub>i</sub> /A <sub>r<sub>2</sub></sub> , W/ft <sup>2</sup>	23.2
A <sub>r</sub> , ft <sup>2</sup>	86
End of Eclipse	
S, W/ft <sup>2</sup>	0
$\sigma$ , deg	0
T <sub>structure</sub> , °C (°F)	-157 (-251)
T <sub>dish</sub> , °C (°F)	-157 (-251)
T <sub>radiator</sub> , °C (°F)	20 (68)
Q <sub>i</sub> /A <sub>r<sub>2</sub></sub> , W/ft <sup>2</sup>	30.3
A <sub>r</sub> , ft <sup>2</sup>	66

Table 3-32. Operational Platform No. 1 Weight Summary

	Weight (kg)
Platform	4,358
Structure	1,592
Thermal Control	161
Attitude Control	1,173
Electric Power	718
Avionics	146
Contingency (15 percent)	568
Payload	2,283
No. 2.1 HVT C-Band	1,145
No. 3 TV Distribution	515
No. 11 Interplatform Link	130
No. 31 DMSP Data Relay	195
Contingency (15 percent)	298
Total Platform and Payload Weight	6,641
Low Thrust OTV (offloaded) <sup>1</sup>	19,326
Total Separation Weight from Orbiter at LEO	25,967
OTV ASE	2,566
Margin Available for Payload ASE <sup>2</sup>	951
Total Liftoff Weight in Shuttle Orbiter <sup>3</sup>	29,434

<sup>1</sup>OTV Weights: Burnout = 2843 kg, in-flight losses = 260 kg, main propellants = 16223 kg.

<sup>2</sup>Preliminary estimate of payload ASE = 685 kg.

<sup>3</sup>Shuttle can insert 29484 kg in LEO.

If Payload No. 1.2 could be moved from Module 2 to Module 3, it would bring Module 2's weight below 19,505 kg, while Module 3 would not go above this. ACS propellant tanks are sized for the total platform weight and an 8-year capacity. Module 1, when launched, can control the entire platform for two years, until the platform is resupplied with ACS propellant for an additional eight years. Module 1 ACS has three tanks, Module 2 has four tanks, and Module 3 has eight tanks. This was done to meet the OTV capability and the available stowage volume in the Orbiter.

Table 3-33. Operational Platform No. 2 Weight Summary

	Weight (kg)
Platform	4,228
Structure	1,466
Thermal Control	277
Attitude Control (6-year supply)	929
Electric Power	909
Avionics	146
Contingency (15 percent)	551
Payload	2,427
No. 1.1 DTU, km Band	1,600
No. 7 Air Mobile	260
No. 11 Interplatform Link	130
No. 27 RF Interferometer	120
Contingency (15 percent)	317
Total Platform and Payload Weight	6,655
Low Thrust OTV (offloaded) <sup>1</sup>	<u>19,349</u>
Total Separation Weight from Orbiter at LEO	26,004
OTV ASE	2,566
Martin Available for Payload ASE <sup>2</sup>	<u>914</u>
Total Liftoff Weight in Shuttle Orbiter <sup>3</sup>	29,484

<sup>1</sup>OTV Weights: Burnout = 2843 kg, in-flight losses = 260 kg, main propellants = 16246 kg.

<sup>2</sup>Preliminary estimate of payload ASE = 685 kg.

<sup>3</sup>Shuttle can insert 29484 kg in LEO.

3.1.8.2 Center of Gravity. Using the center of gravity information from the "Baseline Tug Definition Document," Rev. A, dated June 26, 1972, by MSFC, and the arrangement of Figure FO-1, Sheet 4), the center of gravity for the OTV and platform were developed for shuttle launch, abort landing ( $LH_2$  and  $LO_2$  dumped), and nominal return with the payload airborne support equipment and the OTV airborne support equipment. Figure 3-57 shows these centers of gravity and the allowable cargo center of gravity limits of the Shuttle.

Table 3-34. Operational Platform No. 6 Weight Summary

	Weight (kg)
Platform	3,897
Structure	1,068
Thermal Control	187
Attitude Control	1,173
Electrical Power	815
Avionics	146
Contingency (15 percent)	508
Payload	2,185
No. 1.2 Direct-to-User, Ka-Band	1,040
No. 11 Interplatform Link	130
No. 19 Visual and IR Radiometer	500
No. 54 DOD FHF Experiment	230
Contingency (15 percent)	285
Total Platform and Payload Weight	6,082
Low Thrust OTV (offloaded) <sup>1</sup>	18,373
Total Separation Weight from Orbiter at LEO	24,455
OTV ASE	2,566
Margin Available for Payload ASE <sup>2</sup>	2,463
Total Liftoff Weight in Orbiter <sup>3</sup>	29,484

<sup>1</sup>Expendable L.T. OTV weights: Burnout = 2843 kg, in-flight losses = 260 kg, main propellant = 15270 kg.

<sup>2</sup>Preliminary estimate of payload ASE = 862 kg.

<sup>3</sup>Shuttle can insert 29484 kg in LEO.

3.1.9 STRESS ANALYSIS. All spacecraft considered in this study must be designed to withstand the following major loading conditions:

- Shuttle launch and landing loads. These loads can be reacted by a properly designed supporting cradle.
- Deployment loads. Deployment rates of various structural elements can be made low enough so that induced loads are not critical.
- LEO to GEO transfer loads.

Table 3-35 . Operational Platform Alternative #4 Weight Summary

	Weight (kg)		
	Module 1	Module 2	Module 3
Platform	(11,656)	( 6,036)	( 5,059)
Structure	2 184	2,119	1,196
Thermal Control	405	0	0
Attitude Control	1,577	2,858	3,076
Electric Power	5,780	197	52
Avionics	190	75	75
Contingency (15 percent)	1,520	787	660
Payload	( 5,044)	(14,459)	( 6,380)
Payload	4,386	12,573	5,548
Contingency (15 percent)	658	1,886	832
Total Module and Payload <sup>1</sup>	16,700 <sup>3</sup>	20,496 <sup>3</sup>	11,439 <sup>3</sup>
Airborne Support Equipment	1,670	2,050	1,144
Total Liftoff Weight <sup>3</sup>	18,370	22,545	12,583

<sup>1</sup>L.T. reusable OTV can insert 16878 kg to GEO.

<sup>2</sup>Shuttle can insert 29484 kg in LEO.

<sup>3</sup>Average weight = 16,212.

- d. Docking and/or servicing loads. General Dynamics' soft-docking approach minimizes docking velocities such that the resulting loads are not critical.
- e. On-orbit ACS loads. These loads can be minimized, consistent with operational requirements, by limiting thruster force and torque.

The LEO to GEO transfer loading condition was chosen for the purpose of preliminary sizing since this loading condition is generally the most severe. Alternatives #1 and #4 were designed to be deployed at LEO and transferred to GEO in this state except for the solar panels, which are to be retracted.

For Alternative #1, the transfer vehicle is an expendable OTV with maximum T/W = 0.07. A dynamic factor of 2.0 was used. Bending moments and shears on masts and beams were calculated based on estimated weights. We have a computer program that calculates the minimum size Astromast or tube that can carry specified loads. Using this, we determined the sizes that would have zero margins of

Table 3-36 . Operational Platform Alternative #4 Payload Weight

No.	Description	Payload			Weight (kg)
		Module 1	Module 2	Module 3	
1.1	Customer Premises Service Ku-band				5,732
1.2	Customer Premises Service Ka-band				2,996
2.1	High Volume Trunking C-band	2,797			
2.2	High Volume Trunking Ka-band				1,205
3	TV Distribution				515
4	Tracking and Data Relay, S and Ku-band				425
5	Educational TV				620
6	Direct-to-Home TV	645			
7	Air Mobile				260
9	Land Mobile	684			
11	Interplatform Link	130			
12	Data Collection	130			
17	Lightning Mapper				320
18	Atmospheric Sounder				185
27	RF Interferometer				120
31	DNSR Data Relay				195
33	Material Exposure				10
34	ACOSS/HALO Demonstration				1,200
36	Advanced On-board Signal Processor				350
39	Solar Flare Monitor				100
40	Solar Flare Isotope Monitor				13
41	Energetic Proton/Heavy Ion Sensor				8
43	Magnetic Substorm Monitor				10
44	Charged Particle Monitor				5
51	Cryogenic IR Radiator				120
52	BOSS Evaluation				150
53	Gemini Evaluation				820
54	EHF System				230
55	Aircraft Laser Relay				320
56	Fiber Optics Demonstration				12
71	Earth Optical Telescope				1,100
73	Chemical Release Modification				
	Observations				200
78	Cryo-Cooled Limb Scanner				450
79	LLL TV				300
81	Microwave Sounder				150
Payload Weight		4,386	12,573	5,548	

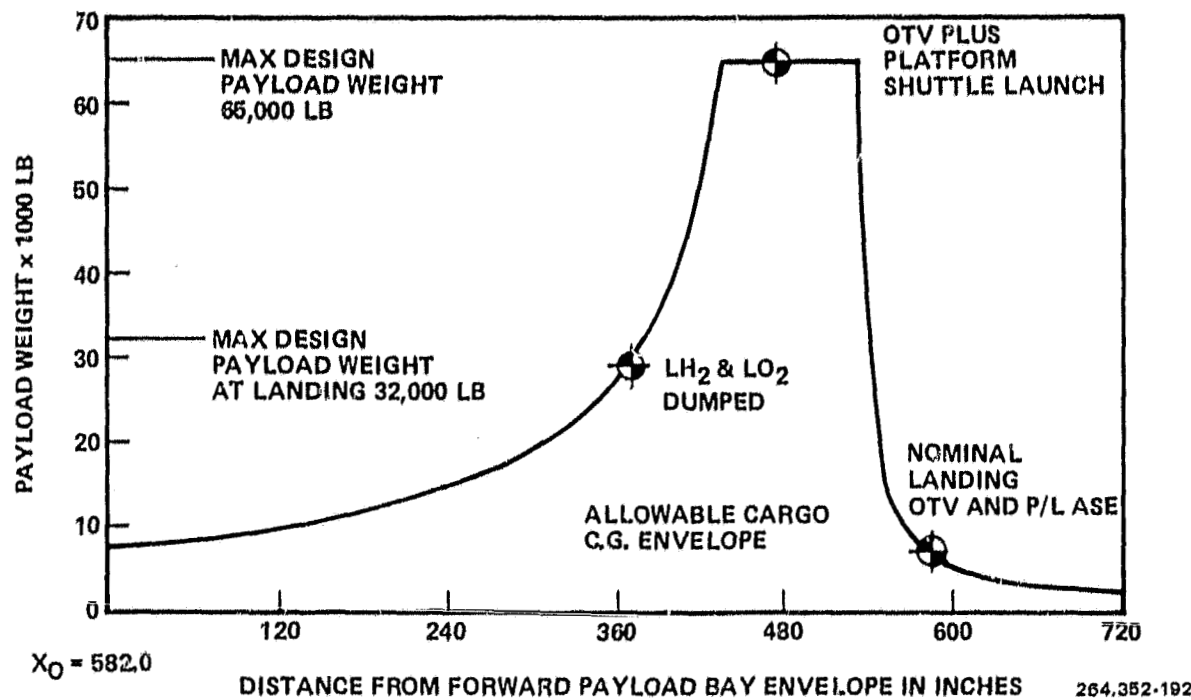


Figure 3-57. Cargo Center of Gravity Limits (Along X-Axis)

safety. These sizes are listed in Table 3-37 along with corresponding stiffnesses. In all cases, these sizes are less than dimensions chosen by designers for weight and packaging studies and therefore we conclude that the proposed designs have positive margins of safety and the stiffnesses are greater than the values shown. An iteration using design dimensions was not made within the budget and schedule. It is expected that many parts will be designed by stiffness and/or manufacturing limitations, so that final sizing must be part of future studies.

For Alternative #4, the procedure was slightly different. Initially the two-stage, standard engined, reusable OTV with maximum T/W = 0.31 was specified. A dynamic factor of 2.0 was again used. GDS deployable truss beams of graphite composite materials were used. Overall truss dimensions and tube sizes, as proposed by designers for weight and packaging studies, were used to calculate wall thicknesses required to give zero margins of safety. We found that if some members were made of solid rods, instead of tubes, the margin of safety was still negative. For this reason, we decided to try T/W = 0.05 and tube wall thicknesses required for zero MS were calculated. These are shown in Table 3-38 and appear to be reasonable. A redesign was then made based on the reusable, low thrust, two-stage OTV with maximum T/W = 0.035. Without resizing the tubes, this yielded margins of safety equal to 0.43 as shown in Table 3-38.

**Table 3-37. Alternative #1 Minimum Structural Sections**

Section Location	Type of Section*	Diameter**	Thickness**	EI ( $\text{Nm}^2$ )	JG ( $\text{Nm}^2$ )	Margin of Safety
<b>Number 1 Western</b>						
IPL MAST	Single Tube (GE)	2.54 cm	0.051 cm	679.0	160.0	0.00 <sup>+</sup>
Central Mast (Yaw Axis)	Articulated Astromast (GE)	0.22 m	—	$3.16 \times 10^5$	$9.29 \times 10^3$	0.05
25m Wrap-Rib Antenna Mast	Supermast Astromast (F)	0.42m	—	$2.80 \times 10^6$	$8.24 \times 10^4$	0.62
16.8m Wrap-Rib Antenna Mast	Supermast Astromast (F)	0.32m	—	$9.15 \times 10^5$	$2.69 \times 10^4$	0.02
Wrap-Rib Antenna Feed Supports (Each)	Single Tube (GE)	10.2 cm	0.203 cm	$1.75 \times 10^5$	$4.11 \times 10^4$	0.07
Solar Array Masts (Each)	Supermast Astromast (F)	0.32 m	—	$9.15 \times 10^5$	$2.69 \times 10^4$	0.03
<b>Number 2 Western</b>						
IPL Mast	Single Tube (GE)	3.18 cm	0.045 cm	$1.18 \times 10^3$	276.0	0.00 <sup>+</sup>
Central Mast (Yaw Axis)	Single Tube (GE)	4.47 cm	0.062 cm	$4.50 \times 10^3$	$1.06 \times 10^3$	0.00 <sup>+</sup>
Solar Array Supports (Each)	Two Tubes (GE)	6.88 cm	0.094 cm	$4.56 \times 10^4$	$1.07 \times 10^4$	0.00 <sup>+</sup>
6m Wrap-Rib Antenna Masts (Each)	Single Tube (GE)	4.97 cm	0.069 cm	$6.89 \times 10^3$	$1.62 \times 10^3$	0.00 <sup>+</sup>
Interferometer Masts (Each)	Supermast Astromast (F)	0.33 m	—	$1.23 \times 10^6$	$3.62 \times 10^4$	0.03
<b>Number 6 Western</b>						
IPL Mast	Single Tube (GE)	3.86 cm	0.109 cm	$5.10 \times 10^3$	$1.20 \times 10^3$	0.00 <sup>+</sup>
Solar Array Supports (Each)	Two Tubes (GE)	3.78 cm	0.106 cm	$9.30 \times 10^3$	$2.18 \times 10^3$	0.00 <sup>+</sup>
4m Wrap-Rib Antenna Masts (Each)	Single Tube (GE)	2.47 cm	0.069 cm	845.0	198.0	0.00 <sup>+</sup>
DoD EHF Experiment Support	Two Tubes (GE)	4.73 cm	0.133 cm	$2.29 \times 10^4$	$5.37 \times 10^3$	0.00 <sup>+</sup>

\*GE = GY70/X30 graphite epoxy ( $O_2$  / ± 24); F = fiberglass.

\*\*Sizes shown are minimum permissible for zero margin of safety. Design values are greater — See Sections 3.1.3.1 and 3.1.9.

Table 3-38. Alternative #4 Minimum Structural Sections

Section Number	Type of Section	Truss Depth (m)	Axial Tubes		Transverse Tubes		$EI_{xx}$ ( $\text{Nm}^2$ )	$EI_{yy}$ ( $\text{Nm}^2$ )	$JG$ ( $\text{Nm}^2$ )	Margin of Safety
			d mm(IN)	t mm(IN)	d mm(IN)	t mm(IN)				
1	OOA Type Truss (GE)*	5.00	50.8 (2.000)	1.78 (0.070)	28.7 (1.130)	0.23 (0.009)**	$7.35 \times 10^8$	$3.67 \times 10^8$	$2.36 \times 10^7$	0.43
2	OOA Type Truss (GE)	2.29	45.0 (1.770)	0.58 (0.030)	25.4 (1.000)	0.23 (0.009)**	$5.83 \times 10^7$	$2.91 \times 10^7$	$2.47 \times 10^6$	0.43
3	OOA Type Truss (GE)	0.93	18.4 (0.723)	0.61 (0.024)	10.4 (0.408)	0.23 (0.009)**	$3.19 \times 10^6$	$1.55 \times 10^6$	$1.68 \times 10^5$	0.43
4	OOA Type Truss (GE)	2.95	57.9 (2.280)	1.91 (0.075)	32.8 (1.290)	0.38 (0.0150)	$3.10 \times 10^8$	$1.56 \times 10^8$	$8.81 \times 10^6$	0.43
5	OOA Type Truss (GE)	0.62	12.3 (0.484)	0.41 (0.016)	6.93 (0.273)	0.23 (0.009)**	$6.31 \times 10^5$	$3.16 \times 10^5$	$5.02 \times 10^4$	0.43
6	OOA Type Truss (GE)	0.76	15.0 (0.590)	0.48 (0.019)	8.48 (0.334)	0.23 (0.009)**	$1.36 \times 10^6$	$6.83 \times 10^5$	$9.15 \times 10^4$	0.43
7	Supermast Astromast (F)	0.33 (diameter)	N/A	N/A	N/A	N/A	$1.23 \times 10^6$	$1.23 \times 10^6$	$3.62 \times 10^4$	0.47

\*GE = GY70/X30 graphite epoxy ( $O_2/ \pm 24$ ); F = fiberglass.

\*\*Minimum gage = 0.009 in.

The dimensions of Item 2 in Table 3-38 represent the actual dimensions of the initial GDC deployable truss beam, which has been built and is being tested (see Figure 3-9). The proportions have been worked out carefully to assure compact packaging and efficient deployment. These proportions include tube diameters and fitting proportions. In the design of Alternative #4 (Figure 3-58) other beam sizes are needed also (see Items 1, 3, 4, 5, and 6 in Table 3-38) but detailed designs have not been worked out for these sizes. For this reason we assumed tube diameters and lengths to be scaled exactly in proportion to beam depth and we calculated the corresponding wall thicknesses to carry the loads as explained previously. This procedure has accounted for the unconventional diameters and thicknesses shown in Table 3-38. In an actual design, the proportions would have to be worked out in detail for each different truss cross section and more conventional dimensions might be chosen to accommodate production tooling and actual thicknesses of layup layers of the graphite composite laminations. Nevertheless the figures shown demonstrate feasibility and provide a basis for weight estimating.

**3.1.10 STRUCTURAL DYNAMICS.** Structural vibration modes of the Alternative #4 platform were determined using the finite element model shown in Figures 3-59 and 3-60. The model consisted of 65 grid points and 64 structural elements for a total of 390 structural degrees of freedom. Each payload was modeled as a rigid mass (including rotary inertia effects) lumped at the payload's center-of-gravity. The properties of the structure were obtained from the data listed in Table 3-38.

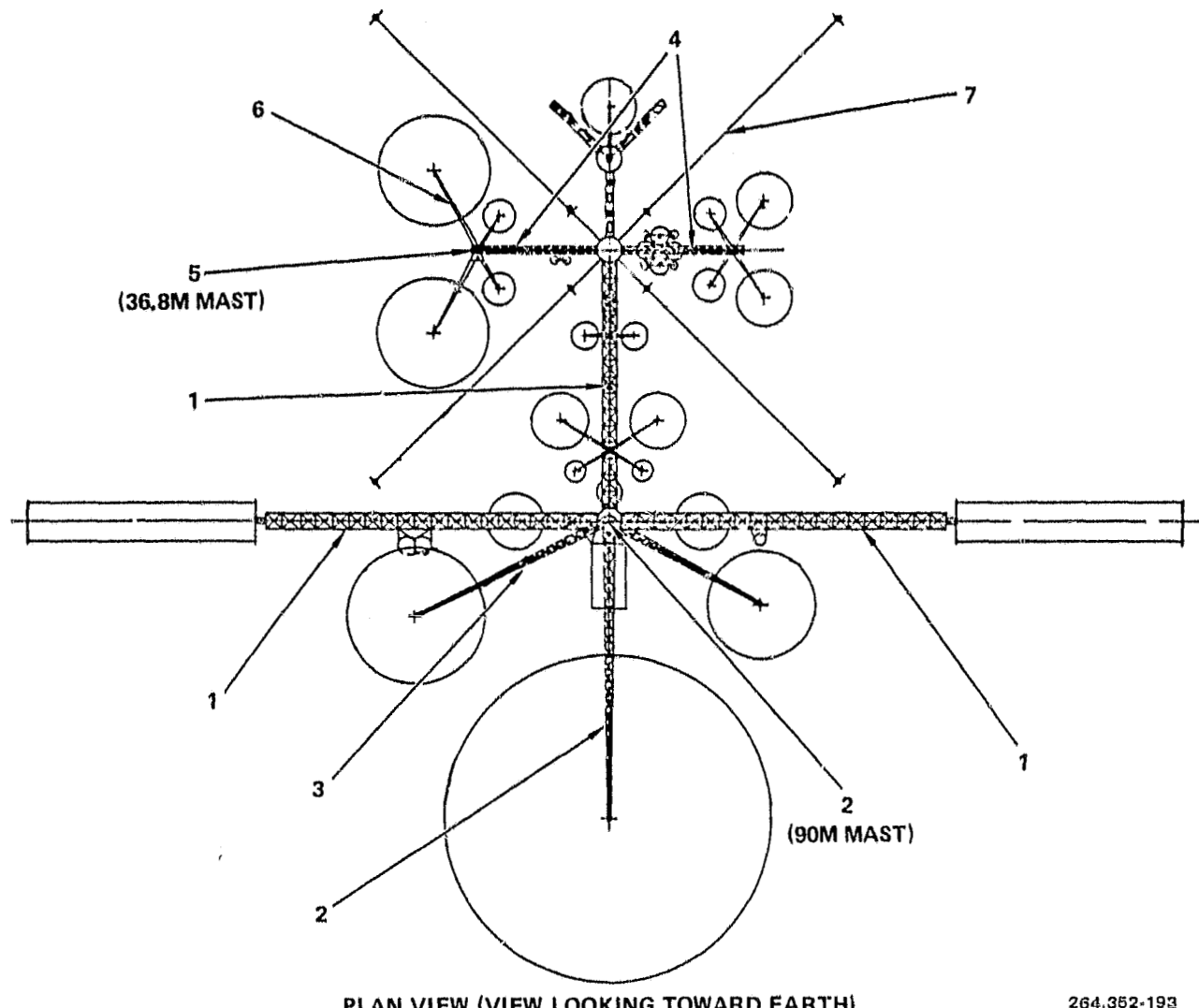
The modal frequencies of all modes up to 0.1 Hz were determined and are listed in Table 3-39. The first eleven mode shapes are described in Table 3-40 and a typical mode shape is shown in Figure 3-61.

### **3.1.11 RELIABILITY.**

**3.1.11.1 Introduction.** Previous satellite programs have emphasized the importance of incorporating reliability/availability analyses and design influence from the conceptual through the operational phase of the total system. Reliability will be designed into the geostationary communication platform system to guarantee trouble-free operation during its expected long life.

Discussion will center on the reliability/availability approach to the design, areas of concern at the subsystem level, and recommendations to assure a highly effective system.

**3.1.11.2 Reliability Considerations.** Since failures have occurred on communications satellites in the past, it is reasonable to assume that similar failures will occur in the future. Actual error in design or problems associated with quality control can result in a reliability less than had been planned.



PLAN VIEW (VIEW LOOKING TOWARD EARTH)

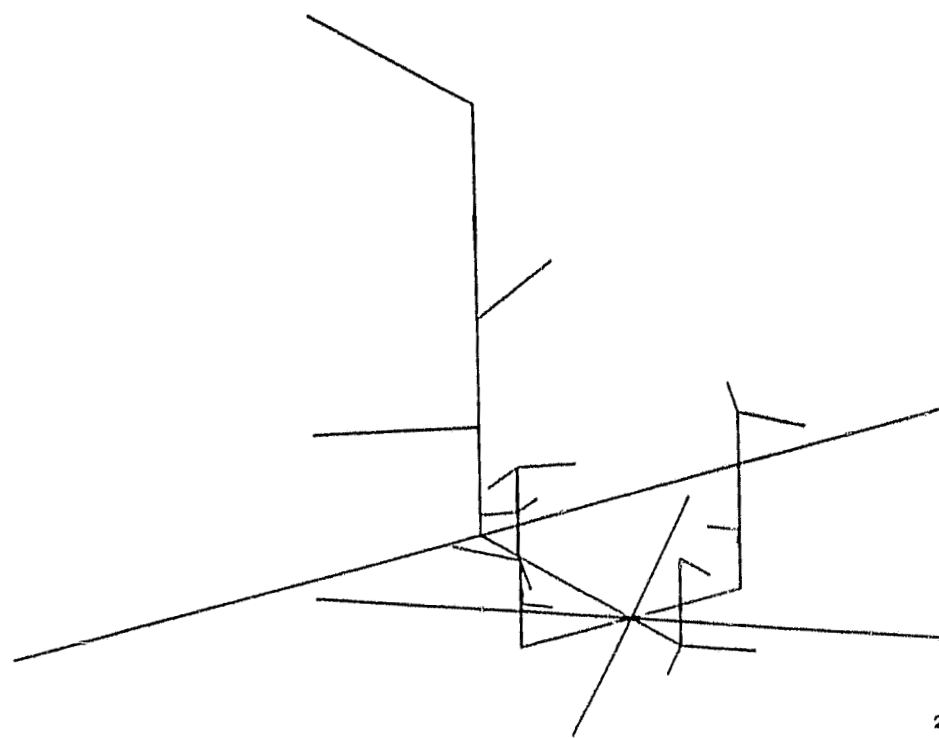
264.352-193

Figure 3-58. Alternative #4 Representative Structural Sections

Experience indicates a large portion of failures are design failures, indicating a possible need for servicing of communications satellites. Areas of concern include communications system, electric power solar array bearings, positioning thruster, orientation, initial erection, orientation propellant, orientation propellant relief valves, orientation earth sensor, telemetry, and command decoder and momentum wheels. Problems may arise from wearout characteristics; gradually the fuel supply will be reduced, batteries may exhibit reduced charge retention, and prime power will approach its end of life rating due to solar cell radiation damage.

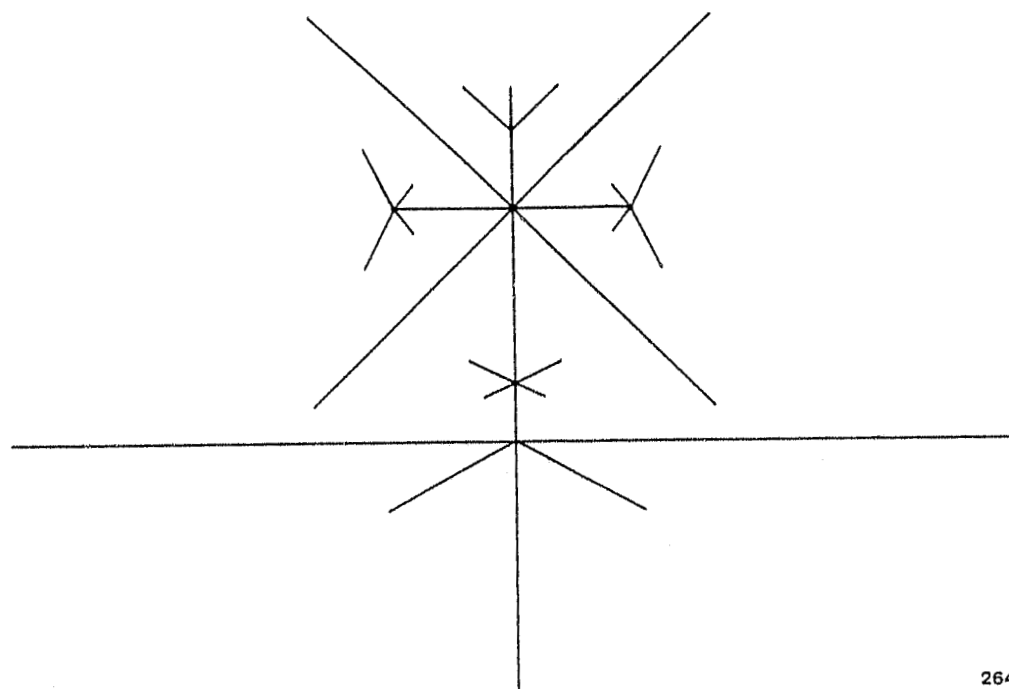
In obtaining high reliability in a communication satellite, several approaches during its design phase must be followed painstakingly.

- a. Reliability in every area must be pursued by all concerned.



264,352-194

Figure 3-59. Isometric View of the Alternative #4 Platform Finite Element Model



264,352-195

Figure 3-60. Top View of the Alternative #4 Platform Finite Element Model

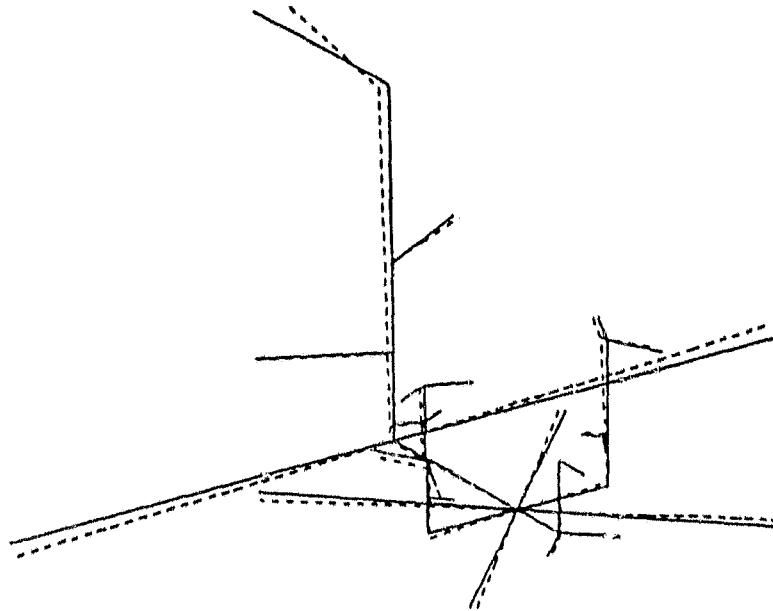
Table 3-39. Modal Frequencies of the Alternative #4 Platform

Mode	Frequency (Hz)	Mode	Frequency (Hz)
1-6	0.000	15	0.063
7	0.019	16	0.066
8	0.023	17	0.067
9	0.030	18	0.074
10	0.043	19	0.078
11	0.044	20	0.085
12	0.046	21	0.088
13	0.048	22	0.092
14	0.059	23	0.098

Table 3-40. Description of the First Eleven Mode Shapes

Mode	Frequency (Hz)	Description of Mode Shape
1-6	0.000	Rigid Body Modes
7	0.019	Torsion of Module 1 Mast
8	0.023	Fore-Aft Torsion of Payload 2.2 Support
9	0.030	Torsion of Payload 1.2 Mast
10	0.043	Coupled Torsion of Payloads 2.2 and 81 Masts
11	0.044	Torsion of Platform Center Beam

- b. Individual parts must be sufficiently derated or planned for use at some small fraction of their designed capacity.
- c. Wide design margins both in operating parameters and in operating environment must be incorporated in subsystems.
- d. Redundant elements must be incorporated into circuits correctly, where their presence offers the highest potential for increased reliability.
- e. The operational environment, that of space at a planned altitude, must be understood quantitatively and its effects anticipated.
- f. Mechanical factors such as the packaging of components, their thermal connections, and their shielding must be precisely designed with adequate margins.
- g. Testing at three levels - components, subsystem, and system - must be rigorous, realistic and carefully planned, including design for testability in the satellite.



HIGH TRAFFIC MODEL - WESTERN HEMISPHERE - ALTERNATE 4  
MODAL BEFORE SUBCASE 7 MODE 7 FREQ 0.018869

264.362-196

Figure 3-61. Typical Mode Shape of the Alternative #4 Platform

In space technology, three types of parts are used depending on the time-cost versus reliability trade that is made.

- a. Commercial parts are those manufactured for standard applications in over-the-counter radios, television sets, and the like.
- b. Military parts are those produced on a production line in which materials and processes are controlled by appropriate military specifications, for example, MIL-STD-105 for quality control and MIL-STD-202 for testing.
- c. High-reliability parts are produced on lines where materials and processes are very strictly defined and controlled and whose handling, packing, storing, transporting, and mounting are rigidly specified. All parts are tested under load for 200 hours, for example, before they are accepted. This eliminates the infant mortality rate or failures that occur during initial system operation resulting from the application of underrated or defective components and from human errors.

**3.1.11.3 Availability Considerations.** A prime design consideration for the geostationary platform system is to attain a high level of operational availability. Availability is an indication of the ratio of the amount of time that a user can successfully use the system to the amount of time he wants to use it. Users are willing to pay for higher availability levels, and due to the high construction/deployment cost, a high availability level is a requirement.

Unfortunately, the term is not uniquely defined for a complete system and, though most people have the same general understanding about it, questions can arise as to just how it should be evaluated quantitatively. For example, when someone speaks of the availability of the geostationary platform system, does he mean:

- a. The entire ground and platform communication system?
- b. The platform system only?
- c. A priority channel?
- d. With or without servicing?
- e. Scheduled, unscheduled, or both?
- f. With or without module replacement?
- g. With or without platform replacement?

An important step, before making major design commitments, will be to clarify these points.

Availability can also have a different interpretation, depending on the design configuration; for example, one large platform will be analyzed differently than a constellation of smaller platforms in the same orbital slot that are required to communicate with one another.

The choice among competing configurations, strictly from an availability and reliability viewpoint, would be one large platform offering economy of scale, with the ability to replace failed modules on a scheduled replenishment trip and on an unscheduled basis if the need arises, while maintaining the highest availability levels on primary channels.

Since the communications satellite system must be capable of operating for 16 years, a serviceable satellite built with replaceable modules that can rendezvous with an unmanned servicer and replace any failed modules can provide many benefits. Some of these would include increased satellite availability, increased reliability, decreased life cycle costs, replacement of worn-out items, installation of updated equipment, and correction of design failures. The advantages of on-orbit servicing appear to be the greatest when there are several similar satellites in orbit in formation or in close proximity to each other, when the program time is long relative to the satellite mean time to failure, and when the satellite availability requirement is high.

Depending on which configurations are chosen for a continuing study, the most applicable availability analysis will be developed.

Experience has shown (especially with Intelsat) that high availability of a satellite communication system can be achieved, through proper design and operating scenarios. The Intelsat system uses a "continuity of service" figure

of merit estimate using circuit hours instead of equipment hours. The figure of merit is similar to an availability factor considering both the satellite and earth terminal system for an average earth-terminal-satellite-earth-terminal path. For the five year period of 1970-1974 this figure of merit was between 0.9988 and 0.9995 on a global basis.

The geostationary communications platform system, due primarily to its 16 year life requirement, will require a greater level of design flexibility and complexity than on existing systems in order to match Intelsat's availability record. To attain high availability levels for a 16 year platform system will require designs to incorporate: high reliability of each subsystem, the allowance for graceful degradation, the elimination/reduction of single point catastrophic failure modes, development of advanced technology subsystems, automatic switching, on-board processing and control, ground to satellite override capability, minimization of the probability of fault propagation through the system, and the option of removing/replacing failed modules in orbit.

There are various ways to achieve high reliability at the subsystem level. Some involve the use of redundancy, active or standby, fault tolerant designs, high-reliability parts, derating, and functional partitioning.

The application of redundancy properly conceived, is one of the strongest tools for enhancing the reliability of the satellite. In fact, for an unattended system, the principles of redundancy provide the increase in expected lifetime that make our present space technology possible and, in particular, satellite communications relays economically feasible. There are, however, dangers in the use of redundancy that must be avoided. If short circuits are more likely than open circuits as the cause of failure in a unit, for example, then simple paralleling of redundant units will increase the failure rate; the redundant part should be placed in series. If a redundant component also requires a switch or relay circuit, the effects of this additional complexity must be included. Each element of the circuit must be scrutinized for the effects of additional components. Redundancy, in and of itself, will be impractical for a long lived system. Initial estimates indicate that increasing the subsystem reliability by redundant elements (e.g., valves, computers, thrusters) alone, impose weight, cost, and volume burdens that are prohibitive for the optional configurations.

The optimal use of redundancy is at the piece part or submodule level. This, combined with high reliability parts and derating techniques, will keep redundancy at the module level to a 2 or 3 module maximum. Proper use of functional partitioning can increase subsystem reliability beyond that of a multiple redundant subsystem. The employment of fault tolerant subsystems tied with the capability of the subsystem to detect critical faults within itself and to automatically repair, isolate, or switch to an alternate path greatly increases reliability while minimizing additional complexity, with its accompanying penalties.

Subsystems will be designed for graceful degradation, especially in the power subsystem (viz; batteries and solar cells) and in the attitude control subsystem (viz; fuel consumption). Combining this with other subsystems, designed such that a reduction in supplied power or internally or externally caused damage, will still allow the subsystem to continue to operate, albeit at a reduced capacity. With gradual degradation of the subsystem telemetered to the ground, it can become a candidate for replacement during a scheduled fuel/battery replenishment trip.

Through proper design techniques and reliability analysis, catastrophic single point failure modes should be eliminated or reduced to an acceptable probability of occurrence. No single failure should result in a mission in-orbit abort.

To obtain and maintain high availability levels, certain subsystems will require an advancement in the state of the art to minimize currently projected excessive redundancy levels. Additionally, it would seem practical to spend the time and money substantially enhancing a given subsystem to achieve a high availability, rather than distributing the same funds over all of the subsystems. Candidates for this enhancement will be discussed in several of the following sections.

To prevent fault propagation through the system, a reliable fault detection, isolation, and switching capability must be an integral part of the design. This will allow redundant units to be brought on line immediately and problem equipments removed from influencing the remaining portions of the platform. In the event of multiple failures, the offending units would be functionally removed, resulting in platform degradation, but not in platform failure.

Designing the system for automatic switching, on-board processing, and control with the option of ground to satellite override capability, in case of a failure not correctable by the satellite, will enhance availability levels substantially.

Finally, servicing, including module replacement, whether scheduled, unscheduled, or both, reflects flexibility of the design resulting in an availability increase.

#### 3.1.11.4 Reliability Subsystem Considerations.

Electrical Power System. The solar array is modular in its construction. The array consists of modules of solar cells connected in parallel. Each module contains six strings of 250 solar cells in each string connected in series and forming one panel. Each cell is connected with a bypass shunt diode. In case of failure, only one cell would be lost in the series string instead of 250. Two panels are connected in parallel.

Array reliability cannot be determined from a parts count, since it is not possible to specify that a given number of failed cells fail the array, while one fewer failed cell does not fail the array. The system will be modeled and optimized to determine the required redundancy. The array is designed for

expected radiation degradation, a 5 percent load margin, and a 10 percent design margin for unknowns, which will enhance the reliability.

The solar array is failure tolerant because design allows diode switching around failed solar cells so that high reliability levels are maintained despite random solar cell failure occurrences. It is degradation tolerant because it allows for some random solar cell failures in the system and for the system to still be operational.

Each platform has four batteries in parallel. Each battery has 72 battery cells in series. Each cell is connected with a bypass shunt diode. In case of failure, only one cell would be lost in the series string instead of 72. Each battery is designed with a certain amount of reserve if distributed fairly evenly over all batteries, that is, not all in one battery.

The battery is failure tolerant because design allows diode switching around failed battery cells so that high reliability levels are maintained despite random battery cell failure occurrences. It is degradation tolerant because it allows for some random battery cell failures in the system and for the system to still be operational.

In the switching mechanism, the most probable failure modes are opens and shorts. The mechanism most often found is contamination, which manifests itself as either particulate matter or corrosion products. The conductive materials obviously produce varied conductance paths or shorts as well as switch lockup because of wedging or jamming. The nonconductive material results in contact interference or open, as well as switch lockup. Switch screening inspections and tests are recommended to discover failures before actual part implementation. MIL-STD-202 has many effective tests ranging from temperature cycling to hermeticity and radiographic inspection.

Solder connections are an area of concern in any electrical power system. One of the most prevalent modes of failure is the cracking of connections due to thermal fatigue. In many instances, it is very difficult to distinguish between solder cracking as a result of thermal fatigue and those as a result of poor workmanship. Thermal fatigue cracks will predictably occur on sequentially manufactured items and will also propagate with storage time. Solder cracks due to poor workmanship will appear randomly on sequentially produced items. These failures can be reduced by applying and controlling appropriate design criteria. The following list of criteria can be used as a guide to minimize these problems.

- a. Use only silicone or polyurethane based conformal coatings of minimum thickness.
- b. Avoid gold-plated boards. Use solder plated or solder coated boards.
- c. Do not use rigid encapsulating system to secure and protect connected parts on printed wiring boards.

- d. Resilient spacers should be of minimum thickness between the solder connected part and printed wiring board.
- e. Do not hard mount parts to printed boards with mechanical fasteners unless leads are parallel to the board and of sufficient length as to provide strain relief. Also, do not hard mount parts by using minimum lead length inserted through feedthrough holes.
- f. Use terminals only when necessary and then only use terminals designed to be used on printed wiring boards.

Telemetry, Command, and Control. Coded command signals transmitted from the ground control station to the spacecraft are used to reset clocks, execute spacecraft maneuvers, recalibrate instrumentation, adjust transmitters, reposition steerable antennas, actuate switching devices, override preprogrammed signals, change telemetry commutation rates, or activate a variety of other decision mechanisms and telemetry devices. The telemetry link may, in fact, be considered as the return path of the command/control link, whether it transmits verification of command status of equipment, or actual diagnostic-data. Commands may also be used for partial control and fault correction within the spacecraft to enhance reliability.

Command receiver performance is critical to system success and must be designed for the highest reliability. These receivers are characterized by low sensitivity, high selectivity, and wide dynamic range to avoid saturation. Selectable fixed frequencies, each with narrow bandwidth, permit operational flexibility and make available a choice of several command bands for alternate channel arrangements.

Two redundant command receivers usually are used, with the outputs cross-connected to the decoders. Failure detection features built into the receivers would allow the gain of one receiver to double should the other fail. Similarly, the outputs of dual digital decoders could be combined in parallel, although each may have a separate address.

Attitude Control System. Two types of control that may be required are control of the location of the satellite in orbit or orbit velocity, and control of the satellite attitude. The control system must be extremely reliable since it must operate throughout the life of the satellite.

The satellite's attitude can be controlled by torqued gyros or reaction wheels. When the wheel inside the satellite is accelerated or decelerated, it creates a torque in the opposite direction. Since the torque created by the wheel will be a product of its inertia and its angular acceleration, relatively lightweight wheels can be used if they can be driven at sufficient speed and means must be incorporated to prevent their overspeeding.

A probable failure mode is bearing wearout of the reaction wheels. A new technology of magnetic bearings, with no wear characteristics, will be considered a prime candidate for the platform, thus increasing design reliability.

Another new technology that will be considered is pulsed plasma thrusters to replace the thrusters now in use. They have a reported reliability of 0.95 as a probability that they will operate within specification after 10 years.

Thermal Control System. The influence of structure on mass equilibrium temperature and thermal gradients within the system are an important consideration in the mechanical design of the spacecraft. The only effective means of achieving temperature control is to adjust the spacecraft radiation balance so that the absorbed energy is balanced by the radiated energy at the required temperature. The fundamental areas of concern are internal power dissipation and heat generation, and the ratio of absorption to emission of the external surface.

The system contains radiators, pumps, and valves. The most probable failure mode is leakage. Deterioration of the contacting surfaces, due to wear, damage during installation, chemical attack, misalignment, etc., will result in imperfect sealing resulting in internal leakage. All valves with the exception of relief and check valves are actuated by an external mechanical force that is transferred to the movable member by a stem or riser. This actuation mechanism is subject to failure by seizure as the result of corrosion, contamination, or failure. The required opening into the valve body for entry of the operating stem is an additional source of leakage due to inadequate design and packing.

Primary considerations in the selection of valves includes knowledge of the physical property of materials from which the valve is manufactured in order to assure compatibility with applicable fluids, temperatures, and pressure limits.

Summary. The areas of concern will be reduced and the reliability increased by selecting high reliability parts, extensive quality assurance testing, good quality control, redundancy, fault tolerance, and parts derating.

A computer analysis of the subsystems indicates the design will require funding for research and development and extensive testing to attain high reliability and maintain high availability levels through the life of the platform system.

A review of all new technology as related to the geoestationary platform should be made including integrated circuits, magnetic bearings, and pulsed plasma thrusters. Extensive testing will be performed to obviate failure modes.

**3.1.12 RADIATION ENVIRONMENT.** A study of the radiation environment at geostationary altitude is included in this section. Though the levels are considerably less than at lower altitudes in the van Allen belt, the long lifetime requirement of 16 years makes consideration of this factor mandatory.

As a starting point for this discussion, Appendix K which is basically unchanged from that for Intelsat IV and V, will be used. This environment is conservative and as a worst case can be scaled directly to a 16 year mission (assuming two solar flare cycles for the proton fluence). Since it is conservative (primarily in using the solar flare proton fluence from cycle 19), a more reasonable environment would be obtained by scaling the electron environment to 16 years, but using the flare proton results for only 1 solar cycle. More recent data for the electron environment at synchronous altitude has been provided in the NASA AEI-7HI/LO radiation model. This model indicates greater fluences above 3.5 MeV than the AE-4 model on which Appendix K is based. More data, being acquired on the P78-2 (SCATHA) satellite, will provide a better specification in the not too distant future. The analytic representation of the environment as expressed in the appendix are between the AE-4 and AEI-7 LO values and are adequate for our purposes for several reasons: 1) the influence of the electron environment above 3 MeV is small compared to that from the low energy electrons and solar flare protons for a lightweight solar array; 2) experimental uncertainty is greatest in the electron environment in this high energy region; and 3) the uncertainty in predicting the solar flare proton fluence is at least as great as that in measurements of the high energy electron region.

Laboratory simulation of a space environment on solar cells with known and tested radiation behavior is fraught with uncertainties. Specifying a simulation for cells not yet designed is even more daring. As a first approximation, lightweight array cell configurations will be assumed for 10  $\Omega$ -cm silicon solar cells with presently known characteristics and calculations will be based on a paper by Rostron, reproduced in Appendix L for convenience. The cell configurations (Table 3-41) will be limited to three sets, but subdivision will allow further configurations to be derived. Only the significant components of the radiation environment will be included: electrons and solar flare protons. Table 3-41 gives the 1 MeV electron equivalent fluences/cm<sup>2</sup> associated with a year or cycle exposure to the electron or solar flare proton environment. Since the substrate provides no greater protection than the coverslides, the equivalent fluences are specified for both front and back contributions. The values in Table 3-41 are assembled in Table 3-42 to represent the three configurations for a 16 year mission including both the worst case (2 solar flare cycles) and the expected case (1 solar flare cycle). It is seen that proton damage dominates the predicted equivalent fluence and that arrays with thin substrates are particularly susceptible to proton damage when the protection falls below 50  $\mu$ m thickness.

As a second approximation, predicted structure modifications for future cells are used. Heavily doped cells may achieve high efficiencies but are very sensitive to both electron and proton damage. High resistivity cells (light

Table 3-41. Solar Cell Configurations

Configuration		Electron	Proton
1) 2 mil Coverslide	Front	$6.0 \times 10^{13}/\text{yr}$	$2.0 \times 10^{15}/\text{cycle}$
	Back	5.5	1.0
	Total	$11.5 \times 10^{13}/\text{yr}$	$3.0 \times 10^{15}/\text{cycle}$
2) 2 mil Coverslide	Front	$6.0 \times 10^{13}/\text{yr}$	$2.0 \times 10^{15}/\text{cycle}$
	1 mil Substrate	6.0	4.0
	Total	$12.0 \times 10^{13}/\text{yr}$	$6.0 \times 10^{15}/\text{cycle}$
3) 4 mil Coverslide	Front	$5.0 \times 10^{13}/\text{yr}$	$0.8 \times 10^{15}/\text{cycle}$
	2 mil Substrate	6.0	2.0
	Total	$11.0 \times 10^{13}/\text{yr}$	$2.8 \times 10^{15}/\text{cycle}$

Table 3-42. Solar Cell Configuration Totals

Configurations	1	2	3
Electrons	$1.8 \times 10^{15}$	$1.9 \times 10^{15}$	$1.8 \times 10^{15}$
Protons	$3 + 6 \times 10^{15}$	$6 + 12 \times 10^{15}$	$2.8 + 5.6 \times 10^{15}$
Total	$5 + 8 \times 10^{15}$	$8 + 14 \times 10^{15}$	$5 + 7 \times 10^{15}$

doped) display a different damage mode but, at least with present understanding, are much less influenced by protons when under AM0 illumination. Since proton damage is the dominant degradation source, the injection level effects that reduce the effective proton damage are of greatest importance. The 1 MeV equivalent fluence could, therefore, in general, be much smaller for the proton environment. However, 50  $\mu\text{m}$  thick coverslides allow a much greater percentage of low energy protons to transit the cell and the damage from these protons is less sensitive to injection levels (References 55 and 56).

Future cells on thin deployed arrays could very well have grids on the backs rather than full metal coverage as presently employed. This would allow greater emittance and lower absorption of long wavelength light. The lower total metal on the back would reduce the radiation protection from the back but could actually reduce any damage from micrometeoroids. This threat is small for conventional arrays but is increased by an order of magnitude for the geostationary platform ultralightweight array design. The micrometeoroid environment in Section 2.5 of Appendix K indicates about 1 crater/ $\text{m}^2$  every three days. Over 16 years in orbit about 2000 holes/ $\text{m}^2$  will penetrate the cell

junctions, both front and back. Nearly a third of these will leave craters 500  $\mu\text{m}$  across. Data on micrometeoroid damage to solar cells is not common and some of that which is available is not valid. For the most part a clean puncture or crater is not expected to influence cell performance. Even a fracture is not going to be damaging; but if a crater is generated through metalization, the possibility exists for shorting a cell. Unmetalized backs are therefore preferred if substrate thickness cannot reduce the probability of micrometeoroid penetration.

Ultraviolet damage is not likely to be worse on future cells than present and a loss factor of  $2.5 \pm 0.5 \text{ mA/cm}^2$  is reasonable.

In summary, a 1 MeV electron equivalent fluence of  $6 \pm 2 \times 10^{15}/\text{cm}^2$  is a good number for radiation simulation of solar cells in an ultra light solar array. More work on damage from penetrating micrometeoroids is necessary since thin coverslides and substrates greatly increase the probability of degradation from this source.

### 3.2 TRANSPORTATION SYSTEMS

In the Task 2 system trade studies we defined and evaluated more than 150 platform system concepts that employed the Shuttle and 19 different OTV configurations/operating modes to launch to LEO and transfer to GEO. We found that platform design and program costs are directly coupled to the choice of transportation means and that transportation costs are a significant fraction of total program costs. The percentage of transportation costs versus total space segment program costs ranged from 22 percent to 65 percent over the span of OTV/platform concepts, and the average for all cases was 40 percent. For Alternative #1, the ratio is 34 percent.

**3.2.1 TRANSPORTATION REQUIREMENTS.** Transportation requirements are of two types: 1) delivery of the platform modules to their assigned orbital locations, and 2) delivery of servicing items for periodic logistics missions. In both cases, the space Shuttle is employed to place an OTV mated with a platform module or servicing items into a circular parking orbit at 296 km (160 n.mi.) altitude, inclined 28.5 degrees. The Shuttle can deliver 29,484 kg (65,000 lb) of cargo to this reference orbit.

**3.2.1.1 Program Schedule.** Twelve module delivery missions and 16 logistics missions are scheduled over the initial 16 years of the program mission, as shown in Figure 3-62. A nominal launch schedule is shown for logistics flights; specific dates would be scheduled in accordance with actual needs as determined during the course of the program. If a high level of payload updating activity is required, some additional logistics flights would be required. Logistics traffic requirements and mission planning are analyzed in detail in Section 3.3.

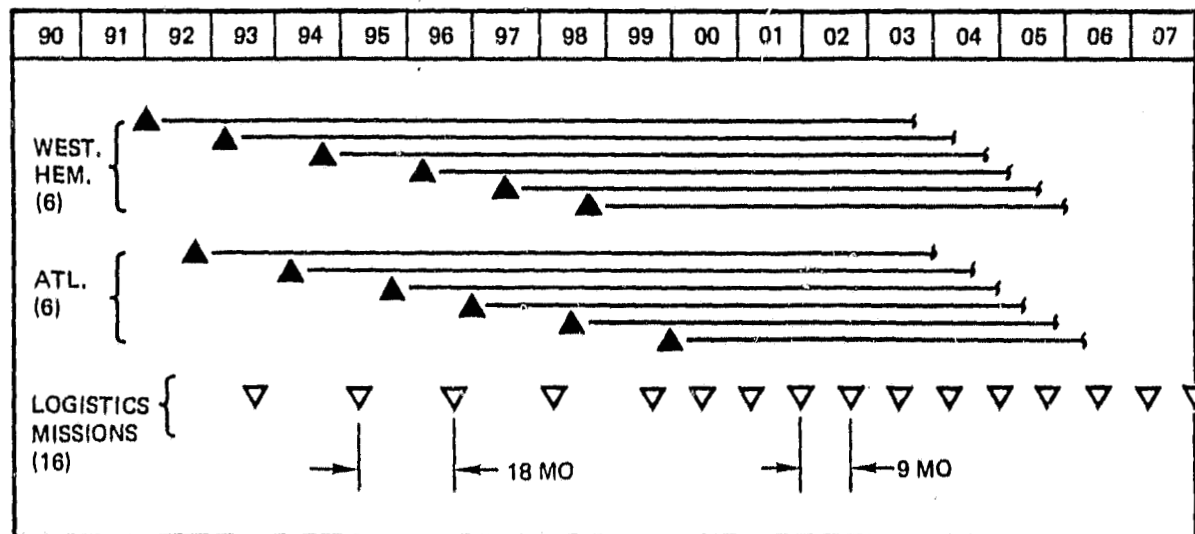


Figure 3-62. Program Schedule

**3.2.1.2 Platform System Description.** For platform system concept Alternative #1, the communications and secondary payload set for the nominal traffic model is accommodated on 12 platforms. Six are located at 110°W longitude to serve the Western Hemisphere, and six are located at 15°W longitude to serve the Atlantic area. The delivery of each of the modules is time-phased as shown in Figure 3-62 to meet the projected communications traffic demands.

This concept employs the single Shuttle (per module) launch mode; i.e., the mated OTV and platform module (packaged in its launch configuration) together occupy the Shuttle cargo bay. The OTV and platform, along with associated ASE, must conform to the Shuttle weight, size and cg constraints as specified in JSC 07700, Vol. XIV.

The OTV that was selected for the module delivery mission for Alternative #1 is the single stage OTV, using a low thrust engine, used in the expendable mode. For the single Shuttle launch mode, propellant is offloaded from the OTV to meet the Shuttle's 29,484 kg (65,000 lb) cargo weight limit. Shuttle/OTV performance capabilities, constraints, and costs were furnished by NASA (Reference 57).

When the OTV/platform assembly is delivered to the parking orbit by the Shuttle, the assembly is rotated out of the cargo bay and positioned relative to the Orbiter while the platform elements are deployed and checked out by the crew. Subsystems and payloads are preattached and prewired to the maximum extent consistent with Shuttle volume constraints. Certain installation tasks may be accomplished by planned EVA where this mode yields an advantage in

reducing platform complexity or cost and/or in increasing reliability. Unplanned EVA is also available as a backup operating mode to correct anomalies.

When the platform and OTV checkout are satisfactorily completed, the assembly is released from the Orbiter and the OTV begins the LEO to GEO transfer phase.

The OTV transfers the platform to a designated delivery point near its assigned orbital slot using a multiple perigee burn, single apogee burn trajectory. Preliminary delivery point RSS accuracy requirements are as follows:

Position:  $\pm 10$  km

Velocity:  $\pm 3$  m/s

Orientation: Nadir  $\pm 1$  degree

When the earth station command and control link is established and the platform ACS is activated and acquires its references, the OTV releases the platform without imparting significant velocity or attitude perturbations, backs away to a safe distance, and then lofts itself to a supersynchronous orbit where it cannot interfere with geostationary platforms or other satellites.

Each of the two assigned orbital slots ( $110^{\circ}$ W and  $15^{\circ}$ W) will eventually be occupied by six platform modules, arranged in a rotating circular constellation that will maintain them well within a  $\pm 0.1$  degree area as viewed from the earth, yet will maintain minimum separation distances and minimize orbit adjustment propellant usage. This is accomplished by placing each of the modules in orbits that deviate slightly from geostationary orbit (slightly inclined and slightly elliptical) with the proper nodal point phasing. The platform on-board propulsion system is used to control the placement of each platform module into its desired orbit, and then maintain its relative position. Values of orbit eccentricity of  $e = 0.00011$  and inclination of  $i = 0.0125$  degree will result in a circular constellation with a diameter on the order of 18 km.

Alternative #1 is designed to require a minimum of servicing while assuring high system availability. Platform subsystems are designed for 16 years of life and employ a high degree of redundancy of critical elements. The RCS, which provides both attitude control and stationkeeping propulsion, is sized to carry an eight-year supply of propellant and will be replenished at intervals less than or equal to eight years. Batteries are packaged in modules that can be replaced in orbit by an unmanned servicing vehicle. Battery usable life is currently projected to be about 10 years; therefore, as few as one servicing flight could theoretically suffice for a 16 year platform mission, given a large enough servicing vehicle. Payload equipment can either be designed for long life through high redundancy or for repair or replacement via logistics flights; this choice is a user option. However, if users elect to service or update payloads, the number of logistics flights will be increased beyond that shown in Figure 3-62.

The OTV that has been chosen for the logistics missions is the single stage OTV with a standard thrust engine, used in the reusable mode. The teleoperator maneuvering system (TMS) that is employed as the servicing vehicle is also recovered for reuse. Definition of the TMS was provided by NASA (References 58 and 59).

**3.2.2 MODULE DELIVERY TRANSPORTATION ANALYSIS.** The Alternative #1 concept was jointly selected by General Dynamics Convair and NASA to further define and evaluate the smaller size range of platforms that could use a single stage OTV and one Shuttle launch per platform module. (A conceptual design has been started for Alternative #4 - see Section 3.1.3.2. A transportation analysis should be performed on Alternative #4 in the future tasks.) The Shuttle launch mode and OTV capability places two major constraints on platform design: 1) the OTV mass delivery capability to GEO determines the number of platforms required to accommodate the payload set, and 2) having chosen an OTV, launch mode determines the volume in the Shuttle bay available for packaging the deployable platform for the earth-to-LEO transportation phase.

**3.2.2.1 Earth-to-LEO Mission Phase.** Each platform module, packaged in its launch configuration, is integrated with the OTV at the vertical processing facility (VPF). Following checkout and interface verification, the OTV/platform module assembly is transported in the payload canister to the launch pad and is transferred to the payload changeout room (PCR). The PCR is then rotated to mate with the Orbiter and the assembly is loaded into the Orbiter on the launch platform.

Transportation analyses were initially made using a reference platform weight\* of 6895 kg. This is the OTV capability specified by NASA in Reference 57. While this work was in progress, conceptual designs and corresponding weight estimates were being made. Thus additional transportation analyses were made later (see Section 3.2.2.4) using data from the conceptual designs as they became available. The conceptual designs are identified as follows:

Alternative #1	Platform 1
	Platform 2
	Platform 6
Alternative #4	Module 1
	Module 2
	Module 3

Figures 3-63 and 3-64 illustrate launch configuration packaging concepts for two of the platform modules assigned to the 110°W orbital slot.

---

\*Not to be confused with weights estimated for actual design concepts (see Tables 3-32 through 3-34).

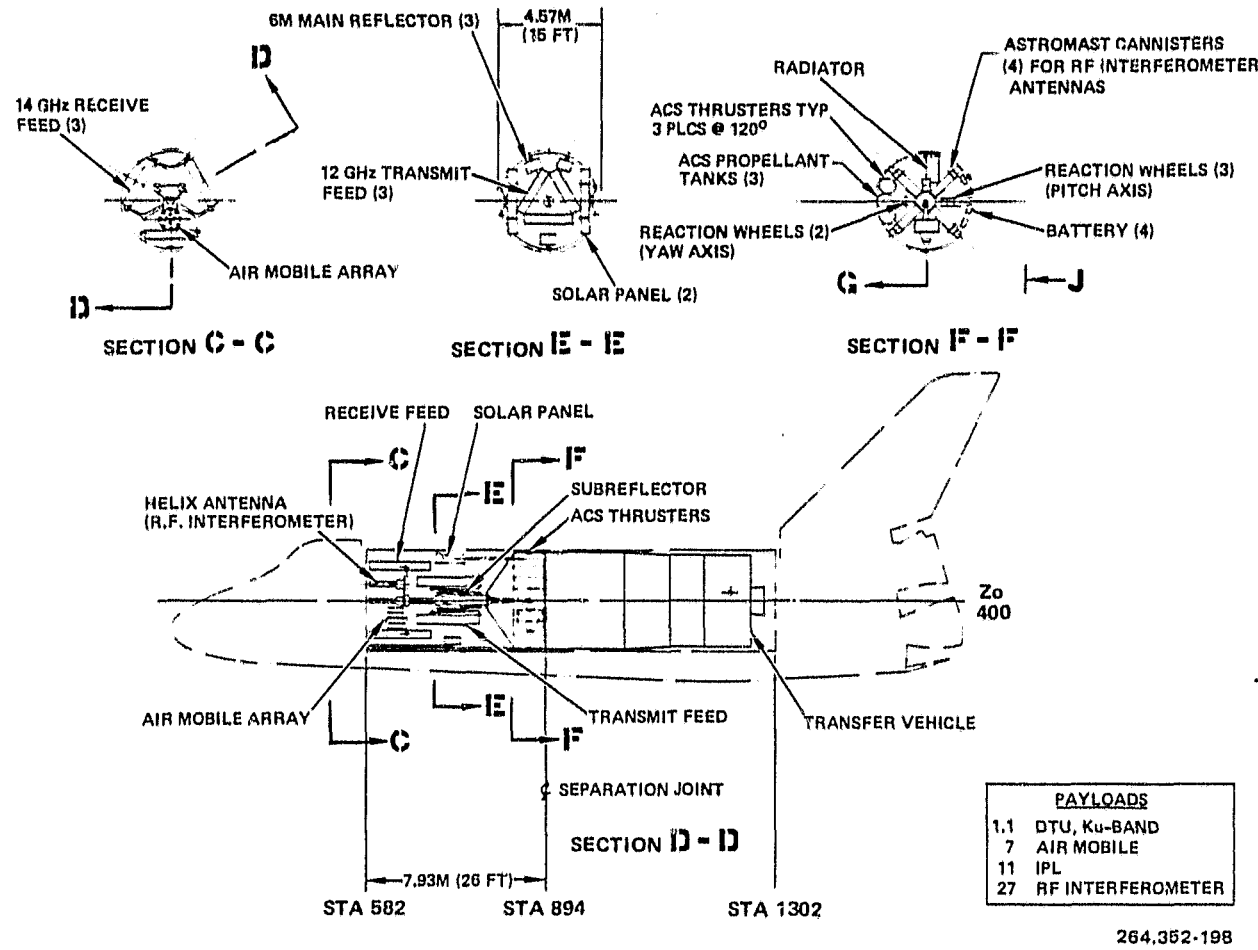


Figure 3-63. Alternative #1, Platform 2, Launch Configuration

The liftoff mass statement for the OTV with a reference platform (6,895 kg) is given in Table 3-43. The maximum permissible platform ASE mass for this configuration is 265 kg. Although the OTV propellant tanks are capable of loading 24,306 kg (53,585 lb) of propellants, it is necessary to off-load 7,390 kg (16,293 lb) in order to meet the Shuttle's 29,484 kg (65,000 lb) cargo weight constraint. This parameter directly determines the delivery mass capability of the OTV to GEO, and thus the maximum platform mass.

Detailed descriptions of the earth-to-LEO flight and the LEO platform construction and checkout operations are presented (for typical delivery flight) in Section 3.3 (refer to Table 3-57). The nominal time required for the earth-to-LEO mission phase and payload deployment and checkout is approximately 62.5 hours (through OTV/platform release from the Orbiter).

**3.2.2.2 LEO-to-GEO Mission Phase.** The OTV transfers the platform to the designated delivery point using a 7 perigee burn, single apogee burn trajectory. The OTV operates in the low thrust mode, with a maximum thrust-to-weight ratio at burnout of  $T/W = 0.07$ . Table 3-44 summarizes the OTV characteristics

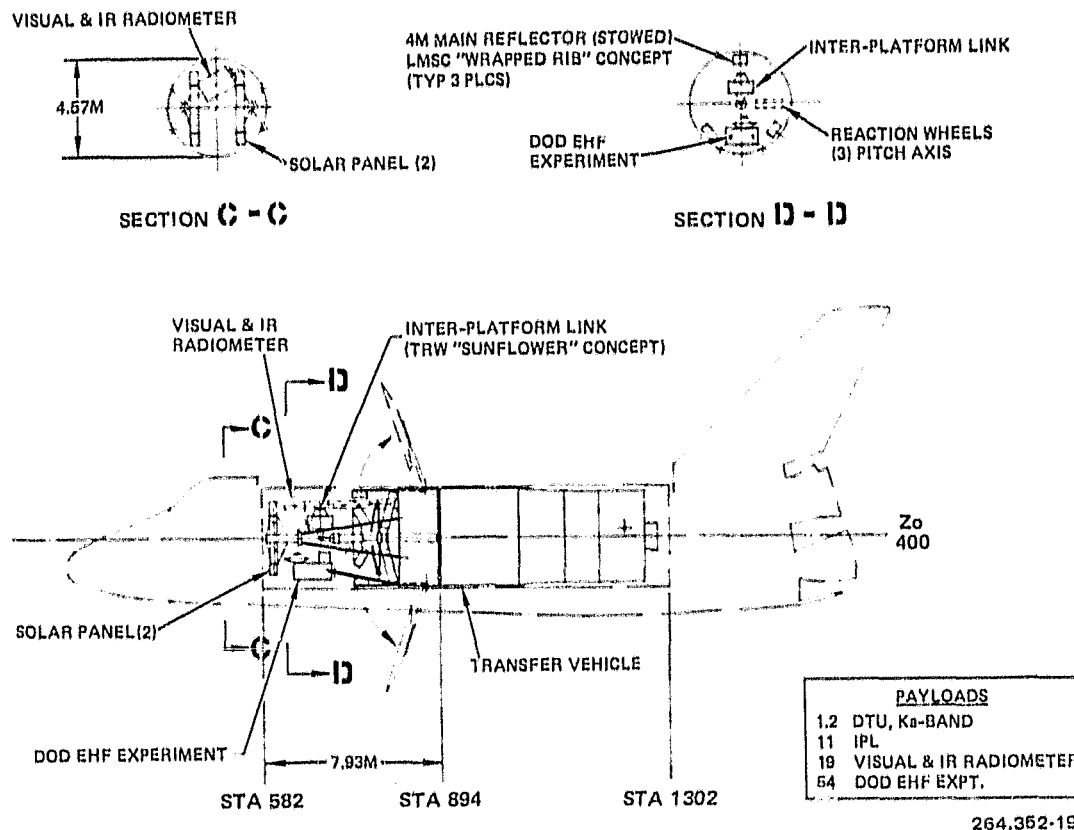


Figure 3-64. Launch Configuration, Alternative #1, Platform 6

for the delivery mission. A description of the events for this mission phase is given in Table 3-57. The time required for LEO-to-GEO transfer and OTV separation is approximately 36 hours. After separation, the OTV is then lofted to a disposal parking orbit at 39,500 km (21,323 n.mi.) altitude (circular).

A vehicle performance analysis for the LEO-to-GEO transfer phase is given in Table 3-45. (In the analysis, propellant usage calculations are performed using conventional units and the results are displayed in both conventional and SI units.)

For the performance analysis, the RCS  $\Delta V$  requirements (which are on the order of 70 fps) are lumped in with the main engine requirements. This simplifying assumption does not contribute any significant error to the analysis results (i.e., about 6 lb).

During the 2.5 day period spent in LEO the OTV propellant boiloff rates are:

$$\text{LO}_2 = 24.3 \text{ lb/day} (11.04 \text{ kg/day})$$

$$\text{LH}_2 = 17.0 \text{ lb/day} (7.74 \text{ kg/day})$$

$$\text{Total } 41.3 \text{ lb/day} (18.78 \text{ kg/day})$$

Table 3-43. OTV/Platform Launch Mass  
(For 6,895 kg Reference Payloads\*)

<u>Mass</u>		
	kg	lb
Platform Module (including adapters, etc)	6,895	15,200
OTV Stage Burnout Mass**	2,843	6,268
Propellant Mass	16,916	37,292
LO <sub>2</sub> 14,499 kg (31,965 lb)		
LO <sub>2</sub> 2,417 kg ( 5,327 lb)		
ASE Mass	2,830	6,240
OTV      2,566 kg (5,656 lb)		
Platform   265 kg ( 584 lb)		
Totals	29,484	65,000

\*For Design Concept Weights see Tables 3.1.8.1-1, -2 and -3.

\*\*Includes FPR of 202 kg (445 lb).

The total boiloff losses in LEO are thus:

$$\text{LO}_2 = 61 \text{ lb (28 kg)}$$

$$\text{LH}_2 = 42 \text{ lb (19 kg)}$$

$$\text{Total } 103 \text{ lb (47 kg)}$$

The sum of the velocity increments required for the 7 perigee burns is 8200 feet per second, including the additional gravity losses associated with this low thrust trajectory. The apogee burn requires a velocity increment of 6200 fps for circularization, final plane change, and trimming the orbit parameters to deliver the platform module to the designated aim point. Because of the relatively short LEO-to-GEO transfer phase time duration, propellant boiloff during LEO-to-GEO transfer is assumed to be zero. Delivery of the platform thus requires 36,944 lb (16,758 kg) of propellant (plus LEO boiloff losses), and at this point in the mission the usable propellant remaining is 245 lb (111 kg).

**3.2.2.3 OTV Disposal Mission Phase.** After the OTV separates from the platform, it drifts away to a safe distance and then performs a 2 burn coplanar Hohmann transfer to place itself into a 39,500 km (21,323 n.mi.) altitude circular orbit.

Table 3-44. Delivery Mission OTV Characteristics

Physical Size		
Diameter	14.6 ft	(4.47m)
Length (Engine bell retracted)	34 ft	(10.36m)
Main Engine		
Propellants	LH <sub>2</sub> /LO <sub>2</sub>	
Thrust Level	1500 lb	(6672N)
Isp	450 sec	(4413 $\frac{Ns}{kg}$ )
RCS Thrusters		
Propellants	LH <sub>2</sub> /LO <sub>2</sub>	
Thrust Level	25 lb	(111N)
Isp	380 sec	(3726 $\frac{Ns}{kg}$ )
Stage Burnout Mass	6268 lb	(2843 kg)
Hardware	5,223 lb (2369 kg)	
Residuals	600 lb (272 kg)	
FPR	445 lb (202 kg)	

During the 1.5 day stay time at GEO, the OTV propellant boiloff losses are 62 lb (28 kg), thus reducing the remaining propellant mass to 183 lb (83 kg).

The perigee burn velocity increment ( $\Delta V_p$ ) is:

$$\Delta V_p = \sqrt{\frac{K}{r_p}} \left[ \sqrt{\frac{2 r_a/r_p}{1 + (r_a/r_p)}} - 1 \right]$$

where  $K = 1.4076 \times 10^{16} \text{ ft}^3/\text{sec}^2$

$$r_p = 1.3833492 \times 10^8 \text{ ft}$$

$$r_a = 1.5048715 \times 10^8 \text{ ft}$$

$$\frac{r_a}{r_p} = 1.0878464$$

$$\Delta V_p = 210 \text{ ft/sec}$$

Table 3-45. Delivery Vehicle Flight Performance Analysis  
(for 6,895 kg Reference Payload)

1.	Propellant loading at launch is	37,292 lb	(16,916 kg)
2. Flight Performance Analysis			
2.1 Perigee Burns			
a.	$\Delta V = 8200$ fps		
b.	Propellant boiloff in LEO is	103 lb	(47 kg)
c.	Usable propellant mass is	37,189 lb	(16,869 kg)
d.	Starting mass: Stage B. O. *	6,268 lb	( 2,843 kg)
	P/L	15,200 lb	( 6,895 kg)
	Propellant	37,189 lb	(16,869 kg)
	Total	M <sub>S</sub>	58,657 lb
e.	End of burn mass	M <sub>E</sub>	33,308 lb
f.	Mass of propellant burned	M <sub>P</sub>	25,349 lb
g.	Mass of propellant remaining	M <sub>R</sub>	11,840 lb
			( 5,371 kg)
2.2 Apogee Burns			
a.	$\Delta V = 6200$ fps		
b.	Starting mass	M <sub>S</sub>	33,308 lb
c.	End of burn mass	M <sub>E</sub>	21,713 lb
d.	Mass of propellant burned	M <sub>P</sub>	11,595 lb
e.	Mass of propellant remaining	M <sub>R</sub>	245 lb
			( 111 kg)
2.3 Disposal Perigee Burn			
a.	$\Delta V = 210$ fps		
b.	2.2e propellant remaining		245 lb
c.	Propellant boiloff in GEO		62 lb
d.	Usable propellant mass		183 lb
e.	Starting mass : Stage B. O. *	6,268 lb	( 2,843 kg)
	Propellant		183 lb
	Total	M <sub>S</sub>	6,451 lb
f.	End of burn mass	M <sub>E</sub>	6,358 lb
g.	Mass of propellant burned	M <sub>P</sub>	93 lb
h.	Mass of propellant remaining	M <sub>R</sub>	90 lb
			( 41 kg)
2.4 Disposal Apogee Burn			
a.	$\Delta V = 205$ fps		
b.	Starting mass	M <sub>S</sub>	6,358 lb
c.	End of burn mass	M <sub>E</sub>	6,269 lb
d.	Mass of propellant burned	M <sub>P</sub>	89 lb
e.	Mass of propellant remaining	M <sub>R</sub>	1 lb
			( 0 kg)

\*Includes FPR of 445 lb (202 kg)

The apogee burn velocity increment ( $\Delta V_a$ ) is:

$$\Delta V_a = \sqrt{\frac{K}{r_a}} \left[ 1 - \sqrt{\frac{z}{1 + (r_a/r_p)}} \right]$$

$$\Delta V_a = 205 \text{ ft/second}$$

Again, due to the short time span, propellant boiloff during transfer is assumed to be negligible. Disposal of the OTV stage into a supersynchronous orbit thus requires 182 lb (83 kg) of propellant, leaving the flight performance reserve of 445 lb (202 kg) of propellant margin.

**3.2.2.4 Conceptual Design Results.** Mass of each designed platform varies from the reference platform mass because of differences in payloads and subsystems. Also, the ASE required to structurally support the packaged platforms during ascent from earth to LEO will be a function of payload fragility; studies to date indicate that such ASE will be considerably heavier than that previously shown for the reference platform. A comparison of these weight elements is as follows:

Reference Platform	Platform Mass, kg	Platform ASE Mass, kg
Reference	6895	265
1	6641	685
2	6655	648
6	6082	862

Flight performance analyses for the delivery of Platforms 1, 2, and 6 were run using the designed platform and ASE masses and the results are summarized in Tables 3-46 through 3-48, respectively. In all three cases, when the maximum allowable propellant load is used (i.e., Shuttle launch mass = 29,484 kg), flight performance is more than adequate. The propellant mass margins for delivery of Platforms 1, 2, and 6 (and disposal of the OTV stage) are 96 kg, 95 kg, and 576 kg, respectively. These margins are in addition to the FPR of 202 kg.

A potential performance problem will be encountered if the mass of a platform approaches the 6895 kg reference mass and the platform ASE mass approaches the 700 to 900 kg area. To define these limits, a series of performance analyses was run over a range of ASE masses, and the corresponding maximum allowable platform masses were calculated. The results of these analyses are plotted

Table 3-46. Platform No. 1 Delivery Performance Analysis

1.	ASE mass - OTV	= 2566 kg;	Platform	= 685 kg;	Total	= 3,251 kg.
2.	Propellant Loading at Launch is	36,924 lb (16,749)				
3.	Flight Performance Analysis					
3.1	Perigee Burns					
a.	$\Sigma \Delta V = 8,200$ fps					
b.	Propellant boiloff in LEO is			103 lb	( 47 kg)	
c.	Usable propellant mass is			36,821 lb	(16,702 kg)	
d.	Starting mass: Stage Burnout*			6,268 lb	( 2,843 kg)	
	Payload			14,641 lb	( 6,641 kg)	
	Propellant			36,821 lb	(16,702 kg)	
	Total	$M_S$		57,730 lb	(26,186 kg)	
e.	End of burn mass	$M_E$		32,782 lb	(14,870 kg)	
f.	Mass of propellant burned	$M_P$		24,948 lb	(11,316 kg)	
g.	Mass of propellant remaining	$M_R$		11,873 lb	( 5,385 kg)	
3.2	Apogee Burns					
a.	$\Sigma \Delta V = 6,2000$ fps					
b.	Starting mass	$M_S$		32,782 lb	(14,870 kg)	
c.	End of burn mass	$M_E$		21,370 lb	( 9,693 kg)	
d.	Mass of propellant burned	$M_P$		11,412 lb	( 5,176 kg)	
e.	Mass of propellant remaining	$M_R$		461 lb	( 209 kg)	
3.3	Disposal Perigee Burn					
a.	$\Delta V = 210$ fps					
b.	2.2e propellant remaining			461 lb	( 209 kg)	
c.	Propellant boiloff in GEO			62 lb	( 28 kg)	
d.	Usable propellant mass			399 lb	( 181 kg)	
e.	Starting mass: Stage Burnout*			6,268 lb	( 2,843 kg)	
	Propellant			399 lb	( 181 kg)	
	Total	$M_S$		6,667 lb	( 3,024 kg)	
f.	End of burn mass	$M_E$		6,571 lb	( 2,981 kg)	
g.	Mass of propellant burned	$M_P$		96 lb	( 44 kg)	
h.	Mass of propellant remaining	$M_R$		303 lb	( 137 kg)	
3.4	Disposal Apogee Burn					
a.	$\Delta V = 205$ fps					
b.	Starting mass	$M_S$		6,571 lb	( 2,981 kg)	
c.	End of burn mass	$M_E$		6,479 lb	( 2,939 kg)	
d.	Mass of propellant burned	$M_P$		92 lb	( 42 kg)	
e.	Mass of propellant remaining	$M_R$		211 lb	( 96 kg)	

\*Includes FPR of 445 lb (202 kg)

Table 3-47. Platform No. 2 Delivery Performance Analysis

1. ASE mass-OTV	2566 kg,	Platform	648 kg;	Total	3214 kg	
2. Propellant loading at launch is				36,975 lb	(16,772 kg)	
3. Flight Performance Analysis						
3.1 Perigee Burns						
a. $\Sigma \Delta V \approx 8,200$ fps						
b. Propellant boiloff in LEO is				103 lb	(47 kg)	
c. Usable propellant mass is				36,872 lb	(16,725 kg)	
d. Starting mass: Stage Burnout*				6,268 lb	(2,843 kg)	
Payload**				14,672 lb	(6,655 kg)	
Propellant				36,872 lb	(16,725 kg)	
Total	$M_S$			57,812 lb	(26,223 kg)	
e. End of burn mass	$M_E$			32,828 lb	(14,891 kg)	
f. Mass of propellant burned	$M_P$			24,984 lb	(11,333 kg)	
g. Mass of propellant remaining	$M_R$			11,888 lb	(5,392 kg)	
3.2 Apogee Burns						
a. $\Sigma \Delta V \approx 8,200$ fps						
b. Starting mass	$M_S$			32,828 lb	(14,891 kg)	
c. End of burn mass	$M_E$			21,400 lb	(9,707 kg)	
d. Mass of propellant burned	$M_P$			11,423 lb	(5,184 kg)	
e. Mass of propellant remaining	$M_R$			460 lb	(209 kg)	
3.3 Disposal Perigee Burn						
a. $\Delta V = 210$ fps						
b. 2.2c Propellant remaining				460 lb	(209 kg)	
c. Propellant boiloff in GEO				62 lb	(28 kg)	
d. Usable propellant mass				398 lb	(181 kg)	
e. Starting mass: Stage Burnout*				6,268 lb	(2,843 kg)	
Propellant				398 lb	(181 kg)	
Total	$M_S$			6,666 lb	(3,024 kg)	
f. End of burn mass	$M_E$			6,570 lb	(2,980 kg)	
g. Mass of propellant burned	$M_P$			96 lb	(44 kg)	
h. Mass of propellant remaining	$M_R$			303 lb	(137 kg)	
3.4 Disposal Apogee Burn						
a. $\Delta V = 205$ fps						
b. Starting mass	$M_S$			6,570 lb	(2,980 kg)	
c. End of burn mass	$M_E$			6,478 lb	(2,938 kg)	
d. Mass of propellant burned	$M_P$			92 lb	(42 kg)	
e. Mass of propellant remaining	$M_R$			210 lb	(95 kg)	

\*Includes FPR of 445 lb (202 kg)

\*\*Propellant off-loaded to 6 yr. supply

Table 3-48. Platform No. 6 Delivery Performance Analysis

1. ASE Mass - OTV	= 2,566 kg; Platform	= 862 kg; Total	= 3,428 kg
2. Propellant loading at launch is		37,768 lb	(17,131 kg)
3. Flight Performance Analysis			
3.1 Perigee Burns			
a. $\Sigma \Delta V = 8,200$ fps			
b. Propellant boiloff in LEO is		103 lb	( 47 kg)
c. Usable propellant mass is		37,665 lb	(17,085 kg)
d. Starting mass: Stage burnout*		6,268 lb	( 2,843 kg)
Payload		13,408 lb	( 6,082 kg)
Propellant		37,665 lb	(17,085 kg)
Total	$M_S$	57,841 lb	(26,010 kg)
e. End of burn mass	$M_E$	32,561 lb	(14,769 kg)
f. Mass of propellant burned	$M_P$	24,780 lb	(11,240 kg)
g. Mass of propellant remaining	$M_R$	12,885 lb	( 5,844 kg)
3.2 Apogee Burns			
a. $\Sigma \Delta V = 6,200$ fps			
b. Starting mass	$M_S$	32,561 lb	(14,769 kg)
c. End of burn mass	$M_E$	21,226 lb	( 9,628 kg)
d. Mass of propellant burned	$M_P$	11,335 lb	( 5,141 kg)
e. Mass of propellant remaining	$M_R$	1,550 lb	( 703 kg)
3.3 Disposal Perigee Burn			
a. $\Delta V = 210$ fps			
b. 2.2c propellant remaining		1,550 lb	( 703 kg)
c. Propellant boiloff in GEO		62 lb	( 28 kg)
d. Usable propellant mass		1,488 lb	( 675 kg)
e. Starting mass: Stage Burnout*		6,268 lb	( 2,843 kg)
Propellant		1,488 lb	( 675 kg)
Total	$M_S$	7,756 lb	( 3,518 kg)
f. End of burn mass	$M_E$	7,644 lb	( 3,467 kg)
g. Mass of propellant burned	$M_P$	112 lb	( 51 kg)
h. Mass of propellant remaining	$M_R$	1,376 lb	( 624 kg)
3.4 Disposal Apogee Burn			
a. $\Delta V = 205$ fps			
b. Starting mass	$M_S$	7,644 lb	( 3,467 kg)
c. End of burn mass	$M_E$	7,537 lb	( 3,419 kg)
d. Mass of propellant burned	$M_P$	107 lb	( 49 kg)
e. Mass of propellant remaining	$M_R$	1,269 lb	( 576 kg)

\*Includes FPR of 445 lb (202 kg)

in Figure 3-65. Over the ASE mass range of interest, the maximum allowable platform mass can be determined from the following equation:

$$M_p = -0.3696 M_{ASE} + 7941$$

where

$M_p$  = platform mass, kg

$M_{ASE}$  = total ASE mass, kg (includes 2566 kg for OTV)

#### PERFORMANCE PARAMETERS

OTV ASE MASS = 2,566 KG

OTV DISPOSAL AT 39,500 KM

LOW THRUST; 8-BURN TRAJECTORY; Isp = 450 SEC.

PROPELLANT BOILOFF LOSSES INCLUDED

OTV BURNOUT MASS = 2,843 KG (INCL. FPR = 202 KG)

SHUTTLE CARGO LIFTOFF MASS = 29,484 KG

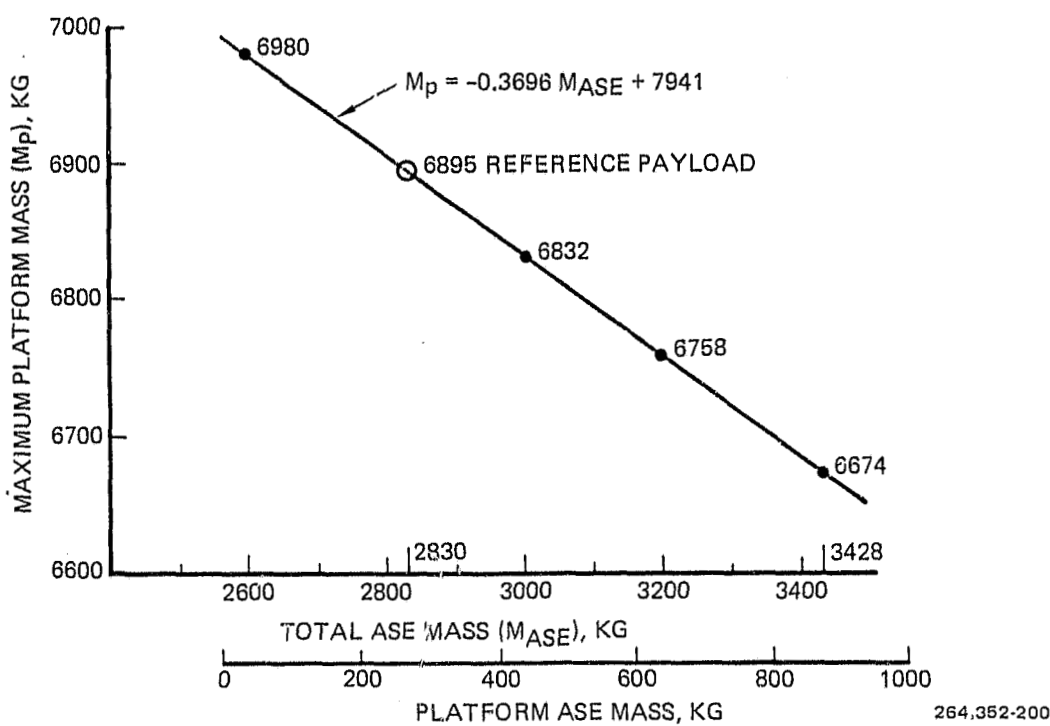


Figure 3-65. Allowable Platform Mass Versus ASE Mass For Delivery Mission

Figure 3-66 shows the same plot of maximum allowable platform mass versus ASE mass with the points for Platform 1, 2, and 6 added. With the present estimates of ASE mass, Platforms 1 and 2 have mass margins of 98 kg and Platform 3 has a margin of 592 kg. Conversely, with the present estimates for platform mass, the platform ASE mass could be increased by 265 kg for Platforms 1 and 2, and by 1602 kg for Platform 6.

PERFORMANCE PARAMETERS  
 OTV ASE MASS = 2,566 KG  
 OTV DISPOSAL AT 39,500 KM  
 LOW THRUST; 8-BURN TRAJECTORY; ISP = 450 SEC.  
 PROPELLANT BOILOFF LOSSES INCLUDED  
 OTV BURNOUT MASS = 2,843 KG (INCL. FPR = 202 KG)  
 SHUTTLE CARGO LIFTOFF MASS = 29,484 KG

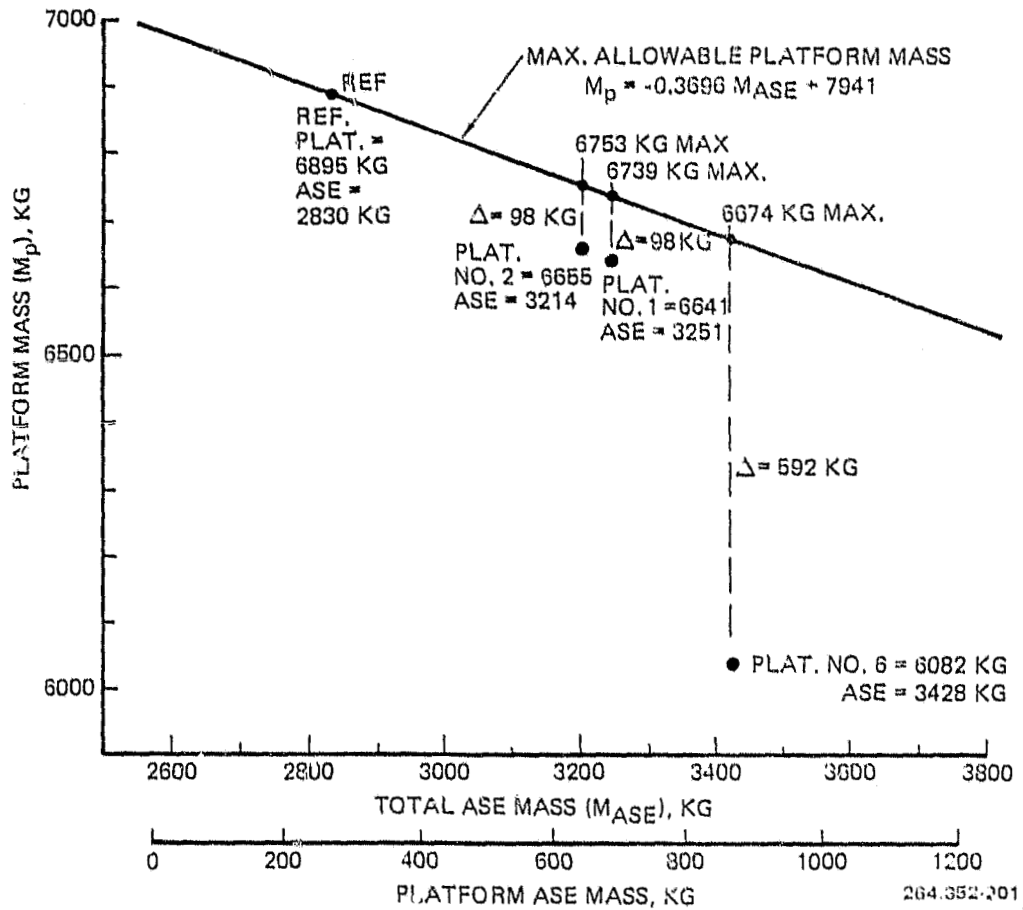


Figure 3-66. Alternative #1, Platform Mass Versus ASE Mass Characteristics

For the platform and ASE masses as designed here, other alternatives for the delivery mission that would make use of excess performance could be to dispose of the OTV in a higher orbit, or to further offload OTV propellant so that the Shuttle cargo mass at liftoff is less than the 29,484 kg used for these performance analyses.

**3.2.3 LOGISTICS MISSIONS TRANSPORTATION ANALYSIS.** The logistics flight concept for Alternative #1 is structured around reusability of both the OTV stage and the TMS in order to minimize the per-flight operating costs while affording frequent servicing opportunities.

The performance capabilities of the single stage OTV to deliver/retrieve payloads to/from GEO are plotted in Figure 3-67. This figure applies to the single Shuttle launch case, i.e., the OTV and its payload are mated on the ground and together occupy the Shuttle's cargo bay. Again, OTV propellants must be offloaded to meet Shuttle weight constraints, but payload packaging volumetric constraints are not encountered for the types of consumables to be carried.

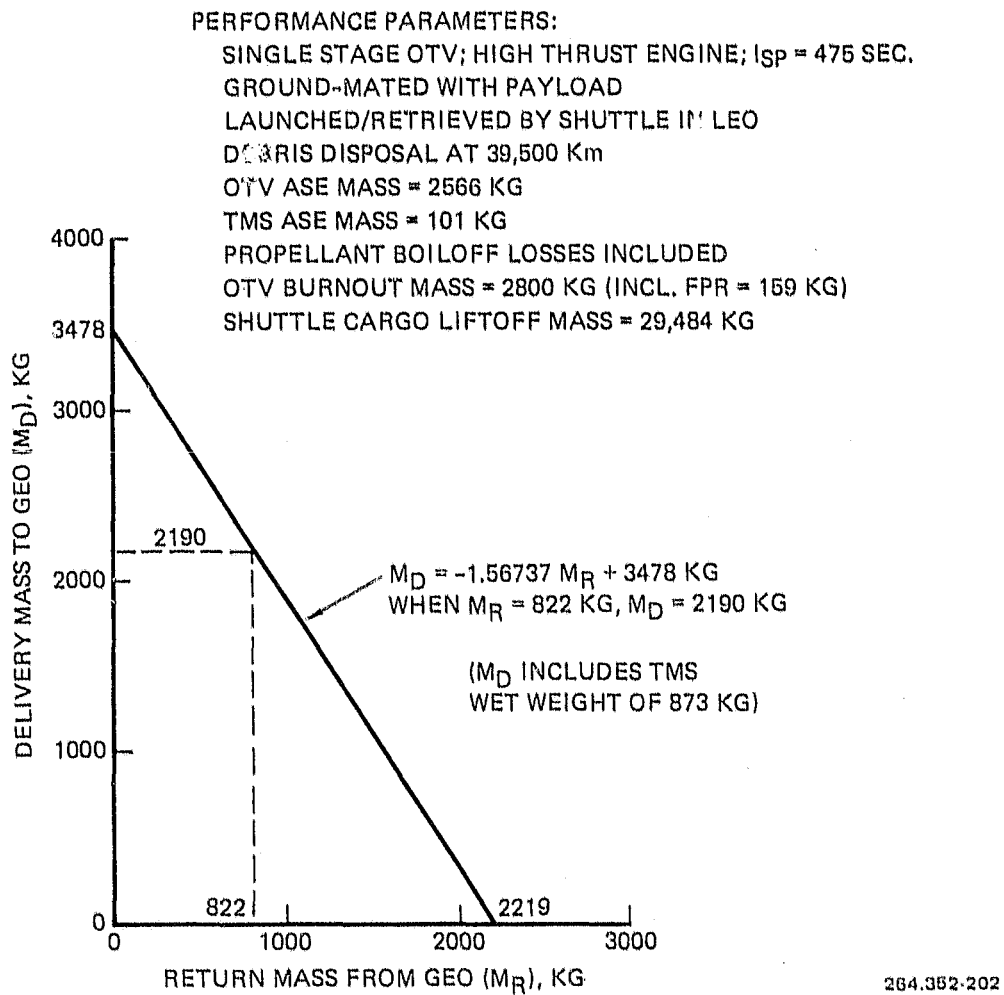
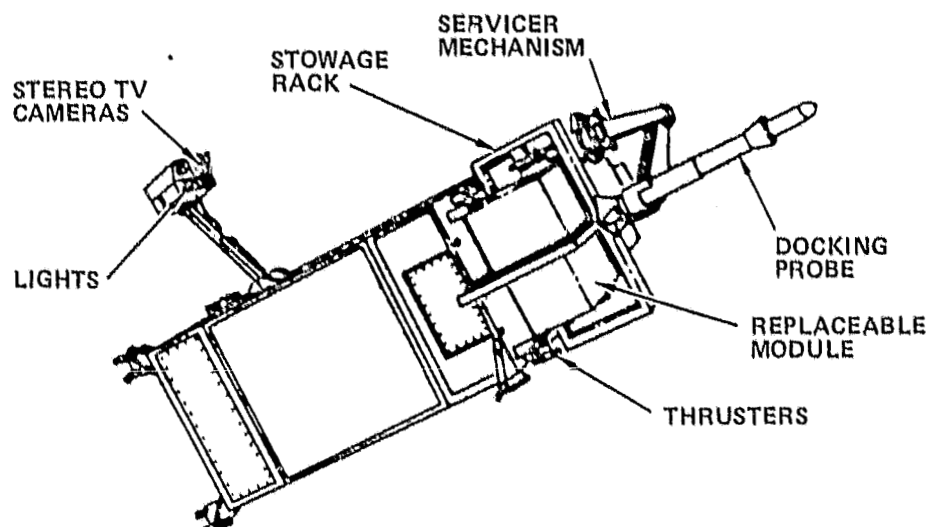


Figure 3-67. OTV Delivery/Return Mass Capabilities for GEO Logistics Flights

**3.2.3.1 Earth-to-LEO Mission Phase.** For the logistics flights, the OTV payload consists of the TMS carrying the platform resupply items required for each of the servicing missions, i.e., batteries, propellant bottles, and platform payload equipment (optional).

The TMS is a multipurpose system that consists of a core vehicle and a family of mission-peculiar kits used to adapt the TMS for the specific functions to be performed. The TMS, outfitted with kits to perform servicing missions, is

illustrated in Figure 3-68 (see Table 3-58 also). The TMS attaches to the front of the OTV with four latches similar to those used for pallet mounting in the cargo bay. Additional consumables are mounted on the sides of the core vehicle at the mounting stations for the four add-on hydrazine propulsion kits that are used when orbit transfer AV is required. These kits are not used for platform logistics missions.



264.352-203

Figure 3-68. Dedicated TMS Servicer Configuration

The prelaunch ground processing flow is similar to that described for the OTV/platform, i.e., integration with the OTV in the VPF and on-pad loading into the Orbiter. One additional step is the hydrazine loading of the TMS in a fueling facility.

The weight statement for the OTV and its payload at liftoff is given in Table 3-49. From the OTV performance capability plot in Figure 3-67, it is determined that when the TMS is returned dry (822 kg) the OTV can deliver 2199 kg to GEO, including the wet weight of the TMS (873 kg). This leaves a balance of 1317 kg available for consumables on each logistics flight.

For the typical logistics flight shown in Table 3-49 carrying two propellant bottles and three batteries, the total consumables mass is 1312 kg. The OTV propellant load is thus 21,832 kg (48,130 lb).

A detailed analysis of a typical logistics flight is given in the Logistics Plan in Table 3-56. The earth-to-LEO mission phase is accomplished in approximately 2.5 hours (through OTV separation from the Orbiter).

Table 3-49. Logistics Mission Launch Mass

Element	<u>Mass</u>	
	kg	lb
TMS	873	1,925
Dry Weight	822 kg (1813 lb)	
Propellant	15 kg ( 112 lb)	
Consumables		
2 bottles	946 kg (2086 lb)	1,312
3 batteries	366 kg ( 807 lb)	2,893
OTV Stage Burnout Mass*	2,800	6,173
Propellant	21,832	48,130
LO <sub>2</sub>	18,713 kg (41,254 lb)	
LH <sub>2</sub>	3,119 kg ( 6,876 lb)	
ASE		
OTV	2,566 kg (5,656 lb)	2,667
TMS	101 kg ( 223 lb)	5,879
		—
Totals	29,484	65,000

\*Includes FPR of 159 kg (350 lb)

3.2.3.2 LEO-to-GEO Mission Phase. The OTV transfers the TMS to the platform constellation location using a 2 perigee burn, single apogee burn trajectory. The characteristics of the single stage OTV as configured for the logistics missions are given in Table 3-50. The OTV operates in the high thrust mode and the maximum thrust-to-weight ratio at the end of the apogee burn is  $T/W = 0.63$ . The time required for phasing, orbit transfer, and rendezvous with the platform constellation is approximately 20 hours (Table 3-56).

A vehicle performance analysis for the logistics mission is given in Table 3-51. Again, RCS requirements are lumped in with the main engine propellant requirements, and boiloff losses are estimated to be 41.3 lb/day (18.78 kg/day). The total LEO-to-GEO velocity increment required is 14,011 fps, and the propellant requirement is 35,455 lb (16,082 kg) plus boiloff losses of 38 lb (17.2 kg) during the 19.5 hour transfer ellipse. The propellant remaining is 12,637 lb (5,732 kg).

Table 3-50. Logistics Mission OTV Characteristics

Physical Size		
Diameter	14.6	( 4.47m)
Length (Engine bell retracted)	34.0 ft	(10.36m)
Main Engine		
Propellants	LH <sub>2</sub> /LO <sub>2</sub>	
Thrust Level	15,000 lb	(66,723N)
Isp	475 sec	( 4,658 $\frac{NS}{kg}$ )
RCS Thrusters		
Propellants	LH <sub>2</sub> /LO <sub>2</sub>	
Thrust Level	25 lb	(111N)
Isp	380 sec	( 3,725 $\frac{NS}{kg}$ )
Stage Burnout Mass	6,173 lb	( 2,800 kg)
Hardware	5,223 lb (2,369 kg)	
Residuals	600 lb ( 272 kg)	
FPR	350 lb ( 159 kg)	

3.2.3.3 Debris Disposal Mission Phase. After the TMS completes servicing the platforms at GEO, the TMS (carrying empty propellant bottles and old batteries removed from the platforms) redocks with the OTV and is carried to the 39,500 km (21,323 n.mi.) disposal orbit.

While parked at GEO during the 47.5 hour servicing mission operations, propellant boiloff losses are 83 lb (38 kg), and the remaining propellant load is 12,554 lb (5,694 kg). The velocity increment required is 415 fps and the propellant required is 579 lb (263 kg). The propellant remaining after the apogee circularization burn at 39,500 km is 11,976 lb (5,432 kg).

3.2.3.4 OTV/TMS Recovery Mission Phase. After releasing the spent batteries and propellant bottles in the disposal orbit, the OTV with the TMS attached transfers back to LEO for recovery by the Shuttle. The OTV circularizes 20 n.mi. above and 130 n.mi. ahead of the Orbiter, and the Orbiter performs the necessary maneuvers to rendezvous with the OTV and capture it. The return phase requires 11,972 lb (5,430 kg) of propellant, leaving a margin of 4 lb (2 kg), in addition to the FPR of 350 lb (159 kg). The nominal mission elapsed time to this event is about 95 hours (Table 3-56).

Table 3-51. Logistics Vehicle Flight Performance Analysis

1.	LEO-GEO Transfer Phase		
1.1	Perigee Burns		
a.	$\Sigma \Delta V$ required = 8112 fps (phasing, x'fer ellipse & mid-course corr)		
b.	Initial propellant load is 48,130 lb (21,832 kg)		
c.	Earth-to-LEO boiloff is negligible		
d.	Starting mass:	Stage burnout*	6,173 lb ( 2,800 kg)
		TMS (wet)	1,925 lb ( 873 kg)
		Consumables	2,893 lb ( 1,312 kg)
		Propellant	<u>48,130 lb</u> ( <u>21,832 kg</u> )
	Total	$M_S$	59,121 lb (26,817 kg)
e.	End of burn mass	$M_E$	34,786 lb (15,779 kg)
f.	Mass of propellant burned	$M_P$	24,335 lb (11,038 kg)
g.	Mass of propellant remaining	$M_R$	23,795 lb (10,793 kg)
1.2	Apogee Burns		
a.	$\Sigma \Delta V$ required = 5899 fps (GEO insertion, rendez. & braking)		
b.	Propellant boiloff during transfer is:	38 lb	( 17 kg)
c.	Remaining propellant load is:	23,757 lb	(10,776 kg)
d.	Starting mass is	$M_S$	34,748 lb (15,762 kg)
e.	End of burn mass	$M_E$	23,628 lb (10,718 kg)
f.	Mass of propellant burned	$M_P$	11,120 lb ( 5,044 kg)
g.	Mass of propellant remaining	$M_R$	12,637 lb ( 5,732 kg)
2	Debris Disposal Transfer Phase		
2.1	Perigee Burn		
a.	$\Delta V$ required is 210 fps		
b.	Propellant boiloff during GEO operations is 83 lb		( 38 kg)
c.	Remaining propellant load is	12,554 lb	( 5,694 kg)
d.	Starting mass:	Stage burnout*	6,173 lb ( 2,800 kg)
		TMS (dry)	1,812 lb ( 822 kg)
		Bats. & Empty Bots	1,067 lb ( 484 kg)
		Propellant	<u>12,554 lb</u> ( <u>5,694 kg</u> )
	Total	$M_S$	21,606 lb ( 9,800 kg)
e.	End of burn mass	$M_E$	21,311 lb ( 9,667 kg)
f.	Mass of propellant burned	$M_P$	295 lb ( 134 kg)
g.	Mass of propellant remaining	$M_R$	12,259 lb ( 5,561 kg)

\*Includes FPR of 159 kg

Table 3-51. Logistics Vehicle Flight Performance Analysis (Contd)

---

2.2	Apogee Burn			
a.	$\Delta V$ required = 205 fps			
b.	Propellant boiloff during transfer is negligible			
c.	Starting mass	$M_S$	21,311 lb	( 9,667 kg)
d.	End of burn mass	$M_E$	21,027 lb	( 9,538 kg)
e.	Mass of propellant burned	$M_P$	284 lb	( 129 kg)
f.	Mass of propellant remaining	$M_R$	11,976 lb	( 5,432 kg)
3.	OTV/TMS Recovery Phase			
3.1	Apogee Burns			
a.	$\Sigma \Delta V$ required = 5776 fps (xfer.orbit inj. & mid-course corr.)			
b.	Propellant boiloff during debris disposal phase is negligible.			
c.	Starting mass: Stage burnout*		6,173 lb	( 2,800 kg)
	TMS (dry)		1,812 lb	( 822 kg)
	Propellant		<u>11,976 lb</u>	<u>( 5,432 kg)</u>
	Total	$M_S$	19,961 lb	( 9,054 kg)
d.	End of burn mass	$M_E$	13,683 lb	( 6,206 kg)
e.	Mass of propellant burned	$M_P$	6,278 lb	( 2,848 kg)
f.	Mass of propellant remaining	$M_R$	5,698 lb	( 2,585 kg)
3.2	Perigee Burns			
a.	$\Sigma \Delta V$ required = 8231 fps (phasing & circularization)			
b.	Propellant boiloff during transfer is negligible			
c.	Starting mass is	$M_S$	13,683 lb	( 6,206 kg)
d.	End of burn mass	$M_E$	7,988 lb	( 3,623 kg)
e.	Mass of propellant burned	$M_P$	5,694 lb	( 2,583 kg)
f.	Mass of propellant remaining	$M_R$	4 lb	( 2 kg)

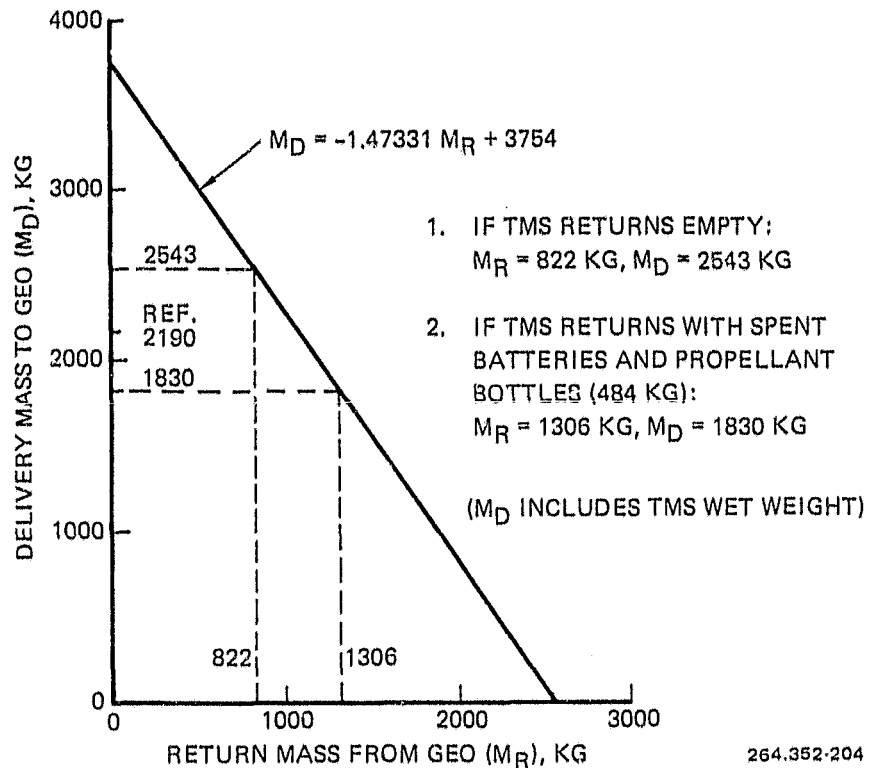
---

\*Includes FPR of 159 kg.

3.2.4 DEBRIS DISPOSAL OPTIONS. Disposal of the spent batteries and propellant tanks (and, optionally, replaced payload equipment) at a super-synchronous disposal orbit was baselined for the transportation analysis task. However, several other options are possible and are evaluated in this section.

3.2.4.1 Debris Stored on Platform. If the empty propellant tanks and spent batteries can be stored aboard the platforms rather than being transferred to the 39,500 km disposal orbit, the savings in OTV propellant will allow an increase in the consumables delivered on each logistics flight. Figure 3-69 illustrates the OTV delivery versus retrieval mass capability for this mode of

**PERFORMANCE PARAMETERS:**  
 SINGLE STAGE OTV; HIGH THRUST ENGINE;  $I_{sp} = 475$  SEC  
 GROUND MATED WITH PAYLOAD  
 LAUNCHED/RETRIEVED BY SHUTTLE IN LEO  
 OTV ASE MASS = 2566 KG  
 TMS ASE MASS = 101 KG  
 PROPELLANT BOILOFF LOSSES INCLUDED  
 OTV BURNOUT MASS = 2800 KG (INCL. FPR = 159 KG)  
 SHUTTLE CARGO LIFTOFF MASS = 29,484 KG



264.352-204

Figure 3-69. OTV Delivery/Return Capabilities Without Supersynchronous Debris Disposal

operation. For a return mass of 822 kg (dry TMS) the delivery capability is 2543 kg. This is an increase in delivery capability of 353 kg per logistics flight compared to the 2190 kg capability shown in Figure 3-67. However, storing the spent batteries and propellant tanks aboard the platforms will cause an increase in the amount of hydrazine used by the platforms' RCS systems because of the additional platform mass during the eighth through sixteenth years of platform life. This requires some additional propellant resupply on the logistics flights, but there is still a net gain in consumables delivery capability of about 19 percent over the baseline.

**3.2.4.2 Debris Returned to Earth.** A second option is to return the empty propellant tanks and spent batteries to LEO by keeping them attached to the TMS during the OTV/TMS recovery mission phase. However, this increase in

return mass causes a significant decrease in delivery mass capability. For example, for the typical logistics flight discussed in Section 3.2.2, the extra mass of the batteries and empty propellant tanks (484 kg) would increase the mass returned to LEO by the OTV to 1306 kg.

This would decrease the delivery mass capability to 1830 kg (Figure 3-69), a reduction of 360 kg per logistics flight compared to the 2190 kg capability shown in Figure 3-67. This amounts to a 27 percent reduction in net consumables per flight and would increase the number of logistics flights required by 38 percent.

**3.2.4.3 Debris Disposal by TMS.** As an alternative to using the OTV to carry the TMS and debris to the 39,500 km disposal orbit, it could be possible to use the TMS for this function if it were outfitted with a small  $\Delta V$  kit. Table 3-52 summarizes the flight performance analysis for this mission. The amount of propellant required to transfer the TMS and spent consumables to 39,500 km and then return the TMS to the OTV waiting at GEO is 126 kg. The mass of a small  $\Delta V$  kit to provide the required impulse is 27 kg (dry). This would increase the return mass of the TMS to 849 kg. From Figure 3-69, the delivery mass capability would then be:

$$M_D = -1.47331 (849) + 3754$$

$$M_D = 2503 \text{ kg}$$

Of this amount, the wet mass of the TMS with the added  $\Delta V$  kit would be 1026 kg leaving a net consumables delivery capability of 1477 kg per flight. This is an increase of 160 kg over the 1317 kg baseline mission capability, or about 12 percent improvement.

**3.2.5 SPACE BASED TMS OPTIONS.** The use of a ground-based TMS was baselined for the logistics transportation analysis task. However, the significant delivery penalty imposed by returning the TMS from GEO to LEO indicated that a spacebasing mode should also be considered for the TMS.

**3.2.5.1 Debris Stored on Platform.** Referring again to Figure 3-69, we see that if the TMS remains at GEO with the platform constellation and the spent consumables remain on the platform, the return mass carried by the OTV is zero and thus the delivery mass capability is 3754 kg. A storage rack to carry the consumables would weigh about 20 percent of the weight of the consumables or 1/6 of the total mass delivered. Thus the rack would weigh 626 kg and the consumables would weigh 3128 kg. However, the extra mass loading of the debris stored on the platform during the last 8 years would require additional RCS propellant. Also, the TMS host platform would require extra structure and subsystems support, thus increasing its mass and RCS propellant requirements. Together, it has been estimated (Section 3.3.2) that the additional propellant resupply penalty would be about 108 kg per flight, so that the net consumables delivered would be 3020 kg per flight, an increase of 129 percent over the baseline capability.

Table 3-52. TMS Debris Disposal Mission - Flight Performance Analysis

---

1.	Transfer from GEO To Debris Disposal Orbit		
a.	$\Sigma \Delta V = 415$ fps		
b.	Isp = 235 sec		
c.	Starting Mass:		
	TMS w/ $\Delta V$ kit	1,872 lb	( 849 kg)
	Spent Consumables	1,067 lb	( 484 kg)
	$\Delta V$ Propellant	<u>278 lb</u>	<u>( 126 kg)</u>
	$M_{S_1}$	3,217 lb	(1,459 kg)
d.	Ending Mass	$M_{E_1}$	3,045 lb (1,381 kg)
e.	Propellant Burned	$M_{PB_1}$	172 lb ( 78 kg)
f.	Propellant Remaining	$M_{R_1}$	106 lb ( 48 kg)
2.	Transfer from Debris Disposal Orbit to GEO		
a.	$\Sigma \Delta V = 415$ fps		
b.	Isp = 235 sec		
c.	Starting Mass:		
	TMS w/ $\Delta V$ Kit	1,872 lb	( 849 kg)
	$\Delta V$ Propellant	<u>106 lb</u>	<u>( 48 kg)</u>
	$M_{S_2}$	1,978 lb	( 897 kg)
d.	Ending Mass	$M_{E_2}$	1,872 lb ( 849 kg)
e.	Propellant Burned	$M_{PB_2}$	106 lb ( 48 kg)
f.	Propellant Remaining	$M_{R_2}$	0 lb ( 0 kg)

---

This extra capacity could be used for additional payload updates without extra flights, or else could be used to reduce the number of logistics flights.

3.2.5.2 Debris Returned to Earth. If we desire to return the debris to earth the debris (484 kg) and the storage rack (407 kg) must be carried on the return flight. For this return mass of 891 kg, the delivery mass capability is 2441 kg. This includes the storage rack (407 kg); therefore, the consumables delivery capability is 2034 kg per flight. Again, some additional RCS propellants would have to be resupplied for the TMS and for the TMS host platform. This

penalty has been estimated at 58 kg per flight (Section 3.3.2) and the net consumables supplied would be 1,976 kg, an increase of 50 percent over the baseline of 1317 kg.

### 3.2.6 CONCLUSIONS AND RECOMMENDATIONS. This section presents a summary of the transportation system analyses and recommendations.

**3.2.6.1 Delivery Missions.** The three platforms of Alternative #1 for which design layouts have been made and mass properties have been estimated (1, 2, and 6) have been shown to be compatible with the mass delivery capability of the single stage OTV used in the low thrust, expendable mode in a single Shuttle launch. The delivery mission also includes disposal of the OTV in a supersynchronous circular orbit (39,500 km altitude) where it will not interfere with subsequent platform operations.

The performance analyses for Platforms 1, 2, and 6 assumed that the Shuttle cargo weight at liftoff was the maximum allowable (29,484 kg); the end-of-mission propellant margins were 96 kg, 95 kg and 576 kg, respectively. Platform ASE mass and propellant boiloff during the mission were both included in the analyses.

The Task 3.1 platform design effort encountered great difficulty in packaging the platforms in the Orbiter cargo bay along with the OTV for a single Shuttle launch. The baselined single stage OTV as defined in Reference 57 allows only 7.9m cargo bay length for the packaged platform.

Since these delivery missions are performed with the OTV propellant tanks offloaded, the OTV is occupying valuable space in the cargo bay. Since the OTVs used for the platform delivery missions are used in the expendable mode, they could be better matched to this mission by reducing the LH<sub>2</sub> tank length by about 1.1 meter. This would increase the allowable length of the packaged platform to 9m, an improvement of about 15 percent.

OTVs designated for single Shuttle launch delivery missions should be matched to the mission propellant requirements rather than employing fixed tankage sizes, originally based on the OTV and its ASE comprising the full Shuttle cargo capacity of 29,484 kg.

Reducing the length of the LH<sub>2</sub> tank should be possible with no additional cost to the program; all of the other OTV subsystems (and LO<sub>2</sub> tankage) would be unaltered. The increased cargo bay length made available for the packaged platform will help to reduce the packaging design difficulty made evident in Task 3.1.

**3.2.6.2 Logistics Missions.** Six logistics flight options were analyzed and proven feasible, including both ground-based and space-based TMS operating modes. The basic logistics flight requirements and approaches were developed

in the Logistics Plan in Section 3.3, and the performance analyses of these approaches plus several more options were evaluated. Table 3-53 summarizes the performance analyses of the six options.

The logistics mission options employ the single stage OTV in a reusable mode. The baseline system description requires 16 logistics flights with the TMS over a 16 year period. Each flight requires a single Shuttle launch. The expended debris (spent batteries, empty propellant tanks, etc.) are always disposed of in one of several ways. The space-based TMS operating mode options yield a much higher net consumables delivery capability than the ground-based options (i.e., 129 percent and 50 percent improvements). This mode implies that a dedicated TMS would be assigned to each of the platform constellations; however, the economic viability of this operating mode has been verified in the analyses presented in Section 3.3.2.

Return of the debris to LEO for return to earth imposes large penalties in delivery capabilities for both the ground based and space based TMS operating modes. However, the ability to conduct failure analyses of returned equipment could provide very valuable information that could be applied to the design of new equipment that would exhibit improved reliability and/or longer life.

Further studies are needed to evaluate the possible benefits of the space-based TMS operating mode and the ability to return platform and payload equipment to earth.

### 3.3 LOGISTICS PLAN AND MISSION MODEL

This task establishes a feasible logistics plan for the geostationary platform. The logistics plan is comprised of a mission model with a flight schedule and identification of flight payloads, OTV and servicing vehicle, operational modes, sequences of events, and timelines.

The logistics plan is based on a geostationary platform concept of two satellite constellations, one over the Atlantic at 15°W and one serving the Western hemisphere at 110°W. Each constellation has six satellites and has the appearance to an observer on earth of rotating about a vertical axis at a fixed longitudinal point with all six satellites on the circumference of an 18 km diameter circle. We describe this configuration as a "Merry-Go-Round." (This is achieved by six orbital planes, each with an eccentricity of 0.00010965, inclination of 0.012565 degree, and assumed argument of 270 degrees. The ascending nodes are placed 60 degrees apart with the time of perigee passage sequentially every 3,989 hours.

The platforms are designed for a nominal 16-year lifetime with an 8-year supply of attitude control and stationkeeping propellants and batteries onboard when initially placed in orbit. There is a logistics plan ground rule to resupply the

Table 3-53. Summary of Logistics Flight Options

Mass Parameters	Debris Disposal Options					
	1 Debris Disposal at 39,500 km by OTV (Baseline)	2 Debris Retained on Platform	3 Debris Returned at Shuttle at LEO	4 Debris Disposal Returned at 39,500 km by TMS with ΔV Kit	5 Debris Retained on Platform	6 Debris Returned to Shuttle at LEO
Return Mass, kg	822	822	1306 <sup>2</sup>	849 <sup>3</sup>	0	891 <sup>4</sup>
Delivery Mass, kg	2190	2543	1830	2503	3754	2441
Wet TMS Mass, kg	873	873	873	1026	0	0
Storage Rack Mass, kg	0	0	0	0	626	407
Consumables Delivered per Flight, kg	1317	1670	957	1477	3128	2034
Delivery Penalties per Flight, kg	0	Extra N <sub>2</sub> H <sub>4</sub> propellant = 105 kg/flt (Ref Table 3-54)	0	0	Extra N <sub>2</sub> H <sub>4</sub> for platform + TMS resupply = 108 kg/flt (Ref Table 3-55)	Extra N <sub>2</sub> H <sub>4</sub> for platform + TMS resupply = 58 kg/flt (Ref Table 3-55)
Net Consumables Delivered per Flight, kg	1317	1565	957	1477	3020 <sup>5</sup>	1976 <sup>5</sup>
Δ from Baseline, Percent	-	+19	-27	+12	+129	+50

<sup>1</sup>Dedicated TMS required at each constellation; launched on first logistics flight to each constellation.

<sup>2</sup>Dry TMS (822) + debris (484).

<sup>3</sup>Dry TMS (822) + dry ΔV kit (27).

<sup>4</sup>Debris (484) + storage rack (407 kg).

<sup>5</sup>Reduce by 873 kg for 2 TMS delivery flights.

expendable propellants and batteries only (no new payloads, equipment, or maintenance servicing is to be scheduled). The resupply flight schedule is also ground-ruled to provide a flight every 18 months during the first eight years, and every 9 months during the next eight years. Thus, if unscheduled payload placement is desired or unscheduled servicing is required, then a planned logistics flight will be available for these contingencies. The "bumped" logistics payload can subsequently be flown with the addition of a Shuttle flight.

During this study, we considered many operational logistic options. Trade studies were conducted when sufficient data were available; however, often only a reasonable selection was made on a reference basis so that the study could continue. These options are listed so that subsequent studies may be undertaken to properly recommend the best operational mode.

**3.3.1 MISSION MODEL.** The buildup of the satellite constellations starts in 1992 with the Western Hemisphere constellation and proceeds at the rate of one satellite added each 16 months until the constellation is completed in 1998; concurrently, the Atlantic constellation is initiated in 1993 and is completed (6 satellites) in 1999. This schedule is presented as Figure 3-70 with each platform identified.

SCHEDULE																		
PLACEMENT FLIGHTS	92	93	94	95	96	97	98	99	00	01	02	03	04	05	06	07	08	
WESTERN HEMISPHERE CONSTELLATION	1	2	3	4	5	6												
ATLANTIC CONSTELLATION	7	8	9	10	11	12												
LOGISTIC RESUPPLY FLIGHTS		▽	▽	▽	▽	▽	▽	▽	▽	▽	▽	▽	▽	▽	▽	▽	▽	

264.352-205

Figure 3-70. Logistics Mission Model

The logistics flight schedule is also identified on Figure 3-70, starting in 1993 at 18-month intervals until 1999, and then every 9 months thereafter. This schedule provides resupply sufficient for a 16-year lifetime to each platform. Additional logistic flights are required to provide a constellation lifetime of 16 years or more.

The payload assignment and power requirements for each platform are as identified in Table 3-22. The maximum platform weight is referenced at 6895 kg.

**3.3.2 LOGISTICS PLAN.** The logistics plan is based on the mission model and ground rules described above. Details of the plan are developed based on the selected OTV, servicing vehicle, expendables resupply requirements, and selected operational modes as discussed below.

**3.3.2.1 OTV.** After completion of Task 2 (concept selection) the OTV selection was made from NASA-provided choices. Selected were the "d" concept (low-thrust, expendable) for the platform delivery operations, and the "q" concept (high-thrust, reusable) for the logistic operations. These "d" and "q" concepts are achieved by the same OTV, as shown on Figure 3-71, which can be used in different modes to perform both high and low thrust missions. The performance characteristics, as provided by NASA, are presented in Table 3-54 and are based on an advanced engine concept.

The OTV low-thrust geosynchronous payload placement reference value is 6895 kg based on an expendable OTV flight. However, performance was recalculated to account for placing the spent OTV into a disposal orbit (2000 n.mi. above GEO) and to account for ASE weight associated with platform support during Shuttle launch. The resulting performance is as presented in Figure 3-72 for both five-burn and nine-burn GEO transfer trajectories (includes one apogee burn) as a function of the Orbiter payload chargeable weight. Start, stop, and propellant boiloff losses are included in the effective specific impulse of 450 seconds.

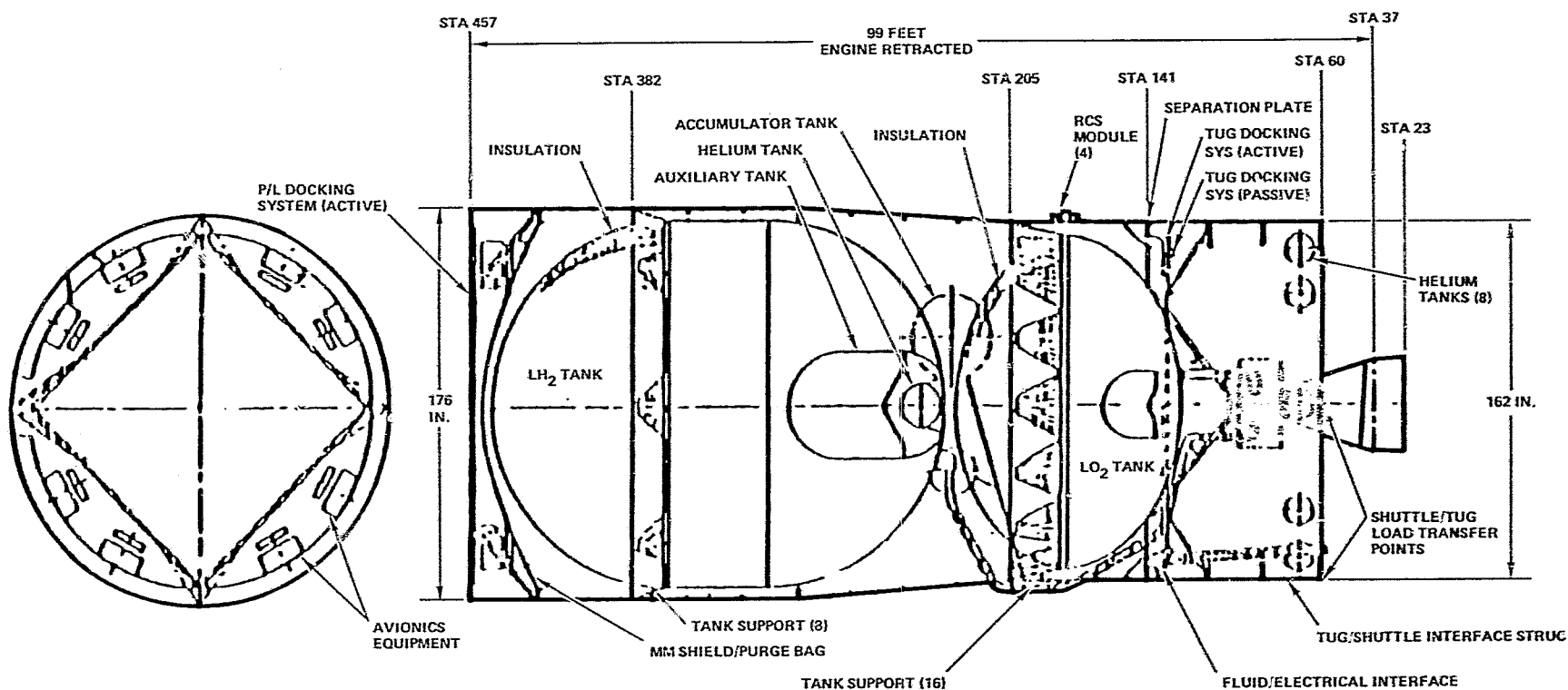
**3.3.2.2 Servicing Vehicle.** The TMS is used as the servicing vehicle for this study. The TMS is illustrated in Figure 3-73 configured for the servicing operations. The TMS servicing configuration requires additional subsystems, including the servicing manipulator, docking probe, TV, and navigation kits. The geostationary platform's N<sub>2</sub>H<sub>4</sub> bottles and battery replacements are attached to the TMS, as illustrated. TMS propellants are all internal (core) for the servicing mission.

TMS performance characteristics are presented in Table 3-55. The TMS ASE equipment is assumed to be 50 percent of nominal Orbiter-attached mode values since the TMS will not be controlled from the Orbiter (reduced AFD equipment), and the TMS is mounted on the OTV and uses OTV cabling (reduced TMS-unique Orbiter cabling).

Control of the TMS during servicing will be from the ground Payload Operations Control Center (POCC) with the command and control communications link passing through the on-orbit geostationary platform.

**3.3.2.3 Resupply Requirements.** The geostationary platform resupply requirements are based on the planned 16-year lifetime of the platform and the 8-year initial on-board supply at launch. The only planned replenishment requirements for platform are batteries and hydrazine (N<sub>2</sub>H<sub>4</sub>) attitude control and stationkeeping propellants.

\*See Tables 3-32, 3-33 for concept design weights.



264 352 69

Figure 3-71. OTV Configuration

Table 3-54. OTV Performance Characteristics

OTV Weights	Platform Placement Flight (Low Thrust)		Logistics Flight (High Thrust)	
	Jettison Weight	2843 kg ( 6268 lb)	2800 kg ( 6173 lb)	2369 ( 5223)
Dry and Contingency	2369	( 5223)	2369	( 5223)
Hardware	( 2116)	( 4665)	( 2116)	( 4665)
Contingency (Structural)	( 253)	( 558)	( 253)	( 558)
Nonusable Residuals	474	( 1045)	431	( 950)
Trapped Propellants and Gases	( 58)	( 127)	( 58)	( 127)
He Pressurant	( 214)	( 473)	( 214)	( 473)
Main Engine Reserve (FPR)	( 202)	( 445)	( 159)	( 350)
Nominal Propellant (24,302 kg capacity)	17008 kg	(37502 lb)	21808 kg	(48086 lb)
OTV ASE	2565 kg	( 5656 lb)	2565 kg	( 5656 lb)
Main Engine				
Thrust	6673 N	( 1500 lb)	66726 N	(15000 lb)
Specific Impulse	450 sec		475 sec	
Propellants	LO <sub>2</sub> /LH <sub>2</sub>		LO <sub>2</sub> /LH <sub>2</sub>	
Mixture Ratio	6:1		6:1	
RCS Engine				
Specific Impulse	380 sec		380 sec	
Propellants	LO <sub>2</sub> /LH <sub>2</sub>		LO <sub>2</sub> /LH <sub>2</sub>	

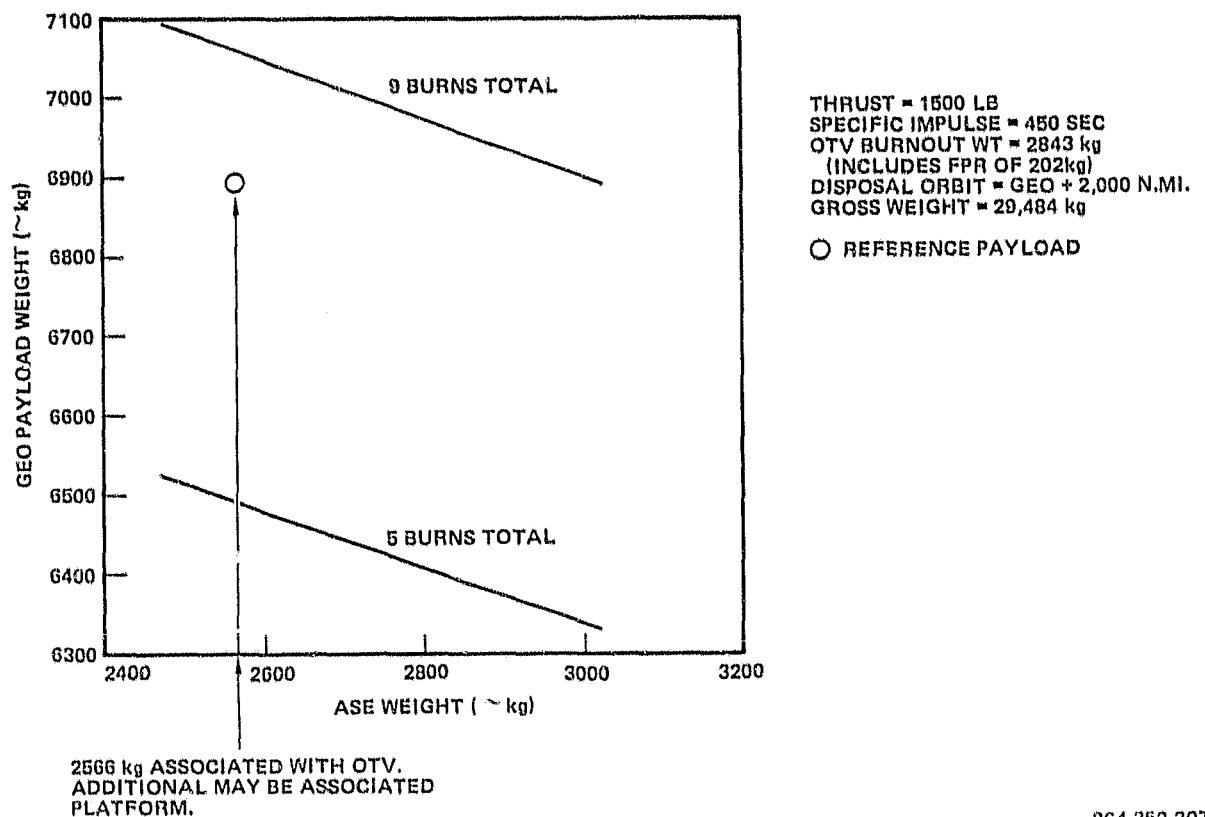


Figure 3-72. OTV Low Thrust Performance (Expendable OTV)

The impulse requirements for inclination control are 87.5 kg-sec per day for a 6895 kg platform. Impulse requirements for longitude control are 10.3 kg-sec per day at 15°W (Atlantic constellation) and 3.8 kg-sec per day at 110°W (Western Hemisphere constellation) for a 6895 kg platform. This results in  $N_2H_4$  usage requirements of 155.2 kg/year for the Atlantic constellation and 144.9 kg/year for the Western Hemisphere constellation, based on geostationary platform RCS average specific impulse of 230\* sec. Thus, an average eight-year supply of hydrazine is 1242 kg for a 6895 kg platform in the Atlantic constellation.

It was determined that three  $N_2H_4$  bottles per platform provide good logistics capability with the selected OTV/TMS vehicle. A resupply  $N_2H_4$  bottle with a 414 kg usable propellant capacity results in a wet inert weight of about 59 kg (including tank, valves, regulators, tank support platform, quick connect, sensors, and helium pressurant) as shown on Table 3-56. Thus, a loaded  $N_2H_4$  bottle weighs about 473 kg each. Package size is about 1.1m diameter for each bottle plus support platform.

\*Section 3.1 used thermal augmentation to get  $I_{SP}$  = 300 seconds and save weight.

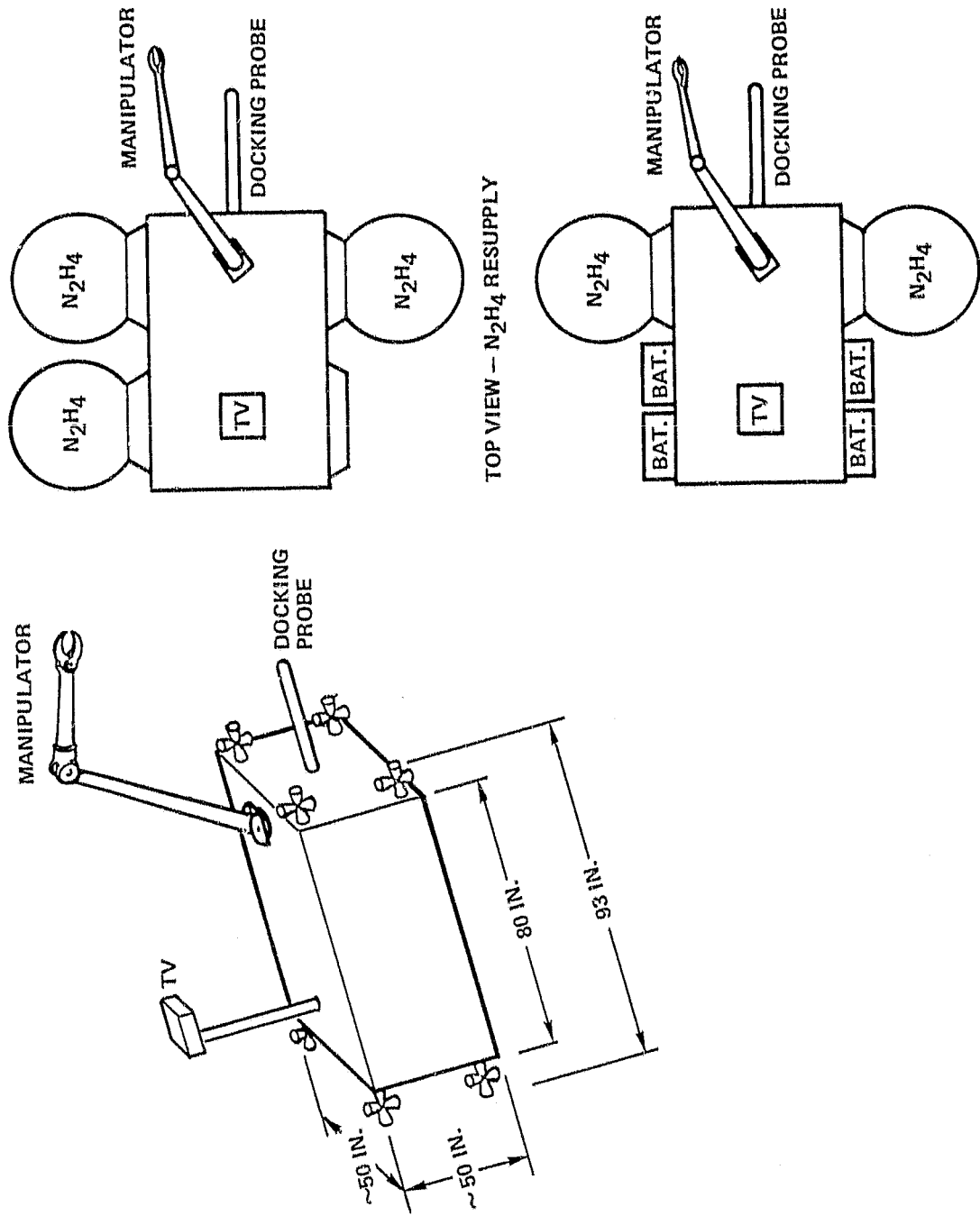


Figure 3-73. Teleoperator Maneuver System (Platform Resupply Configuration)

TOP VIEW - N<sub>2</sub>H<sub>4</sub> AND BATTERY RESUPPLY  
264.352.208

Table 3-55. Teleoperator Maneuvering System Characteristics

System	
TMS Launch Weight	<u>873</u> kg
Usable Propellant (90 Percent)	51
TMS Return Weight	<u>822</u> kg
Core (Dry)	636
Docking Probe Kit and Storage Attachments	60
Service Mechanism Kit	52
TV and Navigation Kit	68
Residual Propellant and Pressurization	6
TMS Equipment on AFD (50 Percent Nominal)	37 kg
TMS Cargo Bay Cables (50 Percent Nominal)	64 kg
Specific Impulse	
$N_2H_4 = 235$ sec	
Thrust = 31 → 13 Newtons/Thruster	
125 → 53 Newtons Total	

The battery logistic requirements are based on five batteries for Platforms 2, 5, 8, and 9. The other eight platforms require only four batteries each. Each battery weighs 122 kg, including wiring connectors, pack rack, harness, and thermal housing, as listed in Table 3-56. Package size is about 0.20 by 0.51 by 1.32m per battery.

3.3.2.4 Logistic Options. During the logistics plan development, many alternative operational modes were considered. A trade study was conducted when appropriate data was available, and a selection made so that a reasonable logistics plan could be developed. These logistic options are listed in Table 3-57, alternative modes for each option are identified and the reference case used in this study is identified. The rationale for the selection or other brief comments are stated in Table 3-57 and are discussed below.

Table 3-56. Resupply Logistic Weights

Propellant Bottles		Batteries	
Gross Weight	<u>473 kg</u>	Gross Weight	<u>122 kg</u>
Usable N <sub>2</sub> H <sub>4</sub>	414 kg	Battery (Ni-H <sub>2</sub> , 96 cells)	94
Resupply Bottle	59 kg	Wiring Connectors	5
N <sub>2</sub> H <sub>4</sub> Residuals	8	Pack Rack	12
He	1	Harness, Plug-in	3
Tank	40	Thermal Housing	8
Valves, Regulators, Lines, Sensors	1		
Tank Support Platform	7		
Quick Connect Mechanisms	2		

Servicing of more than one platform per flight was chosen since increased versatility will be realized. Servicing of only one constellation was chosen at this time since OTV payload (delivered propellant and battery weight) is reduced by servicing both constellations.

A tradeoff of the hydrazine propellant transfer mode was conducted. A comparison was made between the transfer of propellant between tanks (bottle-to-bottle transfer) and the removal of one bottle and replacement with another (bottle replacement). For the bottle-to-bottle propellant transfer of 1242 kg N<sub>2</sub>H<sub>4</sub> replacement, the resupply bottle system (single tank and pressurization subsystem) will weigh about 249 kg, while a bottle replacement mode will result in about 177 kg of propellant bottles. Thus, there is a net weight of 72 kg advantage to the bottle replacement mode; there will be less system complexity and fewer operational events required to perform the bottle replacement.

The blowdown N<sub>2</sub>H<sub>4</sub> pressurization mode was chosen since the blowdown system is less complex than the constant pressure mode. However, a slight performance gain can be achieved with a constant pressure system if a specific impulse gain of 5 percent is realized.

The TMS was chosen as the geostationary platform servicing vehicle since it is a planned STS vehicle, design data with performance characteristics are available, and its performance is adequate for the servicing operations.

Table 3-57. Alternative Logistics Considerations

Ref.	Alternatives (✓ Reference)	Comments
1	Platforms serviced per flight <ul style="list-style-type: none"> <li>• One</li> <li>✓ • More than one</li> </ul>	Provides more versatility
2	Constellations serviced per flight <ul style="list-style-type: none"> <li>✓ • One</li> <li>• Two</li> </ul>	Preferred to eliminate multiple OTV transfers
3	N <sub>2</sub> H <sub>4</sub> Propellant Transfer <ul style="list-style-type: none"> <li>✓ • Bottle Replacement</li> <li>• Bottle to bottle transfer</li> </ul>	Less complexity and lower logistics weight (72 Kg/ft)
4	N <sub>2</sub> H <sub>4</sub> Propellant Pressurization <ul style="list-style-type: none"> <li>✓ • Blowdown</li> <li>• Pressurization</li> </ul>	Less complexity
5	Servicing Vehicle <ul style="list-style-type: none"> <li>✓ • TMS (Teleoperator Maneuvering System)</li> <li>• Other</li> </ul>	Planned vehicle
6	Package Storage During Transfer <ul style="list-style-type: none"> <li>✓ • Attached to TMS</li> <li>• Stored in rack</li> </ul>	Reduces operations and added TMS propellant tanks (attachment location) not required.
7	Location of OTV during servicing <ul style="list-style-type: none"> <li>✓ • Locate in center of constellation, maneuver with TMS</li> <li>• Maneuver with OTV</li> <li>• Other</li> </ul>	Center available for OTV usage convenient for TMS operations

Table 3-57. Alternative Logistics Considerations (Contd)

Ref.	Alternatives (✓ Reference)	Comments
8	TMS Basing ✓     ● Return ● Store on Orbit	<ul style="list-style-type: none"> <li>● Standard operations, lower initial cost</li> <li>● Program total cost is \$209M less</li> </ul>
9	Debris Disposal ✓     ● Use disposal orbit ● Store on platform <span style="border: 1px solid black; border-radius: 50%; padding: 2px;">Recommended</span>	<ul style="list-style-type: none"> <li>● Reference</li> <li>● Increases platform RCS logistics requirements. Reduces number of logistics flights for \$39M cost reduc.</li> </ul>
	● Return to Orbiter	<ul style="list-style-type: none"> <li>● Reduces GEO payload delivery capability, significant increase in costs</li> </ul>
10	Debris Transfer Method ✓     ● OTV ● TMS ● Expendable propulsion unit	Maximum net useful logistics weight delivered to platform
11	Disposal Orbit Debris ✓     ● Unattached ● Debris depot	No plans at this time for a debris depot.

The attachment of the logistics supply packages directly to the TMS was selected instead of using a separate storage rack attached to the OTV. The TMS does not require its external N<sub>2</sub>H<sub>4</sub> propulsion tankage kits, so these TMS structural interface locations are available for attaching the logistic packages. Additionally, the TMS has adequate performance to maneuver among the platforms in a constellation with all logistics packages attached. Consequently, operations are minimized by not having to return to the OTV for each separate package.

The "parking" of the OTV during the TMS servicing operations was selected to be in the "center" of the constellation with all servicing maneuvers performed by the TMS. The TMS (unattached to the OTV) was selected to perform the

maneuvering and docking operations with the platforms because of its lower mass and operations fine maneuver and control capability. The "center" spot "parking" of the OTV was selected because it is available and results in an orbit different from all the other constellation satellite orbits.

The TMS was selected to be earth-based since operations are standard (less initial risk) in that the TMS is ground serviced and maintained between each flight. If the TMS were to be based at GEO (attached to one of the platforms), the TMS would also have to be resupplied with maneuvering propellants and obtain power from one of the platforms between resupply periods. However, the advantage of the GEO basing mode would result in a 121 percent greater logistics payload delivered per OTV flight and, consequently, would lower operational costs since seven fewer Shuttle flights would be required to resupply the required quantity of logistics payload. Space-basing the TMS will reduce program cost by \$209M (1980 \$) as detailed in the TMS basing mode trade study of Table 3-58.

The expended geostationary platform debris (empty N<sub>2</sub>H<sub>4</sub> bottles, spent batteries) were removed from the platform and deposited in a disposal orbit for the reference case since platform retention required additional stationkeeping propellants (122 kg per satellite for an eight-year period). However, the debris should be stored on the platform. The net delivered payload increment is 112 kg per flight greater by retaining the debris (1650 kg payload delivered) than by removing the debris and placing it in a disposal orbit (1433 kg payload delivered) after accounting for the 105 kg per flight increased expendables required for debris retention per resupply flight. Details of this trade study are presented as Table 3-59. Storing expended bottles on the platform results in a program cost reduction of one Shuttle/OTV/TMS resupply flight of \$39M (1980 \$).

The OTV is used to place the debris in the disposal orbit to maximize the logistics weight delivered to the geostationary platform. The TMS does not have the performance capability with its core propellants to deliver the debris and return, while a self-propelled expendable storage rack would require additional weight and cost to provide for autonomous propulsion attitude control and guidance subsystems.

Jettison of the debris in the disposal orbit was used as a reference case since there is no current plan for a debris depot. However, after many such disposal flights without a debris depot, there will have to be care not to have an OTV/debris impact.

**3.3.2.5 Resultant Logistics Plan.** The logistics plan that resulted from the above stated ground rules, mission model, OTV, TMS, logistics requirements, and selected logistic flight systems is presented as Figure 3-74. The initial launch of each platform and the planned logistic flights are as presented in Figure 3-70. The TMS servicing flight to each platform is presented showing

Table 3-58. Trade Study of TMS Basing Mode

	First 8 Years	Second 8 Years
Platform Weight (ground-based TMS)	6,895 kg	7,570 kg
Host Platform TMS Support Weight	82 kg	82 kg
TMS Weight	<u>—</u>	<u>—</u>
Host Platform/TMS Weight (space-based TMS)	<u>6,977</u> kg	<u>8,474</u> kg
Stationkeeping N <sub>2</sub> H <sub>4</sub> for 8-Year Period at 230 seconds		
Space-Based TMS	1,257 kg	1,527 kg
Ground-Based TMS	<u>1,242</u> kg	<u>1,364</u> kg
Increased N <sub>2</sub> H <sub>4</sub> Required for Host Platform of Space-Based TMS	15 kg	163 kg
Increased N <sub>2</sub> H <sub>4</sub> Required Bottle Weight (0.1425)	<u>2</u> kg	<u>23</u> kg
Increased Expendables Weight per Constellation	<u>17</u> kg	<u>186</u> kg
Increased Logistics Transportation Weight for Space-Based TMS Per Constellation		
Expendables	(17 kg + 186 kg)	203 kg
TMS		822 kg
Replace Host Platform TMS Support Weight		<u>82</u> kg
Total Increased Weight Per Constellation		1,107 kg
		<u>x</u> 2 constellations
Total Increased Logistics Transportation Weight for Space-Based TMS		2,214 kg
Logistics Transportation Weight for Ground- Based TMS		<u>24,601</u> kg
Total Logistics Transition Weight for Space- Based TMS		26,815 kg
Payload Capability of OTV		3,757 kg
TMS Propellants Plus Tankage (average per flight)		58 kg
Loss Due to 40 kg Logistics Rack		<u>50</u> kg
Net Logistics Payload Capability of OTV with Space-Based TMS		3,649 kg
Number of Resupply Flights (26,815 ÷ 3,649)		7.3 flights

Table 3-58, Trade Study of TMS Basing Mode, Contd

	First 8 Years	Second 8 Years
Resupply Cost of Ground-Based TMS: 15 Shuttle/OTV/TMS		\$585M
Flights at \$39M		
Resupply Cost of Space-Based TMS		\$376M
2 TMS at \$35M each	\$ 70M	
8 Shuttle/OTV Flights at \$37M each	\$296M	
8 TMS Servicing Operations at \$1M Each	\$ 8M	
Power Conditioning Cost Increase of Host Platform	\$ 2M	
Cost reduction by Space-basing the TMS		<u>\$209M</u>

Resupply debris retained on platform; One TMS per constellation;  
TMS transported to GEO on first resupply flight.

what is delivered to each platform by N<sub>2</sub>H<sub>4</sub> bottle replacement identification number or number of batteries. The initial logistic flights require on-orbit storage of full N<sub>2</sub>H<sub>4</sub> bottles since there will have not been enough stationkeeping propellants expended to utilize a full logistics flight without this on-orbit storage capability. Subsequent flights with the TMS are then used to replace expended bottles with those previously delivered and stored as identified in Figure 3-74.

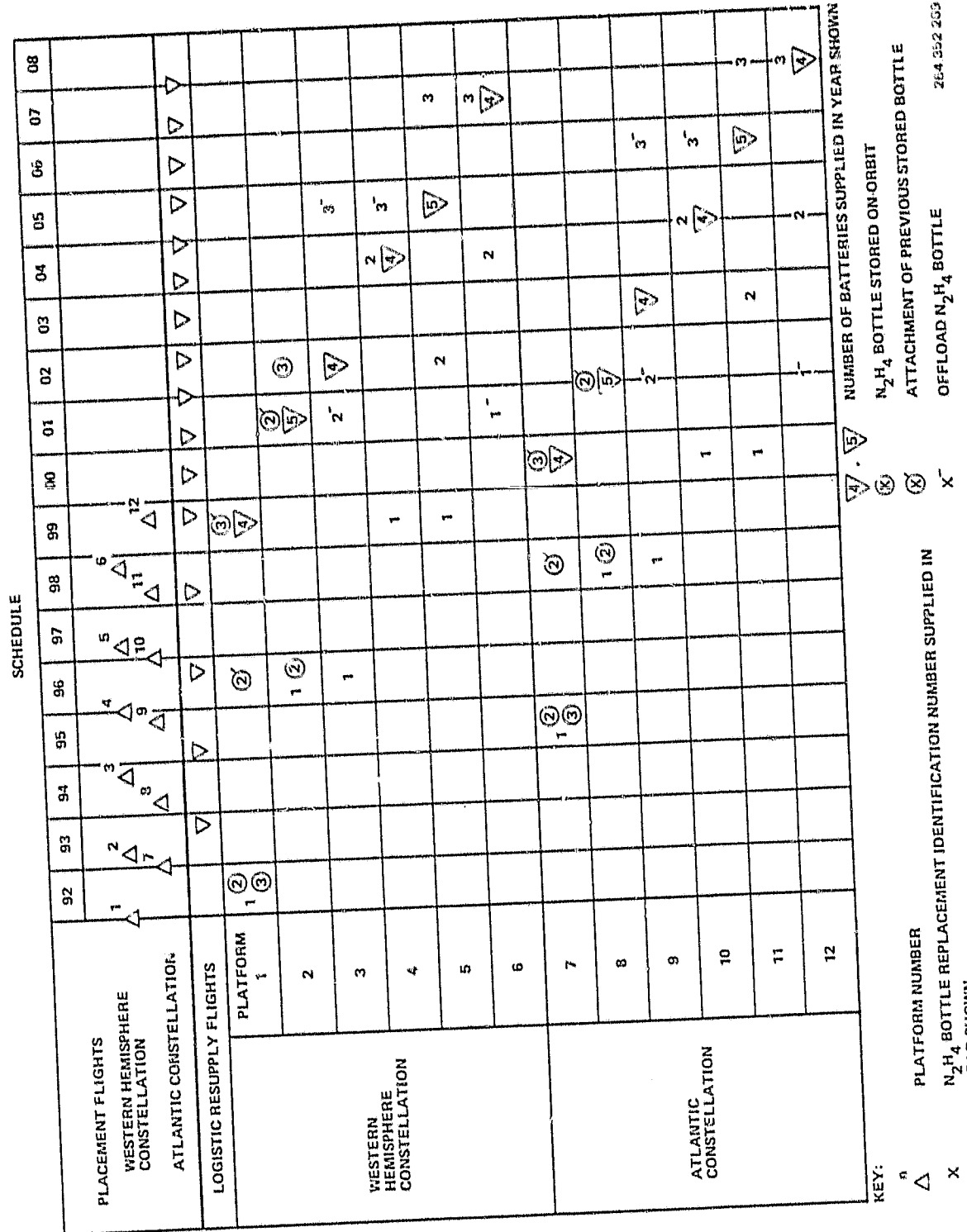
This logistics plan is based on three N<sub>2</sub>H<sub>4</sub> bottles per platform. The bottles are manifolded and valved such that one bottle is expended before the next bottle is used. The logistic flights that transport the required 5 batteries to Platforms 2, 5, 8, and 11 are weight-limited; therefore, the accompanying N<sub>2</sub>H<sub>4</sub> propellant bottles on these flights are offloaded to match the OTV performance capability. Nevertheless, these offloaded bottles provide sufficient propellant for the platforms that they service since these platforms (Tables 3-32 through 3-34) are lighter and require fewer stationkeeping propellants than the "reference" 6895 kg platform. (Subsequent analysis resulted in a need for only four batteries for Platforms 2, 5, 8, and 11.)

The logistics plan is based on the 16-year planned life of the geostationary platform with resupply of only an eight years' inventory of expendables. In reality, the resupply of expendables will continue as long as the platform usage is economically viable. Continuation of constellation operations beyond the 16th year of Platform 1 (10th year of Platform 6) requires additional logistics flights beyond those presented in Figure 3-74.

**3.3.3 FLIGHT OPERATIONS.** The nominal flight time for a typical resupply mission will be completed within five days as shown in Figure 3-75. Summary operations for Orbiter, OTV, and TMS are presented for servicing three

Table 3-59. Trade Study of Debris Disposal Mode  
(Resupply Debris Retained on Platform vs Disposal to GEO + 2000 n.mi.)

Reference Platform Weight	6,895 kg
Satellite Debris Weight	675 kg
3 N <sub>2</sub> H <sub>4</sub> Bottles	177 kg
4 Batteries	488 kg
Attachment of Debris	10 kg
Platform Weight with Debris Retained	7,570 kg
Stationkeeping N <sub>2</sub> H <sub>4</sub> (8 years)	
Debris Retained	1,364 kg per satellite
Debris Removed	<u>1,242</u> kg per satellite
Additional N <sub>2</sub> H <sub>4</sub> Required to Retain Debris on Platform for 8 Years	122 kg per satellite × 12 satellites
Total Additional N <sub>2</sub> H <sub>4</sub> Required for 12 Satellites	1,468 kg for 12 satellites
Average N <sub>2</sub> H <sub>4</sub> Resupply Increase	÷ 16 resupply flights 92 kg / flight
Average Container Increase	<u>13</u> kg / flights
Total Average Required Weight Increase	105 kg / flights
OTV Payload (debris retained)	1,650 kg
OTV Payload (debris removed)	<u>1,433</u> kg
Payload Gain	217 kg
Increase in Required Weight	<u>105</u> kg
Net Payload Gain by Retaining Debris per OTV Flight	112 kg
Total Nominal Resupply Capability (debris removed) (16 flights × 1433 kg / flight)	22,928 kg
Added Required N <sub>2</sub> H <sub>4</sub> (debris retained)	1,464 kg
Added Required Bottle Weight (debris retained)	<u>209</u> kg
Total Resupply Required (debris retained)	24,601 kg
Number of Resupply Flights (debris retained) 24,601 ÷ 1,650	14.9 flights

Figure 3-74. Logistics Plan (Three N<sub>2</sub>H<sub>4</sub> Bottles/Platform)

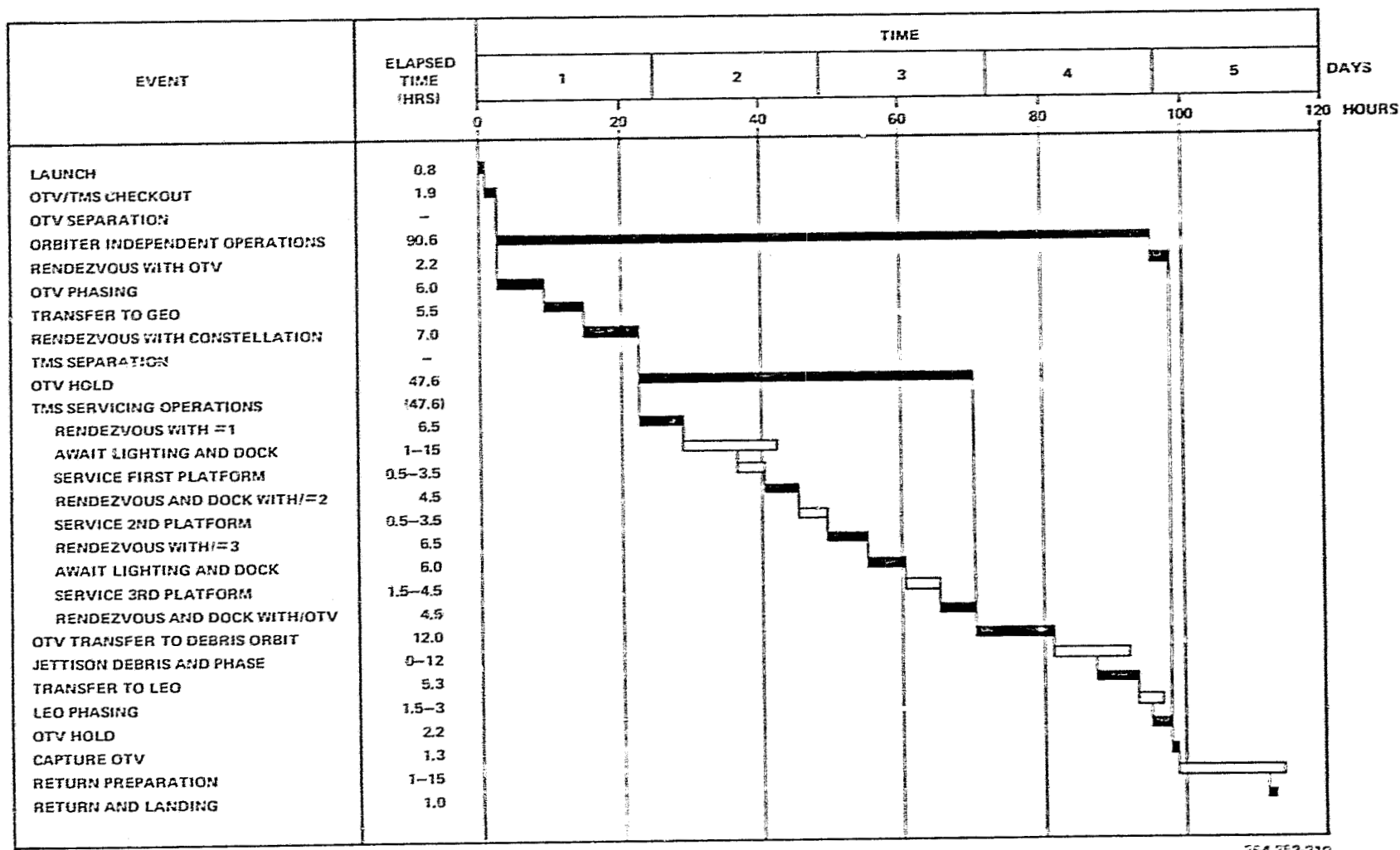


Figure 3-75. Logistics Flight Sequence of Events (Atlantic Constellation)

platforms in the Atlantic constellation. In presenting the sequence of events and times, open bars are used to show the anticipated maximum nominal times expected, with the subsequent event starting at a nominal expected time (contingency events could obviously increase the times presented). This schedule results in two days availability for contingency operations within the nominal Orbiter seven day on-orbit lifetime.

A typical detailed listing of the logistics flight timeline is presented as Table 3-60. Additional flight operations information provided in Table 3-60 includes operation altitudes and values of the velocity maneuvers. Lighting constraints for docking operations was restricted to greater than 15 degrees. Since detailed servicing operations including inspection requirements and time variation could not be included herein, a three hour operations margin at each platform is used.

Typical sequence of events for placement of a platform into geostationary orbit is presented in Figure 3-76. Platform deployment is accomplished within the three-day period, allowing four days within which to perform any contingency operations (based on the seven-day Orbiter lifetime). The expanded events of these platform deployment operations are listed in Table 3-61.

#### 3.4 SPECIALIZED COMMUNICATIONS/INTEGRATION EQUIPMENT

This section addresses the conceptual design of special equipment that will be needed to accomplish the mission requirements. The following functions are included:

- a. Antennas and feeds.
- b. High accuracy pointing equipment.
- c. Switch matrices.
- d. Onboard regeneration.
- e. Interplatform links.
- f. High power amplifiers.
- g. Electromagnetic compatibility (EMC).

**3.4.1 ANTENNAS AND FEEDS.** Antenna systems for very high reuse of the frequency bands are complex. Three major types of antennas can be used for these applications:

- a. The phased array has optimum application when the antenna gain is below about 50 dB and the number of independent beams (both fixed and scanned) is small.
- b. The lens antenna has higher gain and a larger number of independent beams than the phased array, but a high degree of complexity is encountered in the lens.

Table 3-60. Flight Operations - Logistics Flight (Atlantic Constellation)

Event	Start Time (hrs/min)	Event Time (min/sec)	Elapsed Time (hrs/min)
Lift-Off	0	-	0
SRB Separation	:02	-	:02
MECO	:08	-	:08
ET Separation	:08	-	:08
OMS - 1 burn (231 ft/sec)	:09	1:50	:11
Ascent Coast (50 x 150 n.mi.)	:11	32:20	:44
OMS-2 Burn Circularization	:44	1:45	:46
Reconfigure Orbiter Software	:48	12:00	1:00
Enable TMS Discretes	1:00	-	-
Orbiter IMU Alignments	1:00	20:00	1:20
Open Payload Bay Doors	1:20	5:00	1:25
Deploy Radiators/Activate Cooling	1:25	2:00	1:27
Transfer OTV Electrical Power	1:27	-	-
OTV Checkout & Systems Verification	1:28	30:00	1:58
TMS Checkout & Systems Verification	1:28	30:00	1:58
Update OTV Navigation	1:58	:30	1:59
Reorient to OTV Deployment Attitude	1:59	15:00	2:14
Rotate OTV	2:14	4:30	2:19
Activate OTV-Orbiter RF Link	2:19	5:00	2:24
Final OTV/TMS Checkout	2:24	13:00	2:37
Separate OTV	2:37	-	-
OTV Separation Coast	2:37	4:00	2:41
Activate OTV	2:41	1:00	2:42
Coast to First Nodal Crossing	2:42	38:00	3:20
Coast to Phasing Orbit Burn	3:20	180:00	6:20
OTV Phasing Burn (3rd Nodal Crossing) ( $\Delta V = 3025$ )	6:20	5:56	6:26
Phasing Orbit Coast	6:26	185:00	8:41
OTV Transfer Orbit Insertion ( $\Delta V = 5037$ )	8:41	7:36	8:49
Coast to Mid-course	8:49	180:00	11:49
Mid-course Correction ( $\Delta V = 50$ ft/sec)	11:49	0:21	11:49
Coast to GEO	11:49	135:00	14:04
OTV GEO Insertion Burn (15°W, 60 n.mi. range, $\Delta V = 5825$ )	14:04	6:13	14:10
Search & Acquire Constellation	14:10	60:00	15:10
Initial Rendezvous Burn (48 ft/sec)	15:10	0:21	15:10
Coast	15:10	300:00	20:10
Perform Braking Burns (26 ft/sec)	20:10	120:00	22:10
Rendezvous (Center Position, 15°W)	22:10	-	-
Activate TMS	22:10	330:00	22:40
TMS Burn (2 ft/sec)	22:40	-	-
Coast	22:40	300:00	27:40

Table 3-60. Flight Operations - Logistics Flight (Atlantic Constellation), Contd

Event	Start Time (hrs/min)	Event Time (min/sec)	Elapsed Time (hrs/min)
Braking Burns (4 ft/sec)	27:40	60:00	28:40
TMS Rendezvous with Platform #8	28:40	-	
Await Lighting	28:40	0-14 Hours	Avg. 35:40
Maneuver to Docking Position	35:40	60:00	36:40
Dock TMS with Platform #8	36:40	-	
Remove Empty N <sub>2</sub> H <sub>4</sub> Bottle #3	36:40	16:00	36:56
Install Full N <sub>2</sub> H <sub>4</sub> Bottle #3	36:56	16:00	37:12
Operations Margin	37:12	180:00	40:12
Dedock TMS	40:12	-	
Maneuver to Transfer Position	40:12	30:00	40:42
TMS Transfer Injection (6 ft/sec)	40:42	-	
Coast	40:42	120:00	42:42
Braking Burns (10 ft/sec)	42:42	60:00	43:42
TMS Rendezvous with Platform #9	43:42	-	
Maneuver to Docking Position	43:42	60:00	44:42
Dock TMS with Platform #9	44:42	-	
Remove Empty N <sub>2</sub> H <sub>4</sub> Bottle #3	44:42	16:00	44:58
Install Full N <sub>2</sub> H <sub>4</sub> Bottle #3	44:58	16:00	45:14
Operations Margin	45:14	180:00	48:14
Dedock TMS	48:14	-	
Maneuver to Transfer Position	48:14	30:00	48:44
TMS Transfer Injection (2 ft/sec)	48:44	-	
Coast	48:44	300:00	53:44
Braking Burns (4 ft/sec)	53:44	60:00	54:44
TMS Rendezvous with Platform #12	54:44	-	
Await Lighting	54:44	300:00	59:40
Maneuver to Docking Position	59:40	60:00	60:40
Dock TMS with Platform #12	60:40	-	
Remove Battery #1	60:40	16:00	60:56
Install Battery #1	60:56	16:00	61:12
Remove Battery #2	61:12	16:00	61:28
Install Battery #2	61:28	16:00	61:44
Remove Battery #3	61:44	16:00	62:00
Install Battery #3	62:00	16:00	62:16
Operations Margin	62:16	180:00	65:16
Dedock TMS	65:16	-	
Maneuver to Transfer Position	65:16	30:00	65:46
TMS Transfer Injection (6 ft/sec)	65:46	-	
Coast	65:46	120:00	67:46
Orient OTV	67:43	3:00	67:46
Braking Burns (10 ft/sec)	67:46	60:00	68:46
Rendezvous with OTV	68:46	-	

Table 3-60. Flight Operations - Logistics Flight (Atlantic Constellation), Contd

Event	Start Time (hrs/min)	Event Time (min/sec)	Elapsed Time (hrs/min)
Maneuver TMS to Docking Position	68:46	60:00	69:46
Dock TMS with OTV	69:46	-	
OTV Burn to Debris Orbit ( $\Delta V=210$ , low thrust)	69:46	1:30	69:48
Coast to +2000 n.mi.	69:48	720:00	81:48
OTV Burn to Circularize ( $\Delta V=205$ , low thrust)	81:48	1:20	81:49
Jettison Expended Bottles & Batteries	81:49	-	
Coast to Nodal Crossing	81:49	0-12 Hours	87:44
OTV Burn to Return Transfer Orbit  ( $\Delta V = 5726$ )	87:49	3:14	87:52
Coast to Midcourse	87:52	180:00	90:52
Midcourse Correction ( $\Delta V = 50$ ft/sec)	90:52	0:21	90:52
Coast to LEO	90:52	135:00	93:07
LEO Phasing Orbit Burn ( $\Delta V = 3741$ )	93:07	1:32	93:09
Phasing Orbit Coast	93:09	90-180:00	95:24
LEO Circularization Burn (20 n.mi. above, 130 n.mi. in front, $\Delta V=4490$ , $\Sigma \Delta V=8231$ )	95:24	1:25	95:25
Orbiter Rendezvous with OTV	95:25	129:00	97:34
Vent OTV LH <sub>2</sub>	97:34	30:00	98:04
Vent OTV LO <sub>2</sub>	98:04	30:00	98:34
Disable OTV RCS	98:34	-	
Capture OTV with RMS	98:34	2:30	98:37
Return OTV to Cradle	98:37	17:30	98:54
Orbiter Thermal Conditioning & Re-entry			
Phasing	98:54	<12-15 Hours	110:54
Orbit Determination	110:54	1:30	110:56
Orbiter IMU Alignment	110:56	20:00	111:16
Close Payload Bay Doors	111:16	20:00	111:36
Orient to Deorbit Attitude	111:36	10:00	111:46
OMS Deorbit Burn (338 ft/sec)	111:46	2:00	111:48
Orient to Entry Attitude	111:48	10:00	111:58
Coast to Entry Interface	111:58	8:00	112:06
Entry Interface (400K ft)	112:06	-	
Entry Flight Operations	112:06	24:16	112:30
TAEM-Landing Operations	112:30	5:01	112:35
Touchdown (4.7 days)	112:35	-	

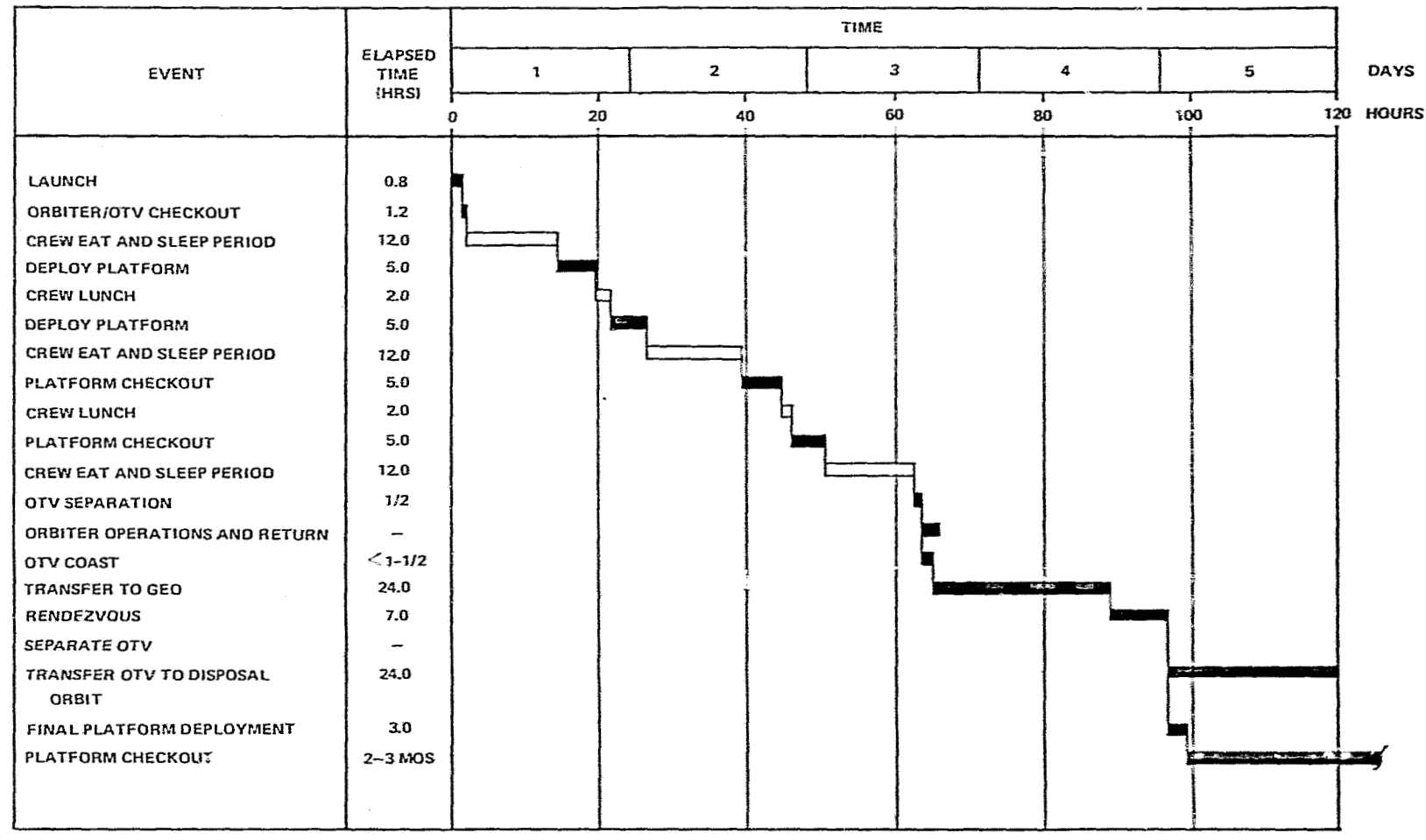
G11  
G2

Figure 3-76. Platform Placement Flight Sequence of Events (Platform 2)

Table 3-61. Flight Operations - Placement Flight (Platform 2)

Event	Start Time (hrs/min)	Event Time (min)	Elapsed Time (hrs/min)
Lift-Off	0	-	0
SRB Separation	:02	-	:02
MECO	:08	-	:08
ET Separation	:08	-	:08
OMS - 1 burn	:09	2:00	:11
Ascent Coast	:11	32:00	:44
OMS - 2 burn circularization	:44	2:00	:46
Reconfigure Orbiter software	:48	12:00	1:00
Orbiter IMU alignments	1:00	20:00	1:20
Open payload bay doors	1:20	5:00	1:25
Deploy radiators/activate cooling	1:25	2:00	1:27
Transfer OTV electrical power	1:27	-	-
OTV checkout & systems verification	1:28	30:00	1:58
Crew eat and sleep period	2:00	720:00	14:00
Rotate OTV to 75° position	14:00	5:00	14:05
Raise central mast	14:05	15:00	14:20
Deploy 6 m main reflectors			
rotate reflector #1 main arm 135°	14:20	20:00	14:40
extend main arm	14:40	10:00	14:50
rotate main reflector support arm 100°	14:50	15:00	15:05
deploy antenna #1	15:05	30:00	15:35
repeat above steps for reflector #2	15:35	75:00	16:50
repeat above steps for reflector #3	16:50	75:00	18:05
Deploy 6 m antenna receive arrays			
rotate feed array #1, 45°	18:05	10:00	18:15
rotate feed array #2, 45°	18:15	10:00	18:25
rotate feed array #3, 45°	18:25	10:00	18:35
Crew lunch	18:35	120:00	20:35
Deploy 6 m antenna transmit arrays			
rotate feed array #1, 120°	20:35	30:00	21:05
rotate feed array #2, 120°	21:05	30:00	21:35
rotate feed array #3, 120°	21:35	30:00	22:05
Deploy subreflector			
rotate subreflector #1 support arm 45°	22:05	5:00	22:10
rotate inner reflector 135°	22:10	10:00	22:10
rotate outer reflector 180°	22:20	15:00	22:35
repeat above steps for subreflector #2	22:35	30:00	23:05
repeat above steps for subreflector #3	23:05	30:00	23:35

Table 3-61. Flight Operations - Placement Flight (Platform 2), Contd

Event	Start Time (hrs/min)	Event Time (min)	Elapsed Time hrs/min)
Deploy RF interferometer			
extend astromast #1, 52 m	23:35	15:00	23:50
extend astromast #2, 52 m	23:50	15:00	24:05
extend astromast #3, 52 m	24:05	15:00	24:20
extend astromast #4, 52 m	24:20	15:00	24:35
Deploy solar arrays			
rotate array arm #1, 90°	24:35	10:00	24:45
extend solar panel, 18 m	24:45	30:00	25:15
rotate array arm #2, 90°	25:15	10:00	25:25
extend solar panel, 18 m	25:25	30:00	25:55
Crew eat and sleep period	26:00	720:00	38:00
Deploy radiator			
rotate radiator housing 90°	38:00	5:00	38:05
extend radiator 15 m	38:05	45:00	38:50
Power up and check out subsystems, telemetry thru ground stations (platform oriented along nadir axis)	38:50	240:00	43:00
Crew eat	43:00	120:00	45:00
Continue subsystems checkout	45:00	240:00	49:00
Retract solar panels	49:00	60:00	50:00
Crew eat and sleep	50:00	720:00	62:00
Activate OTV-Orbiter RF link	62:00	5:00	62:05
Reorient to OTV deployment attitude	62:05	15:00	62:20
Final OTV checkout	62:20	13:00	62:33
Separate OTV	62:33	-	62:33
OTV separation coast	62:33	4:00	62:37
Activate OTV	62:37	1:00	62:38
Coast to initial burn point	62:38	< 90:00	64:00
Transfer to geostationary orbit (8-burn total)	64:00	24 hours	88:00
Search and acquire constellation	88:00	60:00	89:00
Initiate rendezvous burn	89:00	-	89:00
Coast	89:00	300:00	94:00
Perform braking burns	94:00	120:00	96:00
Rendezvous	96:00	-	96:00
Orient to platform attitude	96:00	15:00	96.15
Separate OTV from platform	96:15	-	96:15
Deploy solar panels	96:15	81:00	97:35
Power up platform	97:35	55:00	98:30
Deploy inter-platform link antenna			
extend antenna mast 9 m	98:20	10:00	98:40
deploy antenna	98:40	20:00	99:00
Initiate platform checkout	99:00	-	99:00
Platform checkout	-	2-3 months	-
Initiate platform operations	-	-	-

c. The reflector has very good multibeam and high gain capability.

The greatest disadvantages of the reflector antenna are the scanned beam characteristics. For most high gain applications the reflector antenna is used. Large amplitude taper and offset reflector geometries are used to reduce antenna pattern sidelobes. Scanning of the reflector has been improved by increasing the illumination taper on the reflector by exciting a number of elements for the scanned beam. Additional feed elements are also excited to cancel the larger ring type sidelobes that form on the side of the scanned beam toward the axis of the antenna. Dual reflector antennas are receiving increased attention for their improved scan capability. Current Cassegrain antenna systems provide scan angles near six degrees. Improved shaping of the reflector surfaces will further increase the maximum scanned beam angle. A major disadvantage of the dual reflector antenna is the enlargement of the feed assembly aperture. Improvements in scanned beam performance and in a number of other areas of antenna performance are required.

**3.4.1.1 Antenna Geometry.** The requirements specified for the CPS and HVT services necessitate offset antenna geometries that can provide low sidelobes, low cross-pol and minimum scan loss performance. Offset configurations (Figures 3-77 and 3-78) are normally used to eliminate scattering from feeds and supports structures which are detrimental to sidelobes and cross-pol requirements. Large effective f/D ratios are used to minimize the scan loss.

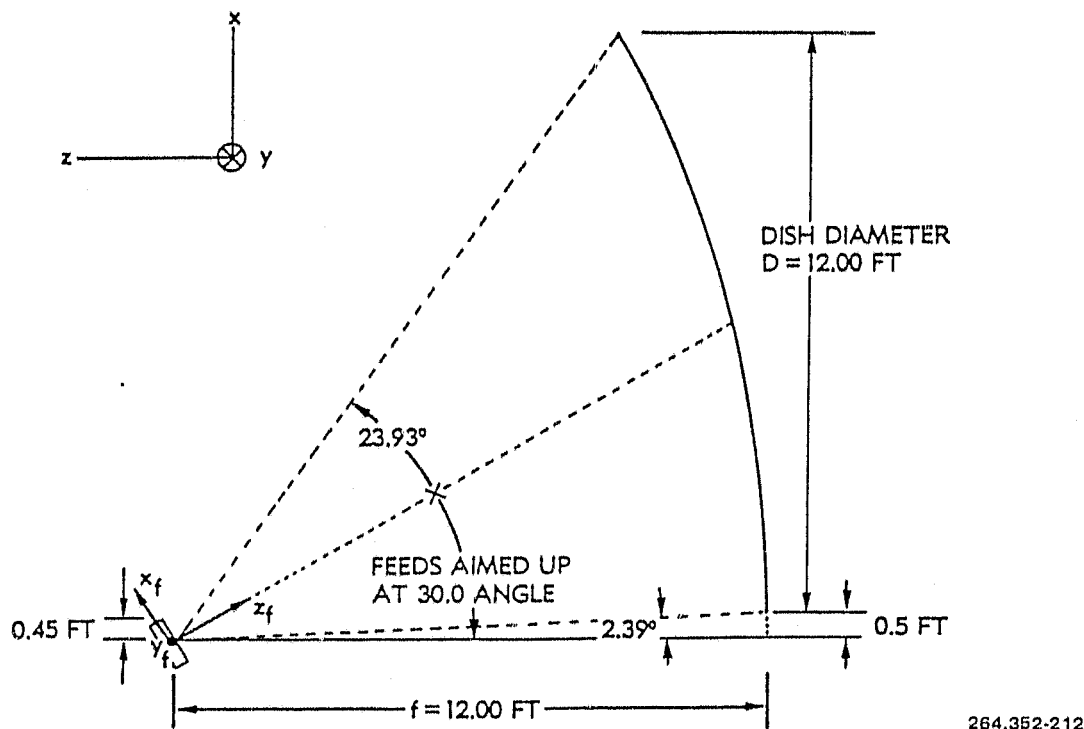


Figure 3-77. Single Offset Reflector Configuration

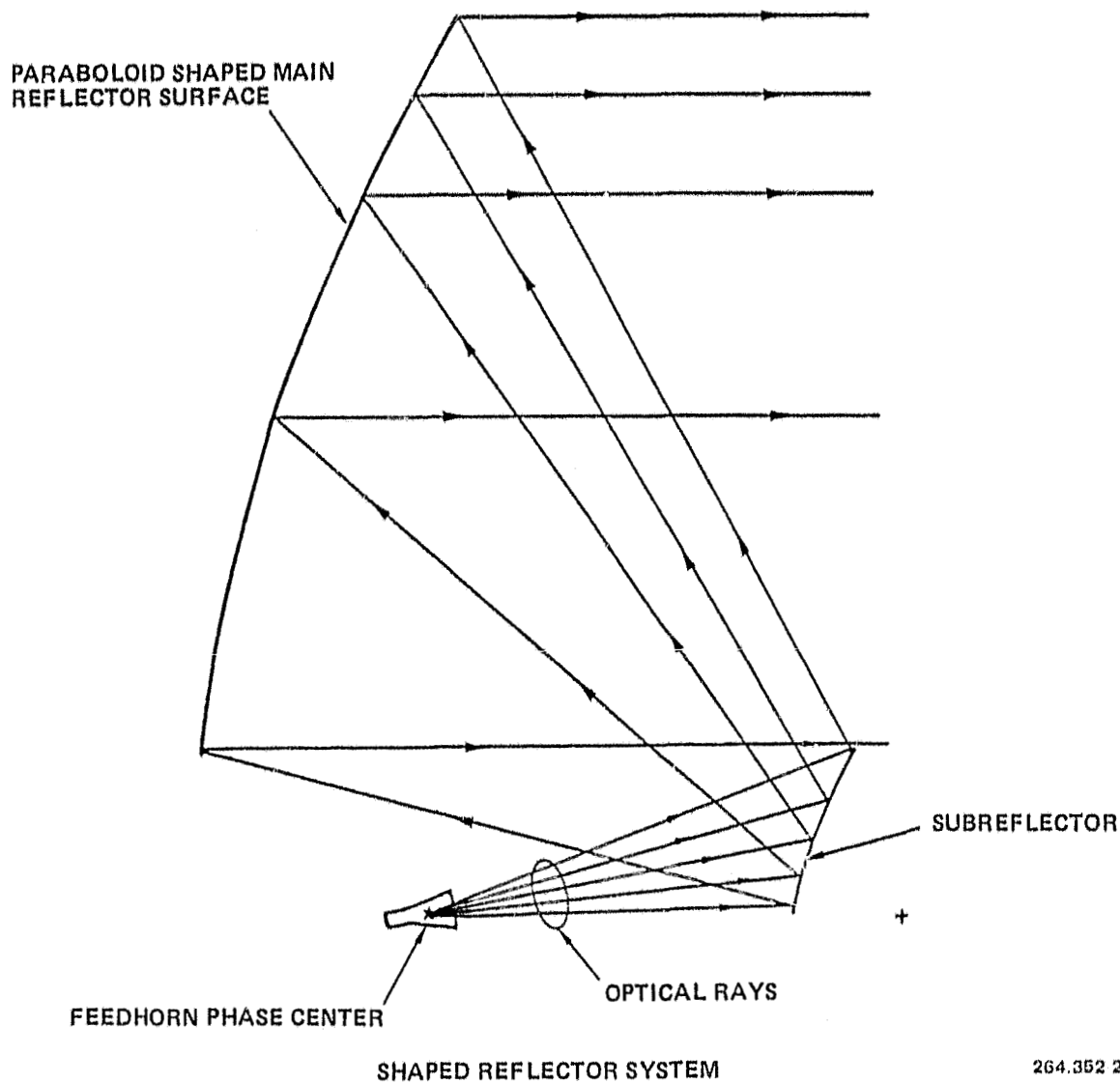


Figure 3-78. Dual Offset Reflector Configuration

Present dual offset reflector systems will not meet the scanning requirements of the CPS and HVT coverages. Reflector systems of this type tend to be angle limited in scanning rather than the number of scanned beamwidths of the single reflector. At angles greater than 6 degrees severe scanning loss occurs. Efforts to increase the reflector system's field of view to as large as  $\pm 10$  degrees are presently being made. This work has concentrated on solving for optimum feed locations and shaping subreflectors for improved scanning performance. To date, a solution that can provide  $\pm 8$  degrees of minimal scan loss has not been found. Continued effort in this area should produce a solution consistent with the time frame of the geostationary platform.

264.352 213

**3.4.1.2 Reflector Surface Tolerances.** The surface tolerances of a reflector place a fundamental limitation on the sidelobe levels that are achievable. Present day solid reflector technology would not be acceptable for Ka-band CPS coverage in terms of the isolation required. In addition, deployable reflectors, which are presently being considered, would further degrade the performance. A continued effort in development of improved surface tolerances will be necessary for the successful implementation of the Ka-band coverage.

Low sidelobe requirements are extremely important for the CPS service. Even with optimum reflector illuminations, the sidelobe performance and antenna gain can be severely degraded by reflector surface tolerances. Figures 3-79 and 3-80 indicate the loss in gain and degradation in sidelobe performance that can occur from the surface inaccuracies of the reflector. Figure 3-80 indicates that for a 0.053 rms (ins) surface tolerance at Ku-band sidelobes can be 5 dB greater than predicted levels. This much variation in the sidelobe levels would make it very difficult to maintain the C/I ratios for CPS services.

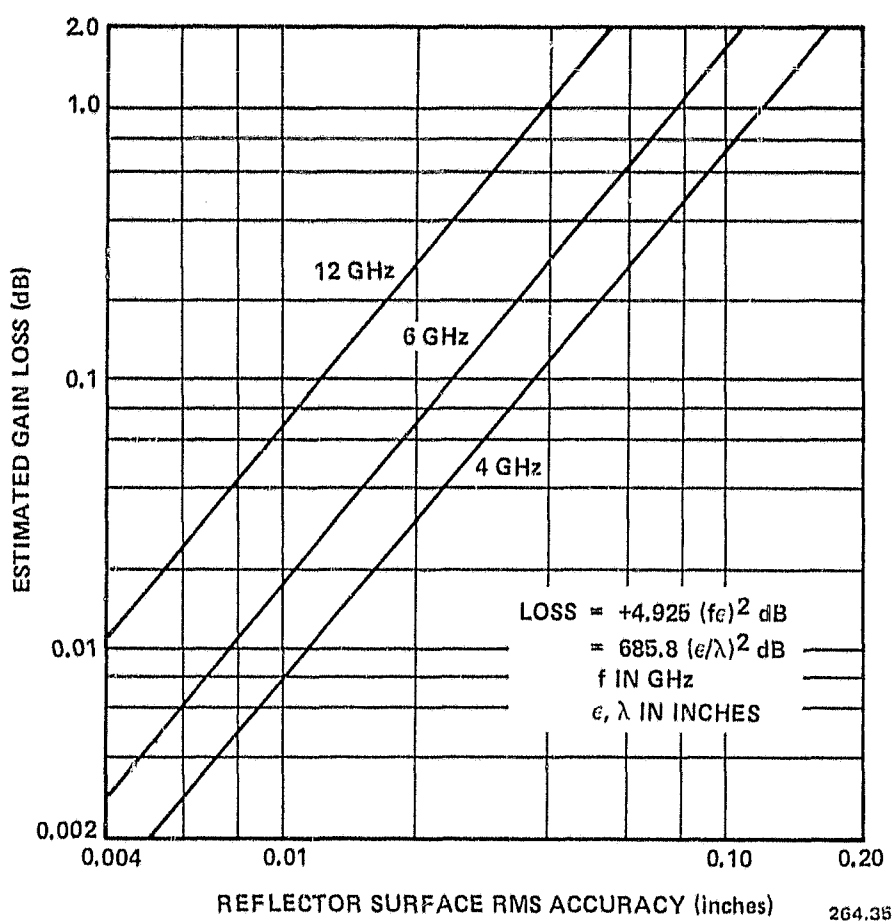
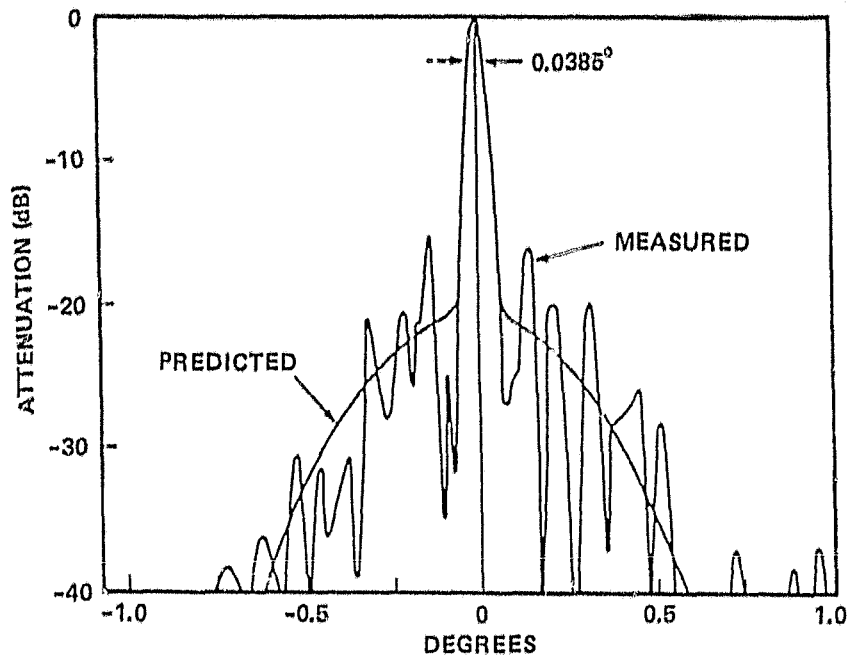


Figure 3-79. Reflector Gain Loss Versus Surface Tolerances

264.352-214

MEASURED PATTERN SHOWING EFFECT OF SURFACE  
TOLERANCE ON SIDELOBE LEVELS  
AT 15 GHz AND 0.053 RMS (ins)



264.362-216

Figure 3-80. Sidelobe Degradation Due to Surface Tolerances

**3.4.1.3 Feed Systems.** Generating a component beam from a single horn will not produce acceptable isolation between nonadjacent scanned beams. The only feasible way of implementing the three frequency system would be to use a cluster of possibly 7 or 9 horns to form each component beam. By tapering the amplitude distribution of the horns a very low sidelobe beam can be formed. The horn cluster must be able to operate over large bandwidths (50 percent) and generate very little cross-pol interference. Feed systems operating at Ku-band over a 30 percent bandwidth have already been built. But a feed system consistent with the Ka-band requirements will need further development.

The proper choice of a feed element is necessary for maintaining low cross-pol. The ideal Huygen's source that will generate no cross-pol on a symmetrically fed reflector can be approximately realized by a corrugated horn or dual mode (Potter horn) as shown in Figures 3-81 and 3-82. Despite its superior performance, the corrugated horn tends to be too large to be used as an array element. The Potter horn has been used in arrays and has been shown to perform very well. The Potter horn tends to be bandwidth limited but recent work, which incorporates dielectric rings in the horn, has increased the usable bandwidth. The Potter horn generates a pattern with symmetrical E and H planes and very low cross-pol in these planes. Maximum cross-pol is generated in the 45 degree cut planes. A typical radiation pattern is shown in Figure 3-83.

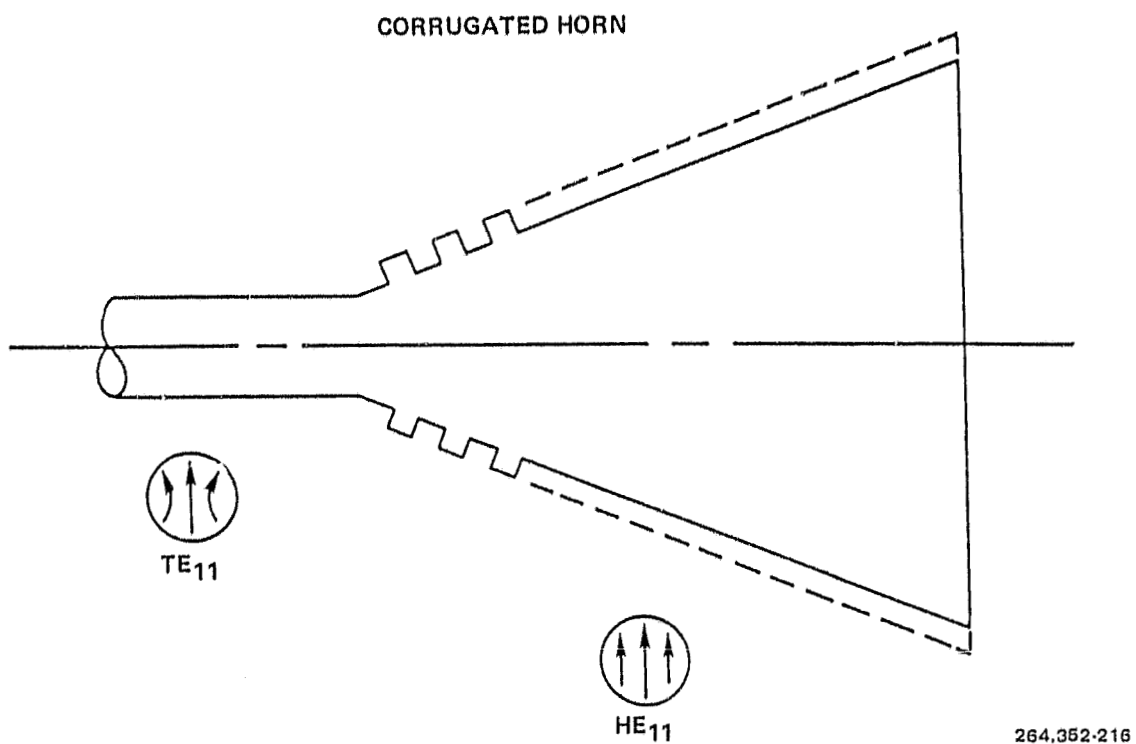


Figure 3-81. Corrugated Horn With Hybrid Modes

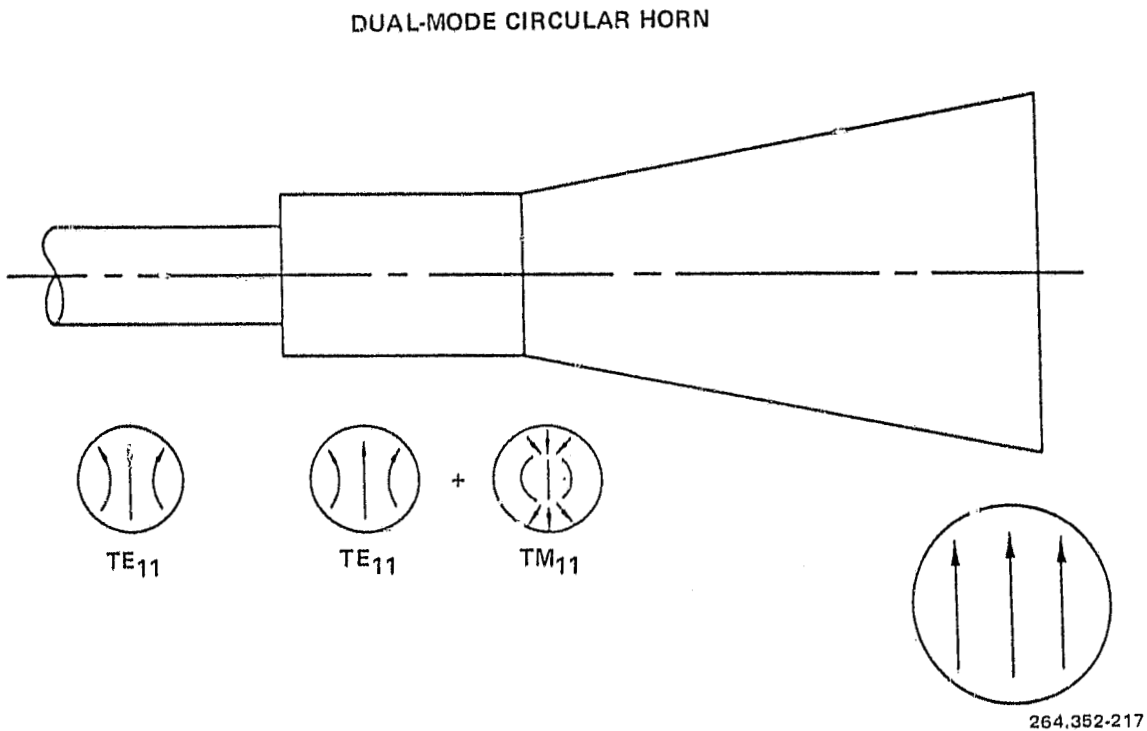
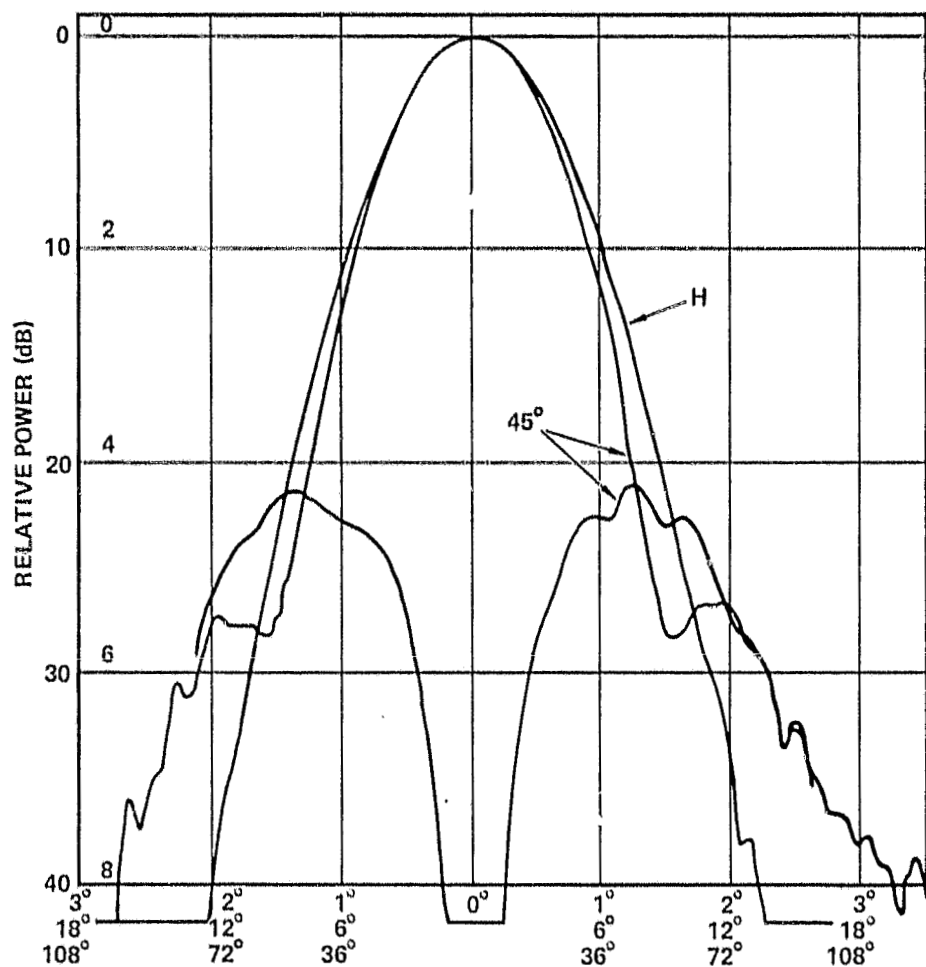


Figure 3-82. Dual Mode Potter Horn



264.J52-218

Figure 3-83. Measured Pattern of Broadband Horn, H and 45° Plane, 6.0 GHz

When using a cluster of horns to obtain high C/I ratios each horn is properly weighted in amplitude to create a tapered distribution on the reflector aperture; this generates a low sidelobe component beam. Figure 3-84 illustrates the problem of using a single horn to generate a component beam. In Figure 3-84, a cluster is actually used but the excitations on the outer ring are small and response shown would be similar to that of a single horn. Two additional 3 dB beamwidths have been added to the figure. In Figure 3-84, the receive C/I ratio of beam 1 into beam 3 is at worst case 22 dB. Assuming an average of 6 interferers into each beam, the worst case C/I may be as low as 14.3 dB. More realistically, this number will be about 18 dB. On transmit the C/I ratio (within the 3 dB contour) is 19 dB. The minimum C/I could be as low as 12 dB, but a more likely value would be about 15 dB. The beam in Figure 3-84 is generated from a horn at the reflector focus. When scan loss is taken into account these numbers will degrade even further.

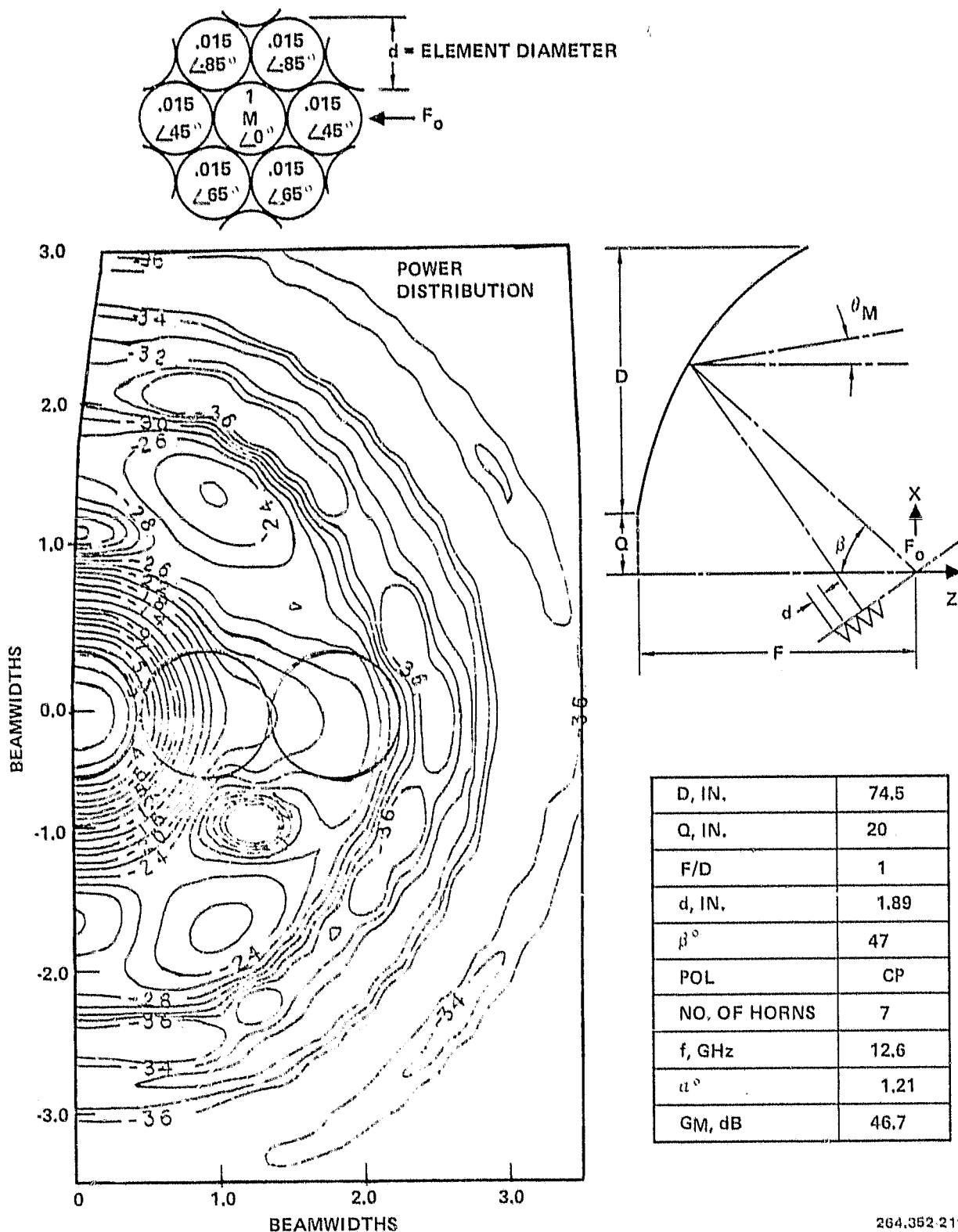


Figure 3-84. Secondary Pattern of a Single Horn with Low Amplitude Peripherals Excited (Additional Beams Shown Separated by One and Two Beamwidths)

In Figure 3-85, the component beam is generated by a 7 horn cluster. Two additional 3 dB component beams have been placed on the figure. The amplitudes of the horns are adjusted to form a tapered distribution across the aperture of the seven horns. This tapered distribution produces a low sidelobe beam. For the case shown, the receive C/I for beam 1 into beam 3 is 26 dB. This represents a 4 dB improvement over the single horn case. It should be pointed out that the beam in Figure 3-85 has been scanned 6° in elevation. For beams scanned only a few degrees, higher C/I ratios are possible. With small scan angles receive C/I ratios of 30 dB are obtainable. Assuming an average of 6 interferers the receive C/I ratio for Figure 3-85 would be approximately 23 dB. For transmit the total C/I will be about 20 dB. These two values may be improved by 2 or 3 dB if more optimum horn excitations are used and the scanning is reduced. The horns used in the cluster were dual mode Potter horns, which have been optimized to operate over approximately a 40 percent bandwidth. The cross-pol performance of this horn cluster is shown in Figure 3-86. Such a horn cluster, which can operate over a 50 percent bandwidth and exceed the isolation performance of that shown, will be necessary for the CPS services. Figure 3-87 depicts a typical feed network for a broadband seven horn cluster. The three auxiliary horns are used for sidelobe suppression in a preferred direction.

**3.4.1.4 Scanning Performance.** The CPS services will require an antenna that can provide up to  $\pm 9$  degrees of scan with a minimum of degradation in performance. Figure 3-88 shows the degradation in gain versus scan angle for the seven horn cluster discussed previously. Of greater importance is the degradation in sidelobe levels as the scan angle is increased. This could have serious effects on the isolation levels between beams. For best performance a large f/D ratio must be used along with an optimized feed cluster.

**3.4.1.5 Antenna Pointing Requirements.** Based on a 0.35 degree beamwidth, (required for the low traffic model) at the very minimum a pointing accuracy of 0.05 degree should be maintained. This will probably necessitate an RF tracking system such as the one shown in Figure 3-89. This type of monopulse system is being used on present satellite systems and has been shown to be able to achieve 0.05 - 0.075 degree pointing accuracy. For pointing accuracies better than 0.05 (which may be necessary), especially with the high traffic model further optimizations of this system must be developed.

**3.4.1.6 Conclusions.** For the CPS and HVT services to be properly implemented, a very small rms surface tolerance reflector must be used. The optical system must have a large f/D ratio ( $\sim 0.6$ ) and must be fed by a very large feed array consisting of clusters of horn segments forming the component beams.

**3.4.2 HIGH ACCURACY POINTING EQUIPMENT.** Antenna pointing accuracy requirements of 0.03 and 0.05 degree are discussed in Section 3.4.1 and 3.4.5. To operate a tracking/pointing system, a sensor, a controller, and an antenna positioner are needed to close the control loop. For the above mentioned high pointing accuracy requirements, a monopulse sensor is ideal for detecting

3.4 GHz  
 $d = 5.44$  IN.  
 RCP, MAIN

$TE_{11} + q TM_{11}$   
 $n = 7$   
 $P_o = 0$  dB  
 $P_k = -4.77$  dB,  $k = 1, 2, \dots, 6$

$D = 162$  IN,  
 $F/D = 1.617$   
 $Q = 90$  IN.  
 $\theta_{ma} = 5.63^\circ, \theta_{me} = 0.05^\circ$   
 $G_o = 39.96$  dB

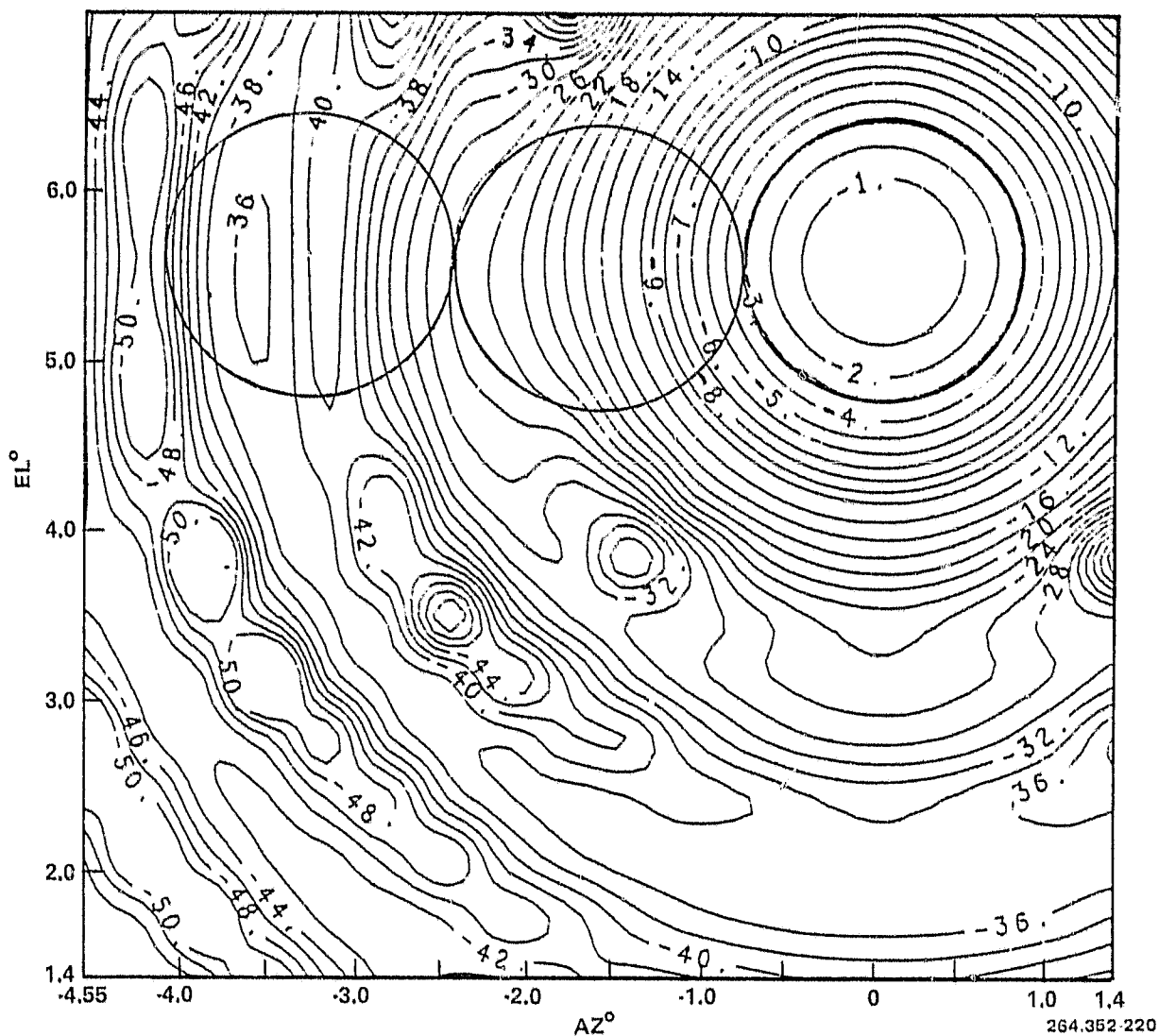


Figure 3-85. Main Polarized Gain Contour Plot for the Geometry Shown on Figure 3-84 Using 7 Component Beams (Center Horn Is At 0 dB Level, Outside Horns Are At -4.77 dB Level with  $TE_{11}$  Mode Excitation)

pointing errors along two orthogonal directions. The key advantage of this type sensing system is its use of the communication antenna as a sensor to point that same antenna, eliminating several types of pointing errors presented in other configuration.

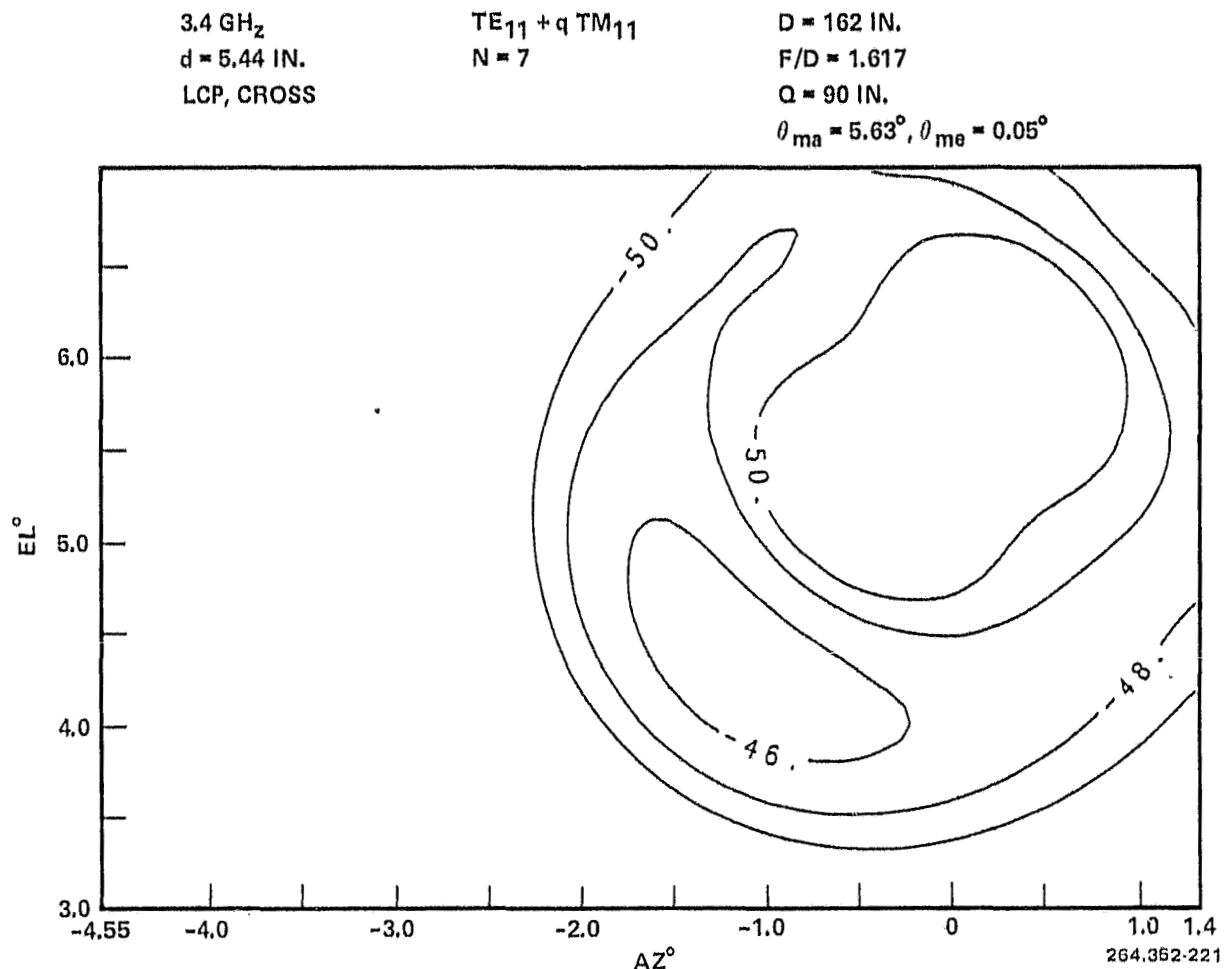


Figure 3-86. Cross Polarized Gain Contour Plot For the Geometry Shown on Figure 3-84 Using 7 Component Beams (Center Horn Is At 0 dB Level, Outside Horns Are At -4.77 dB Level with TE<sub>11</sub> Mode Excitation)

A representative monopulse sensor, as shown in Figure 3-89, can be used to detect antenna pointing errors which will be processed by a controller and generate commands to an antenna positioner. The sensed error signals will be processed by a controller and generate a command to an antenna positioner. This positioner may consist of a double gimbal with adequate angular freedom. Each step motor drives a gear set with certain reduction ratio, such that the resulting step size is proper for the required pointing accuracy.

The SBS/ANIK-C type spacecraft uses a monopulse sensor that provides an attitude determination accuracy of 0.01 degree ( $3\sigma$ ) and the control loop can achieve an antenna pointing accuracy in the order of 0.05 degrees. The associated antenna drive has an angular quantization of 0.0025 degree. The step

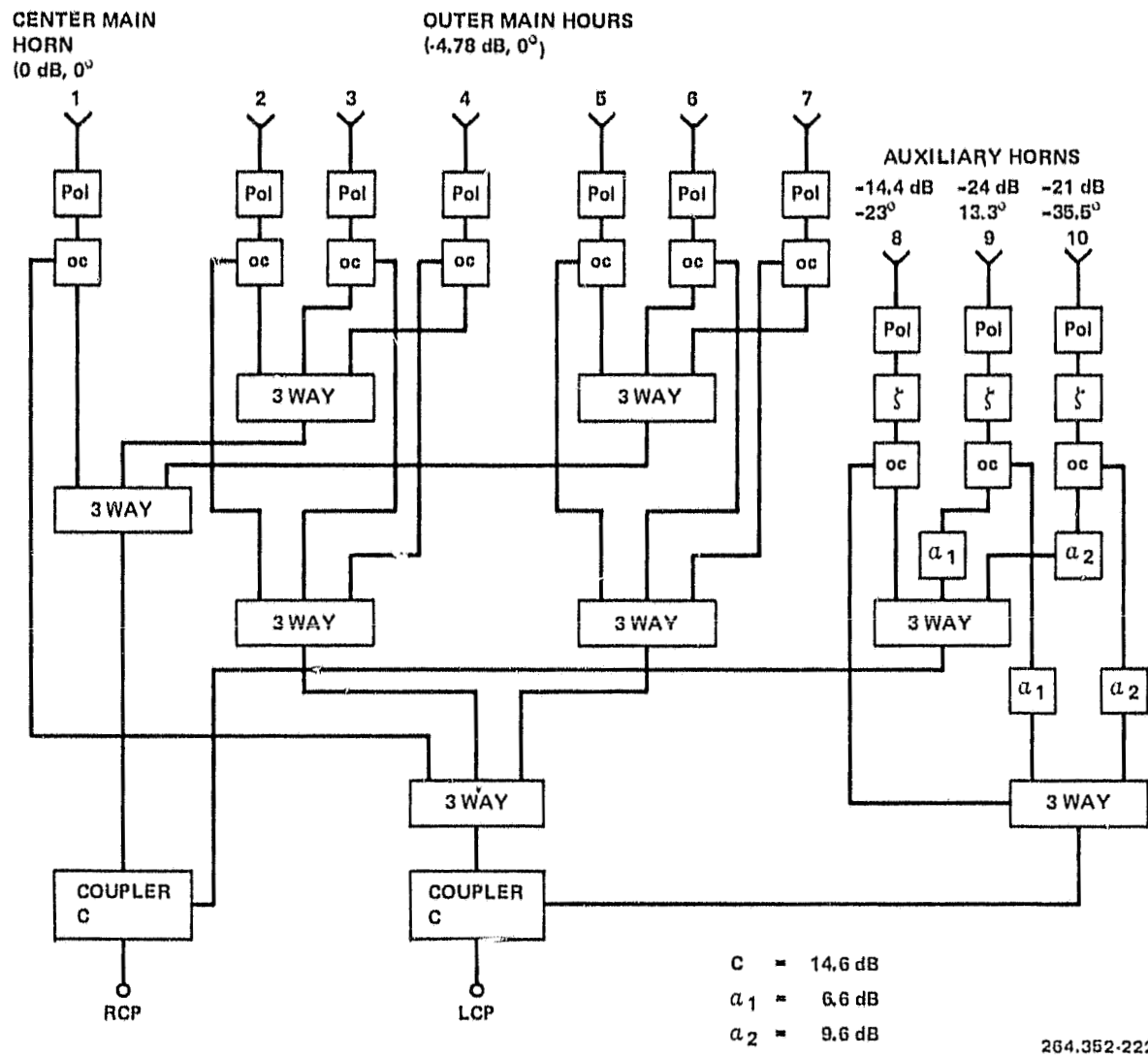
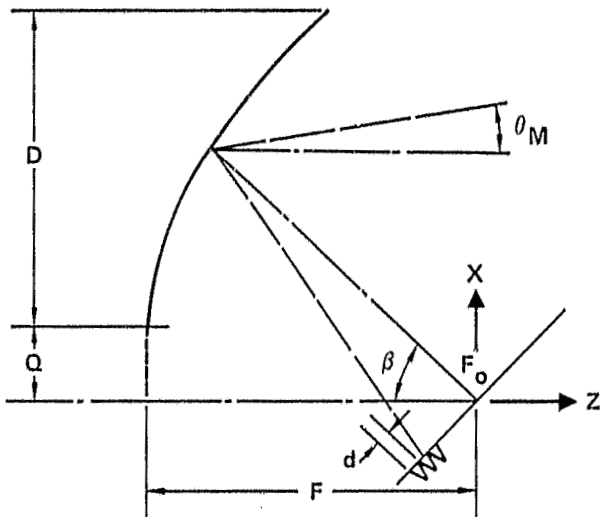


Figure 3-87. BFN Layout For the Experimental Broadband Feed

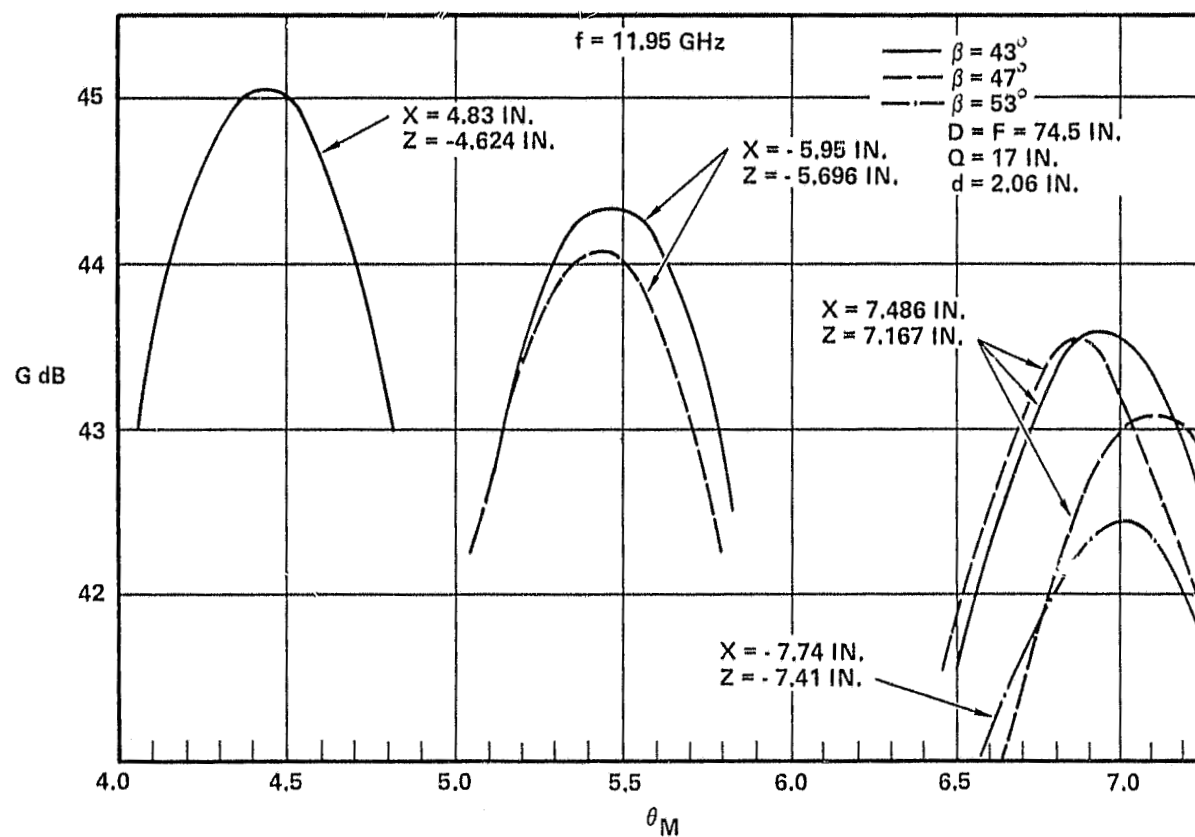
size of the pointing mechanism and the performance of the control loop suggest that technology similar to that used by SBS can, with some refinement, be developed to fulfill the stringent antenna pointing requirements for application to the geostationary platform.

**3.4.3 SWITCH MATRICES.** The geostationary platform will require a variety of matrix switches. A considerable amount of effort is being directed towards development of these switches. Several companies presently engaged in this type of work are:

- COMSAT Labs - 8 by 8 wideband microwave switch matrix (MSM) at 4 GHz as well as a baseband switch matrix (BSM) are under development.

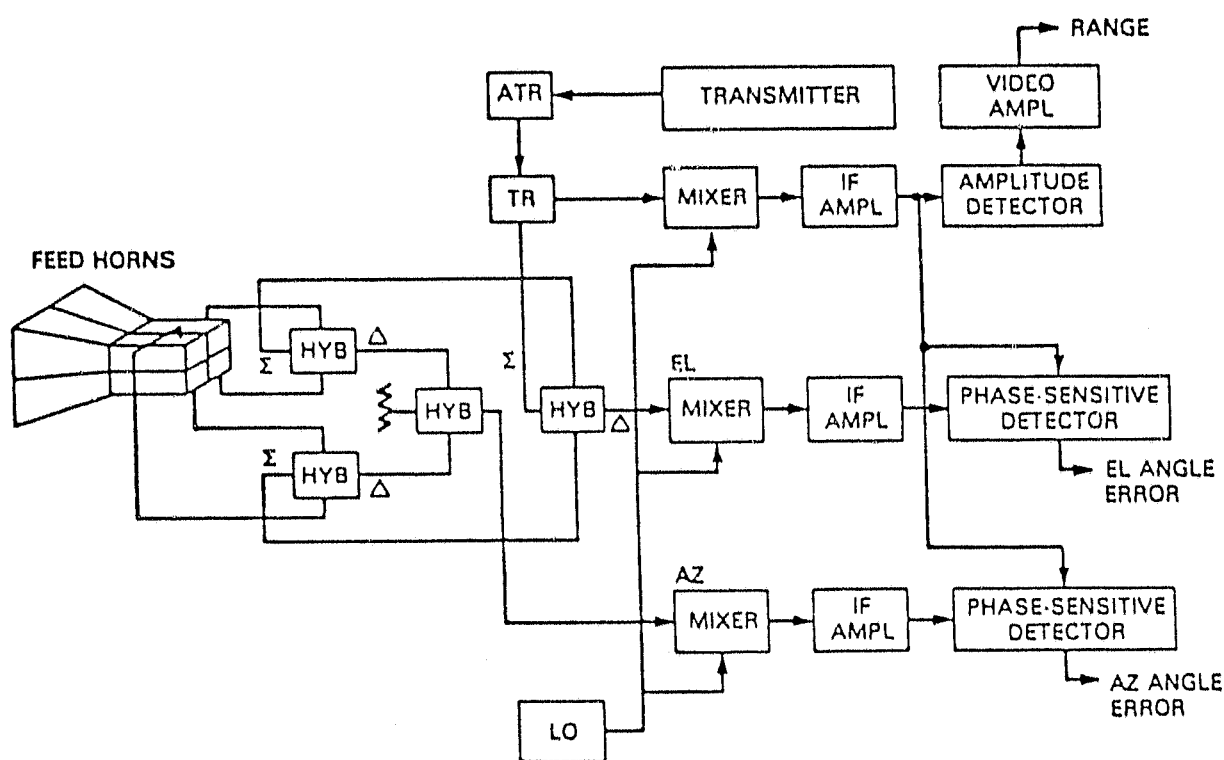
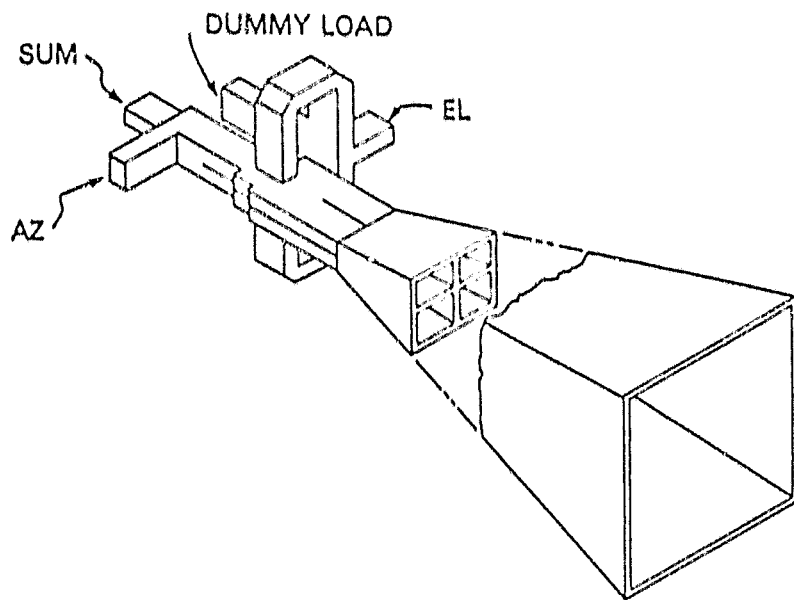


BASIC GEOMETRY OF OFFSET PARABOLOID ANTENNA



264.352-223

Figure 3-88. Patterns of Scanned Beams Versus  $\theta_M$



264.352-224

Figure 3-89. Monopulse Tracking Network

- b. TRW - 4 by 4 MSM for the TDRSS satellite.
- c. Hughes Aircraft Corporation - 8 by 8 MSM at 4 GHz.
- d. Nippon Electric Company - delivered a 4 by 4 IFSM at 140 MHz.

The major problem areas are:

- a. Reliability - the reliability of the switches and a means of effective redundancy must be established.
- b. Isolation.
- c. Insertion loss.
- d. Switching time.
- e. Size - the units tend to be large.
- f. Weight - the units tend to be heavy.

COMSAT's experience indicates that as a first order approximation the weight and power requirements go up as the square of the number of ports.

The implementation of Satellite-Switched Time Division Multiple Access (SS-TDMA) systems such as shown in Figure 3-90 is implicit in the mission. The required transponder for such a system, in this case utilizing a 4 by 4 switch matrix as an example, is shown in Figure 3-91. The heart of such a system (Reference 60) requires an MSM shown in Figure 3-92. The MSM is controlled by a distribution control unit (DCU) shown in Figure 3-93 and an acquisition and synchronization unit (ASU) shown in Figure 3-94 to provide the necessary TDMA references.

Figure 3-95 shows alternative configurations of redundant 8 by 8 matrix switches. Also, a worst case, four consecutive failures, of a redundant 8 by 8 switch matrix using only T-switches is shown. Typical specifications for an MSM are given in Table 3-62.

As a first-order approximation, the weight and power go up as the square of the number of ports. Typical DCU specifications are:

Long-term stability	$1 \times 10^{-8}$ min
Minimum burst time	Dependent upon data rate and frame size but on the order of 6 $\mu$ s for a 750- $\mu$ s frame.

Rozec and Assal (Reference 61) indicate that to obtain at least 50-dB input/output isolation the PIN diodes should be connected in shunt as shown in Inset (A) of Figure 3-96. The switch is designed to produce a low-pass filter, Inset (B) of Figure 3-96, at 0V bias and a reactive termination with 5 mA current, Inset (C) of Figure 3-96.

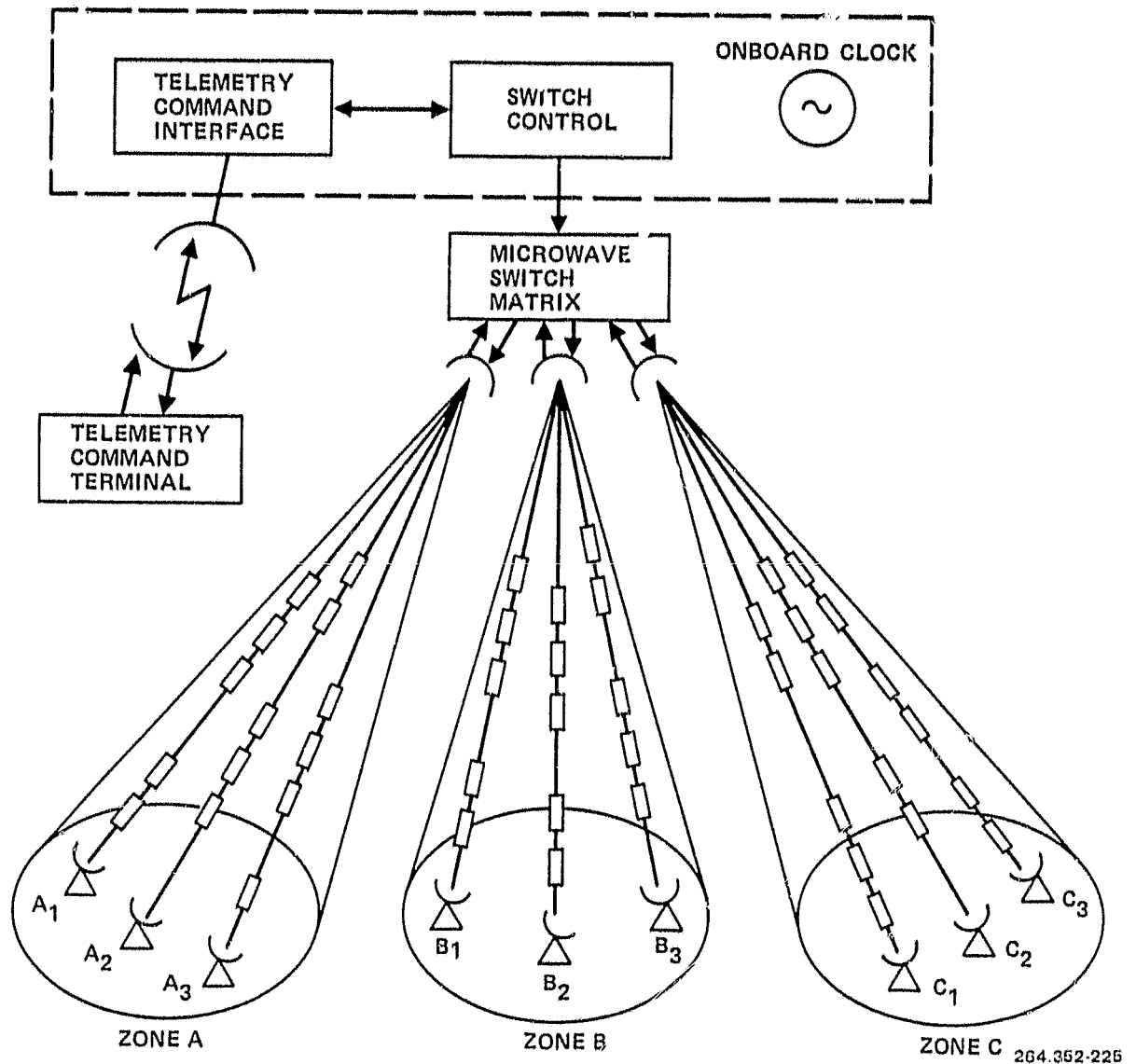


Figure 3-90. SS-TDMA System Concept

As previously stated (reference 60), the reliability of the switches and effective redundancy approaches are yet to be established. Ito, et al. (Reference 62) has computed the probability of survival for an 8 by 8 cross-bar type switch, as shown in Figure 3-97. Theoretically, when the level of redundancy increases, the probability of survival also increases, with an increase in complexity, as shown in Figure 3-95.

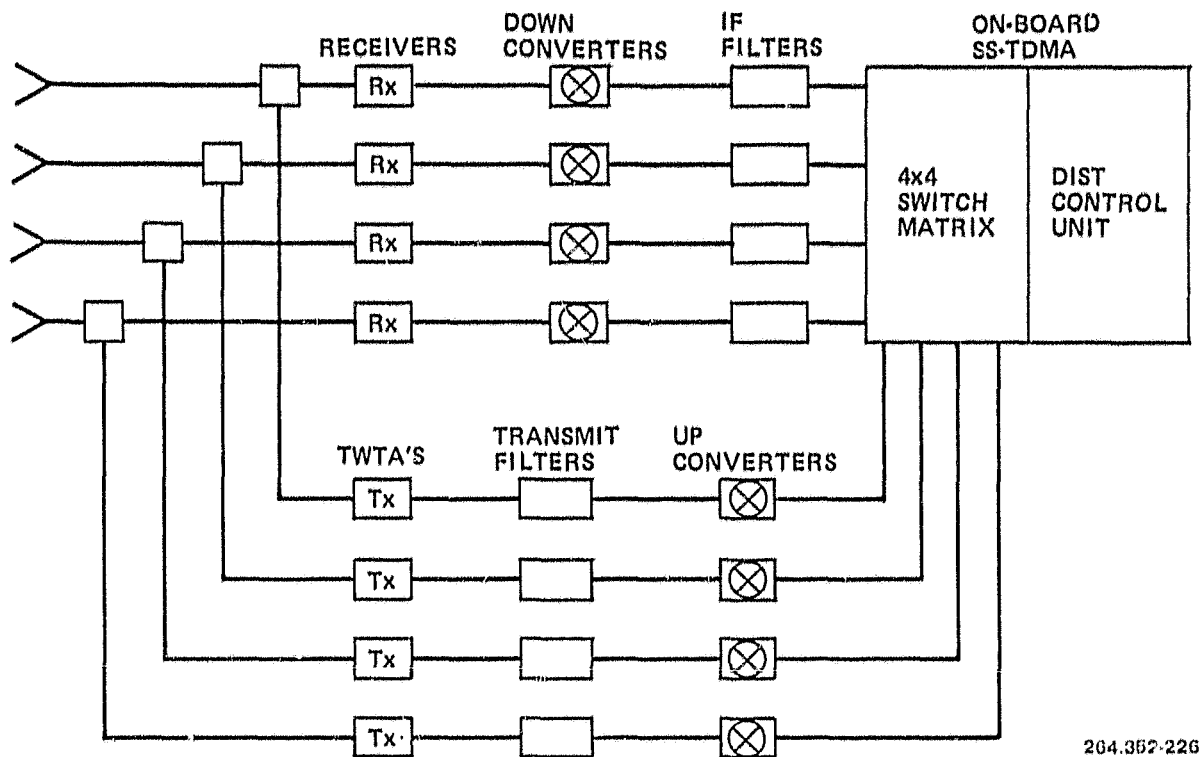


Figure 3-91. Single-Frequency, Multiple-Beam SS-TDMA Transponder

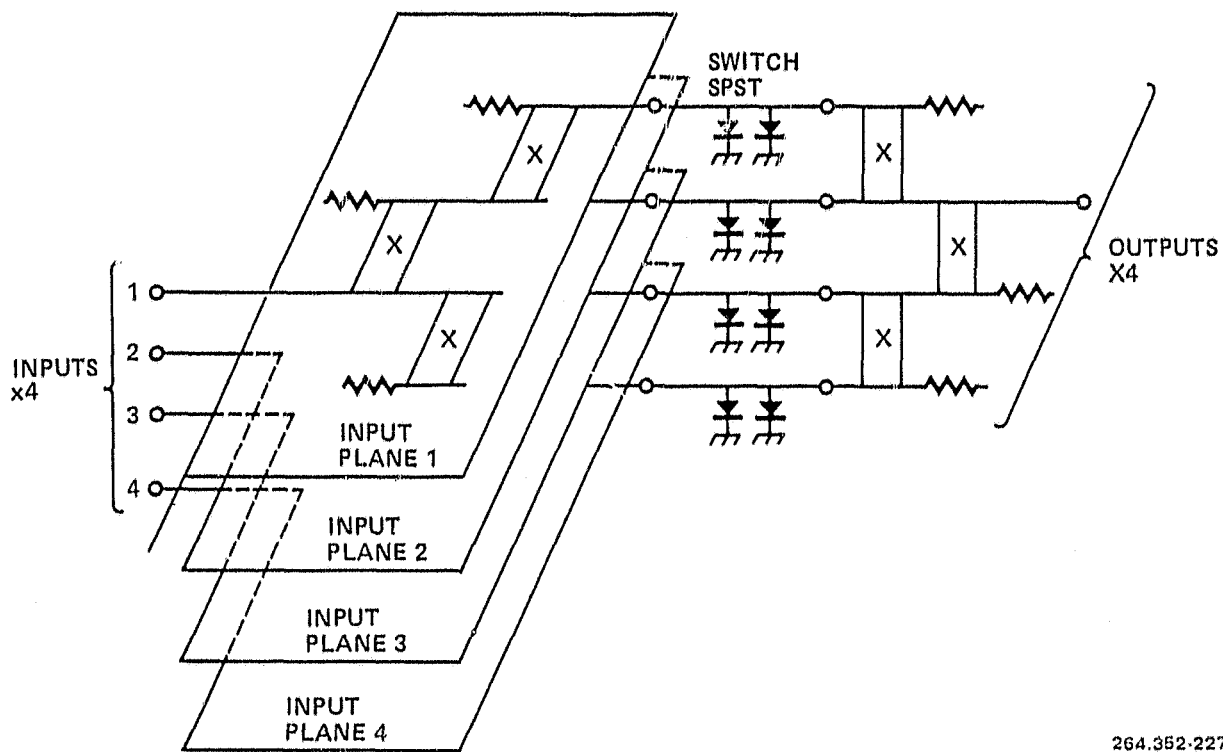
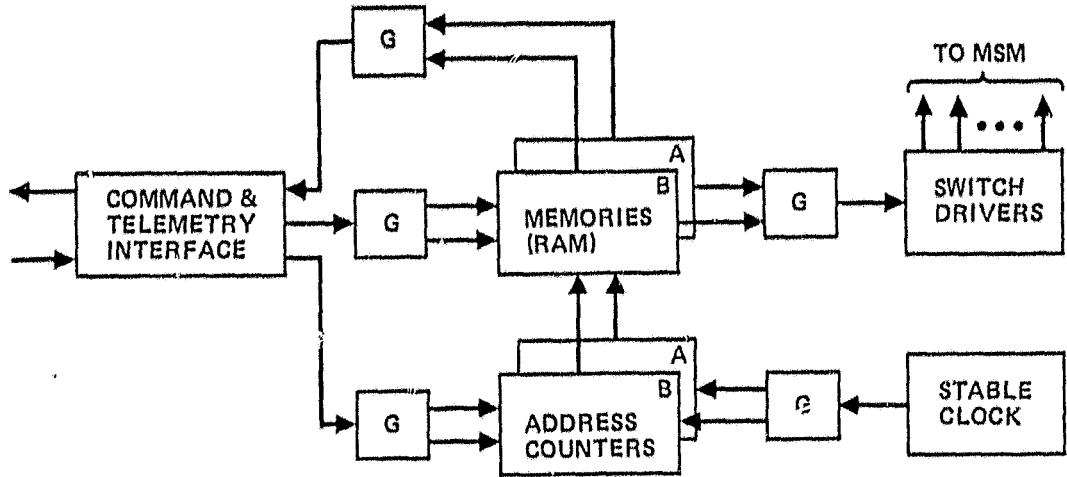


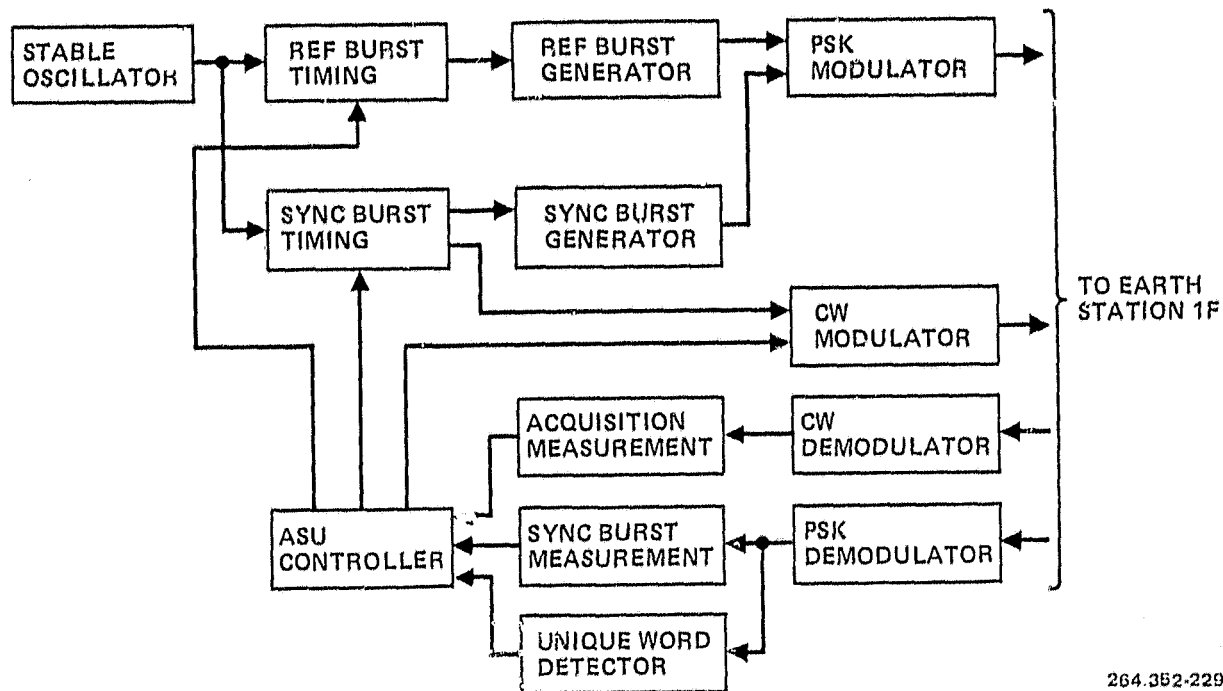
Figure 3-92. Schematic Diagram of the Simplified MSM



[G] = MEMORY SELECT GATE

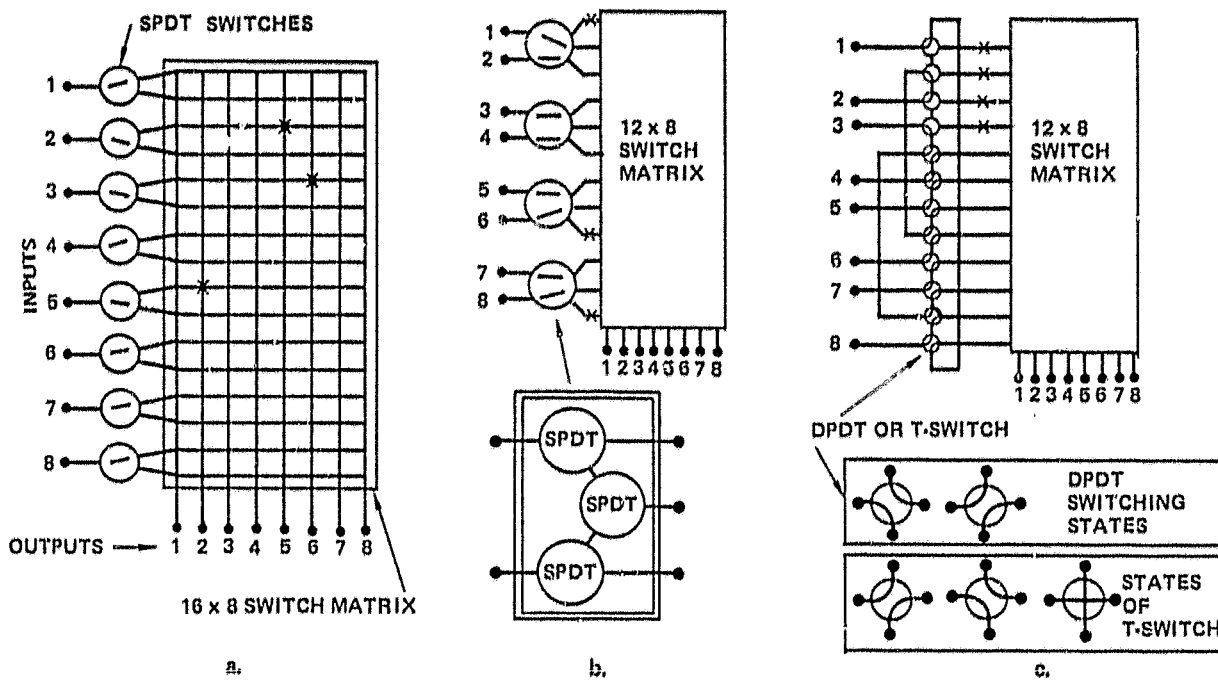
264.352-228

Figure 3-93. Simplified Block Diagram of the DCU

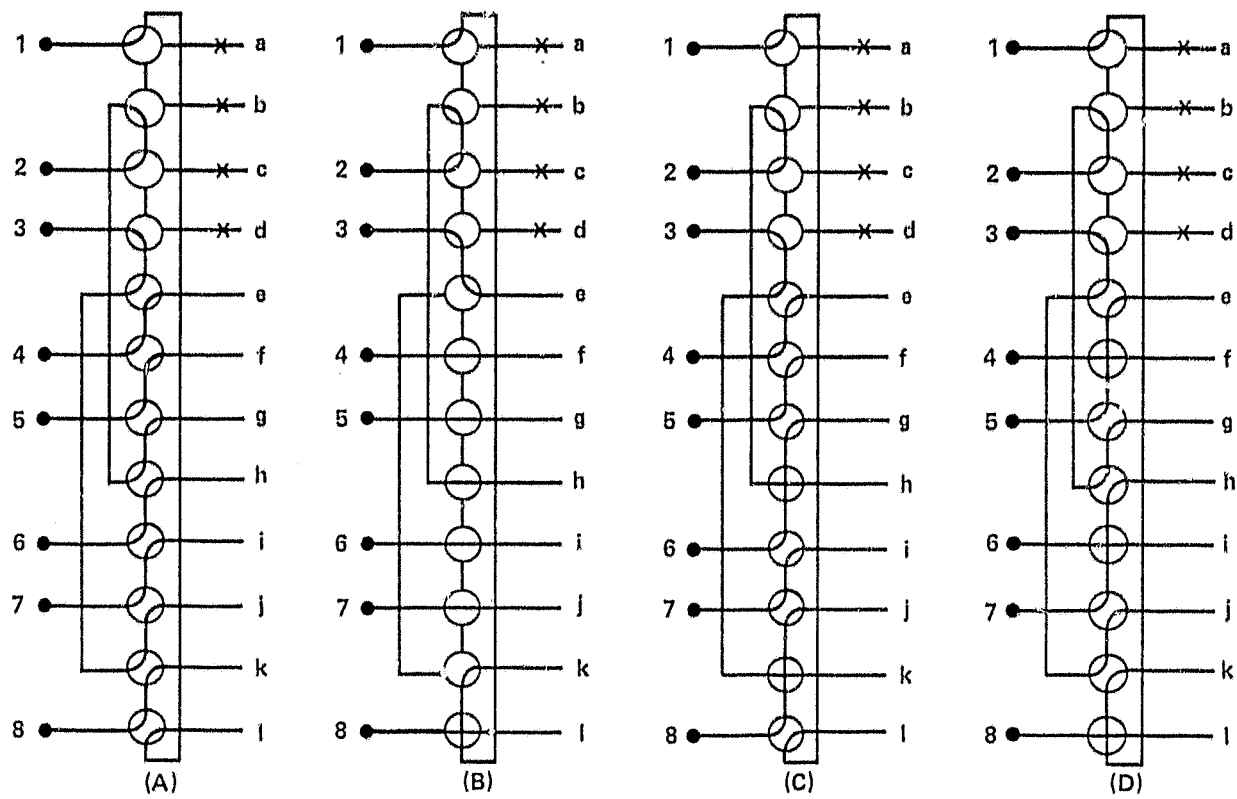


264.352-229

Figure 3-94. ASU Block Diagram



CONFIGURATIONS OF REDUNDANT 8 x 8 SWITCH MATRICES USING LATCHING-TYPE ELECTROMECHANICAL REDUNDANCY SWITCHES



264.352-230

Figure 3-95. Representative Worst Case, Four Consecutive Failures of a Redundant 8 by 8 Switch Matrix Using Only T-Switches

Table 3-62. Typical MSM Specifications

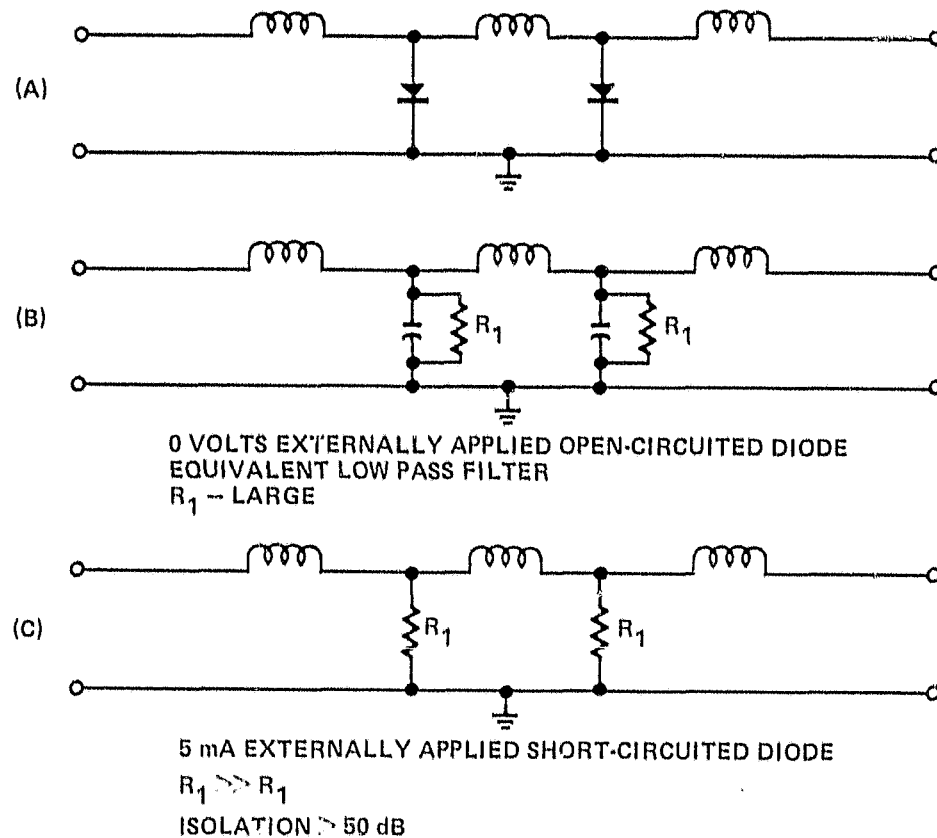
Matrix Type	N by N
Switch Type	SPST - Bias On
Switch Element	PIN Diode
Switched Signals	
Input	±15 dBm
Output	-10 dBm
Insertion Loss	<30 dB
Path-to-Path Variation	<1 dB
Path Isolation	50 dB
Switching Time	<50 ns
Switch Bandwidth	>500 MHz
Size (e.g., 16 by 16)	10.5 cm by 12.1 cm by 12.1 cm
Weight (e.g., 16 by 16)	2.3 kg
Prime Power (e.g., 16 by 16)	8.5W

Baseband switch matrices, an alternative approach, offer the best interface with on-board regeneration schemes. The advantage to SS-TDMA applications is the ability to implement:

- a. Call routing.
- b. Packet switching.
- c. On-board traffic storage for small data users.

The use of linear analog switches enables one to have unrestricted data transfer and incorporate microprocessing. Implementation using MOSFET technology is shown in Figure 3-98. Optical switching is also an attractive alternative offering large arrays for high capacity traffic, low power consumption, negligible EMI, and high isolation. Implementation of such a system is shown in Figure 3-99.

**3.4.4 ON-BOARD REGENERATION.** Various studies by COMSAT and Intelsat have been made and several engineering models have been fabricated in the 6/4 GHz and 14/12 GHz bands. On-board regeneration (OBR) has the advantage of separating uplink and downlink impairments and is easily integrated with baseband switching and processing techniques. On the other hand, it requires traffic standardization, uplink power control, and greater on-board circuit complexity and reliability.



264.362-231

Figure 3-96. PIN Diode Switch

A typical OBR transponder is shown in Figure 3-100.

One configuration explored has been DQPSK on the uplink and CQPSK on the downlink, as shown in Figure 3-101. While the use of DQPSK is not optimum from the viewpoint of theoretical communications [e.g., for bit error rate =  $10^{-4}$ ,  $E_b/N_0 = 8.4$  dB (11.4 if uncorrected) for CQPSK and 13.7 dB for DQPSK], it allows simplified circuitry since carrier recovery is achieved with a one-bit delay of the incoming signal.

One of the major drawbacks of the DQPSK regenerator is the stringent temperature stability requirements on the delay line used for detection. Recent work with barium tetratitanate substrates is encouraging but much more work is necessary. An approach for achieving temperature stability is shown in Figure 3-102.

A CQPSK-CQPSK transponder design is shown in Figure 3-103.

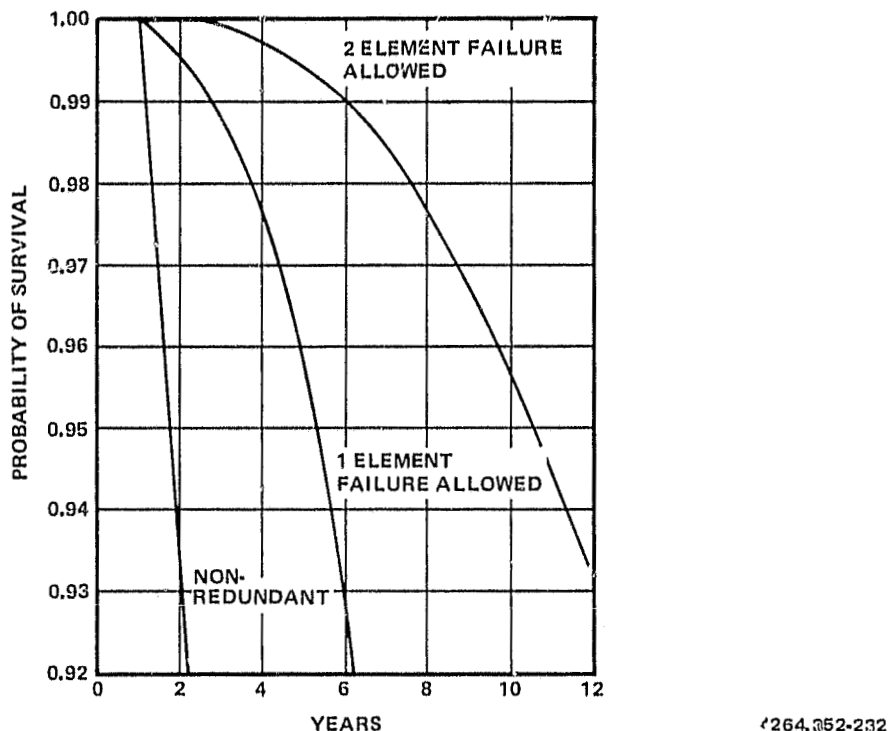


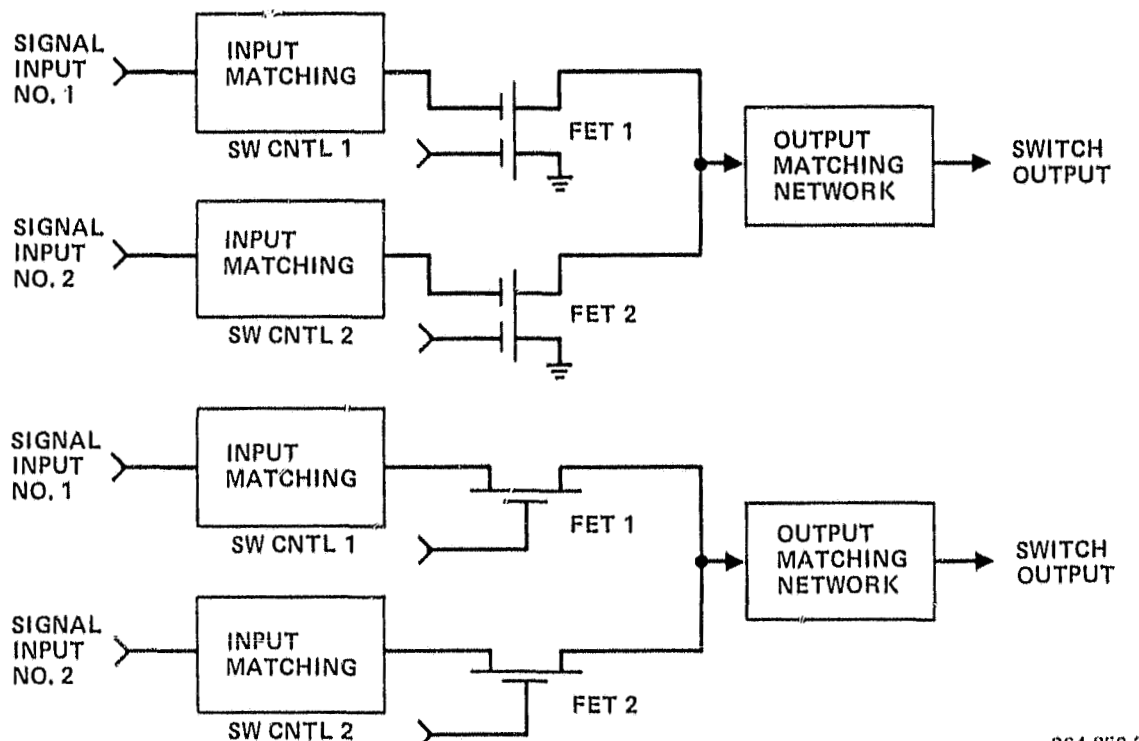
Figure 3-97. Computed Probability of Survival 8 by 8 Crossbar Switch

A comparison of required C/N ratios for a conventional transponder versus either a DQPSK-CQPSK or CQPSK-CQPSK scheme is shown in Figure 3-104. The best performance is CQPSK-CQPSK. However, this requires the greatest on-board complexity.

To meet the requirements of multiple transponders, efforts must be made to develop highly reliable demodulators with lightweight and low-power circuitry.

Finally, if one uses on-board regeneration, uplink fades require uplink power control. The size of the earth terminal transmitter must be such that fades consistent with service grade can be met at the saturation power of the earth terminal HPA.

**3.4.5 INTERPLATFORM LINKS.** The task on IPL is actually a two-part problem. If one assumes that the platform is a single rigid structure, all frequency diversity interconnections can be effectively hard wired into place and one merely need concern himself with 32/25 GHz link between platforms in different orbital positions.



264.362-233

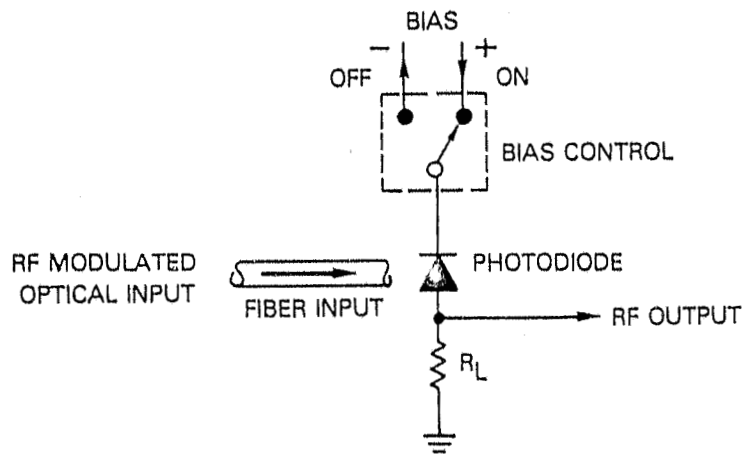
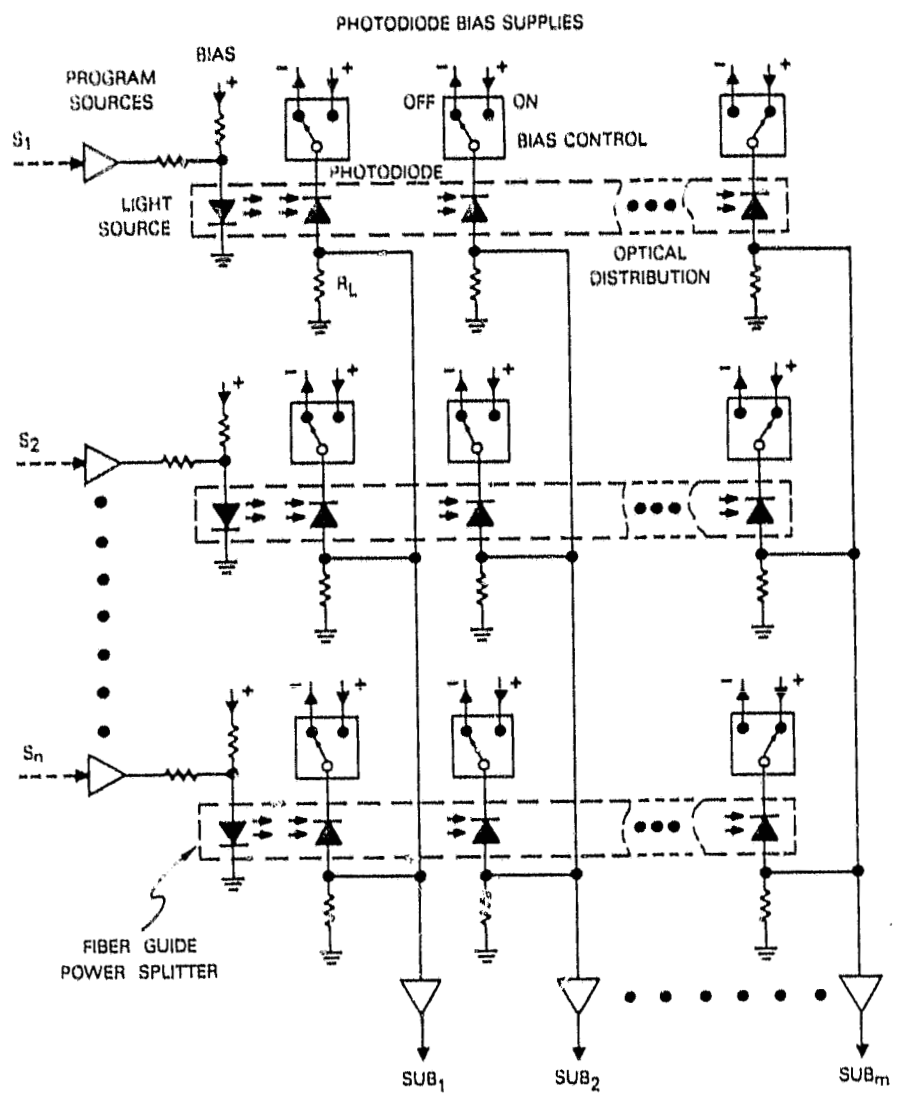
Figure 3-98. MOSFET Switch Implementation

Alternatively, if the platform is a series of modules flying in some formation as to represent a constellation to the earth terminals, then one is faced with a dual problem. One must use an ICL (platform to platform within a constellation) to interconnect the different missions and/or frequency diversity approaches and also an interplatform link between constellation. This approach is used for Alternative #1 and has all of the problems of the rigid platform, vis-a-vis interplatform communications, compounded by the intraconstellation links, which are highly dependent upon the flight formation employed.

The areas requiring development/investigation are as follows:

- Interplatform/intraconstellation relative stationkeeping and the ability to track/point the antennas.
- What missions will require interconnections?
- What/how many frequencies should be assigned to the intraconstellation link? One solution may be the use of a central module as a main switching point for all intermodule switching and stationkeeping.

The answers to items a, b, c will determine the shape of the IPL/ICL system and geometry.



264.352-234

Figure 3-99. Optical Switching Implementation

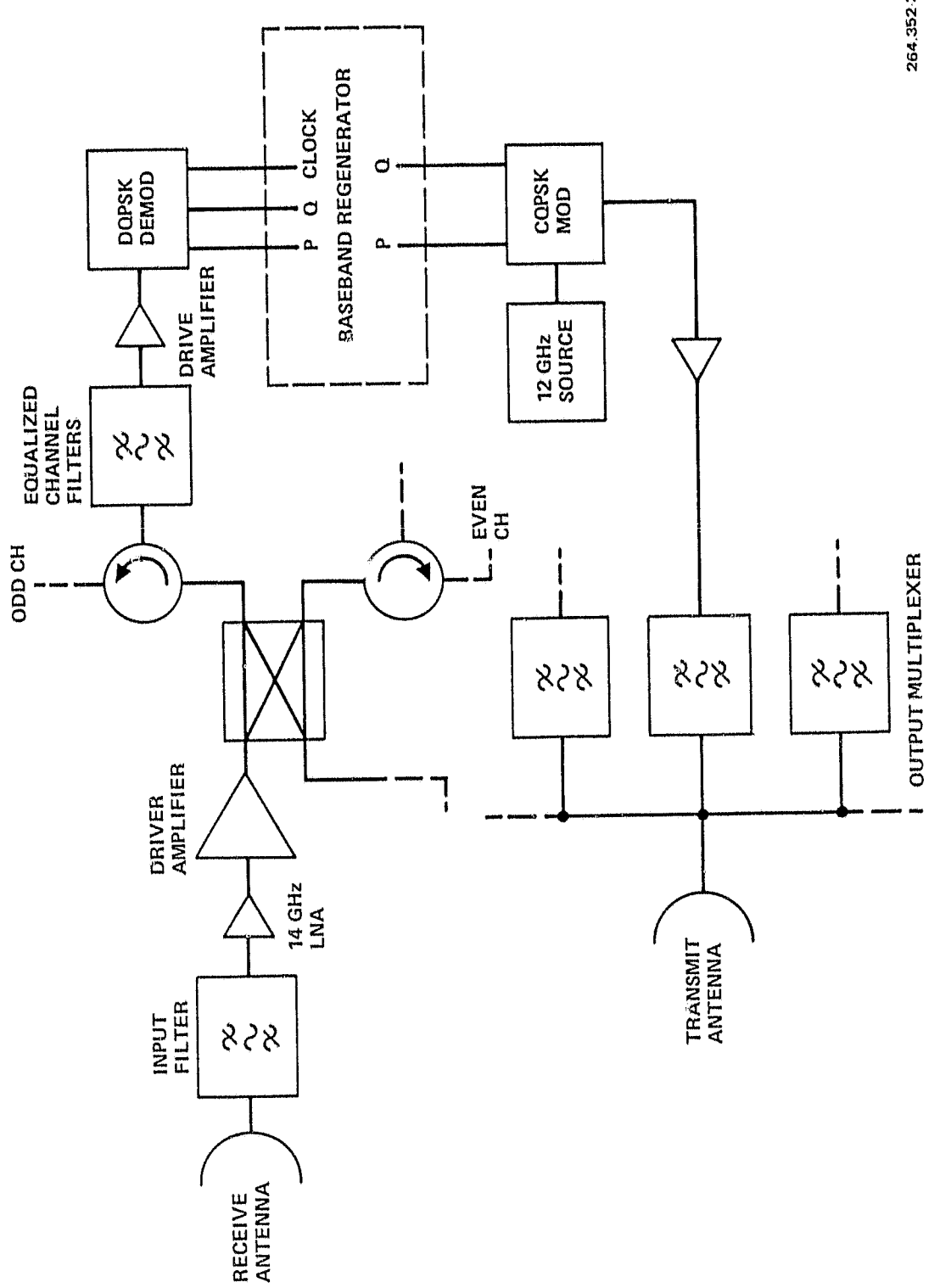
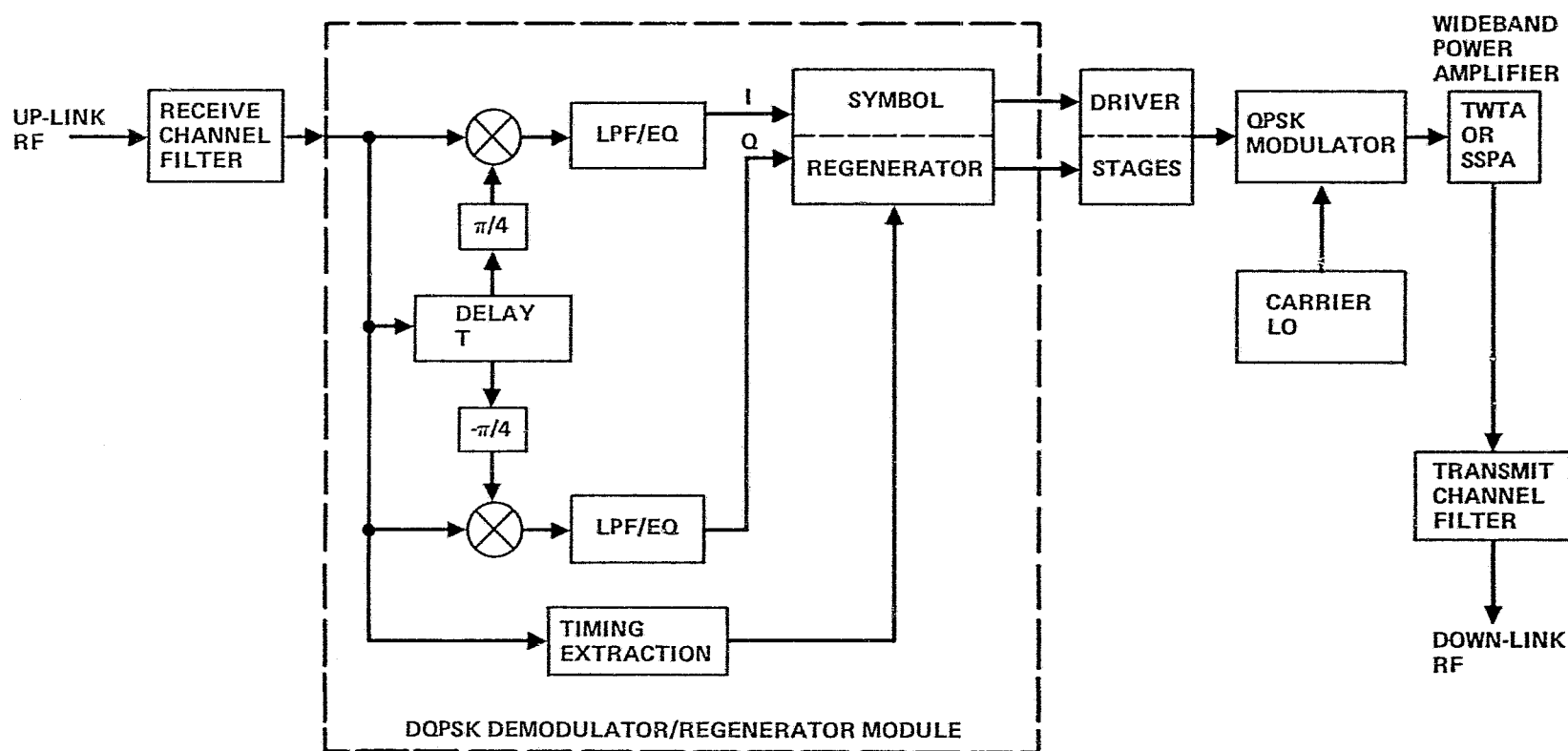


Figure 3-100. On-Board Regenerative Transponder



264.352.236

Figure 3-101. DQPSK-CQPSK Block Diagram

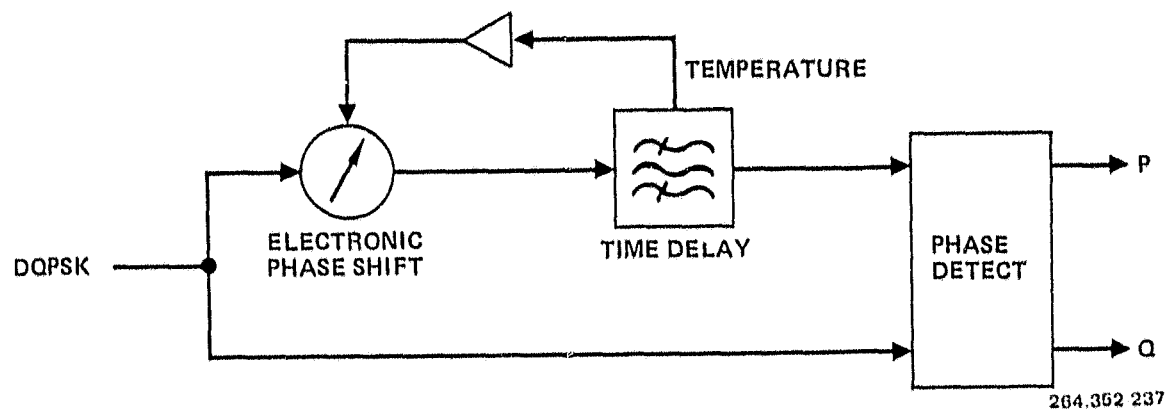


Figure 3-102. Block Diagram of a Temperature Compensated DQPSK Demodulator

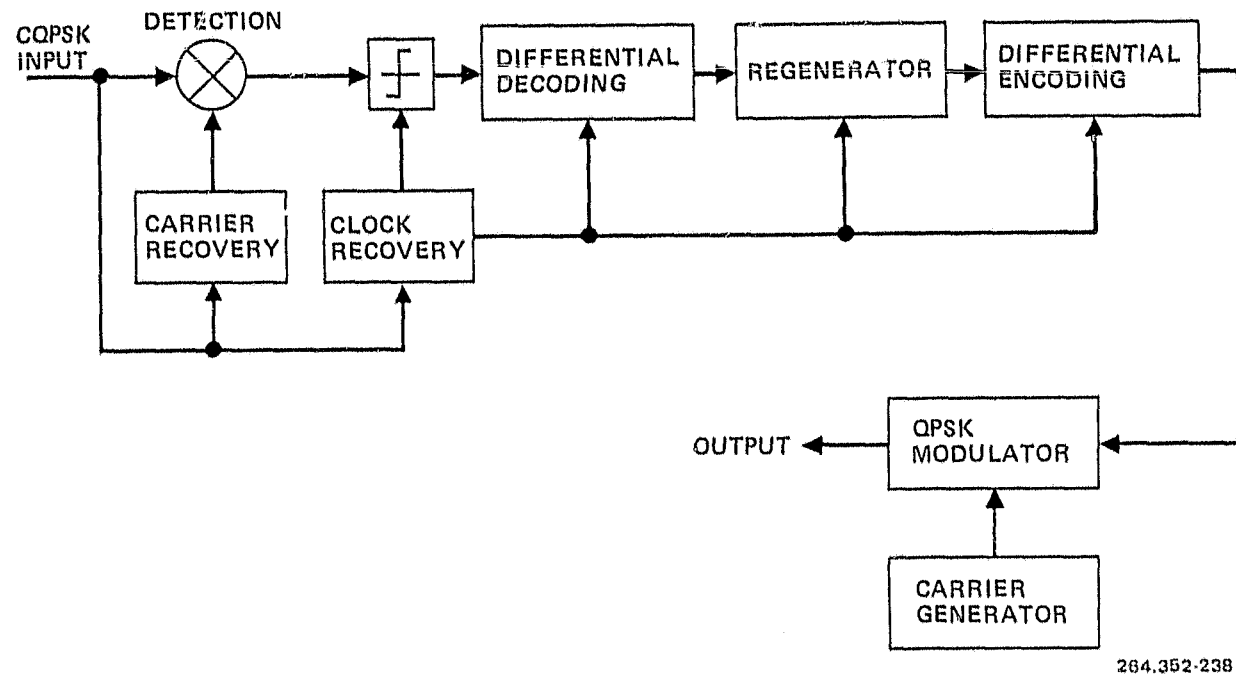


Figure 3-103. CQPSK OBR Block Diagram

Once the system geometry is established, the effect on the traffic handled must be considered. J. H. Deal (Reference 68) indicated that SS-TDMA operation, for example, faces the following impairments:

- Translation oscillator frequency stability in both platforms.
- Doppler frequency offset due to relative satellite/platform motion.

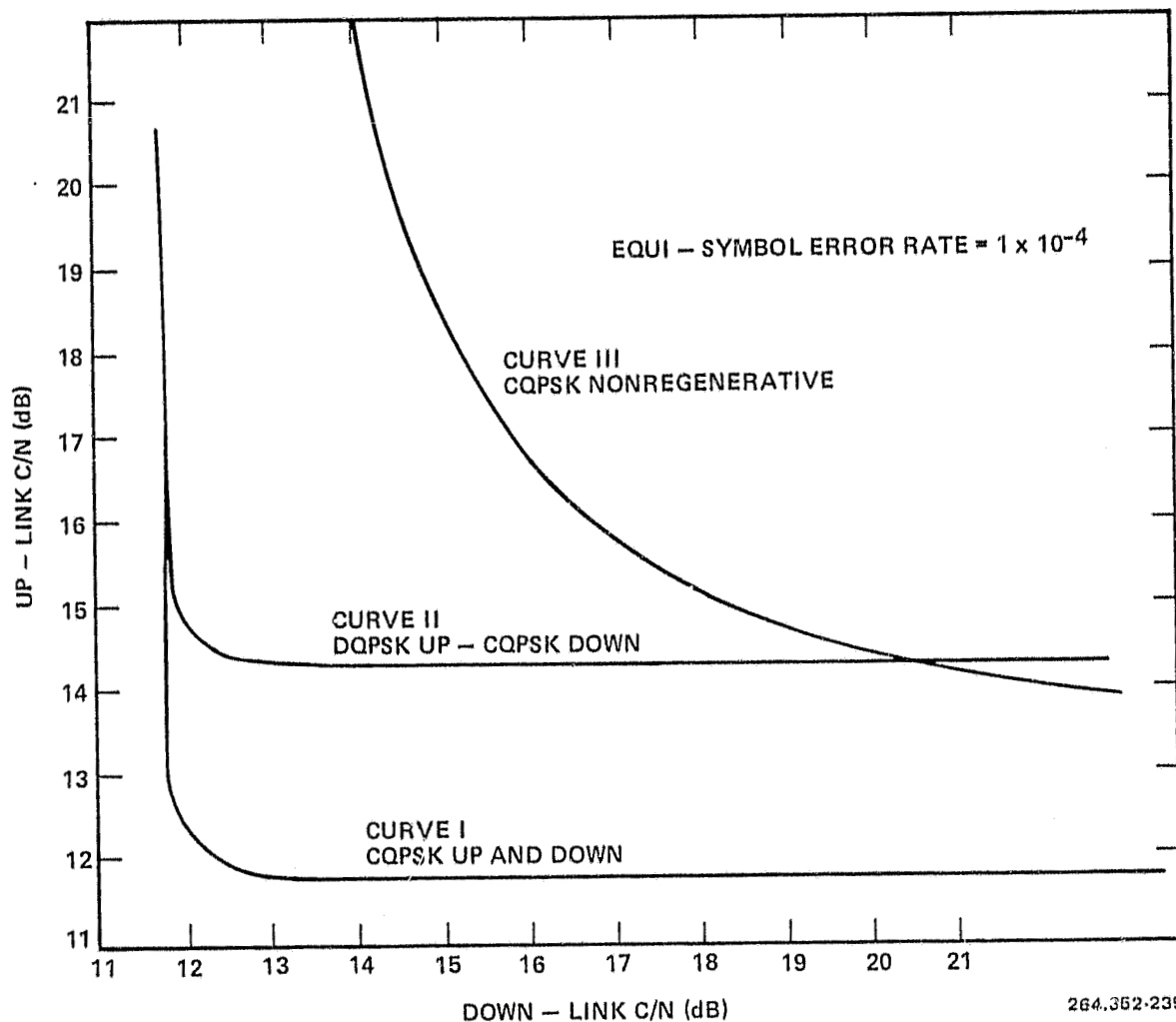
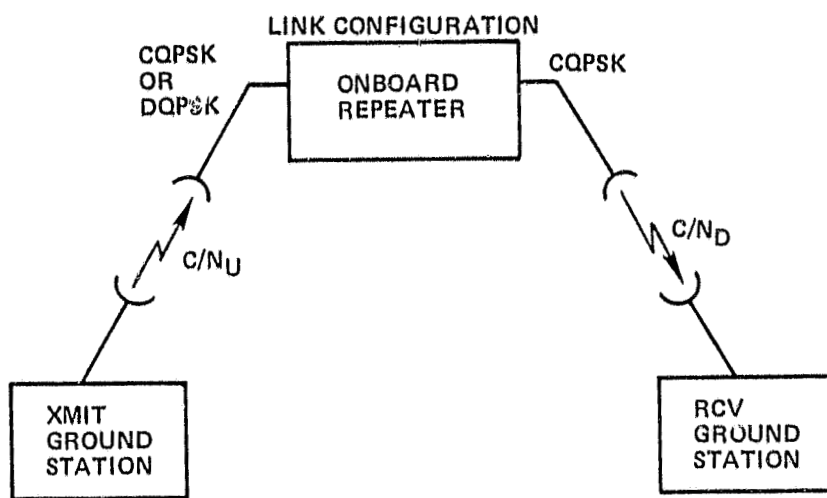


Figure 3-104. Equi-symbol Error Rate Curve for Regenerative Repeaters and a Conventional Transponder

- c. Clock timing instabilities.
- d. TDMA frame and burst synchronization.

Deal concludes that the above problems can be overcome with a slaved network approach, which requires a special reference station and satellite equipment for control of the slaved SS-TDMA switch timing (see Figure 3-105). Similarly, FDM/FM has its related problems as do all other forms of data/analog transmission, all of which require further investigation.

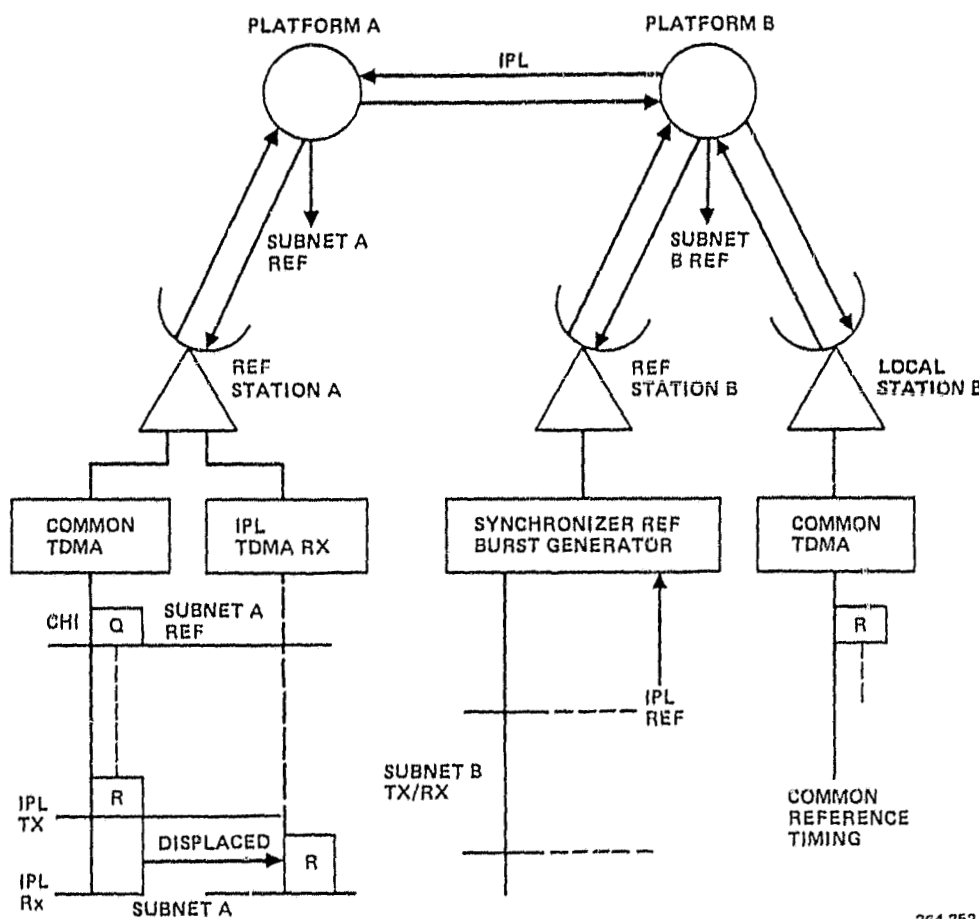


Figure 3-105. SS-TDMA Slaved Subnet Work For an Interplatform Link

**3.4.5.1 IPL-RF Links.** This section applies to both IPLs and ICLs. The choice of frequencies, geometry, and traffic to be switched or interconnected will ultimately determine the shape of the interplatform link. COMSAT Labs (Reference 69) has done considerable work in the area of intersatellite links, which are equally applicable for the interplatform links. Though the approach deals primarily with a 6/4 GHz earth-satellite link, it can be modified to 14/12 GHz and, with certain restraints, to a 30/20 GHz link.

Figures 3-106 shows a general overall link for either FDMA, TDMA, or TV traffic. Figure 3-107 shows a typical platform communication function and Figure 3-108 shows a typical communications platform schematic. The top half of Figure 3-108 shows a modulator/transmitter chain with the signal flow from left to right and from uplink to IPL. The bottom half shows the IPL receiver/demodulator chain from right to left and IPL to downlink.

Two versions of the IPL circuit using FM remodulation and heterodyne repeaters are shown in Figures 3-109 and 3-110, respectively. In both versions, the IPL is essentially transparent. The FM version expands the bandwidth and uses saturated transmitters. The heterodyne repeater operates in a 120-MHz bandwidth with backed-off transmitters.

Figure 3-111 compares (without multicarrier backoff consideration) the power/bandwidth contour for FM with the corresponding point for heterodyne transmission. Heterodyne transmission is assumed to occupy 120 MHz and to require 8 dB output backoff. The EIRP saving can be converted to a range extension for a fixed EIRP; thus, for an RF bandwidth of 820 MHz, a power saving of 9.5 dB (or a range extension by a factor of three) can be realized through FM remodulation.

Crosslink budgets for both approaches, given 15 in. spacing, are shown in Tables 3-63 and 3-64. Two different receive-system noise temperatures and backgrounds are considered.

Tables 3-63 and 3-64 indicate that for a black-sky condition, the low-noise receivers improve the FM remodulation approach more than the heterodyne crosslink. At solar conjunction, the benefit is less, except that the low-noise receiver in the FM system prevents the demodulator from going below threshold, thus giving a benefit of over 3 dB.

The effect on a TDMA link of an IPL is more pronounced and involves changes to the earth terminal and to the platform transponder.

In a normal TDMA network operation, all carriers undergo the same translation. Platform frequency translation errors are compensated in the TDMA terminal by automatic frequency control (AFC) in each receiver using a stable reference pilot frequency transmitted from the ground.

When using an interplatform link, the IPL TDMA carriers experience a separate frequency translation not affecting the local carriers, whose transmission path includes only the local platform. This additional translation requires the use of a separate IPL pilot.

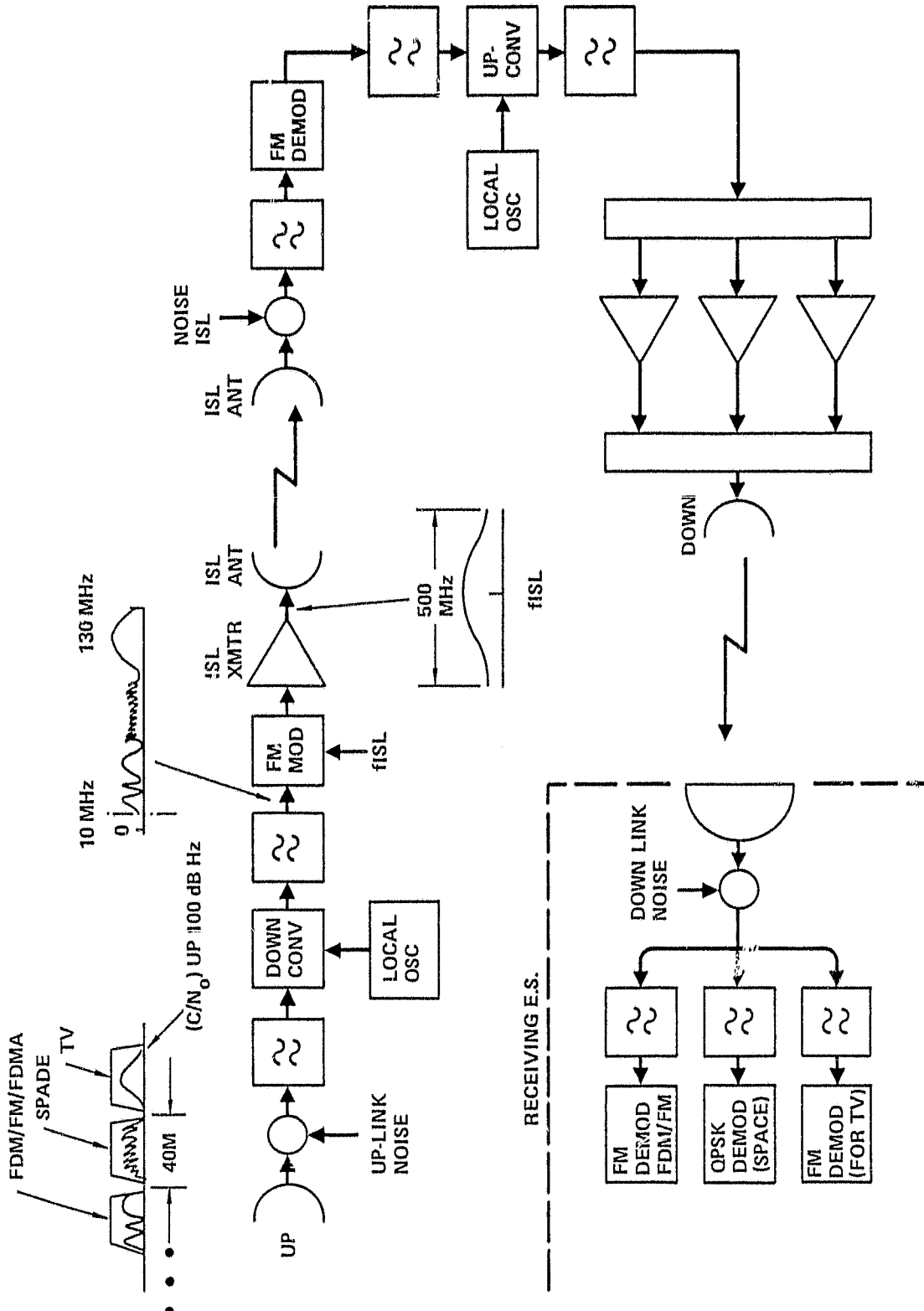


Figure 3-106. General and Overall Link - Ground to IPL to Ground

264.352.241

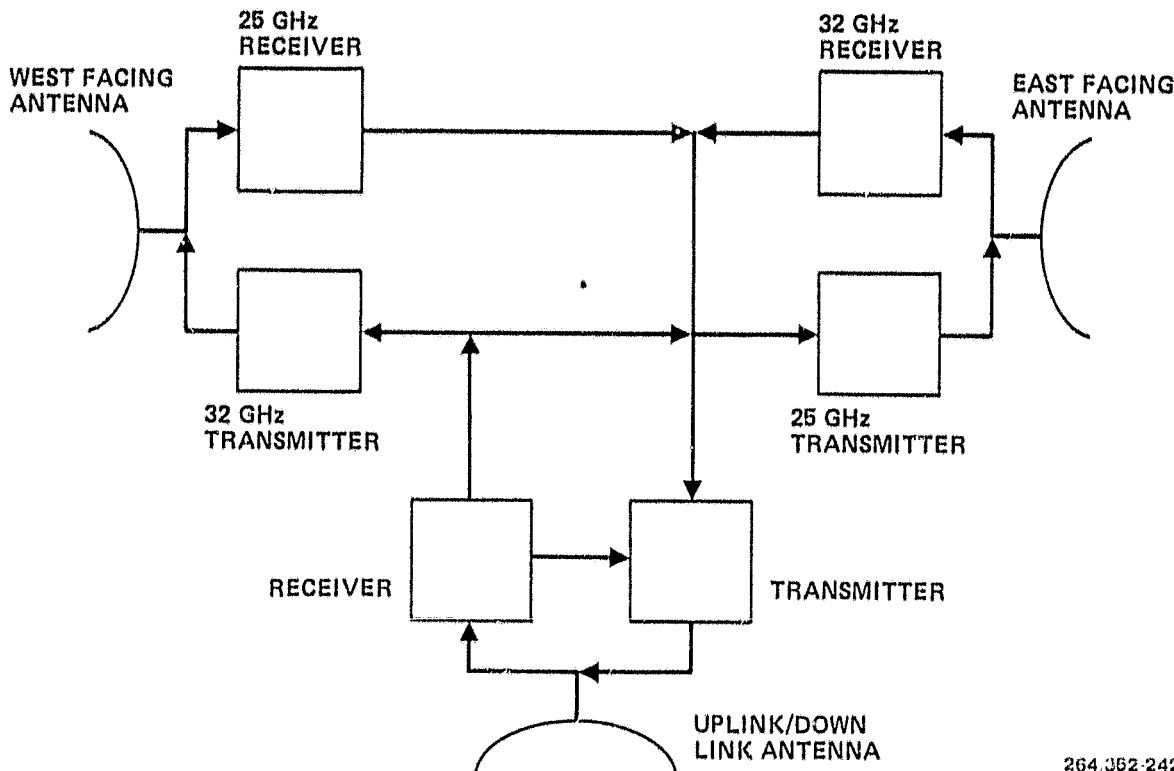


Figure 3-107. Typical Platform - IPL Communications Function

Figure 3-112 is a block diagram of a TDMA terminal IF subsystem with the separate IPL spectrum-centering hardware. The functions of the IF subsystem are as follows:

- The transmitter section accepts carriers from the individual channel units, IPL and local CSC modems, and pilot (for reference mode operations); combines these carriers into a single spectrum; and heterodynes this composite spectrum to the IF.
- The receive section accepts the received spectrum from the earth station IF, heterodynes the spectrum to the TDMA terminal IF, and supplies this spectrum to the channel units and to the IPL and local CSC modems.
- The receive section performs two independent AFC functions to center each half of the received spectrum precisely in the TDMA terminal IF (locked to the terminal pilots). The IPL and local spectra are centered using separate pilots and frequency-centering hardware.

Thus, the receive section performs the inverse function of the transmit section. In addition, downlink Doppler shift and translation frequency offsets are removed by the voltage-controlled local oscillators. The AFC functions are locked to the pilot frequencies received at the edge of each allocated band. This operation ensures that all channel carriers are within specific ranges of the assigned frequency. The desired spectrum is selected and unwanted

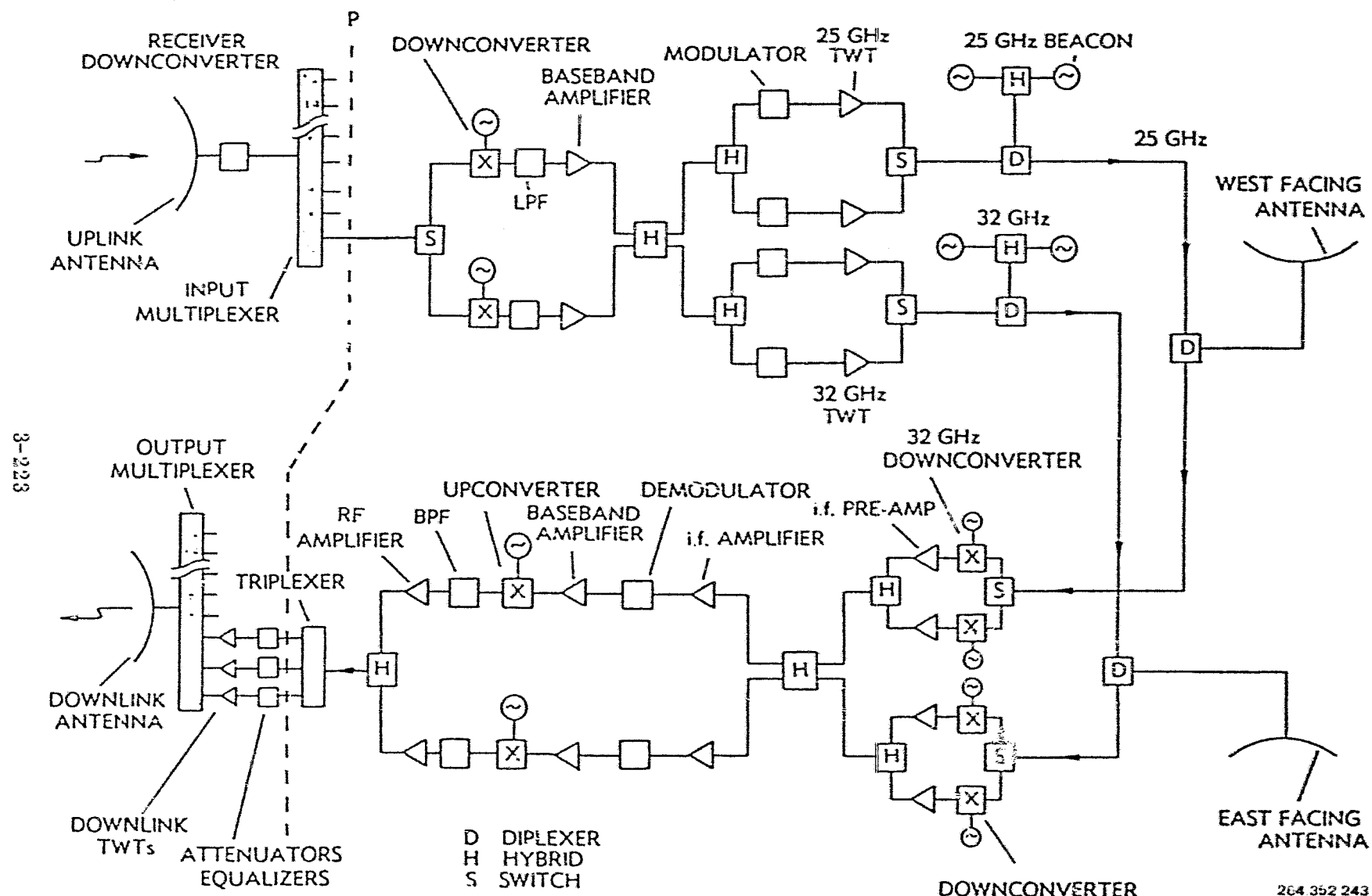


Figure 3-108. Typical Platform Communications Schematic

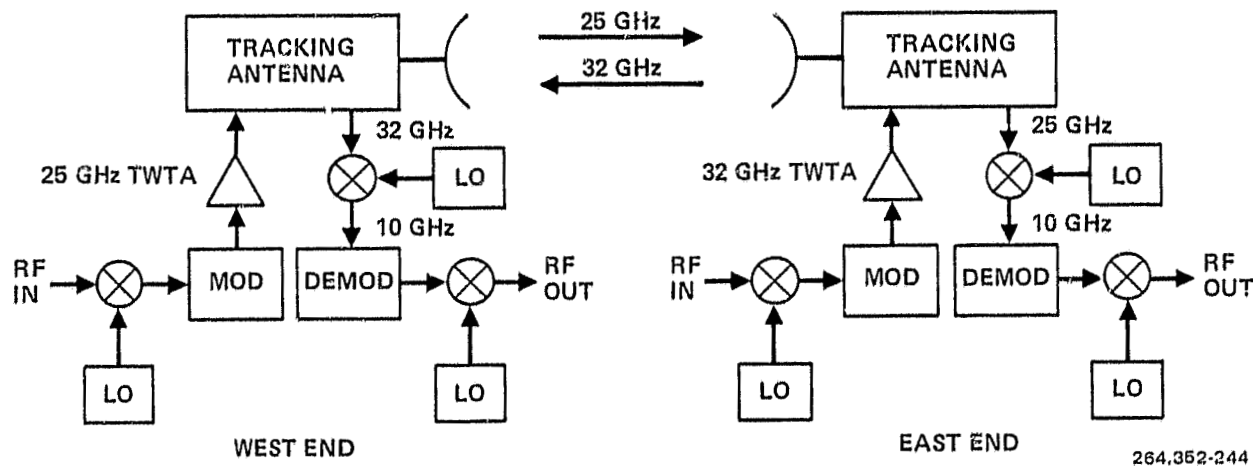


Figure 3-109. IPL Circuit Using FM Remodulation

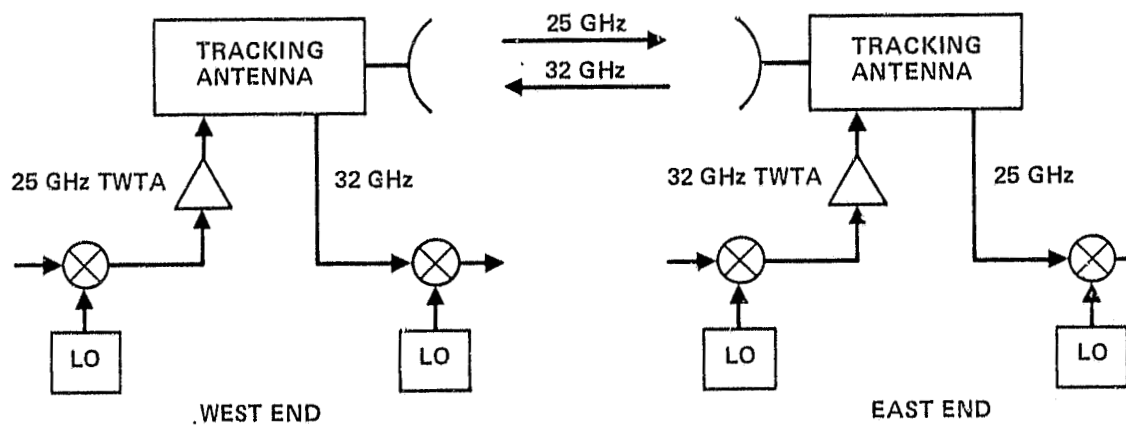


Figure 3-110. IPL Circuit Using Heterodyne Repeater

signals filtered out by the bandpass filter at the IF divider input. The divider serves as a distribution amplifier supplying all channel units and both CSC units with replicas of the received spectrum.

The impact of the TDMA on the IPL transponder configuration is shown in Figures 3-113 and 3-114 for two alternate design, respectively. It is evident from these two schematics that the filtering requirements at the baseband and microwave frequencies are the same; i.e., the filter bandwidths, the frequency selectivities, and the required isolations are identical. Since the only difference is a translation of center frequency from RF to baseband, the lossless filter characteristics are obviously the same. Further, since the product of the filter Q at RF and the percentage bandwidth is approximately equal to the product of filter Q at baseband and the percentage bandwidth, the lossy filter responses are also nearly identical.

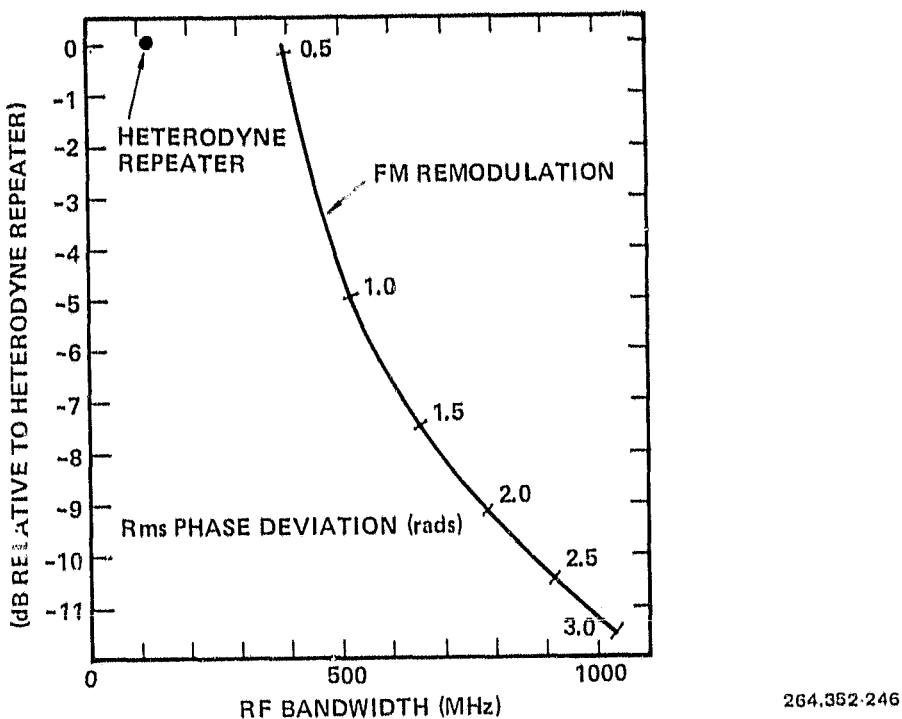


Figure 3-111. Power Versus Bandwidth for FM and Heterodyne Repeaters

Therefore, the choice of the "best" configuration is not self-evident, but must depend on considerations such as power, weight, volume, and ease of manufacture.

A typical transponder layout is shown in Figure 3-115 and a rough weight and power summary is given in Table 3-65.

**3.4.5.2 IPL - Laser Links.** Optical IPL systems are an additional alternative to achieve high data rate links. Feasibility models with 1 gigabit/second data rates (References 70 and 71) are presently being tested and available optical component technology indicate that multigigabit rates are practical.

Among the available laser sources, Nd:YAG laser system has the following advantages:

- a. Inherent simplicity and efficiency of direct photodetection formats.
- b. Availability of wideband modulators and high-gain, low-noise detectors.
- c. GaAlAs laser diode-pumped, lightweight, potentially highly reliable solid-state laser source.

Table 3-63. FM Crosslink

		Receive System Temperature			
		1000 K		3000 K	
		Background	Background	Background	Background
		Black	Sun	Black	Sun
EIRP	dBW	60.0	60.0	60.0	60.0
1/L	dB	-201.4	201.4	-201.4	-201.4
G/T	dB/K	20.0	11.5	15.2	10.4
1/k	dBkHz/W	228.6	228.6	228.6	228.6
1/B (750 MHz)	dB/Hz	-88.9	-88.9	-88.9	-88.9
(C/N) <sub>RF</sub>	dB	18.3	9.8	14.5	8.7
(C/N) <sub>BB</sub> /(C/N) <sub>RF</sub>	dB	6.5	5.5	6.5	1.5
(C/N) <sub>BB</sub>	dB	24.8	15.3	21.0	10.2
C/IM	dB	35.0	35.0	35.0	35.0
C/(N + IM) <sub>IPL</sub>	dB	24.4	15.3	20.8	10.2

On the other hand, a CO<sub>2</sub> laser system requires heterodyne detection with cryogenically cooled optical detectors and optical frequency local oscillators. The CO<sub>2</sub> laser system is thus more complex than Nd:YAG laser system. The lifetime of a CO<sub>2</sub> laser also requires improvement (typically 5,000 hours).

The basic block diagram of a duplex YAG laser optical IPL transceiver is shown in Fig e 3-116.

Nd:YAG and Nd:YAG lasers are frequency-doubled and internally mode-locked in order to generate stable pulse-width of less than 300 p/s at the 1/e<sup>2</sup> intensity point. Furthermore, the internally frequency-doubled YAG laser pulse width is inversely proportional to pulse repetition rate, and shorter pulse width is possible. A GaAlAs laser diode pump is compact, efficient, and potentially more reliable requiring 40 watts prime power and weighing 10 pounds as compared with a K-Rb lamp needing 315 watts and weighing 81 pounds.

An optical receiver is shown in Figure 3-117 and a demultiplex scheme in Figure 3-118.

Table 3-64. Heterodyne Crosslink

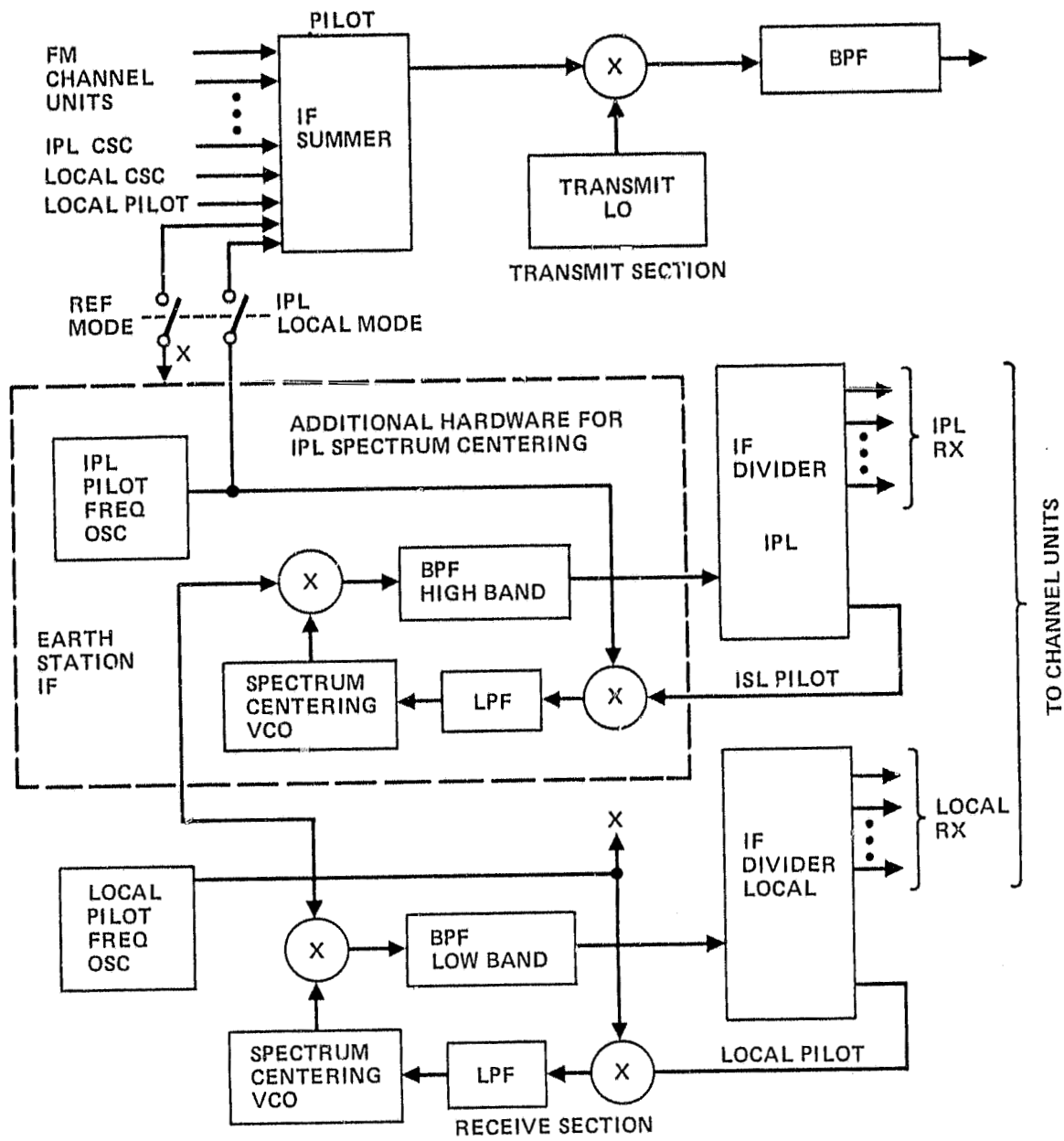
		Receive System Temperature			
		1000 K		3000 K	
		Background		Background	
		Black	Sun	Black	Sun
EIRP	dBW	60.0	60.0	60.0	60.0
1/L	dB	-201.4	-201.4	-201.4	-201.4
G/T	dB/K	20.0	11.5	15.2	10.4
1/K	dBkHz/W	228.6	228.6	228.6	228.6
1/B (120 MHz)	dB/Hz	-80.9	-80.9	-80.9	-80.9
(C/N) <sub>RF</sub> (Saturated)	dB	26.3	17.8	21.5	16.7
Output Backoff	dB	-6.3	-3.4	-4.7	-3.1
C/N	dB	20.0	14.4	16.8	13.6
C/IM	dB	26.1	17.3	19.9	16.7
C/(N + IM) <sub>IPL</sub>	dB	18.2	12.6	15.0	11.8

Maynard (Reference 70) reports that for a spacing of 13,500 km a 2 gigabit/sec link can operate with 6 dB margin. Tests on a 1 gigabit/sec system reportedly yielded an 11 dB link margin.

Data received to date is highly encouraging but further work is still needed.

**3.4.5.3 IPL Antenna Acquisition and Tracking.** For a secured application of the interplatform links, the IPL antennas must have two distinct capabilities:

- Acquisition. The capability to acquire the communications link before starting the IPL operation and the capability of reacquiring the operation after losing the link.
- Tracking. The capability to track the partner IPL antenna during the operation of the communication links.



264.362-247

Figure 3-112. TDMA Terminal IF Subsystem

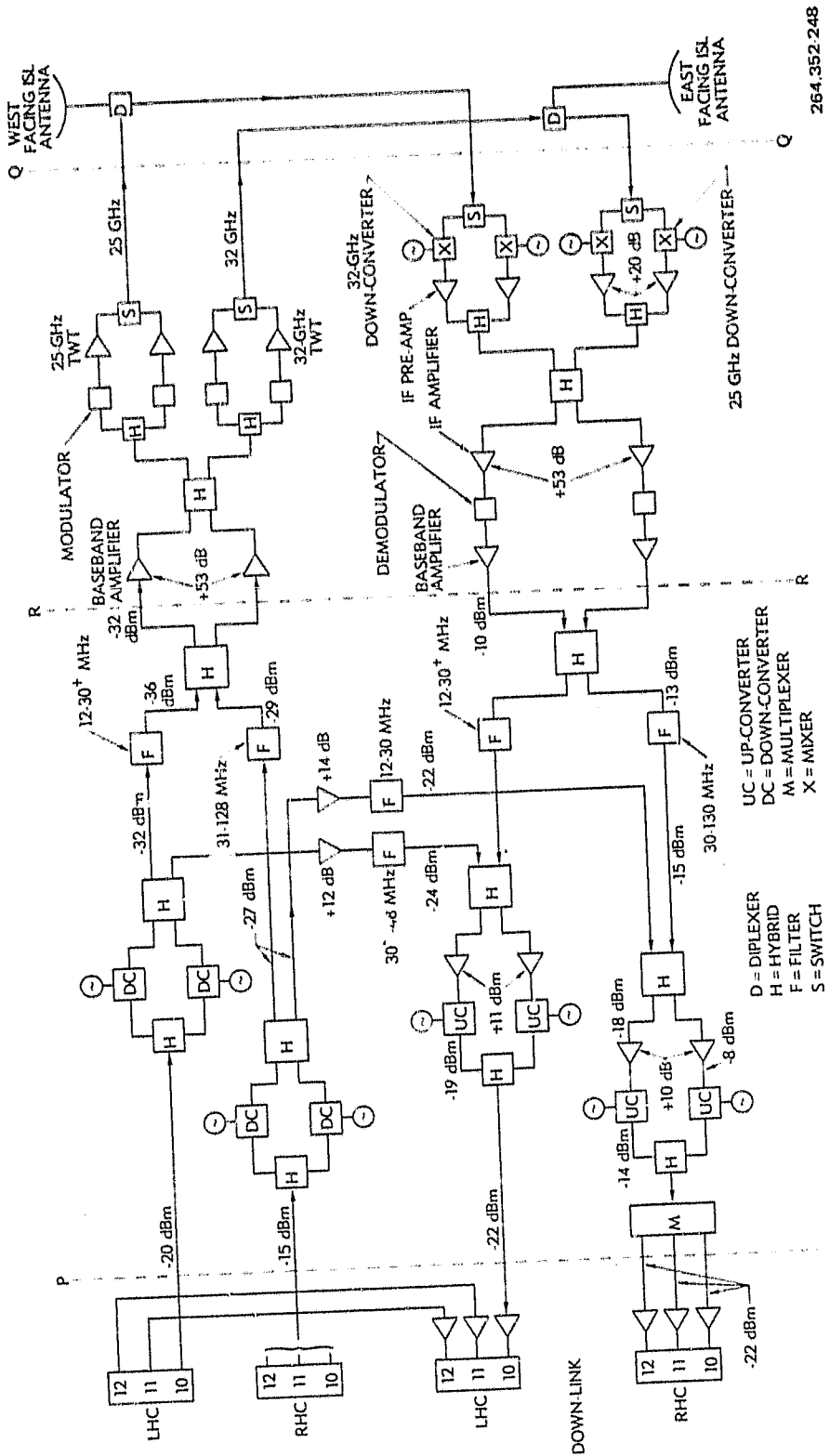


Figure 3-113. IPL Transponder Using Baseband Filters

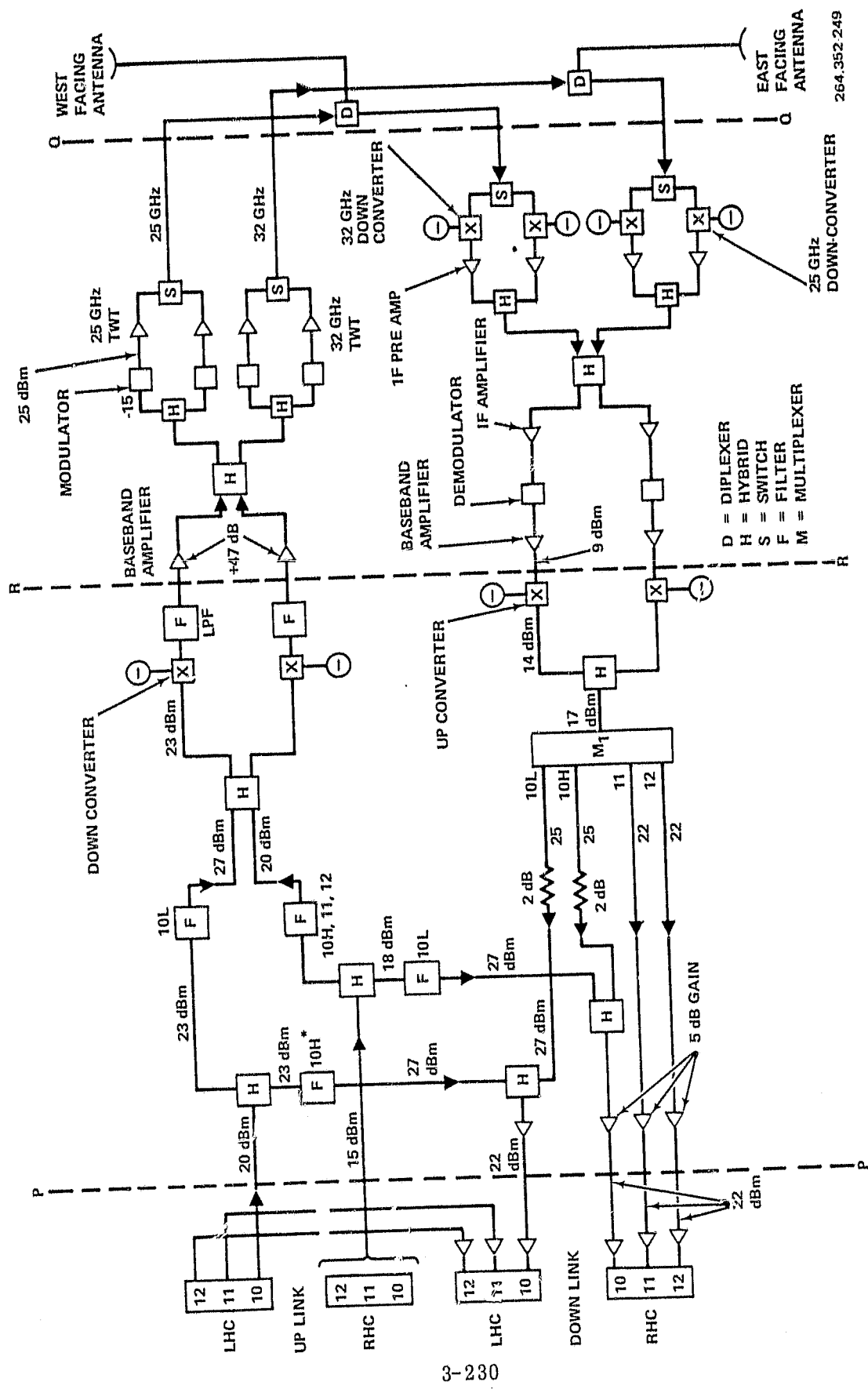


Figure 3-114. IPL Transponder Using Microwave Filters

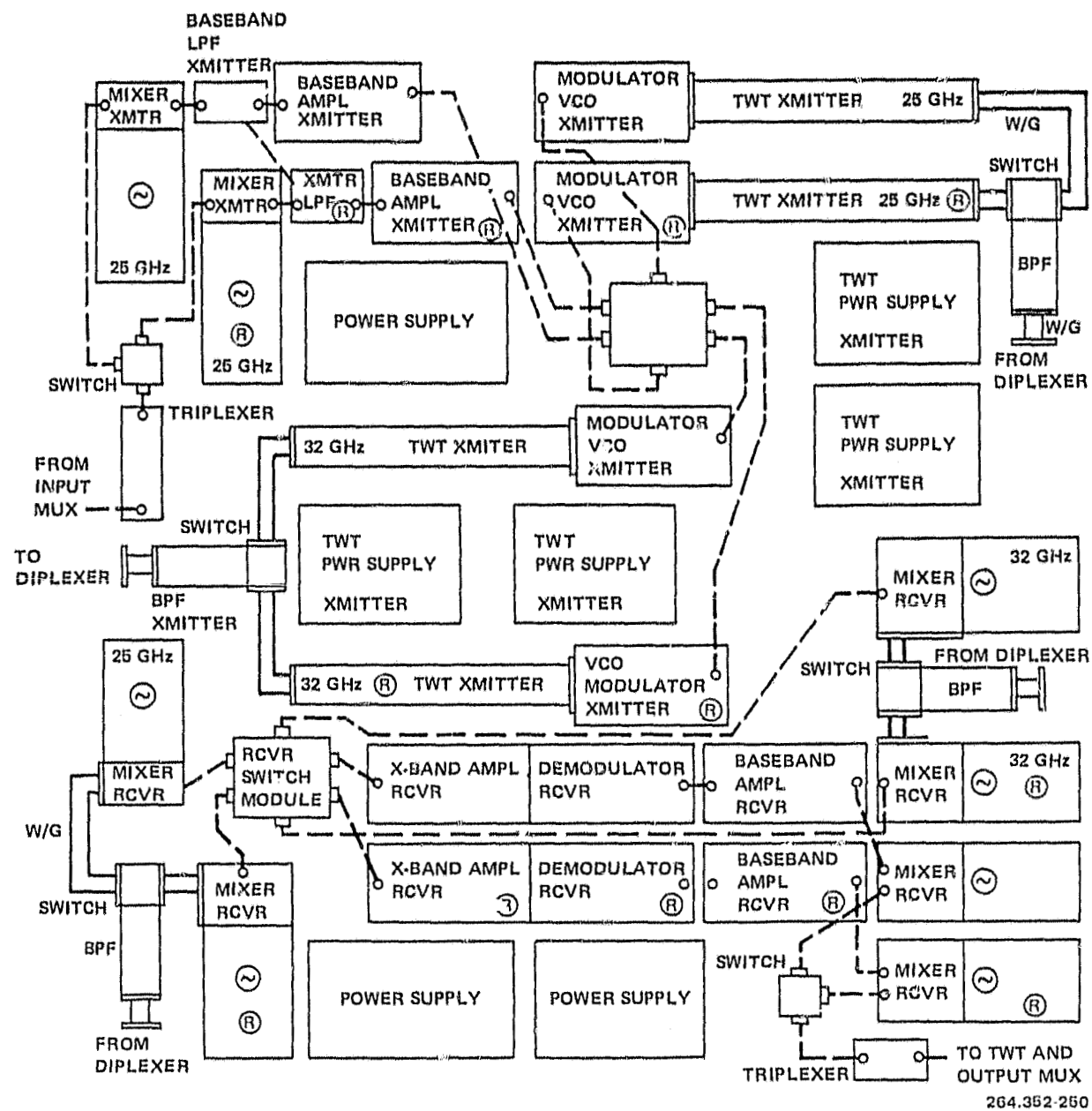


Figure 3-115. Typical Transponder Layout

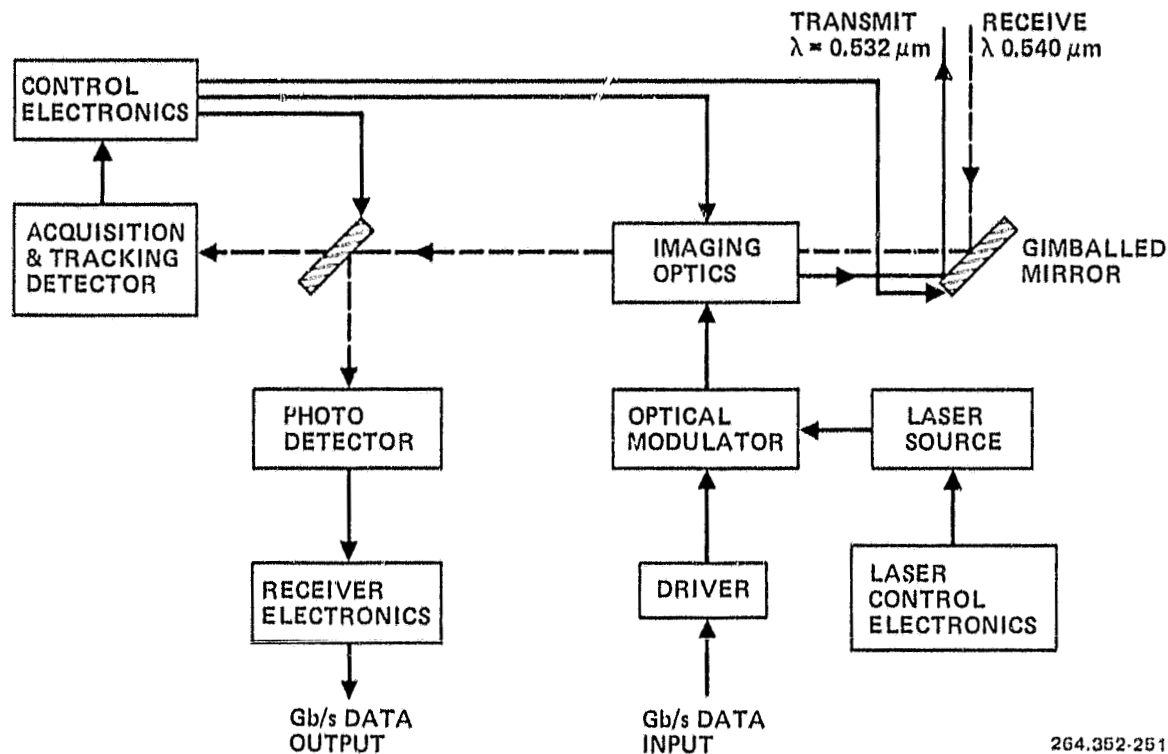
In the acquisition phase, the IPL antenna will be pointed by ground command to its partner antenna before initiation of the acquisition operations. This initial pointing error defines the angular acquisition window and its size is determined by how well the position and attitude errors of the geostationary platforms can be estimated. Acquisition can be carried out by coordinate scanning of the IPL antennas, and the acquisition time will depend on the antenna scanning rates, beamwidth, and size of the acquisition window.

Table 3-65. Weight/Power Summary

Item	Quantity Required	Weight (kg)		Power <sup>a</sup> (W)	
		Each	Total	Each	Combined
<b>Transmitter</b>					
25 GHz	2	3.1	6.2	56	56
32 GHz	2	3.1	6.2	56	
<b>Receiver</b>					
25 GHz	2	2.6	5.2	8	8
32 GHz	2	2.6	5.2	8	
Interconnections, Switches, Filters, and Miscellaneous	—	—	5.5	—	—
<b>Power Supplies</b>					
TWT	4	1.8	7.2	12	12
	2	1.8	<u>3.6</u>	3	<u>3</u>
			39.1		79

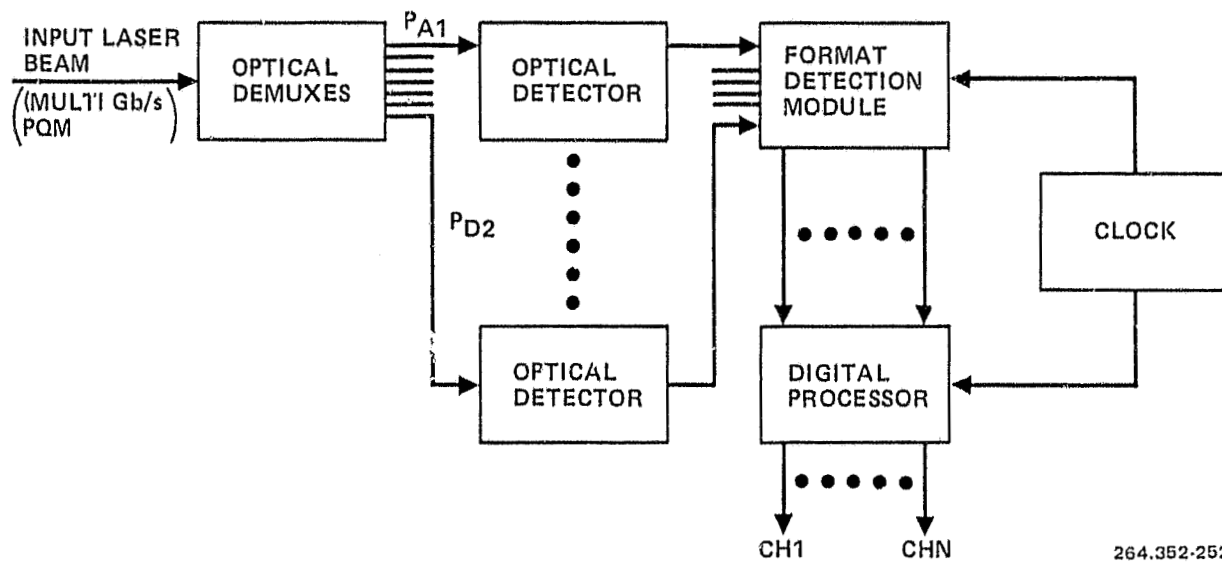
<sup>a</sup>Only one receiver and one transmission are energized at one time.

Angular tracking window is defined by  $\epsilon_V$  and  $\epsilon_H$  along the vertical (north-south) and horizontal directions respectively, and their deviations. Three cases are considered. For a Western Hemisphere platform to an Atlantic platform IPL, there is a longitudinal separation of 95 degrees between them. Assume that the maximum platform attitude errors and position errors are  $\pm 0.1$  and 0.05 degree, respectively, and assume that the maximum altitude error is 9 km. The corresponding tracking window for this case will be  $\epsilon_V = \pm 0.33$  and  $\epsilon_H = \pm 0.26$  degree. Using the same assumptions, a platform to other satellite IPL will have a tracking window of  $\epsilon_V = \pm 1.36$  and  $\epsilon_H = 0.53$  degree. In this case, the orbital arc spacing of 5 degrees has been used. The third case considered corresponds to a module to module IPL, where a spacing of 0.05 degree is assumed. With such a close spacing, the nominal positions of the two modules will be in the same orbit, with the same inclination and the same orbit normal. A ten percent stationkeeping accuracy is a reasonable assumption (Reference 72). By phasing the stationkeeping maneuvers of the two modules, a tracking window for the IPL antenna can be defined. Using the same assumptions on the platform attitude errors and position errors, the tracking window for a module to module IPL will be  $\epsilon_V = \pm 11.5$  and  $\epsilon_H = \pm 3.1$  degrees.



264.352-251

Figure 3-116. Block Diagram of Optical IPL System



264.352-252

Figure 3-117. Optical Receiver Block Diagram

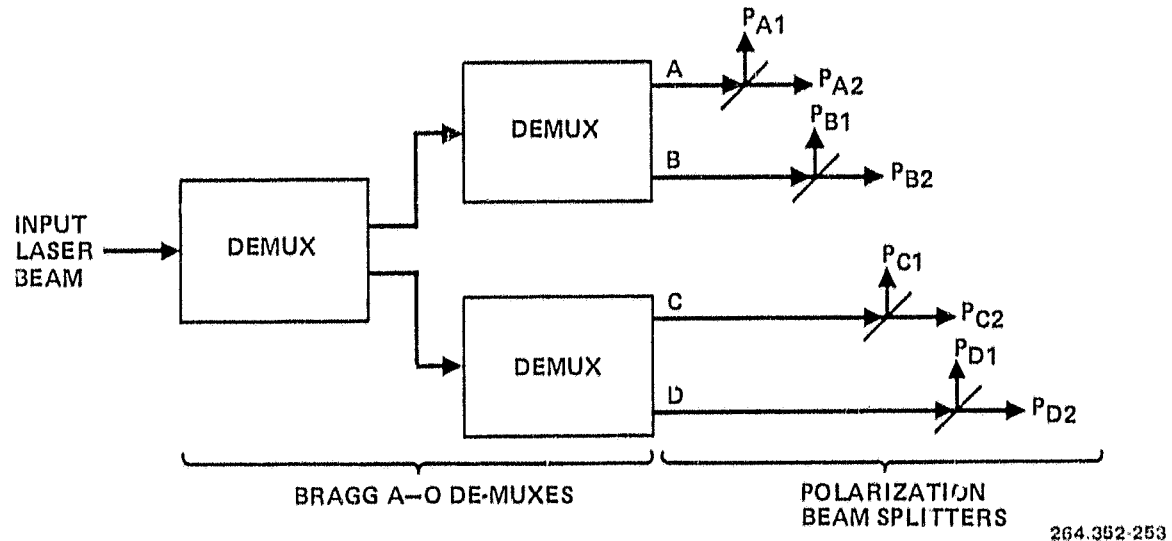


Figure 3-118. Optical Receiver Demultiplex Scheme

Table 3-66 summarizes the above discussion. The tracking windows for platforms with a maximum platform attitude error of  $\pm 0.2$  degrees is also included.

Table 3-66. IPL Tracking Windows

Tracking Window Sizes	Orbit Arc Spacing					
	Maximum Platform Attitude Errors					
	0.05°	5°	95°			
$\Sigma_V$	$\pm 0.1^\circ$	$\pm 0.2^\circ$	$\pm 0.1^\circ$	$\pm 0.2^\circ$	$\pm 0.1^\circ$	$\pm 0.2^\circ$
$\Sigma_h$	$\pm 11.5^\circ$	$\pm 11.7^\circ$	$\pm 1.36^\circ$	$\pm 1.57^\circ$	$\pm 0.33^\circ$	$\pm 0.69^\circ$

Sizes of the tracking windows in Table 3-66 also define the operational ranges for the tracking antennas. For a module to module IPL, the tracking antenna should have a linear operation range of  $\pm 12$  degrees along the vertical direction and  $\pm 3.5$  degrees along the horizontal direction.

To operate a closed-loop tracking (pointing) system, we need a sensor to detect the pointing error, a controller to generate commands, and an antenna positioner to null the tracking (pointing) error to a required accuracy. IPL antennas and some earth facing antennas need a pointing accuracy of 0.03 degrees (References 73 and 74). For such high accuracy pointing requirement, monopulse sensors can be used to detect the pointing error, and a controller

accompanied by a two-axis gimbal will close the control loop. A pointing accuracy of 0.03 degree can be achieved by properly selecting the bandwidth of the control loop and by designing the performance of the pointing hardware.

**3.4.6 HIGH POWER AMPLIFIERS.** The high power amplifiers (HPSSs) required for the 1990 space platform mission fall into two categories:

- a. Satellite TWTA.
- b. Ground TWTA.

The current and projected state-of-the-art (SOA) satellite TWTA's are shown in Table 3-67.

Table 3-67. Satellite TWTA Status

Frequency	Type	Item	Current SOA	1990 SOA
20 GHz	Helix	Saturated Power (watts)	10-20	40-80
		Efficiency (%)	35	38
		Approximate Weight (kg)	2.3	4.5
20 GHz	Coupled Cavity	There is no coupled cavity tube available but a 200 W unit could be developed.		
12 GHz	Helix	Saturated Power (watts)	150-200	150-200
		Efficiency (%)	42	42
		Saturated Power (watts)	400-600	400-600
12 GHz	Coupled Cavity	Efficiency (%)	44	44
		Approximate Weight (kg)	23	23

In the area of ground TWTAs, at 14 GHz helix tubes with saturated powers of 350-700W have been developed and coupled cavity tubes of 700-2,000W have been developed. At 30 GHz, some 300-1,000W developmental model coupled cavity tubes have been built and 30-60W helix tubes could be developed.

At 30 GHz, the couple cavity TWTA appears to be the best approach to achieve the required earth station transmit power, however, the 1 GHz required bandwidth is not readily achievable.

The current available and projected SOA devices are shown in Table 3-68. At 4- and 6-GHz, 2-5W reliable devices are commercially available and higher power units are being tested in laboratories. At 12-14 GHz, the available devices have yet to demonstrate reasonable reliability and above 14 GHz, the present devices are only laboratory test units.

Table 3-68. Solid-State Amplifier

Frequency (GHz)	Type	Current SOA $P_{out}$ /Efficiency (percent)	1990 SOA $P_{out}$ /Efficiency (percent)
4	FET/Bipolar	4-5 W/40	70 W/50
6	FET/Bipolar	2-3 W/30	30 W/35
12	FET	0.5-1 W/15	9 W/25
12	IMPATT	2.5 W/18	
14	FET	0.4 W/15	6 W/25
20	FET	0.2 W/7	3 W/15
20	IMPATT	1.0 W/10	
30	FET	0.1 W/3	1 W/10
30	IMPATT	0.5 W/8	

The foregoing has tabulated current and projected state-of-the-art TWTAs and solid state amplifiers. The communications architecture to date has been based on single carrier per transponder operating at saturation.

The possibility of multicarrier per transponder does exist. This mode of operation requires the output of the TWT to be backed off sufficiently such that they operate linearly and the C/I generated by the nonlinearities are within tolerable limits. Obviously backing off the output of a TWT requires a larger tube if the required power is fixed by link calculations. Strauss (References 75 and 76) has detailed the problem of backoff and efficiency and several possible solutions

to the problem. Figure 3-119 shows a conventional phase drive curve and a comparison of a possible means of extending the linear operating region. Figures 3-120 and 3-121 show the phase drive and C/I characteristic for a 12-GHz double taper helix tube and a 14-GHz coupled cavity tube, respectively. Figure 3-122 shows the C/I versus output power of a 14-GHz helix tube.

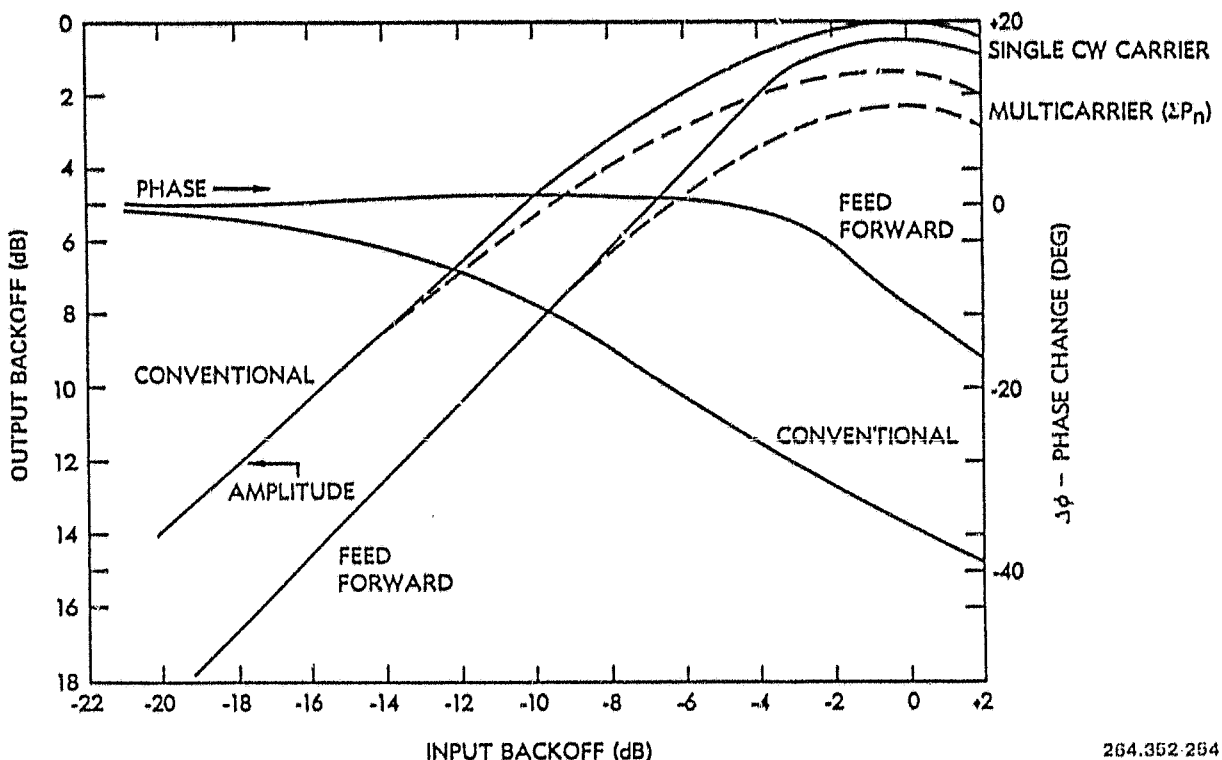


Figure 3-119. Comparison of Conventional Tube Characteristics With a Corrected Network Characteristic

Various possible linearizer approaches are shown in Figure 3-123 and the effect on required output backoff shown in Figure 3-124. Comparison of Figures 3-120 and 3-124 show that for a conventional tube a 6 dB two carrier output backoff will yield a C/I = 17 dB, as opposed to 25 dB for the feed forward linearizer, distortion network. Implementation of these techniques has demonstrated feasibility. Flight designs and reliability evaluation are required.

In the area of solid state amplifiers, IMPATT diode and FET amplifiers are both presently receiving attention. Chou (Reference 77) has recently developed a 10W, 12-GHz IMPATT amplifier. Two alternative circuits are shown in Figure 3-125. Both circuits give the same performance with B yielding 0.5 dB more power due to lower combiner loss. The frequency response is shown in Figure 3-126 and the amplifier performance is given in Table 3-69. The major problem related to the use of IMPATT amplifiers is their low efficiency, in this case 9 percent.

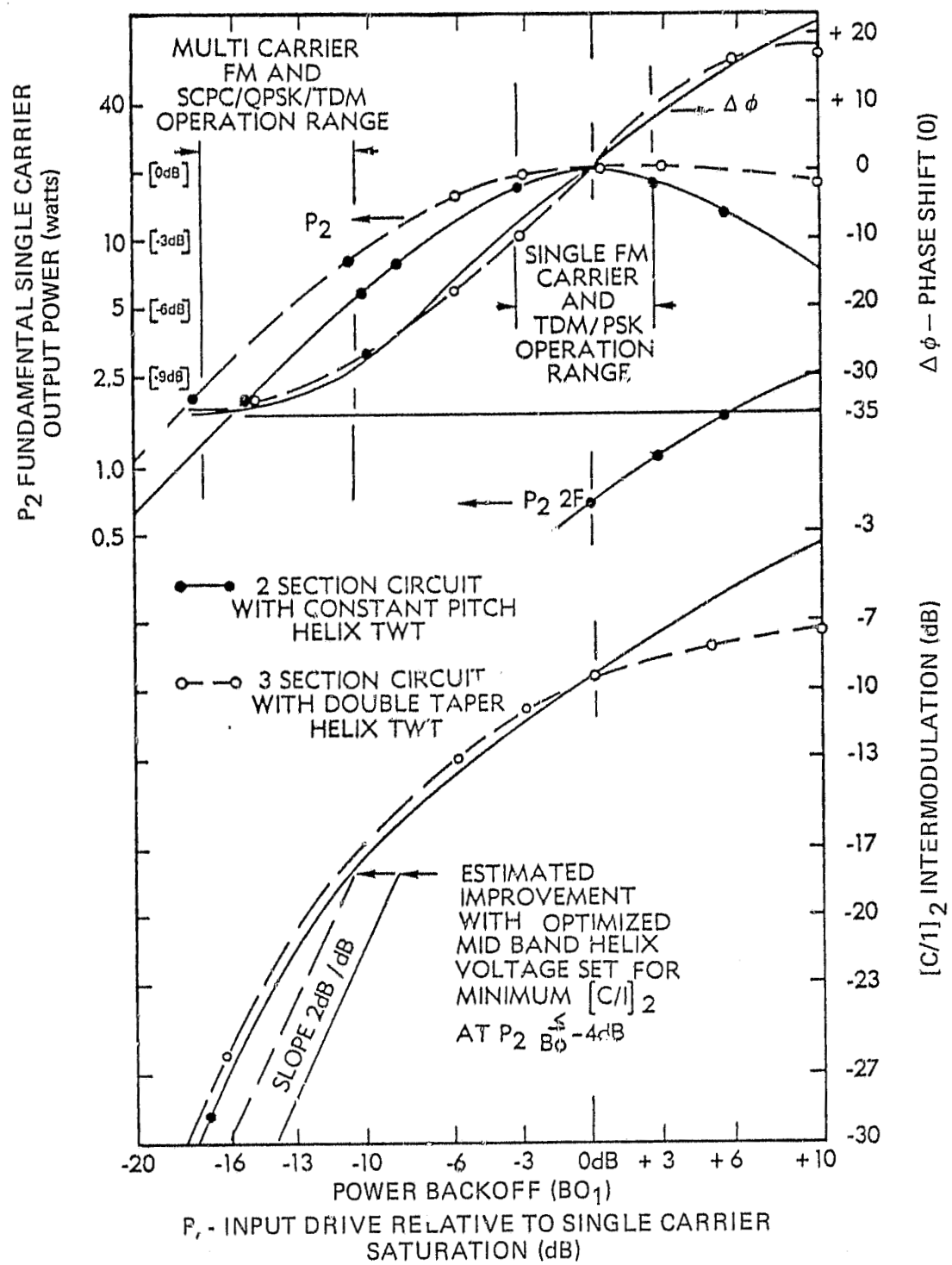


Figure 3-120. 12 GHz Double Tape Helix Tube Characteristics

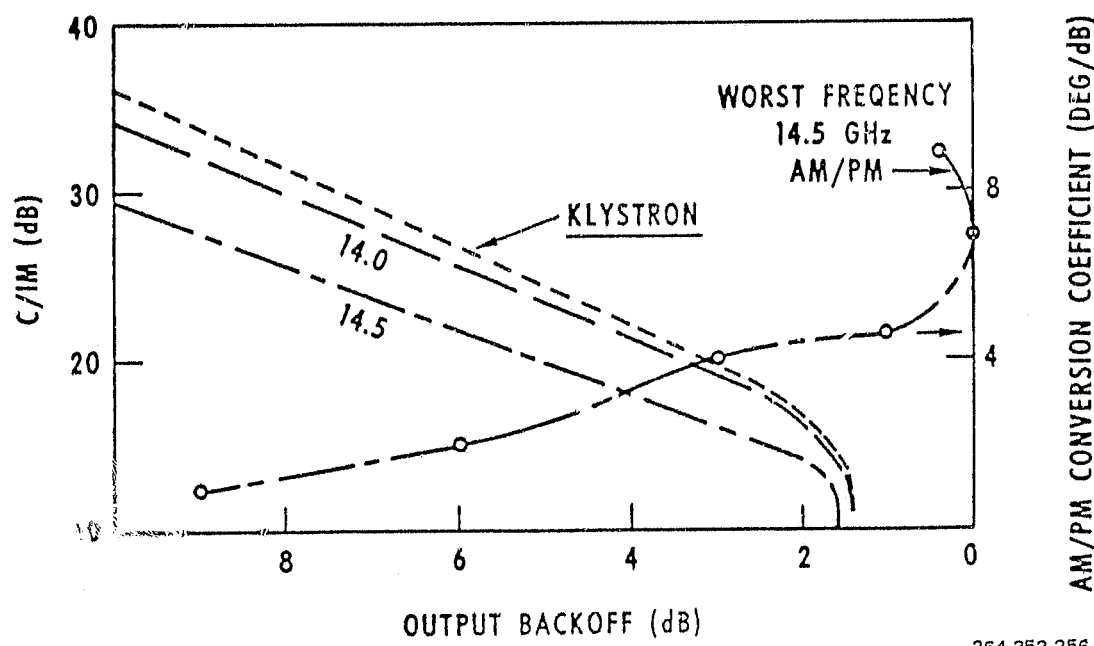
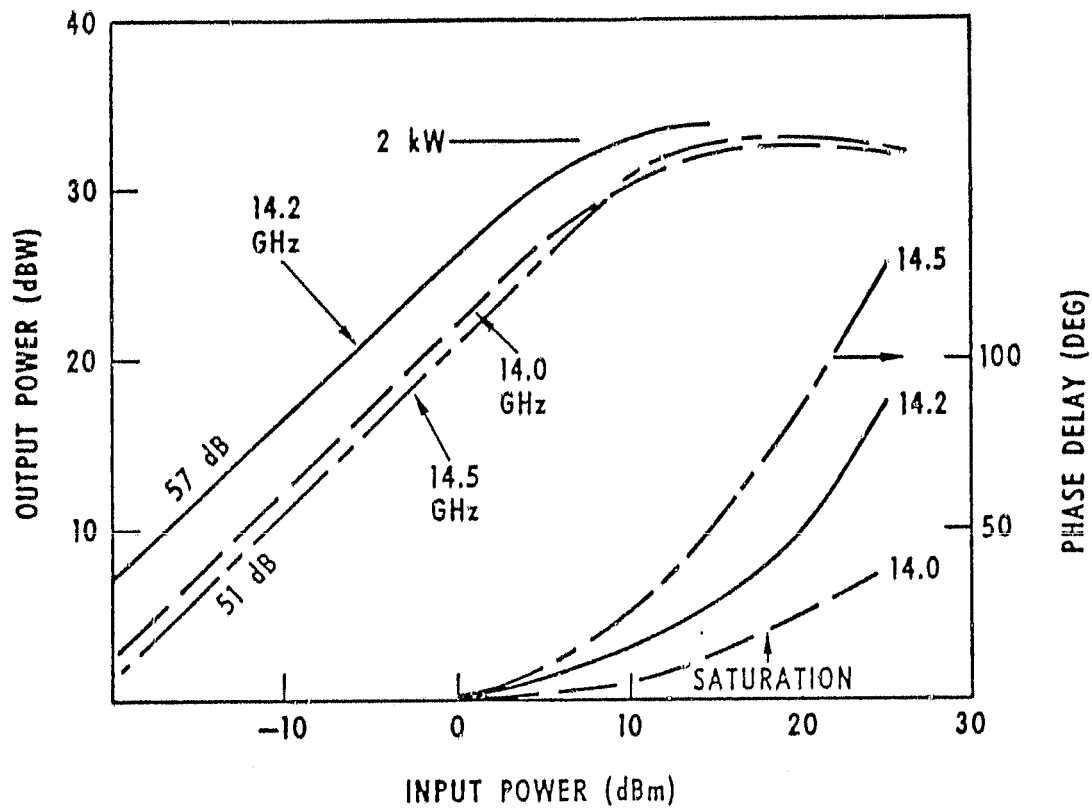
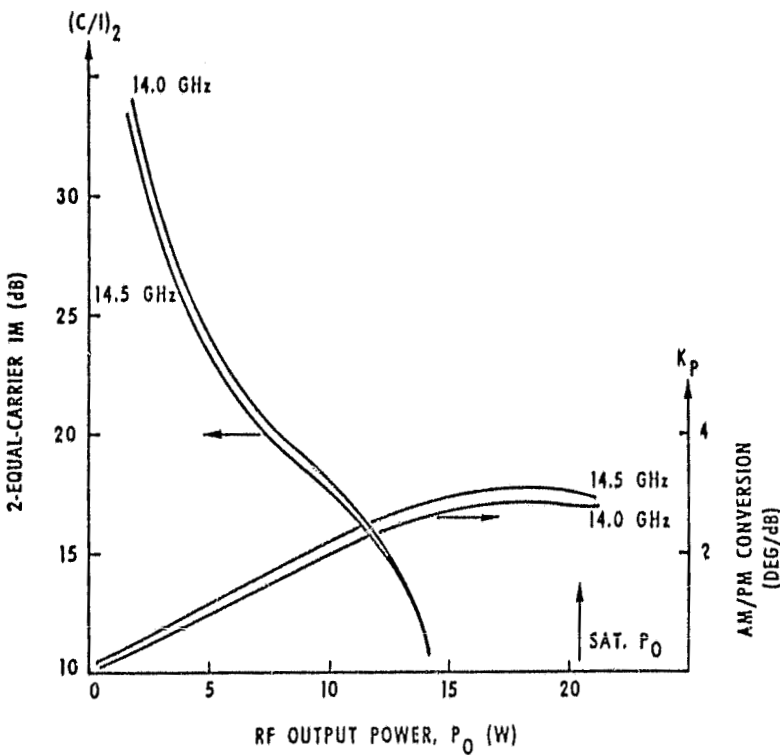


Figure 3-121. 14 GHz Coupled Cavity Tube Characteristics



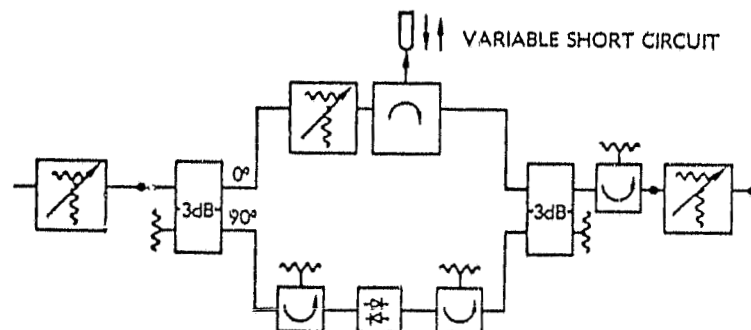
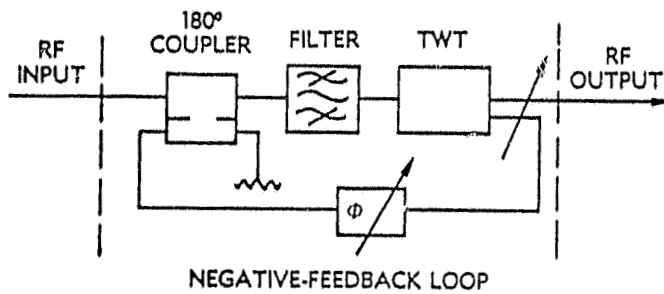
264,352-257

Figure 3-122. 14 GHz Helix Tube C/I Versus Output Power

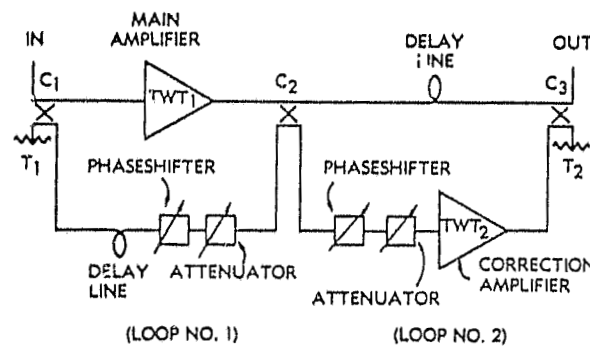
Figure 3-127 shows that a possible 6-GHz implementation of FET amplifiers as well as higher frequency amplifiers is dependent on solving the heat dissipation problems related to the 0.5-1.0 micron FET gates.

**3.4.7 ELECTROMAGNETIC COMPATIBILITY (EMC).** Electromagnetic interference control methods have been worked out for satellites with limited frequency reuse and a limited number of radiating payloads. Future satellite constellations or platforms will have a significant increase in both frequency reuse capability and in the number of radiating payloads that can interfere with one another and within themselves. The possible sources of interference in a system as complex as the GEO platform are legion and each source must be considered separately. The interference coupling media in the complex platform warrants investigation so that design drivers will be devised to present required performance in the final system.

Methods for the elimination of interference and design techniques to incorporate these methods of interference elimination are required for the geostationary platform. Three major classifications of interference occur in the platform: 1) interplatform, 2) interpayload, and 3) intrapayload. The first class of interference is significant between platforms separated by orbital slot separation in the geostationary arc but is very important for closely spaced satellites in close formation. Individual satellites arrayed in a time varying constellation introduce interference from sidelobe illumination and for some formation



THE PREDISTORTION NETWORK CIRCUITRY



CIRCUIT FOR FEEDFORWARD LINEARIZED TWTA

264,352-258

Figure 3-123. Various TWTA Linearizer Approaches

configurations mainlobe illumination of one satellite by other members of the constellation. The interference introduced by each of the other satellite constellation members is highly time dependent in both phase and amplitude. The rejection of in-band and intermodulation interference is difficult under these variable conditions. Further analysis and testing of the coupling between satellite constellation members will require experimental measurements with satellites equipped with antenna systems similar to the baseline configuration. A related interference occurs when a ground station antenna pattern simultaneously illuminates several satellites. The information directed to one satellite becomes a variable interference to an adjacent satellite. If a single large platform is used, the interference can be corrected since a fixed phase amplitude relation occurs.

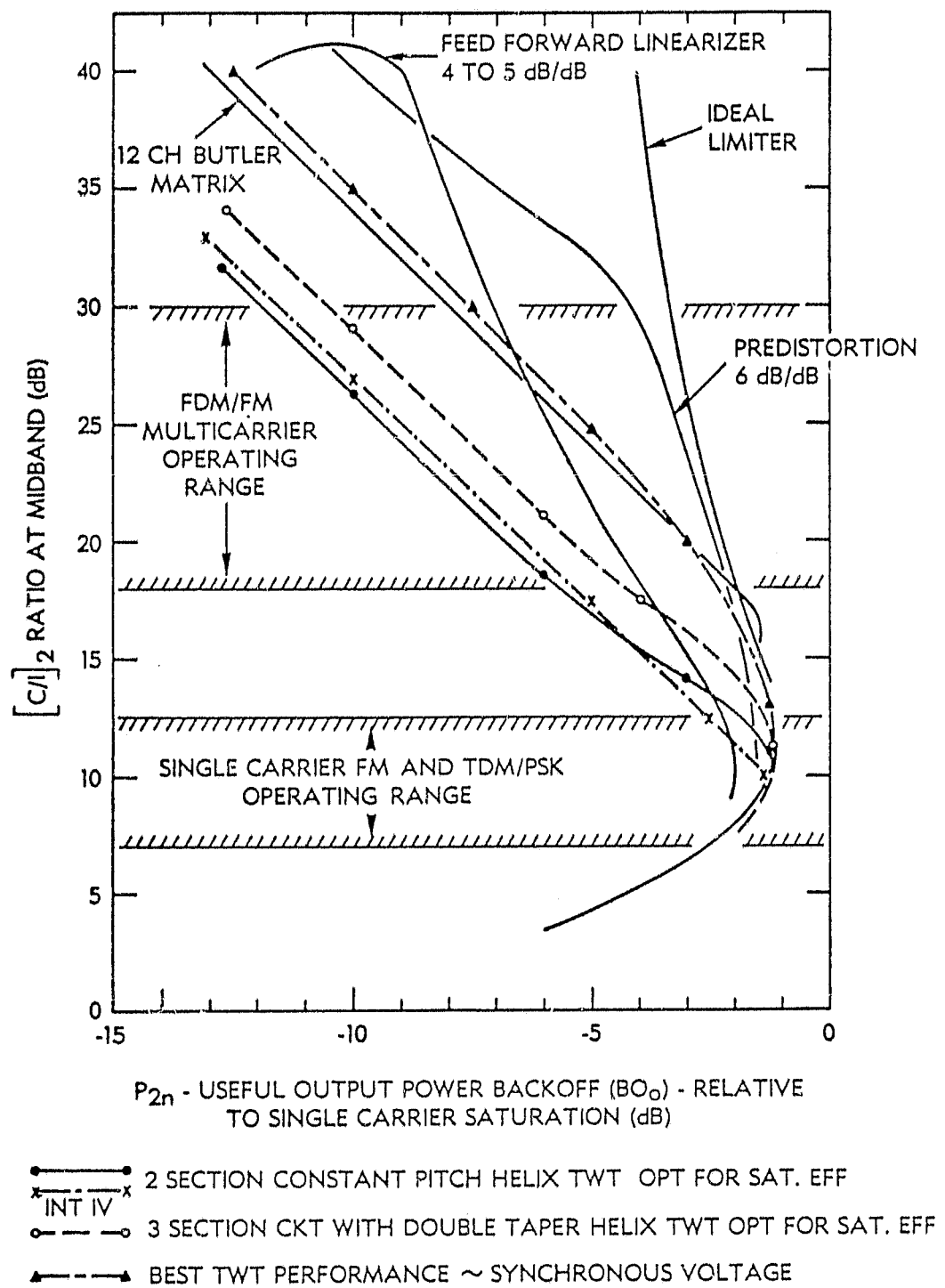
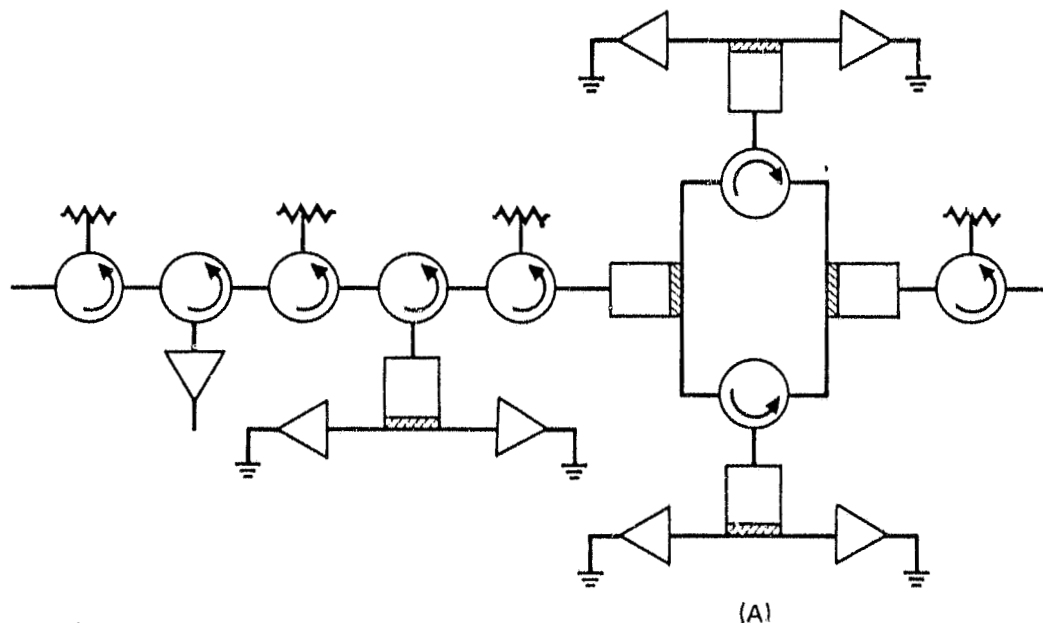


Figure 3-124, Linearized TWT Performance



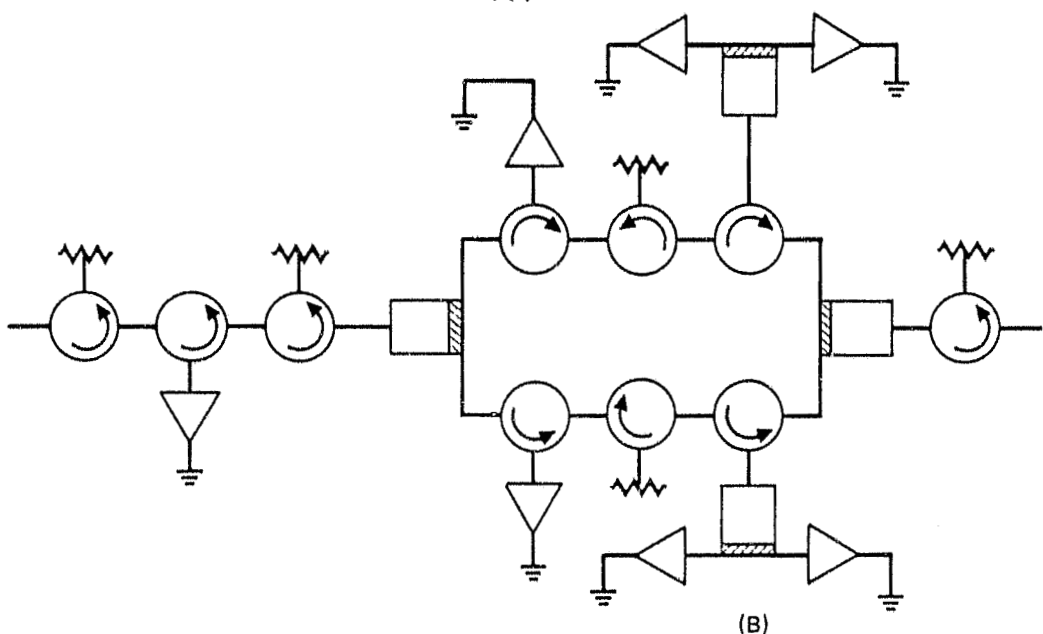
(A)

—► SINGLE DIODE AMPLIFIER MODULE

—□— POWER COMBINER

—○— CIRCULATOR

—○— ISOLATOR



(B)

264.352-260

Figure 3-125. Schematic of 12 GHz IMPATT Amplifiers

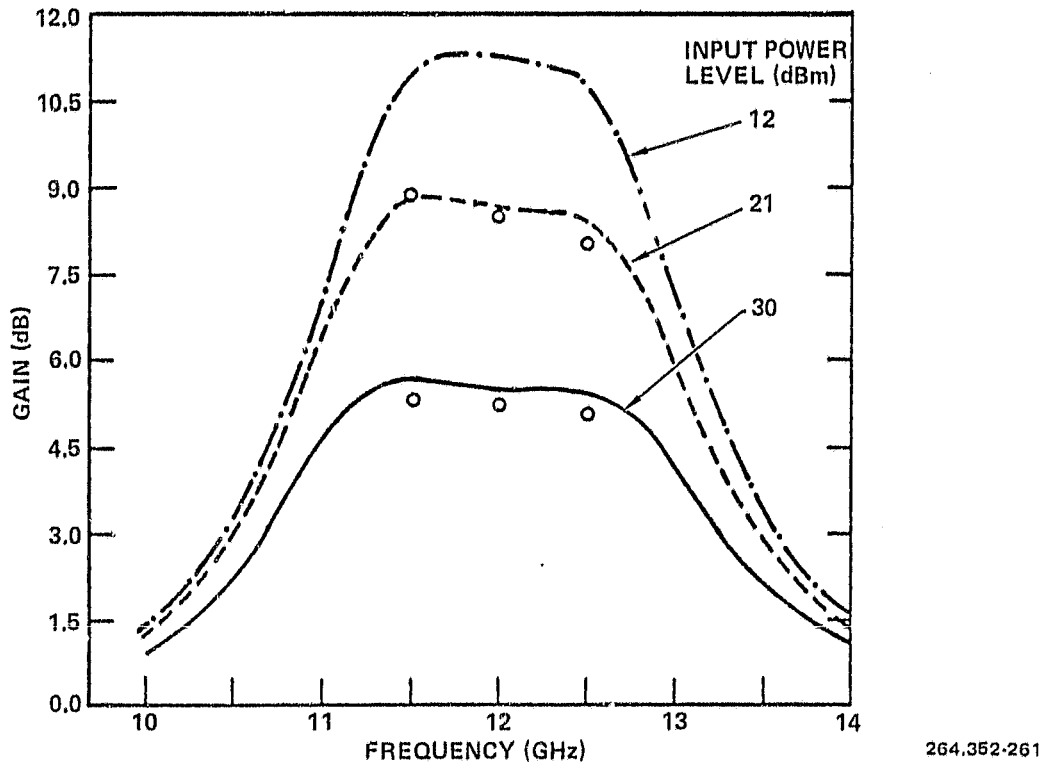


Figure 3-126. Frequency Response of a Double Tuned IMPATT Amplifier

Interpayload interference occurs within a satellite or platform between the many payloads present on the payload. Interference occurs between payloads when the separate payload channels are routed through common switching and processing components as well as through payload peculiar components. Both electromagnetic, including optical, and acoustic coupling mechanisms are present. Intermodulation is also a high interference source depending on the material type and interconnects between components of the antenna reflectors, feeds, and the platform.

Intrapayload interference has sources similar to the interpayload sources with the additional influence of the antenna system isolation. A primary source of interference is introduced by the reflector antenna feed assembly. The antenna feed has coupling between channels caused by overlapping of beams when high reuse of both uplink and downlink frequencies are used. Both the systems architecture and the antenna design are combined to control the intrapayload interference levels.

The elimination of adjacent channel interference presents a major development problem for the filter technology. The CPS and HVT services presently envisioned on the platform have 40 MHz bandwidth transponders at Ka-band. RF filters capable of separating the individual channels at the Ka-band uplink frequency have bandwidths near 0.13 percent. These filters are very narrow and the control of adjacent channel levels will be difficult.

Table 3-69. Amplifier Performance

Frequency	11.7 to 12.2 GHz
Input Power	30 dBm
Output Power	40 dBm (typical)
Net Gain	10 dB
Gross Gain per Single-Diode Module	5.4 dB
Input/Output VSWR	1.25:1 maximum
DC to RF Efficiency	9 percent minimum
Circulator Insertion Loss	0.3 dB per path

EMI testing of the payloads and interpayload switching and processing will be performed on the ground during the design C, D phases to validate performance capability. All of the systems comprising the platform will be tested together in the final stages of design for compatibility. When the platform components are isolated into a constellation of individual satellites, an added nonstationary variable is introduced that cannot be measured in the ground testing.

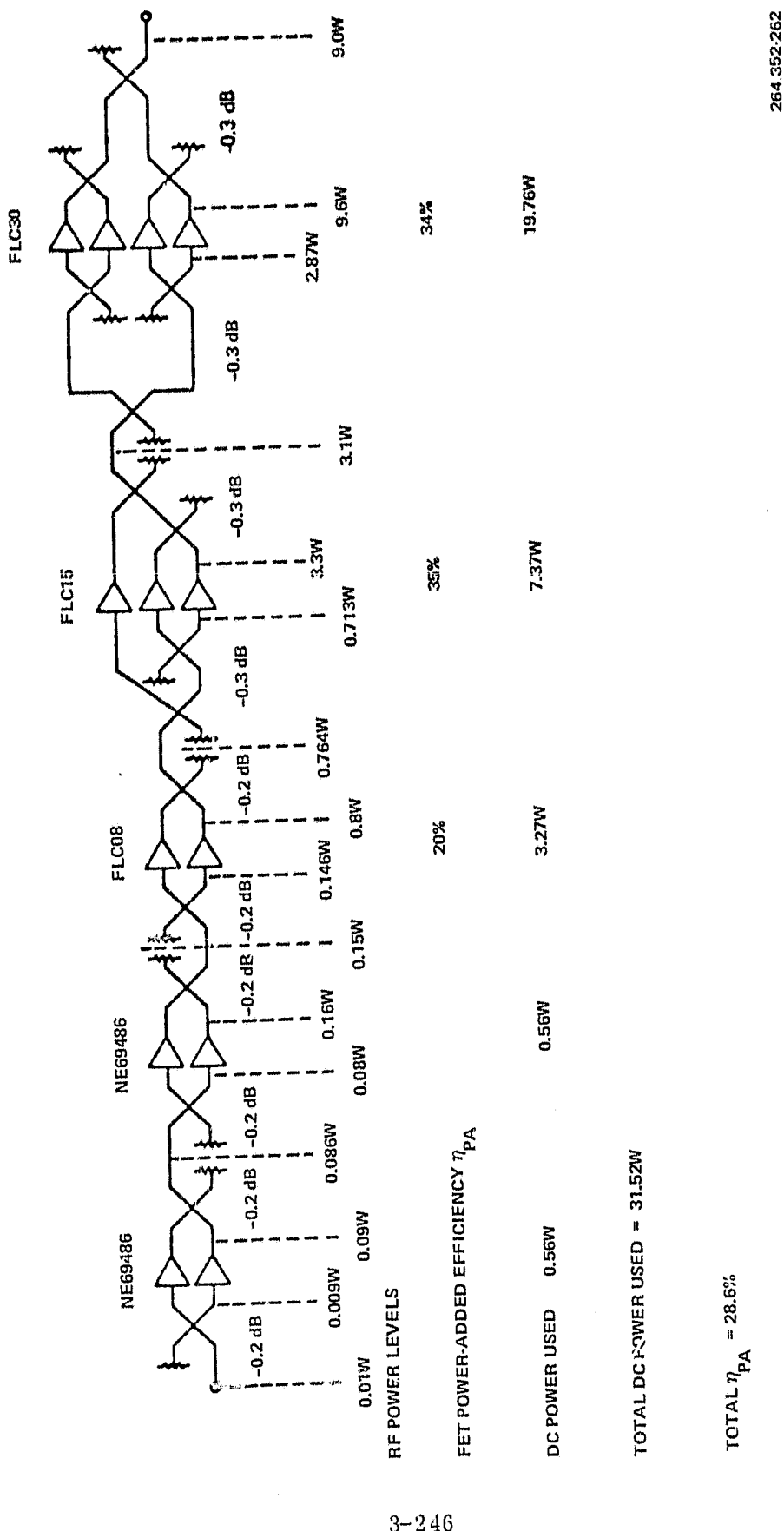


Figure 3-127. High-Power C-Band Amplifier (6 GHz)

### 3.5 REFERENCES

1. L.W. Slifer and W.J. Billerbeck, "Synchronous Orbit Power Technology Needs," NASA Technical Memorandum 80280, April 1979.
2. H. Brandhorst and D. Bernatowicz, Space Solar Cells - High Efficiency and Radiation Damage, Conference Record of the Fourteenth IEEE Photovoltaic Specialists Conference, San Diego, California, 7-10 January 1980.
3. J. Wise, private communication.
4. R. Loo, T. Goldhammer, B. Anspaugh, R.C. Knechtli, and G.S. Kamath, "Electron and Proton Degradation in (Al Ga) As-GaAs Solar Cells," Conference Record of the Thirteenth IEEE Photovoltaic Specialists Conference, 78CH1319-3, Washington, D.C., 5-8 June 1978, pp. 562-570.
5. R.V. Elms and L.E. Young, "SEPS Solar Array Design and Technology Evaluation," Record of the Tenth Intersociety Energy Conversion Engineering Conference University of Delaware, Newark, Delaware, 18-22 August 1975, pp. 1041-1047.
6. H. von Bassewitz and J. Lydorf, "Development Status of the Ultralight-weight Solar Array ULP," Conference Record of the Twelfth IEEE Photovoltaic Specialists Conference - 1976, Baton Rouge, Louisiana, 15-18 November 1976, 76CH1142-9ED, pp. 435-442.
7. S. Wolff, "The Flight of the FRUSA," Conference Record of the Ninth IEEE Photovoltaic Specialists Conference, 72CH0613-0-ED, Silver Spring, Maryland, 2-4 May 1972, pp. 240-253.
8. M. Newns, C.J. Williams and R.L. Crabb, "The ESA Solar Array for Space Telescope," Proceedings of the First European Symposium on Photogenerators in Space ESTEC, Noordwijk, The Netherlands, 11-13 September 1978, pp. 201-208.
9. H. Berbermeier, U. Hoffman and J. Rath, "Development of a Multi-kW Rollout Solar Generator," Conference Record of the Twelfth IEEE Photovoltaic Specialists Conference - 1976, Baton Rouge, Louisiana, 15-18 November 1976, 76 CH1142-9 ED, pp. 418-429.
10. W. Alsbach and H. Losch, "Comparison of Foldout and Rollout Generators in the Multi-kW Range," Conference Record of the Twelfth IEEE Photovoltaic Specialists Conference - 1976, Baton Rouge, Louisiana, 15-18 November 1976, 76 CH1142-9 ED, pp. 430-434.

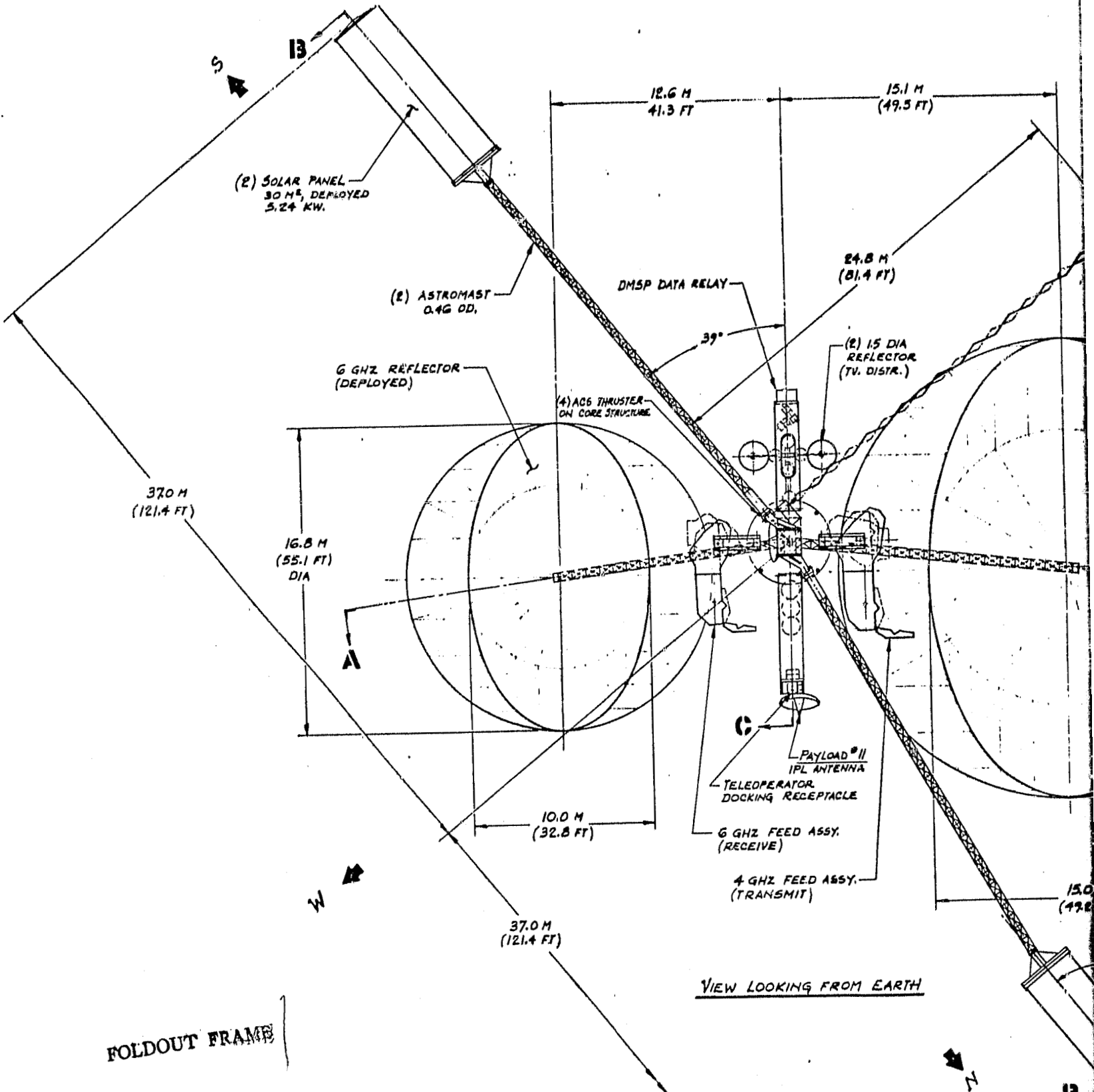
11. L. Chidester, Lockheed Missiles and Space Company, private communication of the beginning of life performance.
12. J.S. Smith, S.S. Sachdev and J.A. Hunter, "Testing of the Communications Technology Satellite Deployable Solar Array System," Conference Record of the Eleventh IEEE Photovoltaic Specialists Conference - 1975, Scottsdale, Arizona, 6-8 May 1975, 75CH0948-ED, pp. 82-83.
13. D.J. Curtin and W.J. Billerbeck, "Development of Advanced Interconnectors for Solar Cells," COMSAT Technical Review, Vol. 4, Number 1, Spring 1974, pp. 53-68.
14. F.C. Treble, A. Dunnet and R.L. Crabb, "Comparative Deep Thermal Cycling of Solar Cell Panels," Conference Record of the Eleventh IEEE Photovoltaic Specialists Conference - 1975, Scottsdale, Arizona, 6-8 May 1975, 75CH0948-ED, pp. 145-152.
15. R.W. Fredericks and F.L. Scarf, "Observation of Spacecraft Charging Effects in Energetic Plasma Regions," Photon and Particle Interactions with Surfaces in Space, edited by R.J.L. Grard, D. Reidel Publishing Co., 1973, pp. 277-308.
16. Alan Rosen, "Spacecraft Charging: Environment Induced Anomalies," AIAA 13th Aerospace Sciences Meeting, 21 January 1975, AIAA Preprint, No. 75-91.
17. D.A. McPherson, D.P. Cauffman, and W. Schober, "Spacecraft Charging at High Altitudes: The Scatha Satellite Program," Spacecraft Charging by Magnetospheric Plasmas, edited by A. Rosen, Progress in Astronautics and Aeronautics, Vol. 47, Cambridge, Massachusetts: MIT Press, 1976, pp. 15-30.
18. B.E. Anspaugh, J.A. Scott-Monck, R.G. Downing, and T.F. Miyahira, "Effects of Electrons and Protons on Ultrathin Solar Cells," Conference Record of the Fourteenth IEEE Photovoltaic Specialists Conference, San Diego, California, 7-10 January 1980.
19. D.J. Curtin and R.W. Cool, "Thermal Cycle and Charge Tests of Solar Array Modules," Proceedings of the Photovoltaic Solar Energy Conference, Luxembourg, Germany, 27-30 September 1977.
20. D.E. Rockey and I. Baker, "Concentrator Designs for Space Photovoltaic Arrays," Conference Record of the Fourteenth IEEE Photovoltaic Specialists Conference, San Diego, California, 7-10 January 1980.

21. V.A. Caluori and H. Oman, "Photovoltaic Solar Power Satellites," Conference Record of the 12th IECEC, Washington, D.C., August 28-September 2 1977, pp. 1378-1385.
22. H. Oman, private communication.
23. R.V. Elms, Jr., "Family of Solar Array Design Options," Proceedings of the 13th IEEE Photovoltaic Specialists Conference, Washington, D.C., 5-8 June 1978, pp. 208-214.
24. Hughes Aircraft Company, "Conceptual Design Study of Concentrator Enhanced Solar Arrays-Interim Final Report," JPL Contract No. 955194, 15 May 1979.
25. Hughes Aircraft Company, "High Efficiency Solar Panel-GaAs Solar Cells," Contract F33615-77-C-3150, 15 January 1980.
26. D.E. Rockey, private communication.
27. NASA CR-898 "Study and Analysis of Satellite Power Systems Configurations for Maximum Utilization of Power" prepared by TRW Systems for GSFC, October 1967.
28. D. Maurer, "Separators," Proceedings of the 1971 NASA/GSFC Aerospace Industry Battery Workshop, pp. 44.
29. D.N. Stager and W.R. Scott, Two Kilowatt Long Life Battery, AFAPL Reports No. 71-43, June 1971.
30. R. Sparks and D. Rusta, "Nickel Cadmium Battery Reconditioning and Long-Term Performance in Geosynchronous Orbit Spacecraft," Proceedings 13th IECEC, 20 August 1978, Vol. 3.
31. W. Billerbeck, "Long-Term Prediction of Power System Performance for Geosynchronous Spacecraft," Proceedings 14th IECEC, August 1979.
32. E. Levy and F. Osugi, "Design and Performance of Intelsat IV Power Subsystem," Proceedings IECEC Conference, 1972.
33. W. Crum and I. Schulman, "TDRSS Battery System Design," Proceedings 14th IECEC, Boston, Massachusetts, August 1979.
34. W. Scott and D. Rusta, Sealed Cell Ni-Cd Battery Applications Manual, NASA Reference Publication No. 1052, 1979.

35. R. Beauchamp, et al: US Patent 3,653,967, April 1972.
36. M. Klein and B. Baker, "Nickel-Hydrogen Battery System," Proceedings 9th IECEC, San Francisco, California, 1974, pp. 118.
37. J.D. Dunlop, et al: "Sealed Metal Oxide-Hydrogen Secondary Cells," Proceedings 9th International Power Sources Symposium, Brighton, England, 1974, pp. 315-329.
38. J.D. Dunlop, "Sealed Nickel-Hydrogen Secondary Battery," to be published in Proceedings 15th IECEC, August 1980.
39. F. Betz, J. Stockel, and A. Gaundt, "Nickel-Hydrogen Storage Battery for Use of Navigation Technology Satellite - 2" Proceedings 11th IECEC meeting, Lake Tahoe, Nevada, 1976.
40. G. Van Ommering, et al: "INTELSAT V Nickel Hydrogen Battery System," Proceedings AIAA 8th Communications Satellite Systems Conference, Orlando, Florida, April 1980.
41. R. Patterson, et al: "Development of Spacecraft Power System Using Nickel-Hydrogen Battery Cells," Proceedings 6th Communications Satellite Systems Conference, Montreal, Canada, 1976.
42. D. Rusta, "Power Source Requirements of Electronic Propulsion Systems Used for North-South Stationkeeping of Communication Satellites," Proceedings 11th IECEC, September 1976.
43. L. Slifer and W. Billerbeck, "Synchronous Orbit Power Technology Needs," NASA/GSFC TM 80280, April 1979.
44. F. Esch, W. Billerbeck, and D.J. Curtin, "Electric Power Systems for Future Communications Satellites," IAF Paper 76-237 presented at the 27th IAF Congress, Anaheim, California, October 1976.
45. E. Levy and F. Osugi, "Design and Performance of INTELSAT IV Power Subsystem," Proceedings 1972 IECES.
46. W. Rintala, D. Briggs, R. Misin, and C. Wiebe, "INTELSAT V Power Control Electronics Systems," Proceedings, 14th IECES, Boston, Massachusetts, August 1979.
47. Electric Power Conditioner Development, Final Report on INTELSAT Contract IS-55 Hawker-Siddeley Dynamics, Ltd., Stevenage, UK.

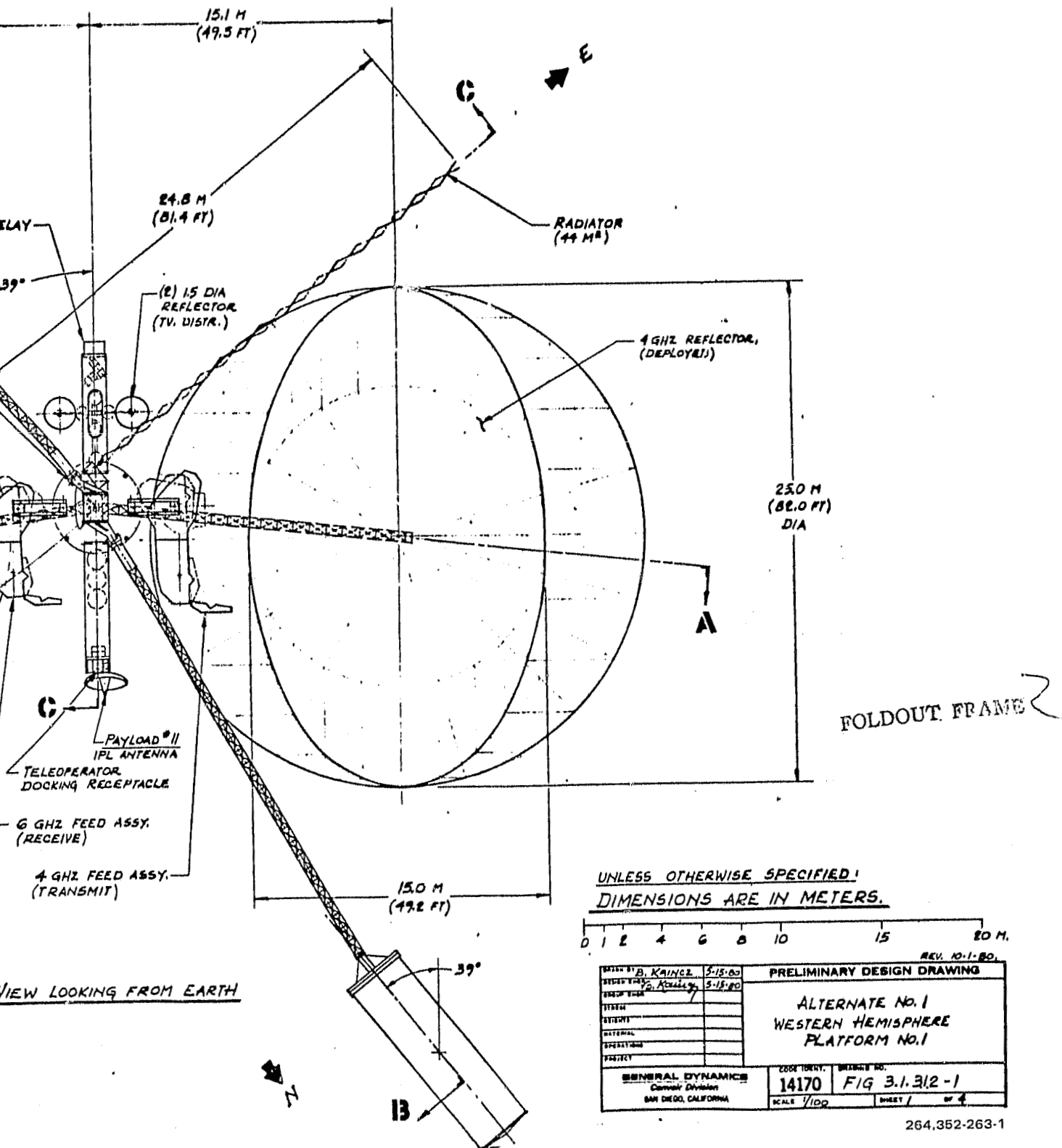
48. R. Hehnem, AC Power Systems in the Kilowatt Range, ESRO Report SP-103, AEG-Telefunken, September 1974.
49. W. Denzinger, Square Wave Power Generation and Distribution, ESRO Report SP-103, Donier-System GmbH, September 1974.
50. W. Muller and W. Denzinger, Square Wave AC Power Generation and Distribution of High Power Spacecraft, ESA Report SP-126, Donier-System GmbH, September 1977.
51. J.C. Evans, An-Ti Chai, and Chandra Goradia, "Planar Multijunction High Voltage Solar Cells," Proceedings, 14th IEEE Photovoltaic Specialists Conference, San Diego, California.
52. "On-Chip Solar Cells Power ICs," Electronic Products Magazine, March 1980, p. 27.
53. Alston, High Voltage Technology, published by Oxford University Press, 1968, p. 56.
54. General Electric Co., SCR Manual, including Triacs and other Thyristors, GE Semiconductor Products Division, 1972.
55. A. Meulenberg, "Damage in Silicon Solar Cells from 2 to 155 MeV Protons," IEEE Photovoltaic Specialists Conference - 1973 p. 89 Proceedings, pp. 359-365.
56. A. Meulenberg, "Proton Damage to Silicon From Laboratory and Space Sources," IEEE Photovoltaic Specialists Conference - 1976, p. 89 pp. 224-228.
57. MSFC Memo PD 01-79-70, "STS Upper Stage Geosynchronous Payload Capability," 6 November 1979 and subsequent updates PD 01-79-72, 17 November 1979 and PD 01-80-16, 4 March 1980.
58. Teleoperator Maneuvering System (TMS) Program Definition Activities, MSFC Report, November 1979.
59. Remote Teleoperator System (RTS) Redefinition Activities, MSFC Report, October 1979.
60. L. Pollack, "Technologies for Future Satellites," Journal of Spacecraft and Rockets, Vol. 17, No. 1, January-February 1980.
61. X. Rozec and F. Assal, "Microwave Switch Matrix for Communications Satellites," ICC Proceedings, Vol. III, June 1976.
62. Y. Ito et al., "Analysis of a Switch Matrix for an SS-TDMA System," Proceedings of IEEE, Vol. 65, No. 3, March 1977.

63. C. Mahle, W. Childs, and A. Berman, "A DQPSK Satellite Transponder Using 14-GHz MIC Technology," EASCON '78 Record, pp. 411-416.
64. Y.S. Lee, "Simulation Analysis for DCQPSK Regenerative Repeater," COMSAT Technical Review, Vol. 7, No. 2, Fall 1977.
65. W. Childs, C. Mahle, and Poturuchi, "An Integrated DQPSK Demodulator for 14-GHz Satellite Communications Applications," IEEE MTT-S International Microwave Symposium, Ottawa, Canada, June 1978.
66. J. Campanella, F. Assal, and A. Berman, "On-Board Regenerative Repeater," ICC '77 Conference Record, Vol. 1 pp. 6.2-121 - 6.2 -125.
67. K. Koga, T. Muratani and A. Ogawa, "On-Board Regenerative Repeaters Applied to Digital Satellite Communications," Proceedings IEEE Vol. 65, No. 3 pp. 401-410, March 1977.
68. J.H. Deal, "Digital Transmission Involving Intersatellite Links," International Conference on Digital Satellite Communications - 4th Montreal, Canada, October 1978.
69. G.A. Welti, "Inter Satellite Link for Multiple Access Telephony" EASCON '78 Record, pp. 432-440.
70. J.A. Maynard et al, "Multigigabit Laser Communications for Satellite Cross-Links," 4th International Conference on Digital Satellite Communications, October 1978.
71. M. Ross et al, "Space Laser Communications," AIAA Conference, 1978.
72. Private discussion with Dr. Gary D. Gordon.
73. Geostationary Platform Systems Concepts Definition Study, Second Interim Review, February 12 February 1980, Report No. GDC-GPP-79-003.
74. Attachment 3 of a letter from Mr. C.D. Pengelley of General Dynamics to Mr. Mel Grossman, 26 February 26 1980.
75. R. Strauss, "Demands on TWT's Tighten as Carrier Density Grows," Microwaves, April 1978.
76. R. Strauss, "The State-of-the-Art of High Power Amplifiers for Satellite Communications above 10 GHz," AIAA/CASI 6th Communications Satellite Systems Conference, Montreal, Canada, April 1976.
77. S.M. Chou, "12 GHz IOW Amplifier Using Gaas IMPATT Divides," COMSAT Technical Review, Volume 9, No. 2B , Fall 1979.



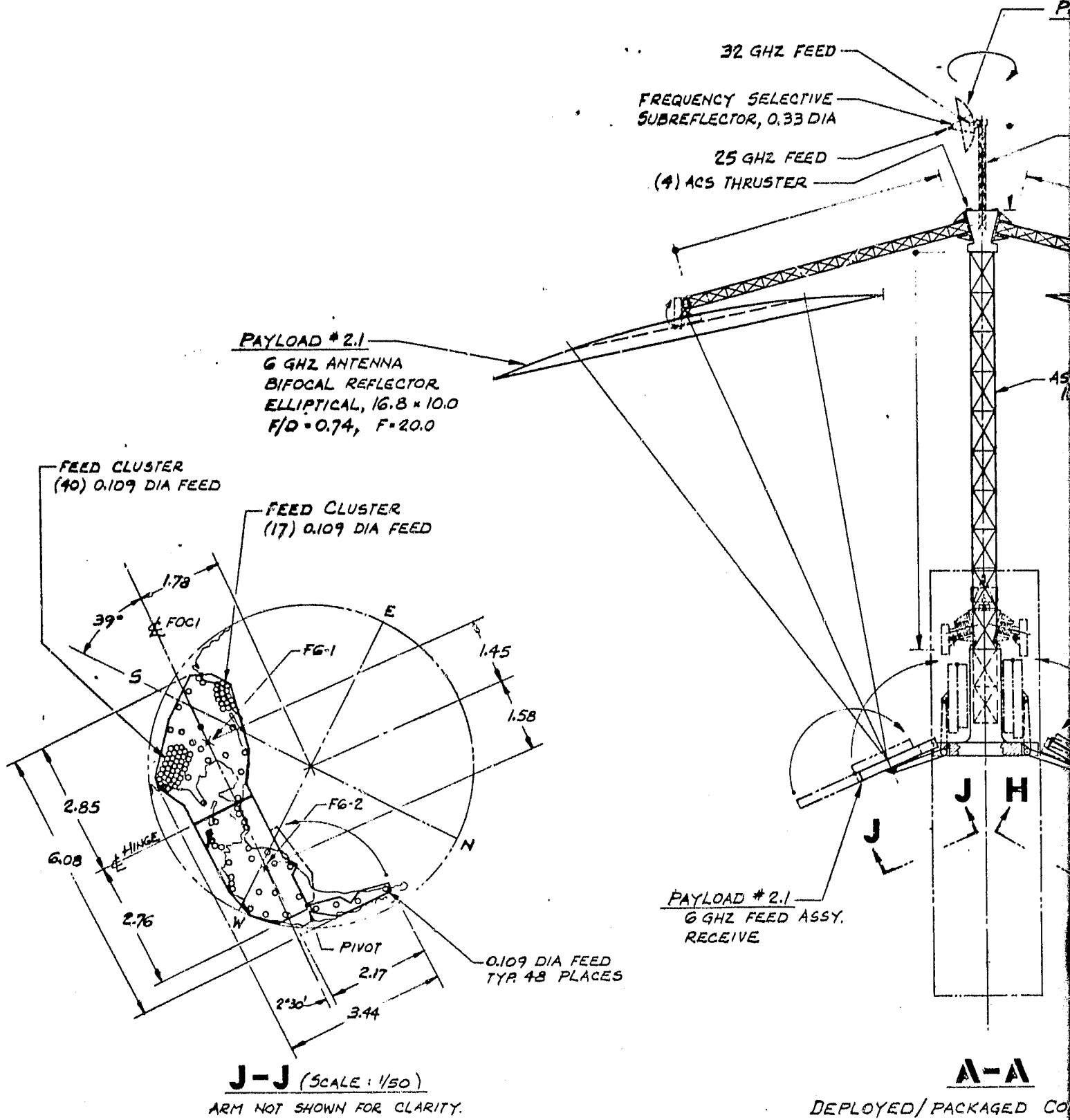
ORIGINAL PAGE IS  
OF POOR QUALITY

### Alternative #1,

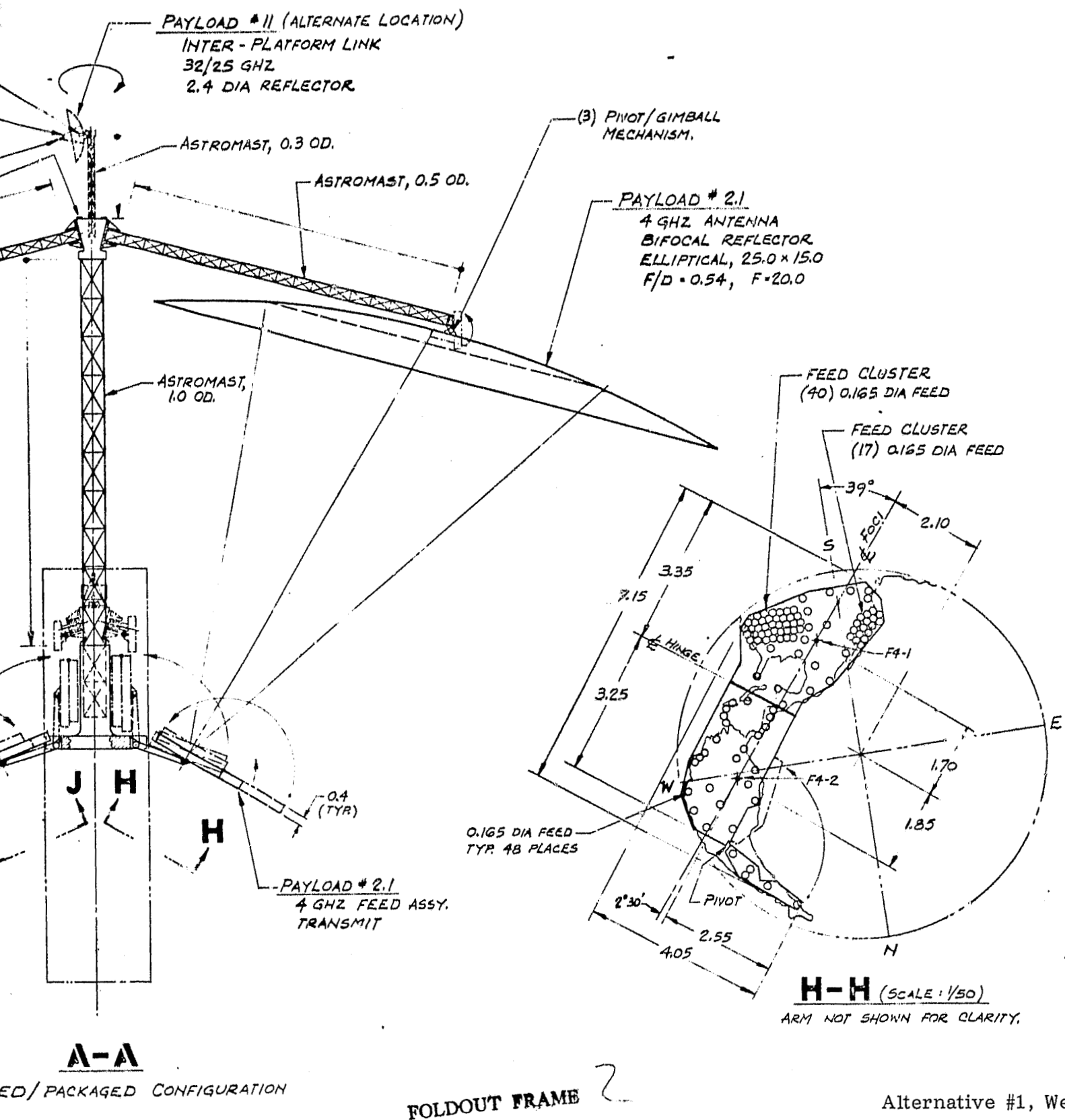


Alternative #1, Western Hemisphere, Platform No. 1

FO-1 (Sheet 1 of 4)



FOLDOUT FF



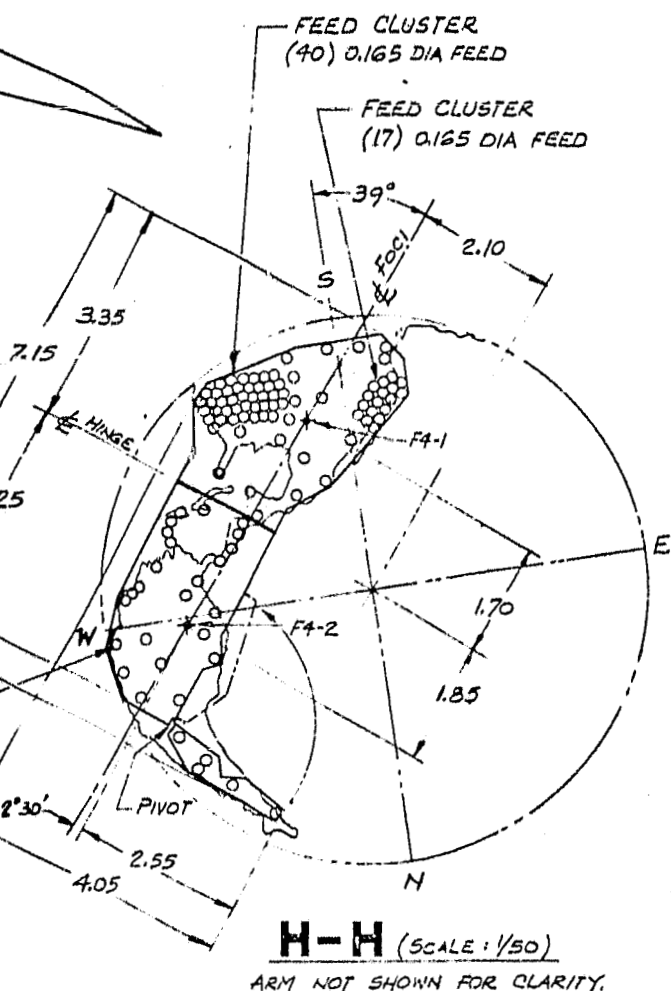
DRAWN BY  
 DESIGN ENG.  
 GROUP ENG.  
 STRESS  
 WEIGHTS  
 MATERIAL  
 OPERATIONS  
 PROJECT  
 GEN

Alternative #1, Western He

PIVOT/GIMBALL  
MECHANISM.

PAYOUT # 2.1

4 GHZ ANTENNA  
BIFOCAL REFLECTOR  
ELLIPTICAL, 25.0 x 15.0  
F/D = 0.54, F=20.0



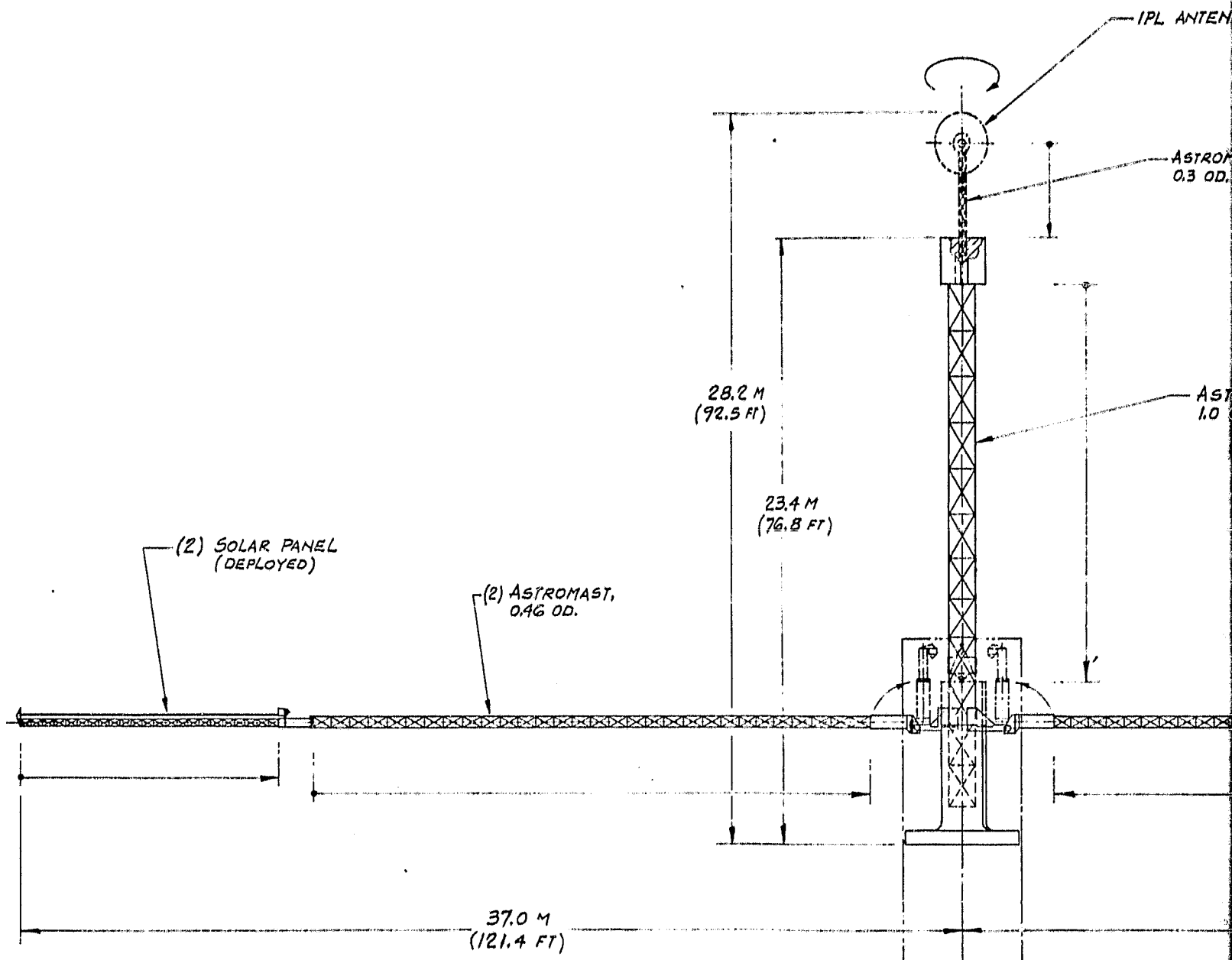
DIMENSIONS ARE IN METERS

0	1	2	4	6	8	10	15	20 M.
REV. 10-1-80								
PRELIMINARY DESIGN DRAWING								
DRAWN BY B. KAINCZ 5-15-80 DESIGN AND B. Kaincz 5-15-80 GROUP HIGH								
STRESS								
WEIGHTS								
MATERIAL								
OPERATIONS								
PROJECT								
GENERAL DYNAMICS Convair Division SAN DIEGO, CALIFORNIA								
CODE LENT DRAWING NO. 14170 FIG 3.1, 312-2								
SCALE 1/50 SHEET 2 OF 4								

Alternative #1, Western Hemisphere, Platform No. 1 264.352-263-2

FO-1 (Sheet 2 of 4)

FOLDOUT FRAME 3



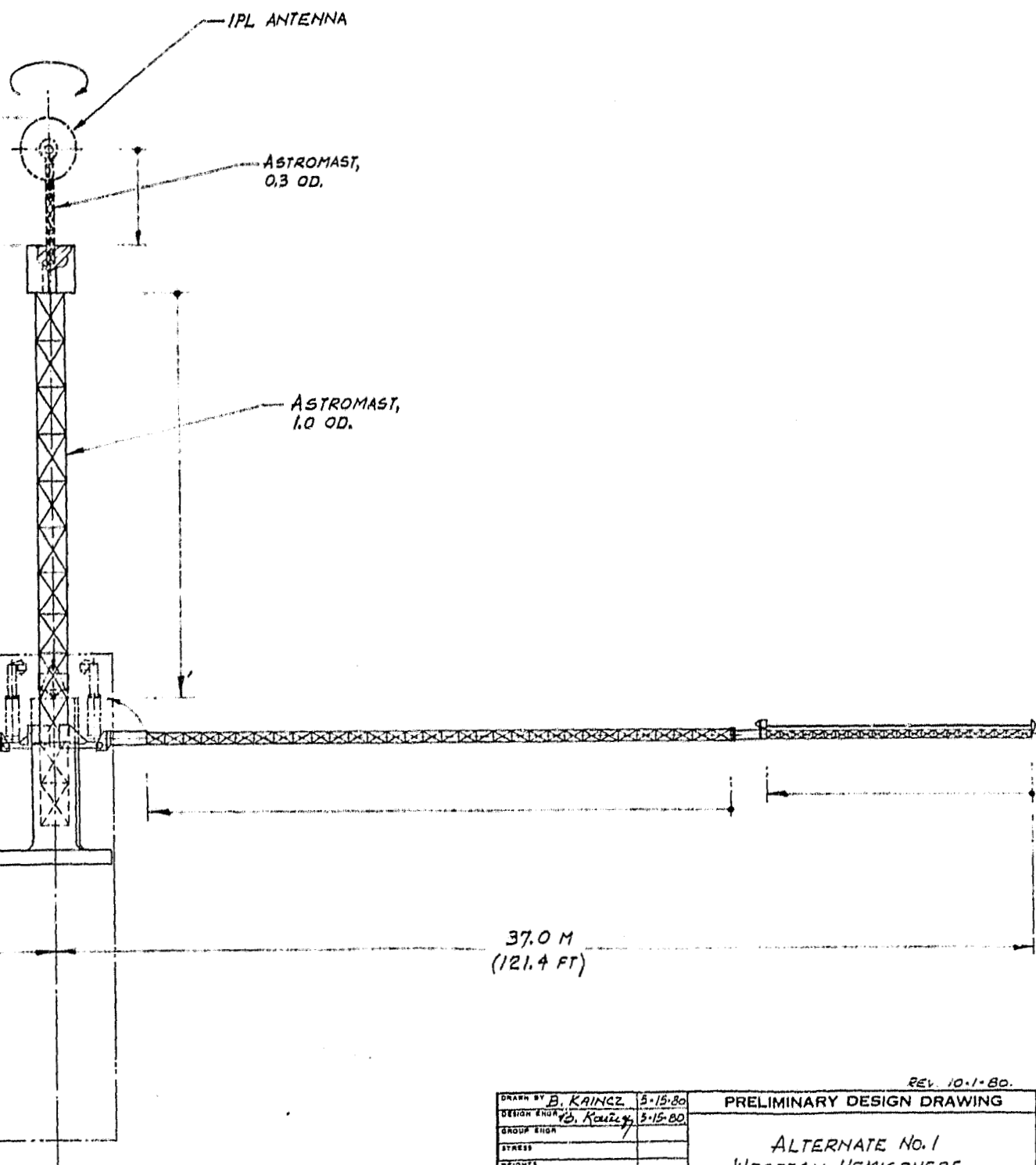
B - 13 (ROTATED 51° CCW.)  
DEPLOYED/PACKAGED Configuration  
(N-S ARMS)

FOLDOUT FRAME

UNLESS OTHERWISE SPECIFIED  
DIMENSIONS ARE IN METERS

0 1 2 4 6 8 10 15

Alternat



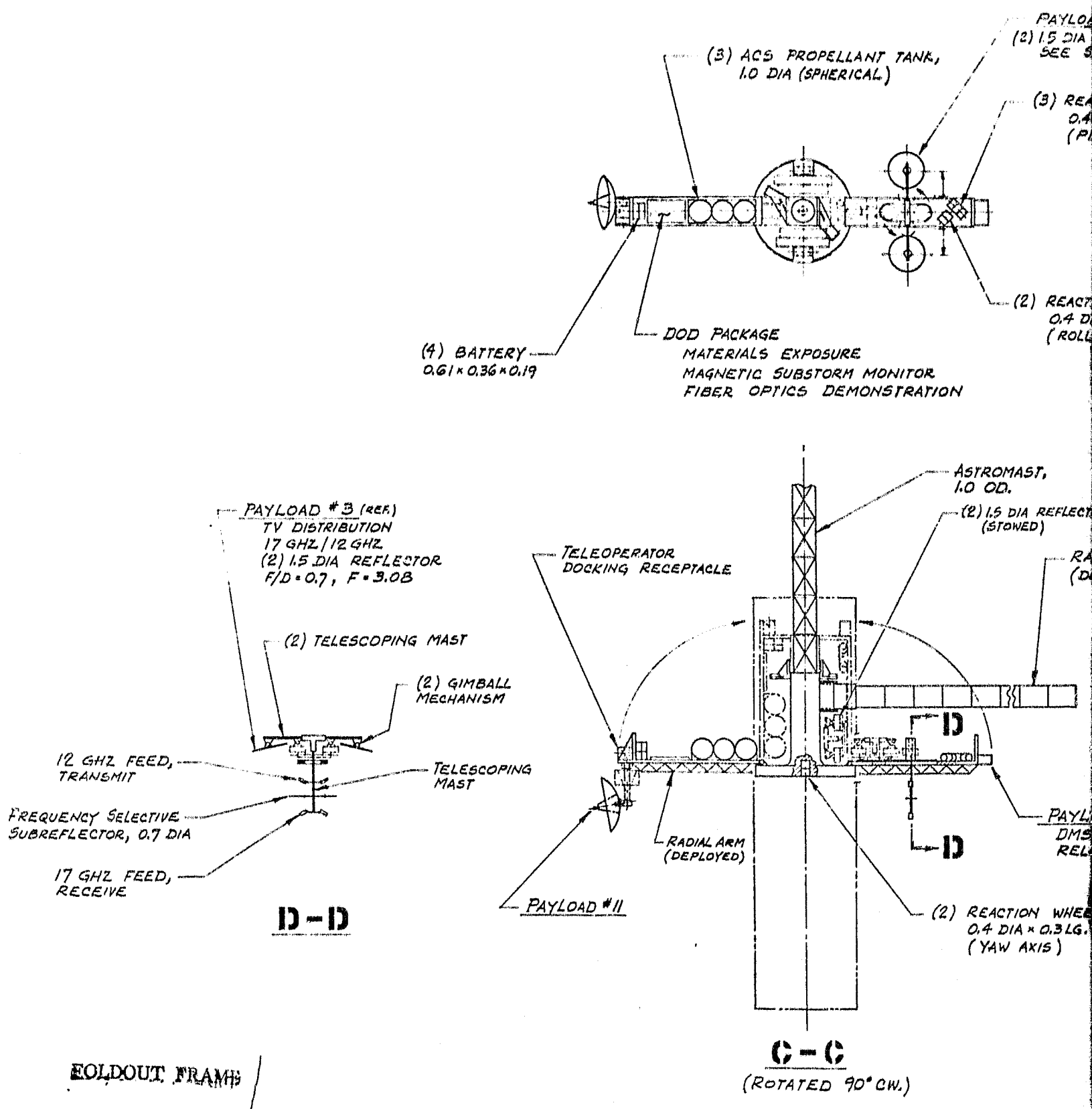
DRAWN BY B. KAINCZ		5-15-80	REV. 10-1-80.	
DESIGN ENGR. B. Kaincz		5-15-80	PRELIMINARY DESIGN DRAWING	
GROUP SIGN				
STRESS				
WEIGHTS				
MATERIAL				
OPERATIONS				
PROJECT				
GENERAL DYNAMICS Convair Division SAN DIEGO, CALIFORNIA		CODE IDENT. 14170	DRAWING NO. FIG 3.1.312-3	
		SCALE 1/100	SHEET 3 OF 4	

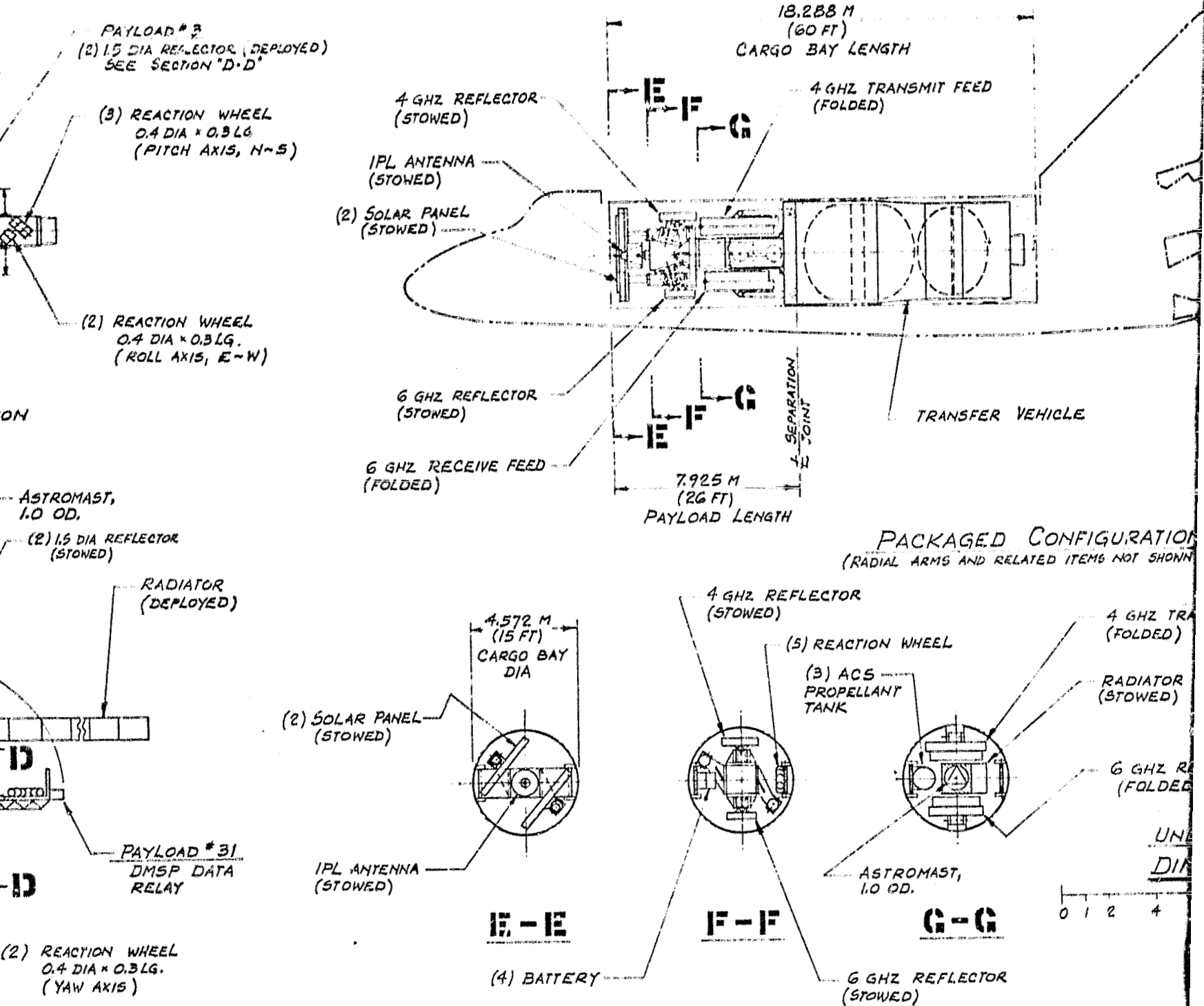
Alternative #1, Western Hemisphere, Platform No. 1

FO-1 (Sheet 3 of 4)

264.352-263-3

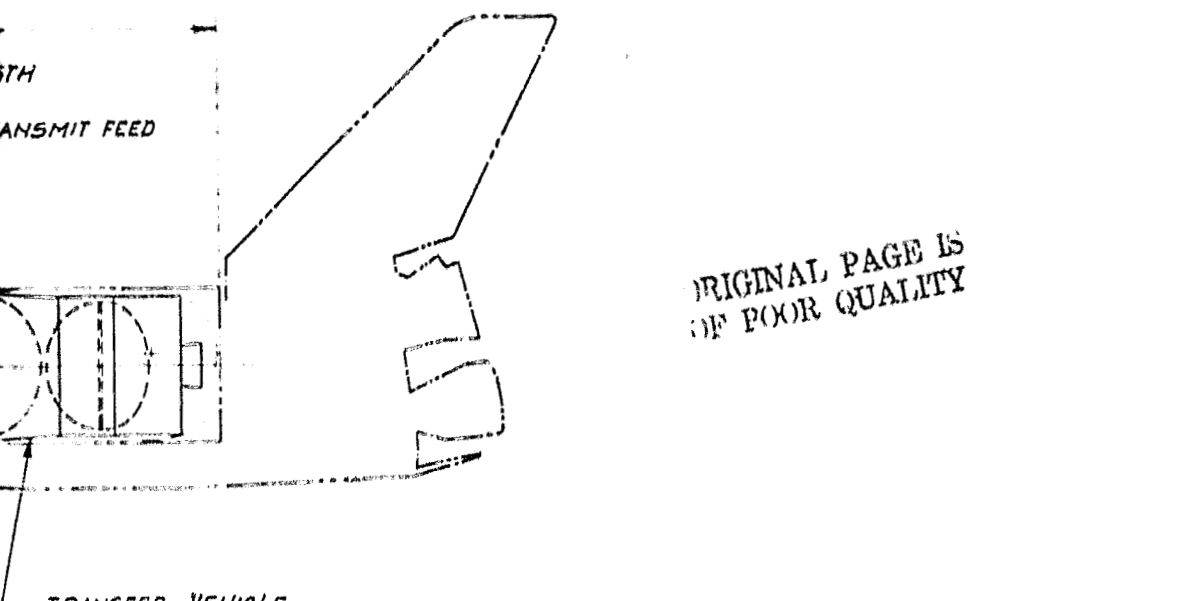
FOLDOUT FRAME 2



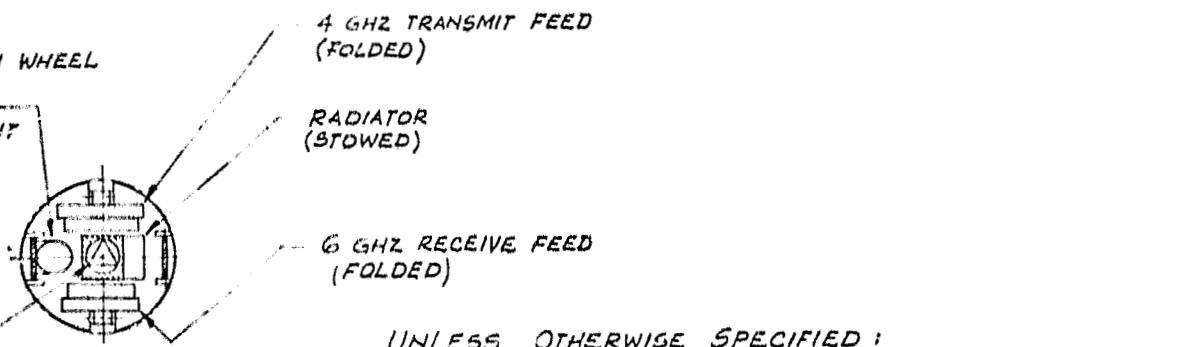


FOLDOUT FRAMES

Alternative #1, Western



**PACKAGED CONFIGURATION**  
(ALL ARMS AND RELATED ITEMS NOT SHOWN FOR CLARITY.)



UNLESS OTHERWISE SPECIFIED:  
DIMENSIONS ARE IN METERS.

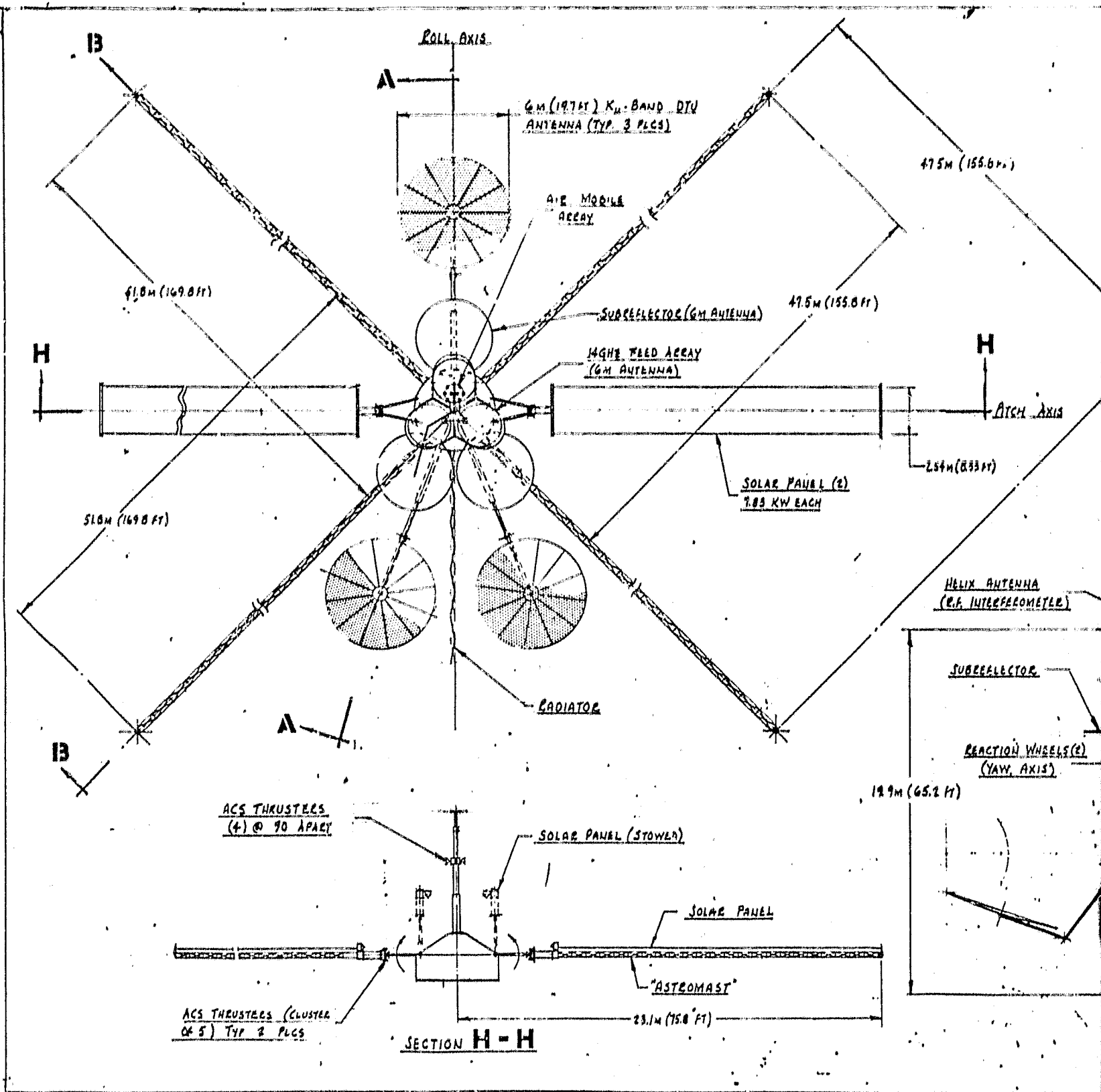
0 1 2 4 6 8 10 15 20M

REV. 10-1-80

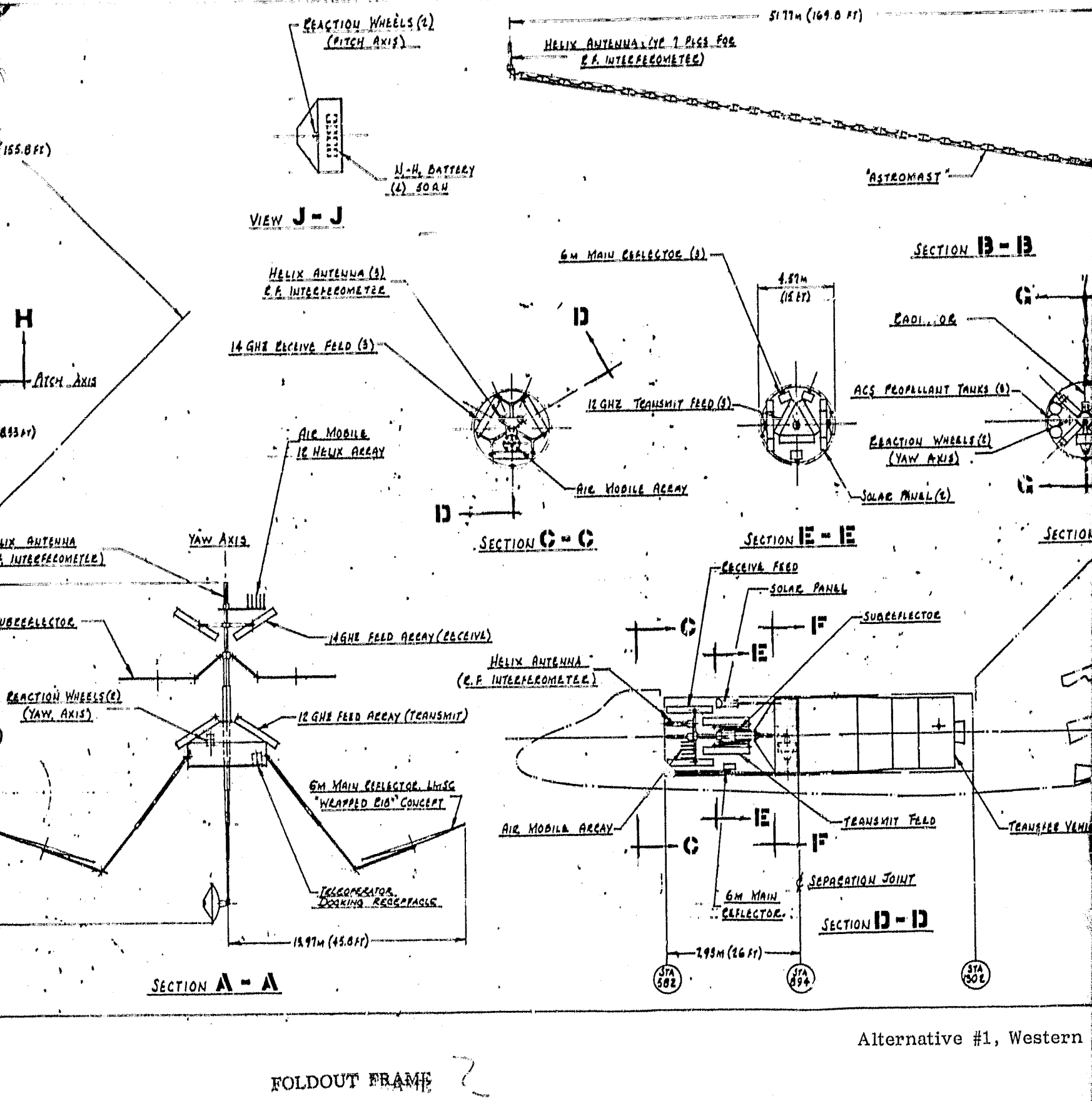
DRAWN BY B. KAINCZ 5-15-80		PRELIMINARY DESIGN DRAWING	
DESIGN ENGR P. Kaincz 5-15-80			
CHECKED BY			
STRESS			
WEIGHTS			
MATERIAL			
OPERATIONS			
PROJECT			
GENERAL DYNAMICS Convair Division SAN DIEGO, CALIFORNIA		CODE IDENT.	DRAWING NO.
		14170	FIG 3.1.312-4
		SCALE 1/100	SHEET 4 or 4

264.362-263-4

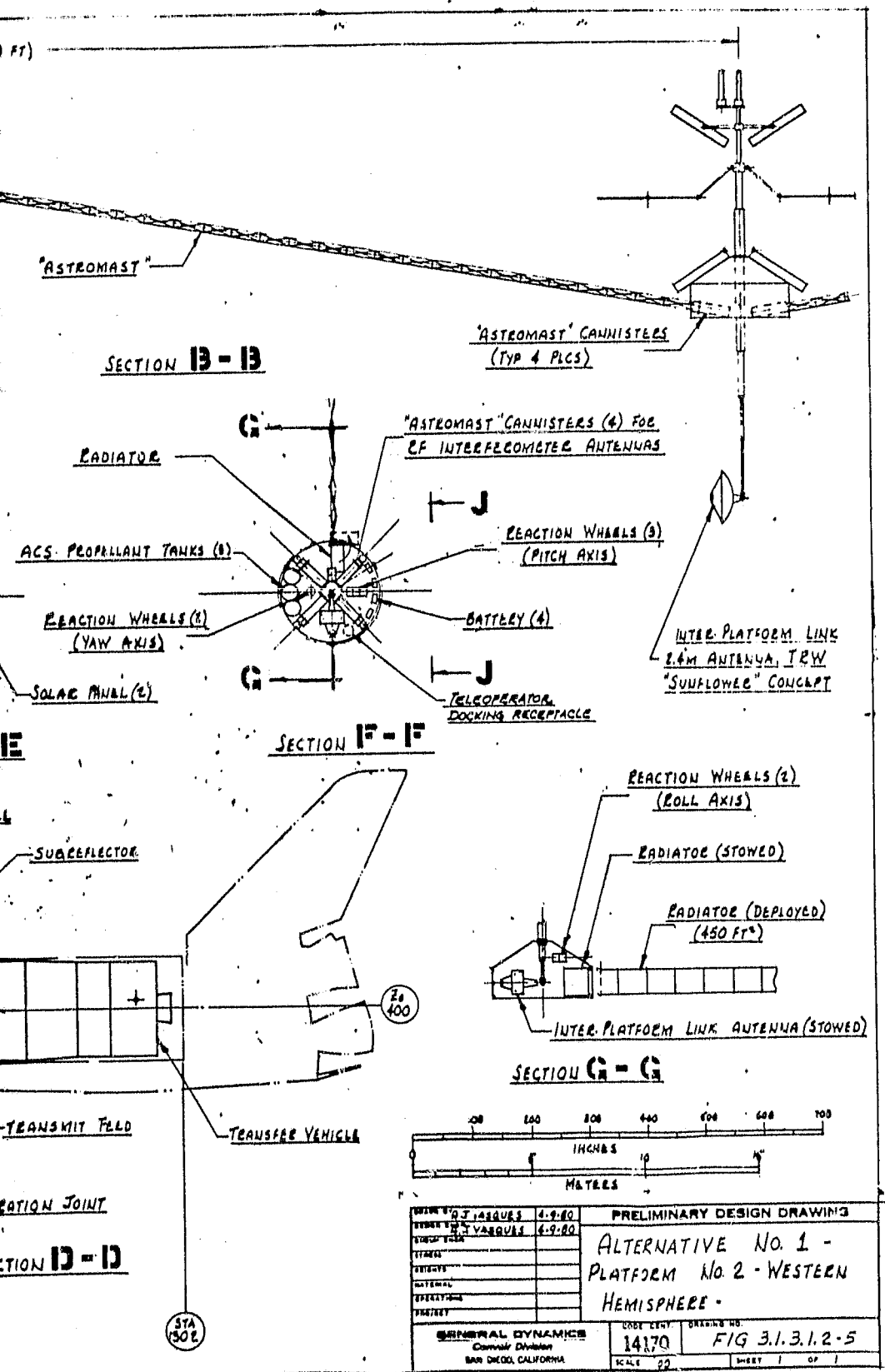
Alternative #1, Western Hemisphere, Platform No. 1  
FO-1 (Sheet 4 of 4)



FOLDOUT FRAME



Alternative #1, Western

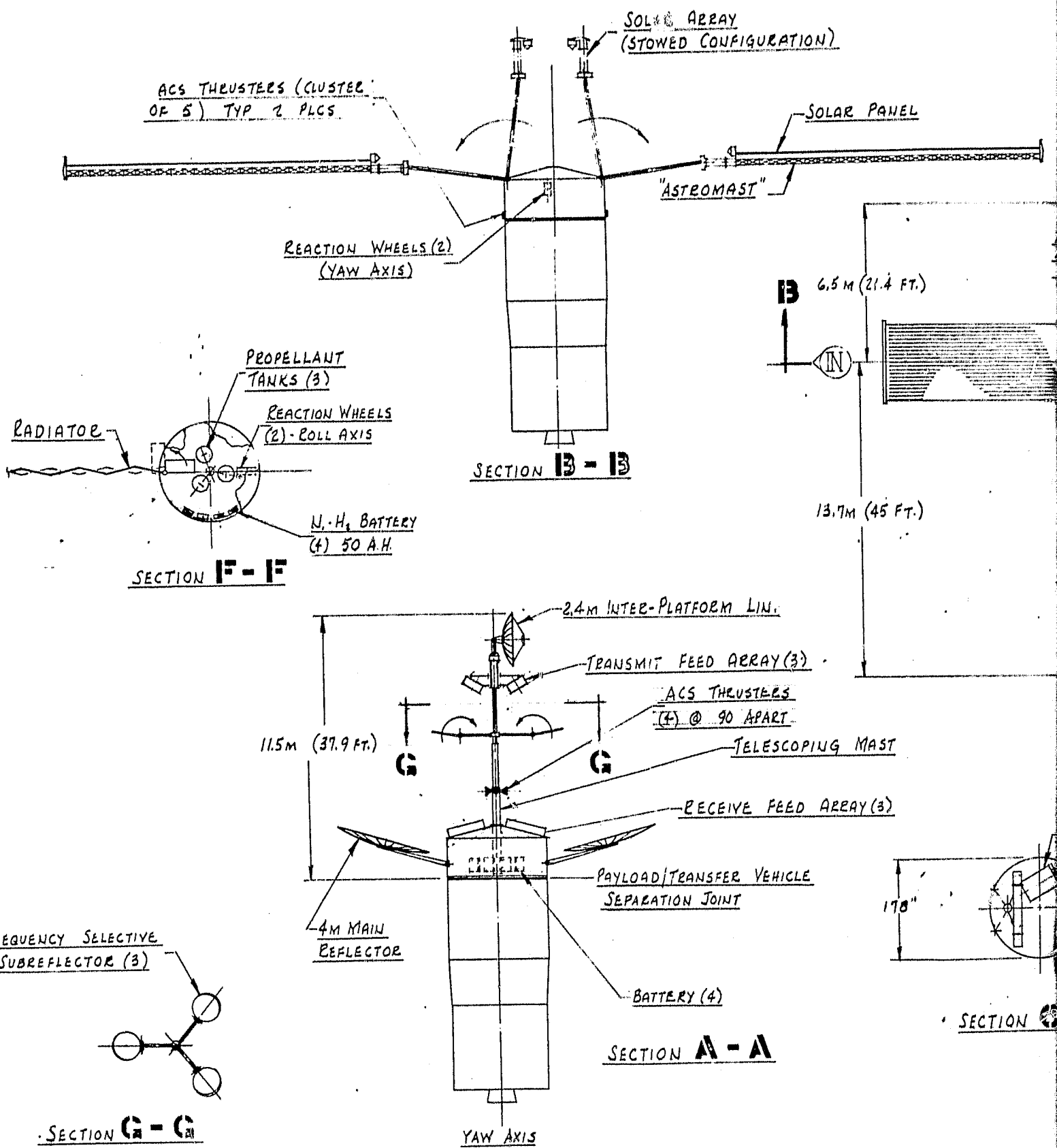


264.362-264

FO-2

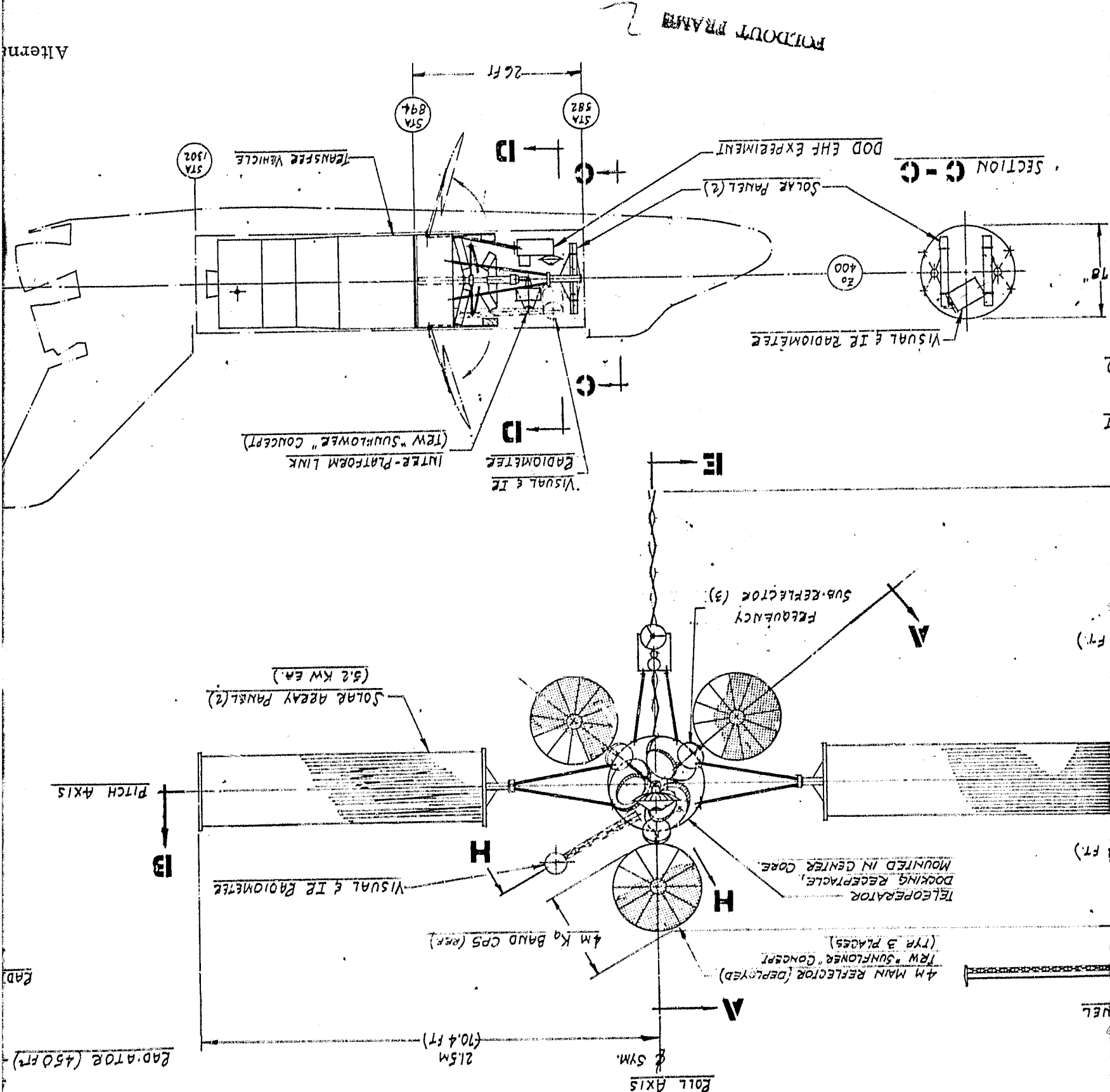
NOT TO SCALE

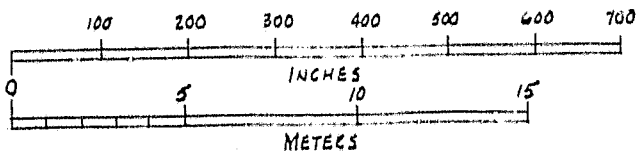
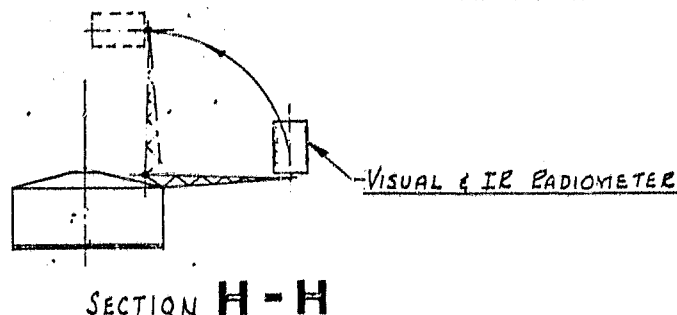
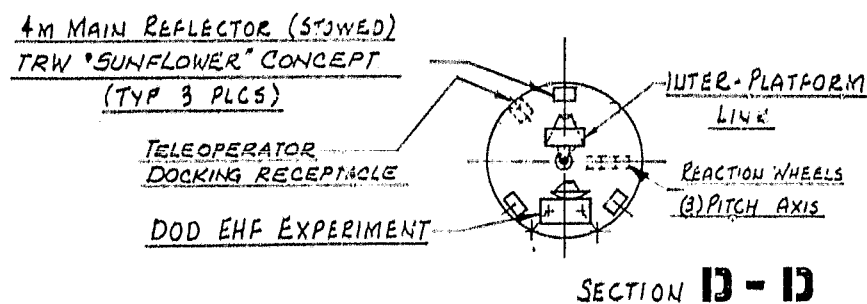
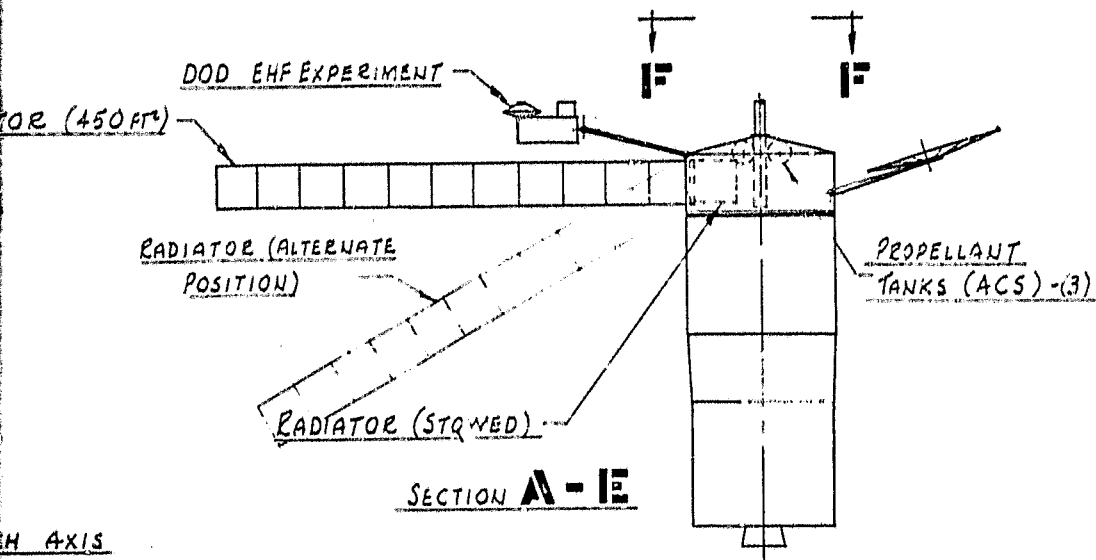
Alternative #1, Western Hemisphere, Platform No. 2



FOLDOUT FRAME

Afternoon





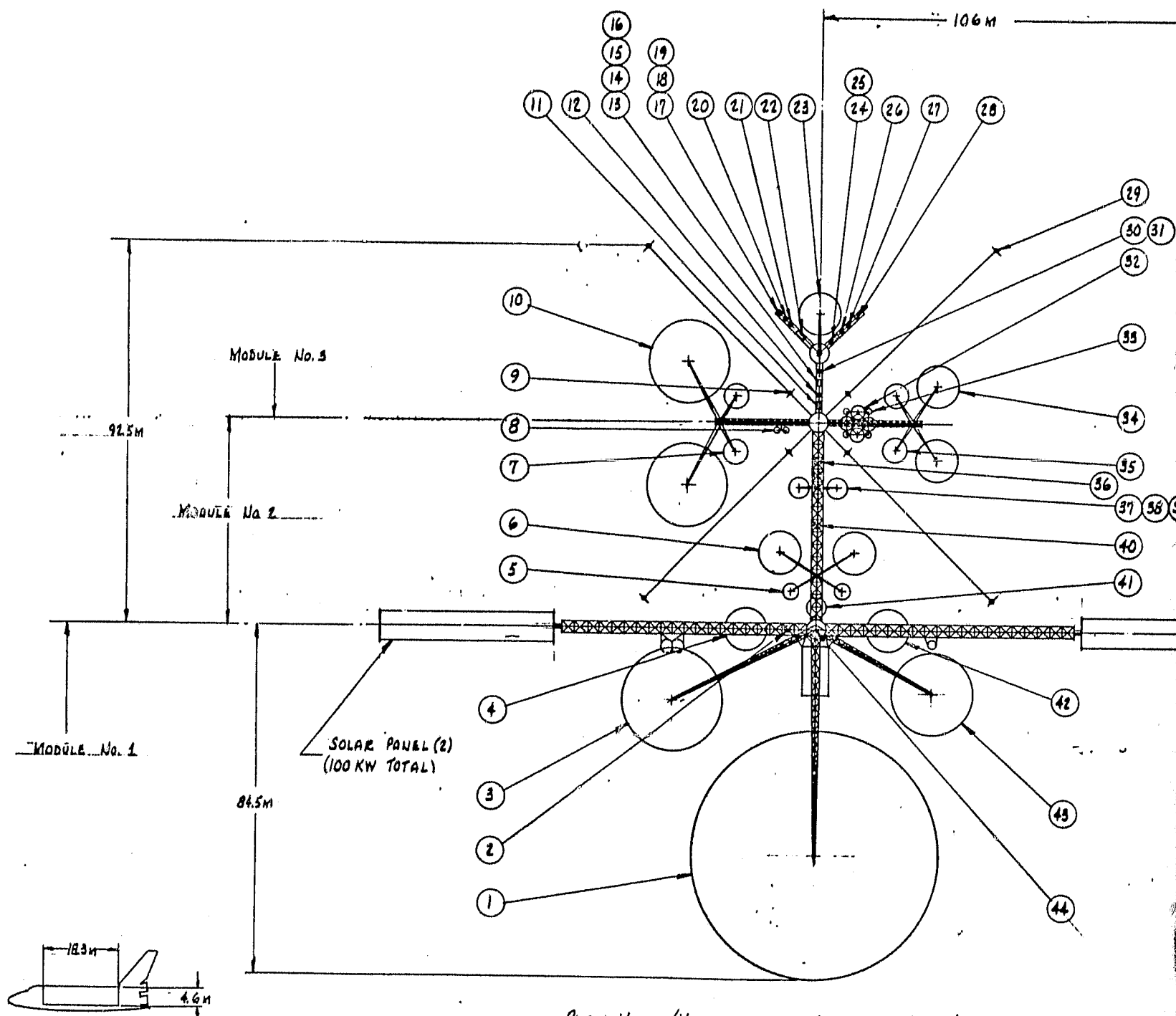
DRAWN BY A.J. VASQUEZ	3-26-80	PRELIMINARY DESIGN DRAWING	
DESIGN ENGR A.J. VASQUEZ	3-16-80		
GROUP ENGR			
STRESS			
WEIGHTS			
MATERIAL			
OPERATIONS			
PROJECT			
GENERAL DYNAMICS Convair Division SAN DIEGO, CALIFORNIA		DATE ISSUED 14170	DRAWING NO. FIG 3.1.3.1.2-6
SCALE 1/100		SHEET 1 OF 1	264,352-265
		REV A 4-17-80	
		REV B 6-19-80	
		REV C 6-17-80	
		REV D 7-7-80	

Alternative #1, Western Hemisphere, Platform No. 6

264,352-265

FO-3

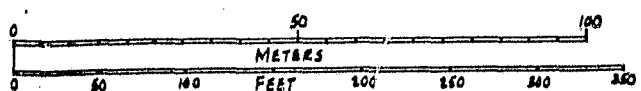
EX-1.DDUT FRAME



FOLDOUT FRAME

Alternative #4,

PAYLOAD NO.	DESCRIPTION	ITEM	SIZE	QTY
1.1	CPS, KU BAND	10	20M	2
		7	6M	2
1.2	CPS, KQ-BAND	6	10M	2
		5	4M	2
2.1	HVT, C-BAND	1	60M	1
		3	25M	1
2.2	HVT, KA-BAND	34	10M	2
		35	6M	2
3	TV DISTRIBUTION	8	1.5M	2
4	TRACKING & DATA RELAY	37	5M	2
		38	2M	1
		39	1.5M(ARRAY)	1
5	EDUCATIONAL TV	32	3M	4
		33	1.5M	4
6	DIRECT TO HOME TV	4	10M	1
		8	1.5M	1
7	AIR MOBILE	40	1M(ARRAY)	1
8	LAND MOBILE	43	20M	1
11	INTER-PLATFORM LINK	44	2.4M	1
12	DATA COLLECTION	42	10M	1
17	LIGHTNING MAPPER	9	HELICIDES	7
18	ATMOSPHERIC SOUNDER	36		
27	EF INTERFEROMETER	29	HELICIDES	7
31	DMSP DATA RELAY	41	5M	1
33	MAT'L'S EXPOSURE	17		
34	ACOSS/HALO DEMO.	28		
36	ADV. ON-BOARD SIG. PROC.	30		
39	SOLAR FLARE MONITOR	13		
40	SOLAR FLARE ISOTOPE MONITOR	14		
41	ENERG. PROTON/HEAVY ION SENSOR	15		
43	MAG. SUB-STOCK MONITOR	18		
44	CHARGED PARTICLE MONITOR	16		
51	CRYOGENIC IR RADIATOR	24		
52	BOSS EVAL.	31		
53	GEMINI EVAL.	26,27		
54	EHF SYSTEM	11		
55	A/C LASER RELAY	12		
56	FIBER OPTICS DEMO	19		
71	EARTH OPTICAL TELESCOPE	20		
73	CHEM. RELEASE MOD. OBSV.	21		
78	CYCO COOLED LIMB SCANNER	25		
79	LLLTV	22		
81	MICROWAVE SOUNDER	23	10M	1



PRELIMINARY DESIGN DRAWING

HIGH TRAFFIC MODEL - WESTERN  
HEMISPHERE - ALTERNATE No. 4

BY A.T. VASQUEZ APPROVED	SCALE 1/500 DATE 5-6-80
COMPAK AEROSPACE DIVISION OF GENERAL DYNAMICS SAN DIEGO, CALIFORNIA	DRAWING NO FIG 3.1, 3.2, 2-1

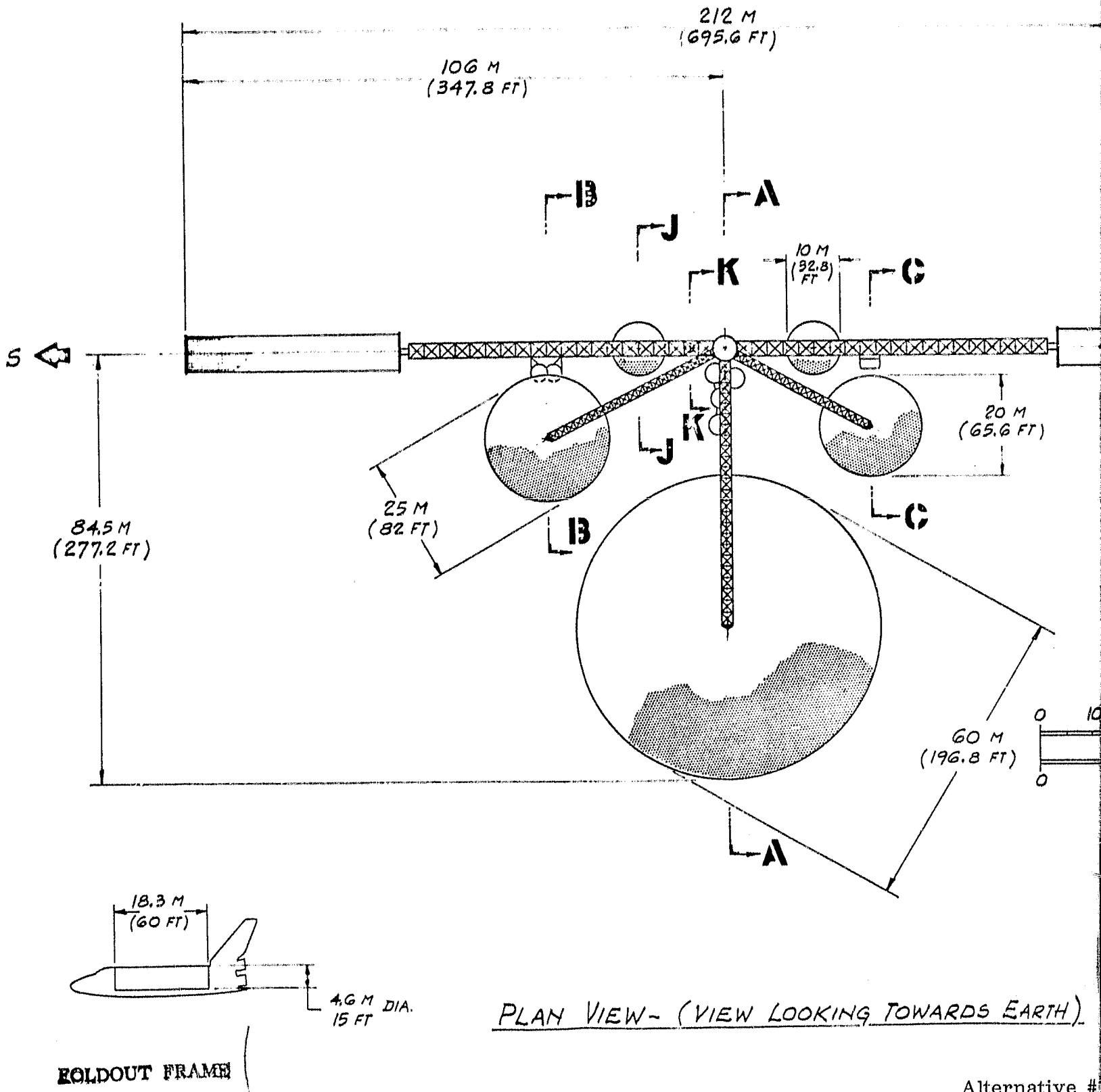
164-15-74

264.352-266

Alternative #4, Western Hemisphere, High Traffic Model

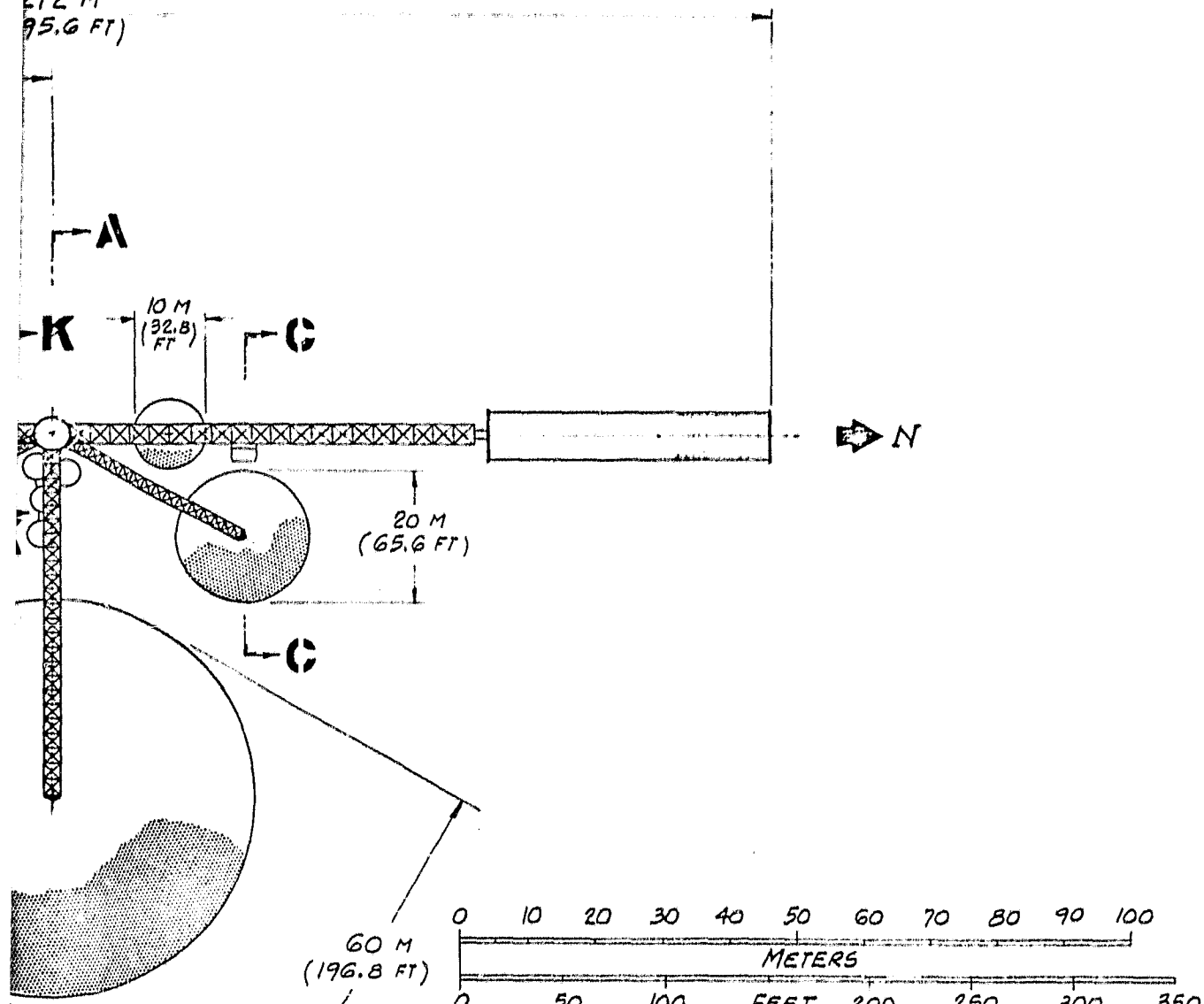
FO-4

ORIGINAL PAGE IS  
IN PINK QUALITY



ORIGINAL PAGE IS  
OF POOR QUALITY

212 M  
(95.6 FT)



VIEW LOOKING TOWARDS EARTH.)

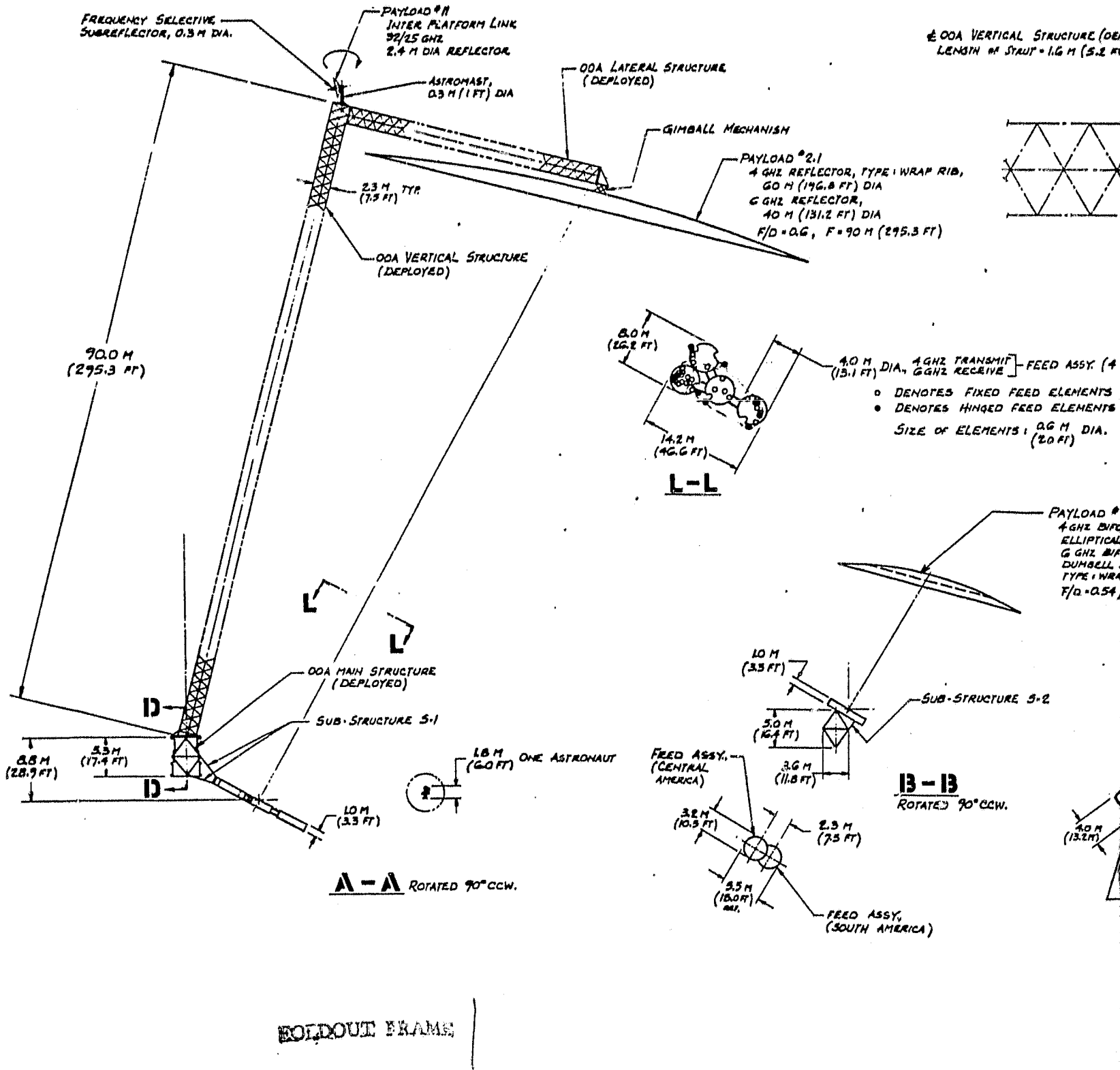
DRAWN BY B. KAINCZ	6-18-80	PRELIMINARY DESIGN DRAWING	
DESIGN ENGR. T. R. Kaincz	6-18-80	ALTERNATE NO. 4	
GROUP ENGR.		WESTERN HEMISPHERE	
STRESS		MODULE NO. 1	
WEIGHTS			
MATERIAL			
OPERATIONS			
PROJECT			
GENERAL DYNAMICS Convair Division SAN DIEGO, CALIFORNIA		CODE IDENT.	DRAWING NO.
		14170	FIG 3.1.3.2.2-2
		SCALE 1/500	SHEET 1 OF 2

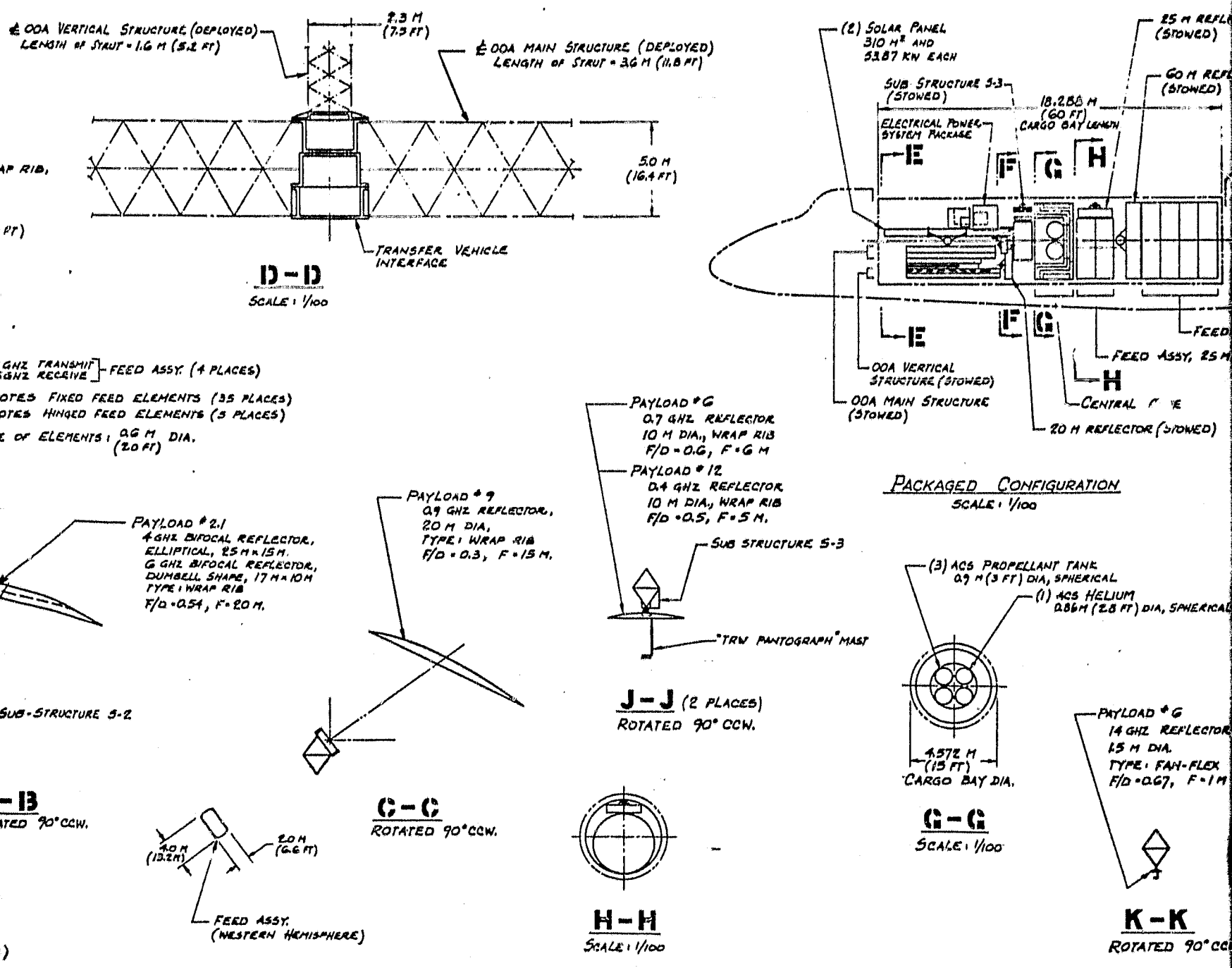
264.352-267-1

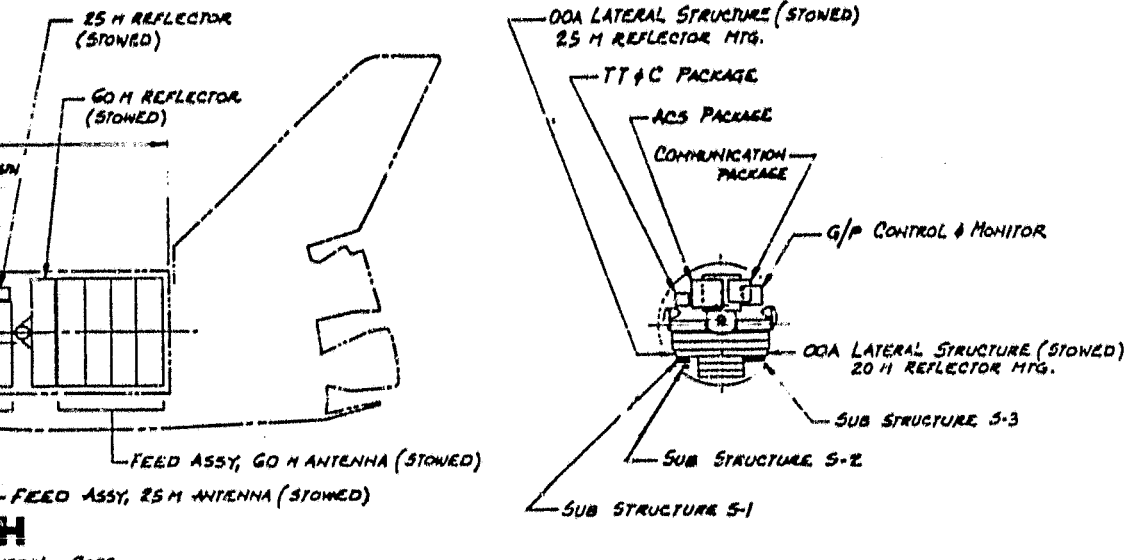
Alternative #1, Western Hemisphere, Module 1

FO-5 (Sheet 1 of 2)

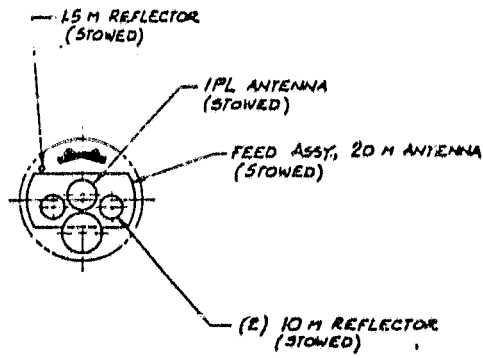
FOLDDOUT FRAME







E - E  
SCALE 1/100



F - F  
SCALE 1/100

Mr. J. Ramez	5/2/69	PRELIMINARY DESIGN DRAWING	
Mr. A. Agius	5/7/69		
DATE ISSUED			
REVISION			
EXPIRES			
ORIGINALS			
REPLICATES			
PRINTED			
GENERAL DYNAMICS CLOUDS DIVISION SAN DIEGO, CALIFORNIA		DRAWING NO.	FIG. 3.1.3.2.2-3
		SCALE 1/250 & ROTATED	HEET 2 - 2

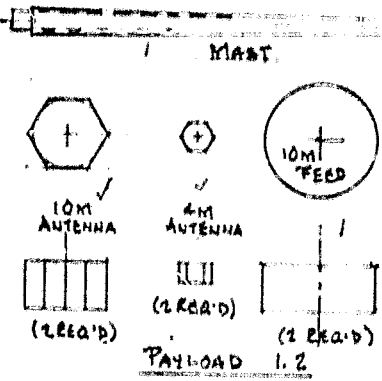
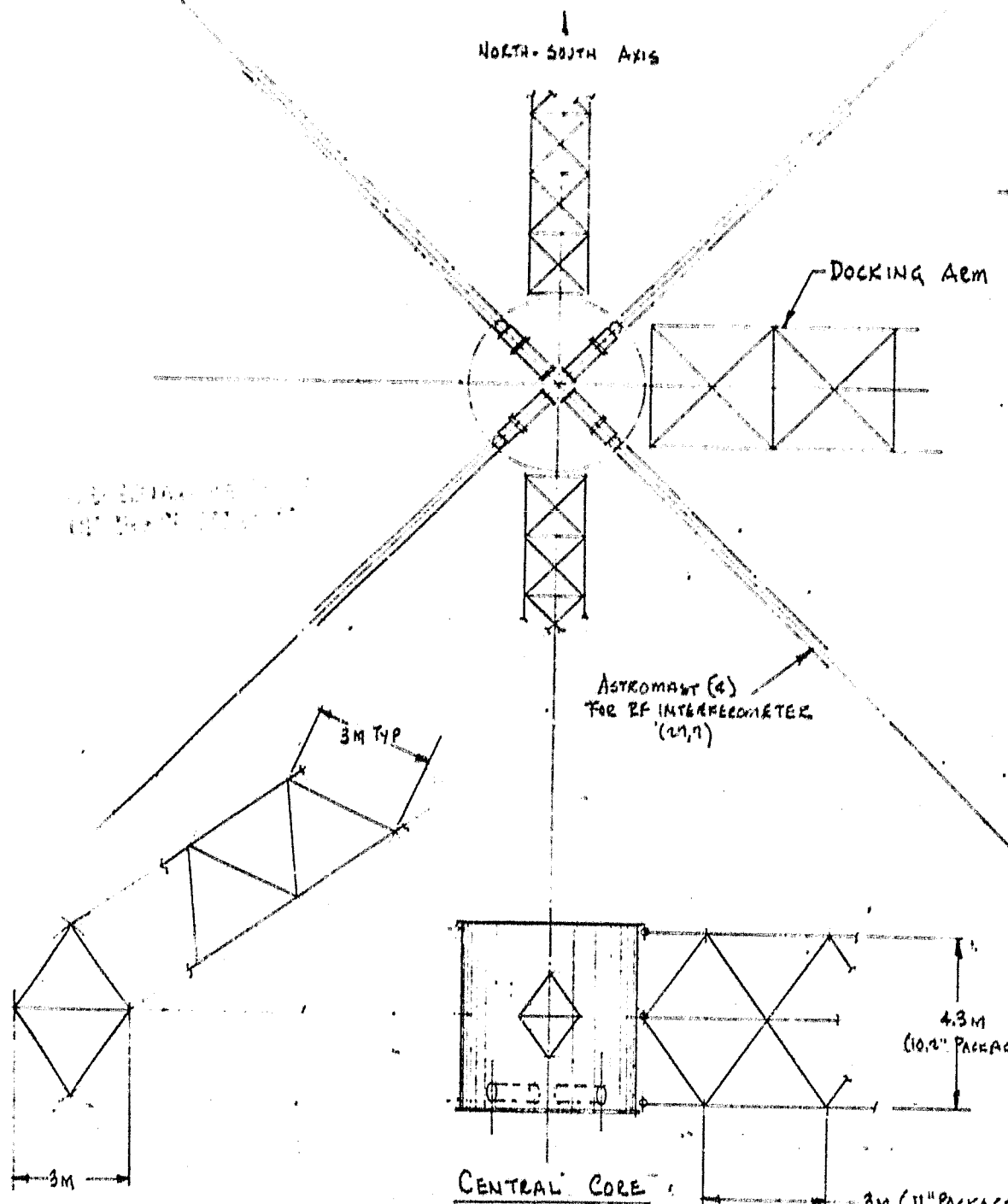
264.352-267-2

K - K  
ROTATED 90° CCW.

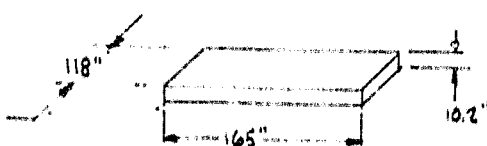
Alternative #1, Western Hemisphere, Module1

FO-5 (Sheet 2 of 2)

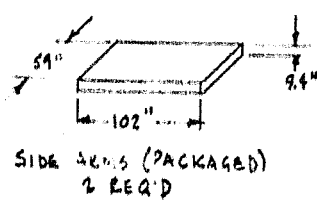
NORTH-SOUTH AXIS



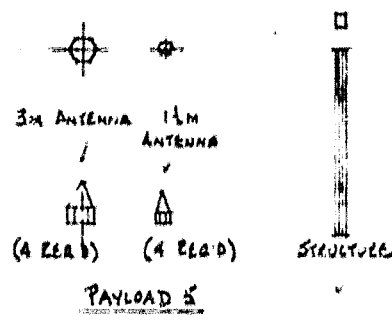
FOLDOUT FRAME



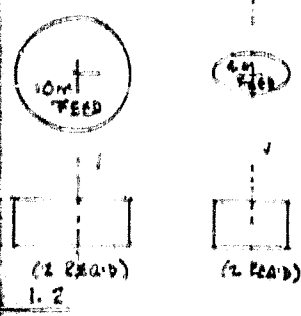
DOCKING ARM (PACKAGED)  
(1 REA'D)



SIDE SKINS (PACKAGED)  
2 REA'D



5M ANT  
PALE



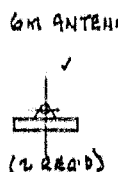
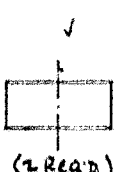
MAST & LATERALS



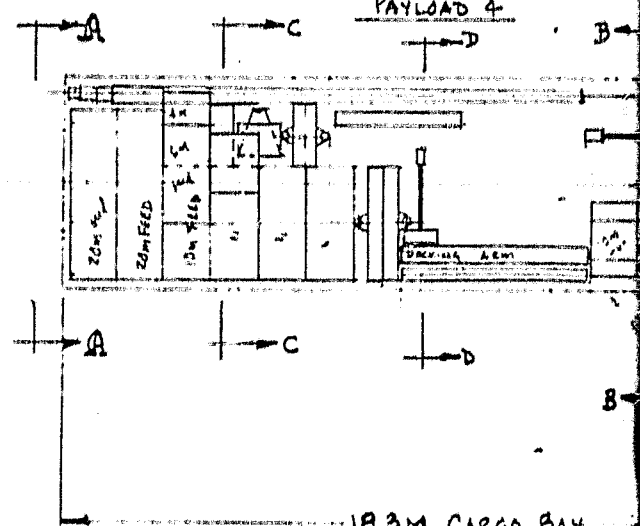
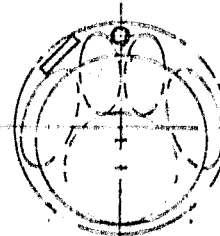
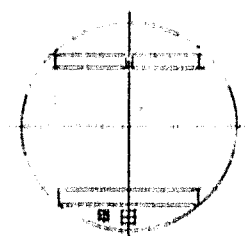
ANTENNA SUPPLIES



5M ANTENNA



PAYLOAD 1.1



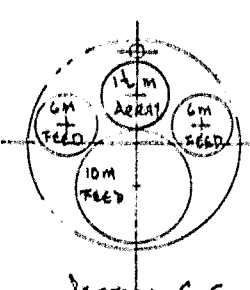
B-

C-

D-

18.3M CARGO BAY

FOLDOUT FRAME



Alte

(2)

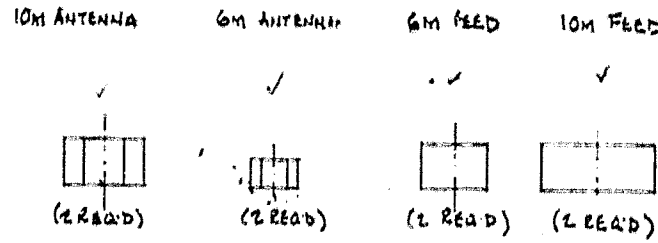
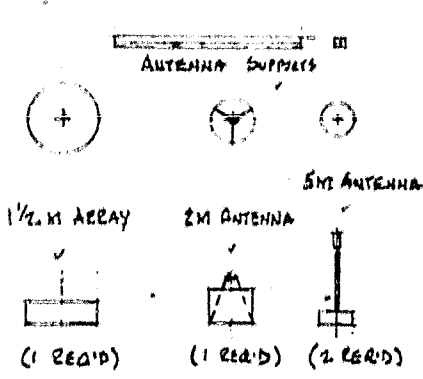
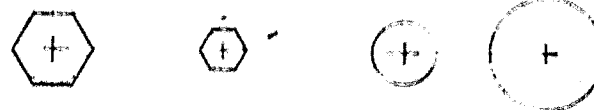
9.4"

(+)

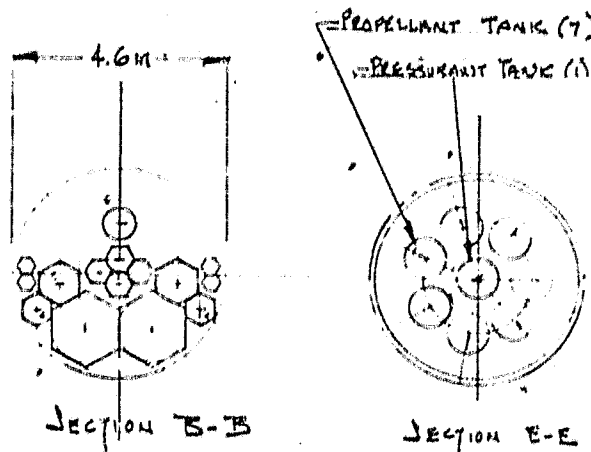


5M ANTENNA (1 READ)  
PAYLOAD 31

MAST (NESTABLE, COLUMN)



PAYLOAD 2.2



18.3 M CARGO BAY

SCALE = 1/100      0 1 2 3 4 5 6 7 8 9 10  
METERS

264.352.268